VOLUME 113 NUMBER 1

THE ASTROPHYSICAL JOURNAL

AN INTERNATIONAL REVIEW OF SPECTROSCOPY AND ASTRONOMICAL PHYSICS

JANUARY 1951

THE ORBIT AND PARALLAX OF PROCYON ... *Strand* 1
THE POLE OF THE GALAXY AS DETERMINED FROM MEASUREMENTS ... 205
MG/SEC ... *Charles L. Sagar and Ralph* 21
DOPPLER-SHIFTED AURORAL HYDROGEN EMISSION ... *Vegard* 50
DISPLACED CALCIUM LINES IN THE SPECTRUM OF HD 190073 ... *Merrill* 55
THE SPECTRA OF VARIABLES OF THE RV TAURI AND YELLOW SEMI-REGULAR TYPES ... *Joy* 60
THE SPECTRA OF R ANDROMEDAE (MAXIMUM) AND MU CEPHEI BETWEEN 7400 AND 8800 A ... *L. H. Aller and J. O. Hynek* 77
HYDROGEN AND HELIUM LINE INTENSITIES IN SOME Be STARS ... *E. Margaret Burbidge and G. R. Burbidge* 84
THE WEAKER LINES IN THE PHOTOGRAPHIC REGION OF SOME A STARS ... *Stephen P. Keenan* 91
INTENSITIES OF THE INTERSTELLAR BAND AT λ 4430 ... *Swings and Struve* 105
TURBULENCE IN THE INTERSTELLAR MEDIUM ... *Aller* 125
SPECTROPHOTOMETRY OF REPRESENTATIVE PLANETARY NEBULAE ... *Aller* 135
A FINDING LIST OF O AND B STARS OF HIGH LUMINOSITY ... *J. J. Nassau and Morgan* 141
ON STELLAR STATISTICS ... *S. Chandrasekhar and Münch* 150
ON THE STELLAR DYNAMICS OF SPHERICAL GALAXIES ... *J. Bel'ze, G. Gamow, and Keller* 164
RADIATION FIELD OF EXTENDED STELLAR ATMOSPHERES ... *Unsöld* 181
PROPAGATION OF SHOCK WAVES IN THE GENERALIZED ROCHE MODEL ... *Pierre A. Crowe, Phyllis A. Fox, Felix Haurwitz, and Kopal* 193
TWO NEW BAND SYSTEMS OF THE *AlO* MOLECULE ... *Herzberg* 310
A NEW BAND SYSTEM OF THE *AlBr* MOLECULE ... *Herzberg* 219
NOTES
PHOTOGRAPHS WITH THE HENYEY-GREENSTEIN WIDE-ANGLE CAMERA ... *Donald Osterbrock and Rudolph Wright* 222
ROTATIONAL STRUCTURE IN THE *R* BRANCH OF THE ATMOSPHERIC NITROGEN OXIDE ... *Elvey* 223
A LIST OF NEWLY DISCOVERED PECULIAR OBJECTS ... *Miss Cannon* 223
CONCERNING ROSS'S PARALLAXES AND SCHLESINGER'S PRIMARIES ... *Ross and Schlesinger* 224

THE UNIVERSITY OF CHICAGO PRESS
CHICAGO, ILLINOIS, U.S.A.

January 1951 Vol. 113, No. 1

THE ASTROPHYSICAL JOURNAL

AN INTERNATIONAL REVIEW OF SPECTROSCOPY AND ASTRONOMICAL PHYSICS

Edited by

W. W. MORGAN
Managing Editor
Yerkes Observatory of the University of Chicago

S. CHANDRASEKHAR

PAUL W. MERRILL
Mount Wilson Observatory of the Carnegie Institution of Washington

HARLOW SHAPLEY
Harvard College Observatory
Cambridge, Massachusetts

N. U. MAYALL
Lick Observatory
University of California

With the Collaboration of the American Astronomical Society

Collaborating Editors:

1949-51

W. BAADE
Mount Wilson Observatory

LEO GOLDBERG
Observatory of the University of Michigan

G. HERZBERG
National Research Council, Ottawa

1950-52

LYMAN SPITZER, JR.
Princeton University Observatory

A. N. VYSSOTSKY
Leander McCormick Observatory

ALBERT E. WHITFORD
Washburn Observatory

The Astrophysical Journal is published bimonthly by the University of Chicago at the University of Chicago Press, 5750 Ellis Avenue, Chicago 37, Illinois, during July, September, November, January, March, and May. ¶Two volumes are published per year, one beginning with the January issue and the other beginning with the July issue. The subscription price is $6.00 per volume or $12.00 per year; the price of single copies is $3.00. (Orders for service of less than a volume will be charged at the single copy rate.) ¶Postage is prepaid by the publishers on all orders from the United States and its possessions. No extra charge is made for postage to countries in the Pan American Postal Union. ¶Postage is charged extra as follows: for Canada, 20 cents per volume, 40 cents per year (total $6.20 per volume, $12.40 per year); on single copies 5 cents (total $3.05); for all other countries in the Postal Union, 50 cents per volume, $1.00 per year (total $6.50 per volume, $13.00 per year), on single copies 10 cents (total $3.10). ¶Subscriptions are payable in advance. Please make all remittances payable to The University of Chicago Press, in United States currency or its equivalent by postal or express money orders or bank drafts.

The following is an authorized agent:

For the British Empire, except North America and Australasia: The Cambridge University Press, Bentley House, 200 Euston Road, London, N.W. 1, England. Prices of yearly subscriptions and of single copies may be had on application.

Claims for missing numbers should be made within the month following the regular month of publication. The publishers expect to supply missing numbers free only when losses have been sustained in transit, and when the reserve stock will permit.

Business correspondence should be addressed to The University of Chicago Press, Chicago 37, Illinois.

Communications for the editors and manuscripts should be addressed to: W. W. Morgan, Editor of THE ASTROPHYSICAL JOURNAL, Yerkes Observatory, Williams Bay, Wisconsin.

Line drawings and photographs should be made by the author, and all marginal notes such as co-ordinates, wave lengths, etc., should be included in the cuts. It will not be possible to set up such material in type.

One copy of the corrected galley proof should be returned as soon as possible to the editor, Yerkes Observatory, Williams Bay, Wisconsin. Authors should take notice that the manuscript will not be sent to them with the proof.

The cable address is "Observatory, Williamsbay, Wisconsin."

The articles in this journal are indexed in the *International Index to Periodicals*, New York, N.Y.

Applications for permission to quote from this journal should be addressed to The University of Chicago Press, and will be freely granted.

Microfilms of complete journal volumes are available to regular subscribers only and may be obtained at the end of the year. Orders and inquiries should be addressed to University Microfilms, 313 North First Street, Ann Arbor, Michigan.

Notice to subscribers: If you change your address, please notify us and your local postmaster immediately. The Post-Office does not forward second-class mail.

Entered as second-class matter, July 31, 1900, at the Post-Office at Chicago, Ill., under the Act of March 3, 1879.
Acceptance for mailing at special rate of postage provided for in United States Postal Act of October 3, 1917, Section 1103, amended February 28, 1925.

[PRINTED IN U.S.A.]

THE ASTROPHYSICAL JOURNAL

AN INTERNATIONAL REVIEW OF SPECTROSCOPY AND ASTRONOMICAL PHYSICS

VOLUME 113 JANUARY 1951 NUMBER 1

THE ORBIT AND PARALLAX OF PROCYON

K. Aa. Strand

Dearborn Observatory, Northwestern University

Received September 1, 1950

ABSTRACT

The orbital motion and the parallax of Procyon have been determined from plates taken at the Yerkes and McCormick Observatories between 1915 and 1949. The parallax has also been determined from a comparison of the astrometric orbit with the radial-velocity variations derived from the measurements of eleven spectra taken with the coudé spectrograph of the 100-inch telescope between 1926 and 1943.

The photographic observations combined with the visual observations made by Aitken and Barnard between 1897 and 1913 give a period of 40.65 years and a semi-major axis of 4".55. With an absolute parallax of +0".287 and a mass ratio of 0.268, the individual masses of the system are 1.74⊙ and 0.63⊙.

I. INTRODUCTION

Procyon = α Canis Minoris = Schaeberle- = ADS 6251; $7^h36^m.7$, +5°21′ (1950), is a visual binary with a period of 40.65 years and a semi-major axis of 4".55, as derived in the present investigation. The combined magnitude on the International photovisual system is 0.45,[1] and the difference between the components is 10.3.[2] The spectrum of the brighter component is F5 IV in the Yerkes system,[3] and the color of the companion has been observed by Kuiper[4] as white.

The most recent investigation of this system was made by Spencer Jones,[5] who obtained the orbit of the bright component relative to the center of mass of the system from a discussion of the meridian observations made between 1755 and 1925 and from a series of high-dispersion spectra taken at the Cape Observatory between 1909 and 1924. Spencer Jones derived a mass for the brighter component which did not agree with the mass-luminosity relation. This deviation was due to the fact that he adopted too large a parallax for the system and found too small a value for the semi-major axis of the relative orbit from a discussion of the visual observations. His orbit did not fully represent the micrometer observations as indicated by the systematic increase with time in the difference between the observed and computed distances after 1902. The results of the present investigation, based mainly on the photographic observations, give a mass of the expected order of value for the brighter component, and the computed motion agrees closely with the micrometer observations of Aitken and Barnard.

[1] G. P. Kuiper, *Ap. J.*, **88**, 477, 1938.

[2] G. P. Kuiper, *ibid.*, **85**, 253, 1937.

[3] W. W. Morgan, unpublished data.

[4] The results kindly communicated in advance of publication.

[5] *M.N.*, **88**, 403, 1926.

II. THE YERKES PHOTOGRAPHIC OBSERVATIONS

Between 1916 and 1949, 104 plates on 66 nights were taken with the 40-inch Yerkes refractor. A special sector with two blades running at different speeds provided a reduction of approximately 10 mag. of the image of Procyon for the plates taken before 1948. This procedure was changed in 1948, after which the plates were taken with a sector giving a reduction of 6 mag., while the additional 4-mag. reduction was provided by the use of an objective grating giving a 4-mag. difference between central image and first-order spectra. As will be seen from the later discussion, the accuracy of the plate solution increased. The exposure time before 1932 was 5 minutes, and after 1939 about 1 minute. The measurements were made by the writer on the Gaertner long-screw measuring machine at the Yerkes Observatory in the direction of right ascension (x) and declination (y) for the approximate equator of the year 2000. Four reference stars of visual magnitudes ranging from 10.3 to 10.8 were used, while the image of Procyon was reduced to 10.2. The standard frame and dependences for the approximate epoch 1947.0 are given in Table 1. The spectra were furnished by Dr. A. N. Vyssotsky.

TABLE 1

REFERENCE STARS FOR YERKES PLATES

No.	AC+5°57	Sp.	Mag.	Diam. (Mm)	x_0 (Mm)	y_0 (Mm)	Dependences
1.....	130	A2	10.3	0.174	−50.76	− 0.90	0.180+0.00089 (t−1947.0)
2.....	132	A9	10.8	.127	−28.55	+64.16	.177− .00088
3.....	147	B1	10.7	.132	+14.41	−53.74	.298+ .00090
4.....	165	F2	10.5	.144	+64.90	− 9.52	0.345−0.00091
Procyon....	148	.....	10.2	0.192	+12.54	− 8.12	.....

Table 2 contains the mean epoch, hour angle, parallax factors in right ascension and declination, elliptical rectangular co-ordinates, the solutions and their residuals in the same order, and the assigned weight, which depended upon the number of exposures and their quality, with allowance for an irreducible night error, when several plates for one night were combined. The elliptical rectangular co-ordinates were derived from the investigation of the orbit discussed in Section V. The scale factor used is 1 mm = 10".655. The four epochs for 1950, each consisting of four plates, were taken after the completion of the investigation and were not used in the computations.

III. THE MCCORMICK PHOTOGRAPHIC MATERIAL

From a preliminary discussion of the Yerkes material it appeared that a satisfactory solution for the orbital motion could not be obtained, owing to the lack of observations between 1928–1930 and 1933–1938. Fortunately, these time intervals were covered by plates taken with the 26-inch refractor at the McCormick Observatory. Dr. H. L. Alden kindly furnished the measurements of these McCormick series of Procyon. He also took a series of new plates in 1948–1949 to strengthen the conversion of the McCormick solutions to the scale of the Yerkes solutions.

Between 1915 and 1949, ninety-seven plates were taken on fifty nights. The plates obtained in 1915–1916 were taken with a sector, reducing Procyon to a magnitude of 7.5, while on the later plates the star was reduced to a magnitude of 8.9 by means of a neutral filter and a sector. The measurements were made by Drs. C. M. Anderson (the plates taken between 1915–1928 and 1935–1942), P. van de Kamp (1929–1932), and Mr. T. Sully (1948–1949) on the Gaertner long-screw measuring machines at the McCormick

TABLE 2

OBSERVING DATA, MEASURED POSITIONS, AND RESIDUALS

EPOCH	H.A. (MIN.)	P_α	P_δ	$\bar{X}$	$\bar{Y}$	X (MM)	Y (MM)	O−C		WT.
								x	y	
1916.247....	+79	−0.964	+0.095	−0.9049	−0.7911	+14.4782	−5.1143	+0.025	−0.029	1.0
.274....	+57	− .988	+ .144	−0.9018	− .7927	+14.4788	−5.1181	+ .059	− .059	1.0
.840....	−02	+ .933	− .230	−0.8369	− .8244	+14.4968	−5.1626	+ .130	+ .069	0.5
.883....	+03	+ .812	− .278	−0.8318	− .8267	+14.4794	−5.1816	+ .011	− .081	0.5
.902....	−21	+ .738	− .294	−0.8295	− .8277	+14.4915	−5.1741	+ .176	+ .019	0.3
17.167....	−05	− .737	− .064	−0.7976	− .8409	+14.4094	−5.1914	− .090	+ .009	1.0
.877....	−02	+ .833	− .273	−0.7076	− .8721	+14.4191	−5.2612	+ .088	− .053	0.5
.885....	+20	+ .805	− .280	−0.7066	− .8724	+14.4112	−5.2621	+ .018	− .054	1.2
.943....	−08	+ .549	− .311	−0.6989	− .8746	+14.3926	−5.2665	− .066	− .043	0.8
.962....	+07	+ .445	− .311	−0.6963	− .8753	+14.3840	−5.2456	− .115	+ .197	0.5
18.153....	−08	− .674	− .092	−0.6709	− .8822	+14.3464	−5.2726	− .064	+ .018	1.0
.183....	−23	− .799	− .033	−0.6670	− .8832	+14.3426	−5.2709	− .048	+ .048	0.7
.230....	00	− .933	+ .059	−0.6606	− .8848	+14.3395	−5.2780	− .009	− .012	1.7
.240....	+28	− .953	+ .081	−0.6592	− .8852	+14.3300	−5.2765	− .098	+ .007	1.2
.260....	+19	− .979	+ .117	−0.6566	− .8858	+14.3306	−5.2769	− .069	+ .011	1.2
.806....	−01	+ .978	− .178	−0.5809	− .9014	+14.3480	−5.3321	− .050	− .020	0.7
.868....	+09	+ .862	− .264	−0.5720	− .9028	+14.3602	−5.3301	+ .157	+ .077	0.7
.871....	+15	+ .853	− .267	−0.5716	− .9029	+14.3368	−5.3395	− .088	− .019	1.0
19.103....	−27	− .416	− .181	−0.5383	− .9077	+14.2975	−5.3523	+ .012	+ .025	1.0
.180....	+09	− .786	− .040	−0.5271	− .9091	+14.2879	−5.3601	+ .068	− .030	0.7
.188....	+12	− .816	− .024	−0.5259	− .9092	+14.2754	−5.3612	− .051	− .038	0.7
.865....	−20	+ .872	− .260	−0.4246	− .9162	+14.2751	−5.4235	− .068	− .051	1.0
.887....	−14	+ .800	− .282	−0.4213	− .9163	+14.2849	−5.4181	+ .071	+ .032	1.0
.898....	−21	+ .757	− .290	−0.4196	− .9163	+14.2759	−5.4263	− .005	− .044	1.0
20.050....	−06	− .588	− .125	−0.3961	− .9165	+14.2205	−5.4370	− .114	− .070	1.7
21.151....	−02	− .665	− .096	−0.2204	− .9016	+14.1673	−5.5153	+ .060	+ .042	0.7
.208....	−11	− .881	+ .017	−0.2112	− .9000	+14.1500	−5.5185	− .028	+ .028	1.4
.861....	−06	+ .883	− .256	−0.1028	− .8751	+14.1541	−5.5752	− .077	+ .062	0.5
.915....	−36	+ .682	− .301	−0.0938	− .8724	+14.1568	−5.5787	+ .042	+ .085	1.0
22.169....	−18	− .745	− .060	−0.0511	− .8589	+14.1131	−5.5857	+ .132	+ .167	0.5
.186....	+10	− .810	− .027	−0.0482	− .8579	+14.1045	−5.5930	+ .069	+ .095	1.0
.803....	−37	+ .980	− .174	+0.0559	− .8157	+14.1012	−5.6610	− .110	− .050	0.5
.849....	−18	+ .906	− .242	+0.0635	− .8121	+14.1179	−5.6500	+ .115	+ .126	1.0
23.152....	−01	− .671	− .093	+0.1144	− .7859	+14.0509	−5.6904	+ .017	− .079	1.4
24.160....	−18	− .704	− .079	+0.2781	− .6735	+14.0046	−5.7747	+ .072	− .079	1.4
27.101....	+76	− .416	− .184	+0.5917	− .1173	+13.8789	−6.0404	.000	− .030	1.0
31.191....	+01	− .836	− .012	+0.2543	+ .6930	+13.6792	−6.4726	+ .005	+ .038	1.0
.213....	+08	− .901	+ .031	+0.2507	+ .6959	+13.6720	−6.4751	− .042	+ .028	0.7
.229....	+02	− .938	+ .064	+0.2482	+ .6978	+13.6775	−6.4710	+ .037	+ .082	0.5
32.226....	+22	− .931	+ .058	+0.0845	+ .8017	+13.6135	−6.5962	− .026	− .051	1.7
.248....	+17	− .968	+ .099	+0.0809	+ .8035	+13.6156	−6.5812	+ .022	+ .124	0.5
39.810....	−31	+ .972	− .191	−0.9954	+ .7363	+13.1313	−7.4133	− .004	+ .030	1.0
.959....	+46	+ .450	− .311	−1.0102	+ .7261	+13.1063	−7.4338	− .003	+ .005	1.7
41.182....	−09	− .803	− .031	−1.1212	+ .6349	+12.9829	−7.5499	+ .034	+ .014	1.2
.212....	−30	− .898	+ .029	−1.1237	+ .6324	+12.9765	−7.5525	+ .018	+ .004	1.2
.217....	+05	− .912	+ .040	−1.1241	+ .6321	+12.9786	−7.5529	+ .047	+ .002	1.0
.220....	+14	− .918	+ .046	−1.1244	+ .6318	+12.9786	−7.5484	+ .051	+ .051	1.4
46.883....	−08	+ .806	− .280	−1.3934	+ .1053	+12.5825	−8.1110	+ .032	− .003	0.3
.943....	−31	+ .536	− .311	−1.3941	+ .0993	+12.5625	−8.1182	− .055	− .012	0.7
47.044....	−41	−0.069	−0.260	−1.3953	+0.0890	+12.5452	−8.1274	+0.014	−0.021	0.7

TABLE 2—*Continued*

Epoch	H.A. (Mn.)	P_α	P_δ	$\bar{X}$	$\bar{Y}$	X (Mm)	Y (Mm)	O−C		Wt.
								x	y	
1947.159....	+04	−0.710	−0.076	−1.3964	+0.0774	+12.5131	−8.1332	−0".052	−0".018	2.0
.175....	−22	− .778	− .044	−1.3966	+ .0758	+12.5056	−8.1322	− .098	.000	2.0
.989....	+11	+ .274	− .307	−1.4000	− .0065	+12.4773	−8.2116	− .025	+ .030	2.0
48.129....	+18	− .568	− .135	−1.3997	− .0207	+12.4394	−8.2136	− .076	+ .099	2.0
.139....	−24	− .618	− .117	−1.3997	− .0217	+12.4574	−8.2344	+ .140	− .117	1.7
.199....	−36	− .861	+ .002	−1.3995	− .0278	+12.4398	−8.2316	+ .070	− .061	1.2
.215....	+38	− .907	+ .035	−1.3995	− .0294	+12.4258	−8.2260	− .053	+ .006	1.7
.229....	+56	− .938	+ .062	−1.3994	− .0307	+12.4298	−8.2175	+ .010	+ .103	1.7
.237....	+18	− .952	+ .078	−1.3994	− .0315	+12.4270	−8.2238	− .010	+ .039	2.0
.851....	+61	+ .902	− .248	−1.3948	− .0936	+12.4220	−8.3009	− .080	− .093	0.7
.879....	+46	+ .819	− .279	−1.3944	− .0964	+12.4248	−8.2992	− .003	− .039	2.0
.922....	+65	+ .638	− .308	−1.3939	− .1007	+12.4182	−8.3037	+ .013	− .038	2.9
.999....	+28	+ .212	− .301	−1.3930	− .1085	+12.3994	−8.3063	− .004	+ .009	2.8
49.002....	+28	+ .193	− .300	−1.3929	− .1088	+12.4010	−8.3096	+ .022	− .025	2.0
.135....	+14	− .602	− .122	−1.3911	− .1222	+12.3679	−8.3154	.000	− .004	3.0
.206....	+17	− .884	− .101	−1.3900	− .1293	+12.3565	−8.3186	+ .017	+ .025	2.7
50.017....	+41	+ .096	− .289	−1.3733	− .2105	+12.3208	−8.4030	+ .026	− .040	2.8
.056....	+17	− .144	− .249	−1.3723	− .2142	+12.3044	−8.4013	− .050	+ .004	2.3
.091....	+20	− .360	− .199	−1.3714	− .2176	+12.3061	−8.4062	+ .058	− .028	2.2
.198....	+36	−0.857	−0.001	−1.3685	−0.2283	+12.2813	−8.4120	+0.021	−0.040	2.6

TABLE 3

Reference Stars for McCormick Plates

No.	McC-7, 104	Sp.	Mag.	Diam. (Mm)	x_s (Mm)	y_s (Mm)	Dependences
1.....	26	M2	9.6	0.12	−49.48	+19.71	0.231+0.00020 (t−1930)
2.....	32a	M0	8.5	.19	−35.79	−31.01	.243+ .00097
3.....	60	K0	9.3	.14	+20.87	+55.15	.248− .00123
4.....	89	K0	8.1	0.23	+64.40	−43.85	0.278+0.00006
Procyon...	.....	.....	.....	.....	+ 2.95	− 1.50	.....

Observatory in the direction of right ascension (x) and declination (y) for the approximate equator of the year 2000. Four reference stars were used, of visual magnitudes ranging from 8.1 to 9.6. The standard frame and dependences for the approximate epoch 1930.0 are given in Table 3. The spectra were furnished by Dr. A. N. Vyssotsky.

Table 4 lists the mean epoch, hour angle, parallax factors in right ascension and declination, the elliptical rectangular co-ordinates of the astrometric orbit discussed in Section V, the solutions in x and y, converted to the Yerkes system as explained in Section IV, the final residuals, and the weights which were assigned on the same basis as those for the Yerkes plates.

IV. THE REDUCTION OF THE McCORMICK SOLUTIONS TO THE YERKES SOLUTIONS

A direct reduction of the McCormick and the Yerkes solutions to the same system was not possible because the Yerkes comparison star No. 1 did not appear on the

TABLE 4

Observing Data, Measured Positions, and Residuals

Epoch	H.A. (Min.)	P_α	P_δ	$\bar{X}$	$\bar{Y}$	X' (Mm)	Y' (Mm)	O−C		Wt.
								x	y	
1915.167	−03	−0.742	−0.064	−1.0175	−0.7209	+14.5817	−5.0150	+0".215	+0".132	1.0
.198	+20	− .852	− .004	−1.0144	− .7231	+14.5626	−5.0283	+ .067	+ .003	1.0
.200	+11	− .861	+ .002	−1.0143	− .7232	+14.5805	−5.0493	+ .261	− .219	1.0
.208	+14	− .885	+ .018	−1.0134	− .7238	+14.5454	−5.0271	− .099	+ .019	1.0
.238	+44	− .953	+ .078	−1.0105	− .7258	+14.5372	−5.0213	− .145	+ .093	1.0
.831	+28	+ .947	− .220	−0.9500	− .7654	+14.5488	−5.0887	− .101	− .015	1.5
.853	−22	+ .901	− .249	−0.9476	− .7669	+14.5547	−5.0909	− .011	− .012	1.7
.858	−60	+ .887	− .255	−0.9472	− .7672	+14.5574	−5.0784	+ .027	+ .129	1.7
.907	+10	+ .712	− .300	−0.9419	− .7703	+14.5311	−5.1049	− .167	− .097	1.4
16.194	+50	− .842	− .010	−0.9107	− .7880	+14.4942	−5.1077	+ .091	+ .051	1.7
.216	+22	− .905	+ .033	−0.9084	− .7892	+14.4691	−5.1154	− .142	− .022	1.0
.232	+26	− .941	+ .066	−0.9066	− .7902	+14.4720	−5.1122	− .092	+ .018	1.7
.264	+28	− .984	+ .129	−0.9030	− .7921	+14.5066	−5.1240	+ .315	− .097	0.7
23.239	+09	− .953	+ .783	+0.1289	− .7778	+14.0336	−5.6969	− .070	− .087	0.7
.247	+13	− .965	+ .094	+0.1302	− .7770	+14.0369	−5.6947	− .026	− .059	1.0
.260	+48	− .980	+ .120	+0.1322	− .7759	+14.0406	−5.6855	+ .025	+ .039	0.7
27.986	+30	+ .293	− .308	+0.5950	+ .0909	+13.8707	−6.1426	+ .063	− .098	1.7
28.035	+12	− .012	− .273	+0.5937	+ .1023	+13.8485	−6.1264	− .067	+ .120	1.4
29.217	+26	− .910	+ .038	+0.5174	+ .3645	+13.7866	−6.2568	+ .068	.000	2.2
.943	−09	+ .533	− .314	+0.4353	+ .5038	+13.7847	−6.3427	+ .013	+ .036	2.1
.954	+19	+ .475	− .314	+0.4339	+ .5058	+13.7795	−6.3450	− .021	+ .023	1.7
30.224	+33	− .927	+ .053	+0.3981	+ .5521	+13.7298	−6.3775	− .012	− .097	1.7
.271	+42	− .988	+ .142	+0.3917	+ .5598	+13.7244	−6.3716	− .027	− .001	1.7
31.153	+43	− .684	− .090	+0.2602	+ .6883	+13.6874	−6.4747	− .003	+ .021	1.7
.800	−14	+ .980	− .173	+0.1554	+ .7621	+13.6978	−6.5508	+ .036	+ .012	2.2
.893	−20	+ .769	− .290	+0.1401	+ .7713	+13.6860	−6.5670	+ .028	− .017	1.7
32.130	+09	− .576	− .132	+0.1006	+ .7934	+13.6282	−6.5840	− .062	+ .046	1.7
.204	+10	− .876	+ .012	+0.0883	+ .7998	+13.6224	−6.5886	+ .009	+ .047	1.7
35.898	−03	+ .746	− .294	−0.5092	+ .9110	+13.4068	−7.0063	− .119	+ .035	1.4
37.220	+72	− .918	+ .044	−0.6941	+ .8760	+13.2823	−7.1504	+ .039	− .080	2.2
.924	+38	+ .629	− .309	−0.7841	+ .8462	+13.2736	−7.2164	+ .072	+ .103	1.3
38.888	+05	+ .786	− .287	−0.8977	+ .7949	+13.2007	−7.3277	+ .016	− .016	1.7
39.134	+45	− .594	− .126	−0.9248	+ .7801	+13.1410	−7.3484	− .036	− .010	2.9
.183	+46	− .808	− .030	−0.9301	+ .7771	+13.1271	−7.3544	− .086	− .045	2.1
.896	+12	+ .756	− .293	−1.0040	+ .7305	+13.1204	−7.4280	− .018	+ .023	1.7
.909	−21	+ .700	− .301	−1.0053	+ .7295	+13.1148	−7.4283	− .051	+ .036	1.7
40.193	+18	− .843	− .009	−1.0329	+ .7096	+13.0478	−7.4586	− .101	− .055	1.3
41.905	+05	+ .717	− .299	−1.1781	+ .5757	+12.9684	−7.6322	+ .017	+ .011	1.5
.962	−08	+ .427	− .314	−1.1822	+ .5710	+12.9656	−7.6468	+ .116	− .080	1.7
42.034	+70	− .005	− .274	−1.1875	+ .5648	+12.9426	−7.6453	+ .050	+ .001	1.7
.036	−06	− .022	− .271	−1.1877	+ .5647	+12.9443	−7.6554	+ .076	− .104	2.2
.066	−30	− .210	− .236	−1.1898	+ .5622	+12.9388	−7.6478	+ .094	− .001	1.7
.080	+03	− .294	− .216	−1.1908	+ .5609	+12.9236	−7.6544	− .033	− .062	1.7
48.182	−01	− .806	− .032	−1.3996	− .0261	+12.4370	−8.2217	− .020	+ .068	2.0
.229	+07	− .937	+ .062	−1.3994	− .0307	+12.4310	−8.2255	− .009	+ .049	2.1
.876	−09	+ .829	− .276	−1.3945	− .0961	+12.4220	−8.2947	− .066	+ .034	1.5
.895	−20	+ .758	− .292	−1.3943	− .0980	+12.4279	−8.2974	+ .033	+ .029	2.4
49.141	+10	− .629	− .113	−1.3910	− .1228	+12.3675	−8.3157	− .021	+ .026	1.3
.198	−36	− .858	.000	−1.3901	− .1285	+12.3639	−8.3264	+ .051	− .064	2.0
.214	+16	−0.905	+0.033	−1.3898	−0.1302	+12.3488	−8.3192	−0.082	+0.021	1.9

McCormick plates, owing to its position under the sector, and the McCormick comparison stars Nos. 3 and 4 were outside the usable field of the Yerkes plates. Since the two series of plates were exposed to different limiting magnitudes, there appeared no possibility of choosing a common set of comparison stars.

In order to obtain the necessary scale and orientation factors for converting the McCormick solutions to the Yerkes solutions, the co-ordinates of the Yerkes comparison stars Nos. 2, 3, and 4 were measured on the McCormick standard plate No. 26687 (1929.943), and the co-ordinates for the McCormick comparison stars Nos. 1 and 2 were measured on the Yerkes standard plates Nos. 12673–12674 (1947.175).

From these measurements the following equations were obtained:

$$X' = +1.9531X - 0.0014Y\,, \qquad Y' = +0.0028X + 1.9498Y\,,$$

where X' and Y' are the values of the X, Y solutions on the McCormick plates reduced to the orientation and the scale of the Yerkes plates. The above values for the scale factors agree well enough with the value 1.947 obtained from the ratio of the scale values normally used for the McCormick (1 mm = 20".748) and the Yerkes plates (1 mm = 10".655).

In order to check the factors derived above and to find the zero-point corrections as well as the correction for differential proper motion between the two reference systems, normal places were formed from plates taken at both observatories at nearly the same epoch. Both series were corrected for a parallax of 0".293 (Yerkes 0.0275 mm; McCormick 0.0141 mm). An additional correction for proper motion was applied to the Yerkes results to bring them to the epoch of the McCormick plates. These corrections were: -0.0628 in x and -0.0941 in y in units of millimeters per year. Additional small corrections were applied for the orbital motion as derived from the provisional orbit.

Table 5 lists the results for the Yerkes normal places in the following order: mean epoch, number of plates, X and Y in millimeters corrected for a parallax of 0".293 (0.0275 mm), X and Y in the fifth and sixth columns corrected for proper motion, and orbital motion to the epoch given in the last column.

Table 6 lists the results for the McCormick normal places in the following order: mean epoch, number of plates, X and Y in millimeters corrected for a parallax of 0".293 (0.0141 mm), X' and Y' in millimeters, using the above conversion factor for orientation and scale. The next two columns give the difference between the Yerkes and the McCormick solutions, while the following two columns give the differences in x and y for the individual normal place as compared with the mean. The agreement in the x co-ordinate is extremely close, indicating no differential proper motion between the two systems and giving a p.e. of the individual normal place of ± 0.0011 mm. The differences in the Y column show the presence of differential proper motion between the systems. A further study of these residuals shows that a term linear with time fails to bring the necessary agreement between the two series of observations and that the introduction of an additional term quadratic with time is necessary to bring the two systems into a close agreement in the y co-ordinate. The residuals from this conversion are given in the last column of Table 6 and indicate a p.e. of the individual normal place equal to ± 0.0011 mm. The factors for reducing the McCormick solutions (X, Y) to those of the Yerkes (X', Y') are thus

$$X' = +1.9531X - 0.0014Y + 13.8542\,,$$

$$Y' = +0.0028X + 1.9498Y + 0.00100\,(E - 1930) + 0.000061\,(E - 1930)^2 - 6.3943\,,$$

where E is the epoch of the observations.

The acceleration term at present cannot definitely be attributed to the McCormick series. However, the computations which follow for the orbital motion show preference

for the application of this term to the McCormick series. To explain this term solely as a spurious acceleration term which depends upon the product of yearly change of the dependences of the reference stars due to the proper motion of the central star and upon the proper motion of the reference stars will necessitate a proper motion of 0.05 mm per year for either McCormick reference stars No. 2 and No. 3, both having the largest yearly changes in their dependences ($\Delta D_2 = +0.0010$; $\Delta D_3 = -0.0012$), or a proper motion of half this amount for each of the stars in opposite directions. It seems unlikely that the proper motions are as large as indicated by this effect.

TABLE 5

YERKES NORMAL PLACES FOR SCALE

Epoch	No. of Plates	X (Mm)	Y (Mm)	X (Mm)	Y (Mm)	Epoch
1916.260...	2	+14.5053	−5.1195	+14.5069	−5.1175	1916.236
23.152...	2	+14.0693	−5.6878	+14.0650	−5.6956	23.249
32.233...	3	+13.6402	−6.5932	+13.6438	−6.5859	32.167
39.884...	2	+13.0992	−7.4166	+13.0979	−7.4184	39.902
48.191...	12	+12.4605	−8.2240	+12.4594	−8.2254	48.206
48.895...	9	+12.4012	−8.2933	+12.4016	−8.2927	48.889
49.170...	8	+12.3826	−8.3166	+12.3809	−8.3187	49.193

TABLE 6

MCCORMICK NORMAL PLACES FOR SCALE

Epoch	No. of Plates	X (Mm)	Y (Mm)	X' (Mm)	Y' (Mm)	Yerkes−McCormick		O−C		
						x (Mm)	y (Mm)	x (Mm)	y (Mm)	y (Mm)
1916.236	4	+0.3342	+0.6553	+0.6515	+1.2786	+13.8554	−6.3961	+0.0012	−0.0207	+0.0004
23.249	3	+ .1075	+0.3605	+0.2092	+0.7032	+13.8558	−6.3988	+ .0016	− .0232	− .0003
32.167	4	− .1070	−0.0988	−0.2091	−0.1929	+13.8529	−6.3930	− .0013	− .0176	− .0012
39.902	4	− .3878	−0.5337	−0.7566	−1.0417	+13.8545	−6.3767	+ .0003	− .0013	+ .0017
48.206	4	− .7157	−0.9572	−1.3966	−1.8683	+13.8560	−6.3571	+ .0018	+ .0183	− .0012
48.889	3	− .7430	−0.9912	−1.4496	−1.9371	+13.8512	−6.3556	− .0030	+ .0198	− .0020
49.193	5	−0.7547	−1.0085	−1.4729	−1.9685	+13.8538	−6.3502	−0.0004	+0.0252	+0.0024

The acceleration can also be attributed to an error in the orientation of the plates relative to the optical axis of the telescope. This would give rise to a similar effect, owing to the change with time in the position of Procyon relative to the comparison stars and the center of the plate.

V. THE DETERMINATION OF THE ASTROMETRIC ORBIT

The X and Y values for the Yerkes (Table 2, seventh and eighth cols.) and the McCormick nightly means (Table 4, seventh and eighth cols.) were corrected for a parallax of 0".293 (0.0275 mm) and 0".291 (0.0273 mm), respectively, assuming an absolute parallax of 0".295 for both systems. In addition, the nightly means were reduced to the epoch of 1930.0, adopting the provisional proper motions:

$$\mu_x = -0.06630 \text{ mm}, \qquad \mu_y = -0.09529 \text{ mm}.$$

The nightly means combined into seasonal means in X and Y were plotted against time in order to derive the time of the periastron passage and the eccentricity from the projected displacement-curves, following the same procedure as that first outlined by K. Schwarzschild for spectroscopic binaries.[6] Normally, the displacement-curves in the two co-ordinates serve as an independent check on the derived values. In this case, however, it was found that the points on the $\Delta\delta$-curve for periastron and apastron fell close to the maximum and minimum displacements, thus making the time of periastron almost indeterminate from this co-ordinate. The periastron was determined as $T = 1927.5$ from the displacement-curve in $\Delta\alpha \cos\delta$. The value of the eccentricity determined from the ratio of the projected distances, center focus, and center periastron in the two displacement-curves was derived to be: $e = 0.39$. Prior to the determination of these values for T and e, the period 40.75 years was found by comparing the position angles observed between 1897 and 1909 with those derived from the displacement-curves.

In order to improve the dynamical elements derived from the graphical method, a series of seventeen orbits was computed. For each orbit a set of dynamical elements was adopted, and the orientational elements were computed from a least-squares solution, using the sum of the squares of the residuals as a criterion for the fitness of the orbit. In this investigation the period was varied between 39.5 and 41.0 years, the eccentricity between 0.32 and 0.44, and the time of periastron between 1927.0 and 1927.7.

This investigation indicated that the following orbital elements gave the closest agreement with the photographic observations, as well as with the visual position angles observed by Aitken and Barnard between 1897 and 1909:

$$P = 40.65\,, \qquad T = 1927.60\,, \qquad e = 0.40\,.$$

The corresponding values for the orientational elements are:

$$A = +0.0901 \text{ mm}\,, \qquad B = +0.0232 \text{ mm}\,,$$
$$F = -0.0287 \text{ mm}\,, \qquad G = +0.1109 \text{ mm}\,.$$

The co-ordinates for the center of gravity were: $c_x = +13.6998$ mm, $c_y = -6.3669$ mm. A change of 0.1 year in P and T and a change of 0.01 in the value of e from the above value showed definite increases in the residuals of the photographic observations.

Since the above elements were derived after assuming the parallax and the proper motion of the system and with equal weights assigned to each normal place regardless of the number of observations it contained, a definitive solution was made in both co-ordinates in which the final corrections were derived for the adopted parallax and proper motion and for the orientation elements, together with the probable errors. Because the photographic observations did not cover a complete period, a correction for this value could not be obtained, and no attempt was made to correct either the eccentricity or the time of periastron passage.

The residuals Δx and Δy between the measured co-ordinates and the provisional values for the parallax, proper motion, and orbital motion give the following equations of condition for the zero epoch 1930.0:

$$\Delta x = \Delta c_x + \Delta c_x' + \Delta B\bar{X} + \Delta G\bar{Y} + \Delta\pi P_\alpha + \Delta\mu_x t\,,$$
$$\Delta y = \Delta c_y + \Delta c_y' + \Delta A\bar{X} + \Delta F\bar{Y} + \Delta\pi P_\delta + \Delta\mu_y t\,,$$

where Δc_x, Δc_y, and $\Delta c_x'$, and $\Delta c_y'$ are the corrections to the zero point for the Yerkes and the McCormick plates; $\Delta\mu_x$ and $\Delta\mu_y$ the component corrections in proper motion; t the time of observations relative to 1930 in units of 10 years; $\Delta\pi$ the correction to the pro-

[6] *A.N.*, **152**, 65, 1900.

visional parallax, P_α; P_δ the parallax factor; ΔA, ΔB, ΔF, and ΔG the corrections to the orientational elements; and X and Y the elliptical rectangular co-ordinates as derived from the dynamical elements given above.

The normal equations are

$$
\begin{array}{rrrrrrr}
+79.00\Delta c_x + & 0.00\Delta c_x' - & 68.62\Delta B - & 21.08\Delta G - & 21.07\Delta\pi + & 37.94\Delta\mu_x = & -0.1228\,\text{mm} \\
+80.30 & - 53.07 & + 15.17 & - 12.16 & + 27.62 & & +0.0699 \\
& + 156.76 & + 8.13 & + 25.87 & - 119.61 & & +0.0269 \\
& & + 62.49 & + 1.56 & + 68.04 & & +0.0322 \\
& & & + 92.33 & - 17.96 & & -0.0687 \\
& & & & + 269.77 & & -0.0212\,, \\
+79.00\Delta c_y + & 0.00\Delta c_y' - & 68.63\Delta A - & 21.08\Delta F - & 9.57\Delta\pi + & 37.94\Delta\mu_y = & +0.0743\,\text{mm} \\
+80.30 & - 53.07 & + 15.17 & - 10.64 & + 27.62 & & -0.1119 \\
& + 156.76 & + 8.13 & + 16.71 & - 119.62 & & +0.0281 \\
& & + 62.49 & - 0.78 & + 68.04 & & -0.0302 \\
& & & + 5.99 & - 12.49 & & -0.0015 \\
& & & & + 269.77 & & -0.0385\,.
\end{array}
$$

The separate solutions in Δx and Δy for the combined Yerkes and McCormick plates lead to the following values expressed in millimeters:

$$
\begin{array}{ll}
\Delta c_x = -0.0024\,, & \Delta A = -0.0002\,, \\
\Delta c_y = +0.0010\,, & \Delta B = -0.0007\,, \\
\Delta c_x' = +0.0003\,, & \Delta F = +0.0008\,, \\
\Delta c_y' = -0.0018\,, & \Delta G = -0.0002\,, \\
\Delta\pi_x = -0.0011\,, & \Delta\mu_x = -0.00009\,, \\
\Delta\pi_y = -0.0023\,, & \Delta\mu_y = -0.00046\,.
\end{array}
$$

After computing their probable errors, these corrections were applied to the provisional values, leading to the following results:

$$
\begin{array}{lll}
c_x = +13.6974 \pm 0.0010\ \text{mm}\,, & A = +0''.958 \pm 0''.009\,, & \\
c_y = -\ 6.3659 \pm 0.0008\ \text{mm}\,, & B = +0''.240 \pm 0''.011\,, & \\
c_x' = +13.7001 \pm 0.0009\ \text{mm}\,, & F = -0''.298 \pm 0''.010\,, & \\
c_y' = -\ 6.3687 \pm 0.0008\ \text{mm}\,, & G = +1''.180 \pm 0''.013\,, & \\
\pi_x = +\ 0''.282 \pm 0''.007\,, & \mu_x = -0''.7065 \pm 0''.0007 & \left.\right\} \text{Yerkes}\,, \\
\pi_y = +\ 0''.268 \pm 0''.026\,, & \mu_y = -1''.0158 \pm 0''.0006 & \left.\right\} \\
\text{p.e. } 1_x = \pm 0''.062\,, & \mu_x = -0''.7065 \pm 0''.0007 & \left.\right\} \text{McCormick}\,. \\
\text{p.e. } 1_y = \pm 0''.047\,, & \mu_y = -1''.0265 \pm 0''.0006 & \left.\right\}
\end{array}
$$

The proper motion of Procyon according to the FK_3 is: $\mu\alpha \cos\delta = -0''.712$, $\mu\delta = -1''.021$, which shows the following dependence–mean proper motion for the reference stars:

$$\mu_x = -0''.005\,; \qquad \mu_y \text{ (Yerkes)} = -0''.005\,; \qquad \mu_y \text{ (McCormick)} = +0''.006\,.$$

The FK_3 proper motions for the center of mass of the system were derived from the observations of the bright component reduced by means of the orbit published by Spencer Jones.

The probable error of unit weight is especially large in the x co-ordinate as compared with the average value of $\pm 0''.035$ normally obtained for other series at both observatories; one likely explanation would be the large reduction of the bright star by means of a rotation sector or a neutral filter. The last eleven nightly means obtained at Yerkes, where the reduction of the bright star was obtained by means of a sector and an objective grating, reduced the probable errors of unit weight to $\pm 0''.031$ and $\pm 0''.028$ for $\Delta\alpha \cos\delta$ and $\Delta\delta$, respectively, thus showing the superior accuracy obtained by this method.

The yearly normal places derived from the Yerkes and the McCormick plates, corrected for the final parallax and proper motions, have been plotted against the orbital motion in Figures 1 and 2.

VI. SPECTROSCOPIC OBSERVATIONS

Dr. W. S. Adams kindly called the author's attention to a series of spectrograms taken at the coudé focus of the 100-inch Mount Wilson telescope. These plates were lent to the author by Dr. Bowen, and a series of seven prism and four grating spectrograms taken between 1926 and 1943 were found suitable for measurement. While the material was insufficient to establish the orbital motion in the line of sight, it was used for the derivation of the parallax of the system, by adopting the orbital motion derived from the astrometric orbit. The plates prior to 1937 were prism spectrograms, while the subsequent ones were taken with Wood diffraction gratings, as described in detail by Adams.[7]

The spectrograms were measured on the small Gaertner machine of the Dearborn Observatory by Dr. (Mrs.) Helen Steel Lillibridge, assisted by Mr. Harry Rymer. The region $\lambda\lambda$ 4175–4272 was chosen for the radial velocities. On each plate thirty-three stellar lines were measured, primarily *Fe* I, chosen for their freedom of blends, medium intensity, and lack of diffuseness, while thirty-one lines in the iron comparison spectrum were measured. The lines were identified by Mrs. Lillibridge. The values for the wave lengths of the lines were the International secondary standards of iron[8] and those published by Burns and Walters,[9] increased by 0.002 A to adjust the vacuum-arc values to the wave lengths observed in air. Each plate was measured in direct and reverse position, with three settings on each line.

In the reduction of readings to wave lengths, the region was divided into two parts at λ 4219, and a linear relation was set up between readings and wave lengths at the ends of the region. The departures of the computed intermediate wave lengths of iron lines from the standard values were then plotted against computed wave length. From the resulting curve, corrections were obtained to the computed wave lengths of the stellar lines. Then $\Delta\lambda/\lambda$, averaged for the thirty-three lines and multiplied by the velocity of light, gave the observed radial velocity.

Table 7 lists the plate number; the epoch; the observed radial velocity, v_o, with its probable error; the average dispersion in the region of measurements; the combined corrections for the heliocentric, diurnal, and barycentric motions of the earth, v_e; and the velocity, v, of Procyon A relative to the sun.

[7] *Ap. J.*, 93, 11, 1941.

[8] *Trans. I.A.U.*, 3, 86, 1929.

[9] *Pub. Allegheny Obs.*, 6, 159, 1929.

We derive the motion in the line of sight in kilometers per second from the orbital elements of the final orbit after adopting a provisional parallax for the system. A comparison of these velocities with the observed velocities will then give the corrections to the assumed parallax and the velocity of the center of the system (v_c). A least-squares solution, based on each observed velocity having unit weight, gave the following values:

$$\pi = +0''.316 \pm 0''.013 \text{ (p.e.)}, \qquad v_c = -4.11 \pm 0.05 \text{ km/sec (p.e.)}.$$

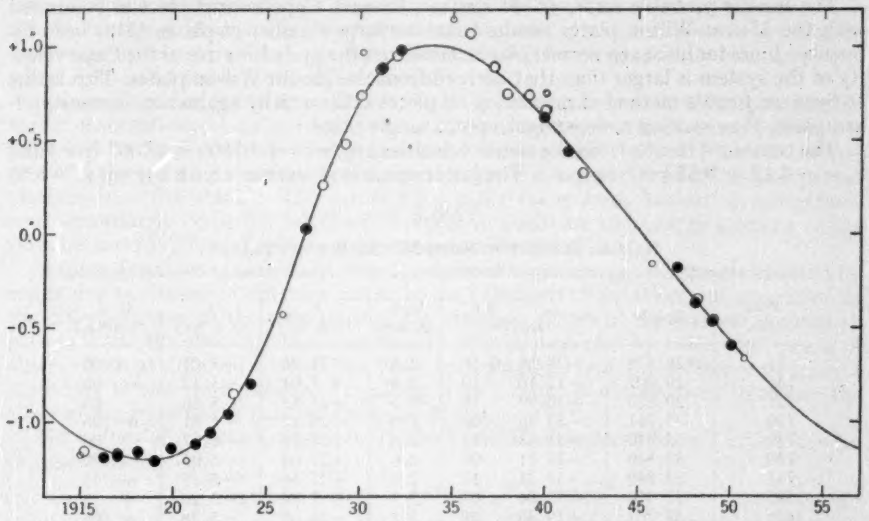

FIG. 1.—The orbital motion in $\Delta\alpha \cos\delta$. The yearly normal places are marked with a dot for the Yerkes plates and with a circle for the McCormick plates. The small circles are the normal places derived from the meridian observations.

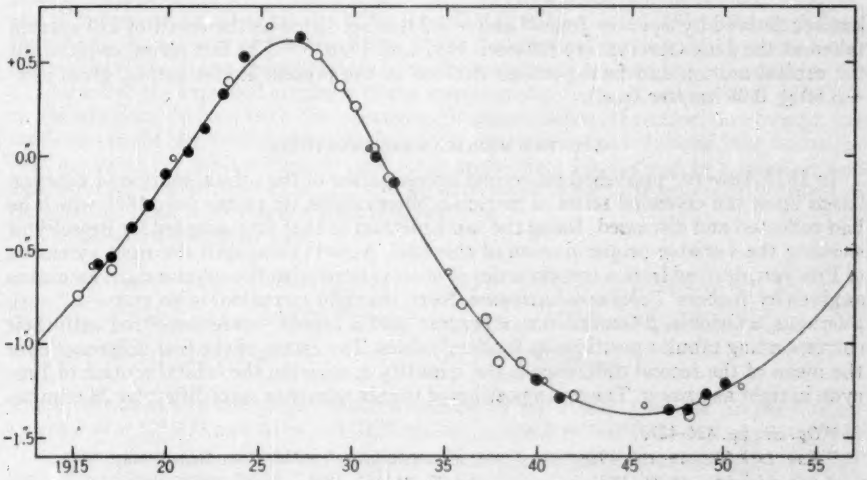

FIG. 2.—The orbital motion in $\Delta\delta$. The symbols are identical with those in Figure 1

The residuals between the observed and computed radial velocities are listed in the last column of Table 7. The probable error for one plate is ±0.09 km/sec.

A similar solution for the radial velocities obtained by Spencer Jones[10] from high-dispersion plates (8.4 A/mm), taken at the Cape Observatory, gave the following results:

$$\pi = +0''.294 \pm 0''.008 \text{ (p.e.)}, \qquad v_c = -4.17 \pm 0.14 \text{ km/sec (p.e.)}.$$

The smaller probable error, ±0.05 km/sec, for each Cape normal place as compared with the Mount Wilson plates results from the large number of plates (119) used by Spencer Jones for his seven normal places. However, the probable error of the Cape velocity of the system is larger than that derived from the Mount Wilson plates. This is due to Spencer Jones's method of measuring all plates differentially against the same standard plate, thus making v_c dependent upon a single plate.

The combined results from the radial velocities are: $\pi = +0''.300 \pm 0''.007$ (p.e.) and $v_c = -4.12 \pm 0.05$ km/sec (p.e.). The latter value is at variance with the value −3.69 km/sec derived by Spencer Jones[10] and −3.2 km/sec listed as the result of 114 spectra taken at the Lick Observatory between 1897 and 1926.[11, 12] The last series, reduced for the orbital motion and final parallax derived in the present investigation, gives $v_c = -3.50 \pm 0.08$ km/sec (p.e.).

TABLE 7

RADIAL VELOCITIES FROM MOUNT WILSON PLATES

Plate No.	Epoch	v_o (Km/Sec)	p.e.	Disp. (A/Mm)	v_c (Km/Sec)	v (Km/Sec)	O−C (Km/Sec)
51.....	1926.878	−28.56	±0.18	2.6	+24.95	−3.61	0.00
136.....	29.002	−12.16	.10	2.6	+ 7.04	−5.12	− .09
221.....	29.870	−30.99	.19	4.3	+25.53	−5.46	− .03
720.....	33.761	−33.98	.08	2.6	+28.17	−5.81	+ .06
739.....	33.840	−33.63	.12	2.6	+27.76	−5.87	.00
740.....	33.840	−33.71	.07	2.6	+27.64	−6.07	− .20
741.....	33.840	−33.31	.10	2.6	+27.56	−5.75	+ .12
1595.....	37.974	−17.04	.06	3.1	+11.84	−5.20	+ .22
1626.....	38.201	+19.30	.08	3.1	−24.68	−5.38	+ .01
1824.....	38.853	−32.21	.06	3.1	+26.73	−5.48	− .17
3309.....	43.934	−22.68	±0.08	2.9	+18.12	−4.56	+0.07

VII. THE MERIDIAN OBSERVATIONS

In 1873 Auwers[13] published his second investigation of the orbital motion of Procyon based upon the extended series of meridian observations up to the year 1870 which he had collected and discussed. Using the same method as that first adopted by Bessel[14] for showing the variable proper motion of this star, Auwers compared the right ascension of Procyon, derived from a certain series of observations with the tabular right ascension as given by Wolfers' *Tabulae reductionum*. Next, the right ascensions of six stars—α Tauri, β Orionis, α Orionis, β Geminorum, α Hydrae, and α Leonis—were compared with their corresponding tabular positions in Wolfers' tables. The excess of the first difference over the mean of the second difference is the quantity q, showing the orbital motion of Procyon in right ascension. The mean position of the six reference stars differs by 28 minutes

[10] *Op. cit.*, pp. 424–427.

[11] *Pub. Lick Obs.*, **16**, 116, 1928.

[12] *Pub. Lick Obs.*, **18**, 66, 1932.

[13] *Monatsberichte d. Akad. Wiss. Berlin*, May, 1873.

[14] *A.N.*, **22**, 151, 1844.

in right ascension and 30′ in declination from the co-ordinates of Procyon. It can therefore be expected that any systematic errors in right ascension depending upon right ascension and declination have practically been eliminated.

For the comparison in declination, Auwers did not find it possible to choose a series of fundamental stars whose mean declination differed little from that of Procyon without having their mean right ascension differ considerably from that of Procyon. The seven comparison stars had a mean position differing 9′ in declination from Procyon's position, while the difference in right ascension equaled 6^h46^m. The observed variation, r, in the declination of Procyon is therefore affected by the systematic error in declination depending upon right ascension in the individual series but is practically independent of errors in the adopted latitude and refraction.

Spencer Jones[5] added to Auwers' lists the observations made since 1870, incorporated earlier observations which had not already been used by Auwers, and revised such values published by him for series of early observations where new reductions had led to improved values. As a basis throughout, Spencer Jones adopted the positions and proper motions from the *P.G.C.*[15] The values for q and r taken from Auwers' investigations were accordingly corrected for the differences in positions and proper motions of the stars between Wolfers' *Tabulae reductionum* and the *P.G.C.*

Spencer Jones also pointed out that the derived variations, q and r, were affected by errors due to the use of different values of the constants of nutation and aberration at the different times in the reductions of the apparent places of the stars to their mean places. While the effect of aberration could safely be neglected by taking the means of observations at different times of the year, Spencer Jones found it necessary to apply a correction to the mean value of r resulting from a series of observations to reduce the effect of nutation to the basis of the value 9″.210.

The values of q and r as found in Tables I and II of Spencer Jones's article can be expressed as follows:

$$q = c_x + \mu_x (t - 1850) + B'\bar{X} + G'\bar{Y},$$

$$r = c_y + \mu_y (t - 1850) + A\bar{X} + F\bar{Y},$$

where c_x and c_y are the corrections to the positions in the *P.G.C.*; μ_x and μ_y the component corrections to the proper motion (counted from the epoch 1850); and A, B', F, and G' the orientational elements ($B' = B$ [sec $\delta/15$]; $G' = G$ [sec $\delta/15$]) of the final orbit, reduced to the equator of 1850.0; X and Y are the elliptical rectangular co-ordinates as derived from the Johannesburg tables from the mean anomaly and the eccentricity.

In view of the expected accuracy of the meridian observations, these would add little to the solutions derived from the photographic observations; therefore, no attempt was made to obtain the orbital elements from the above equations. Instead, the terms depending upon the orbital motion were taken from the orbit derived in Section V, and least-squares solutions for c_x, c_y, μ_x, and μ_y were made to find the general agreement of the adopted orbit with the meridian observations.

The obtained solutions were:

$$c_x = +0^s.0014 \pm 0^s.0011 \text{ (p.e.)}, \qquad c_y = +0''.010 \pm 0''.026 \text{ (p.e.)},$$

$$\mu_x = -0^s.00022 \pm 0^s.00003 \text{ (p.e.)}, \qquad \mu_y = -0''.0021 \pm 0''.0007 \text{ (p.e.)},$$

$$\text{p.e. } 1 = \pm 0^s.023\ (0''.34), \qquad \text{p.e. } 1 = \pm 0''.39.$$

These corrections to the proper motion applied to the *P.G.C.* give the proper motion $\mu\alpha \cos\delta = -0^s.0471$ and $\mu\delta = -1''.029$ against $\mu\alpha \cos\delta = -0^s.0473$ and $\mu\delta = -1''.032$

[15] Lewis Boss, *Preliminary General Catalogue of 6188 stars for the Epoch 1900* (Washington: Carnegie Institution of Washington, 1910).

from the *G.C.*;[16] and $\mu\alpha \cos \delta = -0^s.0474$, $\mu\delta = -1''.029$ from the FK_3 (all computed for the equinox 1950).

Since the corresponding probable errors of unit weight as derived from the residuals listed by Spencer Jones are $\pm 0^s.021$ ($0''.32$) and $\pm 0''.41$, it is seen that both orbits fit the meridian observations equally well. The derived probable errors of unit weight may be compared with the value $\pm 0''.30$ adopted by the *P.G.C.* as the probable error of unit weight for meridian observations in general, since Spencer Jones used this system for weighing the observations. Since the observations of very bright stars are usually the least accurate, neither one of the probable errors can be considered as substantially larger than normal; this shows that the agreement between the meridian observations and the adopted orbit is satisfactory.

The total weights of the meridian observations in right ascension and declination are 599.5 and 411.5, respectively. If these weights are expressed in the same units as for the photographic observations, they become 19.9 and 5.8 as compared with the weights 159.3 for each of the two co-ordinates of the photographic observations. The meridian observations would therefore have contributed little if a combined solution had been attempted. The meridian observations reduced to one period and combined into eight normal places have been plotted in Figures 1 and 2.

VIII. MICROMETRIC OBSERVATIONS OF ADJACENT STARS

Several series of micrometer measures are available of the bright components of Procyon relative to adjacent stars. The most complete observations of this kind are those made by O. Struve[17] between 1851 and 1890 and listed by Spencer Jones (*op. cit.*, pp. 436–437) in his Table IX, together with an early observation by Bessel (1822) and observations by Auwers and Quetelet. The two reference stars were BD+5°1738 (mag. 9.0) and BD+5°1741 (mag. 8.5) preceding and following Procyon at intervals of 24 and 22 seconds of time, respectively, and differing from Procyon in declination by less than 2 minutes of arc at maximum. In the third column of the table Spencer Jones has listed the difference between the declination of Procyon and the mean declination of the two comparison stars.

Adopting the final orbit, we find from a least-squares solution the following values for the zero point and proper motion from the differences in declination: $-70''.66 - 1''.022\ (t - 1870)$. The probable error of unit weight as derived from the residuals is $\pm 0''.20$ as compared with the value $\pm 0''.19$ derived from Spencer Jones's orbit. These errors agree with the probable error of unit weight equal to $\pm 0''.16$ as estimated by Struve himself for the accuracy of his observations. No attempt was made to compare the orbital motion with his less accurate observations of right-ascension differences.

IX. OBSERVATIONS OF THE FAINT COMPANION

The large difference in magnitude between the two components makes the observations of their relative positions extremely difficult even at the time when their angular separations are near maximum. For this reason the complete list of micrometer measures in Table 8 should be used with extreme caution in the evaluation of the semi-major axis of the relative orbit. The fact that neither Barnard nor Aitken saw the companion after 1913 makes it doubtful that observations after that time are real, except for the observations by van den Bos and Finsen, made at the Union Observatory under excellent seeing conditions. The observations of van den Bos and Finsen in 1927–1929 are, however, still quite uncertain, owing to the proximity of the two components, which were in the same relative position as when Burnham looked in vain for the companion in 1888 and 1890 with the 36-inch Lick refractor.

[16] *General Catalogue of 33342 Stars for the Epoch 1950* (Washington: Carnegie Institution of Washington, 1937).

[17] *Obs. Poulkovo*, **10**, 72–76, 1893.

TABLE 8

VISUAL OBSERVATIONS OF PROCYON AND THEIR RESIDUALS (EQUINOX 2000)

EPOCH	OBSERVED p	OBSERVED d	NO. OF NIGHTS	OBSERVER	O−C		
					p	p (Arc)	d
1896.93	320°9	4".63	4	Schaeberle	+ 1°8	+0".15	−0".15
97.00	321.6	4.83	4	Aitken	+ 2.2	+0.18	+0.04
97.16	320.3	4.65	3	Hussey	− 0.1	−0.01	−0.16
97.82	324.9	4.66	6	Schaeberle	+ 0.6	+0.05	−0.21
97.83	327.9	4.80	1	See	+ 3.6	+0.31	−0.07
97.83	329.1	4.82	1	Boothroyd	+ 4.8	+0.41	−0.05
97.88	324.3	4.70	3	Aitken	− 0.3	−0.03	−0.18
98.21	325.8	4.82	3,2	Aitken	− 0.7	−0.06	−0.09
98.21	326.5	4.83	6	Barnard	0.0	0.00	−0.08
98.24	326.5	4.26	1	Lewis	− 0.1	−0.01	−0.65
98.28	325.5	4.50	1	Hussey	− 1.3	−0.11	−0.41
98.88	331.1	4.97	4	Aitken	+ 0.9	+0.08	+0.01
99.07	331.1	4.91	3	Barnard	− 0.2	−0.02	−0.06
99.96	335.0	4.88	3	Aitken	− 1.2	−0.10	−0.15
1900.05	336.5	5.09	6	Barnard	− 0.1	−0.01	+0.06
00.23	338.8	4.83	1	Lewis	+ 1.2	+0.11	−0.21
00.29	332.9	4.60	4	See	− 5.0	−0.44	−0.44
01.20	339.00	5.13	3,2	Aitken	− 3.8	−0.34	+0.05
01.30	338.4	5.00	5	See	− 4.9	−0.43	−0.08
01.88	344.0	5.06	2	Barnard	− 2.4	−0.21	−0.04
02.21	345.4	5.39	2	Lewis	− 2.6	−0.23	+0.28
02.24	347.0	5.11	1	Hussey	− 1.2	−0.11	0.00
02.25	338.9	5.35	3	See	− 9.4	−0.84	+0.24
02.72	351.1	5.33	3	Aitken	+ 0.4	+0.04	+0.20
03.15	351.5	5.16	3	Barnard	− 1.4	−0.13	+0.02
04.29	355.7	4.93	2	Bowyer	− 3.1	−0.28	−0.22
04.80	357.9	5.36	1	Barnard	− 3.5	−0.32	+0.20
05.14	6.7	5.14	1	Aitken	+ 3.6	+0.32	−0.02
05.17	5.8	4.46	1	Lewis	+ 2.4	+0.22	−0.70
05.99	10.7	.....	1	Aitken	+ 3.2	+0.29	.....
06.77	28.7	.....	1	Aitken	+17.2	+1.53	.....
09.16	23.0	5.26	4,3	Barnard	− 0.7	−0.06	+0.10
09.30	23.0	5.04	1	Bowyer	− 0.4	−0.04	−0.12
10.10	24.8	5.21	2,1	Barnard	− 3.8	−0.34	+0.06
11.07	29.3	4.69	2	Jonckheere	− 4.2	−0.38	−0.45
13.14	34.8	.....	1	Bowyer	− 9.5	−0.84	.....
13.16	43.1	5.09	3	Barnard	− 1.4	−0.12	+0.01
14.30	29.5	6.14	1	Bowyer	−21.0	−1.80	+1.11
14.94	30.5	5.25	1	Jonckheere	−23.5	−1.99	+0.25
17.24	47.9	4.12	1	Jonckheere	−19.1	−1.58	−0.70
18.22	59.3	4.63	1	Jonckheere	−13.6	−1.11	−0.07
21.21	94.6	(5. ±)	1	Bernewitz	+ 1.3	+0.10	+0.8±
24.19	106. ±	(5.5±)	1	Dick	−17. ±	−0.94	+2.3±
27.11	199.0	3.06	1	van den Bos	+19.5	+0.75	+0.81
28.98	237.9	2.68	3	van den Bos	+ 7.9	+0.34	+0.23
29.06	252.0	3.99	2,1	Finsen	+20.4	+0.86	+1.52
32.27	278.5	3.57	6	van den Bos	− 1.2	−0.08	−0.10
32.28	276.0	3.96	4	Finsen	− 3.8	−0.24	+0.28

The series of distance measures by Barnard and Aitken were used for the purpose of determining the semi-major axis of the relative orbit. For each of the observed distances, the corresponding distance, d_a, was computed from the final orbit. The factor k, with which d_a has to be multiplied to correspond to the observed relative distances, d_o, provides the semi-major axis of the relative orbit, ka, and the total mass in units of the fainter component, $(M_A + M_B)/M_B = k$.

The values of k are listed in Table 9 for Aitken's and Barnard's observations separately. The fact that k does not show a systematic run with time shows the general agreement

TABLE 9

THE RELATIVE DISTANCES AND THEIR RESIDUALS

EPOCH	d_o	No. of NIGHTS	d_a	k	d_c	$d_o - d_c$
	Aitken					
1897.00.....	4".83	4	1".282	3.77	4".79	+0".04
97.88.....	4.70	3	1.306	3.60	4.88	− .18
98.21.....	4.82	2	1.313	3.67	4.91	− .09
98.88.....	4.97	4	1.326	3.75	4.96	+ .01
99.96.....	4.88	3	1.345	3.63	5.03	− .15
1901.20.....	5.13	2	1.358	3.78	5.08	+ .05
02.72.....	5.33	3	1.371	3.89	5.13	+ .20
05.14.....	5.14	1	1.381	3.72	5.16	− .02
	Barnard					
1898.21.....	4.83	6	1.313	3.68	4.91	− .08
99.07.....	4.91	3	1.330	3.69	4.97	− .06
1900.05.....	5.09	6	1.346	3.78	5.03	+ .06
01.88.....	5.06	2	1.365	3.71	5.10	− .04
03.15.....	5.16	3	1.374	3.76	5.14	+ .02
04.80.....	5.36	1	1.380	3.88	5.16	+ .20
09.16.....	5.26	3	1.381	3.81	5.16	+ .10
10.10.....	5.21	1	1.378	3.78	5.15	+ .06
13.16.....	5.09	3	1.358	3.75	5.08	+0.01

between the final orbit and the observations of these two excellent observers. For Aitken's observations we find $k = 3.73 \pm 0.02$ (p.e.) and for Barnard's 3.75 ± 0.01 (p.e.), showing no marked systematic difference between the two observers. The mean value, $k = 3.738 \pm 0.011$ (p.e.) was adopted, and we find, accordingly, that the semi-major axis of the relative orbit is $4".548 \pm 0".015$ (p.e.) and $M_B/(M_A + M_B) = 0.268 \pm 0.001$ (p.e.).

The last column of Table 9 lists the differences between the distances observed by Aitken and Barnard and those computed from the astrometric orbit multiplied by the adopted value k. Assigning a weight equal to 1 for a single night's observation and a weight of 2 for the mean of two or more nights' observations, we find that the residuals indicate a probable error of $\pm 0".10$ for a distance measure of unit weight. The corresponding error for the same observers for the position angles (tangential deviations $d \sin [v_o - v_c]$) was found to be $\pm 0".16$, if we omit the single night's observation by Aitken in 1906, which is obviously erroneous.

These values for the errors are remarkably small as compared with a probable error of $\pm 0''.12$ found by the writer[18] as the average expected error for visual observations of pairs with separations between 2″ and 9″ and with relatively small differences in magnitude.

It has already been mentioned that the position angles observed between 1897 and 1909 were effective in determining the period of the orbit. The same observations proved the correctness of the adopted eccentricity, as can be seen from Figures 3 and 4, where the cosine and sine of the observed position angles are plotted against the final orbit and against one of the provisional orbits with an eccentricity of 0.35.

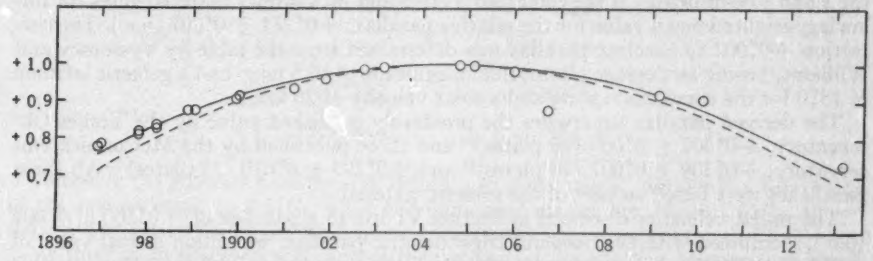

FIG. 3.—Cosines of the visually observed position angles (*circles*) plotted against *a*, a solid curve representing the cosines of the position angles for the final orbit ($e = 0.40$), and *b*, a dotted curve representing the same quantities for a provisional orbit ($e = 0.35$; same period and periastron passage as the final orbit).

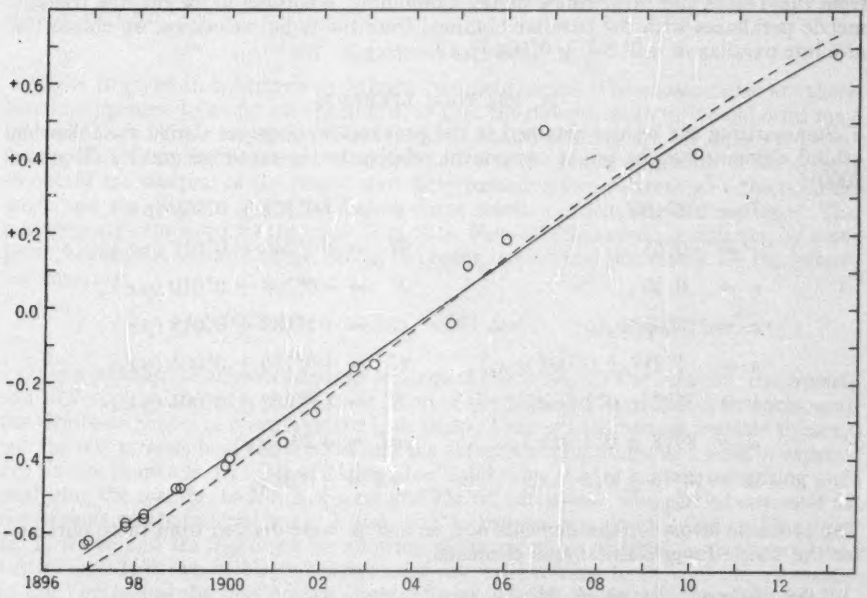

FIG. 4.—Sines of the visually observed position angles (*circles*) plotted against *a*, a solid curve representing the sines of the position angles for the final orbit ($e = 0.40$), and *b*, a dotted curve representing the same quantities for a provisional orbit ($e = 0.35$; same period and periastron passage as the final orbit).

[18] *A.J.*, **49**, 166, 1942.

The last three columns of Table 8 contain the residuals between the observed and computed values for all published observations. Some of the large discrepancies either are contradicted by the observations of Aitken and Barnard made at nearly the same time or were made after Barnard considered the pair too difficult to measure. The observations prior to 1914 give probable errors of $\pm 0''.25$ and $\pm 0''.19$ for the position angles and distances, respectively, for observations of unit weight.

X. THE PARALLAX OF THE SYSTEM

A combination of the results listed in Section V for the relative parallax derived from the x and y co-ordinates of the combined Yerkes and McCormick material gives the following weighted mean value for the relative parallax: $+0''.281 \pm 0''.007$ (p.e.). The correction $+0''.002$ to absolute parallax was determined from the table by Vyssotsky and Williams,[19] using an average photovisual magnitude of 10.5 mag. and a galactic latitude of $15°.0$ for the comparison stars and a solar velocity of 20 km/sec.

The derived parallax supersedes the previously published value by the Yerkes Observatory, $+0''.307 \pm 0''.009$ (15 plates)[20] and those published by the McCormick Observatory, $+0''.309 \pm 0''.007$ (16 plates)[21] and $+0''.293 \pm 0''.010$ (23 plates).[22] All three parallaxes were based on part of the present material.

The radial velocities discussed in Section VI led to a parallax of $+0''.300 \pm 0''.007$ (p.e.). Combined with the absolute trigonometric parallax, we obtain a final value of $+0''.291 \pm 0''.005$ (p.e.). Other adjusted absolute parallaxes derived from photographic series are: Sproul,[23] $+ 0''.288 \pm 0''.014$ (11 plates); Yale,[24] $+ 0''.288 \pm 0''.009$ (22 plates); and Van Vleck,[25] $+ 0''.274 \pm 0''.008$ (48 plates). These three series give a mean absolute parallax of $+0''.281 \pm 0''.005$, thus showing a close agreement with the parallax obtained from the Yerkes and McCormick plates. Combining, according to weight, the trigonometric parallaxes with the parallax obtained from the radial velocities, we obtain the absolute parallax of $+0''.287 \pm 0''.004$ (p.e.).

XI. THE FINAL ELEMENTS

Summarizing the results obtained in the previous sections, we derive the following orbital elements for the bright component relative to the center of gravity (Equinox 2000):

$$
\begin{aligned}
T &= 1927.60, & A &= +0''.958 \pm 0''.009 \text{ (p.e.)},\\
P &= 40.65, & B &= +0''.240 \pm 0''.011 \text{ (p.e.)},\\
e &= 0.40, & F &= -0''.298 \pm 0''.010 \text{ (p.e.)},\\
n &= 8°.8561, & G &= +1''.180 \pm 0''.013 \text{ (p.e.)},\\
a &= 1''.217 \pm 0''.002 \text{ (p.e.)}, & C &= +0''.710 \pm 0''.004 \text{ (p.e.)},\\
i &= 35°.7 \pm 0°.2 \text{ (p.e.)}, & H &= +0''.002 \pm 0''.004 \text{ (p.e.)},\\
\omega &= 89°.8 \pm 0°.3 \text{ (p.e.)}, & \pi L &= +29.79,\\
\Omega &= 104°.3 \pm 0°.3 \text{ (p.e.)}, & \pi N &= +0.08.
\end{aligned}
$$

The probable errors for the elements a, i, ω, and Ω were derived from those obtained for the Thiele-Innes orientational elements.

[19] *Pub. McCormick Obs.*, **10**, 34, 1948.
[20] *Pub. Yerkes Obs.*, **4**, Part III, 11, 1920.
[21] *Pub. McCormick Obs.*, **3**, 229, 1920.
[22] *Pub. McCormick Obs.*, **8**, 246, 1940.
[23] *Pub. Sproul Obs.*, **4**, 48, 1919.
[24] *A.J.*, **44**, 39, 1934.
[25] *Pub. Van Vleck Obs.*, **1**, 142–145, 1938.

If the above elements are advanced to the equinox 2100, the following corrections for precession and space motions are obtained:

$$\Delta A = -0''.0017, \quad \Delta F = -0''.0105, \quad \Delta a = 0''.000, \quad \omega = -0°.02,$$
$$\Delta B = +0''.0084, \quad \Delta G = -0''.0026, \quad i = +0°.03, \quad \Omega = +0°.52.$$

The orbit of the companion about the primary has the same dynamical elements as those given above, while the remaining elements are as follows (Equinox 2000):

$$A = -3''.582, \quad a = 4''.548,$$
$$B = -0''.898, \quad i = 35°.7,$$
$$F = +1''.112, \quad \omega = 89°.8,$$
$$G = -4''.410, \quad \Omega = 284°.3.$$

Adopting the absolute parallax $+0''.287$ derived in Section X, we obtain a total mass of the system equal to $2.37\odot$, while the individual masses are $M_A = 1.74\odot$, $M = 0.63\odot$. The derived mass for the brighter component is the expected for an F5 IV star.

As there is no observed spectrum of the companion, its effective temperature is not known. From Kuiper's observation of its color, it is probable that its effective temperature does not exceed 10,000° and is not less than 6500°. With the absolute visual magnitude of 13.0 and the appropriate bolometric corrections, the two values of the computed diameter are 0.008 and 0.016. The corresponding densities are 1.8×10^6 and 0.22×10^6 c.g.s.

XII. EPHEMERIS OF PROCYON

Table 10 gives an ephemeris covering a complete period. The chosen dates are those listed by Spencer Jones for his ephemeris, so that the differences from the old orbit may be found from simple inspection. The second and third columns are the values required to be added to the right ascension and declination of the center of gravity of the system to obtain the position of the bright star. The remaining two columns give the position angle and the distance of the faint component relative to the bright component. The positions are computed for the equinox of date. For any other equinox differing by n orbital periods, the values change, owing to proper motion and precession, by the following amounts:

$$\Delta a: +0^s.00025\ \Delta\delta n\ ; \qquad \Delta\delta: -0''.53\ \Delta a n\ ; \qquad \Delta v = +0°.21 n\ .$$

It is a pleasure to acknowledge the support of the Research Corporation, the American Philosophical Society, the Watson Fund of the National Academy of Sciences, and the Graduate School of Northwestern University. Their grants made it possible to carry out the measurements of the spectra and the extensive computations. I wish to express my sincere thanks to Dr. (Mrs.) Helen Steel Lillibridge for her part in measuring and analyzing the spectra; to Mr. R. Spong and Mr. T. Littlejohn, who carried out most of the tedious computational work. I also wish to express my appreciation to Directors H. T. Alden and Ira S. Bowen for allowing me to use their material in the present investigation. It is impossible to acknowledge my indebtedness to each of the observers at the Yerkes and the McCormick Observatories, whose observations over the span of more than thirty-five years have made this investigation possible. I am especially grateful to Dr. G. Van Biesbroeck, who has always emphasized the importance of including continuous photographic series of binaries in the parallax program.

TABLE 10

EPHEMERIS OF PROCYON

Date	$\Delta\alpha$	$\Delta\delta$	v	d
1908.0.....	−0ˢ.028	−1″.32	17°.3	5″.17
09.0.....	− .035	−1.28	22.4	5.16
10.0.....	− .043	−1.22	27.5	5.15
11.0.....	− .050	−1.16	32.7	5.14
12.0.....	− .056	−1.08	37.9	5.11
13.0.....	− .062	−0.99	43.2	5.08
14.0.....	− .068	−0.89	48.5	5.04
15.0.....	− .072	−0.79	53.9	4.99
16.0.....	− .076	−0.67	59.4	4.93
17.0.....	− .079	−0.54	65.2	4.84
18.0.....	− .080	−0.41	71.1	4.73
19.0.....	− .080	−0.27	77.4	4.59
20.0.....	− .079	−0.12	84.0	4.43
21.0.....	− .076	+0.03	91.4	4.21
22.0.....	− .070	+0.18	99.5	3.96
23.0.....	− .062	+0.32	108.9	3.65
24.0.....	− .051	+0.44	120.2	3.29
25.0.....	− .037	+0.54	134.5	2.90
26.0.....	− .020	+0.60	153.2	2.53
27.0.....	− .002	+0.61	177.3	2.26
28.0.....	+ .017	+0.54	204.7	2.24
29.0.....	+ .034	+0.42	229.9	2.46
30.0.....	+ .047	+0.26	249.7	2.82
31.0.....	+ .057	+0.08	264.8	3.21
32.0.....	+ .064	−0.11	276.6	3.58
33.0.....	+ .067	−0.29	286.3	3.90
34.0.....	+ .068	−0.47	294.7	4.17
35.0.....	+ .067	−0.62	302.1	4.39
36.0.....	+ .064	−0.77	308.9	4.57
37.0.....	+ .060	−0.89	315.2	4.71
38.0.....	+ .054	−1.01	321.2	4.83
39.0.....	+ .048	−1.10	327.0	4.92
40.0.....	+ .041	−1.18	332.5	4.99
41.0.....	+ .034	−1.25	337.9	5.04
42.0.....	+ .026	−1.30	343.2	5.08
43.0.....	+ .018	−1.34	348.5	5.11
44.0.....	+ .010	−1.37	353.7	5.14
45.0.....	+ .002	−1.38	358.8	5.15
46.0.....	− .006	−1.38	4.0	5.16
47.0.....	− .014	−1.36	9.1	5.17
48.0.....	− .023	−1.34	14.2	5.17
49.0.....	−0.031	−1.30	19.3	5.17

THE POLE OF THE GALAXY AS DETERMINED FROM MEASUREMENTS AT 205 MC/SEC*

CHARLES L. SEEGER AND RALPH E. WILLIAMSON
School of Electrical Engineering, Cornell University and David Dunlap Observatory, University of Toronto
Received July 15, 1950

ABSTRACT

The position of the pole of the galaxy was determined from measurements of galactic radiation at a frequency of 205 megacycles per second. The radiation is found to be highly concentrated along a small circle close to the galactic equator. The co-ordinates of the pole are 266°.8 ± 4°.5 galactic longitude and 87°.43 ± 0°.34 north galactic latitude, referred to the 1900 I.A.U. pole. The small circle has a north polar distance, θ, of 91°.28 ± 0°.18.

The characteristics and calibration of the radio telescope employed in these measurements are described. The observational technique and the treatment of the data are presented in detail. There is a discussion of the sources of error in the observations and an analysis of the reliability of the results.

Two alternative hypotheses are suggested to explain the serious deviations of θ from 90°. The first, judged the less likely, would require changing the accepted height of the sun above the galactic plane from 10 or 20 parsecs to a value of several hundred parsecs. The alternative is to disregard the theoretical calculations of the opacity of the galaxy for the radiation at 205 mc which have been made on the basis of currently used formulae representing free-free transitions in the interstellar medium as the sole source of the opacity.

An observational value of approximately unity per kiloparsec is derived for the mean absorption coefficient in the plane of the galaxy at 205 mc.

INTRODUCTION

Now that the phenomenon of radio frequency radiation from the galaxy is well known and its potential usefulness as an additional tool for analysis of the structure of the galaxy is coming to be recognized, it is desirable to have precise information concerning the distribution of galactic radio frequency radiation with respect to both direction and frequency. The ideal goal would be a complete specification of the function $I_\nu(l, b)$ describing the specific intensity of a given frequency, I_ν, as a function of galactic longitude, l, and latitude, b, together with a quantitative statement of its statistical characteristics if it is found to vary in time. Though several preliminary surveys of the approximate distribution of galactic radiation at frequencies between 20.5 and 480 mc/sec have been published,[1] the present state of our knowledge of galactic radiation falls far short of this goal.

The present lack of detailed information of high accuracy exists because investigations of galactic radiation in the radio frequency spectrum are at least as complicated and as difficult as those investigations familiar to astronomers concerned with absolute spectrophotometry in the optical region of the spectrum. There is an added difficulty which must be overcome in making measurements of specific intensity at radio frequencies. The angular resolutions of the antennas practicable in radio telescopes is of the same order of magnitude as the angular dimensions of the radiating regions in the galaxy. Because of this restriction, the accurate determination of the actual distribution of specific in-

* This research was carried out at the Radio Astronomy Observatory of the School of Electrical Engineering of Cornell University, which was jointly sponsored by Cornell University and the Office of Naval Research, under U.S. Navy Contract N6onr-264-T. O.6, NR 077-321, and performed with the cooperation of the David Dunlap Observatory of the University of Toronto.

[1] Karl G. Jansky, *Proc. I.R.E.*, **21**, 1387, 1933; Grote Reber, *Ap. J.*, **100**, 279, 1944; L. A. Moxon, *Nature*, **158**, 758, 1946; K. F. Sander, *J. Inst. Elect. Eng.*, **3A**, **93**, 1487, 1946; Jack W. Herbstreit and Joseph R. Johler, *Nature*, **161**, 515, 1948; J. S. Hey, S. J. Parsons, and J. W. Phillips, *Proc. R. Soc. London, A*, **192**, 425, 1948; Grote Reber, *Proc. I.R.E.*, **36**, 1215, 1948.

tensity as a function of direction presents a problem which is certainly of a high order of complexity and perhaps not even uniquely solvable in principle. Thus it is necessary, as in more conventional branches of astronomy, for the observer to proceed with caution. He must frame precise observational problems with reference both to their astrophysical importance and to their suitability for radio telescopes.

One such problem is the quantitative determination of how well the galactic radiation agrees with generally accepted ideas of the position of the galactic plane. Until now, only one such quantitative determination was available.[2] It made use of data obtained by Reber at 160 mc and also at 480 mc. Reductions of these data indicated a high order of internal consistency, but they were gathered in a purely preliminary survey and hence might possibly contain systematic errors of direction as great as 1°. Also the galactic radio radiation at various frequencies must be considered separately. The present investigation is at a frequency of 205 mc/sec.

Galactic radiation appears to arrive chiefly from a zone a number[3] of degrees wide near the galactic equator. The specific problem set for solution in this paper is to determine the centroid (that is, the mean galactic latitude) of the 205-mc galactic signal at all galactic longitudes accessible from the latitude of the observing station and to find the optimum small circle on the celestial sphere best fitting these observations. This small circle may be characterized by three parameters: l' and b', the galactic co-ordinates of the north pole of the small circle, and θ, the north polar distance of the small circle from the pole characterized by l' and b'.

At first glance it may seem somewhat surprising that a radio telescope with a comparatively broad antenna pattern can be used for the successful determination of the centroid of galactic radiation. Actually, as shown in Appendix I, the important factors are not so much the dimensions of the antenna pattern as the stability and sensitivity of the receiver and amplifier circuits and the accuracy of the geometrical motions for pointing the antenna in different directions.[3]

Data gathered during a number of months of testing the radio telescope used in the present investigation showed the stability of the 205-mc receiving equipment to be reliable to a small fraction (approximately 1 per cent) of the maximum galactic signal. In order to utilize fully this high degree of stability of the electrical equipment, it was necessary to have all angular displacements of the moving parts of the radio telescope reproducible and accurate to approximately 0°.1. An effort was made at all points in the design of the observational program and in the computing procedure to preserve this accuracy.

EQUIPMENT

The radio telescope used in this determination of the galactic pole was situated at latitude 42°29'.3 north; longitude $5^h05^m48^s.6$ west. This is near the middle of a large, flat plateau which is about five miles north of the Cornell campus. This position was found to be relatively free from radio interference and to provide a uniform, low horizon out to a distance of several miles. The radio telescope consisted of two chief parts, the radio receiver and the antenna.

THE RADIO RECEIVER

The radio receiver used in the measurements reported here was the first one constructed at Cornell especially for the reception of solar and galactic noise. In over-all electrical design, this receiver was a normal high-frequency superheterodyne, consisting of a radio frequency amplifier, a frequency converter, an intermediate frequency ampli-

[2] Ruth J. Northcott and Ralph E. Williamson, *J.R.A.S. Canada*, **42**, 269, 1948.

[3] In this connection it is pertinent to remember that military and RDF installations have often made quite successful use of antennas with broad acceptance patterns for the purpose of precision radio direction finding.

fier, a linear detector, a back-bias arrangement and direct-current amplifier, and a 0–5-Ma Esterline-Angus recording galvanometer. Figure 1 shows the complete receiver, with the exception of the filament power supply. Figure 2 is a block diagram of the entire receiving system.

The width of the receiver passband, between half-power points, was 4.5 ± 0.5 mc

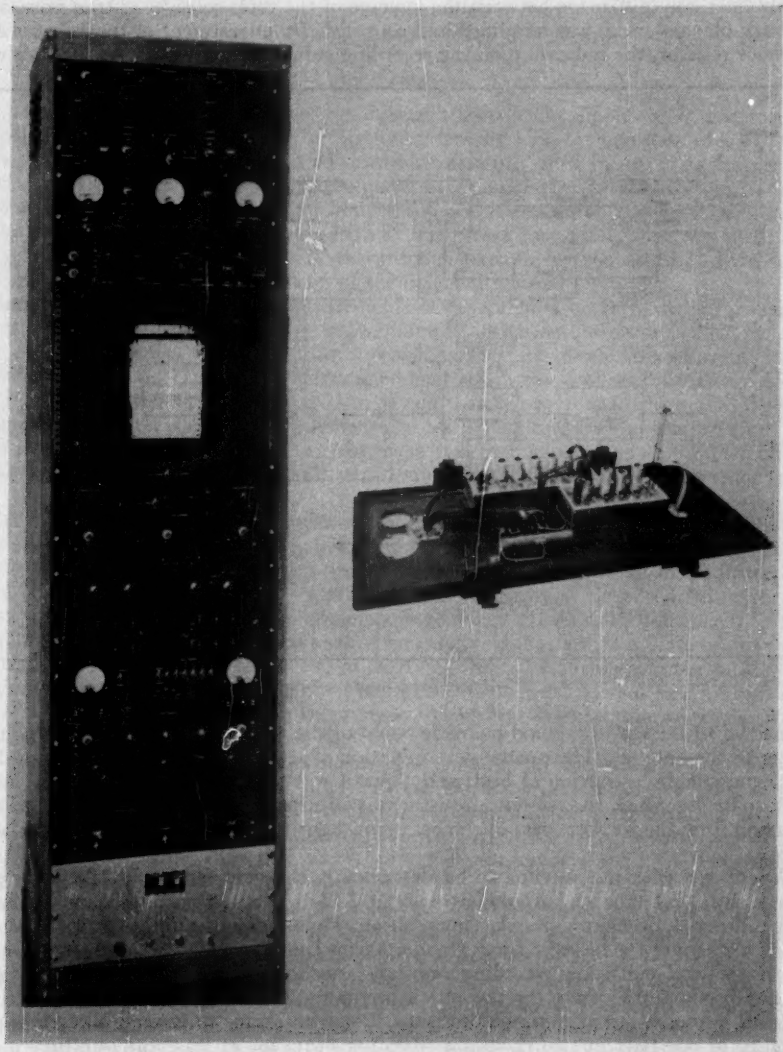

FIG. 1.—205-Mc receiver and auxiliary apparatus. The radio frequency amplifier and converter unit (*lower right*) was mounted close to the antenna. The rest of the equipment was housed in the near-by Quonset hut.

and the center frequency was 205 ± 1 mc. The time constant of the recording galvanometer was approximately 0.4 seconds for a paper speed of 12 inches per minute. The noise figure[4] of the receiver was approximately 12. In normal operation the gain of the receiver was adjusted to provide a detector output noise of 2.0 volts, average value, when the antenna was replaced by an arbitrary reference resistor. This receiver noise was balanced out by an appropriate back-bias battery potential. When the input of the receiver was connected to the antenna, any difference between the average of the total receiver output noise and the back-bias potential was amplified and recorded. By adjustment of the value of the reference resistor, the indication on the recording galvanometer, when the receiver was

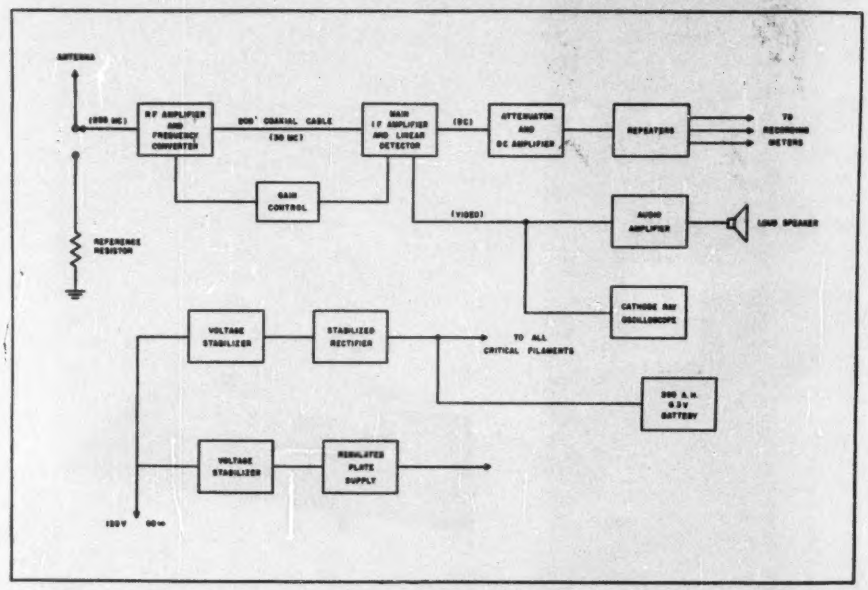

FIG. 2.—Block diagram of receiving system

connected to the resistor, could be made equal to the reading obtained with zero input power to the antenna. The precise determination of zero antenna input power is a difficult experimental operation at best, and, since it was not particularly necessary in the work to be described, the reference resistor was adjusted to give a reading equal to that obtained from the weakest part of the heavens (slightly to one side of the north galactic pole).

When used with the antenna to be described in the next section, this receiver produced a total detector output voltage of about 2.14 volts when the antenna was pointed in the direction of maximum galactic radiation. Thus the maximum galactic signal was only 7 per cent of the receiver noise. Computations based on the above noise figure, high-frequency band width, and recording time constant showed this maximum galactic signal to be only about 150 times the theoretical minimum detectable power for this receiver. Thus, to preserve a maximum of precision, it was necessary to provide a receiver gain stability of one part in two thousand (0.05 per cent) for at least the duration of any single set of measurements, since the only means of distinguishing a change in signal level

[4] H. T. Friis, *Proc. I.R.E.*, **32**, 419, 1944, and correction, *ibid.*, p. 729.

from a receiver gain variation was to sandwich the signal reading between two noise readings when connected to the reference resistor.

Figure 3 illustrates the gain stability of the entire receiver. The total receiver noise output was 2.0 volts, but a full-scale deflection on this record was only 0.05 volts. The magnitude of the trace jitter agreed well with the predicted value for this receiver under conditions of perfect gain stability. This high order of gain stability was achieved chiefly by stabilizing the plate and filament power supplies to better than 0.01 per cent and never shutting down the equipment except in cases of tube failure.

THE ANTENNA

The antenna used for these observations was a forty-eight dipole array, constructed by placing two SCR-268 azimuth receiving mattresses side by side (see Fig. 4). This 17-foot-square antenna was mounted on an alt-azimuth mechanism so as to provide vertical polarization with respect to the horizon. This polarization was chosen to minimize altitude-pointing errors arising from multipath reception at low antenna altitude angles. Direct-reading azimuth and altitude dials, least count 0°.1, were installed, and the relationship of the major axis of the antenna pattern to true north and the local vertical was determined as a function of the dial indications.

Besides routine ground-level measurements of the antenna pattern, careful measurements of the high-altitude angle pattern were made, using the quiet sun as a source at a time when the sun was well away from any comparably strong galactic source of radio frequency radiation. Thus it was determined that this array possessed a pattern $15° \times 15° \pm 0°.5$ for altitude angles greater than 8° and that the pattern of the main lobe was symmetric to better than 0°.25. Furthermore, as a result of sweep measures on the quiet sun, it was found that the entire antenna and mount could be pointed by direct reading of the dials to a precision of better than $\pm 0°.2$ for altitude angles greater than 12°.

Table 1 shows the result of a typical set of measurements of the azimuth of the sun. Azimuth sweeps were made on a day when the sun was quiet. If a burst of solar radiation occurred during a sweep, the sweep was discarded. The sweeps were made in closely timed pairs in opposite directions.[5] The azimuth of the sun was measured by averaging several pairs of equal-amplitude points on each peak and taking the average of these as the azimuth of the maximum of the peak. Then an average azimuth was found for each pair of + and − sweeps. The G.C.T. of each peak was measured from the tape. The position of the sun at the time of each peak and the average position of the sun for each pair of sweeps were calculated. In these observations and calculations, all values were rounded off to the nearest one-tenth degree.

A similar test of the altitude-pointing accuracy was made, even though the observational technique to be employed in obtaining the galactic-pole data did not require the same order of precision as that in azimuth measures. This altitude-pointing test revealed a constant correction of +0°.5 to all dial readings and a variable correction of the same sign, due to ground reflections, which was a maximum of +1°.5 for a dial reading zero and negligible for dial readings above 12°.

The minor lobe response of this antenna was measured, and the response of each first-order side lobe was found to be at least 16 decibels below the response of the main lobe. All other minor lobes were down by more than 20 decibels.

The antenna was mounted on a platform provided with leveling adjustments. A level with a least count of 0°.08 was mounted on the rotating vertical column. Azimuthal rotation was obtained from an induction motor and gear assembly of sufficient torque that only large gusts of wind made scarcely noticeable momentary variations in the rate of rotation. The position of the antenna in azimuth was inserted on the records automati-

[5] A positive (+) sweep, or gauge, is one for which the sense of rotation is N-E-S-W.

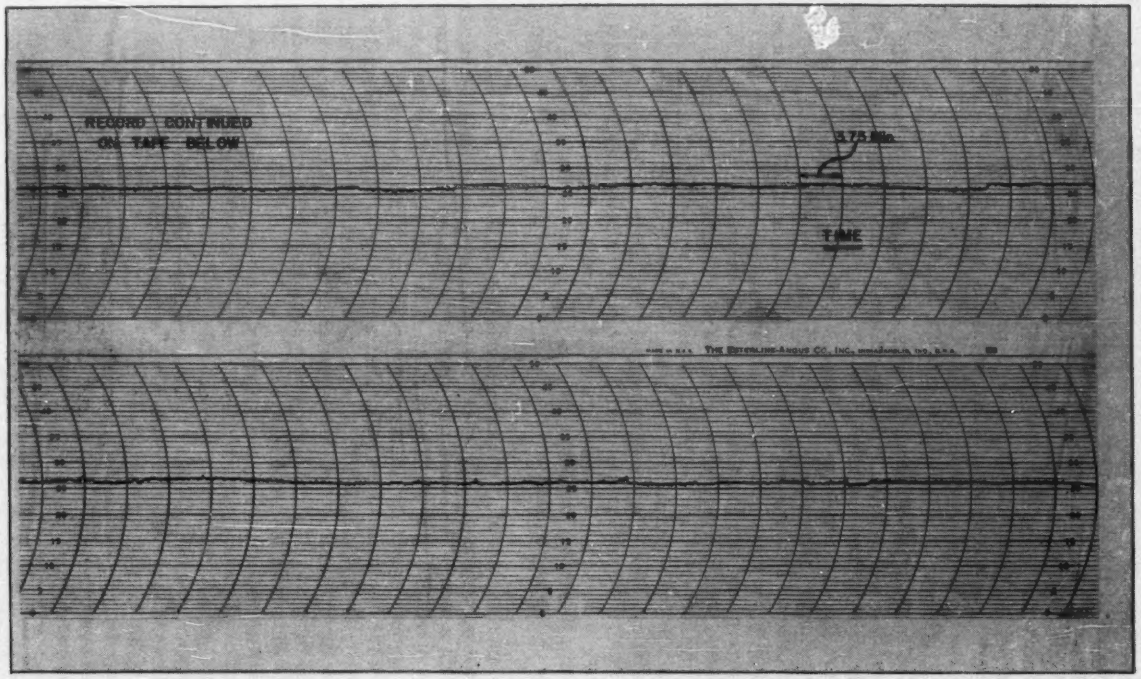

FIG. 3.—Typical record illustrating over-all stability of the 205-Mc receiving system. The traces show the difference between the detector output voltage and the E.M.F. of a 2-volt battery. Full scale on the record is 50 mv. The mean value of the jitter is about that expected on theoretical grounds. The drift was due to a change in ambient temperature of about 5° F.

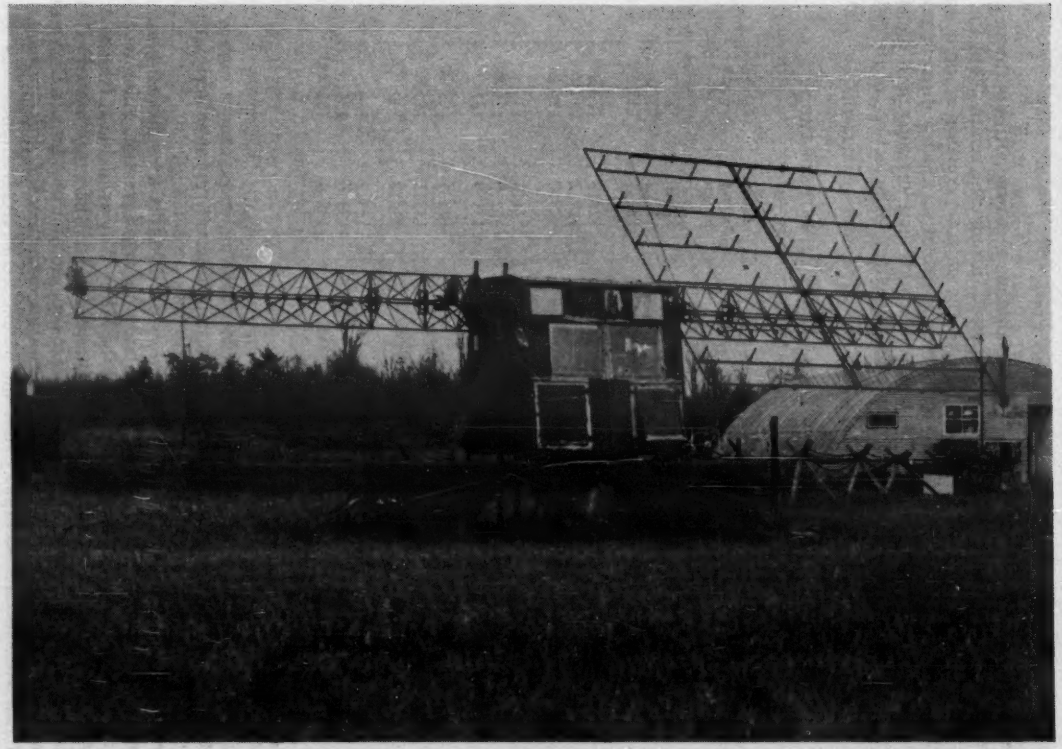

FIG. 4.—48-dipole antenna array and alt-azimuth mounting

cally by using a carefully adjusted toothed wheel and switch assembly positively attached to the vertical column in such a way that there was no play as great as 0°.1.

OBSERVING PROCEDURE

The general observing plan was to sweep the antenna at a fixed altitude through 360° in azimuth at times when the galactic equator passed through the zenith. Thus the path of the center of the antenna beam would cross the galactic equator at right angles, minimizing the labor of data reduction, reducing the extent to which a discrete galactic source could affect the position of the apparent centroids, and lessening both the effects of direct thermal radiation from the ground and the effects of reflections of the galactic

TABLE 1

A TYPICAL SET OF OBSERVED AND CALCULATED AZIMUTHS OF THE SUN

Sweep Direction	Calculated Azimuth of Sun	Observed Azimuth of Sun	Difference (C−O)*	Sweep Direction	Calculated Azimuth of Sun	Obseved Azimuth of Sun	Difference (C−O)*
+	119°.5	119°.4		+	127°.0	127°.2	
−	119.8	119.2		−	127.2	127.0	
Mean	119.6	119.3	+0°.3	Mean	127.1	127.1	0.0
+	120.5	120.4		+	128.9	129.4	
−	120.7	120.3		−	129.2	129.0	
Mean	120.6	120.4	+ .2	Mean	129.0	129.2	− .2
+	122.3	122.7		+	131.7	131.9	
−	122.5	122.5		−	132.0	131.5	
Mean	122.4	122.6	− .2	Mean	131.9	131.7	+ .2
+	123.5	123.8		+	133.3	133.5	
−	123.7	123.5		−	133.5	133.4	
Mean	123.6	123.6	.0	Mean	133.4	133.4	.0
+	124.7	125.0		+	135.2	135.5	
−	124.9	124.9		−	135.6	135.3	
Mean	124.8	125.0	−0.2	Mean	135.4	135.4	0.0

* Mean of calculated *minus* observed is $+0°.01 \pm 0°.035$ (p.e.).

radiation by the ground. Furthermore, it made use of the higher pointing accuracy of the azimuth motion in the determination of the most critical quantity, the galactic latitude of the centroids.

The details of the observing program were worked out as a compromise among a number of conflicting factors. The sun was rapidly nearing a position which would prohibit for several months the observation of all the Milky Way available at Ithaca. A large number of individual observations was desirable for a satisfactory statistical determination of the position of the galactic pole. Finally, the time constant of the recording milliammeter made a slow rate of azimuthal rotation desirable; for, if the antenna swept past the radiation source so rapidly that the period of the received pulse was of about the same order of magnitude as the damping period of the recording galvanometer, the record would be distorted in shape and the maximum would appear to occur at a later azimuth. The observing procedure was as follows:

1. The dates and periods of observation, with notes on the weather, are shown in Table 2.

2. The duration of each 360° azimuthal gauge was approximately 6 minutes.

3. The sense of rotation was opposite for consecutive gauges. The intention was to produce a number of pairs of gauges of opposite sense but of approximately the same celestial path, thus minimizing the effect of the time constant of the recording pen.

4. Gauges were made in steps of 4° of the altitude indicator, reading over the range 0°–64° inclusive. Because of the angular width of the main antenna lobe and the angular width of the galactic radiations, higher altitude gauges were omitted.

5. The starts of consecutive gauges were spaced by 10-minute intervals, allowing the observer about 4 minutes to perform necessary adjustments and to record the events.

6. The alignment of the equipment with the local vertical was checked before and after each 2-hour observing period.

7. The recording tape, driven by a 60-cycle synchronous motor, ran at the relatively fast rate of 12 inches per minute to minimize reading errors.

TABLE 2

DATES AND CIRCUMSTANCES OF THE OBSERVATIONS

Run No.	Greenwich Date (October, 1948)	Tape No.	G.C.T.		Weather
			Start	Finish	
1a	17	O-171	0025	0245	Cloudy
1b		O-174	0530	0815	
2a	18	O-177	0012	0245	Snow, rain, and high winds
2b		O-179	0530	0838	
3a	19	O-182	0035	0255	Cloudy, cold
3b		O-184	0530	0805	
4a	20	O-187	0000	0235	Rain, heavy clouds
4b		O-189	0535	0805	
5a	20–21	O-192	2345	0230	Cloudy
5b	21	O-194	0515	0800	

8. Time marks accurate to a fraction of a second were placed on the margin of the record by means of a chronograph pen. This pen was controlled by the operator, who listened, at appropriate times, to the standard time transmission of radio station WWV.

9. An azimuth mark was automatically placed on the record for every 3° of rotation, starting with a mark for true north. One mark was omitted each 60°, and the observer labeled the azimuth by hand to avoid ambiguity and to provide a double check.

10. The receiver was switched from the antenna to the reference noise source for about 4 minutes after each gauge, so as to observe the performance of the electronic equipment.

11. Except for the few seconds required to make the time marks, the observer was listening to the combined receiver and galactic noise. This greatly minimized the likelihood of mistaking any interfering terrestrial radiation for galactic radiation and provided an additional important check on the electrical performance of the entire equipment.

Since the primary record for each gauge was 10 feet in length, it was desirable, during most of the observations, to make parallel records at only 3 inches per minute. These latter monitor records proved to be very valuable because the observer was able, at a single glance, to stay in close touch with the over-all development of the observations. Several of these monitor records have been reproduced in Figure 5.

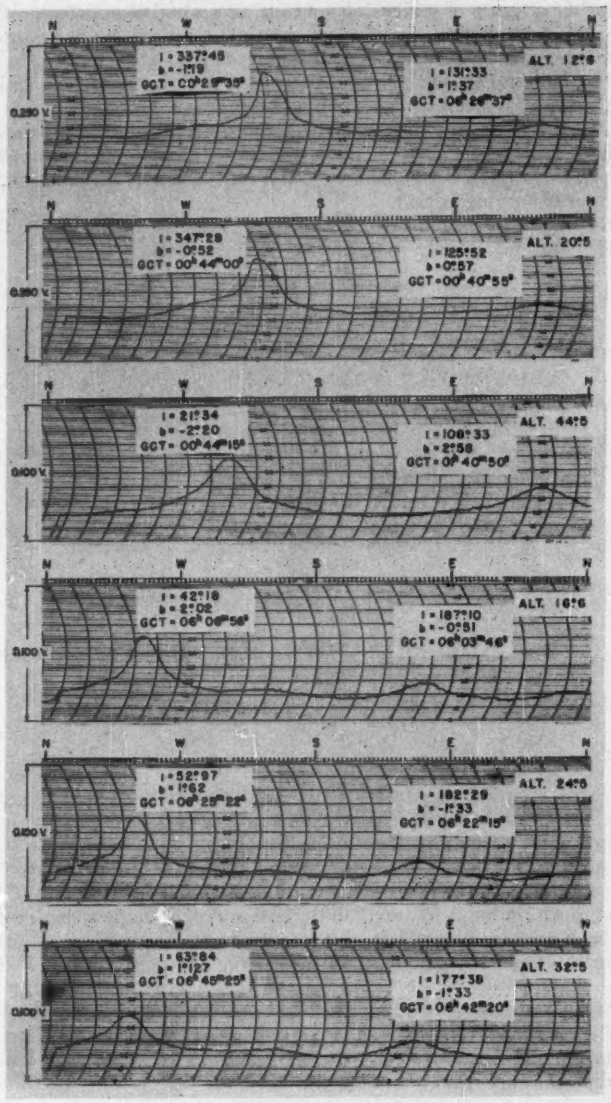

FIG. 5.—Typical monitor records taken on the night of October 20, 1948. The ordinate scale is average detector output voltage, the abscissa is antenna azimuth angle and increases to the left. The true antenna altitude for each gauge is indicated at the start. The galactic co-ordinates and G.C.T. of each maximum are indicated.

OBSERVATIONS AND REDUCTIONS

It is well to have in mind the actual nature of the quantity which is measured by a radio telescope before considering in detail the exact procedure of obtaining the desired quantities from the observations. The antenna of the radio telescope must be thought of as a device which, when pointed in a given direction, receives radiation not only from that direction but also from other directions. Therefore, the power in the transmission line from the antenna to the receiving set is proportional to the weighted mean of the specific intensity of the incoming radiation from the various directions.

Arranging the problem in spherical co-ordinates, as shown in Figure 6, there are three

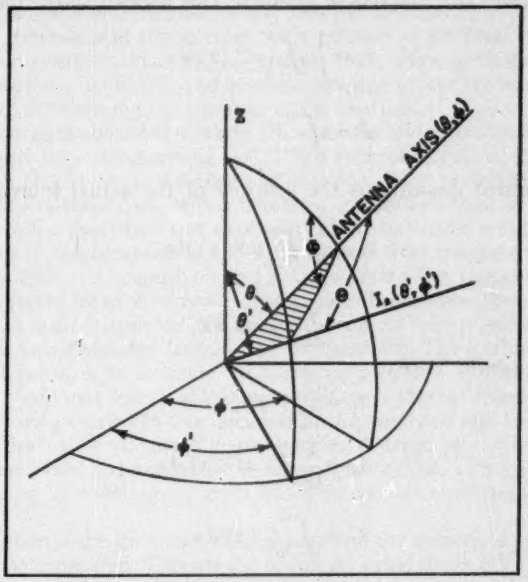

FIG. 6.—Spherical co-ordinate system

functions to be considered. First, $I_\nu(\theta', \phi')$, the angular distribution of the specific intensity at the frequency ν under consideration; next the function $G_\nu(\Theta, \Phi)$, which defines the sensitivity of the antenna in various directions from the central axis of the antenna; and, finally, the function $P_\nu(\theta, \phi)$, which gives the power delivered by the antenna to the receiver for a given pointing direction of the antenna axis corresponding to θ and ϕ. The equation connecting these three quantities is readily seen to be

$$P_\nu(\theta, \phi) = \int_{\phi'=0}^{2\pi} \int_{\theta'=0}^{\pi} I_\nu(\theta', \phi') G_\nu(\Theta, \Phi) \sin \theta' \, d\theta' \, d\phi' . \quad (1)$$

The observing procedure was chosen, in part, so that equation (1) might be simplified and thus reduce the computational labor. For the particular case considered here, the pole of the co-ordinate system is identified with the zenith. For a given sweep of the antenna, the angle θ is fixed and equal to the complement of the altitude of the sweep. The angle ϕ is the azimuth toward which the antenna axis is directed at any moment.

Both $I_\nu(\theta', \phi')$ and $G_\nu(\Theta, \Phi)$ are essentially independent of frequency when considered in relation to the receiver band width of 4.5 mc. Equation (1), therefore, reduces to a function of a single running variable, ϕ, which is now replaced by x. Bearing in mind that both the source and the antenna pattern are of small angular extent and are of the general shape of the Gaussian distribution-curve, equation (1) may be rewritten

$$P(x) = \int_{-\infty}^{\infty} S(x - x') G(x')\, dx' . \tag{2}$$

The function $P(x)$ is the one recorded on the tape in the course of the observation. Thus it is possible, in principle, to form the quantity $\bar{x}_p$, giving the centroid of the distribution of the received power as a function of azimuth. This is given by the following equation:

$$\bar{x}_p = \frac{1}{P} \int_{-\infty}^{\infty} xP(x)\, dx , \tag{3}$$

where

$$P = \int_{-\infty}^{\infty} P(x)\, dx . \tag{4}$$

However, the desired quantity is the centroid of the actual source distribution $\bar{x}_s$, given by

$$\bar{x}_s = \frac{1}{S} \int_{-\infty}^{\infty} xS(x)\, dx , \tag{5}$$

where

$$S = \int_{-\infty}^{\infty} S(x)\, dx . \tag{6}$$

It is shown in Appendix II that

$$\bar{x}_p = \bar{x}_s + \bar{x}_g , \tag{7}$$

where

$$\bar{x}_g = \frac{1}{G} \int_{-\infty}^{\infty} xG(x)\, dx \tag{8}$$

and

$$G = \int_{-\infty}^{\infty} G(x)\, dx . \tag{9}$$

It should be noted that equation (7) is independent of any stringent assumption about the form of the functions P, G, and S. Furthermore, the term $\bar{x}_g$ arises only from a lack of symmetry of the antenna pattern with respect to the geometrical axis of the antenna, and, as already shown, this antenna was extremely symmetric. Indeed, from comparisons of the observed and computed azimuths of the quiet sun obtained on several different days at a number of different altitudes, it was found experimentally that, for the radio telescopes used,

$$\bar{x}_g \ll 0^\circ.1 . \tag{10}$$

In view of the negligible nature of this correction, the apparent azimuth was taken to be the true azimuth.

While the observing schedule was intentionally arranged so that the plane of the galactic equator would coincide approximately with a vertical circle in order to minimize certain observational errors and to simplify the computations, it still required considerable labor to convert the readings actually obtained on the tapes into the desired quantities for computation. Specifically, the desired quantities were the altitude and azimuth of the point corresponding to the centroid of the galactic signal for each crossing of the plane of the galaxy and the G.C.T. of this transit.

The following procedure was adopted as a convenient approximation for locating the centroid. Several pairs of equal-amplitude points on either side of the maximum were located. The azimuth of each of these points was read to one-tenth of a degree and the average taken. The number of pairs of points taken was usually three or more, and they were distributed about the points of maximum slope. The position of this average was marked on the tape and the corresponding G.C.T. read off to the nearest second.

The average position thus determined from the tape was not, in fact, the centroid defined by equation (5). A little reflection will show that, for the case of any symmetric record, the average and the centroid must coincide. Though the actual traces were not, in general, markedly asymmetric, still it was felt to be worth while, in view of the high systematic accuracy required, to make an empirical investigation of the deviation between the average and the centroid for asymmetric distributions. This was done by determining the centroid and the average for a number of artificial distributions with asymmetry characteristics similar to, but greater than, those actually observed. In no case was the deviation significant, and so the averaging procedure was taken as an acceptable means of determining the position of the centroid.

At this stage the data consisted of some 320 azimuths and altitudes of centroids of the galactic signal with the corresponding G.C.T. for each observation. Two independent, systematic, rough checks of all the observational data were performed at this time to insure the accuracy of these data, which had been transcribed from over a mile of tape.

The next step in the procedure was to obtain galactic latitudes and longitudes for the observed positions of the centroids of the signal. These were computed in the following way: First, the altitude and azimuth of the I.A.U. galactic poles, precessed to the equinox of date, were computed for each separate observation. From these computations and the observed azimuths and altitudes of the centroids, it was then possible to calculate directly the galactic longitudes and latitudes of the centroids. The method of computation followed made it possible to institute an independent check of the computations by calculating in two different ways a side common to two different spherical triangles. All these calculations were carried to five decimals in the functions and to thousandths of a degree in angle, to insure adequate guard figures. A large planisphere, built on the principle of the astrolabe but graduated to convert from time, altitude, and azimuth to galactic co-ordinates by overlapping grids was used for test checking to an accuracy of about 1°.

The angle Ψ between the direction of the gauge and the galactic equator at the point of crossing was also computed. Though the optimum value for Ψ is 90°, it had not been practical to arrange the observations so that this value was obtained for each individual transit of the galactic plane. Because of the size of the antenna pattern and because of the asymmetry and extent of the distribution of the galactic radiation both along and normal to the galactic equator, if Ψ should depart seriously from 90° for any gauge, the apparent azimuth of the centroid might differ greatly from the true azimuth. To deal with these data in a convenient manner, normal points were formed by dividing the data into sixteen roughly equal intervals of galactic longitude and, for each group of points thus formed, calculating a mean galactic longitude and a mean galactic latitude.

It was felt worth while to take account of the fact that not all the observations were of equal value. Matters which were deemed to affect the accuracy of the observations were the over-all strength of the galactic signal, the tilt angle Ψ, and whether or not the general appearance of the tape indicated that irrelevant sources of electrical disturbances had been present. In particular, it was found that observations made at the lowest altitude were not always reproducible and hence were of dubious value. The scheme used in weighting the points was the following: All observational points corresponding to strong signals and a good tilt angle were given double weight. Observations made at 0° altitude and observations for which the tilt angle was less than 70° were all given zero weight. Observations giving evidence, by the character of the trace on the tape, of being untrust-

worthy were also given zero weight. These latter points were judged at the original time of reading the tapes. Sometimes the untrustworthiness was recognized to be the result of variation of the signal itself. Thus several records for the region near the radio star Cyg A were discarded. Sometimes, for no known reason, the record was nearly unreadable. All other observations were taken as having weight unity in forming the normal points.

The next step in the procedure was to obtain, by the method of least squares, that small circle on the celestial sphere which best fitted the normal points. The co-ordinates of the normal points were in no case far from the galactic equator, and this made possible a simplification of the observational equations to a linear form. Letting l_i and b_i be the co-ordinates of the normal point i, and letting l_0 be a trial value for the galactic longitude l' of the pole, the observational equations all take the following form:

$$b_i = X - Y\cos(l_i - l_0) - Z\sin(l_i - l_0)\,. \tag{11}$$

In these equations the quantities X, Y, and Z are the unknowns, and they are related to the desired quantities l', b', and θ in the following way:

$$X = 90^\circ - \theta\,, \qquad Y = (90^\circ - b')\cos\Delta\,, \qquad Z = (90^\circ - b')\sin\Delta\,. \tag{12}$$

The quantity Δ is the correction to l_0, the trial value for the longitude of the pole, and so is defined by

$$l' = l_0 + \Delta\,. \tag{13}$$

The quantities X, Y, and Z are all in degrees; and, once they have been determined by solving the normal equations, it is a simple matter to derive l', b', and θ and to convert l' and b' to right ascension and declination of date. These co-ordinates can then be precessed to 1900 for comparison with the position of the I.A.U. pole. The quantity θ is invariant with precession.

It was thought desirable to estimate the accuracy of the three quantities l', b', and θ. The estimate was arrived at in the following way. The weights of X, Y, and Z, the unknowns in the normal equations, were calculated by ordinary methods of least squares in terms of an observation of unit weight. To find a value for the probable error of an observation of unit weight, the root mean square deviation of the normal points from the small circle (represented by the values of l', b', and θ) was derived. This was expressed as the probable error of an observation of unit weight. From these data the probable errors of the three quantities l', b', and θ were computed by ordinary formulae for the propagation of errors. These probable errors were transformed into errors of right ascension and declination of the pole. It is felt that probable errors obtained in this way are at any rate impersonal and hence are of some value in assessing the internal consistency of the observations. The final results, for the equinox of 1900.0, are shown in Table 3.

TABLE 3

CO-ORDINATES OF THE GALACTIC POLE AS DETERMINED BY MEASUREMENTS AT 205 MC
(Equinox of 1900.0)

$$l' = 266^\circ.8 \pm 4^\circ.5\,, \qquad \alpha = 12^h39^m.36 \pm 0^m.89\,;$$

$$b' = 87^\circ.43 \pm 0^\circ.34\,, \qquad \delta = +25^\circ 26' \pm 20'$$

$$\theta = 91^\circ.28 \pm 0^\circ.18\,.$$

Table 7 lists the co-ordinates and weights of the normal points.[6] The normal points and all observations of nonzero weight are shown in Figure 7. The co-ordinates are

[6] A complete tabular summary of all the observations and computations is available on request.

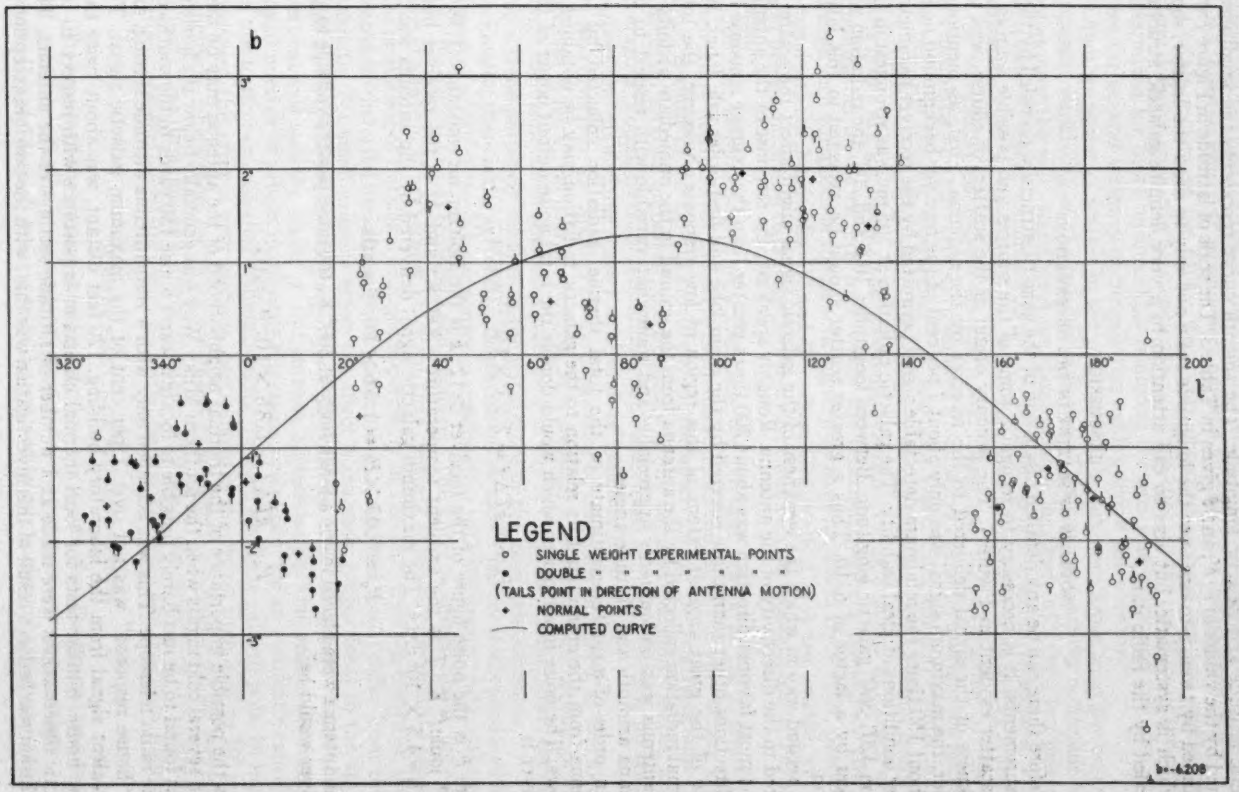

FIG. 7.—Positions of individual sweep maxima (1948 I.A.U. galactic co-ordinates)

galactic latitude and galactic longitude. The smooth curve represents the small circle defined by the values of l', b', and θ given in Table 3. The scale of latitude in Figure 7 was expanded by twenty-to-one over the longitude scale not only to show the scatter, some of which is systematic, but also to call attention to a very definite galactic structure revealed by the radio data.

DISCUSSION

SOURCES OF SCATTER IN THE OBSERVATIONS

Before there can be any detailed discussion of the galactic structure revealed by these measurements, it is necessary to recognize some of the sources and possible sources of the scatter evident in Figure 7. The primary origin of the scatter, of course, was the weakness of the signal delivered to the receiver by the antenna. First, as mentioned earlier, the maximum signal was only about 7 per cent of the receiver background noise, or about 150 times the minimum detectable signal permitted by the receiver parameters under conditions of ideal stability. The galactic radiation at 205 mc was strongest in the region 320°–360° galactic longitude. Between longitudes 100° and 200° the radiation was weaker by a factor of 6–10. Thus a greater scatter should be expected in this latter region.

A second way in which the weakness of the galactic signal might affect the scatter is related to the directivity of the antenna. Roughly speaking, the response of the antenna in the most favored direction was about 200 times greater than the average response for all directions other than those covered by the main lobe and first-order side lobes. Because of the great angular extent of this region of low response, however, the total thermal radiation collected by the antenna from the ground in the immediate vicinity of the antenna was undoubtedly appreciable and somewhat variable with respect to the antenna azimuth and altitude angles.

An order-of-magnitude estimate of the total thermal radiation collected by the antenna from the ground and its relation to the galactic radiation may be obtained as follows: The noise input power which would double the total noise output power of this receiver is

$$P_0 \simeq FkT\Delta f = 2.23 \times 10^{-13} \text{ watts},$$

where F is the noise figure of the receiver $\cong 12$; k is the Boltzmann constant $= 1.38 \times 10^{-23}$ joule/° K; T is the ambient temperature $= 300°$ K; and Δf is the receiver band width $= 4.5 \times 10^6$ c.p.s. The maximum galactic signal delivered by the antenna was

$$P_g \simeq 0.07 \times P_0 = 1.56 \times 10^{-14} \text{ watts}.$$

If the antenna were placed inside a black body at 300° K, the noise power available to the receiver would be[7]

$$P_a = kT\Delta f = 1.86 \times 10^{-14} \text{ watts}.$$

Thus the possible importance of the thermal neighborhood of the antenna may be seen.

On several cold nights when the southern Milky Way was generally below the horizon, it was found to be just barely possible to locate a warm house 150 yards to the southwest of the radio telescope. This was achieved only with a zero antenna altitude setting, and the "house response" was not over 1 per cent of the maximum galactic signal. The equivalent signal from the laboratory building, 120 feet distant, was about twice that of the house. Similar tests for local thermal objects of importance with respect to the galactic observations were made at a number of altitude settings of the antenna. The conclusion reached as a result of this investigation was that, with the possible exception of

[7] R. E. Burgess, *Proc. Phys. Soc. London*, **53**, 293, 1941.

gauges made at zero altitude, the presence of local thermal irregularities could be ignored. For this reason 0° gauges were omitted a priori from the pole solution.

Certain regions of the Milky Way were observed at both low and high altitudes. There does not appear to be a systematic altitude effect in the positions of the centroids determined for these regions. This reinforces the previous conclusion and also emphasizes the general accuracy of the pointing calibration of the antenna.

Another source of scatter in the positions of the centroids arose from the occasional apparent variability of the galactic radiation. This was particularly noticeable in the region near the radio star Cyg A, at about galactic longitude 45°. On a few gauges the total galactic signal was observed to vary by a factor of 2 in about 10 seconds. For this reason these gauges were discarded. Subsequent intensive observation of Cyg A and some of the other radio star regions has shown that a large part of the variations are the result of a modulation by the earth's atmosphere which is most prominent when the radio stars are near the horizon. Furthermore, it has been found that, when the radiation from Cyg A is highly variable with this radio star at an altitude of 30° or more, many other parts of the sky are likely to be apparently variable, though usually to a lesser extent.[8] Examination of the records from which the centroids were computed indicates that, though such variations of the galactic signal may have increased the scatter, particularly around galactic longitudes 45° and 80°, where Cyg A and Cas A are located, yet there is at present no reason to believe that this effect was very serious relative to the over-all measures.

Another possible source of scatter was the physical flexing of the antenna and a momentary hesitation of the drive mechanism under the impact of very strong gusts of wind. Because of the careful monitoring of the observations, the relatively slow rate of azimuthal rotation employed, the frequency of the automatic azimuth marks, and the averaging process used in determining each individual centroid, there is no reason to suspect any appreciable scatter as a result of buffeting by the wind.

No correction was applied to the longitudes of centroids obtained at low altitudes because of refraction near the horizon. It is doubtful whether refraction could produce a longitude distortion or scatter as great as 2° in any of the data. Furthermore, the observing scheme purposely minimized the importance of the longitude measures.

Finally, there is the systematic displacement of individual centroids produced by the apparent width of the galactic source in combination with the angular rate of the gauges and the period of the recording galvanometer. The antenna turned about the vertical axis at a rate of 1° per second. Since the time constant of the recorder was 0.4 seconds, if the amplitude of the signal changed appreciably in 1 second, then the record on the tape would be distorted and the apparent azimuth of a centroid would differ from the true azimuth. For small azimuth errors the effect is inversely proportional to the apparent half-width of the source and proportional to both the rate of antenna rotation about the vertical axis and the cosine of the antenna altitude angle. One reason for making an equal number of gauges in opposite directions was to provide an automatic cancellation of this form of error in the computations for the position of the galactic pole. In Figure 7, however, this error is very obvious, particularly in the region from 320° to 10° galactic longitude, where there are two more or less parallel sets of points, each set representing a particular direction of antenna rotation. Thus it is the opinion of the authors that rather considerable reliance may be placed on the relatively fine details of Figure 7.

GENERAL RESULTS OF THE OBSERVATIONS

The results of the present investigation leave no doubt that the general source of 205-mc galactic radiation is intimately connected with the structure of the galaxy. Table 4 shows the positions of galactic poles determined from a variety of astronomical observa-

[8] A paper describing these observations of Cyg A is now in preparation.

tions by F. F. M. van Tulder.[9] The relation of the 205-mc pole to these other poles is shown in Figure 8. The circles and the rectangle indicate the probable errors of the determinations.

Table 5 gives the positions of the galactic poles as computed by Northcott and Williamson[2] from Reber's observations of galactic noise at 160 and 480 mc. The results of the present determination are included for comparison. Figure 8 suggests that there is nothing in particular to distinguish the positions of the poles of galactic radio noise from the galactic poles determined in other ways. Note, for example, the agreement with the determination, No. 22, from the zone of avoidance of extragalactic nebulae and with the determination, No. 11, obtained from the distribution of B0 stars not in the local group but within 1250 parsecs of the sun. It is probably safe to say that the source of the

TABLE 4

GALACTIC POLES DETERMINED FROM VARIOUS OBJECTS
(Adapted from van Tulder*)

No.	l'	b'	Type	No.	l'	b'	Type
1	191°	87°.1	cB0–cA6	16	304°	89°.0	Wolf-Rayet
2	298	88.8	cB0–cA6				
3	14	84.5	cA7–cK	17	131	89.0	Open clusters
4	6	87.0	cA7–cK	18	0	89.4	Open clusters
				19	357	88.5	Open clusters
5	26	88.1	δ Cephei				
6	343	87.8	δ Cephei	20	161	84.2	Planetary nebulae
7	349	88.5	δ Cephei				
				21	41	85.2	Planetary nebulae
8	193	87.0	B1–B2				
9	346	88.1	B1–B2				
10	12	88.2	B1–B2	22	253	86.2	Extra-galactic nebulae
11	269	88.3	B0				
12	305	88.7	B0	23	290	88.0	High velocities
13	181	88.2	B0–B5	24	281	89.4	Stars far from galactic plane
14	305	89.5	B0–B5				
15	301	88.9	O				

* F. F. M. van Tulder, *B.A.N.*, No. 353, p. 1, 1942.

TABLE 5

GALACTIC POLES DETERMINED FROM MEASUREMENTS OF RADIO NOISE ON THREE FREQUENCIES
(Equinox of 1900)

Frequency (Mc)	Observer	R.A.	Declination	θ	Range in Gal. Long.	Normal Points
160	Reber*	$12^h34^m.5 \pm 1^m.1$	$+27°.10 \pm 0°.26$	$91°.61 \pm 0°.20$	325°–210°	12
205	Cornell	$12\ 39.4 \pm 0.9$	$+25.43 \pm 0.34$	91.28 ± 0.18	326 –196	16
480	Reber*	$12\ 40.9 \pm 2.7$	$+29.10 \pm 0.87$	90.72 ± 0.54	330–55; 150–180	10

* Northcott and Williamson, *J.R.A.S. Canada*, **42**, 269, 1948.

[9] F. F. M. van Tulder, *B.A.N.*, No. 353, p. 1, 1942.

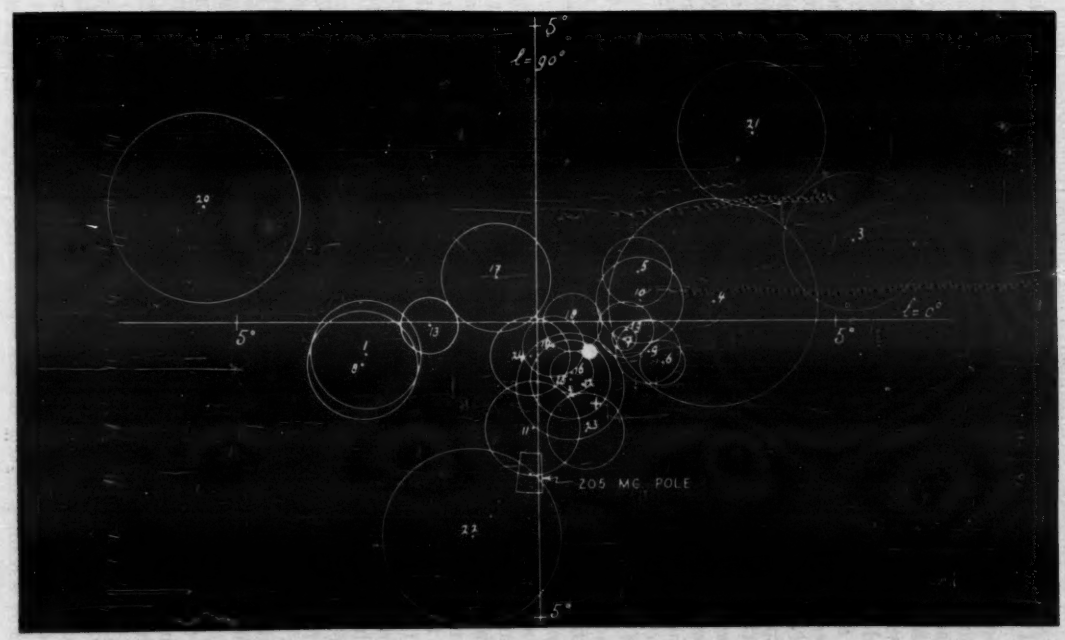

FIG. 8.—Position of the 205-Mc radio pole relative to the galactic poles computed by F. F. M. van Tulder

205-mc radiation has little connection with the phenomenon of Gould's Belt.[10] The pole of Gould's Belt is approximately 15° away from the north galactic pole, whereas the pole of the 205-mc radiation is only 2°.5 distant and in a different direction.

The radio observational material exhibits a high internal consistency, and, partially in consequence of this, the radio determinations show a considerably smaller probable error than most of the determinations from photographic data.[11]

THE OBSERVATIONAL VALUE FOR θ

One provocative result of the radio observations is the fact that the mean galactic latitude of the radiation at 205 mc differs significantly from zero degrees. Reference to Table 5 shows that a similar effect was also apparent in the reductions of Reber's data at both 160 and 480 mc. It is well known from various astronomical observations that the sun appears to occupy a position somewhat to the north of the galactic plane. For the height of the sun above the galactic plane, van Tulder[9] suggests a best value of about 13 parsecs. Now if it is assumed that the sources of the general background galactic radio radiation, whether stellar or interstellar in nature, are more or less uniformly distributed in the immediate neighborhood of the plane of symmetry for other galactic phenomena and if it is assumed that the value of θ is not influenced greatly by the presence of a few intense radio stars, then a mean distance to the effective sources of the radio radiation can be computed. This value turns out to be approximately 750 parsecs at a frequency of 205 mc.

In spite of the dearth of precise information on the spatial and frequency characteristics of galactic radio radiation, considerable effort has been expended by a number of well-qualified persons to develop a satisfactory hypothesis concerning the origin of these puzzling radiations. One of the more persistent suggestions is that the radio radiation is a manifestation of the free-free transition phenomenon operating in the interstellar medium. If the source of the radio radiations is the interstellar medium, then, according to the theory of radiation from a thin slab in local thermodynamic equilibrium, the mean distance to the effective sources should be directly comparable with the distance to an opacity of approximately unity. However, it is not difficult to show that, on the theory of free-free transitions, such a distance must be at least ten times as great as the one just derived, if it is not to conflict violently with present astronomical data on the interstellar electron gas.

There is, of course, an alternate way of considering this phenomenon. Assuming that the galactic radiation is to be identified with radiation from the electron gas in interstellar space, at least 10,000 parsecs must be taken as a fair value for the distance corresponding to unit opacity. This is quite definitely a minimum value, and it is difficult to see how it could be made smaller, at least on the generally accepted theory of free-free transitions.[12] But if this is the average distance to the source of the radiation, then it follows that the sun must be at least several hundred parsecs above the central plane of the radiating medium in order to give the observed value of $-1°$ for the mean galactic latitude of the radio signal.

In this way one is led to see the crucial nature of the conclusion that the centroid of the galactic radiation departs noticeably from a great circle on the celestial sphere. If we accept this conclusion, we must either disregard the theoretical calculations of the opacity of the galaxy for the radiation at 205 mc on the basis of currently used formulae representing free-free transitions as the sole source of the opacity, or we must change our

[10] Bart J. Bok, *The Distribution of the Stars in Space* (Chicago: University of Chicago Press, 1937).

[11] It would be interesting to perform a version of the radio determination of the galactic pole at infrared wave lengths. This could be done by using infrared photocells at the slightly blurred focus of a large mirror.

[12] A. Unsöld, *Naturwiss.*, **7**, 194, 1947.

ideas about the height of the sun above the median plane of the galaxy (assuming, of course, congruence between the median plane of the radio source and the galactic plane). It is our belief that the former alternative is much to be preferred and that we should tentatively accept a value for the absorption coefficient of the order of unity per kiloparsec. This preference is encouraged by other evidence of an observed value for the galactic opacity at 205 mc of the same order of magnitude.[13]

It becomes of considerable importance, then, to test in any way possible the reliability of the value of θ which has been derived. In this connection, particular attention should be paid to the unavoidable gap in the observations which occurs between 200° and 320° galactic longitude. This portion of the Milky Way is not visible as far north as Ithaca. In principle, at least, the comparatively low probable error of θ indicates that no difficulty is to be expected about the determination of this quantity because of the gap in galactic longitude. At the same time, it was felt worth while to make an additional computational test of the reality of the value obtained for θ by asking how well the present data can be represented by a solution in which it is assumed that there is no deviation of the centroids of the galactic signal from a great circle. This is equivalent to requesting the probable errors of l' and b' under the assumption that $X = 0$ in equation (11). Following conventional least-squares methods, new probable errors were computed for l' and b', and the results are exhibited in Table 6, along with the probable errors from

TABLE 6

COMPARISON OF PROBABLE ERRORS OF l' AND b' FOR TWO ALTERNATIVE HYPOTHESES ABOUT X

	$X \neq 0$	$X = 0$
l'	±4°.5	±15°.7
b'	±0°.3	± 0°.8

the more general solution. It can be seen that the probable errors for the position of the pole are more than doubled by requiring the observations to fit a great circle rather than the optimum small circle. Since the method of determining the probable errors takes into account the fact that there are three adjustable parameters in one of the solutions and only two in the other, this cannot be a source of the difference of the probable errors in the two cases. The conclusion to be drawn from this is, presumably, that the observations are definitely better fitted by a small circle corresponding to an X of about $-1°$ than they are by the corresponding great circle. However, in view of the considerable astrophysical interest in the exact value of θ, a final decision must await observations made in latitudes such that the gap in galactic longitude is greatly lessened or completely done away with. Also, in order to study only the general background radio radiation, it will be necessary to subtract the effects, discussed below, of the intense radio stars near the galactic plane. The observational techniques required for this separation are known and not very difficult.

DEVIATION OF THE NORMAL POINTS FROM THE COMPUTED CURVE

Several of the deviations of the normal points from the computed curve are unquestionably significant. Three of these deviations appear to be adequately accounted for by the presence of three radio stars near the galactic plane. Thus Cyg A, an intense

[13] R. E. Williamson, *J.R.A.S. Canada*, **44**, 12, 1950. Thus, from the table in this reference, the total galactic opacity normal to the plane is of the order of 0.2 for 205-mc radiation. Any reasonable estimate of the geometrical extent of the radiating layer will give an absorption coefficient in fair agreement with the number suggested in the present work.

discrete source at 45° galactic longitude, has a galactic latitude of only +5°, and Figure 7 shows clearly the systematic deviation of the neighboring centroids in the direction of positive galactic latitude. Similarly, Cas A, an even more intense radio star at galactic longitude 79° and galactic latitude −2°, seems to exert an influence on the positions of the centroids in its neighborhood. The somewhat weaker radio star Tau A at galactic longitude 154° and galactic latitude −4° appears to be a logical cause for the deviation of the normal point at longitude 161°.

Cyg A, Cas A, and Tau A complete the present census of strong radio stars in the immediate vicinity of the galactic plane, between 320° and 200° galactic longitude. This leaves the very obvious excursions of several other normal points unexplained. In par-

TABLE 7

CO-ORDINATES, WEIGHTS, DEVIATIONS, AND INTERNAL PROBABLE ERRORS OF NORMAL POINTS

Normal Pt. No.	Weight	Galactic Longitude	Galactic Latitude	Deviation of Normal Point from Computed Curve	Probable Error of Normal Point from Internal Consistency
1*.....	19	331.194	−1.617	+0°.601	±0°.06
2.....	20	340.600	−1.520	+0.228	.07
3*.....	20	350.814	−0.953	+0.354	.06
4.....	18	0.880	−1.358	−0.068	.06
5*.....	20	11.921	−2.141	−2.350	.06
6.....	19	25.195	−0.659	−0.364	.21
7*.....	19	44.369	+1.590	+0.941	.11
8.....	20	66.256	+0.568	−0.317	.09
9*.....	19	87.204	+0.325	−0.941	.16
10*.....	19	107.112	+1.949	+0.663	.08
11*.....	20	122.070	+1.883	+1.124	.10
12*.....	20	133.817	+1.381	+0.817	.14
13*.....	20	160.820	−1.652	−1.171	.10
14.....	20	171.604	−1.224	−0.320	.09
15.....	20	181.210	−1.546	−0.005	.09
16.....	20	190.800	−2.235	−0.112	±0.20

* Normal points whose deviations from the computed curve are greater than five times their internal probable error.

ticular, the first five normal points (l = 331°, 341°, 351°, 1°, 12°) in the Sagittarius to Aquila portion of the Milky Way suggest a definite galactic structure. Considerable importance may be attached to the deviations of these centroids because the general galactic radio radiation is most intense in this region and, therefore, the positions of these centroids are the most precise.

The reality of the deviations of the normal points from the computed curve may be examined in another way. Consider the dispersion of the individual observations used in forming a given normal point about that normal point. From this dispersion, an internal probable error for the normal point can be derived. If the excursion of the normal point from the computed curve is of the same order of magnitude as this internal probable error, the conclusion is that there is no significant deviation of the normal point from the smooth over-all structure as given by the computed curve. Conversely, a deviation which is large compared to the internal probable error gives strong evidence of the intrinsic importance of this departure from the smooth curve. Table 7 exhibits the findings of such calculations.

Finally, the probable error of a normal point relative to the computed curve is 0°.89, while the mean of the internal probable errors of the normal points is only 0°.092.

ASYMMETRY OBSERVED NEAR GALACTIC LONGITUDE 345°

It was found that, in general, the radio sources are distributed quite symmetrically in galactic latitude on either side of the central maxima. There is one apparent exception to this rule, however, in a region extending for perhaps 50° along the galactic plane and centered at about galactic longitude 345°. These are very approximate figures, though the asymmetry is quite apparent. The top two monitor records reproduced in Figure 5 demonstrate this apparent asymmetry. The lower skirts of the larger humps are quite unequal.

This asymmetry indicates an apparent extension of appreciable radio sources to north galactic latitudes perhaps as high as +20° or +30°. Reber's observations at 480 mc[14] show a qualitatively similar northern extension. The 205-mc data at hand do not permit a clear interpretation of this asymmetric distribution. There may be one or more weak radio stars or other relatively discrete sources of radio frequency radiation sufficiently close to the northern side of the main galactic concentration that the angular resolving power of the radio telescope was insufficient to produce a definite separation in the observations. Or there may be a real, but very distant, extension of a general source in the direction of the north galactic pole. Because of the method employed in transcribing the data from the tapes, this low-intensity asymmetry is believed to have had only a minor influence on the positions of the centroids in this region.

MAXIMUM RELATIVE INTENSITY AND APPARENT WIDTH OF THE CENTROIDS AS FUNCTIONS OF GALACTIC LONGITUDE

Since, initially, these observations of the galactic radio emission were intended for use only in the determination of the galactic pole and since this was the first serious test of the capabilities of this radio telescope, only cursory attention was paid to the absolute power calibration of the equipment. Despite this fact, certain additional data were obtained and are included here because of their general interest, although they are of considerably lower accuracy than are the data relative to the centroids of the galactic signal as a function of galactic longitude. These additional observations must be regarded as being of a provisional nature.

The relative maximum intensity of the galactic radiation as a function of galactic longitude is shown in the lower half of Figure 9. The ordinate of this curve corresponds to the maximum signal obtained on a gauge. The zero of this curve is approximate, since it corresponds only to the lowest signal obtainable from that part of the celestial sphere visible at Ithaca. However, there is reason to believe that this zero is not in error by more than five scale units. The primary maxima of this relative intensity-curve coincide with the longitude of the center of the galaxy. The secondary maxima occur at longitudes agreeing with the positions of the radio stars Cyg A, Cas A, and Tau A. Apart from these points, the variation appears to be quite smooth. The ratio of the intensity of the 205-mc radio emission from the galactic center to the emission from the anticenter is probably not less than 5 to 1 and not over 10 to 1.

It is possible to arrive at an order-of-magnitude estimate of the specific intensity of the galactic radiation in the following way. When the radio telescope was directed at the quiet sun at a season when galactic radiation was not entering the radio telescope in appreciable quantity, the relative intensity was approximately 140 units. Furthermore, when the radio telescope was directed toward the sun, the flux at the antenna came from a solid angle determined by the angular diameter of the radiating portion of the sun at this frequency, which may be taken to be approximately 0°.8. However, when the radio

[14] Grote Reber, *Proc. I.R.E.*, **36**, 1215, 1948.

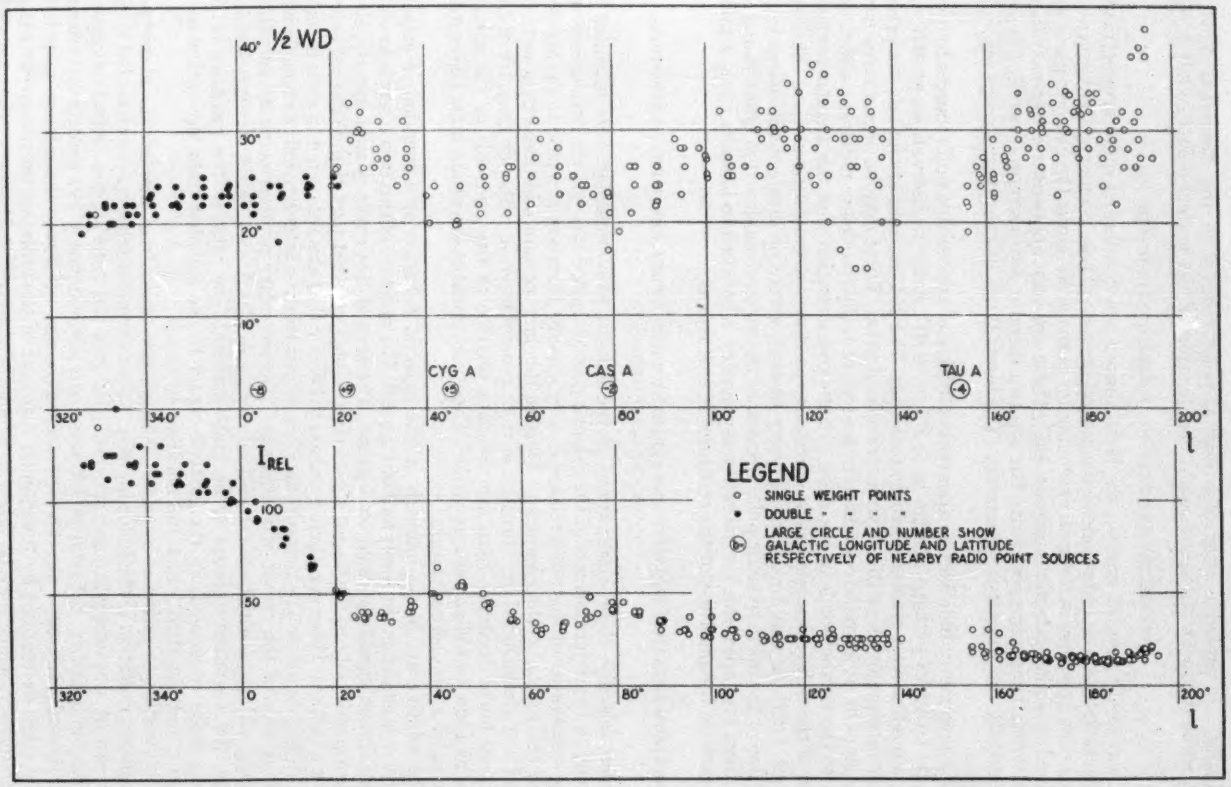

FIG. 9.—Apparent half-width and relative intensity of 205-Mc radio radiation versus galactic longitude

telescope was directed at a portion of the galaxy, the flux at the antenna was partly determined by the half-width of the antenna pattern, which was 15° for this radio telescope. Making use of these facts, we can derive the following simple expression for the specific intensity of the galactic radiation in any galactic longitude as compared with the specific intensity of solar radiation for the frequency concerned:

$$\frac{(I_\nu)\,\text{gal.}}{(I_\nu)\,\text{sun}} \simeq \frac{(I_{\text{rel}})\,\text{gal.}}{(I_{\text{rel}})\,\text{sun}} \times \left(\frac{0.8}{15}\right)^2 = \frac{(I_{\text{rel}})\,\text{gal.}}{140} \times \left(\frac{0.8}{15}\right)^2 = 2 \times 10^{-5}\,(I_{\text{rel}})\,\text{gal.}$$

Taking the radiation temperature of the sun as 10^6 °K and (I_{rel})gal. for the galactic center as 125, we get a radiation temperature for the galactic center as follows:

$$(I_\nu)\,\text{gal. cen.} \simeq 20\,(I_{\text{rel}})\,\text{gal.} = 20 \times 125 = 2500°\text{K}\,.$$

This is in quite satisfactory agreement with the value interpolated from Townes's discussion[15] of galactic measures by Franz, Jansky, Reber, and Hey, Parsons, and Phillips. It cannot be too strongly emphasized that the above computations are not a result of absolute calibrations and are included merely as an order-of-magnitude estimate to give additional meaning to the data represented in Figure 9.

Data were taken from the tapes for the purpose of calculating approximate half-widths for the radiating region of the galaxy in the various galactic longitudes. To do this, a minimum was established by drawing a straight line between the minima on either side of the galactic plane. A line parallel to this was then drawn halfway from the minimum to the maximum value of the signal. The difference in azimuth of the two "half-signal" points was then read from the azimuth calibration marks. From this a rough value of the width in galactic latitude of the observed distribution was computed for each sweep by the following equation:

$$\Delta b = \Delta Z \sin \Psi \cos h\,.$$

In the above equation Δb is the apparent half-width in galactic latitude of the power distribution, ΔZ is the observed half-width in azimuth as read from the tape, Ψ is the tilt angle defined earlier, and h is the altitude of the sweep. The results of these computations are shown in the top half of Figure 9. The ordinate of this curve is the apparent width of the galactic source between the two half-intensity points. Thus no attempt was made to correct for the finite width of the antenna pattern in order to obtain an approximate half-width for the actual intensity distribution of the galactic radiation. Such refinements must await further observations.

An interesting feature of the half-width-curve of Figure 9 is that it exhibits no general trend for a widening of the radiating region toward the direction of the galactic center. As a matter of fact, the apparent trend is in the opposite direction, so that wide, but faint, radiating regions of the galaxy are indicated for galactic longitudes near the anticenter rather than the center. Again, the provisional nature of this conclusion must be stressed.

A rough estimate of the actual half-width of the galactic radiation can be obtained by application of the following equation:

$$\Theta_p^2 = \Theta_s^2 + \Theta_a^2\,.$$

In this equation Θ_a represents the half-width of the antenna pattern, Θ_s represents the half-width of the true source distribution, and Θ_p represents the half-width of the observed distribution. This equation would be exact if all the distributions mentioned were of the Gaussian type. Since this is not strictly true, the equation must be regarded only as a good approximation. The quantity Θ_p may be read from Figure 9, and the quantity Θ_a

[15] Charles Hard Townes, *Ap. J.*, **105**, 235, 1947.

is 15°. It appears that the true half-widths of the radiating regions of the galaxy may lie between 10° and 25° and that a reasonably accurate value at 0° galactic longitude would be approximately 15° from the half-intensity point on one side of the galactic plane to the half-intensity point on the other side of the galactic plane for 205-mc radiation.

Both the low value found for the ratio of the intensities of the radio emission from the direction of the galactic center to the emission from the direction of the anticenter and the uniformity with galactic longitude of the width of the radiating regions is slightly corroborative evidence of the low value for the mean distance to the effective radio sources just computed from the value of θ. For, if the mean distance to the effective sources were of the order of 10–20 kiloparsecs or more, then a distribution of the radio sources would be required by the present data which placed a large proportion of the total radio sources of the galaxy at the periphery of the galaxy, and there is as yet no evidence to suggest a distribution which would be so unlike the distributions of other galactic phenomena.

Furthermore, these geometrical distributions and the smooth intensity distribution do not appear to offer any evidence that the sun is either in or near a possible spiral arm of the galaxy.

CONCLUSION

As a result of the data and interpretations discussed here and the investigation by Williamson,[13] there are now two sets of observations which strongly suggest a value for the mean absorption coefficient in the plane of the galaxy of the order of unity per kiloparsec for a frequency of 2×10^8 cycles per second ($\lambda = 1.5$ meters). It is difficult to see how this value for the absorption coefficient can be reconciled with the present form of the hypothesis that the chief source of the general galactic radio emission is the free-free transition process operating in the interstellar medium. Moreover, the apparent uniformity with galactic longitude of the width of the chief radio frequency emission region near the galactic plane and the smooth and not very great variation of the maximum intensity of the radiation with galactic longitude tend to support a belief in the nearness of the effective sources.[16]

It must be remembered, however, that the data reported here are restricted to the region of the celestial sphere between 320° and 200° galactic longitude. Though this does not appear to be a serious restriction, yet it would be well to consider the conclusions based on these observations as tentative in nature until more complete data are available or other corroborative evidence appears. And, after all, the techniques and facts of radio astronomy are in an early stage of development, so that a patient and judicious attitude is appropriate.

The authors wish to thank their associates on the Cornell University Radio Astronomy Project for their generous assistance in this investigation. W. E. Gordon and B. M. Fannin contributed to the organization and execution of the observations. S. M. Colbert perfected the mechanical arrangements and designed and installed the angular measuring devices and much of the auxiliary electronic equipment. R. D. Wilson constructed the high-frequency portion of the receiver. Particular credit is due Mrs. John Tryon, who performed nearly all the tape measurements and subsequent computations, and whose care and excellent judgment were invaluable throughout the reductions and analysis. Dr. D. A. MacRae, of the Warner and Swasey Observatory, participated in the early stages of this investigation and was a source of continuous encouragement and

[16] Though it was convenient to use freely such terms as "opacity of the galaxy," etc., the authors wish to make it clear that they do not hold any definite opinion concerning the stellar or interstellar nature of the sources of the general galactic radio radiation phenomenon. Two as yet unanswered questions are of the utmost importance in this respect. Have the discrete, and probably near, point sources unduly influenced the value of θ? And are the radio stars and the general galactic radio radiation merely the near and the distant manifestation of the same phenomenon?

helpful suggestions. Appreciation is expressed to Dr. H. G. Booker for criticism of this paper. Thanks are due Dr. C. R. Burrows, director of the Cornell School of Electrical Engineering, and Dr. F. S. Hogg, director of the David Dunlap Observatory, for their advice and encouragement.

APPENDIX I

Factors Governing Pointing Accuracy

To gain some insight into factors governing the accuracy of pointing on an extended source with a broad antenna pattern, we can make use of the one-dimensional approximation introduced in equation (2). The angular distribution of the source intensity, $S(x)$, and the response of the antenna pattern, $G(x)$, must be particularized to some convenient analytical form; all the important features of the problem will be retained if we assume each of the functions to be Gaussian:

$$G(x) = \frac{G}{\theta_a\sqrt{\pi}}\, e^{-(x/\theta_a)^2}, \tag{A.1}$$

$$S(x) = \frac{S}{\theta_s\sqrt{\pi}}\, e^{-(x/\theta_s)^2}. \tag{A.2}$$

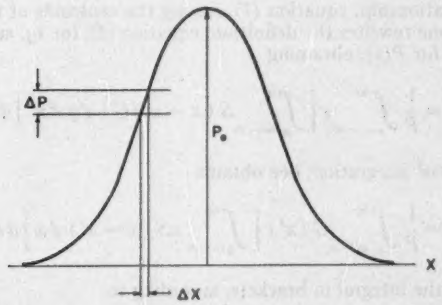

Fig. 10.—Showing the pointing error Δx resulting from a small uncertainty ΔP in the power output as a radio telescope scans a source.

For these functions, the observed power distribution as the source is scanned by the antenna, will be (cf. eq. [2])

$$P(x) = \frac{GS}{\sqrt{\pi}\,(\theta_s^2+\theta_a^2)}\, e^{-[x^2/(\theta_s^2+\theta_a^2)]} \equiv P_0\, e^{-[x^2/(\theta_s^2+\theta_a^2)]}. \tag{A.3}$$

The recording milliammeter fed by the receiver gives a graphical representation of the function $P(x)$—rather, it would do so except for minute fluctuations caused by the irregularities of the amplifier. Suppose these are of the order of ΔP. We must concern ourselves with the question of what uncertainty Δx is to be expected in the measured azimuth, due to a power-fluctuation of magnitude ΔP. From Figure 10,

$$\Delta x = \frac{1}{dP/dx}\,\Delta P. \tag{A.4}$$

If we evaluate dP/dx from equation (A.3) at the point of maximum slope, which is approximately where measures were actually made on the records, we obtain, as a guide, the following relationship:

$$\frac{|\Delta x|}{\theta_a} = 1.166\,\sqrt{1+\left(\frac{\theta_s}{\theta_a}\right)^2}\,\frac{|\Delta P|}{P_0}. \tag{A.5}$$

Since a 1 per cent stability of the value of θ_a for practical antennas is a trivial achievement, it is readily seen that the important factors governing the value of Δx are the stability and sensitivity of the receiver which affect ΔP and P_0 directly.

To apply the above relation to the situation actually encountered in the observing program, where

$$\frac{|\Delta P|}{P_0} \sim 0.01\,, \qquad \theta_s \sim 20^\circ\,, \qquad \theta_a \sim 15^\circ\,,$$

we have

$$|\Delta x| \sim 2 \times 0.01 \times 15 = 0^\circ.3\,. \tag{A.6}$$

It is to be expected, then, that one determination of the centroid for a given longitude, resting on the mean of three or more pairs of determinations, subject to errors of the order of Δx, should be accurate to a small fraction of a degree. Furthermore, the person reading the records will automatically tend to reduce the effective value of ΔP because the eye easily recognizes a mean value in the relatively fine granulations of the record.

APPENDIX II

Relationship of Centroids of $S(x)$, $G(x)$, $P(x)$

To establish the relationship, equation (7), among the centroids of the three distributions, $S(x)$, $G(x)$, and $P(x)$, one rewrites the definition, equation (3), for $\bar{x}_p$, substituting in it the expression, equation (2), for $P(x)$, obtaining

$$\bar{x}_p = \frac{1}{P}\int_{x=-\infty}^{\infty} x\left[\int_{x'=-\infty}^{\infty} S(x-x')\,G(x')\,dx'\right]dx\,. \tag{B.1}$$

By inverting the order of integration, one obtains

$$\bar{x}_p = \frac{1}{P}\int_{x'=-\infty}^{\infty} G(x')\left[\int_{x=-\infty}^{\infty} xS(x-x')\,dx\right]dx'\,. \tag{B.2}$$

Changing variables of the integral in brackets, according to

$$y = x - x' \qquad \text{and} \qquad dy = dx\,, \tag{B.3}$$

it becomes

$$\left[\int_{y=-\infty}^{\infty} (y+x')\,S(y)\,dy\right] = [S\bar{x}_s + Sx']\,. \tag{B.4}$$

Substituting equation (B.4) in equation (B.2), one has

$$\bar{x}_p = \frac{1}{P}\int_{x'=-\infty}^{\infty} G(x')\,[S\bar{x}_s + Sx']\,dx'\,,$$

$$\bar{x}_p = \frac{S}{P}\left[\bar{x}_s\int_{-\infty}^{\infty} G(x')\,dx' + \int_{-\infty}^{\infty} x'G(x')\,dx'\right],$$

$$\bar{x}_p = \frac{SG}{P}\,[\bar{x}_s + \bar{x}_g]\,. \tag{B.5}$$

Now integration of equation (2) over all x shows that

$$P = \int_{x=-\infty}^{\infty}\int_{x'=-\infty}^{\infty} S(x-x')\,G(x')\,dx'\,dx\,;$$

or, making use of the transformations (B.3) and integrating first over y as in equation (B.4), then over x', one arrives at the relation

$$P = GS\,. \tag{B.6}$$

In view of this, equation (B.5) becomes

$$\bar{x}_p = \bar{x}_s + \bar{x}_g\,, \tag{B.7}$$

which is the desired relation.

DOPPLER-SHIFTED AURORAL HYDROGEN EMISSION

A. B. MEINEL
Yerkes Observatory
Received October 10, 1950

ABSTRACT

Spectra obtained during the intense auroral storm of August 18 and 19, 1950, showed that the $H\alpha$ emission observed at the magnetic zenith is asymmetrically displaced to the violet. The violet wing is shifted approximately 71 A, indicating a velocity of impact of 3300 km/sec. The $H\alpha$ emission observed at the magnetic horizon is symmetrical and undisplaced but considerably broadened. These observations clearly establish that protons precipitate into the upper atmosphere during auroral storms. These protons must provide the primary energy source for the auroral emissions.

OBSERVATIONS

The occurrence of a major auroral storm during the two nights of August 18 and 19, 1950, made it possible to utilize the night-sky grating spectrograph[1] to study the auroral spectrum in the region of $H\alpha$. This spectrograph has a dispersion of 247 A/mm and a resolution of 28 μ with an equivalent slit-width of 21 μ. This dispersion is sufficient to separate the region of $H\alpha$ from the adjacent (6, 3) and (7, 4) bands of the first positive system of N_2 at 6624 A and 6543 A, respectively.

Eight spectra were obtained during the course of the auroral storm. Three were secured with the spectrograph pointed 20° south of the astronomical zenith, which is the direction of the magnetic zenith at the Yerkes Observatory. The other spectra were obtained with the spectrograph pointed toward the north magnetic horizon. In both cases an image of the sky 30° long was projected on the slit of the spectrograph.

The spectra of a homogeneous arch in the magnetic horizon taken on August 18, 1950, showed strong $H\alpha$. A spectrum of a flaming curtain taken later the same night did not show $H\alpha$. Early on the following night a homogeneous arch appeared in the magnetic zenith. This spectrum also showed strong $H\alpha$. A flaming corona that followed the disappearance of the arch did not show $H\alpha$ in any appreciable intensity. Spectra obtained of other auroral features in the magnetic horizon this night showed $H\alpha$ in moderate intensity. The features from which the hydrogen emission was strongest could not be ascertained because of a great display of rapidly changing features.

REDUCTION

A cursory examination of the spectra was sufficient to show that $H\alpha$ was shifted to the violet in the spectra obtained in the magnetic zenith. A distinct gap was apparent between the violet edge of the (6, 3) first positive band of N_2 and the red edge of $H\alpha$. Subsequent microphotometer tracings confirmed this examination.

The $H\alpha$ region of the auroral spectrum, taken on Eastman 103*a*-F plates without a filter, is shown in Figure 1. The second-order N_2^+ band at 3914 A appears to the red of $H\alpha$. Spectra *a* and *d*, obtained from the magnetic horizon, show a broadened but undisplaced $H\alpha$ line. The first positive bands of N_2 are weak and do not materially affect the profiles. Spectrum *c*, obtained from the magnetic zenith, shows the asymmetrical violet-displaced $H\alpha$ line. Spectrum *b* is of a flaming aurora and is used as a comparison for the effect of the nitrogen bands.

Microphotometer tracings were made at several places along the wide spectra. The average of four separate microphotometer traces for each type of spectrum is shown in Figure 2. The ordinates on these tracings were changed by a small factor in order to

[1] A. B. Meinel, *Ap. J.*, 111, 555, 1950.

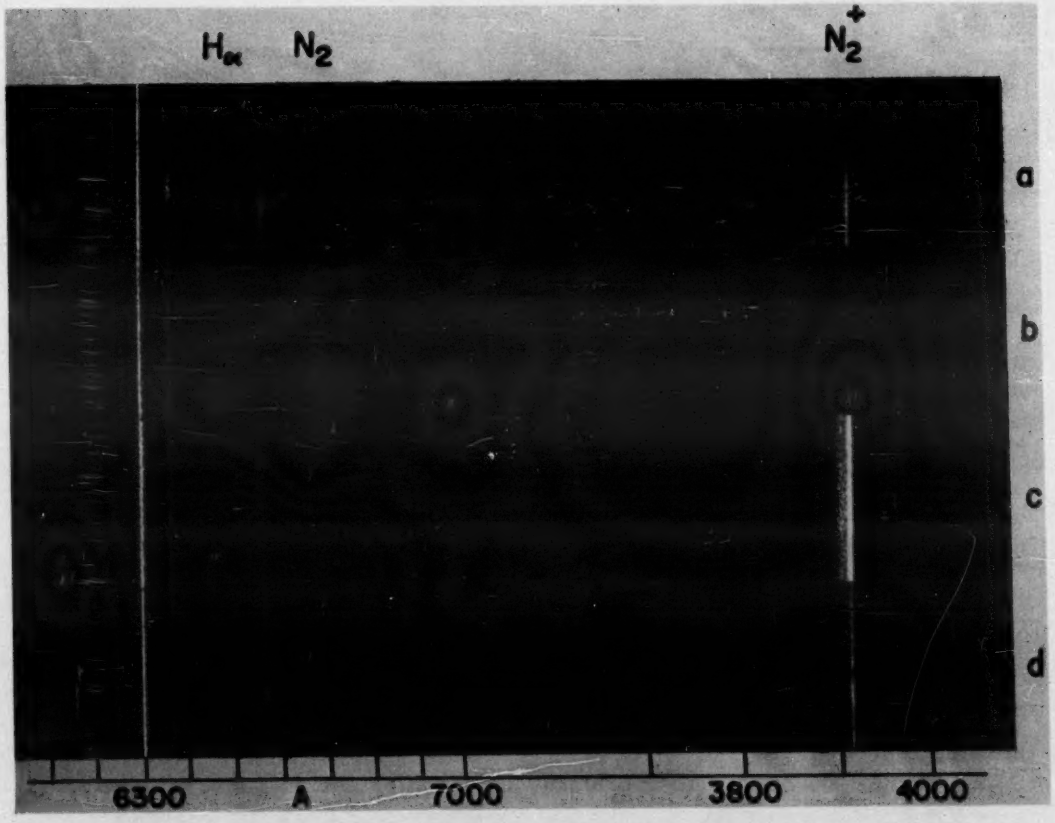

FIG. 1.—The *Hα* region of the auroral spectrum. *a*, *b*, and *d* from magnetic horizon; *c* from magnetic zenith

make the first positive bands between 6580 A and 6680 A of equal intensity. Since each spectrum plate had been pre-exposed to a moderate density, the ordinates represent intensities closely. The $H\alpha$ profiles were corrected for the presence of the first positive bands by subtracting the curve for the aurora without $H\alpha$. The resultant corrected profiles are shown in Figure 3.

ANALYSIS

The presence of hydrogen Balmer emissions in aurorae has been known for some time. These emissions were first found by Vegard and Störmer. The presence of these emissions, however, was generally overlooked by others. A major step toward the general acceptance of the hydrogen identifications was through the extensive observations of Gartlein,[2] who found that the emissions ascribed to $H\alpha$, $H\beta$, and $H\gamma$ showed the same relative intensities throughout a wide range of intensities. Gartlein suggested that the exceptional broadness of these lines could be ascribed to Doppler broadening due to motion of the atoms scattered into the line of sight. Vegard[3] has obtained observations that support this interpretation. Both Gartlein and Vegard, however, were unable to measure any Doppler shift for the broadened hydrogen lines. Vegard[3] states that $H\beta$ is shifted, indicating a Doppler velocity, although his table of measured wave lengths does not bear out any shift greater than the probable error of the other wave lengths.

The current observations, made with respect to the geomagnetic co-ordinates, has enabled an unambiguous evaluation of the nature of auroral hydrogen. The profile of $H\alpha$ in the magnetic zenith is very asymmetrical, with the entire line shifted to the violet. The violet wing indicates a velocity of approach of 3300 km/sec at one-tenth the maximum ordinate. The tail may extend as far as 4000 km/sec. The maximum ordinate is displaced 450 km/sec. This velocity profile can be interpreted only as being due to the deceleration of the incident protons by the atmosphere. The profile cannot indicate a real velocity spread of the incident particles because of their simultaneous arrival in the auroral zone. We can therefore state that the velocity of the protons before entering the upper atmosphere is

$$V_H \geq 3300 \text{ km/sec}$$

The nature of the hydrogen lines observed in the vicinity of the magnetic horizon by Gartlein and Vegard was therefore correctly ascertained. Upon entering the atmosphere, the high-velocity stream of protons is scattered by the atmospheric gases, thereby giving appreciable velocity components at right angles to the incident stream.

The high velocity of the incident protons is greater than has been deduced from indirect phenomena. The time delays between sun-spot meridian passage or solar flares and the occurrence of auroral storms indicates velocities in the range of 800–1600 km/sec. It is also greater than the velocities of 1000 km/sec measured by Richardson[4] and by Bruck and Ruttlant[5] from violet-edge absorption in the solar *Ca* II lines. This discrepancy could be explained if the particles traveled on curved trajectories from the sun to the earth or if the particles were accelerated between the equatorial-ring current of Alfven, Martyn, and others and the earth.

The long-standing problem of the penetration of solar corpuscles into the atmosphere appears to be resolved by the current observations. It was long recognized that electrons of energies equivalent to a few thousand kilometers per second would be stopped in the highest layers of the atmosphere. Likewise, even protons of energies near 1000 km/sec

[2] *Trans. Amer. Geophys. Union*, **31**, No. 1, 7, 1950.

[3] *C.R.*, **230**, 1884, 1950.

[4] *Trans. Amer. Geophys. Union*, **25**, 558, 1944.

[5] *M.N.*, **106**, 130, 1946.

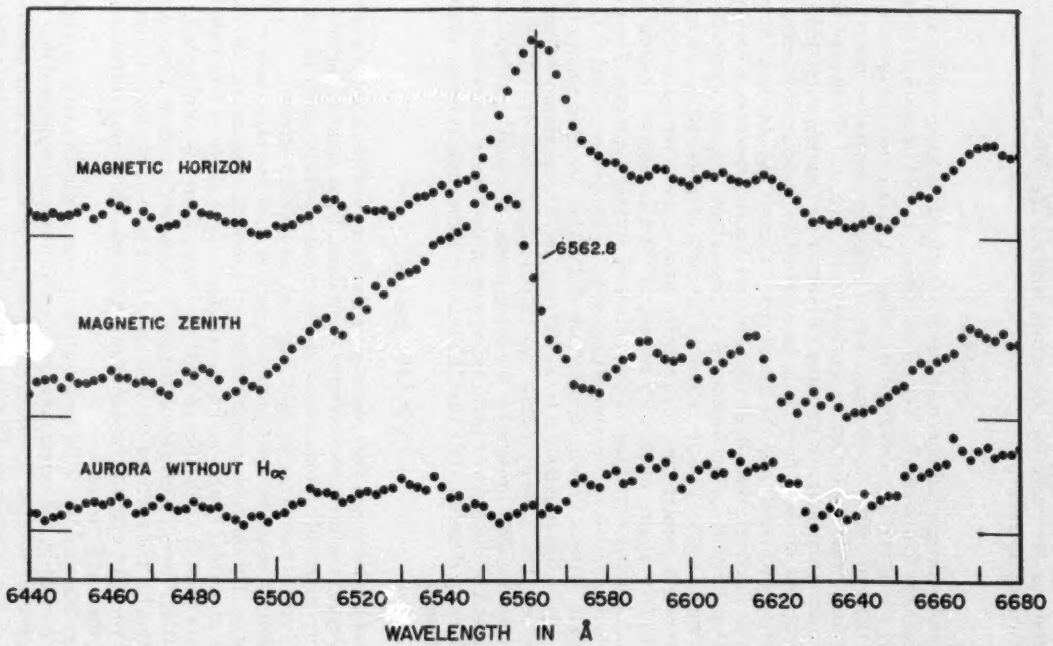

FIG. 2.—A microphotometer tracing of $H\alpha$ in the auroral spectrum. *a*, arch, magnetic horizon; *b*, arch, magnetic zenith; *c*, flames, magnetic horizon.

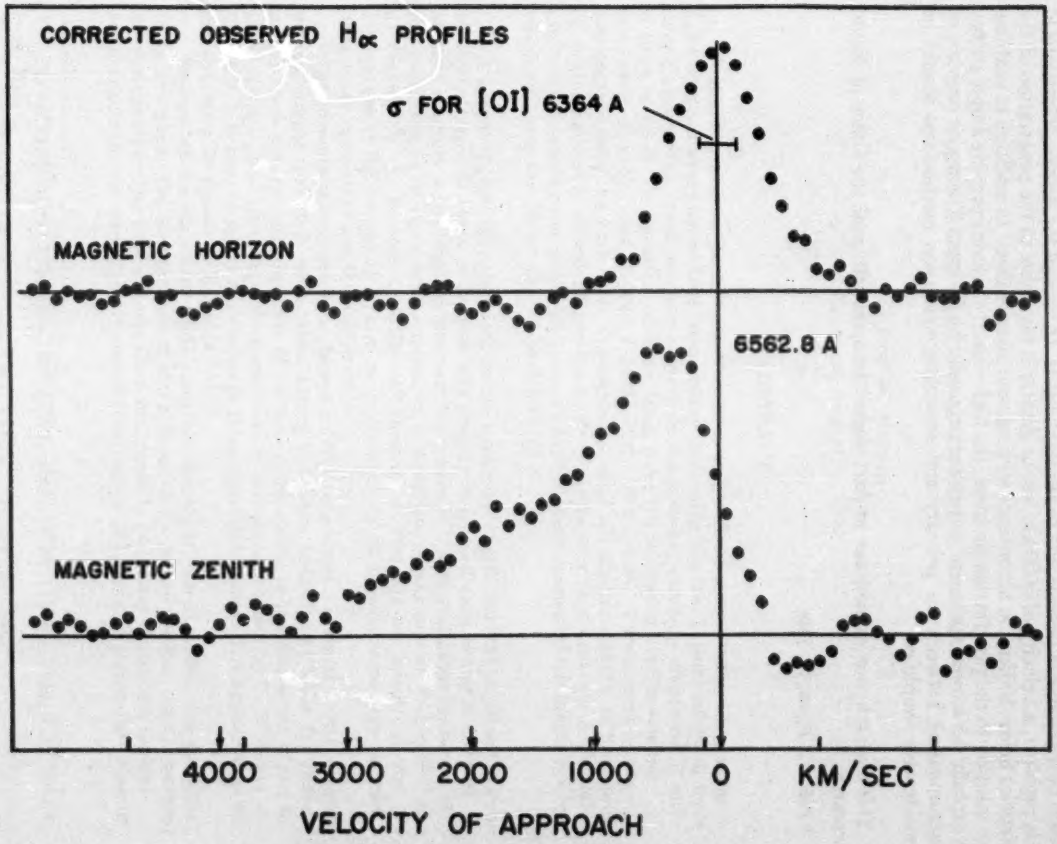

FIG. 3.—Observed *Hα* profiles corrected for first positive bands of N_2

would be incapable of penetrating to auroral heights. In view of the former discussions of this problem, a velocity of 3000 km/sec or greater is favorable to the penetration of the particles below 100 km, in accordance with auroral observations. In addition to enabling the solution to the penetration problem, the high-velocity protons provide ample energy to explain the auroral spectrum, suggested originally by Swings.[6] The major problem of discriminating between the primary and secondary excitation mechanisms should be considerably simplified

This research was carried out in part under the sponsorship of the Office of Naval Research.

[6] *Pub. A.S.P.*, **60**, 18, 1948.

DISPLACED CALCIUM LINES IN THE SPECTRUM OF HD 190073

Paul W. Merrill
Mount Wilson and Palomar Observatories
Received August 1, 1950

ABSTRACT

Numerous narrow dark lines of neutral and ionized metals have been measured with a dispersion of 10 A/mm. Many, including the D1, 2 lines of Na I, have bright edges. The chief interest centers in the intense, strongly displaced H and K lines of Ca II. Components of these lines have the following displacements (km/sec): 0, -147, -181, (-200), (-296), -323, -358, (-396). Three pairs of displacements have the ratio 2:1. The explanation of the displacements on the basis of motions radially outward from the surface of the star is discussed. A formal alternative explanation might lie in some atomic phenomenon which displaces by small amounts the ^2S or the ^2P levels in Ca II.

A bright H_α line was detected in the spectrum of HD 190073[1] at Mount Wilson in 1927. Bright D lines of sodium and greatly displaced dark H and K lines of ionized calcium were found in the next few years.[2] These and other features of the spectrum have since been studied with moderate dispersion at Victoria[3,4] and at Yerkes[5,6,7,8]. In 1946 C. S. Beals[4] obtained at Victoria two spectrograms, dispersion at H_γ 11 and 15 A/mm respectively, which showed numerous narrow dark lines of neutral and ionized metals.

The present investigation is based chiefly on a short series of coudé spectrograms, dispersion 10 A/mm, taken during the years 1943-1950 (Table 1). These plates show a surprising number of narrow components in the displaced H and K lines of Ca II, and like the high-dispersion spectrograms taken by C. S. Beals at Victoria,[4] bring out many narrow dark lines of other metals. The appearance of the spectrum is shown in Figures 1-4.

Except for the displaced Ca II lines and the Mg II line at λ4481, the metallic lines are weak. The undisplaced H and K lines of Ca II are weaker than in normal A-type spectra. The rich narrow-line spectrum is peculiar; it is not a typical shell spectrum but more nearly resembles that of θ Leonis, a sharp-line star of

---

1 BD +5°4393; MWC 325; R.A. $19^h\ 58^m.1$, Dec. +5°28' (1900); mag. 7.9; Spectrum Ape.

2 P. W. Merrill, Mt. W. Contr., No. 461; Ap. J., **77**, 51, 1933.
3 C. S. Beals, Jour. R. A. S. Can., **36**, 145, 201, 1942.
4 C. S. Beals and Miriam S. Burland, Canadian Jour. Research, **A27**, 169, 1949.
5 Swings and Struve, Ap. J., **91**, 546, 1940.
6 Struve and Swings, Ap. J., **96**, 475, 1942.
7 O. Struve, Pub. A. S. P., **54**, 11, 1942.
8 O. Struve, Ap. J., **106**, 358, 1947.

the main sequence classified[9] A4, absolute magnitude +1.0. More than fifty dark lines of Fe I were measured. Other neutral metals identified are Mg I, Al I, Si I, Ca I, V I, Cr I. Lines of the following ionized metals have been measured: Mg II, Si II, Ca II, Sc II, Ti II, V II, Cr II, Fe II, Ni II, Sr II, Ba II. Many of the absorption lines, especially those of Fe II and Ti II, have emission edges of greater or less intensity (probably of variable intensity). The range of intensities of the dark lines, both within multiplets and from one multiplet to another, seems abnormally low. Possibly emission tends to equalize the observed intensities. In fact, in some lines the dark core is scarcely visible and the line then appears as a slightly widened emission line. This is especially true in the ultraviolet where Struve has recorded many such lines.[7] The following lines in the green and yellow are bright: Na I λλ5890, 5896; Fe II λλ4923, 5018, 5169, 5197, 5234, 5276, 5316.

TABLE I

Measured Displacements of Dark Lines
km/sec

PLATE Ce	DATE	Fe I		Fe II		Ti II		MISC.		MEAN	
3281	1943 Nov. 13	-0.8	50*	+0.2	28*	-1.1	27*	-0.9	41*	-0.6	146*
3497	1944 July 8	-1.4	52	-1.4	25	-1.2	31	-1.2	40	-1.3	148
4322	1946 July 13	-1.1	34	-1.1	22	+0.3	25	-1.2	32	-0.8	113
4423	1946 Sept. 15	-1.4	38	-0.2	18	-1.0	23	-1.2	25	-1.0	104
4733	1947 June 30	-0.6	28	-0.9	18	-0.3	22	0.0	24	-0.4	92
5315	1948 Sept. 12	-0.7	31	-0.3	57	0.0	18	-0.6	22	-0.4	128
5683	1949 June 12	0.0	53	+0.8	24	-0.3	26	-0.5	39	0.0	142
6235	1950 May 23	-0.2	12	-0.4	2	-0.4	4	-1.0	14	-0.6	32
Mean		-0.81		-0.42		-0.54		-0.82		-0.66	

* Number of lines.

The bright sodium lines, D1 and D2, like many other metallic lines, have nearly central minima (Fig. 5). In the D lines it is possible that weak interstellar lines may be involved. Of the two emission components in each line, the longward is the stronger, that of D2 rising about 35 per cent above the continuous spectrum. The profiles given by Beals and Burland[3], based on plates with 34 A/mm, appear to be consistent with my results, indicating that no large changes in structure have occurred.

The measured displacements of the metallic lines, including λ4481 of Mg II, are in good agreement (Table 1). The lines of Fe II and Ti II may have very small positive displacements (about 0.005A), with respect to other lines. No dependence on excitation potential is in evidence. The mean velocity is nearly the same on all plates and agrees with earlier determinations by Merrill and by Struve. Hence it appears that the radial velocity of the star as a whole has been constant since 1928. This means that if a close companion exists, the plane of the orbit must be nearly at right angles to the line of sight; hence currents of gas with velocities having large components in the line of sight would not be expected.

9 Adams, Joy, Humason, and Brayton, Mt. W. Contr., No. 511; Ap. J., 81, 187, 1935.

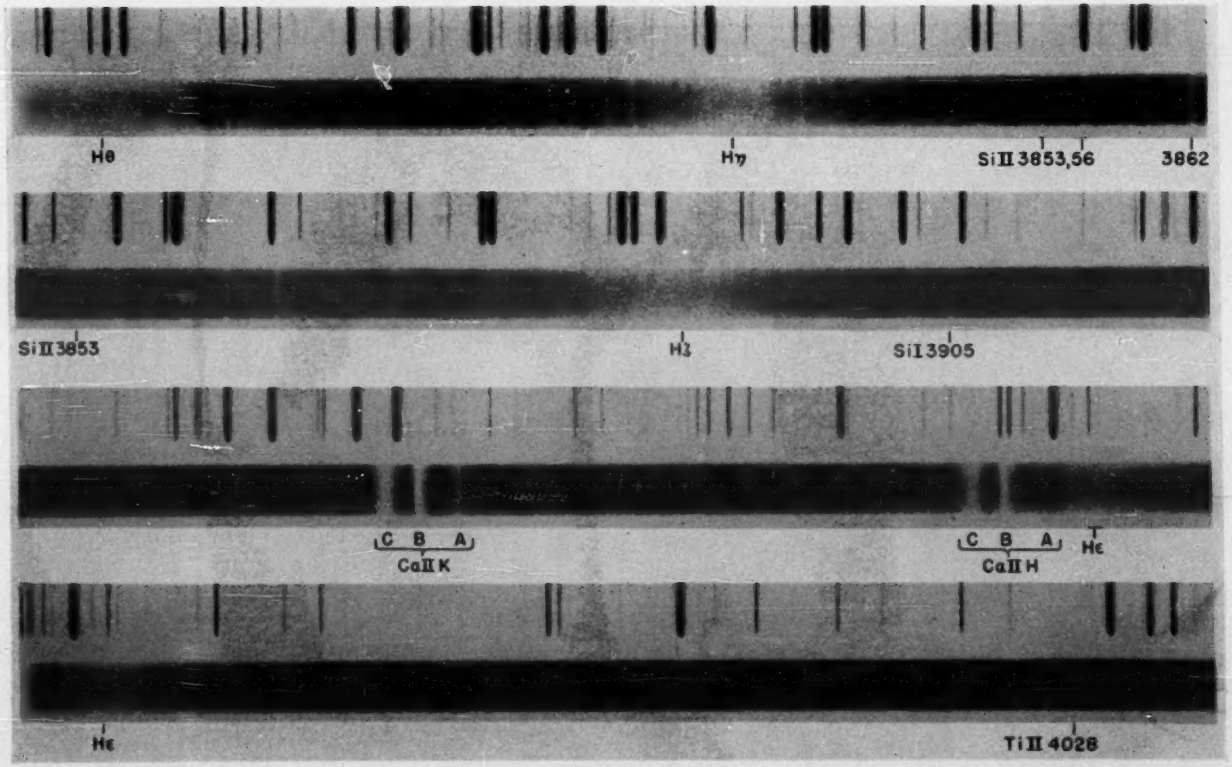

FIG. 1.—The spectrum of HD 190073, Ce 4423; λ3800–λ4030

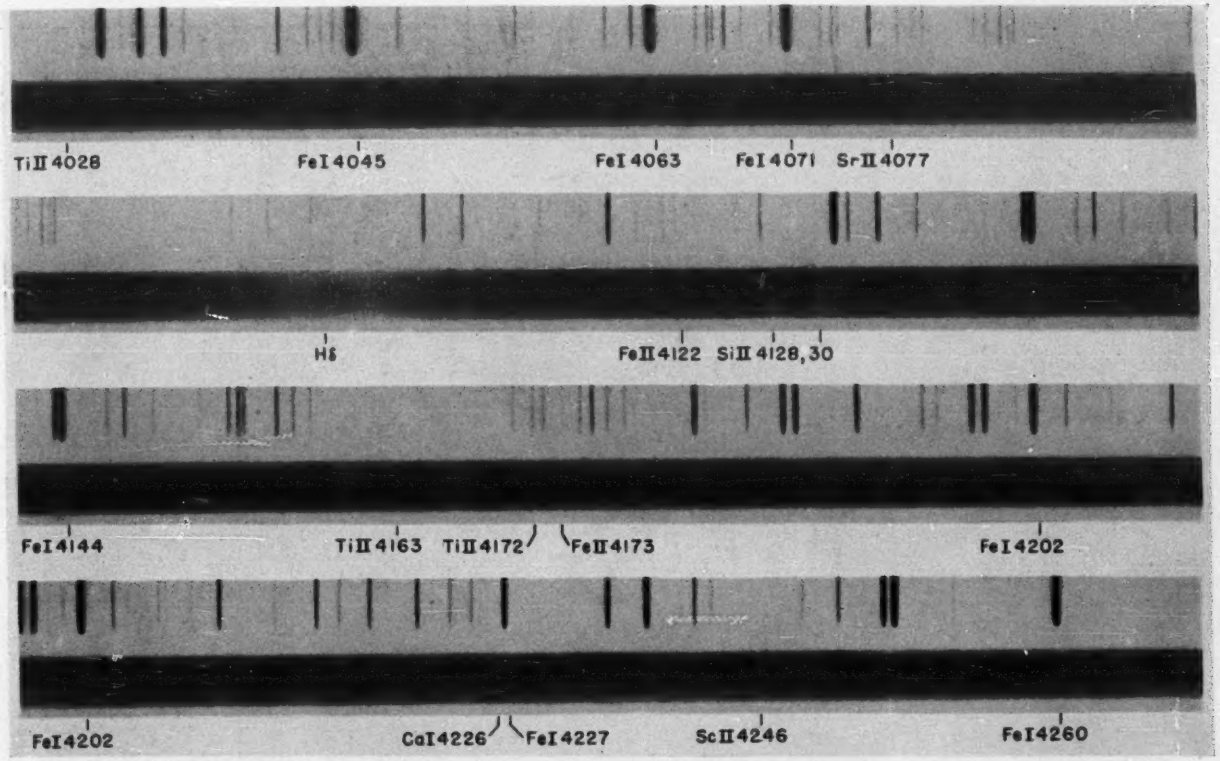

FIG. 2.—The spectrum of HD 190073, Ce 4423; λ4030–λ4260

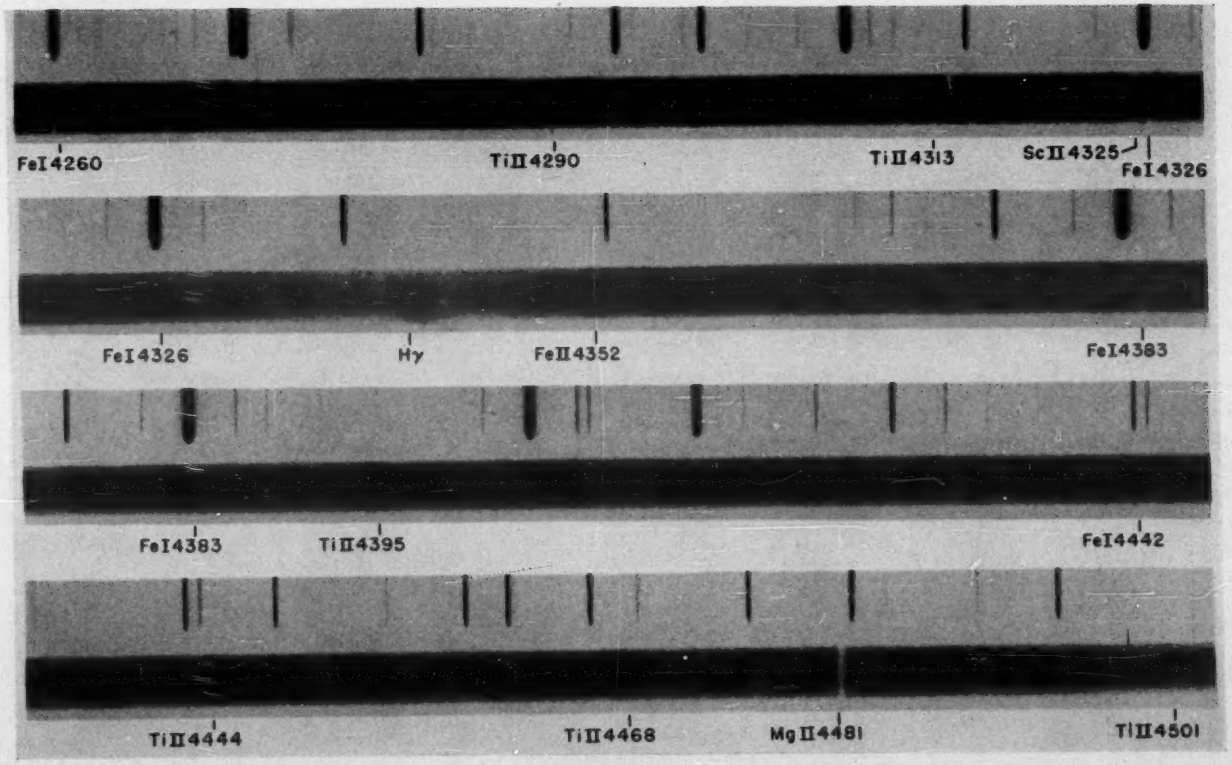

FIG. 3.—The spectrum of HD 190073, Ce 4423; λ4260–λ4500

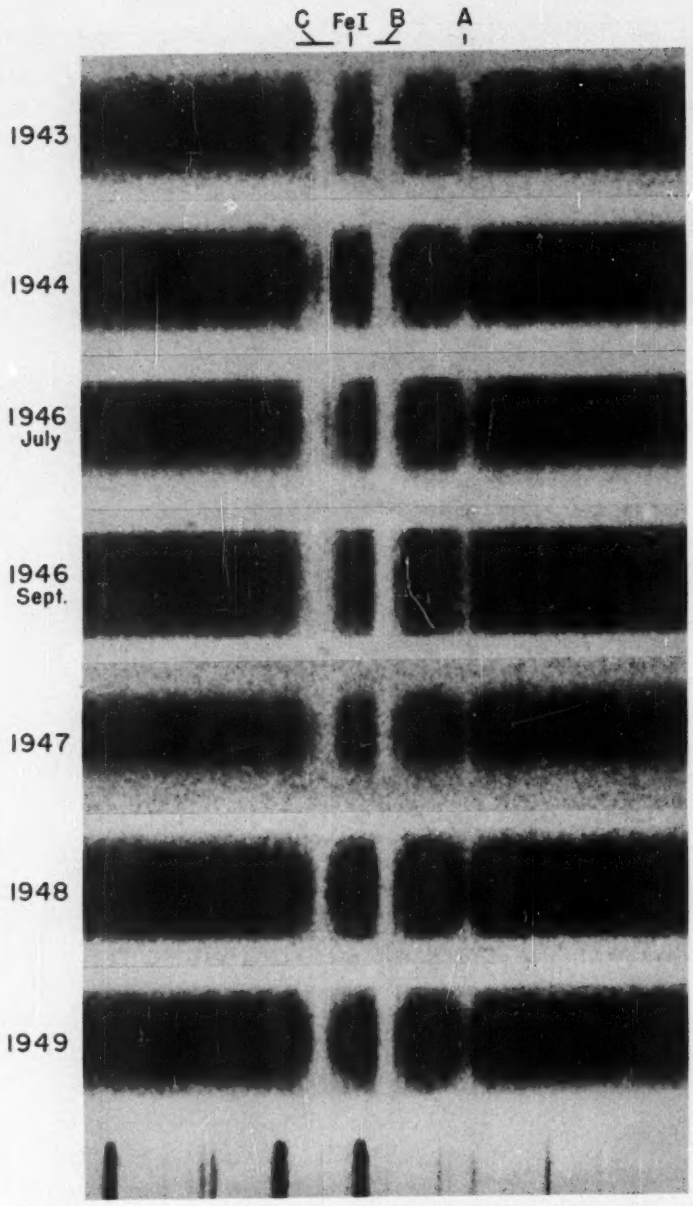

FIG. 4.—The K line of *Ca* II on various plates of HD 190073

With the dispersion of the recent Mount Wilson spectrograms, the H and K lines of ionized calcium reveal an intricate structure with five to eight components, some of which change in intensity and sharpness from year to year (see Fig. 4). The components thus far observed fall into three groups: A, the undisplaced line; B, lines with displacements between 150 and 200 km/sec; C, lines with displacements between 300 and 400 km/sec. The measured displacements of individual components are recorded in Table 2.

The undisplaced line is of moderate intensity. On several plates its appearance is that of a very sharp core with narrow wings. This effect might possibly be caused by the superposition of a weak interstellar component on a slightly broadened stellar line; but the galactic latitude, -14°, and the absence or low intensity of the interstellar sodium lines indicate that the contribution of the interstellar calcium component must be small. The over-all displacement of the Ca II lines is -0.1 km/sec, differing but slightly from the radial velocity of the star, -0.7 km/sec.

The displaced calcium lines are intense and present a most extraordinary appearance (see Figures 1, 4, and 6). Some of the components are very narrow, others are wide with rectangular profiles. With a few apparent exceptions, the

Fig. 5.—Photometric tracing of the sodium lines. The scale of the original negative was 15 A/mm. Ce 6239.

wider components have steep edges like interstellar or circumstellar lines, suggesting that they are actually composed of several narrow subcomponents. The great sharpness of many of the individual components is an important fact to bear in mind in seeking a physical interpretation.

Component B1 is very sharp indeed; it runs throughout the whole series practically without change. The whole general pattern is, in fact, quite persistent; but numerous small changes do occur in the widths and intensities of the subcomponents, especially in group C. Component B3 is strong and wide; on the first two coudé plates a weaker component B4 is seen barely separated from it. A most remarkable fact is that each component of group B has in Group C a corresponding component with twice the displacement. This does not mean that C is the duplicate of B with twice the scale. There are decided differences in structure; for example, the B group does not show a component corresponding to C2.

In novae and in stars of the P Cygni type a displaced absorption line lies at the shortward edge of an emission line whose center is in a position corresponding to the radial velocity of the star as a whole. The displacement of the dark line is ascribed to the motions of atoms radially outward from the surface of the star; and circumstances offer abundant proof of this interpretation.

The same interpretation has been applied to the displaced dark lines in shell spectra. These lines are occasionally multiple; they usually change in position or intensity in intervals of weeks or months; they may or may not be accompanied by emission; there is sometimes evidence of acceleration as the atoms move outward.

The application of this hypothesis to the strong, complex, and nearly fixed pattern of components exhibited by the H and K lines of HD 190073 raises difficult questions. Why should such violent and discrete motions persist for many years in the upper atmosphere of a star? Circumstances seem to rule out a set of expanding shells; the distance traversed would be too great. In 20 years several of

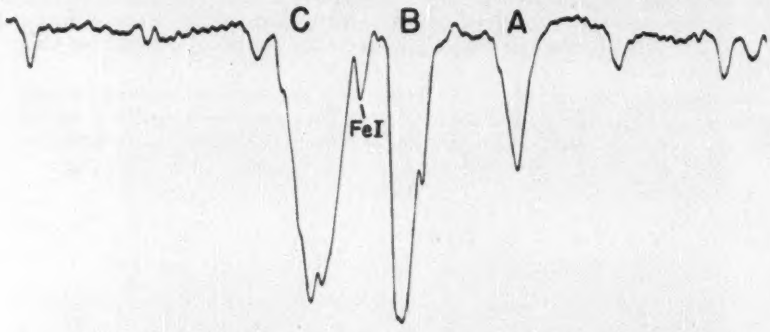

Fig. 6.—Photometric tracing of the K Line of Ca II. Ce 4423.

the fastest shells would have moved outward more than 1000 astronomical units, a distance which is very large compared to the probable radii of the initial shells. In a given expanding shell the number of atoms per square centimeter in the cone joining the observer to the star varies inversely as the square of the radius. Hence the lines should weaken rapidly as the radius of the shell increases, but the displaced Ca II lines in the spectrum of HD 190073 have not changed radically in more than 20 years. Placing the origin of the lines in detached interstellar clouds having high translational velocities would not seem to offer a satisfactory physical solution. We must rather consider a succession of atoms passing upward from the photosphere through fixed or nearly fixed circumstellar zones in which the observed lines are produced; in outer regions under different physical conditions the atoms are lost to us because they cannot produce observable spectral lines. But why should outward accelerations lead to numerous discrete and narrow ranges of velocity? Why are the lines so strong? Why should the motions be limited to atoms of ionized calcium?[10] Why should the ratio 2:1 occur?

A formal alternative explanation might lie in an atomic phenomenon which displaces by small amounts (a few thousandths of an electron volt) the ^2S and/or the ^2P levels of Ca II. High metastable levels in Ca I or very loose bindings of Ca II ions with other particles might be mentioned but I am not aware that either

10 It is barely possible that at times some hydrogen atoms have velocities comparable to those of the ionized calcium atoms. But the profiles of the hydrogen lines lack sharp detail and are decidedly variable; significant correspondence to the Ca II profiles is not very obvious.

circumstance is plausible. If the displacements are caused by an atomic phenomenon of this general sort, we might expect $\Delta\lambda$ to vary with λ^2 instead of with λ as in displacements caused by radial velocity. The measured ratio of $\Delta\lambda$ for H to that for K does indeed appear to be nearer to $(\lambda_H/\lambda_K)^2$, 1.02, than to λ_H/λ_K, 1.01, but the accuracy of measurement, especially of the weaker H line within the wing of H_ϵ, is not sufficient for a definite conclusion. Because some of the components are sharp, considerably higher dispersion might settle the question. No other observed lines have shown the displaced components. If the infrared lines Ca II ^2D - ^2P, $\lambda\lambda$8498, 8542, and 8662 have them, suitable spectrograms with moderate dispersion would be of great interest, but the wide Paschen lines of hydrogen might make the exposures unduly long.

Probably most astronomers would agree with Beals[3] 'that the most promising line of approach to the problem of these complex line profiles is to be found in a study of the forces responsible for the radial motions of atoms ejected from the star.'

TABLE 2

Displacements of Calcium Lines
km/sec

PLATE	YEAR	A	GROUP B			GROUP C			
		NORMAL	1	3	4	1	2	3	4
V 205	1932	(-6)	----	(-175)	----	----	(-323)	----	----
1979	1937	-3	----	-177	----	----	-317	----	----
C 7690	1941	+3	----	-181	----	----	-321	----	----
Ce 3281	1943	-2	-148	-177	-203	----	-320	----	(-420)
3497	1944	-1	-148	-176	-196	----	-313	-354	----
4322	1946	+1	-147	-183	----	-294	-331	-356	-387
4423	1946	+1	-148	-183	----	----	-328*	----	-390
4733	1947	0	-146	-183	----	(-310)	----	-354	----
5315	1948	0	-145	-181	----	(-302)	-326	-364	-407
5683	1949	0	-146	-182	----	-297	-331	-363	?
5821†	1949	+1	-145	-181	----	-293	-325	-356	----
6235	1950	-1	-149	-182	----	----	-326	-358	----
Mean (km/sec)		-0.1	-147.0	-181.0	(-200)	(-296)	-323	-358	(-396)
$\Delta\lambda$ (A)		0.00	-1.93	-2.39	-2.63	-3.90	-4.25	-4.71	-5.21
$\Delta\nu$ (Wave No.)		0.0	+12.4	+15.2	+16.8	+25.0	+27.2	+30.2	+33.4
ΔE (10^{-3}volts)		0.00	1.54	1.88	2.08	3.10	3.37	3.74	4.14

* May consist of three blended components having about the same displacements as those on the preceding plate.

† This plate was taken on August 6, 1949 by H. W. Babcock to whom I am indebted for the privilege of using it. The spectrum closely resembles that on the preceding plate taken two months earlier.

THE SPECTRA OF VARIABLES OF THE RV TAURI AND YELLOW SEMIREGULAR TYPES

L. ROSINO
Yerkes Observatory
Received July 16, 1950

ABSTRACT

Spectrograms of low dispersion and photometric observations have been obtained for a number of variables of the RV Tauri and yellow semiregular types. A revised list of members of the RV Tauri class is given, together with a preliminary description of certain spectroscopic similarities of the members of the class. A division of the RV Tauri stars into two groups is suggested. A period-luminosity relationship is found for some kinds of variable stars located in globular clusters. Attention is called to the remarkable spectroscopic variations of AC Her. The latter appears to be related to the carbon stars.

In the past, many investigations have been carried out to determine certain general characteristics of the spectra of variable stars from which it might be possible to enable an experienced observer to identify an intrinsic variable from a few scattered spectrograms alone.[1]

Particularly interesting, from this point of view, are the so-called "semiregular" variables of intermediate period; these stars lie between the classical cepheids and the Mira-type stars. Classification from predominantly photometric data has not been completely successful up to now because the periods of several physically different groups overlap, while the light-curves are more or less irregular and at times appear completely erratic.

However, if we consider not only the light-curves but also the available spectral types, all these variables can be classified into three distinct groups—the RV Tauri variables; the yellow semiregulars of spectral class F, G, or K; and the red semiregulars of classes M and N. The study of their spectroscopic properties is important because of the possible relationship between these stars and the adjacent groups, the cepheids (either classical or of the type of W Virginis), and the long-period variables. Spectra of the red semiregulars of small amplitude have been recently examined by P. C. Keenan;[2] we shall deal here with the RV Tauri variables and yellow semiregulars.

We shall adopt the following criteria for the RV Tauri type of variation: (*a*) Most of the time the variable follows a light-curve, with well-marked alternate deep and shallow minima, which occasionally interchange. (*b*) Irregularities in the light-curve or period, absence of shallow minima, erratic variations, etc., may be present—provided that they are only secondary and transitory characteristics of the general light-curve. (*c*) The mean brightness may be constant, or variable with a long period. (*d*) The mean spectral type is F, G, or K.[3] The last condition is necessary to prevent the inclusion of spurious members of completely different type; some long-period variables of class Me or Ne have light-curves with deep and shallow minima. As a rule, when spectral types are not available, the criterion that the period should not be longer than 150 days can be used.

The members of the RV Tauri class, according to the above definition, are listed in Table 1. There are only twenty-five variables in this table, about twice as many as were given by B. P. Gerasimovič more than twenty years ago. In the *General Catalogue of*

[1] A. H. Joy, *Pub. A.S.P.*, **54**, 15, 1942.

[2] *Ap. J.*, **95**, 461, 1942.

[3] These criteria do not differ substantially from those assumed in *Harvard Ann.*, **113**, 1, 1942, by C. P. Gaposchkin, V. K. Brenton, and S. Gaposchkin.

TABLE 1

VARIABLES OF THE RV TAURI TYPE

VARIABLE	l	b	PERIOD (DAYS)	MAGNITUDE		MEAN AMPL.	SPECTRAL RANGE	OBSERVER	MEAN RADIAL VELOCITY (KM/SEC)	NOTES
				Max.	Min.					
EZ Aql.	7°	+ 5°	38.6	*11.6*	*13.6*	*0.8*	cK0	. . . . .	. . . . .	
RY Ara. . . .	306	− 9	143.5	9.2	12.1	2.9	G–K0	Cannon	. . . . .	1
UY Ara. . . .	299	−15	57.2	11.1	12.2	1.1	G	. . . . .	. . . . .	
TW Cam. . .	116	+ 6	85.6	10.4	11.6	1.2	F8 *Ib*–G8 *Ib*	Rosino	. . . . .	2
RX Cap. . .	358	−25	67.9	11.6	13.7	1.3	. . . . .	. . . . .	. . . . .	
GK Car. . . .	258	+ 3	55.6	12.5	14.0	1.5	. . . . .	. . . . .	. . . . .	
EQ Cas. . . .	82	− 7	58.4	11.9	13.6	1.7	. . . . .	. . . . .	. . . . .	
RU Cen. . . .	263	+17	64.7	8.8	10.3	1.5	G2–K2	Shapley	. . . . .	1
SX Cen. . . .	266	+14	32.8	9.9	12.4	1.5	F5	Cannon	. . . . .	1
CN Cen. . . .	260	+ 1	51.0	12.5	14:	1.5	G4	. . . . .	. . . . .	
DF Cyg. . . .	44	+ 8	49.8	10.8	15.2	1.8	cG7–cK2	Joy	. . . . .	3
V 360 Cyg. . . .	44	−13	70.4	10.8	13.3	2.5	. . . . .	. . . . .	. . . . .	
SS Gem. . . .	156	+ 2	89.3	8.8	10.2	1.4	F8 *Ib*–G5 *Ib*	Rosino	. . . . .	4
SU Gem. . .	153	+ 6	50.1	*9.9*	*12.2*	*1.5*	K0–M3	Cannon	. . . . .	1
AC Her. . . .	17	+13	75.2	7.1	9.4	1.1	F4p *Ib*–Rp	Rosino	−32	5
EP Lyr.	28	+ 6	83.3	10.2	11.6	1.4	. . . . .	. . . . .	. . . . .	
U Mon.	193	+ 5	92.3	6.8	8.2	1.4	F8e *Ib*–K0p *Ib*	Rosino	+35	6
TT Oph. . . .	348	+27	61.1	9.9	11.7	1.4	F5pe	Adams-Joy	. . . . .	
UZ Oph. . . .	356	+22	87.4	10.5	13.1	1.8	F8–K5	Gerasimo-vič	. . . . .	
AR Pup. . . .	222	− 2	75:	8.7	10.9	2.2	Rp	Rosino	. . . . .	
R Sge.	25	−11	70.8	9.0	11.5	1.2	G0 *Ib*–G8 *Ib*	Rosino	+10	7
AI Sco.	322	− 5	71.8	9.4	11.6	. . . .	. . . . .	. . . . .	. . . . .	
R Sct.	356	− 2	144:	6.1	8.6	2.5	G0e *Ia*–K0p *Ib*	Rosino	+40	8
RV Tau. . . .	142	−11	78.6	9.8	13.3	1.3	G2e *Ia*–K3p	Rosino	. . . . .	9
V Vul.	36	−10	76.0	9.0	11.0	1.5	G1 *Ia*–*Ib*—G8 *Ia*–*Ib*	Rosino	−10	10

NOTES TO TABLE 1

1. The spectral types were derived from Harvard plates taken for the *Henry Draper Catalogue*.

2. No spectral types were previously available.

3. Joy (*Pub. A.S.P.*, **44**, 386, 1932) writes: "The spectrum is like that of R Scuti at maximum. The enhanced lines are very strong. Six plates have been obtained. . . . On plates γ 18070 and C 5751 the hydrogen lines are very weak and may be cut down by the presence of incipient emission. No bright lines or titanium bands have been detected."

4. Russell (*Ap. J.*, **66**, 128, 1927) gives the spectral range G1–G8.

5. Sanford (*Ap. J.*, **73**, 364, 1931) found a spectral range F1–K4. He observed striking changes during each period in the G band and in all the absorption features of the spectrum; hydrogen lines were present in absorption at all times, with associated emission during certain phases from principal minimum to maximum. Some peculiarities of this star to which we shall refer later, particularly the *CH* characteristics and the strength of *CN*, have not been noted by Sanford. His spectra with a dispersion of 37 A/mm at $H\gamma$ were obtained mainly for the study of the radial velocities.

6. Sanford (*Ap. J.*, **77**, 120, 1933) observed *TiO* bands and strong hydrogen lines in absorption at the deep minimum and hydrogen lines in emission during increasing light. Spectral range F7–G8.

7. cG7, according to Sanford (*Ap. J.*, **79**, 77, 1934): "G-band most intense at the minima and least intense at the maxima. The absorption at $H\gamma$ shows two maxima near the phases of light minima and two minima with the phases at or slightly preceding the light maxima."

8. McLaughlin, in an extensive study of R Sct based on 303 spectrograms (*Pub. Obs. U. Michigan*, **7**, 57, 1938), found a spectral variation gG0–K0 with marked *TiO* bands at minimum, as strong as in an M4–M5 star. The G band and *Ca* 4227 were weak at maximum and very strong at minimum. During increasing brightness he found hydrogen lines in emission, the intensity of which was associated with the magnitude at the preceding minimum and with the magnitude range.

9. Almost nothing was known about the spectrum of this star. Two Harvard plates gave spectral types K2 and K.

10. Sanford (*Ap. J.*, **79**, 81, 1934) observed *TiO* bands at minimum. Spectral type cG5p.

Variable Stars by Kukarkin and Parenago several other stars are attributed to the RV Tauri class; additional observations are needed, however, before these identifications can be accepted with certainty. Table 1 is incomplete, but we believe that no spurious members have been included.

The first three columns in Table 1 contain the name of the variable and its galactic co-ordinates; the fourth column gives the photometric period, which is defined as the mean interval between two deep minima. If we consider the significant period to be the interval between two successive maxima, as for cepheids and long-period variables, we must take half the values given in the fourth column. The fifth and sixth columns contain the apparent photographic magnitudes at maximum and minimum and the mean photographic amplitudes; the few visual values are given in italics. The amplitude is defined as the mean difference between the magnitude of the variable in a deep minimum and the magnitude in the following maximum. As we have noted, the mean brightness can be variable with an amplitude of several magnitudes, so that the total range does not necessarily coincide with the mean amplitude. The seventh and eighth columns give the adopted spectral range and the observer. The ninth column contains the average radial velocity of the center of mass, according to R. F. Sanford[4] (AC Her, U Mon, R Sge, and V Vul) and to D. B. McLaughlin[5] (R Sct). All the stars examined by these authors show a velocity variation with the same period as the photometric variation, in the sense that, roughly, the velocity-curve seems to be a reflection of the light-curve, shifted so that the radial-velocity maxima generally follow the photometric minima. The observations are scattered, however, and it is difficult at the present time to derive a correlation between the photometric and radial variations. The last column refers to the notes to the table.

There are several variables that, although certainly related to the RV Tauri stars, cannot be included in Table 1 because their light-curves do not fulfil all the imposed conditions. The spectral types are F, G, or K, and the light-curves sometimes show double maxima, but they have too long periods and ill-defined alternations of deep and shallow minima or long intervals of erratic changes of light. Table 2 contains the most regular and important of these stars, previously called "yellow semiregulars." The different columns have the same meaning as in Table 1. The period is now defined as the mean interval between two successive maxima. The mean radial velocities of WY And, AG Aur, UU Her, and SX Her were derived by A. H. Joy,[6] that of SV UMa by Redman.[7] Table 2 is certainly not complete, but we hope that no spurious members have been included.

Spectra of RV Tauri variables and yellow semiregulars have been obtained in the past with various instruments, from objective-prism cameras to spectrographs of high dispersion, and they have been classified with different criteria. The references and short abstracts of the most important papers are given in the notes to Tables 1 and 2. From November, 1949, to July, 1950, we observed as many of the stars in Tables 1 and 2 as possible, with the one-prism spectrograph attached to the 40-inch refractor. This instrument gives a dispersion of 123 A/mm at $H\gamma$. Eastman 103*a*-O plates were used.

In order to obtain the phases at which the spectra were taken, the stars on the program were followed on the Eastman 33 emulsion with the 6-inch UV camera. Photographic magnitudes were then derived through the comparison stars given in *Harvard Ann.*, **113**, 1. The light-curves obtained in this way are, in general, well defined, so that there are no serious uncertainties about the phases of the spectrograms or the run of the light-variation. The spectrograms were compared with Morgan's standard spectra of supergiant stars and in some cases with those of cepheids.

[4] *Ap. J.*, **73**, 364, 1931; **77**, 120, 1933; **79**, 77, 1934.

[5] *Pub. Obs. U. Michigan*, **7**, 57, 1938; *Ap. J.*, **94**, 94, 1941.

[6] *Pub. A.S.P.*, **46**, 51, 1934. [7] *M.N.*, **92**, 116, 1931.

In addition to the Yerkes material, fifteen spectrograms of RV Tauri stars and semiregular variables, taken with the 82-inch reflector of the McDonald Observatory, were made available through the kindness of Dr. W. P. Bidelman. Thirteen of these spectrograms have a dispersion of 76 A/mm at $H\gamma$; two (of R Sct) of 25 A/mm.

In the spectral classification of the RV Tauri variables we have avoided as far as possible the use of the lines of hydrogen and *Ca* 4227, since these, in most cases, are abnormal. The spectral class was assigned mainly from the appearance of the G band, from the ratio λ 4271:violet side of the G band and from a general comparison with the standards. The data pertaining to the individual spectroscopic and photometric observations are given in Table 3. Figures 1 and 2 reproduce some of the light-curves with the spectral types observed at different phases. The spectral ranges derived from the present observations are contained in the seventh column of Tables 1 and 2. The variables of the RV Tauri type observed here have the following characteristics:

a) They are stars of high or very high luminosity (Morgan's class I*b* or I*a*).

b) The maximum excitation and the earliest spectral types are reached halfway

TABLE 2

YELLOW SEMIREGULAR VARIABLES

Variable	l	b	Period (Days)	Magnitude		Mean Ampl.	Spectral Range	Observer	Mean Radial Velocity (Km/Sec)	Notes
				Max.	Min.					
WY And...	79°	−14°	107.2	9.5	10.6	1.1	cG5e	Joy, Rosino	−181	1
AC Aqr.....	18	−34	67.2	11.2	12.0	0.8	F8	.....	.....	2
XY Aqr....	23	−68	72.7	9.4	10.1	0.7	G0	.....	.....	2
SZ Aqr.....	5	−61	108.5	10.1	12.3	2.2	K5e	Cannon	.....	
AG Aur....	135	+17	96.0	10.8	12.4	1.6	G0e I*b*–K0ep	Rosino	+196	3
UY CMa...	192	−13	116:	10.8	12.8	2.0	G4	Becker	.....	
SX Her.....	8	+45	103.2	9.0	11.1	2.1	gG3e–K0p	Joy	+ 20	4
UU Her....	28	+41	72–90	8.5	10.6	2.1	F2 I*b*–cF8	Rosino, Joy	−132	5
TX Oph....	353	+26	138?	9.8	12.1	2.3	G0	.....	.....	2
AZ Sgr.....	330	− 9	113.5	11.2	12.8	1.6	F9	.....	.....	2
SV UMa...	120	+55	75.3	9.0	10.3	1.3	G1 I*b*–K3p I*a*	Rosino, Keenan	−102	6

NOTES TO TABLE 2

1. Joy (*Pub. A.S.P.*, **46**, 51, 1934) gives the spectral class cG6e. His spectrograms show very strong interstellar H and K.

2. The spectral class has been taken from the *General Catalogue of Variable Stars*, by Kukarkin and Parenago.

3. Joy (*Pub. A.S.P.*, **46**, 51, 1934) gives the spectral type cG5e. He found strong interstellar sodium, from which he derived a distance of at least 2000 parsecs.

4. Joy (*Ap. J.*, **75**, 127, 1932) describes the spectral variations of SX Her as derived from twenty-one spectrograms taken at different light-phases. Hydrogen lines in emission were observed on thirteen spectrograms. They were found to reach their greatest strength slightly before maximum and to disappear at the time of minimum, giving place to absorption lines. *TiO* bands were observed at minimum when the spectral class was K0.

5. The variable follows two different periods, which interchange. When the 90-day period is dominant, the light-curve is of the RV Tauri type, with alternating deep and shallow minima; when the period of 72 days prevails, the light-curve presents cepheid-like oscillations, with an amplitude ranging from more than a magnitude to a few tenths of a magnitude. Joy (*Pub. A.S.P.*, **46**, 51, 1934) gives a spectral class of cF8.

6. Keenan (*Ap. J.*, **95**, 463, 1942) writes: "... the line ratios suggest high luminosity, but all lines in the spectrum are so weak that the application of luminosity criteria is uncertain. There is some similarity to the spectra of V Vul and R Sct." Spectrum, K3p I*a*.

TABLE 3

PHOTOMETRIC AND SPECTROSCOPIC OBSERVATIONS

JD 2430000+	m_{pg}	Sp	Notes
		U Monocerotis	
3255.96	.....	F8 I*b*	1
258.84	.....	G0e I*b*	10
264.71	6.8	.....	
266.78	.....	G5 I*b*	1
270.94	.....	G5 I*b*	1
273.83	.....	G8 I*b*	1
278.60	7.3	.....	
279.74	.....	G8 I*b*	2
288.58	7.8	.....	
289.66	.....	K0p I*b*	3, 4
292.58	8.3	.....	
293.75	.....	K0p I*b*	3, 4
301.60	7.2	.....	
309.71	6.7	G0e I*b*	10
322.58	6.9	.....	
323.60	.....	G2 I*b*	1
329.74	6.95	.....	
331.70	.....	G2 I*b*	2
332.65	7.05	.....	
335.57	.....	G2 I*b*	2
337.70	.....	G2 I*b*	2
339.63	7.05	.....	
345.65	.....	G1e I*b*	10
347.75	6.95	.....	
349.74	.....	G0e I*b*	10
354.69	6.8	.....	
359.59	.....	G0?	6
373.57	7.2	G5 I*b*	2
383.58	7.7	.....	
386.58	7.6	.....	
387.58	.....	G8?	
393.58	7.0	G0e I*b*	10
404.60	.....	G0e I*b*	7
		V Vulpeculae	
3256.57	.....	G2–G5	1
385.78	9.6	.....	
409.78	9.8	.....	
417.77	11.2	.....	
421.86	11.3	.....	
422.85	11.2	G8 I*a*–I*b*	8
429.83	11.2	.....	
439.88	8.9	.....	
443.77	9.1	G1 I*a*–I*b*	1
		RV Tauri	
3249.79	.....	G8 I*a*	
263.60	12.0	.....	
264.82	11.9	K3p	8, 9

JD 2430000+	m_{pg}	Sp.	Notes
		RV Tauri (*cont.*)	
3278.55	11.0	.....	
279.56	.....	G2e I*a*	10
280.54	10.9	.....	
287.48	10.7	.....	
288.55	10.8	.....	
289.56	.....	G8 I*a*	10
290.60	11.0	.....	
292.54	11.0	.....	
301.54	11.5	.....	
309.56	11.1	.....	
315.54	10.7	.....	
322.60	10.7	.....	
323.67	.....	G5e	7, 9
329.71	11.4	.....	
332.75	11.5	.....	
339.63	11.9	.....	
343.63	11.9	.....	
347.73	11.9	.....	
354.63	11.5	.....	
359.59	11.5?	G5e	10
		R Scuti	
1999.70	.....	G2 I*a*	1
2445.66	.....	G5 I*a*	1
643.99	.....	K0p	4
650.94	.....	K0p	4
671.92	.....	G0	1
672.96	.....	G0e	10
3347.97	7.2	K0p I*b*	4
385.79	6.1	.....	
389.90	.....	G0 I*a*	1
393.79	.....	G0 I*a*	1
403.78	6.4	.....	
409.81	6.4	.....	
417.79	6.4	.....	
420.82	.....	G2 I*a*	1
429.75	6.6	G5 I*a*–I*b*	1
439.85	6.7	.....	
446.79	.....	G8 I*a*–I*b*	2
448.76	.....	G8?	
458.69	.....	G8p I*a*–I*b*	2, 8
		AG Aurigae	
3251.96	.....	G0e	11
278.65	10.5	.....	
280.87	11.0	G2e	11
288.48	10.8	.....	
292.60	10.8	.....	
301.61	11.2	.....	

TABLE 3—*Continued*

JD 2430000+	m_{pg}	Sp	Notes
		AG Aurigae (*cont.*)	
3308.89	.....	G5–G8	
309.58	11.5	.....	
315.56	11.8	.....	
329.75	12.5	.....	
332.65	12.4	.....	
339.66	12.1	.....	
343.65	12.1	.....	
349.76	.....	K0ep	4, 11
354.66	11.4	.....	
373.66	10.9	G0e I*b*	11
383.62	10.8	.....	
386.60	11.0	.....	
393.65	10.8	G0e I*b*	10
		WY Andromedae	
3251.67	.....	G5e	10
		TW Camelopardalis	
3258.79	.....	F8 I*b*	2
265.69	10.4	.....	
275.58	.....	G0 I*b*	
279.60	10.9	.....	
288.47	10.8	.....	
289.75	.....	F9 I*b*	14
292.57	10.6	.....	
301.58	10.5	.....	
309.60	10.8	.....	
315.56	11.1	.....	
322.61	11.3	.....	
323.75	.....	G5	
329.76	11.7	.....	
332.64	11.6	.....	
335.66	.....	G8 I*b*	14
339.64	11.5	.....	
347.80	10.8	.....	
354.65	10.5	.....	
386.63	10.4	.....	
		SS Geminorum	
3262.78	.....	G0 I*b*	
263.64	8.8	.....	
264.69	8.8	.....	
278.58	9.9	.....	
279.82	.....	G2–G5 I*b*	12, 13
280.54	9.9	.....	
287.49	10.0	.....	
292.56	9.95	.....	

JD 2430000+	m_{pg}	Sp.	Notes
		SS Geminorum (*cont.*)	
3293.67	.....	G5 I*b*	12, 13
301.56	9.15	.....	
309.58	9.4	G2 I*b*	
315.55	9.7	.....	
317.57	.....	G2–G5 I*b*	5
329.72	9.9	.....	
331.71	.....	G2–G5 I*b*	13
332.63	9.9	.....	
335.66	.....	G2–G5 I*b*	13
337.74	.....	G2–G5 I*b*	13
339.63	9.8	.....	
343.62	9.6	.....	
345.61	.....	G0 I*b*	3, 13, 15
347.74	9.3	.....	
349.70	.....	G0 I*b*	3, 15
354.62	9.1	.....	
359.64	9.5	.....	
373.53	10.1	.....	
383.59	10.0	.....	
386.65	9.8	.....	
387.63	.....	F8 I*b*	
393.59	9.2	.....	
		R Sagittae	
3250.57	.....	G0 I*b*	2, 12
385.80	10.7	.....	
409.78	10.4	.....	
417.75	11.1	.....	
420.85	11.4	.....	
421.84	.....	G8 I*b*	
422.85	11.4	.....	
439.86	11.0	.....	
448.85	.....	G5?	6
461.75	.....	G2 I*b*	14
		SV Ursae Majoris	
2660.70	.....	G1 I*b*	1
3288.54	10.6	.....	
292.61	10.4	.....	
301.63	10.5	.....	
308.98	.....	G5?	
309.61	10.5	.....	
347.80	10.5	G2–G5 I*b*	
354.68	10.6	.....	
377.67	10.2	.....	
383.65	10.3	.....	
389.72	10.3	G2 I*b*	
393.60	10.4	.....	

TABLE 3—*Continued*

JD 2430000+	m_{pg}	Sp	Notes
	UU Herculis		
3079	.....	F2 I*b*	
329.77	9.5	.....	
347.87	9.3	F5 I*b*	3, 13
354.74	9.2	.....	
361.78	.....	F2 I–II	
365.80	9.1	.....	
373.74	9.1	F2 I–II	
377.78	9.2	F2 I–II	
385.69	9.3	.....	
387.70	.....	F2 I–II	
393.65	9.4	.....	
403.76	9.4	.....	
404.66	.....	F2–F5	13
409.71	9.4	.....	
417.71	9.3	.....	
429.82	9.5	.....	
438.84	8.8	.....	
443.63	.....	F2 I*b*	
	AC Herculis		
3347.94	8.1	Rp (G2)	16, 13, 17
365.81	8.4	.....	

JD 2430000+	m_{pg}	Sp.	Notes
	AC Herculis (*cont.*)		
3373.78	8.3	.....	
377.80	8.4	.....	
378.86	.....	Rp (G5)	3, 13, 17
385.70	8.5	.....	
387.74	.....	Rp (G8)	9, 13, 17
389.79	.....	Rp (G8)	9, 13, 17
393.75	9.0	Rp (K0)	9, 13, 17
403.72	9.1	.....	
417.72	8.2	.....	
420.85	.....	Rp (G2)	3, 13, 17
421.81	8.1	.....	
429.80	8.5	Rp (G5)	3, 13, 17
439.85	8.7	.....	
443.70	8.4	F4p	3, 15
446.83	8.4	F4p	3, 15
448.79	8.4	G0p	3, 15
458.64	.....	Rp (G2)	9, 13, 17
461.65	.....	Rp (G5)	9, 13, 17
	AR Puppis		
3274.42	.....	Rp	18

NOTES TO TABLE 3

1. Hydrogen lines weakened by emission.
2. Hydrogen lines slightly weakened.
3. Veiled.
4. *TiO* bands.
5. The spectrum is overexposed.
6. The spectrum is weak.
7. Hydrogen lines greatly weakened or in faint emission.
8. Incipient *TiO* bands.
9. Strong *CN*.
10. Hydrogen lines in emission
11. Hydrogen lines strong in emission.
12. *Ca* 4226 weak.
13. Hydrogen lines abnormally strong.
14. Hydrogen lines slightly enhanced.
15. Hydrogen lines broadened.
16. *CH* star. The spectral peculiarities are described in the text. Equivalent spectral types are given in parentheses.
17. Strong *CH*.
18. *CH* star? Strong G band, neutral lines greatly weakened, very strong λ 4325.

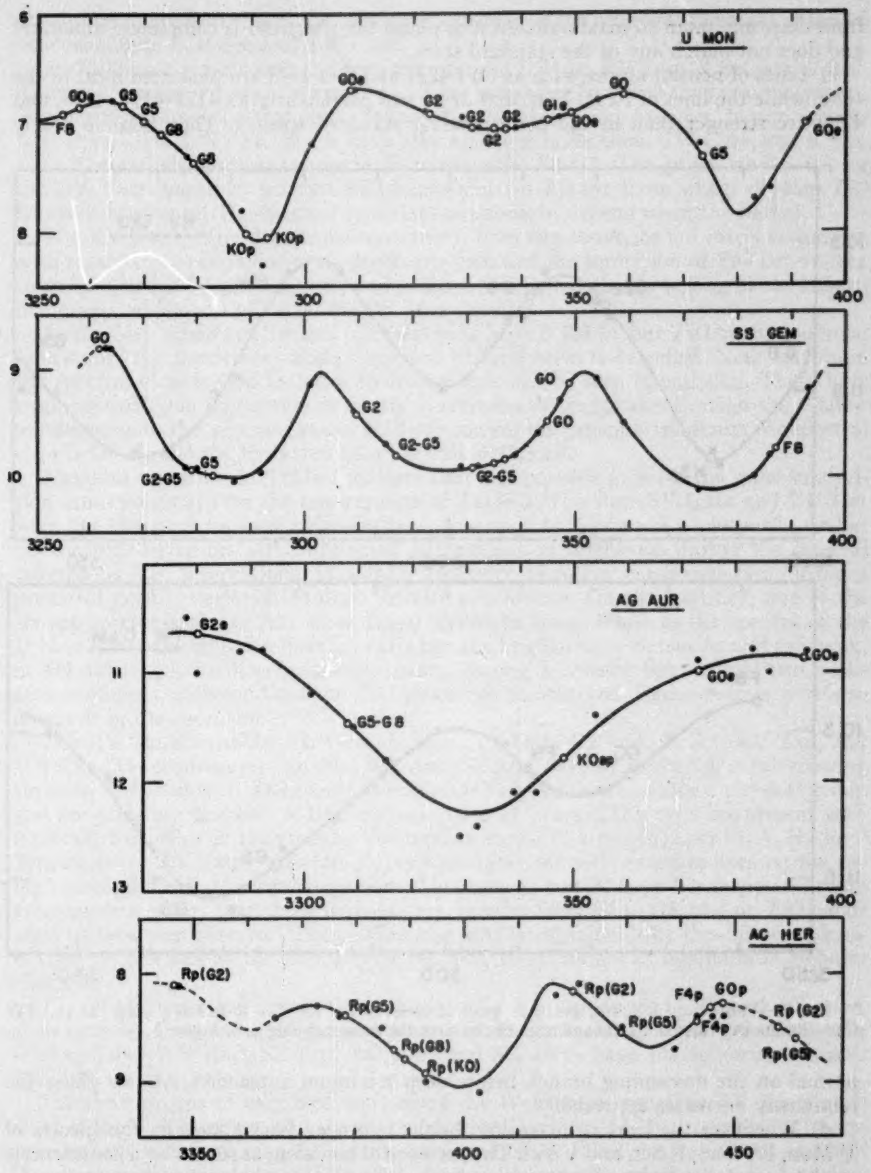

FIG. 1.—Photographic light-curves and spectral variations of U Mon, SS Gem, AG Aur, and AC Her. The dots indicate the observed magnitudes, and the open circles the phases of the spectrograms. Equivalent spectral types are given in brackets for AC Her.

from deep minimum to maximum. At this phase the spectrum is completely abnormal and does not match any of the standard stars.

c) Lines of neutral atoms, such as *Ca* I 4227 and *Fe* I 4143 are weakened most of the time, while the lines of *Fe* II, *Ti* II, and *Sr* II, and particularly λλ 4171–4178, 4215, and 4290 are stronger than in the corresponding standard spectra. They become nearly

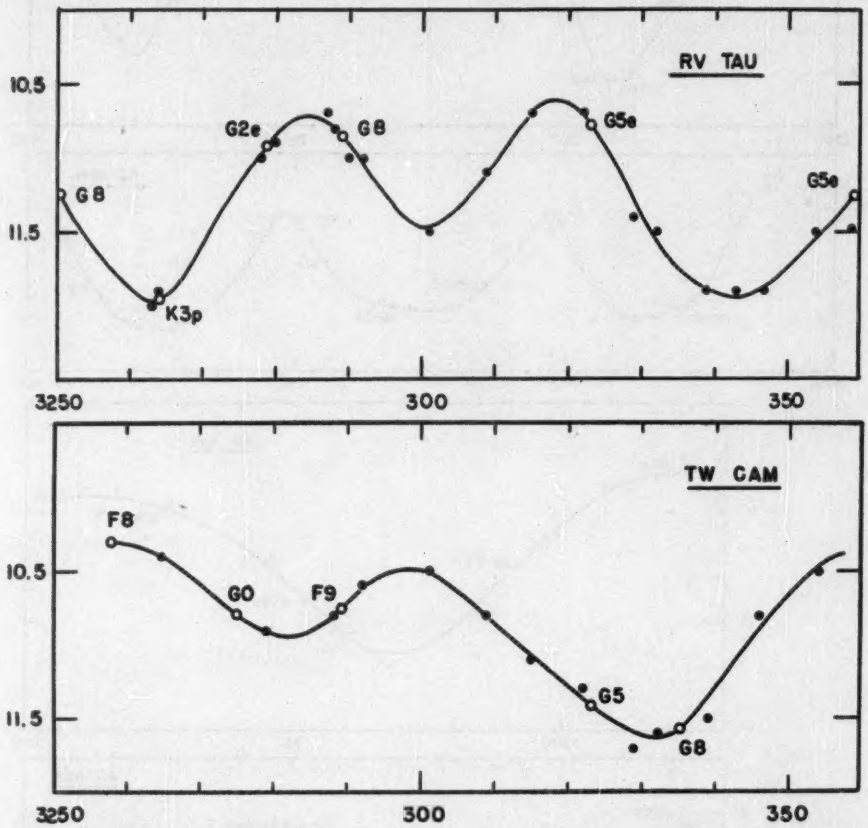

FIG. 2.—Photographic light-curves and spectral variations of RV Tau (luminosity class I*a*) and TW Cam (luminosity class I*b*). Dots and open circles have the same meaning as in Figure 1.

normal on the descending branch before deep minimum is reached. At this phase the luminosity decreases appreciably.

d) Whenever the light is increasing, bright hydrogen lines appear in the spectra of U Mon, RV Tau, R Sct, and V Vul. The presence of emission, as shown by a considerable weakening of the hydrogen absorption lines, is in evidence also for a time during decreasing brightness and disappears only for the few days preceding deep minimum. The stars SS Gem, TW Cam, and R Sge do not show emission on our low dispersion plates; on the contrary, the hydrogen lines are considerably strengthened. They become broad and hazy during increasing light, and faint emission may be associated with the strong

absorption features at this phase. A slight weakening of the hydrogen lines was observed near maximum in R Sge and TW Cam.

e) *TiO* bands appear near the deep minimum in U Mon, RV Tau, R Sct, and V Vul. There is a tendency toward stronger and more persisting bands as the period increases. The corresponding spectral class, defined by the absorption features, is not usually later than K0–K3. No *TiO* bands have been observed in SS Gem, TW Cam, and R Sge.

f) The earliest spectral types are, in most cases, F8–G1. The latest are G5–G8 for the RV Tauri variables without *TiO* bands and G8–K3 for those which develop *TiO* bands at minimum. The spectral type does not seem to depend upon the period.

The RV Tauri variables can be considered, from the above, to fall into two groups, with regard to the behavior of the hydrogen lines and the formation of *TiO* bands. The stars SU Gem, TT Oph, UZ Oph, and perhaps DF Cyg probably belong to the bright-line group, which will be called the "U Mon group."

At the deep minimum the spectral class of U Mon is K0 I*b*, but *TiO* bands as strong as in an M3 star are present, and all spectral features seem to be veiled. Near maximum the spectral class is G0e I*b;* weak hydrogen lines can be seen in emission. These lines reappear weakly in absorption or faintly in emission during phases through the shallow minimum up to the next maximum. Halfway toward the principal minimum the spectral class is G5 I*b*, and the hydrogen lines are still weakened.

The data contained in Table 3 indicate that it is possible to make the same subdivision into two groups for the semiregulars of Table 2. The stars SV UMa and UU Her were not observed to show emission lines; however, both were in a phase of peculiar photometric variation with only small fluctuations in brightness during the interval covered by our observations. It will be necessary to follow these variables during a period of normal variation to draw definite conclusions. On the contrary, five of the six spectrograms of AG Aur show bright hydrogen lines. While in the spectra of the U Mon group the emission lines appear when the brightness is increasing and are weak, in AG Aur they are still very strongly present during decreasing light. About two weeks after minimum, emission lines and *TiO* bands can be observed. Emission lines were also observed in the spectrum of WY And.

The RV Tauri variables SU Gem, U Mon, TT Oph, UZ Oph, R Sct, RV Tau, and V Vul and the semiregular variables WY And, SZ Aqr, AG Aur, and SX Her (all showing emission lines and with *TiO* bands at minimum) appear to constitute a physical group and are probably members of Baade's population II. Stars of this type are present with a certain frequency in the globular clusters, as shown in a recent paper by A. H. Joy.[8] There are five RV Tauri variables in Joy's group 4—all with emission lines on the rising branch and with photometric periods of between 51 and 90 days. Their spectral types are, however, earlier than those derived here, ranging from F4 to G5, and no *TiO* bands seem to have been observed. These differences may be explainable by the different classification criteria and by the difficulty of reaching the variables at minimum in globular clusters.

Two of the semiregular variables in Joy's group 5, with periods of 103 and 106 days, show emission lines and *TiO* bands at minimum. It is interesting to note that the four semiregulars—WY And, SZ Aqr, AG Aur, and SX Her—have the following periods: 107, 108, 96, and 103 days.

The three groups of variables, comprising the W Virginis stars, the RV Tauri variables of the U Mon group, and the yellow semiregulars like AG Aur, constitute a homogeneous sequence if we take the significant period of the RV Tauri variables to be half the photometric period given in Table 1. A period-luminosity relation can be found by the use of the absolute median photographic magnitudes of the variables in globular clusters; this is illustrated in Figure 3. The zero point is defined by assuming that the

[8] *Ap. J.*, 110, 2, 1949.

median absolute photographic magnitude of the RR Lyrae variables is zero. The maximum luminosity is reached for periods of 35–40 days (periods of double variation, 70–80 days). This relation seems to be satisfied by the variables of Tables 1 and 2, with the sole exception of R Sct. The variables RV Tau and V Vul, with luminosity class I*a* or I*a*–I*b*, have periods of 38–39 days (photometric periods, 76–78 days), while U Mon with a period of 46 days (double period, 92 days) is only slightly more luminous than I*b*, and the semiregulars, like AG Aur or SX Her, are in the luminosity class I*b* or I–II.

Table 1 contains a very peculiar star, AC Herculis. There is no question about its inclusion in the list of RV Tauri variables, because all the conditions imposed are satisfied by the light-curve and the spectrum at maximum is type F. Its spectral variation, however, is completely peculiar and deserves a detailed description. A few days after maximum the spectrum is characterized by the presence of hydrogen lines as strong and

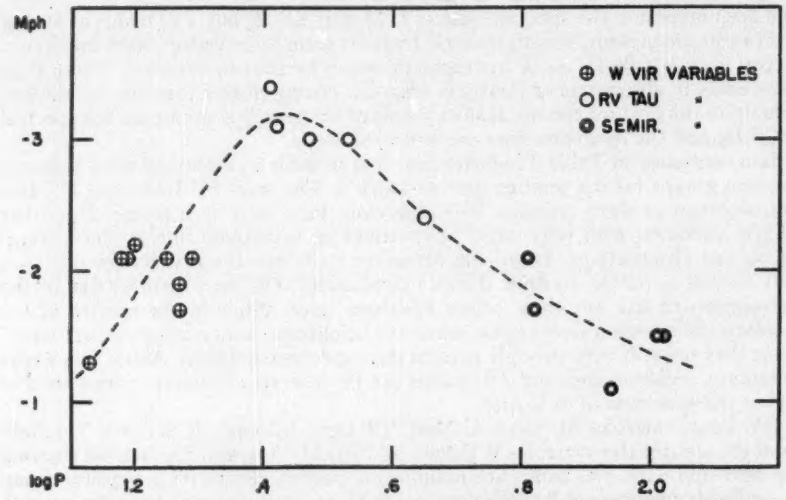

FIG. 3.—The period-luminosity relation for W Vir type, RV Tauri type, and yellow semiregular variables in globular clusters. *Ordinates*, the absolute mean photographic magnitude; *abscissae*, logarithm of the period (in days). Half of the photometric period is plotted for the RV Tauri variables.

sharp in absorption as in an F2–F5 I*b* star. On the other hand, the G band of *CH* is present with an unusually great intensity, as marked and broad as in a late G-type star. All other lines, down to λ 4000, are weakened, with the sole exception of a strong absorption feature at about λ 4325. These peculiarities are accentuated a week later, and, in addition, there appears a very strong *CN* band from λ 4215 toward the violet.[9] The *Ca* 4226 line and all lines of neutral atoms up to λ 4000 are almost obliterated on plates of low dispersion, and *Sr* II 4077 is abnormally weak. The *CN* band becomes still stronger as the brightness approaches the deep minimum, so that it is difficult to obtain the region of the spectrum on the violet side of λ 4215 with sufficient density. The same peculiarities can be observed during the decrease of light toward a shallow minimum, but the *CN* band is less intense. The strength of the *CH* and *CN* bands and the almost complete obliteration of most of the absorption lines indicate that AC Her is a peculiar carbon star. It can be included in that small group of carbon stars which have been

[9] Dr. W. W. Morgan called my attention to the strength of the *CN* and *CH* bands and to the most interesting peculiarities of this variable.

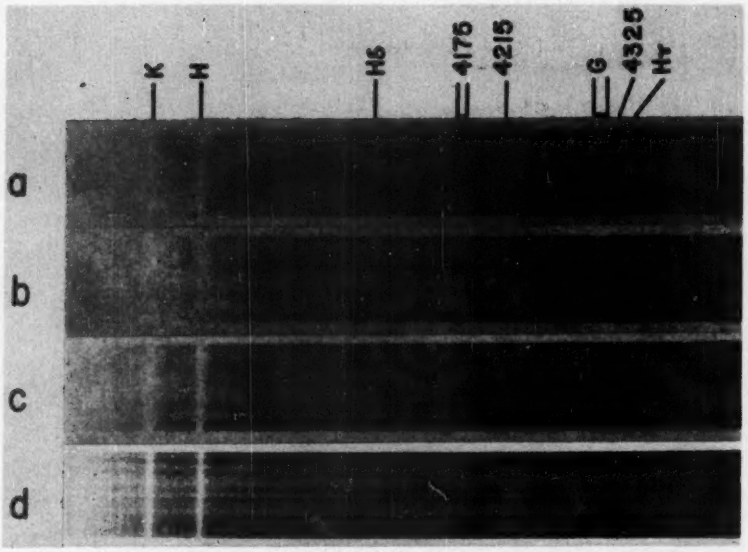

FIG. 4.—Spectrograms of the peculiar carbon variable AC Her. The phases of the spectra are listed below, together with the last three digits of the Julian dates. *a*, 348, near maximum light; *b*, 388, about halfway between maximum and deep minimum on the descending branch; *c*, 430, near a shallow minimum; *d*, 444, on rising branch, between shallow minimum and maximum. Note the remarkable weakening of all lines and the suppression of the G band on the lowest exposure. Spectrogram *b* shows a well-marked absorption of *CN*, together with an exceedingly strong G band.

described by Keenan and Morgan[10] and are called "*CH* stars." As Keenan[11] has pointed out, most of the absorption features in the spectra of *CH* stars coincide with band lines of the *CH* system. In particular, the intensity of the line at λ 4325 is due not to the iron line, which is very faint, but to the narrow and strong band of *CH* at λλ 4323–4324. The spectral types of AC Her in these phases have been described in Table 3 as "Rp." Rough equivalent types have been derived from the general appearance of the spectrum.

The changes in the spectrum of AC Her when the brightness is increasing are striking. A general veiling greatly weakens all lines, while H and K are sharp and abnormally narrow. The G band is weak and discontinuous as in an F2–F5 star, and the hydrogen lines are weak and greatly broadened. The spectrum is therefore completely different from that during decreasing light. The *CH* features and the *CN* band reappear as soon as the brightness starts decreasing. A set of spectrograms of AC Her is reproduced in Figure 4.

In conclusion, I wish to express my deepest gratitude to Dr. W. W. Morgan, who proposed this problem to me, for many helpful suggestions and for his continued and stimulating interest in the course of the investigation.

[10] *Ap. J.*, **94**, 501, 1941. [11] *Ap. J.*, **96**, 101, 1942.

THE SPECTRA OF R ANDROMEDAE (MAXIMUM) AND MU CEPHEI BETWEEN 7400 AND 8800 A*

L. H. ALLER† AND P. C. KEENAN
Indiana University and Perkins Observatory
Received August 17, 1950

ABSTRACT

Spectra of R Andromedae at its 1946 maximum and of μ Cephei have been measured in the photographic infrared region. Wave lengths, identifications, and estimated intensities are given for the atomic absorption lines as well as for a number of band heads of the infrared system of *CN*. The only strong emission features noted in R And at maximum are the lines of *Ca* II at λλ 8498, 8542, and 8662. The intensities of the atomic lines imply that R And is less luminous than μ Cep but is brighter than an ordinary M-type giant.

The atomic lines in the spectrum of R Andromedae (Se) between 3340 and 6832 A have been studied by Merrill,[1, 2] but no description of the line spectrum of an S-type star in the photographic infrared region has been published. The measurements presented here were made on a fairly well-exposed spectrogram of R And taken near its maximum in 1946. This long-period variable is well suited for a comparison of the line spectra of stars of types S and M, since its temperature at maximum is high enough to make the molecular bands relatively weak at this phase.

A good comparison to R And is furnished by μ Cephei (M2 I*a*), which was chosen not only because the bands of *TiO* have about the same strength in the two spectra but also because the S-type stars are known to resemble supergiants in the intensities of many of the enhanced lines in the blue and green regions of their spectra. In addition, μ Cep is of interest in itself as one of the most luminous of the late-type stars. Its spectrum is slightly variable in the intensities of the *TiO* bands, and weak hydrogen emission has been reported by McLaughlin[3] at two of its irregular maxima in light, but no marked changes in the metallic absorption lines have been recorded.

The spectrograms which were measured were taken on Eastman I-N plates (hypersensitized) with the long camera on the Cassegrain grating spectrograph of the Perkins 69-inch reflector. Although the scale of these plates, 25 A/mm, is not comparable to that provided by coudé arrangements, it is adequate for identification and comparisons of the stronger lines in the infrared region. The data of observation are given in Table 1. At the time of observation the visual magnitude of R And was estimated as 6.9, which was about normal for the phase of approximately 20 days past the predicted time of maximum.

Since the radial velocities of both R And and μ Cep are known to vary, it was necessary to use the least-blended lines on the measured spectrograms to derive velocities for the given dates of observation. The velocities found were -14 km/sec for R And and $+18.0$ for μ Cep. These are not far from the published mean values of -11.3 km/sec for R And[1] and $+16.0$ km/sec for μ Cep.[3]

The measured wave lengths, intensities, and identifications of the lines in the two stars are given in Table 2. The scale of intensities is arbitrary but was made consistent for the two stars by direct comparison of the plates. In the column of identifications, the

* *Contributions from the Perkins Observatory*, No. 27.

† Now of the University of Michigan. A research grant from Indiana University made participation in this program possible.

[1] *Ap. J.*, **105**, 360, 1947.

[2] *Ibid.*, **107**, 303, 1948.

[3] *Ap. J.*, **103**, 35, 1946.

multiplet designations (in parentheses) and the laboratory intensities are taken from the *Revised Multiplet Table*[4] wherever possible; where the symbol "*MIT*" appears, the wave lengths and intensities are from the *MIT Wavelength Tables*.[5]

Identification of the lines was aided by Miss Davis' valuable table of lines in the spectrum of the M2–M3 giant β Pegasi.[6] In addition, the study of the infrared solar spectrum by Babcock and Moore[7] facilitated the recognition of the telluric bands of water vapor and the infrared system of *CN* bands. These *CN* bands are much more prominent in late-type spectra than has been generally recognized. Additional Perkins plates show that they remain fairly strong in supergiants to types as late as M3 or M4, and in β Peg they account in part for some of the absorption features left unidentified by Miss Davis or assigned to *TiO*. Among the strongest are the bands at λλ 7872, 7894, 7923, 7933, 7963, 8017, and 8044. They are stronger in μ Cep than in R And but can be easily seen with even moderate dispersion in the spectra of both stars.

TABLE 1

RECORD OF OBSERVATIONS

Star	Plate No.	Date	U.T.	Observer	Exposure (Min.)
R And.....	Gα 1853	1946 Nov. 6	3:10	Keenan	180
μ Cep.....	Gα 1412	1945 Dec. 8	23:05	Decker	30
μ Cep.....	Gα 1413	1945 Dec. 8	23:59	Decker	60

In the spectrum of R And, the only emission lines observed were those of the *Ca* II triplet at λλ 8498, 8542, and 8662. The appearance of these in emission is normal for long-period variables near maximum light, though they seem to be more conspicuous in those of type S than in M-type stars.

Although *Fe* and *Ti* contribute the great majority of the atomic lines observed in the photographic infrared, enough unblended lines from the neutral atoms of nine elements were present to permit the intensity comparisons collected in Table 3.

The lines strengthened in R And all belong to elements of the fifth period, while the lines of the lighter metals are weakened or have about the same intensity as in the M-type star. These features of the infrared spectrum are consistent with those studied by Merrill in the ordinary photographic region. From his comparison lines and bands in R And and R Leonis (M8e) Merrill concluded that "the elements *Y* and *Zr* (atomic numbers 39 and 40) are relatively more abundant in R Andromedae."[1] He further pointed out the correlation of relative abundance in stars of types S and M with position of the elements in the periodic table, in the sense that lines of relatively heavy elements are favored in S-type spectra. The results presented here, together with the strengthening found by one of us[8] for the *LaO* bands in S-type stars, offer further confirmation of these conclusions.

The relative weakening in R And of the *Fe* lines compared to those of *Ti*, *V*, etc., offers a special problem. The weakening is most conspicuously displayed by the strong infrared multiplet (60), $a^5P - z^5D^\circ$, which has an excitation potential of 2.2 volts for its lower levels (see Table 4). These lines are known to be among the most sensitive lumi-

[4] C. E. Moore, *Princeton Contr.*, No. 20, 1945.

[5] G. R. Harrison, *Massachusetts Institute of Technology Wavelength Tables* (1939).

[6] *Ap. J.*, 106, 28, 1947; *Mt. W. Contr.*, No. 733.

[7] *The Solar Spectrum, λ 6600 to λ 13495* (*Carnegie Inst. Pub.*, No. 579, 1947).

[8] P. C. Keenan, *A.J.* (abstr.), 55, 74, 1950.

TABLE 2

WAVELENGTHS AND INTENSITIES

μ Cep		R And			
7323.75	4	e + Atm		23.97	4
7326.57	3	Ca	(44)	26.15	400 + Atm
7344.56	7	Ti	(97)	44.72	4
7351.16	1 n	Fe	(1273)	51.16	2 n
		Fe	(1275)	51.56	4
		Ti	(272)	52.16	1
7356.81	8 w	Cr	(93)	55.94	200
		Ti	(97)	57.74	3
7363.39	7 w	Ti	(97)	64.11	2 + Atm
7366.64	2 s	Ti	(96)	66.60	1
7369.83	2 n	Eu I		69.69	200 ?
		Fe	(1250)	70.16	1 ? + Atm
7382.63	3	Fe	(266)	82.63	p, e
		Fe	(1188)	82.99	1 n
7385.74	2 n	Ni	(84)	85.24	1
		Ni	(286)	86.21	7
		Fe	(1275)	86.39	8 n
7389.96	4 n	Fe	(1077)	89.42	80
		β Peg		90.41	6
7393.66	2	Ni	(109)	93.63	10
7400.42	3	Cr	(93)	00.23	150
		Fe	(204)	00.87	p, e
7406.21	2	Si	(23)	05.85	300
		Y II	(25)	06.23	2
7409.38	2	Si	(23)	09.11	100
		Ni	(139)	09.39	8
7411.17	2	Fe	(1077)	11.18	100
7414.74	3 Bl	Ni	(62)	14.27	3
		Ni	(62)	14.51	2
		Si	(23)	15.37	15
7418.04	3 nn	Co	(89)	17.38	10
		Fe	(1001)	18.67	5
7423.39	5 w	Ni	(139)	22.30	15
		Ti	(97)	23.17	2
		Si	(23)	23.54	500
		Si	(23)	24.63	20
7432.08	5 w	Fe	(1189)	31.94	p
		Ti	(142)	31.98	p
7440.44	2	Ti	(225)	40.60	3
		Fe	(1273)	40.98	2 n
7442.79	1 n	Re		42.75	2 ??
		Fe	(1002)	43.03	2
		Fe	(1309)	43.26	p ?
7445.59	3	Fe	(1077)	45.78	200
		Fe	(107)	45.70	p ?

TABLE 2

WAVELENGTHS AND INTENSITIES (cont'd)

λ Cep		R And		Identification		
7456.70	1 nn			Ti	56.35	p, e
				β Peg	56.59	20
				Co	57.36	200 e ?
7462.03	7			Fe (204)	61.53	1
				Cr (93)	62.37	100
7470.48	2 nn			Ti	70.05	p, e, etc.
7475.00	2 nn			Ti (142)	74.94	p
7479.42	1 n			Zr	79.58	3, etc.
7481.80	1			Fe (266)	81.74	p, e
7483.79	3			La II (1)	83.48	30 ?
7489.45	1 n			Ti (225)	89.61	2
7491.35	2 s			β Peg	91.37	12
				Fe (1077)	91.68	12
7495.22	6			Fe (1077)	95.09	400
				Ti (225)	96.12	2
7506.32	1-			Zr	06.51	2 ?
				Fe (1137)	07.30	8 ?
7511.01	4			Fe (1077)	11.04	800
7518.63	1-			Sm II	18.32	15 ??
7522.94	3-			Ni (126)	22.78	3
7525.24	1			Ni (139)	25.14	3
7531.30	2			Fe (1137)	31.17	60
7540.44	2 n			Fe (266)	40.44	p, e etc.
7546.60	3 n			Fe (unc)	46.18	4
				e ?	46.63	-3 n
				e ?	47.00	-3 nn
7555.15	4 w	55.63 :	1 n :	Zr (23)	54.73	5
				Ni (187)	55.60	5
7562.77	1	↓		Fe (1251)	63.03	1 n ?
7565.27	1			Co	64.96	20
				β Peg	65.37	2 w
7569.23	3	This region underexposed for R And		Fe (1077)	68.93	30
7574.47	4-			Ni (156)	74.08	7
				Co	74.58	100 ??
		↑		β Peg	74.70	-2
7583.92	4			Fe (402)	83.80	50
				Eu	83.91	400 ??
7586.16	3 s			Fe (1137)	86.04	150
7589.85	3 w Bl			Ti0	89.42	25
7664.45	10			K (1)	64.91	10 + Atm O_2
7698.39	6	98.73	5	K (1)	98.98	10

TABLE 2

WAVELENGTHS AND INTENSITIES (cont'd)

μ Cep		R And		Identification		
7714.63	2 n	14.46	1	Ni (62) Ni (109)	14.27 15.63	3 7
7723.29	2 n	23.45	2	Fe (108)	23.20	4
7727.61	1			Ni (156)	27.66	10
7743.04	1 n			Fe (1306) TiO Co (183)	42.71 43.06 43.27	4 n 15 5 ?
7748.54	4 n	49.53	3 nn	Fe (402) Ni (156) TiO	48.28 48.93 49.2	125 10 15
7767.63	1 n	66.64	1 nn	Fe (957)	66.72	p, e ?
7773.29	1	72.98	2	TiO e Rh I	73.3 72.68 72.90	10 -3 100 ? MIT
7780.70	2- n	80.40	0 n	Fe (1154)	80.59	300
7789.14	3	89.04	1	Ni (62)	88.95	2
7797.53	1	Obs.	0	Ni (201)	97.62	3
7799.99	0	99.21	4	Si (81) Rb (1)	7800.00 00.23	4 n 10
7808.33	2 w	?		Fe (1303) Fe Unc	07.97 08.04	p, e 6 n
7811.09	1 n	?		Mg (43)	11.14	p, e ?
Obs	0 ?	7816.23	0 n	Zr	16.32	2 MIT
7820.65	2 nn	Obs	0 wn	Zr TiO	19.35 20.11	10 MIT 7
7828.46	1+	Obs	0	TiO	28.08	10
7832.19	3	31.69	3 n	Fe (1154)	32.22	400 Note 1
7835.58	1 Bl	34.92	1 n	Al I Al I β Peg	35.33 36.15 34.55	50 sp? MIT Note 2 40 sp? MIT 9
7840.49	1 n	40.59	2 n	TiO	39.3	10
7850.06	3 +w	49.33	4+	Zr (40) CN Si (81)	49.38 49 50.5	15 2 ?
7852.59	3 n	52.83	3	Ti (34)	52.74	p, e
?		7856.93	1 n	β Peg	56.90	10
7862.94	3 ww Bl	64.89	1 nw	TiO Zr	60.7 64.37	10 2 MIT (In R And)
7869.54	1	69.95	3	TiO Zr (41)	68.3 70.00	7 12
7873.12	3	72.75	3-	CN Atm	72.7, 72.9, 73.4	

TABLE 2

WAVELENGTHS AND INTENSITIES (cont'd)

μ Cep		R And		Identification		
7875.24	1			CN	74.9, 76.0	
7881.81	3 nn	81.54	3 n	Yt II(32)	81.90	25 ?
				Zr	82.18	4 MIT
				CN	80.8, 82.8	
7884.92	3 s	84.88	3-s	Ti (34)	85.00	p, •
7889.88	On			CN	90.6	?
7894.91	5-	Obs.-diffuse 1t		CN	94.5	
				Ti (34)	95.50	p + Atm
		98.09	0			
7901.07	1	01.34	1-	TiO	00.9	4
				CN	01.9	+ Atm
Obs.	0-	04.07	0	Fe (403)	04.12	p, •
7909.03	4 n	08.63	4	TiO	07.44	12
				Cr (316)	08.30	20
				Co (189)	08.68	6 ??
				CN	09.6	
Obs ?	0-	10.69	2-	LaO	10.50	150(In R And)
				Cr (316)	10.50	18
7913.12	6	13.12	3+	Fe (12)	12.87	6
				Si (35)	13.47	10
7917.62	4 w	17.29	3 nn	Ni (109)	17.48	7
				Cr (316)	17.85	18
				Si (57)	18.38	200
				CN	17.7, 18.2 (In μ Cep)	
7920.39	1	20.53	1	CN	20.2	+ Atm
7923.51	3 w	23.42	1 n	CN	23.0	+ Atm
7926.41	0 } Bl	Obs	2	CN	26.3	
7928.08	2 }			CN	27.9	+ Atm
7930.49	1	30.57	0	β Peg	30.35	1
				Mg (42)	30.83	p, •
7933.25	3	33.27	3	TiO	32.9	7
				CN	33.2, 33.5	
7937.79	4 n	37.90	2 nn	Fe (1136)	37.17	700
				CN	37.7	
7941.61	0 n	Obs	0 n	Fe (508)	41.84	p, • ?
				Cr (300)	42.02	25
				CN	42.1	
7944.23	3 }	44.92	4	TiO	43.2	8
				Ti (308)	43.93	1 ?
				Si (57)	43.94	500
	Bl			Zr (40)	44.65	15(In R And)
				CN	44.4	
7945.72	3 }			Fe (1154)	45.88	600
7949.24	3	48.82	3 n	TiO	48.6	8 ?
				Ti (125)	49.17	3
7953.27	1 n	Obs. ?		TiO	53.2	6
				Ni (266)	53.11	1 ?

TABLE 2

WAVELENGTHS AND INTENSITIES (cont'd)

μ4 Cep		R And		Identification		
7956.62	1 n	56.39	1 n	Zr (41) CN	56.69 7 56.7, 57.0	
7960.52	2 n	Obs	2	Atm Zr	59.98 8	MIT
7963.10	2	Obs	2	CN	63.3	
7965.45	2	65.58	3	CN Fe (1305) β Peg Nd	65.1 65.52 p, 65.73 10 65.70 6	• MIT ?
7970.70	0	Obs.	0	Re	70.87 15	??
7977.40	0	?		CN	77.2	
7978.76	3 s	Obs } Bl	1	Ti (151) Ti (308) CN	78.78 4 78.88 4 79.79	?
Obs	1 n	81.65 }	1	•	81.54 -3	
7985.12	2	83.75	2 n	CN	84.6, etc.	
7987.61	4	87.51	3	Co (89) CN TiO	87.36 5 88.0 88.05 4	
Obs. Bl	0	7991.83	1	• β Peg	91.71 -2 91.68 -2	
7995.16	4	94.98	5	TiO CN	96.0 2 95.0, 95.6	
7999.57	5 w	99.49	5 w	Fe (1136) CN	98.97 700 99.8	
8003.47	3 n	03.25	3	Sc I Atm	03.27 2	MIT ?
?		8005.27	0	β Peg	05.25 0	TiO ?
8007.78	1 wn	07.66	2	TiO (?) + Atm		
8012.22	3 n	12.38	3 n	β Peg • •	12.02 2 12.27 -1 12.48 -1	w TiO ?
Obs. Bl)		8015.27	1	β Peg	15.77	TiO ?
8017.02)	3 w	17.32	1	CN	17.0	
8021.15	3 n	20.83	3	•	21.44 -3	+ Atm
8025.60	7	25.21	7	Ti (151) CN	24.84 2 25.9	
8027.81	5	27.63	5	V (30) Fe (823) Fe (1154)	27.36 30 27.98 p, 28.34 50	•
8030.84	1	Obs	0	•	30.67 -2	+ Atm?
8032.85	0	Obs	0	CN	32.8	+ Atm
8035.28	2	34.89	2	Atm, TiO ?		
8040.55	0 n	39.99	1 n	CN	40.3, 41.7	
8044.20	3	43.81	3 n	CN	43.8, 44.4	+ Atm?

TABLE 2

WAVELENGTHS AND INTENSITIES (cont'd)

μ Cep		R And		Identification			
8047.75	5	47.72	4 s	Fe (12)	47.60	15	
8050.68	2	50.31	2	TiO ?			
8054.24	0 n	53.20	0	CN	54.1		
Not seen		55.79	2	Zr	55.76	4	MIT
				Co (193)	56.00	2	?
Not seen		58.15	0	Zr (41)	58.14	7	
8060.50	J	Obs.	1	e ?	60.70	-3	
8063.16	2	63.08	5	Zr (40)	63.10	10	
8068.02	2	66.60	1 n	CN	67.3		(Note 4)
				Ti (151)	68.24	2	
8070.27	3	70.25	4	Zr (40)	70.12	25	
				CN	70.7		
8072.48	0	?		Fe (106)	72.16	p, e	
				CN	72.4		
8075.14	5	75.08	4	Fe (12)	75.13	4	
				CN	74.4		?
				TiO	74.9	4	
8081.39	3 nw	81.25	4 n	CN	81.55		etc.
8085.22	3	85.03	3 n	Fe (1136)	85.20	500	
8090.22	2 n	90.05	3 nn	Ti	89.76	6	MIT ?
				e	90.46	1	n
8093.25	5	93.59	4	CN	93.0		
				Si (34)	93.32	25	
				V (30)	93.48	100	?
Obs	O-	8114.42	3	Zr	14.28	2	MIT
8116.76	4	17.19	4	V (30)	16.80	200	
8133.01	3	33.29	3	Zr	32.99	80	MIT
				Atm	33.8		
?		44.43	1	V (30)	44.58	50	
8161.58	7	61.83	10	Atm			
				CN	61.45		
8183.24	3	83.38	3 n	Na (4)	83.26	8	
8194.82	5	94.92	3	Na (4)	94.82, .79	10	
Obs.	Blended	8212.52	5 s	Zr (40)	12.59		+ Atm
Obs ?	Bl with Atm	41.49	3	V (30)	41.61	60	
8326.99	5	8326.81	2 n	Fe (60)	27.06	1200	
8331.79	2	Not seen		Fe (1153)	31.94	200	
8334.31	3	Obs	3 n	Ti (33)	34.37	2	+ Atm
8338.37	3	38.87	3 n	Atm	39.0		
				Si (33)	38.43	5	?
				Cr (298)	38.83	5	?

TABLE 2

WAVELENGTHS AND INTENSITIES (cont'd)

μ Cep		R And		Identification			
Obs	2 wn	8343.22	2 wn	Atm	43-4		
				Fe (401)	42.21	p, • ?	
				Fe (1270)	42.95	? •	
8346.02	2 n	Obs	2 nn	Mg (40)	46.13	p, •	
8348.98	4	49.09	3	Cr (56)	48.28	20	
				Fe (12)	49.05	p, •	
				Atm	49.2, 49.4		
8353.22	3	53.37:	4	Ti (33)	53.15	2	
8364.05	5	63.89	4	Ti (33)	64.24	2	
Obs	1 nn	70.27	2 n	Zr (40)	70.21	10	
				β Peg	71.36	3 w	
8377.40	5 s	77.75	5	Ti (33)	77.90	100	
8382.67	7	82.62	7	Ti (33)	82.54	100	
				Ti (33)	82.82	90	
?		85.98	0 n	Ti (182)	86.24	p, ?	
8387.66	6			Fe (60)	87.78	1200(μ Cep)	Bl.
				Zr (40)	89.42	8(R And)	
				Ti (182)	89.48	25	
Obs	0-	94.04	0 n	Atm	94.02	?	
8396.97	4	97.01	4	Ti (33)	96.93	90	
8401.74	2	01.62	1	Fe (108)	01.42	2	
				Fe (1136)	01.68	p, •	
				Ti (224)	02.54	5 ?	
8405.07	1 n	Obs	1	Atm	05.4	?	
8408.09	1 n	07.64	0	β Peg	07.15	0, •	
				Atm	08.8	?	
8412.16	5	12.37	5	Ti (33)	12.36	150	Bl.
8414.06	1	Obs	1	Zr (40)	14.00	7	
8417.29	1 s	16.91	1	Ti (224)	16.97	60	
				Ti (182)	17.54	25	
8418.96	2 wn	Obs	0	Ti (unc)	18.70	10	
				•	19.29	0	
				Ti0	19.1	4	
8424.55	0 wn	---		Ti (182)	24.41	50	
				Fe (12)	25.89	p, •	
8426.46	8	26.41	8	Ti (33)	26.50	200	
8435.21	10	35.47	10	Ti (33)	34.98	300	
				Ti (33)	35.68	300	
8439.01	2 Bl to R	Obs	2±	Ti (224)	38.93	75	
				Fe (1172)	39.60	20	
8450.41	3 n	Obs	3 n	Cr (56)	50.26	15	
				Ti (224)	50.89	75	
?		64.92	3	Zr (40)	64.65	10	
8468.46	4	68.09	2	Fe (60)	68.41	300	

TABLE 2

WAVELENGTHS AND INTENSITIES (cont'd)

μ Cep		R And		Identification		
8471.97	1 nn	Obs	0 nn	TiO	71.97	5
				Fe (1270)	71.75	2
8477.10	2 nw	76.48	3 w	La	76.48	25
				e	77.13	-2
				β Peg	77.59	1
				Probably CN band head		
8488.24	1 n	Obs	2 n	β Peg	88.02	
8498.02	15	97.62	4 Em	Ca II (2)	98.02	300
		98.86	2 Abs			
8510.95	1 n	?		Cr (Unc)	10.97	8
8514.58	6 w	14.92	3	Fe (60)	14.08	150
				Fe (401)	15.08	20
				TiO	14.0	5 ?
8518.43	2 n	18.27	2	Ti (182)	18.05	60
				Ti (150)	18.37	100
8526.40	1 nn	25.62	1 nn	Fe (1270)	25.69	8
				Re	27.73	300 ??
8530.43	1 nn	30.48	1 nn	e	30.17	-3
				β Peg	30.25	2 w
8542.14	18	41.40	6 Em	Ca II (2)	42.09	1500
		42.66	3			
8548.46	2 n	48.83	1	Ti (150)	48.07	100
				Cr (56)	48.83	12
Obs	1	50.28	2 n	Ti (141)	50.54	25
8555.97	2 nn	55.44	3 nn	Cr (56)	55.54	5
				Si (45)	56.64	100
Obs	2 nn	60.30	2 n	β Peg	60.77	0
				Ba	59.95	400 MIT
Obs	0	64.81	0	e	64.62	-3
				β Peg	64.55	0
8569.58	1	68.60	0 n	Ti (209)	69.70	50
8575.31	2	73.18	1 ?	Co	74.57	50
				Co	75.35	50
8582.46	3	81.72	3 n	Fe (401)	82.27	15
				Ba	81.98	50 ?
8597.12	1	97.13 Bl	2 nn	Si (80)	97.00	2
				Ti (236)	98.18	60
8598.66	2			Fe (1153)	98.79	4
Obs	3 nn	02.96	3 nn	β Peg	02.58	1 CN ?
				Ti (141)	00.98	25
				Ti (209)	00.98	
Obs ?		10.3:		Band head ?		
8611.90	3	Obs	1	Fe (339)	11.61	40
8622.11	3 n	21.67	2	Fe (401)	21.61	10
				Bl with weaker line on R		
8642.73	3 wn	41.57	4 n	Cr (56)	43.03	12 Note 5
				Fe (1261)	43.29	p, e

TABLE 2

WAVELENGTHS AND INTENSITIES (cont'd)

μ Cep		R And		Identification		
8648.89	2 n	48.56	2	Si (Unc)	48.89	100
8654.78	1	54.07	1	Fe (623)	54.40	p, •
8662.06	16	61.45 62.55	5 Em 5	Ca II (2)	62.14	1000
8675.17	5	76.18	4	Fe (339) Ti (68)	74.75 75.38	60 150
8679.13	1 n	?		Fe (1286)	79.61	p, • ?
8682.99	Bl on R3	83.58:	5	Ti (68)	82.99	25
8688.64	6	88.58	4	Fe (60)	88.63	1500
8692.26	3	92.26	3	Ti (68)	92.34	100
8699.18	2 n	? The spectrum of R And to the red of this point is too weak for the measurement of faint lines.		Fe (1267) Fe (400)	99.43 98.71	4 p, •
8702.82	2 nn	?		Ni (83) Mn (49)	02.49 03.76	6 500
8707.09	0 n	?		Cr (56)	07.42	7
8710.08	2	09.56	0	Fe (1267)	10.29	20
8713.22	3	12.73	2	Fe (400) Fe (1267) •	13.19 13.19 12.70	10 10 2
Obs	2 nw	29.78	2 nw	Fe (713)	29.17	p, •
8735.00	4	34.77	5	Mn (49) Ti (68) Mg (39)	34.60 34.70 36.0	30 ? 75 1 ?
8751.95	3 nw	Obs	2:	Si (43)	52.17	200 etc.
8757.26	5	56.54	3:	Fe (339)	57.19	25
8763.96	3 n	Obs	?	Fe (1172)	64.00	100 etc.
8766.80	4	66.66	4	Ti (68)	66.64	75
8773.02	4 nw	73.48	3 nw	Al (9) Al (9)	72.88 73.91	15 20
8778.68	3 n	78.82	3 n:	Ti (140) Fe (1050)	78.66 79.12	30 p, • ?
8790.23	2 n	?		Fe (1267)	90.62	10
8793.38	3	92.70:	1:	Fe (1172)	93.38	120
8796.63	2 n	98.28:	1:	Fe (1266) Fe (1286)	96.42 98.05	2 p, • ?
8800.72	1	00.78	4:	Y	00.62	8 MIT
8804.57	4			Fe (106)	04.62	10
8806.74	5			Mg (7) Mg (7) Mg (7)	06.70 06.74 06.77	2 2 10
8838.84				Fe (339) β Peg	38.43 39.19	30 20

NOTES TO TABLE 2

1. λ 7832. The shorter wave length in R And appears to be due to the blending of *Fe* 7832.22 with another line on its violet side.

2. λ 7835. Identification is not certain. Blending on the longward side accounts for the greater wave length in μ Cep.

3. λλ 7978–7981. In μ Cep the sharp line at 7978.76 stands out clearly. In R And there is merely a diffuse blend. Apparently the nearly coincident *Ti* lines are weakened in R And.

4. λλ 8067–8068. In R And the line measured at 8068.0 in μ Cep becomes broader and is displaced toward shorter wave lengths.

5. λ 8642. The *Fe* line is clearly weakened in R And, while the *Cr* line is perhaps stronger than in μ Cep.

nosity criteria in the near infrared and increase steadily in strength from dwarfs to supergiants.[9] At the same time they are quite sensitive to temperature, for they weaken rapidly through the M-type subdivisions later than M5. There is also evidence that in the most luminous cool stars the relative intensities of *Fe* and *Ti* lines are subject to complicated effects of stratification. This was shown strikingly by ρ Cas, in which the *Fe* lines were extraordinarily weak during the 1946 minimum, while *Ti* lines of similar excitation potentials remained strong.[10] The general appearance of the line spectrum of R And

TABLE 3

RELATIVE STRENGTHS OF ATOMIC LINES IN R AND AND μ CEP

Stronger in R And	Roughly Equal in Both Stars	Stronger in μ Cep
Rb	*Ti*	*Fe*
Zr	*V*	*K*
V		*Na*
		Ni

TABLE 4

INTENSITIES OF LINES OF MULTIPLET 60 OF *Fe* I

Line	Lab. Int.	R And	μ Cep	Remarks
8327.06.....	1200	2 n	5	
8387.78.....	1200	4	6	Bl with *Zr* 8389
8468.41.....	300	2	4	
8514.07.....	150	3	6 w	Bl with *Fe* 8515
8661.91.....	600	.....	.....	Bl with *Ca* II 8662
8688.63.....	1500	4	6	

suggests that the weakening of the infrared iron lines in this star as compared to μ Cep is partly due to the lower luminosity of R And.

In the S-type stars, where there is evidence of differences in the abundance of some elements as compared to M-type stars, it is obviously dangerous to attempt estimates of temperature and luminosity from spectroscopic criteria. In view of the fact, however, that the color and the band strengths in R And suggest a temperature of the order of that of α Ori (3100° K), it is probably significant that the intensities of three of the most sensitive features of the infrared spectrum—(1) lines of *Fe*, (2) ultimate lines of *Na* and *K*, and (3) bands of *CN*—are all consistent with the assumption that M_v lies in the range -2 to -4.

[9] Keenan and Hynek, *Ap. J.*, **101**, 265, 1945 (note Pl. III*b*).

[10] P. C. Keenan, *Ap. J.*, **106**, 295, 1947; A. D. Thackeray, *M.N.*, **108**, 276, 1950.

HYDROGEN AND HELIUM LINE INTENSITIES IN SOME Be STARS

E. MARGARET BURBIDGE AND G. R. BURBIDGE
University of London Observatory
and
Mathematics Department, University College, London
Received August 1, 1950

ABSTRACT

Intensity measures of the absorption lines $H\gamma$, $H\delta$, $H\epsilon$, and He I λλ 4471, 4388, 4144, 4026, and 4009 have been made in the spectra of fourteen Be stars, all of which have shown spectral variations in the past. Comparisons are made with previous measures where available and also with the ratios $H\delta/H\gamma$ and the singlet/triplet helium-line ratios of normal B-type stars. 59 Cygni shows a large decrease in intensity of all the lines studied, and numerical values of this decrease are given for each line. Brief descriptions of the spectra are given. The ratio $H\delta/H\gamma$ is approximately constant for the stars studied, except for υ Cyg, 6 Cep, and β Psc, which show emission at $H\gamma$ and have a high value of the ratio. The chief factors affecting the intensities of the lines are discussed.

I. INTRODUCTION

Between July 19 and August 6, 1949, a series of spectrograms of fairly bright Be-type stars was obtained by the writers at the Haute Provence Observatory, France. The program was to measure equivalent widths of hydrogen and helium lines in a selected list of Be stars, given in Table 1, in which the second column gives the HD number, the third

TABLE 1

LIST OF STARS OBSERVED

Star	HD	Spectral Type	No. of Plates	Star	HD	Spectral Type	No. of Plates
θ CrB	138749	B5ne	3	60 Cyg	200310	B3ne	3
66 Oph	164284	B5ne	2	υ Cyg	202904	B3ne	5
12 Vul	187811	B5ne	3	6 Cep	203467	B3ne	4
28(b^3) Cyg	191610	B3ne	3	25 Peg	210129	B8ne	2
25 Vul	193911	B8ne	3	31 Peg	212076	B3e	3
λ Cyg	198183	B6e	3	π Aqr	212571	B1e	2
59(f^1) Cyg	200120	B3ne	10	β Psc	217891	B5e	2

gives the spectral types taken from Merrill and Burwell's catalogue of Be and Ae stars,[1] and the fourth gives the number of plates used for each star. In addition, spectra were taken of γ Cassiopeiae and the shell star HD 217050, but these will be considered at a later date and are not discussed in the present paper.

The stars listed in Table 1 have all undergone spectrum variations in the past, and one of the purposes of measuring their line intensities was to enable these to be compared with future measures and also with past measures where available so that changes in line intensities could be treated quantitatively instead of merely descriptively.

II. INSTRUMENTAL

The apparatus used consisted of the four-prism Tremblot spectrograph (dispersion = 53 A/mm at $H\gamma$) attached to the 80-cm reflecting telescope. Ilford Zenith plates were

[1] *Mt. W. Contr.*, No. 471; *Ap. J.*, **78**, 87, 1933.

used, except for two spectra which were photographed on Kodak II*a*-O plates. The slit-width was about 40 μ, and the range of wave length photographed was about λλ 4500–3600. Since the telescope mirrors were silvered and not aluminized, the intensity fell off very rapidly below about λ 3950; for this reason, lines of wave length shorter than $H\epsilon$ were not measured. The lines studied were $H\gamma$, $H\delta$, $H\epsilon$, and *He* I λλ 4471, 4388, 4144, 4026, and 4009.

The plates were standardized immediately after exposure by means of an auxiliary standardizing spectrograph designed by Barbier.[2] In this apparatus, light from a mercury-vapor lamp enters through a wide slit; two diaphragms in the optical train cause the intensity along each of the resulting wide mercury lines to vary continuously in a calculable manner. Microphotometer tracings of the plates were made by the authors with the Chalonge microphotometer[3] at the Institute of Astrophysics, Paris, and their reduction was carried out at the University of London Observatory. The sensitivity of the Chalonge microphotometer is such that the range "clear glass" to "complete darkness" corresponds to about 40 cm on the tracing.

Calibration tracings were made by running the mercury lines at λλ 4358, 4047, and 3650 through the microphotometer in a direction perpendicular to the dispersion, and three calibration-curves for each of these three wave lengths were constructed for each plate. On the Ilford plates there was a detectable difference between the slopes of the straight-line portions of the curves for the wave lengths λ 4358 and λ 4047 and a very slight difference between λ 4047 and λ 3650. The stellar lines *He* I 4471, *He* I 4388, and $H\gamma$ were reduced using the curve for λ 4358; the lines $H\delta$, *He* I 4026, *He* I 4009, and $H\epsilon$ were reduced using the curve for λ 4047; and for *He* I 4144 an interpolation between λ 4358 and λ 4047 was used. The fact that the calibration wave lengths were not the same as the stellar wave lengths may have introduced slight systematic errors, but it was estimated that these would be considerably less than the accidental errors.

Equivalent widths were then obtained in the standard way by determining the percentage absorption at points on the line contour and measuring the area of the plotted curve with a planimeter.

III. RESULTS

The resulting widths are given in Tables 2 and 3, the unit being the total absorption over 1 A. The number of measures is given for each line, also the mean percentage deviation. These deviations may be compared with the mean percentage deviation of ±9.2 obtained by Miss Underhill for line intensities in B-type stars[4] and the probable errors per cent obtained by E. G. Williams for line intensities in B-type stars.[5] Williams' mean probable errors per cent for groups of lines were as follows: hydrogen, $H\gamma$–$H\zeta$: 5.7, other lines: 7.1; and helium, diffuse triplets: 7.9, sharp triplets: 16.3.

The stars in Tables 2 and 3 are arranged according to spectral type. Table 2 gives the hydrogen lines and Table 3 the helium lines. The lines λ 4471 and λ 4026 belong to the triplet diffuse series of helium, $2^3P^\circ - n^3D$, and the lines λλ 4388, 4144, and 4009 belong to the singlet diffuse series, $2^1P^\circ - n^1D$. The three columns for each line give, first, the equivalent width, *W;* second, the number of measures, *n;* and, third, the mean percentage deviation, *a*.

IV. EFFECT OF BLENDS

Underhill and Petrie[6] have pointed out that intensity measures of *He* I 4026 and *He* I 4144 in B-type stars may be in error because of the blending of the former with the *He* I line λ 4024 ($2^1P^\circ - 7^1S$) and of the latter with *S* II lines. Other lines in the *He* I

[2] *Ann. d'ap.*, **7**, 80, 1944.

[3] *Ann. d'ap.*, **1**, 282, 1938.

[4] *Ap. J.*, **107**, 349, 1948.

[5] *Ap. J.*, **83**, 279, 1936.

[6] *J.R.A.S. Canada*, **38**, 385, 1944.

sharp series occurring in the wave-length range considered here are λλ 4438 ($2^1P^\circ - 5^1S$), 4169 ($2^1P^\circ - 6^1S$), and 3936 ($2^1P^\circ - 8^1S$). The first two of these lines were sometimes just visible on our spectra but were always very weak, and the last line was never visible. Aller[7] gives the following measures of equivalent width of these *He* I lines from high-dispersion spectra of the main-sequence B2.5 star γ Pegasi: λ 4438 = 0.123; λ 4169 = 0.111; λ 4024 (+*O* II) = 0.022; λ 3936 not measured. It is estimated that, although the present measures of λ 4026 may be systematically too large, owing to blending with the line λ 4024, the effect is very small, and the accuracy attainable with the dispersion

TABLE 2

EQUIVALENT WIDTHS OF THE HYDROGEN LINES

Star	$H\gamma$			$H\delta$			$H\epsilon$		
	W	*n*	*a*	*W*	*n*	*a*	*W*	*n*	*a*
π Aqr (B1)	2.41	2	7.9	2.78	2	7.9	2.78	2	12.4
28 Cyg (B3)	3.89	3	5.8	4.11	3	5.6	4.43	3	9.9
59 Cyg (B3)	2.64	8	11.5	2.91	10	11.2	2.87	9	10.3
60 Cyg (B3)	3.36	3	5.0	3.57	3	3.4	3.35	3	1.3
υ Cyg (B3)	3.02	5	7.5	3.60	5	9.4	3.57	5	5.6
6 Cep (B3)	3.09	4	6.2	3.85	4	5.5	4.04	4	8.5
31 Peg (B3)	3.93	3	5.5	4.50	3	4.3	4.32	3	4.5
θ CrB (B5)	6.06	3	9.0	6.85	3	8.1	6.82	3	6.1
66 Oph (B5)	4.85	2	0.9	5.09	2	2.4	5.60	2	1.9
12 Vul (B5)	5.46	3	11.4	5.73	3	6.5	5.91	3	3.1
β Psc (B5)	6.34	2	4.5	7.81	2	1.8	7.12	2	0.6
λ Cyg (B6)	6.84	3	11.1	7.69	3	9.5	6.86	3	10.1
25 Peg (B8)	5.85	2	8.6	6.75	2	7.7	6.63	2	8.9
25 Vul (B8)	4.66	3	6.1	5.07	3	4.8	4.49	3	3.8

TABLE 3

EQUIVALENT WIDTHS OF THE HELIUM LINES

Star	*He* I 4471			*He* I 4026			*He* I 4388			*He* I 4144			*He* I 4009		
	W	*n*	*a*	*W*	*n*	*a*	*W*	*n*	*a*	*W*	*n*	*a*	*W*	*n*	*a*
π Aqr (B1)	0.72	2	0.7	1.02	2	0.5	0.47	2	5.8	0.62	2	10.1	0.44	2	0.6
28 Cyg (B3)	1.70	3	8.9	1.05	3	9.1	.63	3	13.9	.62	3	7.4	.50	3	4.3
59 Cyg (B3)	0.65	8	10.8	0.62	10	10.2	.30	7	19.4	.52	10	7.8	.19	7	11.8
60 Cyg (B3)	1.04	3	2.1	0.99	3	10.7	.48	3	6.7	.63	3	4.9	.39	3	6.2
υ Cyg (B3)	1.07	5	15.8	1.01	5	5.6	.69	4	6.2	.74	5	10.1	.60	5	6.7
6 Cep (B3)	0.78	5	14.6	0.94	4	4.9	.46	3	7.3	.59	3	4.3	.40	4	5.6
31 Peg (B3)	0.96	3	11.9	1.31	3	3.8	.67	3	7.8	.74	3	4.5	.64	3	11.9
θ CrB (B5)	0.92	3	5.7	0.77	3	6.4	.61	3	6.1	.43	3	1.0	.27	3	26.6
66 Oph (B5)	1.46	2	6.5	1.17	2	7.7	.79	1	.....	.80	2	11.3	.70	2	1.7
12 Vul (B5)	1.36	3	9.6	1.27	3	4.7	.60	3	2.9	.79	3	9.8	.54	3	2.9
β Psc (B5)	0.55	2	6.9	0.82	2	2.7	.32	1	.....	.51	2	0.0	.31	1	.....
λ Cyg (B6)	0.92	3	9.9	1.03	3	7.5	.89	2	0.3	.59	3	5.2	.44	2	15.4
25 Peg (B8)	0.48	2	4.2	0.80	2	1.3	.28	2	1.8	.53	2	7.5	.....	.....	.....
25 Vul (B8)	0.48	3	9.7	0.52	3	8.9	0.25	3	4.0	0.39	2	3.2	0.20	3	7.1

[7] *Ap. J.*, 109, 244, 1949.

used does not justify any attempt to make corrections. The same considerations apply to measures of *He* I 4144. The strongest lines of the multiplet $4p^4D^\circ - 4d^4F$ of *S* II are as follows: 4162.70 (10); 4153.10 (10); 4145.10 (9); 4142.29 (8); 4217.23 (3); 4189.71 (6); 4168.41 (5). Laboratory intensities are given in parentheses. These data are taken from the *Revised Multiplet Table of Astrophysical Interest*, by C. E. Moore Sitterly.[8] Aller's measures of equivalent width for *S* II lines in γ Pegasi are as follows: 4217.30 = 0.013; 4189.74 = 0.056 (+*O* II); 4168.41 = 0.014 (+*Fe* III); 4162.70 = 0.028; 4153.0 = 0.024. It is estimated that the addition to the equivalent width of *He* I 4144 due to blending with *S* II lines does not exceed 0.05.

V. BRIEF DESCRIPTION OF THE SPECTRA

Of the fourteen stars in Table 1, only β Psc, 6 Cep, and υ Cyg showed undoubted emission in the wave-length range λλ 4500–3600. In each of these stars emission was present at $H\gamma$ and in none of the other lines measured. In obtaining four of the spectrograms of 59 Cyg, the star was trailed in such a way that the spectra were about twice the width of the rest of the spectra, and on these four it is just possible to see what appear to be very faint emission components at $H\gamma$.

Through the kindness of M. Fehrenbach, subdirector at the Haute Provence Observatory, the authors were enabled to use the 120-cm reflector and large four-prism Tremblot spectrograph for a few nights in August, 1949. With this instrument, the spectra of five stars were obtained in the visual region, and the following is a brief description of the appearance of $H\alpha$ and $H\beta$ in these stars:

β Psc—	$H\alpha$:	Very strong, narrow, single emission superposed on a broad absorption line.
	$H\beta$:	Fairly strong, narrow, single emission on a strong, broad, absorption line.
6 Cep—	$H\alpha$:	Very strong, single emission superposed on a faint, broad, absorption line.
	$H\beta$:	Fairly strong emission superposed on a broad absorption line.
υ Cyg—	$H\alpha$:	Strong emission.
	$H\beta$:	Rather weak emission superposed on a broad absorption line.
59 Cyg—	$H\alpha$:	Strong broad (double?) emission.
	$H\beta$:	Fairly strong double emission ($R > v$) superposed on a broad absorption line.
π Aqr—	$H\alpha$:	Rather weak double emission.
	$H\beta$:	No emission.

Kodak 103*a*-O plates were used. The spectra were obtained merely for descriptive purposes and were not suitable for measurement, since the spectrograph was not in adjustment.

The foregoing descriptions may be compared with those given in Merrill and Burwell's second supplement to their catalogue of Be and Ae stars.[9]

VI. DISCUSSION OF THE MEASURES

a) COMPARISON WITH PREVIOUS MEASURES

Only three of the present list of stars were among those for which E. G. Williams made line-intensity measures.[5] One of these three, 59 Cyg, has undergone considerable change in its spectrum since measured by Williams, for at that time the absorption lines in the range here considered were very much stronger than they were in 1949. A comparison between the present measures (denoted by "B") and Williams' measures (denoted by "EGW") is shown in Table 4. Below the measures for 59 Cyg the quantities (EGW − B)/EGW are given for each line of this star only. These ratios are measures of the reduction in intensity of each line per angstrom of equivalent width.

Bearing in mind the possible errors in each set, it appears that π Aqr and 12 Vul

[8] *Contr. Princeton U. Obs.*, No. 20, 1945.

[9] *Ap. J.*, 110, 387, 1949.

were showing substantially similar spectra in 1949 and when considered by Williams. In 59 Cyg there has been a filling-in of all the lines. It is evident that the physical conditions in the outer regions of this star were different at the times of the two sets of observations. The reduction in equivalent width of the hydrogen and helium lines might be due to incipient line emission or to some such cause as electron scattering. It is difficult to estimate how far continuous emission from free-free electron transitions might be effective.

Münch[10] has shown that electron scattering may produce an apparent decrease in the equivalent widths of stellar lines, since the central parts of absorption lines are filled in by radiation from the neighboring continuum and very extended shallow wings are produced which will probably be largely missed in the measurement of total line intensities. He has pointed out that this apparent decrease of equivalent width will affect weaker lines more than stronger ones, since extended wings of weak lines are more easily missed. Therefore, if we invoke electron scattering to explain the reduction in equivalent width of the helium lines of 59 Cyg, incipient line emission is necessary to explain the additional filling-in of $H\gamma$ and $H\delta$ and possibly of $H\epsilon$ also. But, in any case,

TABLE 4

COMPARISON OF PRESENT MEASURES WITH THOSE OF E. G. WILLIAMS

Star	$H\gamma$	$H\delta$	$H\epsilon$	He I 4471	He I 4026	He I 4388	He I 4144	He I 4009
π Aqr B	2.41	2.78	2.78	0.72	1.02	0.47	0.62	0.44
π Aqr EGW	3.42	2.23	2.88	0.72	1.00	.47	.42	.16
12 Vul B	5.46	5.73	5.91	1.36	1.27	.60	.79	.54
12 Vul EGW	6.08	5.50	5.70	1.18	1.36	.90	.72	.75
59 Cyg B	2.64	2.91	2.87	0.65	0.62	.30	.52	.19
59 Cyg EGW	6.11	6.49	4.50	0.87	0.97	.56	.75	.26
(EGW−B)/EGW	0.57	0.55	0.36	0.25	0.36	0.46	0.31	0.27

the amount of filling-in of the helium lines seems very large to be due to electron scattering alone.

Equivalent widths of $H\gamma$, $H\delta$, and $H\epsilon$ for some of the stars in Table 1 were measured by Günther[11] and intensity measures of $H\gamma$ and $H\delta$ for several of these stars were made by Barbier, Chalonge, and Morguleff.[12] The latter used the "wide-slit" method of intensity determination first described by Öhman,[13] and their measures are not in angstrom units and are not directly comparable with the present ones. However, they have plotted their measures against those of Günther, and there is a linear relation between the two over the range of equivalent width considered here. From this graph we have converted the measures of Barbier, Chalonge, and Morguleff into units of 1 A equivalent width, and these, together with those of Günther, are compared with the present measures in Table 5. Günther's measures are denoted by "G," those of Barbier, Chalonge, and Morguleff by "BCM," and the present measures by "B." It appears that, with the possible exception of λ Cyg, the hydrogen-line intensity of these stars was the same at the times of these different sets of observations.

[10] *Ap. J.*, **108**, 116, 1948.

[11] *Zs. f. Ap.*, **7**, 106, 1933.

[12] *Ann. d'ap.*, **4**, 137, 1941.

[13] *Medd. Upsala*, No. 48, 1930.

b) DETAILED DISCUSSION OF THE HYDROGEN LINES

When the present determinations of the equivalent widths of $H\gamma$, $H\delta$, and $H\epsilon$ are plotted against spectral subdivision, the scatter is very large. However, the ratio of the equivalent width of $H\delta$ to that of $H\gamma$ has a value which does not vary much for the different stars considered here. It is therefore of interest to compare this ratio with other observed values and with the theoretical determination for an absorption-line B-type star.

The profiles and distribution in intensity of the Balmer lines are strongly modified by Stark effect, as is well known. The first detailed theoretical investigation was carried

TABLE 5

COMPARISON OF THE PRESENT MEASURES WITH THOSE OF BARBIER *et al.*

Star		$H\gamma$	$H\delta$	$H\epsilon$	Star		$H\gamma$	$H\delta$	$H\epsilon$
π Aqr	B	2.41	2.78	.....	66 Oph	B	4.58	5.09	.....
	BCM	2.1	2.6	.....		BCM	4.3	4.3	.....
59 Cyg	B	2.64	2.91	.....	β Psc	B	6.34	7.81	.....
	BCM	2.6	3.0	.....		BCM	6.0	7.2	.....
υ Cyg	B	3.02	3.60	3.57	λ Cyg	B	6.84	7.69	.....
	G	2.99	4.34	3.60		BCM	5.5	6.0	.....
	BCM	3.8	4.3	.....					
θ CrB	B	6.06	6.85	6.82					
	G	6.50	7.10	6.60					
	BCM	6.0	6.8	.....					

out by Verweij[14] for the first four Balmer lines, and he compared his results with measures of equivalent width by Williams[5] and Günther.[11] The highest surface temperature considered by Verweij was 16,800°. He used values of the continuous absorption coefficient obtained by Pannekoek,[15] and better values are now available. Also, he used as the basis of his treatment the Holtsmark distribution of static electric fields as responsible for the broadening. A more satisfactory treatment by Mrs. Krogdahl[16] has taken into account the relative motions of the particles responsible for the electric fields. It is necessary, therefore, to see whether this new distribution will have a significant effect in the computation of the total intensities of $H\gamma$ and $H\delta$ for a normal B-type star. However, calculation shows that the use of Mrs. Krogdahl's more exact formulae for these lines gives results which do not depart much from the static Holtsmark distribution for the conditions prevailing for a normal main-sequence B2.5 star.

So, remembering the inaccuracy of Verweij's values of the continuous absorption, his theoretical ratio $H\delta/H\gamma = 1.03$, for $\log g = 4.4$, boundary $T = 16{,}800°$, should be compared with the present measures and other observed values given in Table 6. Miss Underhill's measures show an increase of this ratio toward later spectral subdivisions (as do Günther's and Williams' measures) and indicate that the ratio is lower for higher-luminosity stars. The high value obtained by Miss Underhill for γ Peg is surprising; the value obtained by Aller,[7] 1.35, is even higher. Barbier, Chalonge, and Morguleff[12] found the relationship $H\delta/H\gamma = 1.11$ to hold closely over a wide range of spectral types, including supergiants. Even emission-line stars obeyed this general relation, except those showing strong emission, for which the ratio $H\delta/H\gamma$ was high.

[14] *Pub. Astr. Inst. Amsterdam*, No. 5, 1936.

[15] *Pub. Astr. Inst. Amsterdam*, No. 4, 1935.

[16] *Ap. J.*, 110, 355, 1949.

It will be noted that the three stars of Table 1 which show emission at $H\gamma$—namely, υ Cyg, 6 Cep, and β Psc—have high values of the ratio $H\delta/H\gamma$. Leaving out these three stars, the mean value of $H\delta/H\gamma$ is 1.105, and the individual measures show no tendency toward correlation with spectral subdivision.

c) DETAILED DISCUSSION OF THE HELIUM LINES

In "A Study of Equivalent Widths of Helium Lines in Early-Type Stars," Goldberg[17] discussed the "helium anomaly," i.e., variations from star to star of the ratio of the $2^1P^o-n^1D$ helium lines to the $2^3P^o-n^3D$ lines. This effect has been extensively discussed,[18] and Goldberg showed that the ratio of singlet to triplet equivalent widths may vary considerably from one spectral class to another because of the properties of the

TABLE 6

VALUES OF $H\delta/H\gamma$

Burbidge			Underhill			Williams		Günther	
Star	Sp.	$H\delta/H\gamma$	Star	Sp.	$H\delta/H\gamma$	Sp.	$H\delta/H\gamma$	Sp.	$H\delta/H\gamma$
π Aqr...	B1	1.15	ρ Leo.....	B1 Ib	0.678				
28 Cyg...	B3	1.06	χ^2 Ori....	B2 Ia	0.717	Earlier than B1	0.95	B1–B2...	1.01
59 Cyg...	B3	1.10	σ^3 CMa...	B3 Ia	0.743				
60 Cyg...	B3	1.06	η CMa....	B5 Ia	1.006	Later than B0.5			
υ Cyg...	B3	1.19	β Ori.....	B8 Ia	1.158	($W<3.0$).....	0.97	B3–B5...	1.03
6 Cep...	B3	1.25	ϵ CMa....	B2 II	0.899				
31 Peg...	B3	1.14	γ Peg.....	B2.5 IV	1.278	B0–A ($W>3.0$)	0.98	B8.....	1.06
θ CrB...	B5	1.13	ζ Dra.....	B8 ...	1.080				
66 Oph...	B5	1.11							
12 Vul...	B5	1.05							
β Psc....	B5	1.23							
λ Cyg...	B6	1.12							
25 Peg...	B8	1.15							
25 Vul...	B8	1.09							

curve of growth. From his curves of growth he calculated, for different spectral subdivisions, the ratio of singlet to triplet equivalent width, using mean equivalent widths of the singlet lines λ 4388 and λ 4144 and of the triplet lines $\lambda\lambda$ 4471, 4026, 3820. Williams[19] had derived this ratio from his observations and had plotted it against spectral type and drawn a smooth curve through the points. Goldberg compared his calculated ratios with those read from Williams' smooth curve and obtained good agreement.

In the present investigation *He* I 3820 was not measured, so the ratio [Mean W(4388, 4144)/Mean W(4471, 4026)] was obtained for each of the fourteen stars considered here, and the results are plotted against spectral type in Figure 1, where they are represented by crosses. In order to compare these values with Williams' measures, this ratio has been evaluated for each of Williams' stars, using his measured equivalent widths, and the results are shown as dots in the figure. Goldberg's equivalent widths derived from his curves of growth have been used to calculate the same ratio, and the dashed curve in the figure has been drawn through the points. It will be seen that the crosses lie within the scatter of Williams' points. It has also been investigated whether those of Williams' stars

[17] *Ap. J.*, **89**, 623, 1939.

[18] E.g., Struve, *Ap. J.*, **74**, 225, 1931; **78**, 86, 1933; **82**, 252, 1935; and Struve and Wurm, *Ap. J.*, **88**, 84, 1938.

[19] *Ap. J.*, **83**, 305, 1936.

which have emission lines lie apart from the absorption-line stars in the figure, but no significant differences were found. The conclusion is that, although the helium absorption lines in Be stars are usually weaker than in absorption-line B stars, the singlet/triplet ratio is substantially the same.

The theoretical curve derived from Goldberg's equivalent widths lies slightly low compared to the observed points. This is due to the effect of forming new triplet means, without the line λ 3820. Goldberg's calculated equivalent widths of λ 3820 are smaller relative to the equivalent widths of λ 4471 and λ 4026 than are Williams' measured values for this line. Goldberg has explained the rapid falling-off of his theoretical singlet/triplet ratio toward later spectral subdivisions as a result of using a constant value of the parameter V, while a lower value would have been appropriate for classes B6–B8.

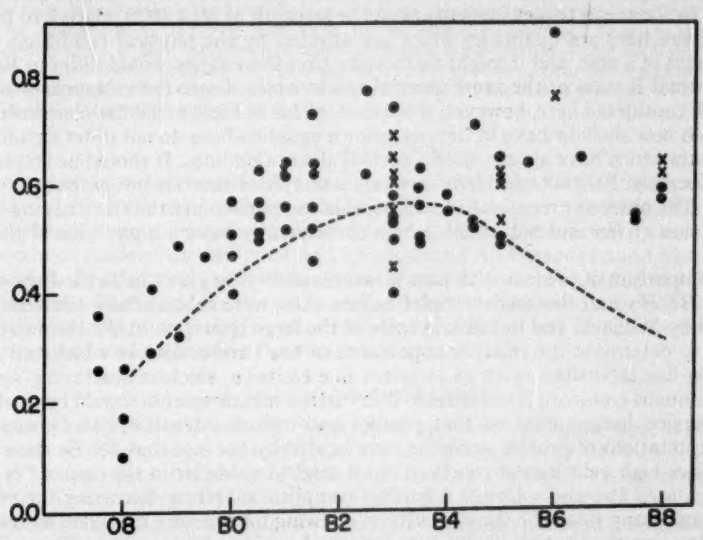

FIG. 1.—[Mean W(4388, 4144)]/[Mean W(4471, 4026)] (*ordinate*) plotted against spectral type (*abscissa*). *Crosses*, measures by Burbridge; *dots*, measures by Williams; *dashed line*, theoretical curve drawn through points obtained from equivalent widths by Goldberg.

A comprehensive theoretical treatment of the helium lines has been carried out by Mrs. Krogdahl.[20] She developed the collision damping theory of Lorentz and Weisskopf and obtained good agreement between theoretical and measured equivalent widths for τ Sco (B0). Miss Underhill[21] has pointed out that a luminosity effect in the line λ 4026 might be expected between intermediate and dwarf B-type stars, the intensities of the forbidden components λ 4025.5 (2P − 5F) and λ 4025.4 (2P − 5G) being very sensitive to field strength. In a recent paper Gusev[22] has used a new procedure to determine the extent of the influence of Stark effect in B stars. He showed that large effects were present in dwarfs and intermediate stars and were almost absent in giants. The average increases due to Stark effect in the intensities of λ 4471 and λ 4026 were 145 and 194 per

[20] *Ap. J.*, **105**, 327, 1947.

[21] *Ap. J.*, **107**, 337, 1948.

[22] *A. J. Acad. Sci. U.S.S.R.*, **25**, 89, 1948. The authors have only had access to the abstract in *Astr. News Letter*, No. 38, 1948.

cent, respectively. The scatter in the singlet/triplet ratios for each spectral subdivision, shown in Figure 1, is probably real and may well be due to these Stark intensity effects.

The present measures show that λ 4026 is the strongest helium line in the following seven stars out of the fourteen in Table 1: π Aqr, 6 Cep, 31 Peg, β Psc, λ Cyg, 25 Peg, 25 Vul. These range from B1 to B8 in spectral type and show, moreover, no correlation between the relative strength of λ 4026 and the amount of emission present in the spectrum, since the seven stars listed above range from β Psc and 6 Cep, which have stronger emission lines than any other star considered here, to λ Cyg, which in 1948 showed no emission even at *Hα*.

d) CONCLUSION

The intensity of $H\delta$ relative to that of $H\gamma$, the ratio of the mean singlet helium-line intensity to the mean triplet intensity, and the strength of *He* I 4026 relative to the rest of the helium lines are quantities which are affected by the physical conditions in the outer regions of a star, and it might be thought that these ratios would differ in Be stars and in normal B stars of the same spectral subdivisions. From the measures of equivalent width considered here, however, it appears, so far as these ratios are concerned, that stars which now show or have in the past shown emission lines do not differ significantly from B stars which have always shown normal absorption lines. It should be emphasized that the fourteen Be stars considered here are a sample of Be stars not notable for strong emission. The obvious exceptions in making this comparison are the stars having noticeable emission at $H\gamma$ and not at $H\delta$, which consequently have a high value of the ratio $H\delta/H\gamma$.

The comparison of present with past measures of 59 Cyg given in Table 4 shows that the ratio $H\delta/H\gamma$ and the singlet/triplet helium ratio were substantially the same when measured by Williams and in 1949, in spite of the large reduction in the line intensities. In order to determine the relative importance of the various factors which can reduce absorption-line intensities, such as incipient line emission, electron scattering, and perhaps continuous emission, it is desirable that further measurements should be made with high-dispersion instruments, so that profiles and central intensities can be measured. The interpretations of profiles would be complicated by the fact that the Be stars all appear to have high velocities of rotation, but it might be simpler in the case of "pole-on" stars, such as β Psc and υ Cyg.[23] A further complication when discussing the effect of electron scattering would be the difficulty in allowing for the very extended wings of the lines in drawing the continuous background on the microphotometer tracings. Further theoretical studies are necessary, for example, on the ratios of the Balmer-line intensities and their modification by physical conditions in stellar atmospheres.

We are grateful to M. Chalonge, of the Institute of Astrophysics, Paris, for pointing out the possibility of working at Haute Provence. We wish to thank M. Dufay, director of Haute Provence Observatory, for permission to work there; also M. Fehrenbach, subdirector, and the members of the staff for their kindness and help during the course of the work. We are grateful for permission to use the Chalonge microphotometer at the Institute of Astrophysics, and to M. Laffineur for his help with this instrument. Also thanks are due to M. Barbier, who supplied us with tables of calibration intensities. Finally, we wish to thank Mr. C. C. L. Gregory, director of the University of London Observatory, for encouragement in the carrying-out of this work. His suggestions concerning variations in Be stars were the starting point of our investigation, which is part of the program on Be stars currently being carried out at the University of London Observatory.

[23] A. Slettebak, *Ap. J.*, **110**, 498, 1949.

THE WEAKER LINES IN THE PHOTOGRAPHIC REGION OF SOME LATE-TYPE STARS

SUZANNE VAN DIJKE BEATTY
Westinghouse Research Laboratories, East Pittsburgh, Pennsylvania
Received July 11, 1950

ABSTRACT

Several thousand lines in the photographic region of the spectra of the sun, α Bootis, 70 Ophiuchi A, β Andromedae, and Lalande 21185 have been compared visually and photometrically on high-dispersion coudé plates. A résumé of the behavior of the elements in the stars is given. Absolute-magnitude effects are evident for atoms of *Na* I, *Ca* I, *Sr* II, and *Ba* II. The increase of intensity of *Cb* I in the giants is considerable. The effect of high- and low-excitation potentials is evident for atoms of *Mg* I, *Cr* I, *Cr* II, *Mn* I, *Fe* I, *Co* I, and *Ni* I. The behavior of *La* II and the singly ionized rare earths can be explained as either an absolute-magnitude effect or an excess of these atoms in the atmosphere of α Bootis. *La* II, then *Eu* II and *Nd* II, show the greatest increase in the giants.

I. INTRODUCTION

In an earlier work by the author[1] a study was made of the K0 giant and dwarf stars α Bootis and 70 Ophiuchi A, with emphasis on the behavior of the fainter lines in the photographic region at a dispersion of 2.9 A/mm. In the present investigation a similar study has been made of the M0 giant and dwarf stars β Andromedae and Lalande 21185 at 10 A/mm. In addition, comparisons have been made at 2.9 A/mm between β Andromedae and α Bootis and between α Bootis and the sun. Thus the behavior of the lines of the different neutral and singly ionized atoms for both K0 and M0 giants and dwarfs can be described and referred to the sun as a standard.

II. DATA AND MEASUREMENTS

The plates of Venus, α Bootis, 70 Ophiuchi A, and β Andromedae were taken in the second order of the grating spectrograph at the coudé focus of the 100-inch telescope at Mount Wilson, giving a dispersion of 2.9 A/mm. One set of plates for β Andromedae and Lalande 21185 was taken at 10 A/mm in view of the low luminosity of the latter star. Microphotometer traces were obtained of the high-dispersion plates at a magnification of 60 and of the low-dispersion ones at a magnification of 100.

In a preliminary survey the lower-dispersion spectra were compared on the Hartmann spectrocomparator over the wave-length range 3990–4375 A. A visual intensity–difference scale was set up and calibrated against estimates made on one hundred relatively unblended lines on similar plates of Venus. The lines were identified and roughly analyzed. It was found that the blending of lines (both physical and optical) is so severe that very few assignments could be made with certainty and many lines have three or more identifications. Furthermore, the continuum as such is quite lacking, owing to the heavy absorption in this late-type spectrum. Consequently, comparisons were made between plates of β Andromedae and α Bootis at 2.9 A/mm from λ 3990 to λ 4300. Additional comparisons were made between α Bootis and the sun from λ 3990 to λ 4650. Thus the intensities of the lines in this wave-length region were compared as a function of temperature, and proportional intensity values could be deduced for the various lines composing blends at 10 A/mm in the M0 stars, and we can compare the K0 and M0 dwarfs and giants with greater certainty.

A scale of apparent difference of intensity from giant to dwarf was established which combined the visual and photometric estimates. In a visual comparison the intensity

[1] *Ap. J.*, **104**, 27, 1946.

scale is affected to a large extent by the complex variation in the differences of the background densities of the plate, by the degree of blending of the individual lines, and, to a slighter degree, by the number of lines in the field. It was found during the study of the K0 stars that simultaneous inspection of the photometric tracings helped minimize these errors.

The identification of the lines was simplified by the use of the *Photometric Atlas of the Solar Spectrum*,[2] the latest revisions of the Rowland table, and the *Finding List and Table of Multiplets*.[3] All the lines appearing on the tracings could be identified in the *Atlas* even when the relative intensities were considerably changed because of temperature and pressure differences.

III. BEHAVIOR OF DIFFERENT ATOMS

In the following section a résumé of the behavior of the various atoms is given, as shown by the weaker lines; *H*, *Ca* II, *CN*, and *CH* are included for the sake of completeness. In the descriptions the expression "unresolved line" refers to a wave length for which more than one identification is given. A "resolved" line in this manner refers to a wave length which is attributed uniquely to a given atomic or molecular transition, regardless of the degree of physical or optical blending in the spectrum. The terms "M giant" and "dwarf" and "K giant" and "dwarf" are used for simplicity, although the results refer specifically to β Andromedae, Lalande 21185, α Bootis, and 70 Ophiuchi A. Four comparisons of spectra were made, between (1) the sun and α Bootis, $\lambda\lambda$ 3990–4650; (2) α Bootis and β Andromedae, $\lambda\lambda$ 3990–4300; (3) α Bootis and 70 Ophiuchi A, $\lambda\lambda$ 3900–4800; and (4) β Andromedae and Lalande 21185, $\lambda\lambda$ 3990–4375. All but the last were obtained at a dispersion of 2.9 A/mm.

Element	Stars Comp.	Behavior
H	⊙–Kg	Strong wings in the sun.
	Kg–Mg	Stronger in the K star.
	Kg–Kd Mg–Md	In the dwarf the lines have strong wings, whereas in the giant they are quite sharp.
Na I	⊙–Kg	The available lines arise from levels with E.P. 2.1 and are stronger in the K giant.
	Kg–Mg	These same lines are somewhat stronger in the M giant.
	Kg–Kd Mg–Kd	Two resolved lines show definite increase in the dwarf. The behavior of the lines is attributed to absolute-magnitude effect.
Mg I	⊙–Kg	The line λ 4571 arising from the lowest level, $3'S$, is enhanced in the K giant. Lines arising from the $3'P^o$ level (E.P. 4.3) are stronger in the sun and have strong wings.
	Kg–Mg	The low-level line is enhanced in the M giant, whereas the high-level lines are enhanced in the K giant.
	Kg–Kd Kg–Md	The low-level line is enhanced in the giant, whereas the high-level lines are enhanced in the dwarf and have wings.
Si I	⊙–Kg	The one line available in the region, λ 4103 (E.P. 1.90), is considerably stronger in the K giant.
	Kg–Mg	This line is stronger in the K giant.
	Kg–Kd	No difference observed.
	Mg–Md	The line is slightly strengthened in the giant.
K I	⊙–Kg	Two lines arising from the lowest level were observed stronger in the K giant.

[2] M. Minnaert, G. F. W. Mulders, and J. Houtgast (Amsterdam: D. Schnabel, 1940).

[3] C. Moore, *Contr. Princeton U. Obs.*, No. 20, 1945.

Element	Stars Comp.	Behavior
	Kg–Mg	These lines were stronger in the M giant.
	Kg–Kd	Both lines were stronger in the giant.
	Mg–Md	No difference noted.
Ca I	⊙–Kg	The strong line λ 4227 (E.P. 0.00) is stronger in the K giant, while the lines arising from the higher levels (E.P. 1.9, 2.5, 2.9) are slightly stronger in the sun.
	Kg–Mg	The line at λ 4227 is stronger in the M giant, the higher-level lines are stronger in the K giant.
	Kg–Kd	All lines observed are stronger in the dwarf, with the exception of λ 4227 and the $4^1P^o - p^2\ ^3P$ transition (E.P. 1.9). These lines are stronger in the giant. The decrease in intensity of the majority of lines from dwarf to giant is one of the outstanding absolute-magnitude effects.
	Mg–Md	All lines are considerably stronger in the dwarf. This is also attributed to absolute-magnitude effects.
Ca II		The H and K lines are the strongest lines in the spectra. The double reversal of the lines is considerably more pronounced in the giants.
Sc I	⊙–Kg	All lines showing a difference of intensity arise from the ground level and are stronger in the K giant.
	Kg–Mg	All lines observed are considerably stronger in the M giant (E.P. 0.00–0.6).
	Kg–Kd	All lines observed are stronger in the giant (E.P. 0.0–1.4).
	Mg–Md	All lines are observed stronger in the giant (E.P. 0.00).
Sc II	⊙–Kg	All lines observed are stronger in the K giant (E.P. 0.00–0.6).
	Kg–Mg	All lines observed are considerably stronger in the M giant.
	Kg–Kd Mg–Md	All lines observed are stronger in the giant (E.P. 0.00–0.6).
Ti I	⊙–Kg	All lines are considerably strengthened in the K giant (E.P. 0.00–2.49).
	Kg–Mg	All lines are considerably strengthened in the M giant (E.P. 0.00–2.49).
	Kg–Kd Mg–Md	All lines are stronger in the giant stars (E.P. 0.00–2.6).
Ti II	⊙–Kg	All lines are stronger in the K giant (E.P. 0.6–1.89).
	Kg–Mg	A few lines were found stronger in the M giant (E.P. 0.6–1.89).
	Kg–Kd	All lines were observed stronger in the giant (E.P. 0.6–2.0).
	Mg–Md	All lines were observed stronger in the giant (E.P. 0.6–2.56).
V I	⊙–Kg	All lines are considerably stronger in the K giant (E.P. 0.0–2.67).
	Kg–Mg	All lines are considerably stronger in the M giant (E.P. 0.0–1.05).
	Kg–Kd Mg–Md	All lines are considerably stronger in the giant stars (E.P. 0.0–2.1).
V II	⊙–Kg	All lines are strengthened in the K giant (E.P. 1.5–2.0).
	Kg–Mg	Several lines are slightly strengthened in the M giant (E.P. 1.5–2.0).
	Kg–Kd	All lines are strengthened in the giant (E.P. 1.5–2.8).
	Mg–Md	Of the eleven lines observed, only two are not blended with low-level lines of *Ti* and *Fe*. These two lines are stronger in the dwarf.

Element	Stars Comp.	Behavior
Cr I	⊙–Kg	All lines are strengthened in the K giant (E.P. 0.00–3.88).
	Kg–Mg	All lines are strengthened in the M giant (E.P. 0.00–3.88).
	Kg–Kd	All lines arising from levels with E.P. less than 3.2 are strengthened in the giant. At somewhat higher values the lines are strengthened in the dwarf.
	Mg–Md	All lines observed were strengthened in the dwarf (E.P. 3.1–5.6).
Cr II	⊙–Kg	Several lines between E.P. 3.8 and 4.0 are stronger in the sun.
	Kg–Mg	Two lines are strengthened in the M giant (E.P. 3.09), and two lines are strengthened in the K giant (E.P. 5.6).
	Kg–Kd	The lines arising from the b^4D level (E.P. 3.1) are slightly strengthened in the giant. Those arising from the b^4F level (E.P. 4.1) are strengthened in the dwarf.
	Mg–Md	Lines arising from the b^4D level and higher E.P. are all strengthened in the dwarf.
Mn I	⊙–Kg	All lines are considerably strengthened in the K giant (E.P. 2.15–3.36).
	Kg–Mg	All lines having an E.P. less than 3.12 are strengthened in the M giant. Three blended lines having an E.P. of 4.33 are strengthened in the K giant.
	Kg–Kd	All the lines observed are strengthened in the dwarf (E.P. 2.2 or greater).
	Mg–Md	All lines observed were strengthened in the giant (to E.P. 2.94).
Mn II		No resolved classified lines are available in the region. The behavior of the atom is indeterminate.
Fe I	⊙–Kg	All lines arising from levels with E.P. less than 3.6 are stronger in the K giant. Above this value, the lines are strengthened in the sun.
	Kg–Mg	All lines arising from levels with E.P. less than 2.2 are stronger in the M giant. Above this value they are stronger in the K giant.
	Kg–Kd	All lines arising from levels with E.P. less than 3.1 are strengthened in the giant, while those arising from higher levels are strengthened in the dwarf. Several multiplets of high E.P. are considerably winged in the dwarf.
	Mg–Md	All lines arising from levels with E.P. less than 3.9 are stronger in the giant.
Fe II	⊙–Kg	Lines arising from the b^4P and b^4F levels (E.P. 2.6–2.8) are stronger in the sun.
	Kg–Mg	Lines arising from the above levels are stronger in the K giant.
	Kg–Kd Mg–Md	Both sets of multiplets are strengthened in the dwarf stars.
Co I	⊙–Kg	All lines are strengthened in the K giant (E.P. 0.0–2.3).
	Kg–Mg	All lines arising from levels with E.P. between 0.0 and 0.6 are strengthened in the M giant. Lines of higher E.P. are indeterminate.
	Kg–Kd	All lines are strengthened in the giant (E.P. 0.0–3.2).
	Mg–Md	All lines arising from levels with E.P. less than 1.04 are strengthened in the giant. One line with E.P. of 3.6 is stronger in the dwarf.

Element	Stars Comp.	Behavior
Ni I	⊙–Kg	All lines are strengthened in the K giant (E.P. 0.00–3.6).
	Kg–Mg	All lines are strengthened in the M giant (E.P. 0.00–3.6).
	Kg–Kd, Mg–Md	Lines arising from levels of E.P. 0.0–1.9 are strengthened in the giant. Lines arising from levels with E.P. greater than 3.3 are somewhat strengthened in the dwarf.
Ni II		No resolved lines are available. The behavior of the atom is indeterminate.
Cu, Zn, Ga, Ge, Rb		The same as above.
Sr I		Only three lines are available, and the results are indeterminate.
Sr II	⊙–Kg	The two ultimate lines in the region, λ 4215 and λ 4078, $5^2S-5^2P^\circ$ (E.P. 0.0) are both considerably strengthened in the K giant.
	Kg–Mg	These lines are both strengthened in the M giant.
	Kg–Kd, Mg–Md	Both lines are considerably strengthened in the giants. The intensities of these lines are often used for the classification of giants and dwarfs.
Y I	⊙–Kg	Four lines arising from the ground level appear stronger in the K giant.
	Kg–Mg	Two lines are observed, and both are strengthened in the M giant (E.P. 0.0).
	Kg–Kd, Mg–Md	Two lines from the ground level are observed and both are strengthened in the giants.
Y II	⊙–Kg	Most lines are severely blended, but indications are that the lines are slightly stronger in the K giant (E.P. 0.1–0.3).
	Kg–Mg	Two lines are considerably strengthened in the M giant (E.P. 0.1–0.3).
	Kg–Kd, Mg–Md	Of the ten unresolved classified lines in the region, only one is slightly strengthened in the K giant. The behavior of the atom is indeterminate.
Zr I	⊙–Kg	All lines are strengthened in the K giant (E.P. 0.0–0.7).
	Kg–Mg	Only one line was found strengthened in the M giant.
	Kg–Kd	All lines observed arise from low levels and are somewhat strengthened in the giant.
	Mg–Md	No differences noted.
Zr II	⊙–Kg	All lines observed are slightly strengthened in the K giant (E.P. 0.7–1.7).
	Kg–Mg	No differences noted.
	Kg–Kd	Lines arising from the a^2D and a^2F levels (E.P. 0.5–0.7) are strengthened in the giant. Lines arising from higher levels show no change in intensity.
	Mg–Md	The lines are badly blended. The behavior of the atom is indeterminate.
Cb I	⊙–Kg	Three low-level lines indicate a strengthening in the K giant, although they are badly blended.
	Kg–Mg	Seven of the twelve lines of the $a^4D-y^4F^\circ$ multiplet show a considerable increase in the M giant.
	Kg–Kd	Two blended lines indicate a strengthening in the giant.
	Mg–Md	Three lines of the multiplet above indicate considerable increase in the giant.
Mo I, *Ru* I		These lines are badly blended and weak but suggest a slight increase in the cooler star of each set.
Rh, Pd, Ag, Cd, In, Sn, Sb, Te, Cs, Ba I		Indeterminate.
Ba II	⊙–Kg	The only line from the lowest level, 6^2S (E.P. 0.0),

Element	Stars Comp.	Behavior
		λ 4554, is very considerably strengthened in the K giant. Other lines from E.P. 0.0 to 2.7 are also strengthened in the K giant.
	Kg–Mg	All lines are considerably strengthened in the M giant.
	Kg–Kd Mg–Md	The line λ 4554 is considerably strengthened in both giants and is particularly sensitive to absolute magnitude. The lines belonging to higher levels (E.P. 2.5–2.7) are unresolved and probably remain constant.
La II	⊙–Kg	All lines are considerably strengthened in the K giant (E.P. 0.00–0.4).
	Kg–Mg	All lines are stronger in the K giant with the exception of λ 4086, which is stronger in the M giant.
	Kg–Kd	All lines observed from E.P. 0.0 to 1.9 are strengthened in the giant. It is noted that in the spectra of the disk and spot no change of intensity is found. The increase here may be due to absolute-magnitude effect.
	Mg–Md	All lines are stronger in the spectrum of the M giant. This again may be an absolute-magnitude effect.
Eu II *Nd* II	⊙–Kg	All lines are considerably strengthened in the K giant, particularly those of *Eu* II.
	Kg–Mg	The lines of *Eu* II show little, if any, change in intensity, while the lines of *Nd* II are slightly strengthened in the M giant.
	Kg–Kd	All lines are considerably strengthened in the giant, particularly those of *Eu* II.
	Mg–Md	All lines are slightly strengthened in the giant.
Ce II, *Pr* II, *Sm* II, *Gd* II, *Dy* II, *Lu* II	⊙–Kg	All lines are strengthened in the K giant.
	Kg–Mg	A few lines are slightly strengthened in the giant, the majority show no change in intensity.
	Kg–Kd	All lines are strengthened in the giant.
	Mg–Md	All lines are slightly strengthened in the giant.
Yb I	⊙–Kg	Several lines indicate a strengthening in the K giant.
	Kg–Mg	Several lines indicate a strengthening in the M giant.
	Kg–Kd	No difference noted.
	Mg–Md	Two lines are strengthened in the dwarf.
CH	⊙–Kg	The $^2\Delta-{}^2\Pi$ band at λ 4300 is considerably stronger in the sun.
	Kg–Mg	This band is stronger in the K giant.
	Kg–Kd Mg–Md	This band is stronger in the dwarf stars.
CN	⊙–Kg	The $^2\Sigma-{}^2\Sigma$ (0, 1) band is stronger in the K giant.
	Kg–Mg	This band is stronger in the M giant.
	Kg–Kd	The $^2\Sigma-{}^2\Sigma$ (0, 0) band is stronger in the dwarf, while the $^2\Sigma-{}^2\Sigma$ (0, 1) band is stronger in the giant.
	Mg–Md	The $^2\Sigma-{}^2\Sigma$ (0, 1) band is stronger in the giant.

IV. DISCUSSION

The behavior of the various atoms as outlined in the preceding section is self-explanatory; however, a few points are particularly noted. The atoms of *Na* I, *Ca* I, *Sr* II, and *Ba* II clearly show absolute-magnitude effects. The increase in intensity of *Cb* I is also very great in the M giants as well as that of the *V* I lines.

The effect of high- and low-excitation potentials is particularly well demonstrated in the behavior of *Mg* I, *Cr* I, *Cr* II, *Mn* I, *Fe* I, *Co* I, and *Ni* I. At given values of the potential, the intensity of the lines changes from an increase in the giant to an increase in the dwarf.

The behavior of *La* II and the singly ionized rare earths indicates a need for further study in other stars of late spectral type. According to the present investigation, the intensity changes can be explained on the basis of absolute-magnitude effect or of an excess of these atoms in the atmosphere of α Bootis. The relative sensitivity of the various atoms shows first *La* II, then *Eu* II and *Nd* II, and then the others. In a study of the K stars alone, this was indicated but not so definite as is now shown.

The behavior of the $^2\Sigma-{}^2\Sigma$ (0, 0) band of *CN* has been discussed[1] and requires further investigation.

Acknowledgment is made to Drs. Walter S. Adams and Paul W. Merrill for suggestions with regard to this work. A portion of this work was completed with the aid of a fellowship from the National Research Council.

INTENSITIES OF THE INTERSTELLAR BAND AT λ 4430

DOUGLAS DUKE
Yerkes Observatory
Received June 16, 1950

ABSTRACT

The central absorption of the broad interstellar band centered near λ 4430 has been measured in some four hundred stars. When combined with spectroscopic parallaxes for the same stars, this material has made possible an investigation of the relationship between band intensity, on the one hand, and color excess and interstellar line intensity, on the other. A good correlation with color excess is found, and a much weaker one with distance; the correlation with the intensity of the interstellar D lines is intermediate between the other two. The band absorption appears to occur, in general, in regions where interstellar reddening is found; there are, however, some exceptions to the very close relationship between band absorption and reddening which seems to exist for the majority of the stars observed.

I. INTRODUCTION

The intensity of the band near λ 4430 has received less attention than that of other interstellar features. Its extreme broadness tends to mask the fact that its total absorption is three to five times that of the interstellar D and K lines. Since the announcement of the band's discovery by P. W. Merrill,[1] C. S. Beals and G. H. Blanchet,[2] F. Sherman,[3] E. H. Baker,[4] and J. Greenstein and L. H. Aller[5] have discussed its intensity. Not more than forty stars are dealt with in any one of these papers, and accurate intensities of the λ 4430 band are known for less than one hundred stars. Most of these are relatively bright objects. This lack of information has made it difficult to generalize about the behavior of the feature with respect to other interstellar parameters.

For these reasons a comprehensive program of observation of early-type stars was undertaken. To test all possible correlations, stars were chosen according to many independent criteria, including large distance modulus, large color excess, availability of other interstellar line measures, and galactic latitude. The extreme broadness of the feature, which makes it difficult to notice the band visually, also makes it possible to study its intensity on low-dispersion plates. Errors due to the finite slit-width in the spectrograph and microphotometer are negligible. In order to obtain the spectroscopic absolute magnitude and hence the distance modulus of a star at the same time as its band intensity, the use of the 6-inch camera attached to the small one-prism spectrograph of the 40-inch refractor of the Yerkes Observatory was decided upon. This combination gives a dispersion of 123 A/mm at λ 4340. Eastman II*a*-O plates were used.

Most of the authors mentioned above used the equivalent width of the band as a measure of its intensity. Only Baker[4] considers the central absorption. Since the band is extremely broad, of the order of 60 A,[5] there are many cases in which it is blended with stellar features. Thus the wings of the band are rather indeterminate. This is especially true in stars of types B0–B2, in which the *O* II lines in the neighborhood of λ 4416 interfere seriously with the determination of the depth of the violet wing of the band. In addition, an error in the location of the stellar continuum enters in approximately the second power in the determination of the equivalent width, but only in the first power in the determination of the central intensity. For these reasons, it seemed preferable to determine the central intensity of the band for this program.

Each plate was calibrated with a tube photometer. In each spectrum the region from

[1] *Mt. W. Contr.*, No. 536; *Ap. J.*, **83**, 126, 1936.
[2] *M.N.*, **98**, 398, 1938.
[3] *Ap. J.*, **90**, 630, 1939.
[4] *Edinburgh Pub.*, **1**, 15, 1949.
[5] *Ap. J.*, **111**, 328, 1950.

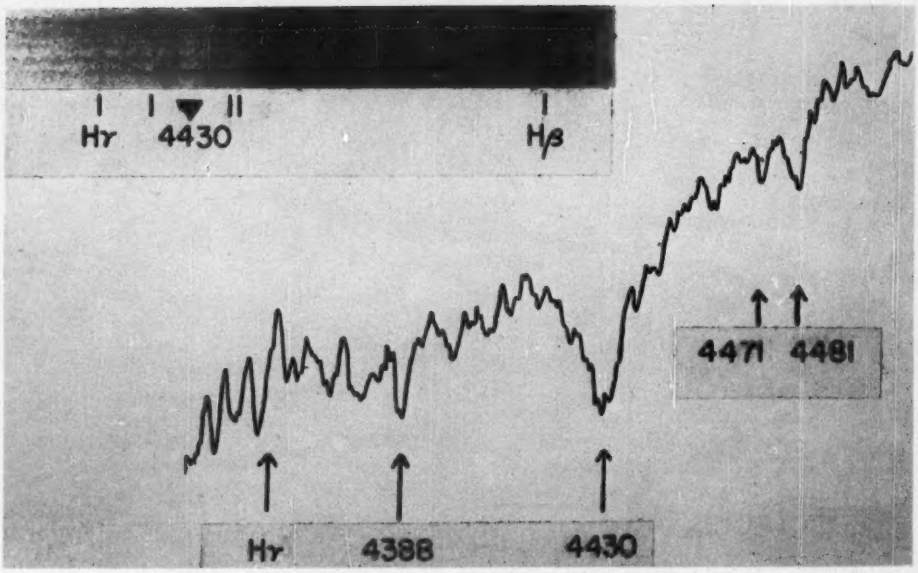

FIG. 1.—The band at λ 4430 in HD 168607; *above*, a spectrogram; *below*, a microphotometer tracing

λ 4250 to λ 4600 was traced at a magnification of one hundred times by means of the photoelectric microphotometer of the Yerkes Observatory. The low-dispersion spectra which are taken at Yerkes for the determination of spectroscopic parallaxes of early-type stars are quite wide, in order to make clearly visible the faint lines of these objects. Since, in general, only one spectrum of each star was available, advantage was taken of the width of the spectra by tracing each half independently. Although this procedure enhances the effect of plate grain, its use provides a check on the results and avoids errors due to imperfections in the plates. Also, the agreement between the two tracings allows a determination of the internal precision of each measure. A reproduction of a spectrogram and of a microphotometer tracing are given in Figure 1.

II. THE CATALOGUE OF THE INTENSITY OF λ 4430 IN 405 STARS

The first column in Table 1 contains the number of the star in the *Henry Draper Catalogue* or the *Henry Draper Extension*. A few stars not in these catalogues are identified in the notes. The second column gives the apparent visual magnitude of the star. Most of these are taken from the catalogue of 1332 B stars.[6] For other objects, either the source of the magnitude is the *Henry Draper Catalogue*, or it is mentioned in the notes.

The spectral types on the system of the Yerkes spectral atlas and spectroscopic distance moduli, corrected for interstellar absorption by an amount equal to seven times the color excess on the system used in the catalogue of 1332 B stars,[6] have been given by Dr. W. W. Morgan[7] or Miss Jane Ramsey[8] for almost all the stars on this program. For the remaining stars, which are indicated by a single asterisk in the last column, these were determined by the author. The data are given in the third and fourth columns of Table 1. For stars for which accurate color excesses are not available, the apparent distance moduli are given in parentheses. No dependable luminosity criteria are known for stars earlier in type than O9. Therefore, the absolute magnitude − 5.0 was adopted for all the early O stars, and the uncertainty in the resulting distance moduli has been indicated by the colons. The probable errors of such an assumption probably do not exceed 1 mag., an uncertainty which does not compare too unfavorably with the determinations for the other types.

The fifth column contains the color excesses of the stars in the color system of the Stebbins, Huffer, and Whitford catalogue of 1332 B stars.[6] Dr. Morgan has suggested that the normal colors for stars of types O–B3 are 0.04 mag. bluer than those used by these authors[9] and that smaller corrections be applied between B5 and B8. In addition, largely on the basis of the observed color of α Cygni, the A-type supergiants (through class A2) seem to be bluer than the dwarfs of the same spectral type; the correction amounts to − 0.05 in the case of the A2 supergiants. Bidelman[10] has mentioned this in his work on the Double Cluster, h and χ Persei. The values of the color excesses given in Table 1 were obtained by subtracting the revised normal colors from the observed colors given in the 1332 B-star catalogue.[6] Several cases in which an estimate of the color is obtained from other sources are indicated by "R" and are discussed in the notes.

The sixth column gives the measured central intensity of the band as the percentage absorption of the continuous spectrum at the same wave length. For very small absorptions the accidental errors become equal to, or greater than, the measured quantity, and most of the determinations of intensities less than 3 per cent are subject to con-

[6] J. Stebbins, C. M. Huffer, and A. E. Whitford, *Mt. W. Contr.*, No. 621; *Ap. J.*, **91**, 20, 1940.

[7] Unpublished. Dr. Morgan has kindly determined preliminary spectral types and luminosities expressly for this investigation.

[8] *Ap. J.*, **111**, 434, 1950.

[9] Other references to this matter are by Oort, *B.A.N.*, Vol. **8**, No. 308, 1938; and van Rhijn, *Groningen Pub.*, No. 51, 1946.

[10] *Ap. J.*, **98**, 61, 1943.

TABLE 1

STARS OBSERVED FOR INTENSITY OF INTERSTELLAR BAND NEAR λ 4430

HD	m_v	Sp.	True $m-M$	E_1 (Mag.)	A_v 4430	Wt.	Notes
108	7.36	O8fp	10.5:	+0.27	7.0	B	
1337	6.12	O9	10.1	+ .07	3.0:	C	
1383	7.8	B1	10.7	+ .23	9.4	C	
1478	7.93	B8:	(10.4)	.....	3.5	B	
1544	8.5	B0:	11.6:	+ .20	12.6	B	
1743	8.7	B0	11.7	+ .23	7.3	B	
1810	8.4	B0.5	10.1:	+ .21	6.5	B	
1976	5.36	B3	6.7	+ .07	4.0	F	
2789	8.3	B2e:	.....	+ .29	6.2	B	
2905	4.24	B1	10.3	+ .16	7.6	B	
3191	8.7	B1:	10.1	+ .29	10.4	A	
3360	3.72	B2	6.6	+ .02	3.0:	C	
3901	4.85	B3	6.2	+ .07	2.0:	F	
3940	7.40	A1	12.1	+ .33	13.0	C	
4142	5.55	B5	6.5	+ .01	2.0:	F	
4180	4.70	B3	7.1	+ .09	2.0:	C	
4717	8.2	A0	11.7	+ .28	7.8	A	
4727	4.42	B5	5.3	+ .02	0	A	
4768	7.9	B5	12.5	+ .26	7.5	B	
4841	7.07	B5	11.7	+ .34	11.0	B	
5458	9.1	B5p	8.9	+ .17	10.8	B	R
5551	7.7	B2	12.4	+ .37	12.4	A	
6300	6.50	B3	7.8	+ .07	2.0:	F	
6675	7.1	B0.5	10.7	+ .20	4.0	B	
7103	8.4	B3	11.2	+ .38	11.0	B	
7252	7.26	B1	9.1	+ .15	7.3	B	
7636	7.6:	B3e	.....	+ .13	5.0	C	R
7902	7.2	B6.5	12.3	+ .20	11.0	D	
9105	7.46	B5	11.4	+ .36	12.0	B	
9311	7.26	B5	11.5	+ .27	9.0	B	
.....	8.7	B3e:	8.5	+ .46:	11.8	B	MWC 14
10898	7.4	B2	11.8:	+ .23	7.4	A	*
12301	5.62	B8	9.9	+ .18	7.0	C	
12953	5.90	A1	11.8	+ .16	7.6	B	
13267	6.36	B5	11.4	+ .19	7.4	B	
13402	8.2:	B0.5:	11.3:	+ .34:	13.8	A	R
13476	6.50	A2	10.2	+ .26	8.2	C	
13621	8.06	B1	(11.1)	.....	5.5	A	
13744	7.8	A0	12.6	+ .31	8.9	A	
13745	7.96	B0	11.4	+ .17	8.5	B	
13841	7.21	B2	13.3	+ .17	8.3	B	
13854	6.42	B1	11.4	+ .21	11.1	A	
13866	7.4	B2	11.9	+ .18	4.4	B	
14010	7.05	B9	12.5	+ .22	7.8	A	
14052	7.98	B1	11.4	.....	8.1	B	**
.....	8.4:	B1	11.4	.....	9.2	F	+56°527**
14134	6.66	B3	11.3	+ .26	8.8	B	
14143	6.66	B2	11.5	+ .30	9.5	B	
14322	6.84	B8	11.4	+ .13	7.3	A	
14433	6.54	A1	11.9	+ .23	8.0	C	
14489	5.22	A2	9.7	+ .14	7.5	B	
14535	7.46	A1	12.3	+ .31	7.9	C	
14542	6.95	B8	12.2	+ .30	9.6	A	
14633	7.3	O9	11.8	− .03	2.0:	C	
14818	6.24	B2	11.3	+ .30	8.2	B	
14899	7.38	B8	11.4	.....	7.8	B	**
14947	8.04	O5f	(12.0:)	.....	15.5:	F	
14951	5.53	B5	6.4	+0.02	2.0:	F	

TABLE 1—*Continued*

HD	m_v	Sp.	True $m-M$	E_1 (Mag.)	A_e 4430	Wt.	Notes
14956	7.32	B2	11.7	+0.40	11.8	A	
15316	7.30	A2	10.0	+ .40	9.0	C	
15497	7.20	B7	11.4	+ .41	10.2	B	
15558	7.82	O6	10.1:	+ .39	12.4	B	
15570	8.0:	O5f	9.7:	+ .47	15.0	B	
15690	7.7:	B2	9.8	+ .42	9.5	B	
15752	8.8	B0.5:	11.3:	+ .35:	11.5	C	*
16243	8.4	B2	11.0	+ .35	12.0	C	
16310	8.4:	B0.5	11.4	.....	10.4	C	**
16778	7.71	A2	11.3	+ .49	9.3	B	
17036	5.80	B9	6.7	+ .01	3.5:	F	
17088	7.54	B9	12.0	+ .37	11.2	B	
17145	8.0:	B6.5	10.7	+ .45	14.5	B	
17505	7.11	O7	10.1:	+ .28	11.2	B	
17857	7.78	B8	11.3	+ .29	10.4	A	
18326	7.91	O8	10.7:	+ .32	9.3	B	
19243	6.54	B2e	.....	+ .30	8.0	A	
19820	7.09	O8	10.6	+ .36	11.0	C	R
20041	5.92	A0	10.9	+ .29	12.5	C	
21212	8.3	B2e	.....	+ .35	11.0	A	R
21389	4.76	A0	10.1	+ .24	7.9	B	
21483	7.06	B3	8.2	+ .34	6.0	B	
21856	5.80	B2	7.1	+ .10	6.0	F	
22253	6.79	B0.5	9.3	+ .22	5.9	F	*
22298	7.8	B2:	.....	+ .30	11.2	C	*
22951	5.04	B1	7.1	+ .15	3.0:	F	
23180	3.94	B1	7.1	+ .17	3.0	B	
23288	5.43	B8	6.3	+ .02	1.0:	C	
23302	3.81	B6	6.3	+ .05	1.0:	C	
23338	4.37	B6	6.3	+ .04	0	C	
23408	4.02	B7	6.3	+ .03	1.0:	C	
23478	6.51	B3	7.1	+ .21	4.2	C	
23630	2.96	B7	6.3	+ .01	1.0:	C	
23675	6.76	B0.5	8.0	+ .34	11.6	B	
24131	5.73	B1	7.1	+ .17	4.3	F	
24398	2.91	B1	7.1	+ .21	4.1	B	
24431	6.70	O8	9.8:	+ .27	7.5	F	
24432	7.02	B5	10.5	+ .29	12.6	A	
24640	5.48	B2	7.1	+ .12	5.7	B	
24760	2.96	B0.5	5.7	+ .06	3.8	B	
24912	4.05	O7	7.1	+ .13	7.2	A	
25090	7.28	B1	9.2	+ .29	9.3	B	
25443	6.75	B0.5	8.8	+ .28	5.8	C	
25539	6.70	B3	7.1	+ .17	4.5	B	
25558	5.33	B3	6.6	+ .08	5.5	F	
25638	7.0	B0	9.6	+ .34:	11.0	F	R
25799	6.87	B3	7.1	+ .15	4.5	F	
25833	6.61	B5	7.1	+ .12	4.5	B	R
25914	8.1	B5	12.8	+ .33	13.6	B	
25940	4.03	B3	6.3	+ .09	3.4	F	
26912	4.32	B3	5.7	+ .09	5.8	F	
27396	4.89	B3	6.0	+ .10	3.0:	C	
27795	7.16	B2	9.4	+ .26	7.0	C	
29309	7.1	B3	(9.1)	.....	7.0	F	
30614	4.38	O9.5	10.0	+ .13	3.4	B	
30836	3.78	B2	7.5	+ .04	1.0:	C	
31327	6.18	B2	8.9	+ 32	7.8	B	
31617	7.34	B2	9.4	+ .14	5.2	C	
32481	8.1	B3p	7.6	+ .27	9.3	C	R
32630	3.28	B3	4.0	+0.03	1.0:	C	

TABLE 1—*Continued*

HD	m_v	Sp.	True $m-M$	E_1 (Mag.)	A_e 4430	Wt.	Notes
34078	5.81	O9.5	8.5	+0.20	6.8	A	
34085	0.34	B8	7.5	+ .00	0	B	
34656	6.71	O7	10.2:	+ .21	5.8	A	
35395	6.83	B0.5	8.9	+ .28	9.2	F	
35708	4.83	B2	7.6	+ .05	5.5	B	
35921	6.71	O9.5	9.5	+ .25	12.0	B	
36371	4.88	B3	8.8	+ .23	7.9	A	
36486	2.48	O9.5	7.5	+ .04	1.0:	C	
36510	4.64	B0	7.5	+ .08	0	C	
36576	5.50	B2	7.1	+ .13	6.0	F	
36819	5.28	B2	6.7	+ .09	4.0	F	*
36861	3.66	O8	8.3:	+ .05	2.0:	C	
37022	5.36	O6	7.5	+ .25	2.5	A	
37041	5.17	O9.5	7.5	+ .11	2.0:	B	
37043	2.87	O9	7.5	+ .04	0	B	
37061	6.8	B1p	.....	+ .25:	6.0	B	R
37128	1.75	B0	7.8	+ .06	0	B	
37468	3.78	O9.5	7.5	+ .11	0	A	
37742	2.05	O9.5	7.5	+ .05	1.0:	C	
38771	2.20	B0.5	7.5	+ .10	2.0:	C	
40005	6.91	B2	8.2	+ .10	4.8	D	*
40111	4.90	B0.5	9.2	+ .10	5.5	F	
41117	4.71	B2	10.4	+ .22	8.6	B	
41398	7.45	B2:	11.9:	+ .22	11.0	C	*
42087	5.76	B2.5	10.2	+ .19	7.6	B	
42088	7.40	O6	11.4:	+ .14	4.5	D	
42560	4.35	B3	5.9	+ .03	1.0:	C	
43384	6.26	B3	10.1	+ .24	10.0	A	
43818	7.03	B0.5	10.2	+ .26	9.2	F	
43836	7.03	B9	9.4	+ .23	8.8	B	
46056	7.96	O8	11.5:	+ .21	10.5	D	R
46106	8.06	B0	.....	+ .26:	10.0	C	R
46149	7.66	O8	11.4:	+ .18	9.5	C	R
46150	6.80	O6	10.2:	+ .23	9.0	B	R
46202	8.16	O9	11.0	+ .17	10.5	F	R
46223	7.14	O5	10.5:	+ .23	9.6	B	R
47129	6.06	O8	10.1:	+ .15	4.2	B	
47240	6.16	B1	9.3	+ .19	8.6	D	
47432	6.13	O9.5	9.5	+ .22	5.5	B	
48279	7.4	O8	10.6:	+ .25	7.0	C	
48434	5.78	B0	9.6	+ .11	4.4	A	
51309	4.39	B3	8.2	.....	2.5:	C	
52382	6.36	B1	10.5	+ .20	8.0	D	
53138	3.12	B3	8.9	.....	2.0:	F	
53367	7.01	B1e:	7.7	+ .31	4.8	C	
53975	6.40	O8	10.8:	+ .08	4.0	C	
54662	6.20	O7	10.4:	+ .12	5.0	B	
55879	5.99	O9.5	10.3	+ .04	1.0:	F	
57061	4.40	O9	9.0	+ .02	1.0:	F	
58050	6.37	B2	10.1	+ .05	3.8	F	
58343	5.20	B3	6.4	+ .09	5.5	F	
58350	2.43	B5	8.7	.....	2.5	D	
63462	4.59	B0.5	7.1	+ .08	3.5	F	
67880	5.54	B3	6.8	+ .08	3.0:	F	
76510	8.0	B1	11.3:	+ .02	3.0:	F	
78584	8.05	B5	9.4:	+ .03	0	B	
87737	3.58	A0	8.0	− .04	1.0:	F	
89688	6.53	B3	8.0	+ .08	2.9	A	
91316	3.85	B1	9.0	+ .05	3.2	A	
93521	6.89	O8:	11.8:	+0.01	1.0:	C	

TABLE 1—*Continued*

HD	m_v	Sp.	True $m-M$	E_1 (Mag.)	A_c 4430	Wt.	Notes
97991	7.28	B2	8.7	+0.08	4.0	F	
119608	7.32	B1	(12.8)	.....	3.1	B	
121968	10.2	B3	11.2:	.....	1.0:	F	*
135485	8.3	B3	(10.3)	.....	5.0:	B	*
141637	4.77	B3	(6.2)	.....	3.4	B	
142114	4.66	B3	(6.2)	.....	2.5:	C	
144218	5.06	B2	6.4	+ .10	6.7	B	
144470	4.13	B1	6.5	+ .08	5.6	A	
145502	4.29	B2	6.4	+ .12	4.8	B	
147165	3.08	B1	6.5	+ .15	5.7	B	
147888	6.56	B5	6.1	+ .21	7.4	B	
147889	8.0	B2	6.3	+ .55	12.0	C	
147933	5.22	B2	6.3	+ .20:	8.2	C	R
148184	4.85	B2p	5.8	+ .22	8.4	F	
149363	7.9	B0.5	10.6	+ .12	6.8	B	
149757	2.70	O9.5	5.7	+ .14	8.8	B	
149881	6.59	B0.5	10.1	+ .07	2.0:	F	
154445	5.62	B2	7.8	+ .13	4.8	F	
156247	6.0	B6	7.0	+ .09	4.0	F	
157857	7.43	O7f	11.3:	+ .15	8.8	B	
158661	8.2	B0.5	11.8	+ .20	6.2	B	
160762	3.79	B3	5.6	+ .03	2.6	F	
161056	6.20	B2	6.2	+ .29	10.4	F	
161961	7.9	B0.5	10.4	+ .22	8.0	F	*
163472	5.73	B2	7.6	+ .16	6.5	D	
163800	6.92	O8	10.0:	+ .27	7.8	B	*
164284	4.81	B2	6.6	+ .10	5.1	F	
164353	3.92	B5	8.9	+ .08	5.4	F	
164402	5.73	O9.5	10.6	+ .13	3.6	B	*
164492	6.91	O8	9.8:	+ .30	6.5	F	
164794	5.86	O5	10.1:	+ .12	4.0	F	
165049	8.07	B2	9.9	+ .33	7.1	C	
165174	6.09	B0	9.1	+ .14	5.2	D	
165319	8.2	B0	12.1	+ .37	14.5	C	
165516	6.22	B1	10.7	+ .16	12.0	C	
165998	8.5	A0:	.....	+ .36:	13.0:	F	*
166182	4.32	B2	7.3	+ .04	2.4	B	
166286	7.58	B1	10.2	+ .25	5.7	C	
166287	7.6	B1	10.6	+ .22	8.2	F	
166540	8.0	B0.5	10.5	+ .22	5.9	F	
166546	7.17	O9	10.2	+ .14	7.8	C	
166628	7.14	B3	10.8	+ .40	14.2	B	
166689	7.34	B1	11.2	+ .16	11.0:	F	
166937	4.0	B8p	(11.0)	.....	6.0	B	
167224	7.9	B2	11.0	+ .14	5.8	B	
167264	5.42	B0	11.0	+ .13	6.0	A	
167263	6.02	O9	10.8	+ .13	8.0	B	
167287	7.0	B0.5	10.3	+ .17	6.8	B	
167375	8.5:	B2	10.5:	+ .14:	7.0	C	R
167659	7.3	O7	10.8:	+ .22	6.3	B	
167771	6.37	O8	10.3:	+ .16	7.2	B	
167815	7.59	B0	10.2:	+ .20	7.4	F	
167838	6.64	B5	11.7	+ .28	17.4	B	
167863	6.57	B8	9.3	+ .04	1.0:	C	
167971	7.34	O8f	8.8:	+ .50	17.6	C	
168021AB	6.9	B0	11.0	+ .23:	9.7	B	R
168607	8.1:	B8	8.8:	+ .90:	22.0	B	*R
168625	8.4:	B2	.....	+ .90:	19.5	F	R
168797	6.04	B3	8.3	+ .11	3.2	B	
169033	5.73	B8	6.0	+0.04	7.1	C	

TABLE 1—*Continued*

HD	m_v	Sp.	True $m-M$	E_1 (Mag.)	A_e 4430	Wt.	Notes
169034	8.6	B3	10.3	+0.68	15.0	F	
169454	6.84	B1	10.3	+ .54	12.0	C	
169753	7.8	B3	9.6	+ .43	10.5	B	
170235	6.23	B2	7.1	+ .16	5.0	B	
170580	6.50	B2	7.3	+ .17	5.5	F	
170650	5.72	B5	8.9	+ .04	3.0:	F	
170714	7.31	B3	7.0	+ .27	5.8	B	
170740	5.80	B2	6.4	+ .27	8.1	B	
170938	8.1	B1	11.6	+ .53	11.5	F	
171012	6.98	B0.5	10.8	+ .32	12.8	C	
171871	7.39	B2	10.8	+ .10	2.0:	F	
172175	9.7	O6f	11.9:	+ .40	8.0:	F	*
173087	6.12	B3	7.0:	+ .08	4.5	F	*
174179	5.78	B3	8.6	+ .02	2.0:	C	
174585	5.77	B2	7.5	+ .05	2.0	F	
175754	7.03	O8	11.5:	+ .07	2.0:	C	
175876	6.73	O6	11.2:	+ .07	6.0	C	
176162	5.36	B5	5.8	+ .08	4.6	B	
176304	6.52	B3	7.0	+ .21	8.3	F	
176818	6.86	B2	8.7	+ .18	7.0	B	
176819	6.55	B2	7.8	+ .18	6.4	C	
176853	6.68	B3	(8.2)	.....	9.2	D	
176871	5.50	B6	7.0	+ .05	3.3	B	
177109	6.22	B5	7.3	+ .06	2.9	F	
177284	9.2	B0p	12.1:	+ .16	11.0	F	
178129	7.8	B5	12.3	+ .27	13.0	A	
178175	5.41	B2e	7.1	+ .11	7.2	B	
179406	5.37	B3	5.7	+ .19	5.4	B	
180126	8.2	B3p	.....	+ .19	3.8	F	R
180554	4.60	B5	5.6	+ .06	2.0:	F	
180968	5.40	B0.5	8.1	+ .14	6.0	F	
181409	6.32	B2	8.9	+ .04	2.8	F	
183143	6.93	B6.5	10.3	+ .55	16.8	B	
183362	6.36	B3	7.8	+ .05	3.0:	C	
184279	6.78	B0.5	9.8	+ .07	7.2	B	
184915	5.04	B0.5	8.1	+ .12	4.0	F	
185507	5.17	B2	6.7	+ .14	3.0	B	
185859	6.44	B0.5	10.3	+ .30	9.8	D	
185915	6.41	B6	6.9:	+ .07	6.0	B	
186980	7.28	O8	11.2:	+ .16	4.1	A	
187320	7.5	B2	10.6	+ .14	7.0	B	
187459	6.35	B0.5	10.0	+ .20	3.2	D	
187567	6.39	B2e	.....	+ .10	2.5	B	R
187879	5.62	B1	8.4	+ .11	4.2	D	
188001	6.29	O6f	10.1:	+ .17	4.6	B	
188209	5.51	O9.5	11.3	+ .10	2.0:	C	
188252	5.70	B2	9.3	+ .06	2.5:	C	
188439	6.15	B0.5	9.7	+ .07	2.0:	F	
188892	4.87	B5	7.7	+ .02	3.5	C	
189066	6.04	B5	7.1	+ .02	2.0:	C	
189178	5.43	B5	8.2	+ .04	3.0	B	
189687	5.15	B3	6.5	+ .07	3.8	F	
190066	6.55	B0.5	9.6	+ .20	6.0	F	
190429br	7.2	O5f	.....	.....	10.5	B	
190429ft	7.8	O9p	.....	.....	10.5	B	
227460	9.9	B1:	9.1:	+ .53	8.0:	F	
190603	5.69	B1.5	10.2	+ .38	10.3	A	
190864	7.8	O6	11.4:	+ .20	8.6	A	
190918	7.01	W+O9:	.....	.....	9.2	A	
190919	7.30	B1	10.6	+0.25	6.2	F	

TABLE 1—*Continued*

HD	m_v	Sp.	True $m-M$	E_1 (Mag.)	A_e 4430	Wt.	Notes
191201	7.12	B0	10.4	+0.19	6.8	A	
191610	4.82	B3	6.4	+ .03	2.0:	C	
191612	7.8	O8	11.0:	+ .25	6.3	A	
228053	8.9	B1	11.2	+ .32	8.5	B	
191746	6.94	B2	8.1	+ .12	3.0	F	
191877	6.11	B1	9.2	+ .13	5.3	F	
192281	7.47	O5f	10.1:	+ .34	7.1	B	
192422	7.10	B0.5	9.4	+ .31	6.0	A	
192639	7.02	O8f	9.9:	+ .30	7.5	B	
193007	8.0	B0.5	.....	.....	6.8	B	
193009	7.02	B2e	.....	+ .18	6.1:	F	
193183	7.12	B1.5	10.3	+ .33	6.5	B	
193237	4.88	Bp	.....	+ .30	7.2	C	P Cyg
193322	5.82	O9	8.9	+ .20	5.2	B	
228841	9.1	O7	11.5:	+ .37	13.5	C	
193426	8.0	B9	(13.5)	.....	14.8	D	
193514	7.29	O8f	9.7:	+ .37	9.0	B	
193536	6.28	B2	8.3	+ .07	3.0:	C	
193793	6.83	WR	.....	.....	8.8	C	
229059	10.2	B1p:	.....	.....	16.0	D	R
194279	7.05	B2	10.3	+ .57	16.5	A	
194335	5.68	B2	9.7	+ .06	1.0:	F	
194839	7.45	B0	9.8	+ .60	12.2	C	
195089	7.24	B3	7.9	+ .11	4.0	C	
195556	4.89	B2	6.9	+ .07	2.5	F	
195592	7.15	O9	9.7	+ .57	11.5	B	
196775	5.92	B3	7.4	+ .05	4.0	C	
197345	1.33	A2	8.5	.00	1.0:	C	
197770	6.36	B2	7.6	+ .27	6.0	B	
198478	4.89	B3	9.4	+ .28	10.2	B	
198846	7.1	O9.5	10.7	+ .14	4.6	C	
198895	8.26	B3	7.1	+ .37	7.5	B	
199140	6.44	B2	10.0	+ .06	2.0:	C	
199216	7.13	B1	9.1	+ .36	6.9	A	
199478	5.76	B8	11.4	+ .22	6.5	B	
199579	6.01	O6	9.0	+ .15	5.4	B	
200120	4.86	B1:	7.7:	+ .03	1.0:	C	
200775	7.20	B3e	.....	+ .30	1.0:	C	
200857	7.16	B3	7.9	+ .39	8.4	C	
201819	6.40	B0	10.3	+ .08	5.1:	F	
202214	5.65	B1:	7.4:	+ .17	6.0	B	
202850	4.28	B9	10.2	+ .07	4.0:	F	
203025	6.41	B3	7.9	+ .21	6.2	B	
203064	5.06	O7	9.3:	+ .11	6.2	F	
203938	7.10	B1	7.6	+ .38	10.0	B	
204172	5.84	B0	10.9	+ .07	2.0:	F	
204403	5.20	B3	8.8	+ .05	1.5	F	
204827	8.3	B0	8.9	+ .41	6.5	B	
205139	5.52	B1	8.8	+ .17	6.7	F	
205196	7.36	B0	10.2	+ .41	9.9	B	
206165	4.87	B2	8.9	+ .26	7.2	A	
206183	7.6	O9	10.5	+ .16	6.9	F	
206672	4.78	B3	7.3	+ .07	1.0:	C	
207198	5.97	O9	9.6	+ .30	8.2	A	
207260	4.46	A2	9.8	+ .26	4.0:	F	
207330	4.26	B3	6.8	+ .07	1.0:	C	
207538	7.03	B0	8.5	+ .29	8.6	A	
207563	6.16	B3	7.5	+ .07	4.5	B	
207673	6.49	A2	10.4	+0.23	6.2:	F	

TABLE 1—*Continued*

HD	m_v	Sp.	True $m-M$	E_1 (Mag.)	A_c 4430	Wt.	Notes
208185	7.7	B2	(9.7)	.....	9.6	B	
208392	7.10	B1:	9.3:	+0.25	8.0	B	
208501	6.01	B8	9.3	+ .39	8.3	B	
208947	6.28	B3	7.0	+ .10	5.6	B	
209339	6.48	B0	9.6	+ .14	5.8:	F	
209454	7.9	B2	8.6	+ .18	5.5	C	
209481	5.50	O9	9.3	+ .15	8.0	C	
209744	6.74	B1	7.9	+ .26	7.5	F	
209975	5.17	O9.5	9.9	+ .15	5.9	A	
210628	6.87	B3	7.0	+ .19	9.5	B	*
210809	7.6	O9.5	11.4	+ .21	8.5	A	
210839	5.19	O6f	8.6:	+ .23	5.6	B	
211924	5.35	B5	5.7	+ .16	4.6	F	
212076	4.93	B2	7.5	+ .08	2.1	F	
212455	8.0	B6	11.7	+ .27	9.8	B	
212571	4.64	B1	6.6	+ .07	2.0:	C	
212978	6.07	B2	8.1	+ .06	3.0	B	
213087	5.66	B0	8.8	+ .27	7.1	F	
213420	4.54	B2	7.0	+ .09	2.0:	C	
213757	8.0	B2	(10.0)	.....	7.0	B	
214080	6.69	B1	(11.9)	.....	3.9	F	
214168	5.83	B2	9.1	+ .10	2.2	B	
214432	7.4	B3	8.2	+ .08	2.5	B	
214680	4.91	O9	8.6	+ .04	1.0:	C	
214993	5.18	B2	8.9	+ .04	1.0:	C	
216014	6.83	B0:	8.8	+ .31	9.5	B	
216200	5.84	B3	6.7	+ .16	2.4	B	
216411	7.16	B1	11.6	+ .40	12.2	B	
216898	8.3	O8	10.8:	+ .36	14.4	C	
216916	5.54	B2	8.8	+ .07	4.0	B	
216927	8.7	B9	13.0	+ .38	14.5	B	
217050	5.20	B5e	.....	+ .03	4.0	D	*
217297	7.36	B2:	7.5	+ .25	9.4	A	
218342	7.46	B0	9.0	+ .36	10.1	C	
218376	4.93	B1	8.4	+ .07	4.2	F	
218674	6.53	B3	7.6	+ .13	5.8	B	
218915	7.06	O9	12.4	+ .17	5.0	B	
219188	6.93	B0.5	10.1	+ .12	3.8	F	
223385	5.61	A2	10.2	+ .34	8.5	B	
223960	6.98	B9	11.7	+ .33	12.4	A	
223987	7.56	B1	10.8	+ .33	10.4	C	
224055	7.16	B3	10.7	+ .43	14.0	A	
224151	6.05	B0.5	8.6	+ .20	5.5	F	
224424	8.4	B1	10.7	+ .46	12.6	B	
224868	7.36	B3p:	7.4	+ .17	6.5	B	
225094	6.26	B3	10.5	+ .25	12.5	B	
225146	8.6	B0	12.6	+ .24	18.4	B	
225160	8.2	O8	11.6:	+0.23	5.3:	F	

NOTES TO TABLE 1

5458 Spectrum may be composite.
7636 Pole-on star.
13402 Color estimated from spectral gradient as compared to other stars with measured colors.
19820 Distance modulus from an unpublished investigation of the color parallax of this star by the author (CC Cas).
21212 Pole-on star.
25638 Double star, color may be in error.
25833 Hydrogen lines very strong.
32481 Hydrogen lines very strong.

NOTES TO TABLE 1—*Continued*

37061 Bond 734, color estimated from spectral gradient by Baade and Minkowski, *Ap. J.*, 86, 123, 1937.

46056, 46106, 46149, 46150, 46202, 46223 These stars are members of a cluster of early-type stars and are believed all to lie at a distance corresponding to a modulus of about 11.0.

147933 Double star, color may be in error.

167375 Magnitude in HD given as 9.7. Magnitude estimated near 8.5 from visual inspection of field. Color excess of several near neighbors adopted also for this star.

168021AB Double star, color may be in error.

168607, 168625 Colors of these stars from Popper and Seyfert, *Pub. A.S.P.*, 52, 401, 1940, as is spectral type of 168625. This pair has the most reddening and 4430 intensity of all the stars in this investigation.

180126 Hydrogen lines very strong.

187567 Pole-on star.

229059 Photographic magnitude given. Red B star in Cygnus rift.

siderable uncertainty. In extremely uncertain cases in which the evidence pointed to the presence of λ 4430, the value 2.0: was assigned. If the evidence for the band was conflicting, the value 1.0: was given. Finally, in cases where the evidence indicated that λ 4430 was absent, the value 0 was assigned.

The seventh column contains an estimate of the precision of the observations of the band. These were derived from the agreement between the two tracings of each star and the amount of confidence placed in the location of the continuum and the central portion of the band. The designation "A" indicates that the probable error of the determination is less than 0.75 per cent of the intensity of the continuum. For probable errors between 0.75 per cent and 1.50 per cent of the intensity of the continuum, the weight is designated as "B," while for weight "C" the probable errors appear to be larger than 1.50 per cent. In addition, the weight designations "D" and "F" refer to measures on plates without calibration, which were taken for other purposes. If these plates contain spectra of stars which also appear on calibrated plates, a fair calibration can be obtained from the intensities of the helium lines near the interstellar band. Such measures have been designated by "D." The weight "F" has been given to measures which have been calibrated by assuming that the intensities of the helium lines are identical in all stars of the same spectral type and luminosity.

Although there do not appear to be any systematic errors in these values, there will certainly be relatively large accidental errors. Accordingly, these measures are of supplementary value only.

An "R" in the last column refers to a note at the end of the table; a double asterisk indicates that the distance modulus has been taken from Bidelman's study of the Double Cluster in Perseus.[10]

III. DISCUSSION

Figures 2 and 3 compare the values given in this paper with those of Baker[4] and of Greenstein and Aller.[5] The values given by Baker for seven O-type stars are undoubtedly of very high weight. For six of these stars the agreement of his results with those in this paper is very satisfactory. Likewise, the agreement of our results with those of Aller and Greenstein is good, except in a few instances. These observers have many plates of most of their stars, and they used a somewhat greater dispersion. On the other hand, as has been pointed out above, the determination of the equivalent width of λ 4430 is more difficult and susceptible to more errors than is the determination of its central intensity. In Figures 4 and 5 a comparison is made of the band intensity–color excess relations from the two papers. The results of Greenstein and Aller have been plotted in Figure 5 against

the improved color excesses of this paper. If we assume that the band intensities are directly proportional to the color excesses, then the spread observed in the intensities must be due to accidental errors. The mean error derived in this way is about 2 per cent, which agrees with the errors estimated from the internal agreement of the measures. This is actually an upper limit to the errors, since we do not know that there is a one-to-one correspondence between reddening and the intensity of λ 4430.

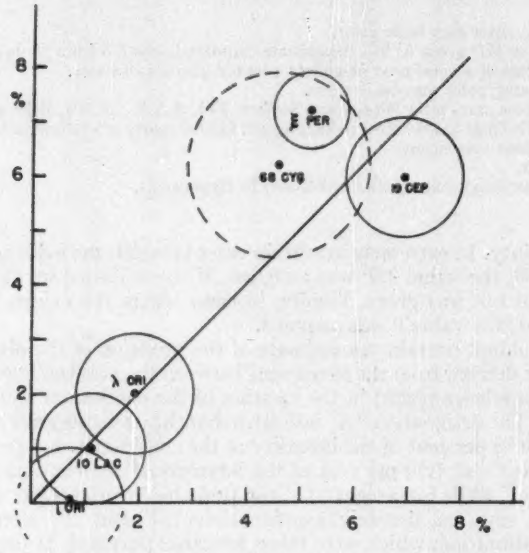

FIG. 2.—Comparison of the results of Baker (*abscissae*) and Duke (*ordinates*). The diameters of the circles indicate the probable error of the ordinates.

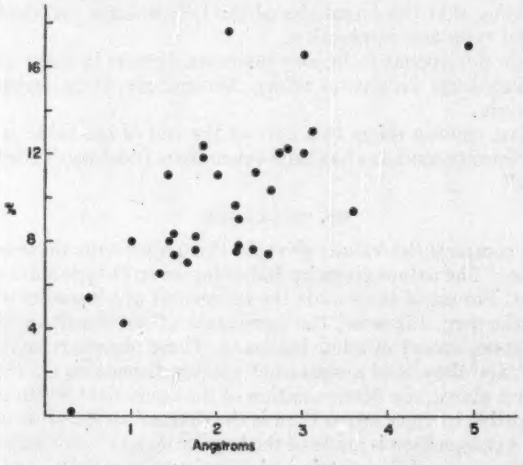

FIG. 3.—Comparison of the results of Greenstein and Aller (*abscissae*) and Duke (*ordinates*).

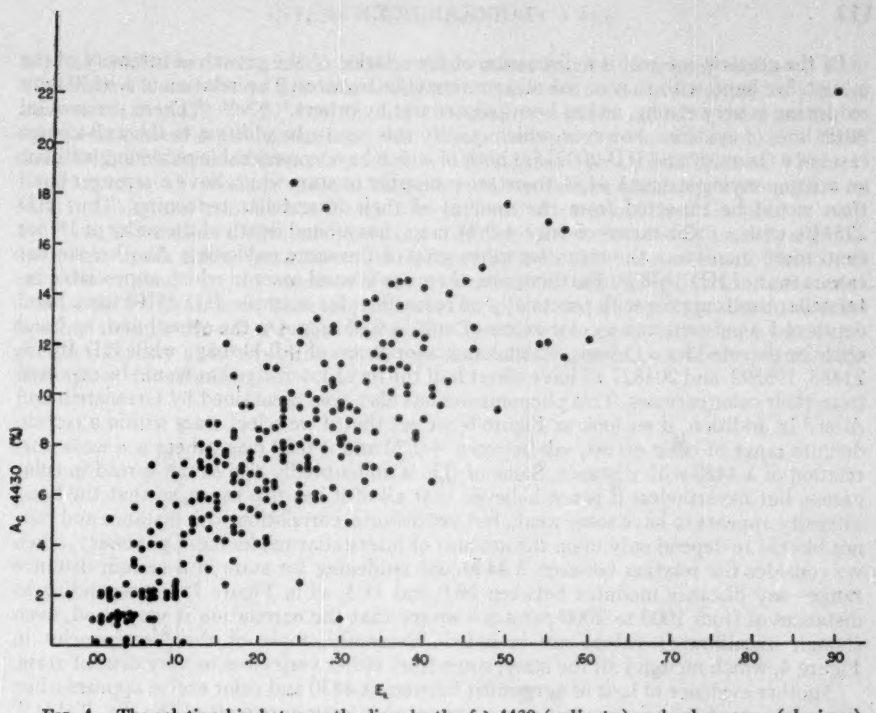

FIG. 4.—The relationship between the line depth of λ 4430 (*ordinates*) and color excess (*abscissae*) as determined from calibrated plates.

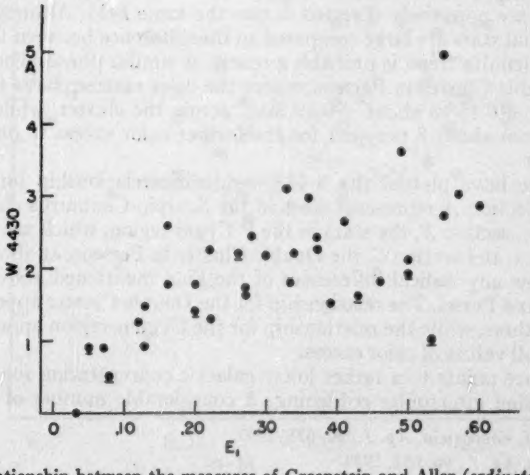

FIG. 5.—The relationship between the measures of Greenstein and Aller (*ordinates*) and color excess (*abscissae*). Underlined points refer to measures of single spectrograms.

Of the greatest interest is a discussion of the relation of the growth of intensity of the interstellar band with that of the other interstellar features. The relation of λ 4430 with reddening is very strong, as has been pointed out by others.[3, 4, 5, 11, 12] There are several other lines of evidence, however, which qualify this result. In addition to the well-known cases of θ Orionis[13] and HD 200775,[14] both of which have considerable reddening without an accompanying strong λ 4430, there are a number of stars which have a stronger band than would be expected from the amount of their interstellar reddening. Thus HD 225146, with a color excess of only +0.24 mag., has a band depth of the order of 18 per cent, more than twice the mean for other stars of the same reddening. Another similar case is that of HD 167838. Furthermore, there are several cases in which appreciable interstellar bands appear with practically no reddening; for example, HD 35708 has a band depth of 5.5 per cent and a color excess of only +0.05 mag. On the other hand, no band could be detected for σ Orionis, which has a color excess of +0.11 mag., while HD 16778, 21483, 195592, and 204827 all have about half the band intensity that would be expected from their color excesses. This phenomenon has also been mentioned by Greenstein and Aller.[5] In addition, if we look at Figure 6, we see that if we select stars within a certain definite range of color excess, say between +0.20 and +0.30 mag., there is a weak correlation of λ 4430 with distance. Some of this is undoubtedly due to the spread in color excess, but nevertheless it is not believed that all of it has this cause, so that the band intensity appears to have some weak, but yet definite, correlation with distance and cannot be said to depend only upon the amount of interstellar reddening. Conversely, when we consider the relation between λ 4430 and reddening for stars in a certain distance range—say distance modulus between 10.0 and 11.5, as in Figure 7, corresponding to distances of from 1000 to 2000 parsecs—we see that the correlation is very good, even though uncalibrated values are included. Evidently, most of the discrepancies in Figure 4, which includes all the stars, come from either very close or very distant stars.

Another evidence of lack of agreement between λ 4430 and color excess appears when the gradients of the two quantities are compared in certain regions of the sky. Table 2, extracted from the catalogue of stars in Table 1, contains the data for ten stars about 300 parsecs from the sun in a region about 4° in diameter at $l = 130°$, $b = -14°$ (the region near o Persei), arranged in order of increasing galactic latitude. We see that the gradients of the quantities are oppositely directed across the same field. Although the probable errors for individual stars are large compared to the difference between the smallest and largest values, a definite trend is probably present. A similar phenomenon occurs in the region of the Double Cluster in Perseus, where the color excesses have the considerable variation of from +0.15 to about +0.40 mag. across the cluster, while the intensities of λ 4430 vary from about 8 per cent for the former color excess to only 10 or 12 per cent for the latter.

In Figure 8 we have plotted the λ 4430-reddening relationship for three physical groups of stars. Section *A* represents stars in the Scorpio-Centaurus cluster, which are relatively near by; section *B*, the stars in the P Cygni region, which are at a distance of about 1000 parsecs; and section *C*, the Double Cluster in Perseus, at about 2000 parsecs. These do not show any radical differences of the kind mentioned above in connection with the stars near o Persei. The relationship for the Double Cluster appears to be a little flatter than the others, while the relationship for the Cygnus region appears to be a little lower for almost all values of color excess.

Further evidence points to a rather lower galactic concentration for λ 4430 than for the material causing interstellar reddening. A considerable number of distant stars at

[11] O. Struve and J. Greenstein, *Ap. J.*, **90**, 625, 1939.

[12] W. W. Morgan, *Ap. J.*, **90**, 632, 1939.

[13] W. W. Morgan, *A.J.*, **51**, 21, 1944.

[14] J. Greenstein, *Centennial Symposia* ("Harvard Observatory Monographs," No. 7, 1948).

large distances from the galactic plane and at various longitudes appear to show λ 4430 bands rather stronger than are comparable with their color excesses. Examples of this are ρ Leonis, HD 14633, 76510, 166182, and 175876. In addition, we have the presence of considerable band depth (about 6 per cent) in the two near-by dwarf B stars, HD 25558 and 26912, with color excesses of less than +0.10 mag. at a galactic latitude of −30°.

The stars of the various spectral classes appear to behave similarly with respect to band intensity and color excess. There is no evidence of a weakening of the band in very hot stars, as has been suspected. There is a slight indication that the Of stars as a group do not have such strong bands as would be expected from their color excesses. This could easily be explained by the presence of some circumstellar reddening due to the material causing the emission lines. The A supergiants exhibit greater scatter about the mean relationship than do the other types. The reason for this is not clear, but it may be due to greater difficulty in locating the continuum and central intensity in these spectra with their many metallic lines.

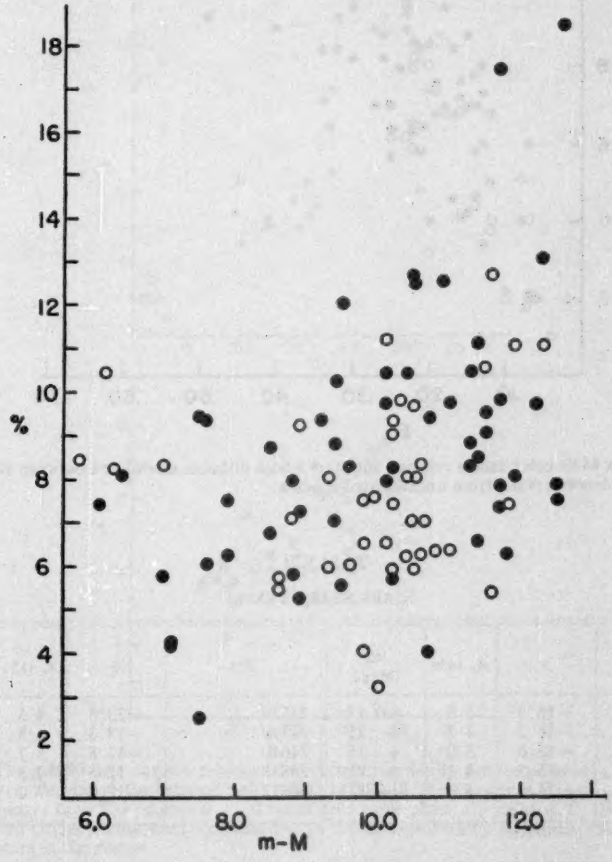

FIG. 6.—The λ 4430–distance modulus relation for all stars having a color excess between +0.20 and +0.30 mag. The open circles represent stars whose distance moduli are uncertain.

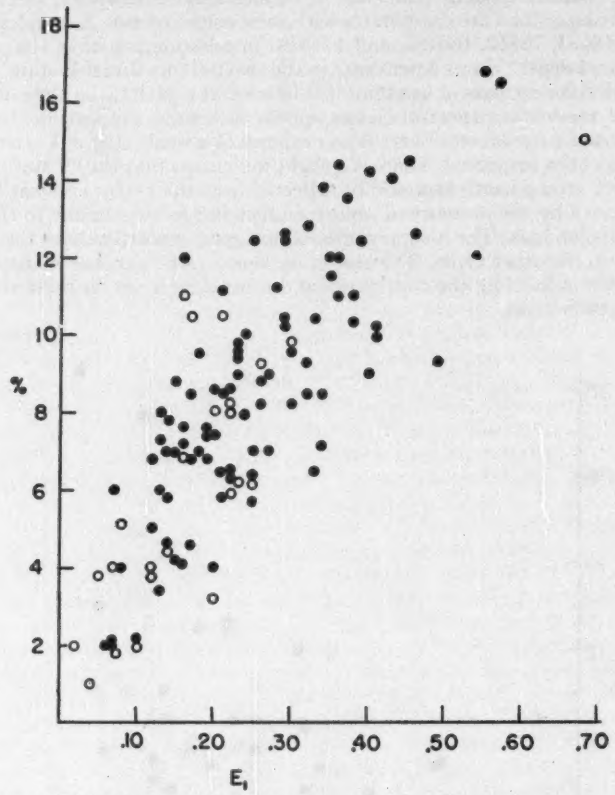

FIG. 7.—The λ 4430–color excess relation for stars whose distance moduli are between 10.0 and 11.5. The open circles denote results from uncalibrated spectra.

TABLE 2

STARS NEAR o PERSEI

HD	b	A_e 4430	E_1 (Mag.)	HD	b	A_e 4430	E_1 (Mag.)
23180	−16°6	3.0	+0.17	25539	−13°5	4.5	+0.17
23478	−16.2	4.2	+ .21	25799	−13.3	4.5:	+ .15
22951	−15.6	3.0:	+ .15	24640	−12.8	5.7	+ .12
24398	−15.5	4.1	+ .21	25853	−12.5	4.5	+ .12
24131	−14.0	4.3:	+0.17	24912	−12.0	7.2	+0.13

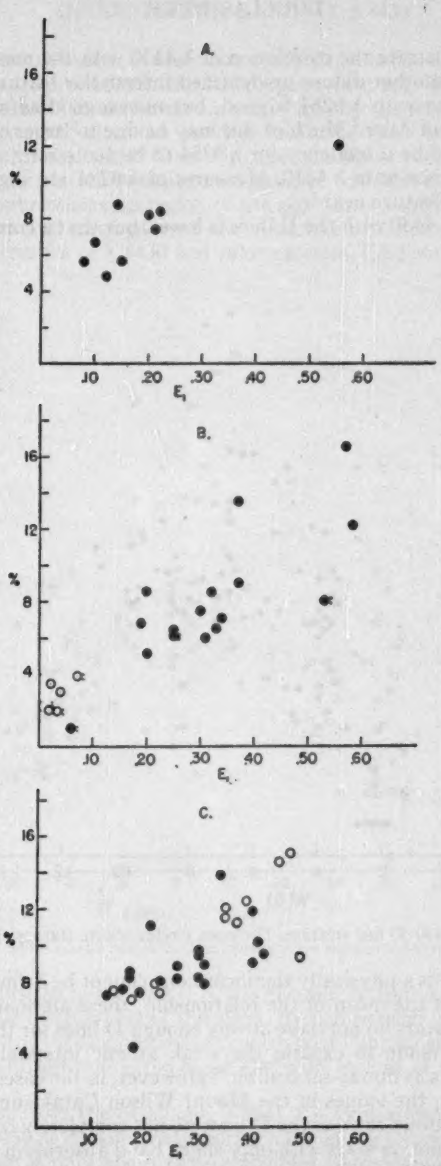

FIG. 8.—The λ 4430-color excess relations for certain physically connected groups. *A*, the Scorpio-Centaurus stars; the star at the extreme right is HD 147889. *B*, the stars near P Cygni; the open circles denote stars nearer than 500 parsecs and not considered to be physically related. *C*, the h and χ Persei region; the filled circles denote stars considered to be cluster members by Bidelman; the open circles indicate other stars in the region.

Figures 9 and 10 illustrate the correlation of λ 4430 with the mean equivalent width of the D lines and of another diffuse unidentified interstellar feature at λ 6284, respectively.[15] The correlation with λ 6284 is good, but not so good as with color excess, as found by Greenstein and Aller.[5] Much of this may be due to larger errors in measures of λ 6284. There seems to be a tendency for λ 6284 to be too strong in the case of the A supergiants in comparison with λ 4430. Measures of λ 6284 are slightly uncertain, owing to an atmospheric feature near by.

The correlation of λ 4430 with the D lines is lower, but that a correlation exists is cer-

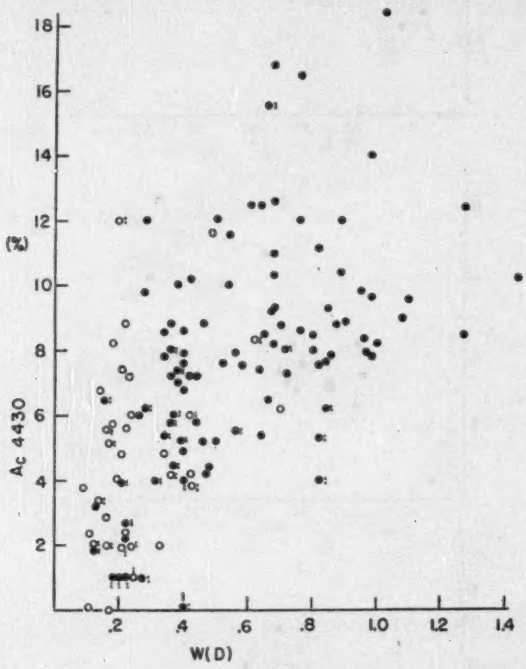

FIG. 9.—The λ 4430–D line relation. The open circles denote stars within 300 parsecs

tain. Whether or not it is a physically significant one cannot be definitely stated. Despite the smooth increase in the mean of the relationship, there are many discordant cases; the near-by reddened stars do not have strong enough D lines for their band intensities. Attempts have been made to explain the weak atomic interstellar lines in near-by strongly reddened stars as due to saturation.[16] However, in the cases of some of the stars in the Scorpius region, the values in the Mount Wilson Catalogue of Interstellar Line Intensities[15] for the doublet ratio of the D lines do not completely confirm this. Also, the presence of strong D lines in stars with only slight band absorption and reddening, such as HD 1337 and 188209,[16] is difficult to explain if a physical correlation between these interstellar features does exist. On the other hand, it must be pointed out that two of the outstanding cases of strong λ 4430 without strong reddening, HD 225146 and 167838, both show strong D lines of the order of 1 A in equivalent width. The comparison of the

[15] Merrill, Sanford, Wilson, and Burwell, *Mt. W. Contr.*, No. 576; *Ap. J.*, **86**, 274, 1937.

[16] L. Spitzer, Jr., *Ap. J.*, **108**, 276, 1948.

equivalent widths does not seem to yield any really definite conclusion as to whether or not the two features are produced in the same regions of space. Here we are troubled by the manner in which the D lines become saturated and by the resulting curve of growth. Dr. Spitzer has suggested[17] that the existing theory be used to relate the equivalent widths and doublet ratios of the D lines with the number of sodium atoms causing the absorption and that this latter quantity be compared with the intensities of λ 4430.

In Figure 11 we have selected a region of the sky where a maximum of data is available for distant stars and have plotted the stars having distances greater than 1000 parsecs with the intensities of λ 4430 and color excesses. Contours have been drawn for

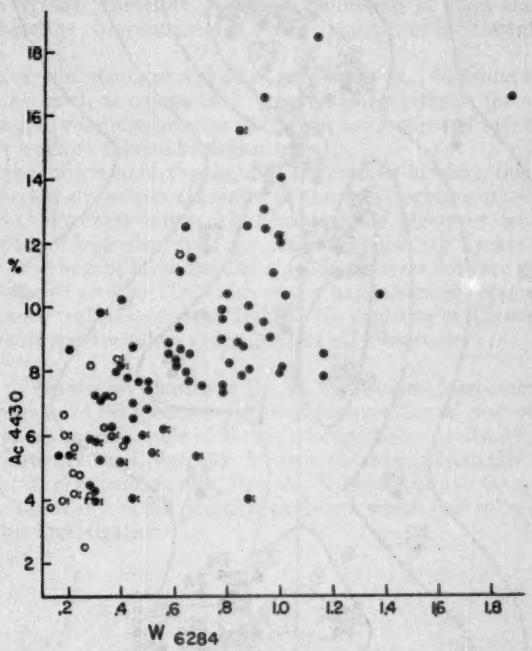

FIG. 10.—The λ 4430-λ 6284 relation. The open circles denote stars within 300 parsecs

λ 4430, although it must be noted that they are necessarily approximations owing to the irregular nature of the distribution of the stars. By comparison with the Ross *Atlas of the Milky Way* and with the isophotometric contours of Pannekoek,[18] it is found that regions of strong band absorption agree in general with regions of maximum interstellar absorption.

A result of interest from the catalogue is that P Cygni appears to have about the same intensity of λ 4430 as do some neighboring stars in the Cygnus region—in particular, HD 193183, which is only about two-tenths of a degree distant. If we assume the same interstellar absorption for these two stars, we find from the spectroscopic absolute magnitude of −5.5 for HD 193183 that the absolute magnitude of P Cygni is −7.7, thus making it one of the brightest known stars in the galactic system. The value given

[17] Privately communicated to the author.

[18] *Leiden Ann.*, 11, 3, 1920.

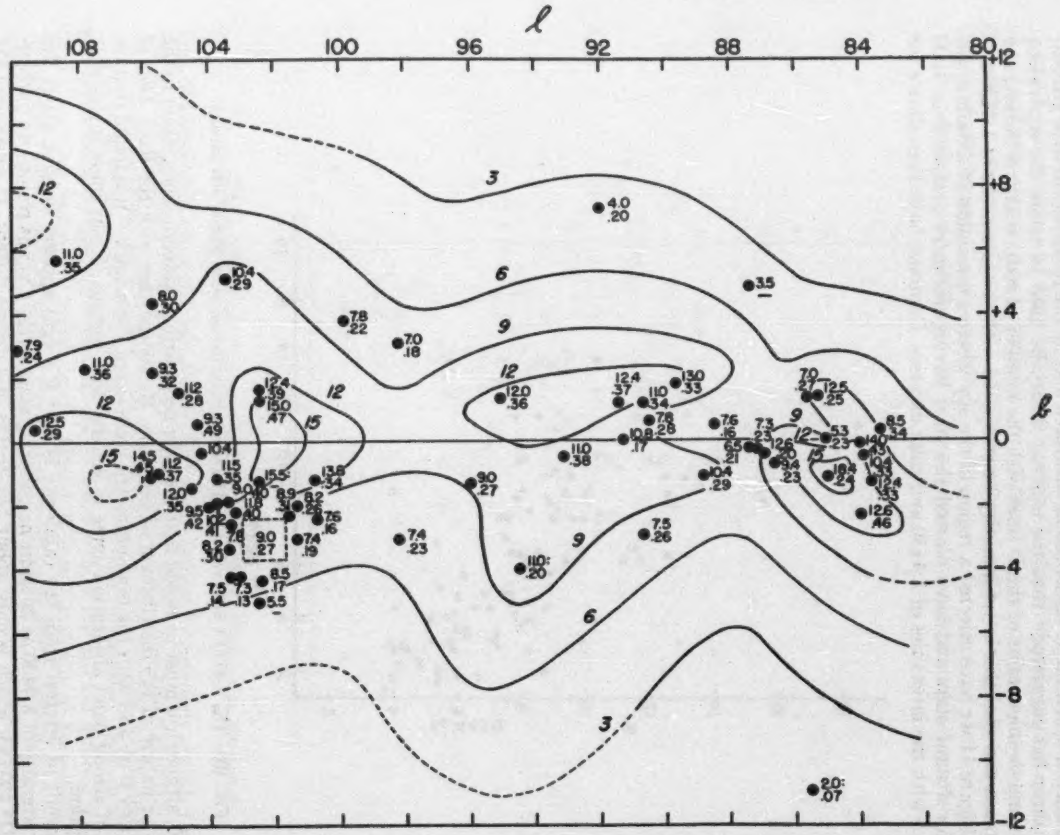

FIG. 11.—Line depths and color excesses for a galactic field. The upper figure is line depth; the lower is color excess. The two values in the square refer to a number of stars too crowded to plot individually. Approximate contour lines for equal values of line depth for λ 4430 have been drawn.

in the catalogue for the absorption of λ 4430 in P Cygni has been given weight "C," owing to the presence of a line of *Fe* III which falls very near the center of the feature, making the value somewhat uncertain.

IV. CONCLUSIONS

The intensities of λ 4430 exhibit an excellent correlation with interstellar reddening, although there is reason to believe that there is not a one-to-one correspondence. The regions of space in which the reddening is produced are therefore also largely those in which the band absorption originates, although they are probably not produced in exactly the same regions. Therefore, when large numbers of stars are considered, there appear cases where the observed ratio of the two quantities is different from the average observed value.

The question of coincidence of regions of production of λ 4430 and the sodium D lines cannot yet be answered, as comparison of equivalent widths of the two features is not an accurate enough procedure because of the unknown effect of saturation of the sharp D lines. Further work on this problem is planned.

The present work sheds no further light on the manner in which this unidentified band is produced. The low-dispersion character of the spectrograms allowed no conclusions to be reached as to the exact nature of the band profile. However, advantage was taken of the large number of high-dispersion spectra available at the Yerkes Observatory from other programs. The best of these spectra of reddened stars indicate an almost perfectly symmetrical V-shaped profile. The width of the band does not appear to exceed 60 A, which is at variance with the result of Baker.[4] No evidence of fine structure was found even on wide coudé spectra taken at the McDonald Observatory.

I should like to express my thanks to Dr. W. W. Morgan for suggesting the problem, for the determinations of the spectral types and luminosities of most of the stars, and for permission to use his extensive file of B-star spectra. I should also like to thank Dr. K. Aa. Strand, of Northwestern University, for an assistantship from that institution during my entire stay at Yerkes, and, finally, Drs. W. P. Bidelman and Guido Münch for their helpful discussion of many of the practical problems which had to be solved toward the completion of this investigation.

TURBULENCE IN THE INTERSTELLAR MEDIUM

L. H. ALLER*
Observatory, University of Michigan
Received September 12, 1950

ABSTRACT

The brightness variation in an extended region of emission nebulosity in Cygnus photographed with the Palomar 48-inch Schmidt is analyzed from the point of view of turbulence theory. The largest eddies appear to be about 5–10 parsecs in diameter. The character of the turbulence spectrum suggests that these large eddies possess a sufficient supply of energy to maintain an equilibrium spectrum. Further studies in this and other regions to fix the character of the turbulence spectrum are needed.

INTRODUCTION

The theory of homogeneous turbulence,[1] developed in recent years by von Karman, Kolmogoroff, Dryden, Heisenberg, Batchelor, Chandrasekhar, and others, largely in connection with aerodynamical problems, promises to be of considerable interest in connection with astrophysical problems. Indeed, important applications have already been made by Schwarzschild and Richardson to the problem of solar granules[2] and to the motions of the gases in the Orion nebula. As formulated so far, turbulence theories have been concerned primarily with velocities, but, since the velocity, pressure, and density of a gas are all interrelated, generalizations can be made to include the effects of turbulence upon densities or pressures. In the present discussion we are concerned not with velocities but with variations in the brightness of emitting gases, brought about primarily by the fluctuations in the density of the emitting material.

The appearance of many regions of the Milky Way gives the impression of widespread turbulence in the interstellar medium. The Sagittarius star cloud, for example, is invaded by wisps of dark absorbing material, whose appearance reminds one of cloud formations in the earth's atmosphere. In the great rift of the Milky Way, in Auriga, and in Taurus, wherever large clouds of absorbing material are found, chaos appears to be the order of things. Bright nebulosity, too, often shows a chaotic structure, although the forms of most reflection or emission nebulosity are governed by the distribution of the illuminating stars as well as by the distribution of the gases. When the gases are sufficiently attenuated and a number of high-temperature stars occur in the region, the extent of patches of faint emission nebulosity may be considerable.

The present study is concerned with bright nebulosity in a region in Cygnus photographed upon a 103*a*-E emulsion through a red Plexiglass filter with the 48-inch Palomar Schmidt camera. The plate was centered at $\alpha = 20^h11^m24^s$, $\delta = +35°27'$; the region with which we are immediately concerned lies on an arc between $\alpha = 20^h1^m.3$, $\delta = 38°.0$, and $\alpha = 20^h13^m.0$, $\delta = 34°.5$ (1950) (see Fig. 1). This area was selected because the bright nebulosity apparently exhibits a random distribution and the effects of differential space absorption do not appear to be serious, through at least the part of the domain actually studied.

Suppose we can measure the intensity distribution, I, along a line drawn through this

* This investigation was made possible by a co-operative arrangement with the Mount Wilson and Palomar Observatories.

[1] See S. Chandrasekhar's Russell Lecture, *Ap. J.*, 110, 329, 1949, for an account of the basic ideas of the theory and important references.

[2] *Ap. J.*, 111, 351, 1950.

FIG. 1.—A region in Cygnus photographed with the Palomar 48–72-inch Schmidt camera. The original plate was centered at $20^{h}11^{m}24^{s}$, $+35°27'$. Only a small portion is reproduced here. The exposure, obtained June 28–29, 1949, was obtained upon a 103*a*-E emulsion through a red filter. Tracings were made along an arc between the arrows. The dark parallel streaks in the lower right corner are due to imperfections in the print used for making the halftone.

region (avoiding the obscured areas). The path will cross many wisps and filaments. If x is the distance along the line drawn in the plane of the sky, then

$$I(x) = \int_{-\infty}^{+\infty} E(z, x)\, dz, \tag{1}$$

where E is the emission per unit volume and z is the distance along the line of sight.

The light incident upon the photographic plate consists primarily of emission $H\alpha$ quanta. This radiation is produced in the well-known mechanism of recombination of protons and electrons in a higher energy level, with subsequent cascading from the third to the second level in hydrogen. The emission, E, is therefore proportional to $N_i N_e$ or, since the material may be presumed mostly ionized, to the square of the density, ρ.

If the turbulence is homogeneous, it may be shown that[3] the turbulence spectrum of $I(x)$ can be regarded as the same as the turbulence spectrum of $E(z, x)$. Hence we can obtain, theoretically at least, the turbulence spectrum for ρ^2. Unfortunately, it is not practicable to derive the turbulence spectrum of ρ from that of ρ^2. If a theory of turbulence in the interstellar medium is available, a prediction of the spectrum of ρ, and therefore of ρ^2 as well, may be made. For the present, therefore, we shall see whether some information on the turbulence spectrum of $I(x)$ (which we interpret as that of ρ^2) can be found.

Actually, since the turbulence produces density fluctuations in a medium which otherwise would be uniform (or at least consist of discrete clouds of uniform density), we are concerned with fluctuations about a mean value. That is, if $I(x)$ denotes the estimated intensity of the emission nebulosity along the line x from $x = x_0$ to $x = x_1$, we choose I_0 so that

$$\int_{x_0}^{x_1} [I(x) - I_0]\, dx = 0. \tag{2}$$

Let us set

$$I' = I(x) - I_0. \tag{3}$$

We shall derive the correlation function $g(r)$ for $I'(x)$ rather than for $I(x)$. In other words, we shall derive the turbulence spectrum of a quantity connected with $\rho^2 - \bar{\rho}_0^2$ rather than simply with ρ^2.

THE CORRELATION FUNCTION $g(r)$

The analysis of the observational data was undertaken in the following fashion. The Palomar plate was too large to be photometered directly, and a positive glass print, preserving as closely as possible the original contrast and of suitable size for the microphotometer, was made by Mr. William C. Miller. Tracings were run across the nebulous patches for a distance of about 21 cm (about 4°) with a magnification of 10×. Underlying the densely packed, thin deflections due to individual stars lay the slowly fluctuating background of the emission nebulosity. The height of the latter was estimated and measured upon the tracings at intervals of 5 mm. We make the assumption that the smoothed galvanometer deflections which we shall call $I(x)$ are, in the first approximation, proportional to the intensity of the original light. Since the fluctuations due to the nebulosity are themselves small, the error arising from the afore-mentioned assumption is probably not more serious than that arising from the uncertainty in the location of the nebulous background or the troubles introduced by space absorption. Strictly speaking, therefore, what we derive is the turbulence spectrum of the smoothed galvanometer deflections, which are correlated with the intensity, which, in turn, is interpreted as being proportional to $\rho^2 - \bar{\rho}_0^2$.

[3] I am indebted to S. Chandrasekhar for this important conclusion.

From a plot of $I(x)$, I_0 was found and $I'(x)$ computed. The next step was to evaluate the correlation function

$$g(r) = \frac{\Sigma I'(x)\, I'(x+r)}{\Sigma I'(x)^2}, \tag{4}$$

where r takes successive values—0, 1, 2, 3, 4, 5, 6, 8, 10, 12, etc. The derived $g(r)$ (see Table 1) starts with a value of 1.0 at $r = 0$ and declines to 0 at about $r = 44$. Thereafter

TABLE 1

THE CORRELATION FUNCTION $g(r)$

r	$g(r)$	r	$g(r)$	r	$g(r)$
0.5	+0.97	10.0	+0.39	50.0	−0.096
1.0	+ .93	12.0	+ .35	60.0	+ .001
1.5	+ .88	14.0	+ .28	70.0	− .24
2.0	+ .84	17.0	+ .16	80.0	− .27
2.5	+ .80	20.0	+ .13	90.0	− .11
3.0	+ .77	22.5	+ .16	100.0	− .37
4.0	+ .69	25.0	+ .20	110.0	− .59
5.0	+ .64	30.0	+ .18	120.0	− .24
6.0	+ .54	35.0	+ .14	130.0	−0.14
8.0	+0.46	40.0	+0.047		

it fluctuates and presumably approaches zero at large r. These fluctuations at large r arise in part from the fact that r becomes comparable with the actual distance over which $I(x)$ is measured. Accordingly, we have replaced the wavy $g(r)$-curve with a smoothed function, which declines from 1.0 at $r = 0$ to zero at $r = 44$, becomes negative, and then gradually returns to zero.

THE TURBULENCE SPECTRUM

The turbulence spectrum $F(k)$ is related to the correlation function $g(r)$ by the expression

$$F(k) = \left(\frac{2}{\pi}\right)^{1/2} \int_0^\infty g(r) \cos k r\, dr, \tag{5}$$

which must be evaluated numerically. To any desired degree of accuracy we may represent the correlation function by a series of straight-line segments of the form

$$g(r) = A_i r + B_i, \qquad r_{i-1} < r < r_i, \tag{6}$$

where $0, r_1, r_2, \ldots, r_{i-1}, r_i, \ldots, r_n$ are the abscissae of the ends of the straight-line segments. Then

$$F(k) = \left(\frac{2}{\pi}\right)^{1/2} \sum_{i=1}^{n} \left[\frac{A_i}{k^2} \cos k r + \frac{1}{k}[A_i r + B_i] \sin k r\right]_{r_{i-1}}^{r_i}, \tag{7}$$

where the bracket is to be evaluated at the two limits of integration and its value for r_{i-1} subtracted from its value for r_i. We further impose the condition[4] that $F(0) = 0$. Hence

$$\int_0^\infty g(r)\, dr = 0. \tag{8}$$

[4] In a private communication, G. K. Batchelor suggests that it is not necessary to impose this condition. Calculations carried out with a smoothed $g(r)$ function which does not fulfil equation (8) show the same general properties of $F(k)$, i.e., the high maximum and steep initial descent.

The adopted values of A and B are given in Table 2.

It is clear from the trend of $g(r)$ that $F(k)$ will have a maximum in the neighborhood of 0.035, and this is confirmed by the calculations (see Table 3). The maximum is, in fact, very sharp. Beyond $k = 0.10$, $F(k)$ falls off more gradually. Within the errors of the analysis, the trend of the spectrum is fairly well represented by k^{-n}, where $n \sim 1.8$ in the interval from $k = 0.1$ to $k = 0.8$. No emphasis can be placed on the exact value of n, for reasons mentioned earlier, but the trend of the turbulence spectrum, with its sharp maximum and steep initial decline, appears to be qualitatively correct. This sharp maximum suggests that there is a sufficient store of energy in the larger eddies to maintain a

TABLE 2

REPRESENTATION OF THE CORRELATION FUNCTION

Interval (Mm on Plate)	B	A	Interval (Mm on Plate)	B	A
0– 6	+1.000	−0.0765	44– 78	+0.220	−0.00500
6–10	+0.765	− .0375	78–120	−0.18	.000
10–16	+0.650	− .0250	120–130	−2.34	+0.018
16–44	+0.377	−0.00857			

TABLE 3

THE TURBULENCE SPECTRUM
(k in Mm^{-1} on the Plate)

k	$F(k)$	k	$F(k)$
0.0	0.0	0.20	2.4
.01	3.9	0.30	1.37
.035	19.3	0.40	0.55
.06	9.0	0.60	0.20
0.10	4.1	1.0	0.05

flow of energy down the hierarchy of eddies. This is the condition necessary for the maintenance of a stationary spectrum.

The linear dimensions of the eddies are a matter of considerable interest. Adopting $k_{max} = 0.035$ as a maximum of the curve, we see that the largest eddies have sizes of the order of $1/k_{max} \sim 3$ cm on the plate, or about 34′. Presumably, these emission nebulosities are excited by high-temperature stars in their neighborhood. Tentatively, we may suppose that the sources of luminosity are the B0–B2 supergiant stars, HD 187459, 190603, 193183, and 194272, whose true distance moduli are given by Morgan as 10.0, 10.2, 10.3, and 10.4. If the diffuse clouds are at a distance of 1000 parsecs, the largest eddy is about 10 parsecs in diameter. At first glance, the dimension seems to be surprisingly large, but we note that on the direct photographs the larger structures are of the order of half a degree in size.

It is to be emphasized that our discussion is of only a preliminary character. Differential space absorption introduces perhaps the greatest uncertainty. Presumably it would be worth while to investigate other regions of the sky and to make additional measures on the same region with photometrically calibrated plates. Does the same type of spectrum hold from point to point in the galaxy? Are the maximum sizes of the turbulence elements the same at various points in the Milky Way?

I want to express my gratitude to Drs. Walter Baade and Martin Schwarzschild for their valuable suggestions in the selection of the observational material; to Mr. William C. Miller for his care in making copies of the Schmidt plate; to Mr. Norman Horwitz, then computing assistant at the University of Michigan Observatory, for some of the extensive numerical calculations; and to Mr. S. Chandrasekhar for many stimulating discussions and helpful suggestions. My interest in this problem was aroused by the Russell Lecture at Ottawa in 1949.

SPECTROPHOTOMETRY OF REPRESENTATIVE PLANETARY NEBULAE

LAWRENCE H. ALLER*
Observatory, University of Michigan
Received June 17, 1950

ABSTRACT

This investigation completes a spectrophotometric study of planetary nebulae initiated some years ago at the Lick Observatory. Special attention is paid to nebulae observed in the λλ 3700–6500 A region by Wyse, to objects with interesting structural features, and to certain stellar nebulae. The observed Balmer decrement agrees with the theoretical predictions by Menzel and Baker for their model *B*, in which all Lyman radiation is assumed degraded into Lyman-α, which alone escapes from the nebula. With the low dispersion employed, most of the central stars show continuous spectra with little evidence of absorption or emission lines. The nuclei of NGC 7026, 6751, and 6905, which show broad Wolf-Rayet emission lines of oxygen, helium, and carbon, are discussed in detail, and relative line intensities are derived.

I. INTRODUCTION

A basic requisite for the understanding of the planetary nebulae is a knowledge of the intensities of the emission lines that comprise their spectra. The brightness of the lines of a given ion differ from nebula to nebula or even within the same nebula in such a way as to reveal important clues to the prevalent conditions of excitation and ionization.

The meaning of the intensity of a nebular emission line merits a moment's attention. First, we would like to have the total intensity of the nebular line—i.e., the total amount of monochromatic energy received from the whole nebula per second by a unit area just outside the earth's atmosphere perpendicular to the line drawn to the nebula. This information should be supplemented by measurements of the distribution of energy throughout the nebular images—the results may be expressed very well by means of isophotic contours such as those published by Berman.[1] Although the total intensity and the isophotic contour give a complete description of the observational data, the emission per unit volume is the item of greatest theoretical interest. An estimation of this quantity requires some knowledge of the spatial structure of the nebula, as well as of its distance. In general, both of these are poorly known.

A number of observers have published measurements of nebular line intensities. Berman observed with the Crossley reflector and quartz spectrograph of the Lick Observatory. Plaskett[2] obtained slit spectra of a number of the brighter objects at the Dominion Astrophysical Observatory. More recently, Bowen and Wyse[3] used the Lick 36-inch refractor and spectrographs equipped with the image slicer. They estimated the intensities of the lines with the aid of scale plates. T. L. Page[4] secured excellent photometric material for a large number of nebulae. He employed the Cassegrain spectrograph of the 82-inch McDonald reflector and a wide slit. A report on the continuous spectra of the planetaries has been published, but an account of the line intensities has not yet appeared.

Some years ago at the Lick Observatory the writer measured the relative total intensities of the nebular lines (and, when possible, the Balmer continuum) in eleven planetary nebulae.[5] In addition to this list, a few objects observed by Stoy were also discussed. The

* The reductions described in this paper were carried out primarily while the writer was at Indiana University.

[1] *Lick Obs. Bull.*, **15**, 86, 1930.

[2] *Pub. Dom. Ap. Obs. Victoria*, **4**, 187, 1928.

[3] *Lick Obs. Bull.*, **19**, 1, 1939.

[4] *Ap. J.*, **96**, 78, 1942.

[5] *Ap. J.*, **93**, 236, 1941.

present investigation comprises a completion of this program. In the present instance, however, the relative total intensities are given for only the stellar planetaries. For the other objects the intensities measured at a particular point (or sometimes two or more points) in the nebula are tabulated, although in a number of instances the total intensities also have been measured.

Section II discusses the selection of the nebulae observed; Section III describes the techniques of observation and reduction; Section IV gives the results, mostly in the form of tables; and Section V treats of the Balmer decrement. A final portion of the paper is devoted to some remarks on the nuclei of the nebulae.

II. SELECTION OF OBJECTS

The observational program was planned in conjunction with quantum-mechanical calculations of the target areas for the collisional excitation of certain of the stronger forbidden lines. Since the transition probabilities are known, it should be possible to utilize such target areas in connection with the observed intensities to get information on the state of ionization and excitation, the electron temperature, and ultimately the composition of the radiating gases.

Particular emphasis was placed on the nebulae studied by Wyse[6]—NGC 2165, 2440, 6741, and IC 5217, which had not been observed in the earlier program. The idea was to supplement the extensive line-intensity measurements in the visual and photographic regions with data for the ultraviolet. Second, there has been included a number of objects of moderate surface brightness that show interesting structural details, e.g., NGC 1535, 2392, 3242, 4361, 6720, 6751, 6778, 6818, 6905, and 7026. Finally, observations were secured of certain stellar nebulae of interest because of their high densities, central stars, and the problem of the Balmer decrement.

In all, 170 spectrograms of 45 planetary nebulae and their nuclei were secured in the 1943–1945 program. Of these objects, 27 have been previously observed by Page and 33 by Wright,[7] and a few have been studied by Minkowski[8] and by Stoy.

For many nebular problems wide-slit spectrograms of the type obtained by Page are probably more useful than slitless plates. Sky fog is greatly cut down, and there is no interference from overlapping stellar spectra. Slitless plates of the larger nebulae are useful only for the stronger, well-separated lines and are capable of giving us no reliable data on the weaker lines or those that fall close to one another. On the other hand, slitless spectrograms often yield more complete information about the structural features of the planetaries and permit the determination of the integrated intensities of the nebular images. The latter data are needed, for example, for the determination of the temperatures of the central stars. A comparison of the line intensities from Page's plates with those obtained in the present series will be of considerable interest, however.

The structural features of a number of planetary nebulae—in particular NGC 1535, 2022, 2392, 2440, 3242, 6309, 6445, 6720, 6751, 6778, 6905, 7026—have been studied on the Crossley slitless spectrograms, and some results have already been published elsewhere.[9] Since these reductions were completed, however, it has become evident that an adequate treatment of the spatial structures of planetary nebulae requires plates taken with a much larger scale, e.g., the slitless spectrograms secured by Olin Wilson at the coudé focus of the 100-inch reflector.[10] Accordingly, reference is made only to the Crossley results for a few of the fainter objects, which cannot be observed at the coudé focus.

[6] *Ap. J.*, **95**, 356, 1942.

[7] *Pub. Lick Obs.*, **13**, 193, 1918.

[8] *Ap. J.*, **95**, 243, 1942.

[9] Cf. the author's *Astrophysics* (Philadelphia: Blakiston Co., in press), chap. xiv.

[10] Cf., for example, the discussion of NGC 6572 and NGC 7662 by Olin Wilson and L. H. Aller, *Pub. A.A.S.*, **55**, 70, 1950.

Limitations imposed by uncertainties in the physical theory.—Recent discussions by Bates, Massey, Fundaminsky, and Leech[11] have shown that the predicted cross-sections for the collisional excitation of the forbidden lines are grossly in error. At the present time it is possible to calculate only a lower limit to the abundances of the ions responsible for the forbidden lines—with no assurance that the real values lie close to this lower limit. For the same reason, electron temperatures derived from a comparison of the 4363 and green nebular lines are open to question, and a precise specification of this parameter is not possible. It is possible, however, that the relative cross-sections are less affected than the absolute values, and for the present we may retain the electron temperatures heretofore assigned. The general character of the excitation in the nebulae, as well as the energy distribution in the continuous spectrum as observed by Page, strongly indicates that T_e must lie in the neighborhood of 10,000° K for most nebulae.

In view of these uncertainties, estimates of ionic densities and the level of excitation and ionization from a study of the emission of [*O* II], [*O* III], [*Ne* V], [*Ne* III], etc., would be insecure. Accordingly, no such discussion is attempted here.

III. OBSERVATIONS AND REDUCTIONS

Photometric procedures.—The observational technique is similar to that employed in the 1938–1939 series.[5] All the plates were secured with the quartz slitless spectrograph at the Crossley reflector of the Lick Observatory. Laboratory standardizations were secured with a spot sensitometer and were supplemented with exposures of the comparison star taken with diaphragms. In the earlier series, π^1 Cygni was employed as the comparison star; in the present investigation the stars observed by Barbier and Chalonge have been utilized.[12] Their list contains objects well distributed over the sky, carefully observed with painstaking spectrophotometric techniques.

Tracings of the plates were made with the Moll microphotometer at the Lick Observatory and with the Beals-type microphotometer at the Yerkes Observatory. Each plate was traced parallel to the dispersion. One trace usually sufficed for the smaller objects; extended objects frequently required several traces through different parts of the nebula. Tracings perpendicular to the dispersion and, in some instances, along the lines of symmetry of the nebula have also been run, in order to study the structural features of certain images in the larger objects.

The construction of deflection log I-curves involved both the sensitometer spots and the widened spectra of the comparison stars. Observations of the comparison star consisted of a series of equal exposures, between each of which the effective aperture of the telescope was varied in a known fashion by means of a diaphragm with circular holes. In the region of low densities the D log I-curves usually coincided; the variations with wave length appeared in the slopes of the straight-line portions. The plates secured on a single night's observations were developed together, and a single set of D log I-curves used was derived. Since development conditions were standardized and plates of a single emulsion number were used, the reduction-curves were very similar from one set of observations to the next.

Vignetting.—In the slitless spectrograph, vignetting is dependent upon wave length. Hence it is necessary that the nebula and comparison star be photographed in the same part of the field. Since the adjustment is made visually and the spectrum of the star appears continuous, slight errors are sometimes made. The position of the bright-line nebula can be adjusted accurately. The plateholder can be slid perpendicular to the direction of dispersion, so that several spectra of the comparison star or of the comparison star and

[11] *Trans. R. Soc. London, A* (in press). For a discussion of possible effects of the revision of the cross-sections on ionic densities, etc., derived from nebular line intensities see L. H. Aller, *Ap. J.*, **111**, 609, 1950.

[12] *Ann. d'ap.*, **4**, 30, 1941.

the nebula can be photographed upon the same plate. Thus the error in the centering of the comparison star can be found. The effect of vignetting was measured as a function of difference in centering upon a series of the plates taken especially for the purpose. In all instances the error in the observations from that cause would appear to be small, amounting to about $\Delta \log I = 0.01$ in the limit. After August, 1944, the corrections have been determined and applied to each night's observations of the comparison stars whenever necessary.

Effect of background continuum.—As previously mentioned, in extended objects the intensity is measured at some particular point or points—usually the brightest portions. In stellar objects the total area under the reduced intensity-curve of the monochromatic image has been measured. Usually, the intensities so derived are in good agreement with those found simply from the heights of the profile on the tracings. In each instance the contribution of the background continuum of the star or nebula must be estimated and subtracted from the measured intensity. This correction is especially serious for the weaker lines and for the Balmer continuum. With respect to the latter, Page's procedure of extrapolating the observed continuum longward of the Balmer limit to shorter wave lengths has been followed. As in the 1938–1939 observations, the tabulated intensity of the 20 A interval of the Balmer continuum is corrected for this underlying continuum. In general, the slitless plates are unsatisfactory for the determination of the energy distribution in the continuum. Slit spectra are required for this purpose.

Type of plates.—Until September, 1944, Eastman 103*a*-O plates were employed. Thereafter, Eastman II*a*-O plates were used. The gain in quality more than offsets the loss in speed. For photometric purposes the plates are less satisfactory than the standard Eastman 33's or Eastman 40's, in that they often show larger random errors.

Sources of error.—Among the sources of error we may mention, first of all, the limitations imposed by the nonuniformity of the photographic emulsion. Second, the calibration-curves are likely to be in error, particularly in the far ultraviolet. Laboratory and comparison-star data may be utilized in the region from about λ 3600 to λ 5000, but farther in the ultraviolet no satisfactory standards are available, and a mean curve has been employed throughout the ultraviolet. The exposure times on the comparison stars and laboratory standards are shorter than those on the nebulae, so that the deflection log I-curves are appropriate to a shorter time interval than the nebular exposures. To correct for the atmospheric extinction, use has been made of Popper's determination of the absorption as a function of wave length. These mean absorption coefficients are reliable for the summer and fall months, but at other times the fluctuations, particularly in the ultraviolet, may become serious. A troublesome feature of photometry on long-exposure slitless spectrograms is the effect of sky fog. At a given point in the spectrum of a nebula, sky light of many different colors is incident. One has to subtract this sky fog from the monochromatic nebular image, and a precise reduction is not possible. Finally, there are practical difficulties in estimating the position of the background continuum and in correcting for the effects of overlapping images.

Precision of the measures.—Perhaps some idea of the precision of the observations may be gained from the internal agreement of the intensities in a given nebula, measured upon different plates and nights. The computed probable error of the intensity of a line depends upon its position in the spectrum and upon its strength. In the region λλ 3700–5000 the probable error of a single measurement of a line stronger than 1.0 (on the scale $H\beta = 10$) is about 10 per cent. Weaker lines show somewhat larger probable errors, partly because of greater accidental errors and partly because of the difficulty in locating the position of the continuum. Ultraviolet lines, such as λ 3341 or λ 3428, also show larger probable errors, of the order of 14–17 per cent. These are the accidental errors; systematic effects are not included.

A detailed comparison with Wyse's intensities for the four nebulae common to our lists shows reasonably good agreement. The fainter lines are systematically measured

slightly weaker in the present set of observations. The differences, however, are much smaller than in the earlier series, in which total intensities were measured and the fainter lines (referred to results obtained with the slit spectrograms) seemed systematically too weak. Perhaps sky fog is responsible for some of these troubles.

IV. THE OBSERVED LINE INTENSITIES

Table 1 gives the designation of the nebula, the α and δ for 1945, the plate number, the exposure time, and, finally, the secant of the zenith distance at midexposure. Tables 2, 3, and 4 give the relative intensities of the principal nebular lines on the scale $H\beta = 10$. Table 2 gives the data for low-excitation objects; Table 3 the results for certain high-excitation nebulae (i.e., objects that show the ultraviolet lines of [*Ne* v] and the Bowen fluorescent mechanism); while Table 4 gives the results for a number of nebulae of low surface brightness or extended surface. For these objects, only the intensity of the strongest lines could be measured. Frequently, the overlapping of images prevented any reliable estimate of the intensities for N1 and N2.

The intensity of the Balmer continuum is expressed in terms of 20 A intervals at the Balmer limit, also on the scale $H\beta = 10$. The tabulated value is corrected for the underlying continuum.

The high-excitation nebulae NGC 2022 and 2392 have recently been the subjects of a detailed spectrophotometric study by Minkowski and the writer. We shall discuss the Lick observations in conjunction with the Mount Wilson data at a later date.

Binuclear nebulae.—NGC 6778 resembles NGC 2440 or 7026, except that its surface brightness is much lower. The *He* II image is small and concentrated perhaps in the nucleus, and the other lines show a binuclear formation. There is no evidence of the spectrum of a central star.

Table 5 gives the intensity distribution along the line joining the two lobes for the [*O* III] λλ 4959–5007, $H(H\beta, H\gamma, H\delta)$, and λ 3727 images of NGC 6778, and the corresponding data (plus that for the [*Ne* III] image in NGC 7026). I have averaged the intensities for the two lobes, since the nebulae possess (very nearly) bilateral symmetry. In NGC 7026, $I(H\beta)$ is taken as 10 at the brightest portion of the condensation—3″ from the center, whereas $I(H\beta)$ is chosen as 10 at 5″ from the center of NGC 6778. I have also calculated the distribution of the emission per unit volume on the assumption that the emitting lobes are roughly spherically symmetrical. It now appears that such a hypothesis is inadequate in even the first approximation. In NGC 7026 the λ 4686 emission is strongly concentrated toward the center, as Wright pointed out many years ago, but I have been unable to find marked differences between the other images. On the other hand, the table shows that the maximum of the image of λ 3727 falls some 2″ or 3″ farther from the center than that of the [*O* III] image. Similar studies have also been carried out for NGC 2440.

Ring nebula.—The high-excitation lines of the Bowen fluorescent mechanism and λ 3203 of *He* II appear in NGC 6905 and 6720, for example, although they are not much above the level of sky fog on the plates. Slitless spectra are not well suited for NGC 6720; I have, however, measured the intensities of the ultraviolet lines with respect to $H\beta$, with the following results:

λ.....	3133	3203	3341	3445
I.....	1.8	1.4	0.7	1.0

If the assumption is made that, to a first approximation, the emitting material in the shell in NGC 6720 is distributed in a spherically symmetrical fashion, one may deduce the emission per unit volume, $E(\rho)$, from the intensity distribution across the monochro-

TABLE 1

OBSERVATIONS OF PLANETARY NEBULAE

Nebula	α	δ	Plate	Date	Exposure (Minutes)	Secant Zenith Distance
Anon.....	$0^h25^m.3$	+55°36′	416	Oct. 14, 1944	120	1.07
			423	Oct. 15, 1944	30	1.06
IC 351.....	3 44	+34 53	417	Oct. 14, 1944	90	1.10
			424	Oct. 15, 1944	20	1.22
II 2003.....	3 52.8	+33 43	418	Oct. 14, 1944	93	1.01
			425	Oct. 15, 1944	75	1.10
			426	Oct. 15, 1944	14	1.03
NGC 1535....	4 11.7	−12 53	454	Nov. 18, 1944	120	1.58
J 320.....	5 2.5	+10 39	472	Mar. 9, 1945	60	1.41
			473	Mar. 9, 1945	21	1.65
NGC 2022....	5 36.6	+ 9 2	450	Oct. 17, 1944	232	1.21
II 2149.....	5 43.5	+46 7	448	Oct. 17, 1944	5, 11	1.41
			449	Oct. 17, 1944	22	1.31
			474	Mar. 9, 1945	5, 12	1.45
			475	Mar. 9, 1945	30	1.58
NGC 2165....	6 19.2	−12 57	427	Oct. 15, 1944	5	2.58
			428	Oct. 15, 1944	20	2.35
			429	Oct. 15, 1944	85	1.89
			464	Nov. 19, 1944	150	1.54
J 900.....	6 22.8	+17 50	462	Nov. 19, 1944	100	1.30
			463	Nov. 19, 1944	20	1.32
			468	Jan. 12, 1945	172	1.08
			469	Jan. 12, 1945	20	1.24
NGC 2392....	7 26.0	+21 2	324	Mar. 19, 1944	120	1.34
			325	Mar. 19, 1944	20	2.44
			430	Oct. 15, 1944	87	1.10
			465	Nov. 19, 1944	90	.....
			470	Jan. 13, 1945	150	1.36
			471	Jan. 13, 1945	20	1.93
NGC 2440....	7 39.5	−18 5	419	Oct. 14, 1944	20	2.46
			420	Oct. 14, 1944	77	2.06
			439	Oct. 16, 1944	5	2.92
			440	Oct. 16, 1944	10	2.79
			441	Oct. 16, 1944	19	2.58
			442	Oct. 16, 1944	90	2.02
			455	Nov. 18, 1944	180	1.82
NGC 3242....	10 22.1	−18 21	313	Mar. 18, 1944	70	1.84
			314	Mar. 18, 1944	60	2.40
			326	Mar. 19, 1944	60	2.10
			327	Mar. 19, 1944	15	2.31
			333	May 20, 1944	10	2.33
			334	May 20, 1944	60	2.54
			456	Nov. 18, 1944	55	1.90
			482	Mar. 11, 1945	30	1.83
NGC 4361....	12 21.7	−18 28	477	Mar. 9, 1945	195	1.93
			483	Mar. 10, 1945	170	1.79
II 3568.....	12 31	+82 53	488	May 8, 1945	50	1.62
			489	May 8, 1945	10	1.66
II 4593.....	16 9.2	+12 13	336	May 20, 1944	17	1.13
			337	May 20, 1944	45	1.11
			345	May 21, 1944	10	1.29
			346	May 21, 1944	18	1.25
			347	May 21, 1944	43	1.18
			478	Mar. 9, 1945	15	1.10
			479	Mar. 9, 1945	20	1.11
II 4634.....	16 58.3	−21 43	340	May 20, 1944	18	2.10
			349	May 21, 1944	18	2.00
			350	May 21, 1944	60	1.97
			491	May 8, 1945	55	2.54

TABLE 1—*Continued*

Nebula	α	δ	Plate	Date	Exposure (Minutes)	Secant Zenith Distance
NGC 6309....	17h10m9	−12°51′	351	May 21, 1944	87	1.57
			352	May 21, 1944	20	1.93
			358	June 22, 1944	120	1.62
			484	Mar. 11, 1945	17	1.91
			485	Mar. 11, 1945	105	1.64
NGC 6445....	17 46	−20 1	506	June 10, 1945	140	1.85
NGC 6567....	18 10.6	−19 5	353	June 18, 1944	47	1.80
			354	June 18, 1944	24	1.79
			492	May 8, 1945	50	2.37
Anon.....	18 15	+10 6	497	June 9, 1945	65	1.46
			515	June 15, 1945	60	1.34
II 4732.....	18 30	−22 42	399	July 22, 1944	120	2.00
			516	June 15, 1945	60	2.13
			517	June 15, 1945	15	2.28
Anon.....	18 47.3	+20 45	498	June 9, 1945	110	1.12
			502	June 10, 1945	20	2.00
			503	June 10, 1945	63	1.62
NGC 6720....	18 52	+32 57	288	Sept. 18, 1943	.....	1.13
			289	Sept. 18, 1943	.....	1.25
			509	June 14, 1945	.....	1.20
NGC 6741....	19 0	− 0 31	291	Sept. 18, 1943	120	1.36
			292	Sept. 18, 1943	30	1.65
			304	Sept. 21, 1943	105	1.44
			431	Oct. 16, 1944	90	1.61
			432	Oct. 16, 1944	20	2.05
NGC 6751....	19 2.9	− 6 3.1	486	May 7, 1945	115	1.47
			518	June 16, 1945	160	1.39
II 4846.....	19 13	− 9 10	355	June 18, 1944	62	1.66
			355	June 18, 1944	20	1.66
			499	June 9, 1945	60	1.66
NGC 6778....	19 15.5	− 1 42	495	June 8, 1945	110	1.29
			526	July 1, 1945	130	1.38
NGC 6790....	19 20	+ 1 23	381	July 16, 1944	90	1.85
			511	June 14, 1945	60	1.29
			512	June 14, 1945	10	1.35
NGC 6803....	19 29	+ 9 57	385	July 17, 1944	30	1.13
			500	June 9, 1945	60	1.14
			501	June 9, 1945	6	1.17
NGC 6807....	19 32	+ 5 21	400	July 22, 1944	40	1.25
			507	June 10, 1945	15	1.20
Anon.....	19 36.5	+15 48	533	July 2, 1945	90	1.64
			534	July 2, 1945	8	1.30
NGC 6818....	19 40.0	−14 18	297	Sept. 20, 1943	115	1.68
			298	Sept. 20, 1943	30	2.08
			375	July 15, 1944	59	1.81
			379	July 16, 1944	180	1.62
			523	June 16, 1945	60	2.22
NGC 6833....	19 48	+48 49	389	July 18, 1944	83	1.10
			410	Aug. 20, 1944	113	1.03
NGC 6884....	20 9	+46 19	361	June 24, 1944	40	1.61
			362	June 24, 1944	20	1.46
			363	June 24, 1944	119	1.21
NGC 6886....	20 11	+19 50	293	Sept. 19, 1943	60	1.30
			294	Sept. 19, 1943	20	1.39
			299	Sept. 20, 1943	105	1.47
			386	July 17, 1944	170	1.08
			387	July 17, 1944	60	1.33
			443	Oct. 17, 1944	147	1.11
NGC 6891....	20 12	+12 33	401	Aug. 22, 1944	80	1.38
			402	Aug. 22, 1944	25	1.62
			433	Oct. 16, 1944	30	1.47
			434	Oct. 16, 1944	70	1.58

TABLE 1—*Continued*

Nebula	α	δ	Plate	Date	Exposure (Minutes)	Secant Zenith Distance
NGC 6905....	20h20m	+19°56′	493	May 8, 1945	138	1.31
			524	June 16, 1945	115	1.07
NGC 7026....	21 5	+47 46	295	Sept. 19, 1943	65	1.37
			365	June 24, 1944	115	1.04
			366	June 24, 1944	25	1.02
			406	Aug. 19, 1944	190	1.03
			422	Oct. 15, 1944	120	1.04
IC 5117.....	21 30	+44 20	390	Aug. 19, 1944	90	1.06
			391	Aug. 19, 1944	30	1.02
			412	Aug. 20, 1944	90	1.37
			413	Aug. 20, 1944	15	1.62
			460	Nov. 19, 1944	120	1.26
Anon.....	21 31	+39 22	368	June 26, 1944	195	1.32
			392	July 18, 1944	70	1.02
			397	July 22, 1944	20	1.10
			411	Aug. 20, 1944	188	1.01
			435	Oct. 16, 1944	60	1.26
II 5217.....	22 22	+50 42	296	Sept. 17, 1943	45	1.74
			370	June 25, 1944	70	1.07
			371	June 25, 1944	10	1.04
			407	Aug. 19, 1944	120	1.07
			408	Aug. 19, 1944	40	1.25
			452	Nov. 18, 1944	120	1.12
Anon.....	22 29.2	+47 28	528	July 1, 1945	110	1.10
			535	July 2, 1945	90	1.35
			536	July 2, 1945	20	1.21
NGC 7354....	22 38.2	+61 0	510	June 14, 1945	120	1.47
Anon.....	23 24.1	+57 54	538	July 2, 1945	75	1.16
			539	July 2, 1945	20	1.11

TABLE 2

LOWER-EXCITATION NEBULAE

λ	Ion	Anon 0h25m	J 320	II 2149	II 3568	II 4593	II 4634	Anon 19h36m
Bac 20 A....	.....	.....	.....	.....	0.88	0.73	0.70	.....
3703.9.....	*H* I	.....	.....	.....	.....	.....	.....	.....
3712.0.....	*H* I	.....	.....	.....	.....	.....	.....	.....
3727.....	[*O* II]	26	2.1	11	0.95	5.9	3.1	3.7
3750.2.....	*H* I	.....	.....	0.73	.....	.....	.....	.....
3770.6.....	*H* I	.....	.....	0.9	.....	.....	.....	0.36
3797.9.....	*H* I	0.33	0.52	0.92	.....	.....	.....	0.53
3835.4.....	*H* I	1.20	0.75	1.2	0.62	.....	.....	0.51
3868.7.....	[*Ne* III]	11	11	2.4	6.6	3.4	6.0	8.9
3889.1.....	*H* I	3.1	2.6	1.5	2.2	1.9	2.0	1.10
3967.4.....	[*Ne* III]	5.5	5.5	2.3	3.0	2.3	4.0	3.3
4026.2.....	*He* I	.....	.....	.....	0.56	.....	.....	0.46
4069+76....	[*S* II]	0.78	.....	.....	0.39	.....	.....	1.1
4101.8.....	*Hδ*	3.3	3.0	3.0	2.5	2.6	2.3	2.0
4340.5.....	*Hγ*	4.7	5.0	5.2	4.2	5.0	3.9	3.4
4363.2.....	[*O* III]	1.6	1.8	0.60	0.88	.....	0.52	1.0
4471.5.....	*He* I	2.1	0.8	0.76	0.43	0.64	0.46	0.65
4634+40....	*N* III	.....	.....	.....	.....	.....	.....	0.26
4685.8.....	*He* II	2.6	.....	.....	.....	.....	.....	0.52
4711.4.....	[*A* IV]	.....	.....	.....	.....	.....	.....	0.58
4740.3.....	[*A* IV]	.....	.....	.....	.....	.....	.....	0.77
4861.3.....	*H* I	10.0	10.0	10.0	10.0	10.0	10.0	10
4959.5.....	[*O* III]	35	34	14	50	18	28	52
5007.6.....	[*O* III]	88	89	41	140	57	78	19.7
C.....	.....	.....	0.27	0	0.27	0.28	0.0	0.36

TABLE 2—*Continued*

λ	Ion	NGC 6567	Anon 18^h15^m	II 4732	Anon 18^h47^m	II 4846	NGC 6790	NGC 6803	NGC 6807
Bac 20 A			0.92		1.30	0.58	0.60	2.4	
3703.9	*H* I		0.22		0.19				
3712.0	*H* I		0.26		0.25		0.21		
3727	[*O* II]	2.3	16	1.6	7.8	4.0	1.3	4.0	2.9
3750.2	*H* I		0.47		0.37	0.49	0.15	0.33	0.38
3770.6	*H* I		0.47		0.41	0.41	0.24	0.47	0.42
3797.9	*H* I		0.50		0.54	0.75	0.31	0.91	0.56
3835.4	*H* I	0.98	0.81	0.91	0.77	0.88	0.40	1.4	0.72
3868.7	[*Ne* III]	5.6		10	1.07	8.7	8.6	9.6	8.4
3889.1	*H* I	2.1	1.1	1.6	1.4	2.1	1.0	2.1	1.4
3967.4	[*Ne* III]	2.7	1.6	3.4	2.0	4.2	3.2	4.8	3.8
4026.2	*He* I	0.53	0.20		0.22	0.43	0.16	0.30	0.4
4069+76	[*S* II]	0.57	0.51		0.19	0.47	0.14	0.56	0.42
4101.8	*Hδ*	2.50	2.6	2.3	2.5	2.7	1.8	2.3	2.7
4340.5	*Hγ*	4.40	5.1	4.3	4.6	4.9	4.1	4.6	4.9
4363.2	[*O* III]	0.57		2.4	0.22	1.4	1.4	0.98	1.1
4471.5	*He* I	0.60	0.27	0.91	0.48	0.94	0.56	0.96	0.65
4634+40	*N* III				0.11		0.21	0.32	
4685.8	*He* II							0.78	
4711.4	[*A* IV]				0.12		0.21	0.62	
4740.3	[*A* IV]						0.29	0.71	
4861.3	*H* I	10.0	10.0	10	10	10	10	10	10
4959.5	[*O* III]	32	0.48	47	13	36	56	38	40
5007.6	[*O* III]	79	1.61		38	97	147	107	
C		0.06	0.14	0.14	0.17	0.04	0.68	0.23	0.17

TABLE 2—*Continued*

λ	Ion	NGC 6833	NGC 6884	NGC 6891	NGC 7026		II 5117	Anon 22^h29^m	Anon 23^h24^m
					Center	Lobes			
Bac 20 A		0.54		1.34	0.51			1.63	
3712.0	*H* I						0.17	0.39	
3727	[*O* II]	1.1	1.1	1.9	3.1	4.7	2.0	4.0	1.0
3734								0.55	0.48
3750.2	*H* I	0.17	0.11				0.22	0.54	0.40
3770.6	*H* I	0.26	0.12				0.35	0.62	0.41
3797.9	*H* I	0.41	0.20	0.22			0.38	0.90	0.49
3835.4	*H* I	0.54	0.42	0.52			0.51	1.0	0.60
3868.7	[*Ne* III]	6.4	6.0	7.3	6.6	7.4	9.3	7.5	4.5
3889.1	*H* I	1.3	0.78	2.3	1.9	2.1	1.2	2.5	1.1
3967.4	[*Ne* III]	2.9	2.6	3.5	3.1	3.6	4.1	4.1	2.8
4026.2	*He* I	0.18	0.07	0.64			0.30	0.61	
4069+76	[*S* II]	0.22	0.06		0.58	0.41	0.60	0.23	
4101.8	*Hδ*	2.0	0.98	2.5	2.2	2.2	2.3	3.5	1.7
4340.5	*Hγ*	3.4	2.23	5.10	3.7	4.4	4.2	5.2	3.6
4363.2	[*O* III]	1.1	0.52		0.18		1.9	0.83	2.2
4471.5	*He* I	0.38	0.40	0.66	0.44	0.56	0.63	1.22	0.74
4634+40	*N* III		0.26	0.25	0.60	0.46	0.54	0.36	
4685.8	*He* II		1.24	0.20	2.8	1.3	1.38		
4711.4	[*A* IV]		0.42		0.27	0.38	0.50	0.30	
4740.3	[*A* IV]		0.49				0.75		
4861.3	*H* I	10	10	10	10.0	10	10	10	10
4959.5	[*O* III]	22	60	3.0	42	40	61	20	13
5007.6	[*O* III]	54	170	8.3	96	84	160		31
C		0.46	0.84	0.66	0.37		0.46	0.0	0.33

matic image, $I(x)$. At a given point x_0 from the center of the projected nebular image, the intensity $I(x_0)$ in the cross-section is given by the integral equation

$$I(x_0) = 2\int_{x_0}^{\infty} \frac{E(\rho)\,\rho\,d\rho}{\sqrt{\rho^2 - x_0^2}}.$$

Solutions of this equation have been given by Von Zeipel, Plummer, and others.[13] Convenient tables for the numerical solution are given by Wallenquist.[14] Chandrasekhar and Münch[15] have shown that the accuracy attainable in the solution for $E(\rho)$ cannot be high. Probably only the general character of the emission function can be derived.

Measurements of the intensity distribution along the major axis of the images of λλ 4686, 3869, 3727, and 4340 are published elsewhere.[9] Whereas the cross-sections of the *H* and *He* II images may be interpreted in terms of a spherically symmetrical emis-

TABLE 3

HIGH-EXCITATION NEBULAE

λ	Ion	IC 351	IC 2003		NGC 1535 Bright Ring	NGC 2165	J 900
			(*a*)	(*b*)			
3133	*O* III	10	8.5	.....	.....	8.8	3.1
3178	*He* I	.....	.....	.....	.....	0.81	.....
3203	*He* II	3.4	2.7	.....	2.3	1.9	1.4
3299	*O* III	.....	.....	.....	.....	0.74	.....
3312	*O* III	1.7	0.84	.....	.....	0.97	0.57
3346	*Ne* V+*O* III	2.1	1.35	1.56	0.8	2.2	1.05
3425	*Ne* V+*O* III	.....	0.70	0.71	.....	6.0	1.8
3444	*O* III	3.0	2.8	3.0	0.95	2.2	1.7
3650(20 A)	*H*	.....	.....	.....	(1.9)	0.7	0.25
3727	[*O* II]	0.87	4.2	5.0	0.80	3.13	5.2
3750.2	*H*	.....	0.5	.....	.....	0.56	0.55
3770.6	*H*	.....	.....	.....	.....	0.40	0.42
3797.9	*H*	0.62	0.48	.....	.....	0.48	0.50
3819	*He* I	.....	.....	.....	.....	.....	.....
3835.4	*H*	0.61	0.81	.....	.....	0.53	0.74
3868.7	[*Ne* III]	9.0	9.0	7.5	7.4	8.7	7.4
3889.1	*H*	1.7	2.0	2.0	2.1	1.8	1.6
3967.4	[*Ne* III]+*H*	3.8	5.0	4.2	3.0	4.3	3.4
4026.2	*He*	.....	0.28	.....	.....	0.18	0.33
4069+76	[*S* II]	.....	0.25	.....	.....	0.20	0.30
4101.8	*H*	2.3	3.0	3.0	2.1	2.65	2.1
4200	*He* II	.....	.....	.....	.....	0.12	.....
4340.5	*H*	5.8	5.0	6.2	4.9	4.6	4.2
4363.2	[*O* III]	1.6	1.2	.....	1.9	2.1	1.3
4471.5	*He* I	2.8	0.37	.....	0.60	0.34	0.40
4542	*He* II	0.32	0.43	.....	.....	0.18	0.27
4634–40	*N* III	0.37	0.34	.....	.....	0.47	0.32
4685.8	*He* II	6.0	5.6	7.5	2.4	6.0	4.7
4711.4	[*A* IV]	0.85	0.49	.....	.....	0.72	.....
4740.3	[*A* IV]	0.77	0.44	.....	.....	0.65	0.40
4861.3	*H*	10.0	10	10.0	10	10	10
4959.5	[*O* III]	44	40	30	.....	53	39
5007.6	[*O* III]	176	136	98	.....	128	126
C	.....	0.12	0.0		.....	0.0	0.17

[13] See, e.g., Smart, *Stellar Dynamics* (Cambridge: At the University Press, 1938), pp. 297–304.

[14] *Upsala Medd.*, No. 65, p. 42, 1936.

[15] *Ap. J.*, 111, 144, 1950, esp. secs. 2 and 3.

TABLE 3—*Continued*

λ	Ion	NGC 2440	NGC 3242 Bright Ring	NGC 6309	NGC 6741	NGC 6886	Anon 21^h31^m	II 5217
3133	*O* III	4.4	7.0	.....	.....	.....	3.5	
3178	*He* I	.....	.....	.....	.....	.....	.....	.....
3203	*He* II	2.0	2.0	.....	1.3	.....	3.0	.....
3299	*O* III	.....	.....	.....	.....	.....	.....	.....
3312	*O* III	0.73	1.1	.....	.....	0.07	.....	.....
3346	*Ne* V+*O* III	6.7	1.6	.....	1.9	2.0	5.6	.....
3425	*Ne* V+*O* III	16	0.55	4.7	4.1	4.4	18.0	.....
3444	*O* III	1.6	3.3	.....	1.7	0.9	1.0	0.6
3650(20 A)	*H*	0.20	0.80	.....	.....	.....	0.48	0.75
3727	[*O* II]	8.3	1.7	4.7	8.2	9.3	4.5	2.0
3750.2	*H*	.....	.....	.....	.....	0.19	0.25	0.29
3770.6	*H*	.....	.....	.....	.....	0.17	0.37	0.32
3797.9	*H*	.....	.....	.....	.....	0.20	0.47	0.52
3819	*He* I	.....	.....	.....	.....	.....	.....	.....
3835.4	*H*	.....	.....	.....	0.74	0.60	0.69	0.60
3868.7	[*Ne* III]	8.3	11.7	9.5	8.6	9.7	6.2	9.8
3889.1	*H*	.....	.....	.....	1.2	1.1	1.7	2.0
3967.4	[*Ne* III]+*H*	3.7	5.0	4.5	3.2	3.3	3.4	4.2
4026.2	*He*	.....	.....	.....	0.62	0.12	0.26	0.20
4069+76	[*S* II]	.....	.....	.....	0.60	0.44	0.28	0.16
4101.8	*H*	2.6	3.2	2.6	3.0	1.7	2.25	2.8
4200	*He* II	.....	.....	.....	0.36	.....	.....	.....
4340.5	*H*	5.2	6.3	4.2	3.7	4.0	4.6	5.5
4363.2	[*O* III]	2.9	.....	.....	1.3	1.5	2.0	1.3
4471.5	*He* I	0.27	0.52	.....	0.50	0.22	0.53	0.62
4542	*He* II	0.30	.....	.....	.....	.....	0.82	.....
4634–40	*N* III	1.0	0.66	.....	0.62	0.42	0.20	0.34
4685.8	*He* II	7.6	5.1	7.7	3.4	4.0	9.0	1.30
4711.4	[*A* IV]	1.6	.....	.....	0.81	0.4	1.0	0.70
4740.3	[*A* IV]		.....	.....	1.32	0.4	0.5	0.74
4861.3	*H*	10	10	10	10.0	10.0	10	10
4959.5	[*O* III]	75	59	40	58	65	29	55
5007.6	[*O* III]	.....	135	101	141	160	75	150
C	.....	.....	.....	.....	0.16	0.49	0.21	.....

sion per unit volume, the [*Ne* III] and [*O* II] images clearly show that the emission departs far from spherical symmetry. In fact, negative values of $E(\rho)$ are required for the region just inside the edge of the ring, in order to represent the observed data. Therefore, departures from spherical symmetry are severe. In view of the filamentary character of this object this result is hardly surprising.

Comments on other nebulae are given in the notes to Table 4.

The structural features of a number of planetary nebulae are being studied in collaboration with Olin C. Wilson, who has obtained slitless spectra with the 100-inch coudé. The present measures may be of value in relating the intensity measures in one monochromatic image with those in another.

V. THE BALMER DECREMENT

Because of the uncertainties in the collisional cross-sections, we are unable to derive ionic abundances and electron temperatures from the nebular line intensities, nor does it seem worth while to calculate electron densities, since the nebular surface brightnesses and distances are so poorly known. Accordingly, our discussion is restricted here to a single problem—the Balmer decrement.

The most detailed observational discussion of the Balmer decrement is that by Ber-

TABLE 4

NEBULAE WITH EXTENDED SURFACES

λ	Ion	NGC 4361*	NGC 6445†	NGC 6571‡	NGC 6778§	NGC 6818		NGC 6905‖	NGC 7354#
						West Side	East Side		
3133	*O* III	.....	.....	.....	.....	.....	.....	2.2	.....
3203	*He* II	.....	.....	.....	.....	.....	.....	2.8	.....
3346	[*Ne* V]	5.4	.....	.....	.....	2.6	4.8	.....	.....
3428	[*Ne* V]	.....	.....	.....	.....	6.7	8.6	.....	.....
3444	*O* III	20	.....	.....	.....	.....	3.2	.....	.....
3650(20 A)	*H*	.....	.....	1.2	0.19	1.0	.....	.....	.....
3727	[*O* II]	.....	20	17	5.8	4.7	6.8	0.87	.....
3868	[*Ne* III]	5	12	7.5	4.6	11	14	5.2	5.5
3889	*H*	.....	.....	.....	2.2	.....	2.0	.....	.....
3967.4	[*Ne* III]	3.7	.....	3.8	2.2	4.5	4.5	2.2	2.6
4101.8	*Hδ*	4.2	.....	3.2	2.8	3.0	2.6	1.6	2.8
4340.5	*Hγ*	9.7	4.1	5.4	4.3	5.9	6.6	2.4	3.6
4363.2	[*O* III]	.....	.....	.....	1.3	.....	2.1	.....	.....
4471.5	*He* I	.....	.....	.....	1.1	.....	.....	.....	.....
4634–40	*N* III	.....	.....	.....	0.8	.....	.....	.....	.....
4686	*He* II	25	5.6	3.2	1.62	8.2	9.3	3.9	6.2
4740	[*A* IV]	.....	.....	.....	.....	.....	1.3	.....	.....
4861	*Hβ*	60	10	10	10	10	10	10	10
4959	[*O* III]		110	160	24	.....	170	78	140
5007	[*O* III]		.....	.....	65	.....	.....	.....	.....

* High excitation. Overlapping of irregular monochromatic images prevents accurate measurements.

† The monochromatic images resemble one another closely. The appearance of NGC 6445 recalls a coral atoll and inclosed lagoon.

‡ Tabulated values are means of two sides of nebulae.

§ Both lobes have the same excitation. Mean values are tabulated.

‖ Mean of measures in three parts of nebula.

The monocromatic images resemble one another closely.

TABLE 5

STRUCTURE OF NGC 7026

Distance	*O* III	*O* II	*Ne* III	Hydrogen	Distance	*O* III	*O* II	*Ne* III	Hydrogen
x	.....	.....	.....	.....	4	81	3.62	4.66	6.51
0	71	2.32	3.31	4.25	5	53.5	2.29	2.33	3.86
1″	70	2.6	4.41	5.85	6	23.8	1.33	0.98	2.3
2	77	3.51	6.62	8.60	7	9.15	0.64	0.417	1.0
3	82	4.72	7.35	10.0	8	4.88	0.29	0.07	0.13

STRUCTURE OF NGC 6778

Distance	*O* II	*O* III	Hydrogen	Distance	*O* II	*O* III	Hydrogen
0	3.7	57.5	8.2	8	3.86	29.4	4.7
1″	3.8	58.5	8.5	9	3.11	20	3.1
2	3.9	62.7	9.2	10	2.2	12	1.8
3	4.0	64.5	9.8	11	1.3	6.3	1.0
4	4.3	63	10.0	12	0.81	3.0	0.36
5	4.8	60	10.0	13	0.49	1.15	.....
6	4.87	53	9.0	14	0.26	.....	.....
7	4.48	42	7.1				

man,[16] who calibrated Wright's intensity estimates with the aid of photometric measurements of his own. He divided the nebulae into three classes, depending on the ratio of N2 to $H\beta$. In order to correct for space absorption, he assumed the interstellar material to be uniformly distributed in galactic longitude and to fall off uniformly with height above the galactic plane. The distance of each nebula had been derived from studies of galactic rotation.[17] With the aid of the distances, line intensities, and galactic latitudes, he made a least-squares solution for the coefficient of absorption per kiloparsec, the exponent n in the assumed law of selective absorption λ^{-n}, and the Balmer decrement for each group. We summarize his results for the Balmer decrement in Table 6. The difficulty with Berman's procedure is that the absorbing material is so unevenly distributed throughout the galaxy that the basic assumptions are not even approximately fulfilled.

TABLE 6

THE BALMER DECREMENT
(After Berman)

λ	I	II	III	λ	I	II	III
4861.....	10.0	10.0	10.0	3969.....	1.25	1.37	1.79
4340.....	4.45	4.80	5.00	3889.....	1.15	1.00	1.24
4101.....	2.13	2.4	2.63	3835.....	0.77	0.52	0.89

In an attempt to overcome some of these difficulties, the nebulae have been divided into three classes: *S*, stellar low-excitation objects; *L*, low-excitation objects with extended surfaces; and *H*, high-excitation objects (those showing ultraviolet *He* II [*Ne* V], or *O* III lines). Smoothed Balmer decrements are derived for each of these objects. If the true decrements are the same for each group, the smoothed intensities should differ from one another only because of differential space absorption. In particular, the nebulae with the slowest decrements should be the least affected by space absorption. Accordingly, the Balmer decrements for each group have been reduced on the assumption that the one with the slowest decrement is essentially unaffected. In this way a set of tentative, observed Balmer decrements may be found.

With observations of this precision, it suffices to take the absorption proportional to $1/\lambda$. Hence one may write

$$\log \frac{I_n}{I_4} = \log \left(\frac{I_n}{I_4}\right)_0 - C\left[\frac{1}{\lambda_n} - \frac{1}{0.4861}\right],$$

where I_n/I_4 is the intensity of the nth line referred to $H\beta$ as 1.0; the subscript "0" refers to the value that this ratio would have if corrected for space absorption; and C is a constant to be determined for each nebula, whose value, computed by least squares, is listed in Tables 2 and 3 for several nebulae. The wave lengths, λ_n, are assumed expressed in microns. With the aid of these C's, it is possible to correct the intensities of the nebular lines for the effects of space absorption.

The mean Balmer decrements, calculated for groups *S*, *L*, and *H*, are compared with the theoretical calculations by Menzel and his colleagues.[18] Models *A* and *B* assume a nebula in which the central star radiates no energy in the Lyman lines. Model *A* is transparent in the lines, so that all the Lyman radiation produced in the nebula by cyclic processes escapes. In model *B*, all Lyman radiation is assumed degraded into Lyman-α,

[16] *M.N.*, **96**, 890, 1936.

[17] L. Berman, *Lick Obs. Bull.*, **18**, 57, 1937.

[18] See J. G. Baker and D. N. Menzel, *Ap. J.*, **88**, 52, 1938; Baker, Menzel, and Aller, **88**, 423, 1938; **89**, 587, 1939.

which alone escapes from the nebula. The Balmer decrement is rather insensitive to the electron temperature; I have chosen a value of 10,000° as representative of typical planetary nebulae. Model *C* refers to a thin nebula (similar to *A*), whose central star radiates like a black body in the Lyman lines. The stellar radiation steepens the theoretical decrement markedly; it would have little influence in a thick nebula.

The Balmer decrement is quite similar for the three groups of nebulae, and there is no clear-cut indication that the high-excitation objects have a systematically different decrement than do the low-excitation objects. The decrements I have found are less steep than those published by Berman but are in substantial agreement with the calculations for theoretical model *B*. This result comes as no surprise, since both models *A* and *C* correspond to thin shells, which should be much fainter than the objects studied in the present survey. It is, of course, possible that slight variations will be found in the Balmer decrements for objects of comparable density and excitation; but, until such differences have been established, it would appear that space absorption remains the chief cause of the variation in the observed decrements, an opinion expressed by Berman some years ago.

VI. THE SPECTRA OF THE CENTRAL STARS

The spectra of the central stars of the planetary nebulae are difficult to observe. Absorption lines originating in the nucleus are often smothered under strong nebular emission, and nuclear emission lines can be observed only when they do not coincide in position with nebular lines.[16]

Stars with continuous spectra.—Most of the central stars showed continuous spectra. Thus Anon 0^h25^m, NGC 6807, II 4732, and probably also NGC 6309 and 6567 showed weak continua probably of stellar origin, with no trace of any stellar emission lines. The well-exposed spectrum of the central star of Anon 18^h15^m showed no trace of any emission lines. A number of central stars, those of IC 351, Anon 18^h47^m, NGC 6790, NGC 6803, Anon $19^h36^m.5$, NGC 6884, and NGC 5217 show λ 4686 *He* II, λλ 4712–4740 [*A* IV], and the λ 4640 group. Probably the λ 4640 lines, as well as the others, originate in the inner portion of the nebula rather than in the star. The central stars of Anon 22^h29^m and 23^h24^m seem to show the λ 4640 group, but not λ 4686. These lines may

TABLE 7

THE BALMER DECREMENT: COMPARISON BETWEEN THEORY AND OBSERVATION

λ	*n*	Observed			Theoretical		
		Low Excitation		High Excitation *H*			
		Stellar *S*	Nonstellar *L*		*A*	*B*	*C*
4861	4	.....	.....	.....	.....	.....	.....
4340	5	5.25	5.66	5.65	5.76	5.1	3.5
4101	6	2.97	3.31	3.13	3.74	3.1	1.6
3969	7	1.93	2.20	1.99	2.55	2.06	0.89
3889	8	1.44	1.50	1.32	1.82	1.43	0.55
3835	9	1.00	1.03	0.93	1.36	1.05	0.36
3797	10	0.74	0.85	0.66	1.05	0.79	0.25
3770	11	0.57	0.56	0.49	0.81	0.59	.....
3750	12	0.45	0.46	0.36	0.65	0.46	.....
3734	13	0.42	.....	.....	0.52	0.37	.....
3722	14	0.38	.....	.....	0.42	0.30	.....
3712	15	0.30	.....	.....	0.35	0.25	.....
3707	.....	0.26	.....	.....	.....	.....	.....

originate in the star itself. On the other hand, J 320 shows λ 4686 but no λ 4640; presumably the emission here is of nebular origin.

The intensity distribution in the continuous spectra of some of the brighter stars has been measured. Table 8 gives the results for NGC 1535, NGC 6891, and II 4593. No correction has been made for space absorption. Preferably, such studies should be made with carefully guided wide-slit spectrograms (to eliminate sky fog) and with somewhat higher dispersion than I have employed.

TABLE 8

INTENSITY DISTRIBUTION IN THE CONTINUOUS SPECTRA OF CENTRAL STARS OF NGC 1535, NGC 6891, AND II 4593

λ	IC 4593	log (I_λ/I_{4386})		λ	IC 4593	log (I_λ/I_{4386})	
		NGC 6891	NGC 1535			NGC 6891	NGC 1535
3300	0.67	.....	0.68	4100	0.21	0.26	0.15
3400	.59	0.74	.59	4200	.19	.21	.11
3500	.53	.67	.51	4300	.16	.16	.09
3600	.47	.58	.43	4400	.13	.12	.07
3700	.41	.49	.36	4500	.11	.09	.06
3800	.35	.42	.30	4600	.08	.06	.04
3900	.30	.36	.24	4700	.05	.03	.02
4000	0.25	0.31	0.19	4800	0.00	0.00	0.00

TABLE 9

THE SPECTRA OF THE NUCLEI OF NGC 6751 AND NGC 6905

NGC 6751		NGC 6905		IDENTIFICATION
λ	I	λ	I	
3203	0.36	3203(prob.neb.)	5	3203 *He* II
3276	0.25	.....	.....	3275 *O* V
3338–3357	0.63	.....	.....	3360 *N* III
~3380	0.39	.....	.....	3381 *O* III+*O* IV
3397–3429	1.3	.....	.....	3411 *O* IV
~3430	0.49	3420–3437	2.9	3429–3445 *O* III
3469–3489	0.55	.....	.....	3483 *N* IV
3696–3722	1.2	3672–3710	2	3708–3750 *O* III, *O* IV, *O* V
3808–3837	0.42	3794–3854	22	3811–3834 *O* VI
3947–3987	0.33	3920–3982	2.3	3965 *O* III
4082–4125	0.55	4096–4141	.....	4070 *O* III 4100 *N* III, *He* II 4123 *O* V
~4200	0.19	.....	.....	4200 *N* III, *He* II
	0.18	.....	.....	.....
4427–4470	0.26	4410–4470	0.76	4441 *C* IV
4492–4572	0.13 0.17	4490–4565	1.2	4512–4540 *N* III? 4542 *He* II 4515 *C* III
4616–4714	10.0	4640–4702	10	4650 *C* III, *C* IV 4686 *He* II

The central stars of NGC 7026, 6751, and 6905 show broad emission lines. In the nucleus of NGC 7026 no lines are found in addition to those near λ 3800 and λ 4650, although there is some suggestion of weak diffuse features in the ultraviolet. The spectrum of the central star of NGC 6751 is of the carbon-sequence, Wolf-Rayet type, with high-excitation lines of carbon, helium, and oxygen in various stages of ionization. Nitrogen, represented by the λ 3483 *N* III group, may be present also. The spectrum of the nucleus of NGC 6905 is similar, although there is no suggestion of any nitrogen. Presumably it and the nucleus of NGC 7026 are typical stars of the carbon sequence, in which the stronger features are the *C* IV λ 4650 and *O* VI λ 3811 groups. Table 9 gives the intensities for the nuclear emission lines of NGC 6751 and 6905. Measures are difficult because of the overlapping nebular spectrum and the faint diffuse character of the stellar lines.

I want to thank Director C. D. Shane and express my gratitude to the late Dr. J. H. Moore, who made it possible for me to obtain these plates at the Lick Observatory. I am grateful to Dr. Otto Struve, then director of the Yerkes Observatory, who allowed me the use of their microphotometer with which many of the tracings were made. Thanks are due to the Graduate School of Indiana University and to the Draper Fund of the National Academy for grants to aid the reduction of the observations. Miss Carolyn Mooshy assisted with the measurement and reduction of the tracings.

A FINDING LIST OF O AND B STARS OF HIGH LUMINOSITY

J. J. NASSAU AND W. W. MORGAN
Warner and Swasey and Yerkes Observatories
Received September 1, 1950

ABSTRACT

A catalogue is given of 918 stars classified on objective-prism plates as being of classes O and B and higher in luminosity than main-sequence stars of classes B2–B5.

The details of the Case survey for early-type stars of high luminosity have been given elsewhere.[1] The survey covered a belt approximately 12° wide, centered on the galactic equator and extending over the northern sky between galactic longitudes 333° and 202°. The plates were taken with the 24–36-inch Schmidt camera of the Warner and Swasey Observatory with a 4° prism. The average limiting magnitude for the various fields is in the neighborhood of 10.0 pg.

The stars, for which a tentative spectral type of OB has been suggested, include the following kinds of objects: (1) O and early B stars of all luminosities; (2) high-luminosity stars of types B2–A3; and (3) certain Be stars which simulate B supergiants on objective-prism plates of low dispersion.

The above listing includes all early-type stars having total intensities for the hydrogen lines weaker than a certain arbitrary limit; this was the principal criterion of classification. In particular, main-sequence stars of types B2 and later should not be present, except for a few borderline cases.

The catalogue (Tables 1–4) is divided into four parts: (1) stars in the *Henry Draper Catalogue;* (2) stars in the *Henry Draper Extension;* (3) stars in the *Bonner Durchmusterung* and not in parts 1 or 2; and (4) stars not in the *Bonner Durchmusterung*. No magnitudes are given for the last group; the objects here are around the tenth magnitude.

It should be emphasized that there is a wide range in luminosity and spectral type in the stars included, and caution should be exercised in attempting to derive distances from average characteristics of the group. A joint program is now in progress at the Yerkes and Washburn Observatories for the determination of accurate absolute magnitudes and color excesses for the stars listed.

The survey was carried out under a grant from the Office of Naval Research.

[1] See papers presented at symposium at the University of Michigan, June, 1950 (*Pub. Obs. U. Michigan*, in press).

TABLE 1

OB Stars in the Henry Draper Catalogue

HD	BD	α (1900)	δ (1900)	m
108	+62°2363	0h 0m.9	+63° 7'	7.36
1070	+58 18	0 9.9	+59 15	8.2
1383	+60 25	0 12.9	+61 10	7.9
1544	+61 38	0 14.6	+61 31	8.0
2451	+61 92	0 23.2	+61 57	8.6
2619	+64 52	0 24.7	+64 43	8.2
2928	+61 113	0 27.5	+61 59	8.7
3191	+60 71	0 30.1	+60 55	8.6
3940	+63 81	0 36.9	+63 45	7.40
4613	+64 83	0 43.0	+65 2	8.9
4694	+63 97	0 43.9	+64 5	8.4
4768	+58 119	0 44.6	+59 7	8.0
4841	+62 160	0 45.4	+63 14	7.06
5005	+55 191	0 47.0	+56 5	7.7
5551	+62 175	0 52.2	+63 11	7.7
5552	+61 187	0 52.2	+61 24	9.0
5689	+62 178	0 53.5	+63 5	9.2
5776	+62 181	0 54.3	+62 30	8.4
6182	+61 200	0 57.8	+61 18	8.6
7103	+61 223	1 6.2	+61 21	8.6
7902	+57 257	1 13.6	+57 40	7.9
8768	+62 254	1 21.4	+62 45	8.0
8965	+59 260	1 23.3	+59 44	7.26
9105	+62 259	1 24.6	+62 51	7.46
9311	+59 271	1 26.6	+60 10	7.26
10063	+55 375	1 33.3	+55 17	7.61
10125	+63 218	1 33.9	+63 40	8.0
10756	+59 318	1 40.1	+60 10	7.71
10898	+57 399	1 41.9	+57 58	8.2
11554	+57 425	1 48.4	+57 24	9.2
11831	+59 364	1 51.1	+59 54	8.0
12302	+58 356	1 55.6	+59 12	8.2
12323	+54 441	1 55.8	+55 8	8.96
12509	+63 281	1 57.6	+63 54	8.0
12567	+63 287	1 58.1	+63 49	8.8
12727	+56 425	1 59.6	+56 34	8.8
12856	+56 429	2 0.9	+56 38	8.4
12867	+57 492	2 1.0	+57 14	9.2
12953	+57 494	2 1.7	+57 57	5.90
12993	+57 498	2 2.1	+57 27	8.6
13051	+56 432	2 2.6	+56 31	8.0
13267	+56 438	2 4.6	+57 11	6.36
13268	+55 534	2 4.6	+55 41	8.2
13338	+57 512	2 5.3	+57 28	9.2
13402	+58 396	2 5.9	+59 4	8.2
13476	+57 519	2 6.6	+58 6	6.50
13494	+55 543	2 6.7	+56 6	9.2
13544	+53 480	2 7.1	+53 27	9.0
13561	+55 547	2 7.3	+56 2	9.0
13590	+63 310	2 7.6	+63 34	8.0
13621	+54 494	2 7.8	+54 51	8.06
13659	+56 462	2 8.1	+56 28	8.9
13716	+57 525	2 8.6	+57 18	8.5
13744	+57 526	2 8.9	+57 50	7.8
13745	+55 554	2 8.9	+55 32	7.96
13758	+57° 527	2h 9m.0	+57°17'	8.9
13831	+56 469	2 9.7	+56 17	8.6
13841	+56 470	2 9.8	+56 34	7.21
13854	+56 471	2 9.9	+56 36	6.42
13866	+56 475	2 10.0	+56 15	7.7
13890	+56 478	2 10.2	+56 19	8.9
13900	+56 479	2 10.3	+56 26	9.0
13969	+56 485	2 10.8	+56 38	8.8
14010	+63 315	2 11.1	+63 58	7.05
14014	+55 567	2 11.1	+55 46	9.0
14052	+56 500	2 11.4	+56 45	8.6
14053	+56 498	2 11.4	+56 33	8.7
14092	+56 507	2 11.7	+56 18	9.5
14134	+56 522	2 12.1	+56 40	6.66
14143	+56 530	2 12.2	+56 43	6.66
14162	+56 535	2 12.4	+56 41	9.4
14250	+56 545	2 13.2	+56 39	8.6
14302	+55 587	2 13.6	+55 52	8.8
14331	+55 590	2 13.9	+55 22	8.81
14357	+56 555	2 14.1	+56 25	8.9
14422	+56 565	2 14.7	+56 56	9.4
14433	+56 568	2 14.8	+56 47	6.54
14434	+56 567	2 14.8	+56 27	8.5
14442	+58 455	2 14.9	+59 6	9.2
14443	+56 570	2 14.9	+56 42	8.6
14501	+57 551	2 15.4	+57 42	9.5
14520	+56 588	2 15.6	+56 38	9.2
14535	+56 591	2 15.8	+56 47	7.46
14542	+56 593	2 15.9	+56 56	6.95
14605	+55 605	2 16.5	+56 8	9.7
14899	+56 621	2 19.2	+56 47	7.42
14947	+58 467	2 19.5	+58 25	8.04
14956	+57 568	2 19.6	+57 14	7.32
15316	+57 576	2 22.8	+57 22	7.30
15325	+56 635	2 22.9	+56 48	8.5
15497	+57 582	2 24.6	+57 15	7.20
15548	+56 647	2 25.0	+56 13	8.9
15558	+60 502	2 25.1	+61 1	7.82
15570	+60 504	2 25.2	+60 56	8.0
15571	+56 648	2 25.2	+56 59	8.0
15620	+57 584	2 25.6	+57 31	8.2
15629	+60 507	2 25.7	+61 5	8.4
15642	+54 569	2 25.8	+54 54	8.0
15690	+56 656	2 26.3	+57 5	7.7
15752	+57 589	2 26.8	+57 58	8.8
15785	+59 513	2 27.2	+60 6	8.41
16243	+57 602	2 31.3	+57 23	8.5
16429	+60 541	2 33.1	+60 51	7.8
16691	+56 693	2 35.5	+56 28	8.4
16778	+59 535	2 36.3	+59 24	7.71
16779	+57 620	2 36.3	+57 24	8.6
16808	+57 622	2 36.7	+57 53	8.9
16832	+56 703	2 36.9	+56 14	9.0
17088	+57 632	2 39.5	+57 19	7.54
17114	+58 518	2 39.7	+58 55	9.2

TABLE 1 (continued)

HD	BD	α (1900)	δ (1900)	m
17145	+57° 634	2h40m0	+57°15'	8.0
17378	+56 718	2 42.2	+56 40	6.53
17505	+59 552	2 43.4	+60 1	7.11
17520	+59 553	2 43.5	+59 59	8.7
17603	+56 728	2 44.4	+56 38	8.6
17857	+63 367	2 47.0	+63 43	7.78
18076	+58 534	2 49.2	+58 41	9.0
18326	+59 578	2 51.6	+60 10	7.91
18352	+60 608	2 51.9	+60 53	7.00
18409	+62 504	2 52.4	+62 19	8.0
19243	+61 525	3 0.7	+62 0	6.54
19820	+59 609	3 6.2	+59 11	7.09
20898	+59 648	3 17.1	+60 8	7.66
20959	+58 600	3 17.8	+59 5	8.2
21212	+61 587	3 20.3	+62 9	8.9
22253	+56 824	3 29.9	+56 23	6.79
23675	+52 714	3 41.9	+52 21	6.76
23800	+52 715	3 42.9	+52 11	6.87
24431	+52 726	3 48.1	+52 21	6.70
24432	+48 1019	3 48.1	+48 45	7.02
25348	+52 752	3 56.6	+53 3	8.2
25517	+43 886	3 58.1	+44 0	8.9
25914	+56 884	4 1.2	+56 50	8.1
31327	+35 930	4 49.7	+36 1	6.18
33357	+41 1101	5 4.6	+42 2	8.2*
33461	+41 1106	5 5.3	+41 6	8.0
33604	+40 1213	5 6.3	+40 5	7.32
34921	+37 1160	5 15.8	+37 35	7.39
35215	+30 873	5 18.1	+30 6	9.11
35347	+29 886	5 19.0	+29 32	8.5
35619	+34 1046	5 21.0	+34 41	9.0
35633	+34 1049	5 21.1	+34 27	8.6
35653	+33 1049	5 21.2	+33 52	7.50
35921	+35 1137	5 23.0	+35 18	6.71
35952	+35 1139	5 23.2	+35 53	8.7
36212	+34 1077	5 25.1	+34 48	8.0
36280	+34 1079	5 25.5	+34 52	9.4
36483	+36 1177	5 26.9	+36 24	7.7
36547	+23 942	5 27.4	+23 16	8.8
36879	+21 899	5 29.7	+21 20	7.8
37032	+34 1118	5 30.5	+34 45	8.1
37614-5	+38 1250	5 34.7	+38 8	8.0
37737	+36 1233	5 35.7	+36 9	8.0
37767	+36 1236	5 35.9	+36 6	8.4
38017	+30 992	5 37.6	+30 53	8.1
38131	+35 1223	5 38.4	+35 8	8.12
38191	+21 958	5 38.9	+21 25	9.5
38658	+28 902	5 42.3	+28 17	8.5
38708	+29 1005	5 42.6	+29 6	8.2
38909	+31 1115	5 44.0	+31 2	8.0
39136	+32 1111	5 45.4	+32 13	9.0
39680	+13 1026	5 49.0	+13 49	7.9
39712	+30 1055	5 49.2	+30 41	8.4
39746	+27 914	5 49.4	+27 42	7.7
40003	+23 1119	5 51.1	+23 25	8.6
40111	+25 1052	5 51.8	+25 57	4.90
40297	+27 938	5 52.8	+27 33	7.9
40589	+27 945	5 54.7	+27 35	6.08
40893	+31 1174	5 56.7	+31 2	9.0
40894	+28 991	5 56.7	+28 40	7.9
41398	+28°1008	5h59m8	+28°56'	7.45
41690	+21 1120	6 1.6	+21 53	8.0
41997	+15 1079	6 3.2	+15 44	8.5
42087	+23 1226	6 3.7	+23 8	5.76
42088	+20 1284	6 3.7	+20 31	7.40
42379	+21 1143	6 5.3	+21 36	7.8
42400	+20 1302	6 5.4	+20 56	6.86
42896	+20 1322	6 8.2	+20 13	9.0
43078	+22 1243	6 9.2	+22 20	8.6
43582	+22 1267	6 11.9	+22 41	9.0
43703	+23 1289	6 12.6	+23 3	8.7
43753	+23 1297	6 12.9	+23 2	8.1
43818	+23 1300	6 13.2	+23 30	7.03
43836	+23 1301	6 13.3	+23 19	7.03
43837	+20 1369	6 13.3	+20 37	8.4
43907	+22 1280	6 13.7	+22 9	8.8
44139	+22 1291	6 15.1	+22 13	8.8
44597	+20 1399	6 17.5	+20 27	9.0
44637	+15 1176	6 17.7	+15 9	7.7
44811	+19 1335	6 18.8	+19 45	8.7
44965	+11 1162	6 19.6	+11 45	7.7
45166	+ 8 1332	6 20.8	+ 8 3	9.6
45314	+14 1296	6 21.6	+14 57	7.09
45626	- 4 1534	6 23.4	- 4 23	9.1
45910	+ 5 1267	6 25.2	+ 5 57	6.70
45995	+11 1204	6 25.6	+11 19	5.83
46056	+ 4 1291	6 26.0	+ 4 54	7.96
46149	+ 5 1282	6 26.6	+ 5 6	7.66
46150	+ 5 1283	6 26.6	+ 5 0	6.80
46223	+ 4 1302	6 27.0	+ 4 53	7.14
46484	+ 4 1319	6 28.6	+ 4 44	7.65
46485	+ 4 1318	6 28.6	+ 4 36	8.3
46559	+ 2 1292	6 29.0	+ 2 28	8.5
46573	+ 2 1295	6 29.1	+ 2 36	8.1
46660	+11 1232	6 29.5	+11 12	7.9
46711	+ 2 1299	6 29.8	+ 2 51	8.9
46783	+ 9 1295	6 30.2	+ 9 56	7.92
46847	+ 2 1302	6 30.5	+ 2 47	8.9
46966	+ 6 1303	6 31.1	+ 6 10	7.3
47129	+ 6 1309	6 32.0	+ 6 13	6.06
47240	+ 5 1334	6 32.5	+ 5 3	6.16
47360	+ 4 1360	6 33.1	+ 4 43	8.3
47382	+ 4 1361	6 33.2	+ 4 42	7.9
47417	+ 7 1386	6 33.4	+ 7 0	7.4
47761	- 4 1607	6 35.1	- 4 36	8.5
47887	+ 9 1344	6 35.7	+ 9 34	7.02
48099	+ 6 1351	6 36.6	+ 6 27	6.20
48279	+ 1 1472	6 37.5	+ 1 49	7.8
48282	-10 1651	6 37.5	-10 24	9.0
48434	+ 4 1414	6 38.3	+ 4 2	5.78
48615	+12 1264	6 39.2	+12 11	8.8
48663	+12 1267	6 39.4	+12 21	8.4
48691	+ 0 1574	6 39.5	+ 0 42	7.7
49330	+ 0 1607	6 42.8	+ 0 53	8.79
49585	+ 0 1624	6 44.0	+ 0 12	9.1
49787	- 5 1815	6 45.0	- 5 24	7.30
49977	-13 1682	6 45.9	-14 0	7.9
49992	- 5 1827	6 46.0	- 5 13	9.2
50064	+ 0 1651	6 46.4	+ 0 25	8.3
50083	+ 5 1448	6 46.5	+ 5 13	6.76

TABLE 1 (continued)

HD	BD	α (1900)	δ (1900)	m
50091	-13°1686	6h46m5	-13° 7'	8.5
50696	+ 0 1691	6 49.2	+ 0 18	8.4
50891	- 3 1643	6 50.0	- 3 34	9.2
51193	- 3 1651	6 51.3	- 3 40	8.7
51452	- 4 1745	6 52.3	- 4 4	8.5
51480	-10 1774	6 52.4	-10 41	6.97
51756	- 2 1856	6 53.5	- 2 53	7.7
52244	-16 1694	6 55.3	-16 3	9.0
52266	- 5 1912	6 55.4	- 5 40	6.97
52382	- 8 1667	6 55.9	- 9 4	6.36
52504	- 2 1884	6 56.4	- 3 0	9.6
52533	- 2 1885	6 56.5	- 2 59	7.9
53032	- 2 1898	6 58.4	- 2 36	9.6
53367	-10 1848	6 59.7	-10 18	7.01
53428	- 8 1729	6 59.9	- 8 42	7.9
53649	- 8 1733	7 0.7	- 8 52	9.1
53667	- 8 1734	7 0.8	- 8 34	7.8
53754	- 8 1737	7 1.1	- 8 39	8.4
53755	-10 1862	7 1.1	-10 30	6.38
53756	-12 1777	7 1.1	-12 40	7.20
53974	-11 1790	7 2.0	-11 8	5.28
53975	-12 1788	7 2.0	-12 14	6.40
54439	-11 1812	7 3.7	-11 42	8.5
54464	- 3 1762	7 3.8	- 3 54	8.6
54493	-12 1809	7 3.9	-12 43	7.00
54662	-10 1892	7 4.6	-10 11	6.20
54764	-16 1802	7 5.0	-16 4	6.03
54786	-15 1672	7 5.1	-15 56	9.2
54879	-11 1822	7 5.5	-11 39	7.9
54911	-15 1681	7 5.6	-15 31	7.03
55036	- 4 1845	7 6.2	- 4 32	7.8
55606	- 1 1603	7 8.5	- 1 54	8.72
55879	-10 1933	7 9.7	-10 8	5.99
56310	-15 1732	7 11.4	-16 3	6.79
56847	-15 1748	7 13.6	-15 27	8.7
57386	- 8 1856	7 15.9	- 8 15	8.1
57682	- 8 1872	7 17.2	- 8 48	6.17
58439	-18 1825	7 20.5	-18 49	6.27
58644	- 8 1909	7 21.4	- 8 54	8.1
59075	-18 1847	7 23.2	-18 17	8.5
59094	-15 1837	7 23.3	-15 53	9.0
60308	-15 1892	7 28.7	-15 14	8.30
60325	-14 1966	7 28.8	-14 7	6.24
60855	-14 1999	7 31.4	-14 16	5.57
61347	-13 2143	7 33.7	-13 38	8.3
62532	-17 2120	7 39.3	-17 42	8.6
159864	-17 4864	17 31.8	-17 46	8.8
160186	-18 4598	17 33.4	-18 21	8.8
163800	-22 4474	17 52.9	-22 30	6.92
163892	-22 4478	17 53.4	-22 27	7.14
164002	-22 4484	17 53.9	-22 33	7.15
164188	-15 4767	17 54.9	-15 48	9.0
164359	-22 4500	17 55.6	-22 7	8.2
164384	-23 13789	17 55.7	-23 10	8.5
164402	-22 4503	17 55.8	-22 46	5.73
164438	-19 4800	17 56.0	-19 6	7.28
164492	-23 13804	17 56.3	-23 1	6.91
164581	-20 4952	17 56.7	-20 44	6.85
164637	-22 4516	17 57.0	-22 43	6.57
164833	-22 4533	17 57.9	-22 50	6.86

HD	BD	α (1900)	δ (1900)	m
164844	-22°4535	17h58m0	-22°34'	8.9
164883	-22 4541	17 58.1	-22 30	7.8
165049	-15 4803	17 59.0	-15 22	8.07
165285	-19 4836	18 0.1	-19 58	8.73
165319	-14 4880	18 0.3	-14 12	8.1
165516	-21 4855	18 1.2	-21 27	6.22
165783	-19 4858	18 2.6	-19 52	8.38
165784	-21 4866	18 2.6	-21 28	6.58
165812	-22 4581	18 2.7	-22 10	7.89
165832	-19 4860	18 2.8	-19 24	10.8
165921	-24 13962	18 3.2	-24 1	7.7
166125	-14 4908	18 4.1	-14 12	9.1
166167	-21 4879	18 4.3	-21 20	9.4
166188	-18 4815	18 4.4	-18 13	9.4
166286	-16 4736	18 4.8	-16 46	7.58
166287	-16 4737	18 4.8	-16 50	7.6
166304	-16 4739	18 4.9	-16 44	9.7
166418	-16 4744	18 5.4	-16 44	8.7
166443	-20 5020	18 5.5	-20 44	8.7
166524	-18 4826	18 5.9	-18 25	9.9
166539	-15 4854	18 6.0	-15 37	8.9
166540	-16 4747	18 6.0	-16 55	8.3
166546	-20 5027	18 6.0	-20 27	7.17
166566	-15 4856	18 6.1	-15 42	8.1
166568	-18 4829	18 6.1	-18 45	10.3
166569	-19 4894	18 6.1	-19 5	9.4
166628	-19 4895	18 6.4	-19 28	7.14
166689	-16 4752	18 6.7	-16 24	7.34
166716	-15 4864	18 6.8	-15 25	7.95
166734	-10 4625	18 6.9	-10 46	8.3
166787	-19 4900	18 7.1	-19 47	8.9
166803	-15 4868	18 7.2	-15 13	8.1
166937	-21 4908	18 7.8	-21 5	4.01
166965	-19 4909	18 7.9	-19 2	9.7
167224	-18 4857	18 9.1	-18 59	8.9
167263	-20 5055	18 9.3	-20 25	6.02
167264	-20 5054	18 9.3	-20 46	5.42
167287	-19 4928	18 9.4	-19 1	8.3
167330	-12 4954	18 9.6	-12 34	8.1
167336	-18 4863	18 9.6	-18 24	9.4
167356	-18 4864	18 9.7	-18 42	6.08
167411	-18 4871	18 10.0	-18 17	8.6
167451	-13 4897	18 10.2	-13 36	7.9
167497	-14 4956	18 10.4	-14 20	9.4
167543	-14 4959	18 10.6	-14 40	8.8
167633	-16 4786	18 11.0	-16 33	8.7
167659	-19 4944	18 11.1	-19 0	8.1
167771	-18 4886	18 11.6	-18 30	6.37
167791	-16 4792	18 11.7	-16 16	9.7
167838	-15 4911	18 11.9	-15 28	6.64
167971	-12 4980	18 12.5	-12 17	7.34
168015	-13 4919	18 12.7	-13 25	8.9
168021	-18 4896	18 12.7	-18 39	6.38
168075	-13 4925	18 12.9	-13 50	8.5
168076	-13 4926	18 12.9	-13 50	8.5
168080	-18 4900	18 12.9	-18 12	8.3
168112	-12 4988	18 13.1	-12 8	8.7
168137	-13 4932	18 13.2	-13 51	9.4
168183	-14 4991	18 13.4	-14 2	8.3
168229	-18 4909	18 13.6	-18 16	9.7

TABLE 1 (continued)

HD	BD	α (1900)	δ (1900)	m
168418	-17°5141	18h14m4	-17° 2'	9.7
168444	-14 5002	18 14.6	-14 53	8.86
168488	-17 5145	18 14.8	-17 42	9.7
168489	-17 5144	18 14.8	-17 48	8.9
168504	-14 5005	18 14.9	-14 0	9.2
168552	-17 5149	18 15.2	-17 11	8.7
168571	-17 5151	18 15.3	-17 26	8.3
168607	-16 4829	18 15.5	-16 25	8.9
168814	-14 5013	18 16.6	-14 26	7.26
168897	-17 5167	18 17.0	-17 30	9.7
168917	-14 5017	18 17.1	-14 25	8.6
168936	-17 5171	18 17.2	-17 43	8.1
169034	-13 4958	18 17.6	-13 39	8.3
169226	-12 5034	18 18.6	-12 15	9.1
169227	-12 5033	18 18.6	-12 17	8.9
169419	-17 5187	18 19.4	-17 35	9.4
169454	-14 5039	18 19.6	-14 2	6.84
169515	-12 5045	18 19.9	-12 45	10.4*
169582	- 9 4729	18 20.2	- 9 49	8.5
169673	-15 4970	18 20.7	-15 41	7.17
169753	- 9 4736	18 21.1	- 9 15	8.9*
169754	-11 4631	18 21.1	-11 25	8.1
170159	-13 4992	18 22.9	-13 4	8.7
170452	-13 5003	18 24.4	-13 1	8.5
170453	-14 5081	18 24.4	-14 17	9.9
170604	-16 4907	18 25.2	-16 39	8.7
170700	-14 5090	18 25.7	-14 11	9.1
170938	-15 5004	18 26.9	-15 46	8.7
171012	-18 4994	18 27.3	-18 26	6.98
171305	- 4 4497	18 29.0	- 4 53	8.60
171589	-14 5131	18 30.6	-14 12	8.8
172175	- 7 4642	18 33.6	- 7 57	9.4
172275	- 7 4645	18 34.2	- 7 27	9.4
172367	- 7 4650	18 34.7	- 7 20	9.7
172488	- 8 4675	18 35.4	- 8 49	7.9
172510	-14 5153	18 35.5	-14 51	8.81
172527	- 4 4548	18 35.6	- 4 11	8.6*
173011	-11 4729	18 38.1	-11 36	8.9
173219	- 7 4689	18 39.1	- 7 13	8.3
173438	- 4 4575	18 40.2	- 4 42	8.1
173783	- 9 4835	18 42.0	- 9 25	9.2
174513	- 7 4740	18 45.7	- 7 54	8.9
175514	+ 9 3928	18 50.6	+ 9 13	8.5
177284	- 2 4840	18 58.9	- 2 10	8.7
177812	+ 3 3893	19 1.1	+ 3 6	8.9
178129	+ 3 3902	19 2.3	+ 3 17	8.0
183143	+18 4085	19 23.0	+18 5	6.93
183561	+26 3566	19 25.1	+26 30	8.0
185418	+16 3928	19 33.9	+17 2	7.42
185859	+20 4218	19 36.1	+20 15	6.44
186745-6	+23 3760	19 41.2	+23 41	7.01
186841	+23 3767	19 41.7	+23 50	8.2
186980	+31 3765	19 42.4	+31 52	7.28
187399	+29 3754	19 44.7	+29 10	7.7
187459	+33 3602	19 45.0	+33 12	6.35
187851	+27 3534	19 47.0	+27 27	7.8
187982-3	+24 3914	19 47.8	+24 44	5.67
188001	+18 4276	19 47.9	+18 25	6.29
189779	+29 3844	19 56.6	+29 37	8.2
189957	+41 3569	19 57.6	+41 43	7.73

HD	BD	α (1900)	δ (1900)	m
190066	+21°4027	19h58m1	+21°52'	6.55
190429	+35 3930	19 59.8	+35 45	6.69
190467	+36 4841	20 0.0	+36 8	8.0
190864	+35 3949	20 1.9	+35 19	8.2
190916	+40 4015	20 2.2	+41 0	7.62
190918	+35 3953	20 2.2	+35 31	7.01
190919	+35 3952	20 2.2	+35 24	7.30
190967	+34 3871	20 2.4	+35 6	7.92
190991	+39 4033	20 2.5	+39 47	8.2
191139	+35 3966	20 3.3	+36 7	8.1
191201	+35 3970	20 3.6	+35 26	7.12
191243	+34 3881	20 3.8	+34 8	6.07
191396	+37 3783	20 4.6	+37 50	8.0
191423	+42 3599	20 4.7	+42 19	7.9
191456	+36 3896	20 4.9	+36 23	8.5
191611	+36 3906	20 5.7	+36 12	8.6
191612	+35 3995	20 5.7	+35 26	8.2
191781	+44 3365	20 6.6	+45 6	9.25
191978	+40 4050	20 7.5	+41 4	7.8
192001	+41 3642	20 7.6	+41 50	7.9
192079	+37 3816	20 8.0	+37 16	8.6
192281	+39 4082	20 9.0	+39 58	7.47
192422	+38 3956	20 9.7	+38 28	7.10
192539	+31 4001	20 10.3	+31 41	7.38
192639	+36 3958	20 10.8	+37 3	7.02
192660	+39 4096	20 10.9	+40 1	7.72
192832	+41 3675	20 11.9	+42 6	8.5
193007	+37 3860	20 12.9	+37 20	8.0
193009	+31 4018	20 12.9	+32 4	7.02
193032	+38 3980	20 13.0	+38 35	8.1
193076	+37 3866	20 13.3	+37 22	8.0
193117	+40 4090	20 13.5	+40 32	9.0
193182	+39 4115	20 13.8	+39 16	6.56
193183	+37 3867	20 13.8	+37 55	7.12
193237	+37 3871	20 14.1	+37 43	4.88
193322	+40 4103	20 14.6	+40 25	5.82
193426	+39 4130	20 15.1	+39 54	8.0
193443	+37 3879	20 15.2	+37 57	7.7
193444	+37 3878	20 15.2	+37 31	9.0
193514	+38 4006	20 15.5	+38 57	7.29
193516	+37 3881	20 15.5	+37 28	8.8
193595	+38 4012	20 15.9	+38 44	9.2
193610	+42 3692	20 16.0	+42 41	7.7
193611	+37 3890	20 16.0	+38 1	9.2
193634	+37 3892	20 16.2	+38 1	7.6
193682	+37 3894	20 16.5	+37 30	8.6
193793	+43 3571	20 17.1	+43 32	6.83
193794	+38 4028	20 17.1	+39 2	9.3
193855	+38 4032	20 17.4	+38 42	8.0
193945	+40 4132	20 17.9	+40 52	8.4
193946	+39 4151	20 17.9	+39 30	9.2
194057	+44 3439	20 18.4	+44 30	7.8
194092	+40 4137	20 18.6	+40 39	8.7
194153	+37 3909	20 18.9	+37 48	9.0
194194	+40 4139	20 19.2	+40 23	8.4
194205	+38 4053	20 19.3	+39 2	9.2
194279	+40 4150	20 19.7	+40 26	7.05
194280	+38 4057	20 19.7	+38 37	9.1
194334	+38 4059	20 20.0	+38 34	9.2
194649	+39 4177	20 21.7	+39 54	9.3

TABLE 1 (continued)

HD	BD	α (1900)	δ (1900)	m
194779	+40°4164	20h22m4	+41° 1'	7.66
194839	+40 4165	20 22.8	+41 3	7.45
195213	+40 4187	20 24.9	+40 28	9.2
195229	+41 3765	20 25.0	+41 40	7.9
195407	+36 4095	20 26.0	+36 39	7.72
195592	+43 3630	20 27.2	+43 59	7.15
195965	+47 3136	20 29.3	+47 53	6.82
196604	+44 3519	20 33.4	+44 34	8.3
197406	+52 2777	20 38.4	+52 14	10.3
198478	+45 3291	20 45.5	+45 45	4.89
198479	+45 3290	20 45.5	+45 16	8.52
198512	+53 2495	20 45.7	+53 32	7.95
198931	+43 3747	20 48.6	+44 3	9.0
199216	+48 3242	20 50.7	+49 9	7.13
199478	+46 3111	20 52.4	+47 2	5.76
199579	+44 3639	20 53.1	+44 33	6.01
200776	+45 3384	21 0.4	+45 56	8.1
200857	+54 2470	21 1.0	+54 51	7.16
202124	+43 3842	21 8.8	+44 7	7.83
202253	+43 3850	21 9.5	+43 28	7.70
203938	+46 3294	21 20.2	+46 44	7.10
204710	+44 3832	21 25.4	+44 29	6.90
204722	+43 3941	21 25.5	+43 54	7.52
205196	+56 2589	21 28.6	+57 4	7.36
206183	+56 2614	21 35.3	+56 32	8.1
206259	+51 3112	21 35.8	+51 54	7.48
206773	+57 2374	21 39.3	+57 17	6.98
207329	+51 3144	21 43.1	+51 39	7.45
207538	+59 2420	21 44.6	+59 14	7.03
207793	+52 3043	21 46.5	+52 14	6.56
208501	+55 2644	21 51.5	+56 8	6.01
208905	+60 2320	21 54.3	+60 49	6.90
209145	+59 2443	21 56.1	+59 50	7.96
209678	+52 3088	22 0.1	+52 43	8.4
209900	+52 3095	22 1.6	+53 1	8.9
209975	+61 2246	22 2.1	+61 48	5.17
210072	+54 2683	22 2.7	+54 46	8.0
210221	+52 3114	22 3.8	+52 49	6.50
210478	+60 2348	22 5.6	+60 30	7.26
210809	+51 3281	22 7.9	+51 56	7.7
210839	+58 2402	22 8.1	+58 56	5.19
211880	+62 2061	22 15.2	+62 43	8.5
211971	+59 2506	22 15.9	+59 38	7.16
212044	+51 3341	22 16.4	+51 21	7.08
212455	+54 2756	22 19.3	+54 44	8.4
212827	+53°2877	22h22m0	+53°16'	8.1
213470-1	+56 2794	22 26.5	+56 43	6.73
215605	+57 2597	22 41.3	+57 20	9.5
215806	+57 2606	22 42.7	+57 46	9.4
215835	+57 2607	22 42.9	+57 33	8.6
215836	+55 2809	22 42.9	+55 54	9.2
216014	+64 1717	22 44.2	+64 32	6.83
216044	+54 2865	22 44.5	+54 36	8.6
216411	+58 2492	22 47.6	+58 28	7.16
216438	+52 3315	22 47.8	+53 11	8.4
216532	+61 2356	22 48.6	+61 54	8.0
216658	+61 2363	22 49.6	+61 36	8.6
216711	+61 2364	22 50.0	+62 4	9.4
216898	+61 2370	22 51.8	+61 46	8.0
216927	+58 2511	22 52.0	+58 22	8.0
217035	+62 2136	22 52.6	+62 19	7.76
217086	+61 2373	22 53.0	+62 12	7.70
217312	+62 2147	22 54.8	+62 32	7.7
217490	+58 2521	22 56.0	+59 5	8.6
217919	+62 2161	22 59.0	+63 10	7.8
218066	+62 2163	23 0.0	+62 51	7.8
218195	+57 2689	23 1.0	+57 43	8.1
218323	+63 1928	23 2.0	+63 46	7.8
218342	+62 2170	23 2.1	+62 41	7.46
218376	+58 2545	23 2.4	+58 53	4.93
219287	+58 2565	23 9.6	+58 51	8.5
220116	+57 2724	23 16.1	+57 43	8.8
220770	+60 2539	23 21.4	+60 53	8.2
223385	+61 2533	23 44.0	+61 40	5.61
223924	+56 3106	23 48.6	+56 16	8.0
223960	+60 2636	23 48.9	+60 18	6.98
223987	+60 2637	23 49.2	+61 3	7.56
224055	+61 2562	23 49.7	+61 17	7.16
224151	+56 3115	23 50.5	+56 53	6.05
224257	+55 3051	23 51.3	+55 26	8.5
224424	+58 2676	23 52.7	+59 9	7.8
224436	+56 3122	23 52.8	+56 32	8.6
224599	+59 2801	23 54.1	+59 29	10.2
224905	+59 2813	23 56.6	+59 54	9.2
225094	+62 2356	23 58.3	+63 5	6.26
225146	+60 2663	23 58.8	+60 33	8.6
225160	+61 2585	23 58.9	+61 40	8.6

*Variable

TABLE 2

OB Stars in the Henry Draper Extension

HDE	BD	α (1900)	δ (1900)	m
236419	+59° 61	0h22m3	+60° 4'	9.0
236589	+55 215	0 52.1	+55 54	9.0
236664	+58 195	1 7.5	+58 33	9.4
236689	+57 240	1 12.3	+57 51	9.0
236740	+59 251	1 20.1	+59 46	8.3
236762	+58° 252	1h24m5	+59°13'	9.3
236768	+58 256	1 25.2	+58 52	9.0
236810	+59 296	1 31.8	+60 4	8.7
236815	+59 297	1 32.8	+59 54	8.5
232522	+54 372	1 39.6	+54 51	8.6

TABLE 2 (continued)

HDE	BD	α (1900)	δ (1900)	m
236894	+57° 409	1h45m.4	+57°57'	8.7
232552	+54 398	1 45.8	+54 51	7.6
232588	+54 448	1 57.1	+54 38	8.5
236935	+57 469	1 57.2	+58 0	9.1
237007	+59 549	2 42.7	+59 59	9.2
237056	+57 681	2 55.0	+57 13	8.7
237090	+59 611	3 7.2	+59 33	9.0
237091	+59 612	3 7.3	+59 33	8.8
237121	+58 587	3 12.7	+58 30	8.3
237204	+56 868	3 52.4	+56 37	9.0
232874	+53 723	3 54.5	+53 27	8.5
237211	+56 873	3 55.3	+56 15	8.9
237213	+55 845	3 56.5	+55 43	8.7
232947	+53 765	4 17.5	+53 11	9.0
232999	+50 1043	4 37.0	+50 23	8.6
242908	+33 1023	5 16.0	+33 25	8.7
242926	+33 1024	5 16.1	+33 13	9.5
242935	+33 1026	5 16.2	+33 19	9.6
245310	+21 901	5 30.4	+21 8	10.6
246901	+33 1138	5 38.3	+33 29	8.9
248587	+19 1111	5 46.5	+19 7	8.9
248893	+22 1090	5 48.0	+22 6	10.0
248894	+20 1158	5 48.0	+20 51	9.2
249695	+30 1071	5 52.2	+30 12	8.9
249845	+32 1146	5 53.0	+32 53	8.3
250028	+25 1065	5 53.8	+25 6	8.9
250163	+19 1166	5 54.4	+19 11	10.2
250289	+23 1148	5 55.0	+23 20	9.2
250290	+23 1149	5 55.0	+23 18	8.6
251117	+28 1001	5 58.7	+28 46	9.0
251311	+23 1183	5 59.4	+23 1	8.8
251726	+19 1210	6 1.0	+19 2	10.0
253049	+20 1305	6 5.8	+20 10	9.4
253214	+20 1309	6 6.4	+20 7	9.4
253247	+18 1123	6 6.5	+18 3	10.0
253659	+16 1046	6 8.1	+16 33	9.7
254042	+24 1176	6 9.8	+24 6	8.8
254699	+23 1286	6 12.3	+23 36	9.3
254755	+22 1273	6 12.5	+22 43	9.0
255055	+23 1304	6 13.6	+23 20	9.1
256276	+22 1311	6 17.7	+22 27	9.1
256413	+19 1331	6 18.1	+19 58	8.9
257971	+11 1191	6 23.1	+11 22	8.9
259431	+10 1172	6 27.6	+10 24	9.0
259440	+ 5 1291	6 27.6	+ 5 52	9.6
259597	+ 8 1388	6 28.1	+ 8 24	8.8
225985	+32 3583	19 45.7	+32 43	9.3
226868	+34 3815	19 54.6	+34 56	10.0
227018	+34 3828	19 56.1	+35 2	9.5
227144	+35 3916	19 57.6	+35 48	10.7
227245	+35 3924	19 58.6	+35 24	10.2
227611	+35 3950	20 2.0	+35 37	9.5
227634	+35 3957	20 2.3	+35 29	7.6
227704	+34 3874	20 2.9	+34 38	9.2
227757	+35 3967	20 3.5	+36 4	9.6
227877	+35 3983	20 4.6	+35 10	9.5
227902	+37 3785	20 4.9	+37 13	9.6
228041	+35 3998	20 6.2	+35 12	9.6
228053	+36 3914	20 6.3	+36 24	9.5
228101	+37 3804	20 6.9	+37 10	8.6
228104	+35°4004	20h 6m.9	+35°35'	9.8
228263	+37 3819	20 8.4	+37 21	9.6
228368	+34 3920	20 9.5	+34 43	9.8
228456	+36 3948	20 10.3	+36 30	10.1
228548	+39 4098	20 11.4	+39 40	10.8
228587	+36 3966	20 11.7	+36 19	10.9
228602	+36 3968	20 11.8	+36 32	10.3
228690	+37 3861	20 12.8	+37 37	9.6
228712	+40 4087	20 13.1	+40 34	9.7
228766	+36 3991	20 13.8	+37 0	9.8
228779	+34 3961	20 14.0	+34 30	10.5
228841	+38 4000	20 14.8	+38 34	8.7
228854	+35 4062	20 15.0	+36 2	9.2
228860	+36 4001	20 15.1	+36 39	10.0
228882	+40 4113	20 15.4	+40 23	10.6
228913	+35 4067	20 15.8	+35 54	10.6
228919	+39 4135	20 15.9	+40 8	10.0
228928	+40 4117	20 16.0	+40 20	10.8
228929	+39 4136	20 16.0	+39 36	10.7
228943	+38 4016	20 16.1	+38 17	10.0
228969	+38 4018	20 16.5	+38 21	10.0
228989	+38 4025	20 16.7	+38 23	10.3
229033	+37 3898	20 17.2	+37 25	9.4
229049	+38 4031	20 17.4	+38 42	10.0
229059	+36 4024	20 17.5	+37 5	10.0
229108	+38 4038	20 18.3	+39 8	10.2
229115	+34 3992	20 18.4	+34 55	10.8
229153	+37 3910	20 19.0	+37 39	10.1
229159	+38 4050	20 19.2	+38 53	9.4
229171	+37 3913	20 19.4	+38 8	9.9
229196	+40 4147	20 19.7	+40 34	9.2
229202	+39 4162	20 19.8	+39 50	10.1
229214	+36 4050	20 20.0	+36 12	9.9
229221	+38 4062	20 20.1	+38 11	10.0
229227	+38 4065	20 20.2	+38 8	10.1
229232	+38 4070	20 20.3	+38 47	10.3
229234	+38 4069	20 20.3	+38 12	9.3
229238	+38 4071	20 20.4	+38 13	9.5
229239	+38 4072	20 20.4	+38 11	9.6
235350	+50 3189	20 42.3	+50 49	9.0
239758	+58 2320	21 41.8	+58 36	9.0
235673	+52 3071	21 54.1	+52 19	9.0
235679	+53 2749	21 55.0	+53 59	8.8
239886	+56 2733	22 8.9	+56 46	8.6
239895	+56 2735	22 9.8	+57 10	8.7
235781	+52 3167	22 13.2	+53 13	8.4
235783	+53 2838	22 13.4	+53 59	8.8
235795	+51 3330	22 15.2	+51 37	8.6
235813	+54 2751	22 18.5	+54 18	8.7
235825	+54 2758	22 19.6	+54 44	9.1
235874	+50 3748	22 28.9	+50 42	9.0
240010	+55 2783	22 34.6	+55 19	9.3
240047	+56 2852	22 41.4	+56 55	9.2
240160	+56 2928	22 57.4	+56 27	9.3
240165	+56 2931	22 58.0	+56 39	9.5
240168	+55 2878	22 58.2	+56 4	8.9
240171	+56 2934	22 58.5	+56 36	9.1
236044	+53 3076	23 2.7	+54 13	9.0
236083	+54 2943	23 12.7	+54 57	9.2
240250	+59 2695	23 13.6	+59 19	8.6
240464	+59 2799	23 53.7	+59 43	9.2

TABLE 3

OB Stars in BD Only

BD	α (1855)	δ (1855)	m	BD	α (1855)	δ (1855)	m
+62° 49	0h11m1	+62°46'	8.7	+60° 493	2h20m0	+60°32'	8.4
+61 39	0 12.4	+61 40	8.9	+62 411	2 20.6	+62 46	8.0
+63 33	0 13.9	+63 48	9.1	+60 497	2 21.0	+60 58	8.6
+60 39	0 14.0	+60 56	9.1	+60 498	2 21.2	+60 54	9.5
+61 74	0 17.9	+61 45	9.3	+60 501	2 21.6	+60 50	9.2
+62 79	0 18.4	+62 38	9.0	+60 512	2 23.0	+60 45	9.5
+60 51	0 18.6	+60 37	9.3	+62 419	2 23.9	+62 57	9.2
+63 48	0 18.6	+63 37	9.0	+62 424	2 25.1	+62 19	8.5
+55 81	0 20.2	+55 36	9.5	+59 562	2 42.3	+59 52	9.5
+61 105	0 23.2	+61 38	8.8	+60 586	2 43.0	+60 3	8.3
+63 61	0 25.2	+63 12	9.3	+60 594	2 45.7	+60 50	9.1
+60 73	0 28.9	+60 34	9.4	+60 596	2 45.9	+60 4	9.3
+63 70	0 32.3	+63 7	9.0	+51 659	2 48.5	+51 31	9.1
+61 153	0 34.6	+61 26	9.2	+51 704	3 5.9	+51 28	9.5
+64 76	0 36.3	+64 28	9.2	+51 710	3 8.4	+51 29	9.4
+60 114	0 41.7	+60 7	9.5	+49 916	3 14.0	+49 7	8.9
+61 175	0 41.9	+61 35	9.1	+55 837	3 46.6	+55 30	9.2
+63 102	0 43.5	+63 53	9.5	+56 864	3 47.6	+56 49	9.2
+62 183	0 52.2	+62 40	9.2	+56 866	3 47.8	+56 41	9.5
+60 180	1 3.1	+60 33	9.4	+55 838	3 49.3	+55 4	9.2
+57 243	1 9.8	+57 27	9.3	+51 921	4 14.3	+51 42	9.1
+57 252	1 10.5	+57 29	9.2	+30 748	4 49.3	+30 28	9.0
+64 156	1 14.0	+64 52	9.2	+43 1168	4 51.8	+43 38	9.0
+62 246	1 15.0	+62 2	8.8	+40 1189	5 0.2	+40 29	8.4
+61 277	1 20.9	+61 59	9.3	+39 1264	5 11.1	+39 10	9.4
+60 261	1 23.0	+60 23	8.7	+42 1286	5 16.2	+42 53	9.4
+59 273	1 23.9	+59 53	8.5	+42 1288	5 17.0	+42 10	9.0
+60 279	1 26.8	+60 14	8.5	+34 1058	5 19.0	+34 33	8.8
+59 286	1 27.3	+59 12	9.0	+35 1141	5 20.3	+35 5	9.1
+57 359	1 30.2	+57 6	9.4	+39 1328	5 22.1	+39 57	9.2
+61 312	1 33.2	+61 44	8.9	+35 1169	5 24.6	+35 42	8.4
+62 297	1 33.3	+62 52	9.2	+33 1103	5 28.3	+33 52	8.3
+55 393	1 34.7	+55 26	9.5	+37 1292	5 32.9	+37 55	8.7
+60 331	1 36.0	+60 30	9.0	+34 1150	5 33.5	+34 16	9.0
+60 333	1 36.2	+60 30	9.0	+34 1162	5 35.6	+34 2	9.0
+60 339	1 36.5	+60 32	8.8	+36 1261	5 38.7	+36 10	8.2
+60 343	1 36.7	+60 32	9.1	+ 5 1340	6 30.7	+ 5 0	9.0
+63 247	1 39.2	+63 37	9.5	- 0 1385	6 32.9	- 0 14	9.5
+54 395	1 42.3	+54 45	9.5	+ 0 1576	6 37.4	+ 0 45	9.2
+63 253	1 43.0	+63 29	9.1	+ 0 1769	6 55.0	+ 0 42	9.3
+54 404	1 43.7	+54 24	9.5	- 0 1618	7 1.6	- 0 48	9.3
+55 441	1 46.4	+55 50	9.4	-22 4543	17 55.5	-22 29	9.1
+63 261	1 46.9	+63 20	9.1	-17 5020	17 58.1	-17 13	9.0
+58 343	1 49.1	+58 14	9.4	-20 5060	18 7.0	-20 23	9.0
+58 351	1 50.7	+58 16	9.5	-12 4970	18 9.6	-12 33	8.7
+63 300	1 59.7	+63 23	9.4	-12 4982	18 10.0	-12 14	9.0
+57 513	2 2.5	+57 25	9.2	-11 4586	18 10.0	-11 21	8.9
+57 515	2 2.6	+57 0	9.3	-20 5108	18 13.7	-20 8	8.7
+54 490	2 4.5	+54 22	9.2	- 9 4713	18 15.9	- 9 58	8.5
+56 473	2 6.9	+56 27	8.7	-14 5037	18 16.8	-14 43	8.2
+56 482	2 7.5	+56 31	8.9	- 8 4617	18 21.3	- 8 39	8.8
+56 484	2 7.6	+56 14	9.1	-11 4667	18 24.2	-11 23	9.0
+56 493	2 8.2	+56 11	9.3	- 0 3584	18 46.1	- 0 44	9.1
+56 589	2 12.6	+56 51	9.1	+ 2 3771	18 56.9	+ 2 54	9.0
+56 606	2 14.5	+56 49	9.0	+14 3887	19 15.0	+14 37	9.5

TABLE 3 (continued)

BD	α (1855)	δ (1855)	m	BD	α (1855)	δ (1855)	m
+14°3898	19h16m8	+14°57'	9.0	+47°3487	21h30m5	+47°16'	9.1
+22 3687	19 18.6	+22 30	8.6	+37 4368	21 30.8	+37 38	9.5
+28 3434	19 35.5	+28 49	8.8	+48 3437	21 31.1	+48 42	8.5
+28 3438	19 36.3	+28 40	8.8	+49 3591	21 35.2	+49 51	9.5
+23 3745	19 36.7	+23 7	8.6	+49 3615	21 40.6	+49 38	8.8
+23 3747	19 37.0	+23 6	9.4	+47 3588	21 47.3	+47 20	8.8
+22 3782	19 37.0	+22 57	8.8	+51 3239	21 58.7	+51 24	9.2
+23 3759	19 39.1	+23 42	8.9	+49 3735	22 0.5	+49 12	9.0
+23 3761	19 39.3	+23 58	8.6	+52 3122	22 3.4	+52 16	9.2
+23 3762	19 39.5	+23 38	9.2	+52 3135	22 6.8	+52 59	9.1
+22 3800	19 39.6	+22 51	9.0	+53 2833	22 10.8	+53 27	9.5
+27 3512	19 40.8	+27 54	8.8	+54 2726	22 11.4	+54 45	9.1
+24 3881	19 41.0	+24 30	9.0	+53 2837	22 11.6	+53 29	9.4
+27 3513	19 41.1	+27 41	8.5	+53 2843	22 13.3	+53 32	9.3
+28 3485	19 43.1	+28 27	8.8	+54 2764	22 18.5	+54 40	9.4
+22 3836	19 44.9	+22 28	9.1	+54 2775	22 20.6	+54 44	9.3
+27 3550	19 48.2	+27 58	9.0	+52 3210	22 21.3	+52 55	9.4
+28 3598	19 57.3	+28 18	9.4	+53 2885	22 21.5	+53 27	9.5
+25 4083	19 58.0	+25 52	8.8	+54 2790	22 24.4	+54 3	9.3
+31 3921	19 58.5	+31 45	8.6	+55 2795	22 37.0	+55 35	9.4
+35 3956	20 0.6	+35 21	8.9	+53 2964	22 37.5	+53 19	9.4
+32 3749	20 8.0	+32 7	9.5	+54 2847	22 38.5	+54 59	9.5
+37 3859	20 11.1	+37 12	9.2	+55 2808	22 40.6	+55 34	9.5
+37 3862	20 11.2	+37 12	9.2	+55 2840	22 49.1	+55 37	9.4
+30 3980	20 12.6	+30 22	8.2	+56 2903	22 49.8	+56 49	9.4
+45 3149	20 16.4	+45 35	9.2	+63 1907	22 50.8	+63 42	9.0
+36 4048	20 18.1	+36 51	9.4	+56 2929	22 55.6	+56 16	9.4
+39 4189	20 21.1	+39 11	9.3	+56 2930	22 56.0	+56 46	9.3
+38 4098	20 22.2	+38 18	9.1	+55 2899	23 0.8	+55 13	9.4
+40 4179	20 22.5	+40 7	9.4	+63 1962	23 10.9	+63 0	8.3
+37 3945	20 22.9	+37 53	9.4	+63 1964	23 11.2	+63 20	8.3
+40 4185	20 23.1	+40 9	9.4	+62 2210	23 12.4	+62 42	8.5
+46 2948	20 24.6	+46 10	9.4	+60 2522	23 14.3	+60 24	8.0
+40 4227	20 28.0	+40 49	8.5	+60 2525	23 15.4	+60 4	9.3
+37 3976	20 28.4	+37 47	9.4	+60 2542	23 20.6	+60 35	8.9
+45 3216	20 29.0	+45 10	8.7	+60 2582	23 28.8	+60 7	8.3
+36 4145	20 30.8	+36 55	8.5	+61 2509	23 36.9	+61 21	8.5
+47 3162	20 35.3	+47 35	9.5	+60 2615	23 37.8	+60 52	8.9
+42 3835	20 37.0	+42 40	8.9	+62 2296	23 40.4	+62 25	8.0
+35 4258	20 40.5	+35 1	9.1	+61 2526	23 40.7	+61 14	8.5
+45 3260	20 40.7	+45 49	9.0	+62 2299	23 41.0	+62 35	9.2
+44 3594	20 44.2	+44 53	9.4	+61 2529	23 41.4	+61 11	8.6
+37 4092	20 48.1	+37 38	9.2	+62 2313	23 44.9	+62 30	8.5
+47 3211	20 48.2	+47 23	9.4	+61 2550	23 45.2	+61 19	9.2
+42 3914	20 51.1	+42 34	8.3	+61 2559	23 46.5	+61 37	9.2
+45 3341	20 52.0	+45 59	9.0	+66 1661	23 50.3	+66 45	8.7
+44 3655	20 53.3	+44 35	9.3	+66 1675	23 54.8	+66 36	9.0
+45 3360	20 55.5	+45 41	9.5	+60 2668	23 58.5	+60 4	8.8
+41 4064	21 10.7	+41 56	8.6	+59 2829	23 59.3	+59 49	9.5
+43 3913	21 19.6	+43 49	8.4				

TABLE 4

OB Stars not in BD

No.	α (1855)	δ (1855)	No.	α (1855)	δ (1855)	No.	α (1855)	δ (1855)	No.	α (1855)	δ (1855)
1	0h31m6	+60°10'	6	3h43m6	+46°27'	11	19h59m8	+35°40'	16	20h16m3	+38°42'
2	0 41.2	+60 12	7	3 47.4	+56 48	12	20 1.6	+35 15	17	20 25.9	+47 22
3	0 44.9	+60 1	8	19 18.1	+29 24	13	20 11.2	+37 14	18	21 8.0	+44 20
4	1 29.6	+57 25	9	19 36.1	+23 7	14	20 13.4	+37 54	19	22 32.3	+54 33
5	2 13.6	+57 40	10	19 40.4	+27 55	15	20 14.4	+38 57	20	22 36.7	+55 58
									21	22 53.3	+56 57

ON STELLAR STATISTICS

S. CHANDRASEKHAR AND G. MÜNCH
Yerkes Observatory
Received September 20, 1950

ABSTRACT

In this paper a method is proposed for treating the fundamental equation of stellar statistics which will take into account the known cloud structure of the interstellar absorbing matter. The method is based on the determination and the interpretation of the fluctuations in the numbers of stars, $N(m)$, per unit solid angle, and brighter than a given apparent magnitude, m, in the various parts of the sky. The marked dependence of these fluctuations on the galactic latitude confirms their relation to the interstellar clouds. Theoretical formulae are derived for the dispersions to be expected in $N(m)$ as a function of the galactic latitude on certain idealized distributions of stars and clouds. The results of star counts tabulated by van Rhijn and by Baker and Kiefer are analyzed in terms of these formulae, and a theoretical prediction based on them is verified. The analysis discloses the importance of taking into account the dispersion in the transparencies of the interstellar clouds as a factor in these considerations.

1. *Introduction.*—The principal quantity with which stellar statistics deals is the number of stars, $A(m)$, of apparent magnitude m, per unit solid angle and per unit magnitude interval in the various parts of the sky; to a less extent it also concerns itself with the mean parallax, $\pi(m)$, of these stars. In tabulating the quantities $A(m)$ and $\pi(m)$, one either includes all stars without regard to their spectral types or includes only such stars as belong to a given spectral type (or a range of spectral types). The latter refinement of subdividing the stars into various spectral classes is customary in the more recent investigations, though the division was not made in much of the earlier work.

As is well known, the quantities $A(m)$ and $\pi(m)$ are related to the luminosity function $\phi(M)$ governing the frequency of occurrence of stars with a given absolute magnitude M, the function $D(s)$ giving the density of the stars at a distance s from the observer and in the direction considered, and the function $a(s)$ giving the absorption in magnitudes by the intervening interstellar matter, by the fundamental equations of stellar statistics, namely,

$$A(m) = \int_0^\infty D(s)\,\phi(M)\,s^2 ds \tag{1}$$

and

$$\pi(m) = \frac{1}{A(m)} \int_0^\infty D(s)\,\phi(M)\,s\,ds\,. \tag{2}$$

In equations (1) and (2) the argument M in the luminosity function, $\phi(M)$, is related to the apparent magnitude, m, by the relation

$$M = m + 5 - 5\log s - a(s)\,, \tag{3}$$

where it is assumed that the distances are measured in parsecs.

If, in making the counts $A(m)$, all stars without regard to their spectral types are included, we must take $\phi(M)$ to mean the general luminosity function; otherwise, $\phi(M)$ should be taken to mean the luminosity function appropriate for the restricted class of stars.

In practice one often considers, instead of $A(m)$, the number of stars,

$$N(m) = \int_{-\infty}^{m} A(m')\,dm'\,, \tag{4}$$

brighter than a given apparent magnitude m. A corresponding integration of equation (3) leads to the integral equation

$$N(m) = \int_0^\infty D(s)\,\Phi(M)\,s^2 ds\,, \tag{5}$$

where

$$\Phi(M) = \int_{-\infty}^{M} \phi(M')\,dM'\,, \tag{6}$$

and the argument, M, in $\Phi(M)$ is still related to m as in equation (3).

Tables of $N(m)$ for various galactic longitudes and latitudes have been given, for example, by van Rhijn.[1]

From the observed counts $N(m)$ (and also from the mean parallaxes, if the latter data are available) stellar statistics seeks to derive information concerning $\Phi(M)$, $D(s)$, and $a(s)$. In practice, $\Phi(M)$ is assumed to be known from a study of the near-by stars, and the principal use to which equations (2) and (5) are put is to determine the density function $D(s)$ and the variation of the absorption $a(s)$ with distance. With regard to $a(s)$, in most of the early investigations the assumption is made that the interstellar matter is uniformly distributed and that there exists a coefficient of interstellar absorption, A (mg kpc), such that

$$a(s) = A\,s \times 10^{-3}\,. \tag{7}$$

In the more recent investigations this assumption of the uniform distribution of the interstellar matter is not made; instead, an attempt is made to determine $a(s)$ from the color excesses of the stars included in the counts. However, any assumption which regards $a(s)$ as a "smooth" function of s in the same sense that the density of stars, $D(s)$, is a smooth function of s is contrary to the well-established fact that interstellar matter occurs in the form of clouds and that, in consequence, $a(s)$ must be considered as a random function subject to fluctuations. In other words, consistent with our present knowledge, we should rather write

$$a(s) = \sum_{i=1}^{n(s)} \epsilon_i\,, \tag{8}$$

where ϵ_i is the absorption in magnitudes by the ith cloud in the line of sight and the summation in equation (5) is extended over all the clouds which occur in the line of sight.

It is currently estimated that the average number of interstellar clouds which a line of sight will intersect is of the order of seven per kiloparsec and that, on the average, each cloud will cut down the brightness of the stars immediately behind it by about 0.2 mag. It is evident from these figures that the fluctuations in $N(m)$ arising from the cloud structure of interstellar matter must be a dominant factor in the problem. This latter fact may, in part, explain why so few results of any definiteness have been obtained by the attempts which have been made so far in inverting the integral equation (5) by numerical methods. However, to avoid any misunderstanding, we should like to state that in our view the essential failure—for so it must be admitted—of the attempts to derive the density function by a numerical inversion of the integral equation (5) cannot be traced entirely to this source; rather, we believe that the failure must be attributed to the fact that the observations which are available are far from having the accuracy necessary for the method of solution adopted to give meaningful results.[2] Thus the observations are known only in the form of histograms, and the derivatives of the observed distribution of $N(m)$, on which the solution sensitively depends, are too imperfectly known to lead to

[1] *Groningen Pub.*, No. 43, 1924.

[2] We are greatly indebted to Dr. Nancy G. Roman for valuable discussions on these and other related problems in stellar statistics.

trustworthy results. Moreover, in the method of solution which is generally adopted, the physical quantities are averaged over such large intervals of distance that we cannot, in principle, expect the method to succeed.

Since the conventional methods of treating the equations of stellar statistics have not yielded concrete results commensurate with the efforts which have been expended on them, we may ask if a reorientation and reformulation of the basic objectives of stellar statistics is not possible which may redirect the investigations in this field along more fruitful lines. It would appear from the investigations of Ambarzumian,[3] Markarian,[4] and the more recent ones of the present authors[5] that results of significance can be obtained by directing our attention to the properties of interstellar clouds—their frequency of occurrence in a line of sight, their mean absorptive power, etc.—and away from the stars.

Since the average number of clouds in the line of sight is of the order of seven per kiloparsec, the actual numbers which will occur in particular instances will be subject to the fluctuations of a Poisson distribution; the pattern of the resulting fluctuations in $N(m)$ should therefore be predictable in principle. Moreover, by considering the fluctuations in $N(m)$ as a function of the galactic latitude, β, we should have a valuable check on the assumptions that may have been made (for reasons of analytical simplicity, for example), since the average number of the clouds in the direction β may be expected to vary as cosec β.

A further consequence of the dominant effect of the fluctuations in the number of clouds in the line of sight is that assumptions concerning $\Phi(M)$ and $D(s)$ will not materially affect the conclusions we may draw about the clouds. In view of this last circumstance, we shall assume in our subsequent analysis that

$$\Phi(M) = \Phi_0 e^{aM} \tag{9}$$

and

$$D(s) = D_0 e^{-s/h}, \tag{10}$$

where Φ_0, D_0, a, and h are suitably chosen constants. In our context neither of these two assumptions is as *ad hoc* as it may seem; for it is true that $\Phi(M)$ in the range of M which contributes to $N(m)$ can be represented with sufficient accuracy by a formula of the form (9). The same remark also applies to assumption (10) if we limit ourselves to distances not exceeding 1000 parsecs in the galactic plane; and for galactic latitudes greater than 30° there are good reasons for believing that a formula of the form (10) provides a suitable approximation.

In this paper we shall derive formulae for the dispersion in $N(m)$ which may be expected on account of the cloud structure of interstellar matter and for certain model distributions of stars and clouds. The analysis in this paper is a generalization and an extension of that contained in the paper by Markarian[4] to which we have already referred. The formulae derived in this paper are applied to van Rhijn's counts,[1] and certain conclusions regarding the mean absorptive power of the interstellar clouds are drawn; these differ from the conclusions Markarian drew from his more limited analysis.

2. *The dispersion to be expected in $N(m)$ for a model distribution of stars and clouds.*—In this paper we shall restrict ourselves to the following model distribution of stars and clouds: Both stars and clouds occur to a distance L in the line of sight. The density of the stars may vary with distance along the line of sight; but the clouds are uniformly distributed and occur in the line of sight on an average of ν per unit distance. On this picture of the distribution of stars and clouds, equation (5) becomes

$$N(m) = \int_0^L D(s)\,\Phi(M)\,s^2 ds, \tag{11}$$

[3] *Abastumani Obs.*, No. 2, p. 37, 1938; No. 4, p. 17, 1940.

[4] *Contr. Burakan Obs. Acad. Sci. Armenian S.S.R.*, No. 1, 1946.

[5] S. Chandrasekhar and G. Münch, *Ap.J.*, 112, 380, 393, 1950; these papers will be referred to hereafter as "Paper I" and "Paper II," respectively.

where

$$M = 5 + m - 5 \log s - \sum_{i=1}^{n(s)} \epsilon_i , \tag{12}$$

and the occurrence of a particular number $n(s)$ of clouds in the distance s is governed by a Poisson distribution with a mean νs.

In our further analysis we shall suppose that the function $\Phi(M)$ can be approximated by a formula of the form (eq. [9])

$$\Phi(M) = \Phi_0 e^{\alpha M} . \tag{13}$$

For $\Phi(M)$ given by equation (13), equation (11) becomes

$$N(m) = \Phi_0 e^{\alpha(5+m)} \int_0^L D(s)\, s^{2-5\alpha \log e} \exp\left\{ -\alpha \sum_{i=1}^{n(s)} \epsilon_i \right\} ds . \tag{14}$$

Letting

$$\alpha = 3 - 5\alpha \log e \qquad \text{and} \qquad Q_i = e^{-\alpha \epsilon_i} , \tag{15}$$

we can write equation (14) in the form

$$N(m) = \Phi_0 e^{\alpha(5+m)} \int_0^L D(s)\, s^{\alpha-1} \prod_{i=1}^{n(s)} Q_i\, ds . \tag{16}$$[6]

In Paper I we introduced the fraction q by which an interstellar cloud cuts down the light of the stars immediately behind it. It is readily verified that q defined in this manner is related to Q by (cf. eq. [15])

$$Q = \exp(2.5\alpha \log_{10} q) = \exp(1.0859\alpha \log_e q) = q^{1.0859\alpha} . \tag{17}$$

By letting $r = \nu s$, we can make the Poisson distribution governing the frequency of occurrence of clouds in the interval $(0, r)$ be

$$\frac{e^{-r} r^n}{n!} . \tag{18}$$

In terms of the variable r, equation (16) can be written in the form

$$\frac{\nu^\alpha}{\Phi_0} e^{-\alpha(5+m)} N(m) = \int_0^\xi D\left(\frac{r}{\nu}\right) r^{\alpha-1} \prod_{i=1}^{n(r)} Q_i\, dr , \tag{19}$$

where

$$\xi = L\nu \tag{20}$$

is the average number of clouds to be expected in the distance L.

The problem now is to evaluate the moments of the quantity defined on the right-hand side of equation (19). We shall show how these moments can be evaluated by using the result established in the following lemma.

Lemma.—Consider the random function

$$g(\xi; x) = \int_0^\xi F(r + x) \prod_{i=1}^{n(r)} Q_i\, dr , \tag{21}$$

[6] If we treat the mean parallaxes, then the equation for $A(m)\,\pi(m)$ will differ from eq. (16) only by the fact that the exponent of s in the integrand will be $\alpha - 2$ instead of $\alpha - 1$ (cf. eqs. [1] and [2]). Consequently, the analysis of the rest of this section will apply to $A(m)\,\pi(m)$ if α is replaced by $\alpha - 1$ wherever it occurs.

where ξ and x are two constants and the Q's occur with a probability given by a function $\Psi(Q)$ $(0 \leqslant Q \leqslant 1)$ and the $n(r)$'s are subject to fluctuations governed by the Poisson distribution $e^{-r}r^n/n!$. Under these circumstances the mth moment, $\mu_m(\xi; 0)$ of

$$g(\xi; 0) = \int_0^\xi F(r) \prod_{i=1}^{n(r)} Q_i dr \tag{22}$$

can be derived from the $(m-1)$th moment $\mu_{m-1}(\xi; x)$ of $g(\xi; x)$ by the formula

$$\mu_m(\xi; 0) = m \int_0^\xi e^{-(1-Q_m)r} F(r)\, \mu_{m-1}(\xi - r; r)\, dr, \tag{23}$$

where

$$Q_m = \int_0^1 Q^m \Psi(Q)\, dQ. \tag{24}$$

Proof.—By definition

$$\mu_m(\xi; 0) = \int_0^\xi dr_m F(r_m) \int_0^\xi dr_{m-1} F(r_{m-1}) \int_0^\xi \cdots \int_0^\xi dr_1 F(r_1) \times \left\{ \prod_{j=1}^{m} \prod_{i=1}^{n(r_j)} Q_i \right\}_{\text{average}}. \tag{25}$$

The integrand in this m-fold integral is a symmetrical function of the variables. We can accordingly use the lemma established in Paper I (eq. [47]) and rewrite the foregoing expression for $\mu_m(\xi; 0)$ in the form

$$\mu_m(\xi; 0) = m \int_0^\xi dr_m F(r_m) \int_{r_m}^\xi dr_{m-1} F(r_{m-1}) \int_{r_m}^\xi dr_{m-2} F(r_{m-2}) \int_{r_m}^\xi \cdots \times \int_{r_m}^\xi dr_1 F(r_1) \left\{ \prod_{j=1}^{m} \prod_{i=1}^{n(r_j)} Q_i \right\}_{\text{average}}. \tag{26}$$

With the integration over the variables arranged in this fashion,

$$r_j \geqslant r_m \quad \text{for} \quad j \leqslant m-1. \tag{27}$$

Under these circumstances

$$n(r_j) - n(r_m) = n(r_j - r_m), \tag{28}$$

and (cf. Paper I, eqs. [52]–[58])

$$\left\{ \prod_{j=1}^{m} \prod_{i=1}^{n(r_j)} Q_i \right\}_{\text{average}} = \left\{ \prod_{i=1}^{n(r_m)} Q_i^m \right\}_{\text{average}} \times \left\{ \prod_{j=1}^{m-1} \prod_{i=1}^{n(r_j - r_m)} Q_i \right\}_{\text{average}} = e^{-(1-Q_m)r_m} \left\{ \prod_{j=1}^{m-1} \prod_{i=1}^{n(r_j - r_m)} Q_i \right\}_{\text{average}}. \tag{29}$$

Using this last result in equation (26) and writing r_j in place of $r_j - r_m$ $(j = m-1, \ldots, 1)$ and r in place of r_m, we have

$$\mu_m(\xi; 0) = m \int_0^\xi dr\, F(r)\, e^{-(1-Q_m)r} \left\{ \prod_{j=1}^{m-1} \int_0^{\xi - r} dr_j F(r_j + r) \prod_{i=1}^{n(r_j)} Q_i \right\}_{\text{average}}. \tag{30}$$

But the quantity in braces on the right-hand side of equation (30) is $\mu_{m-1}(\xi - r; r)$. Hence,

$$\mu_m(\xi; 0) = m\int_0^{\xi} dr F(r)\,\mu_{m-1}(\xi - r; r)\, e^{-(1-Q_m)r}. \tag{31}$$

This is the required relation.

It is evident that by using the relation expressed by equation (31) we can successively evaluate all the moments of $N(m)$. However, in this paper we shall limit ourselves to evaluating only the dispersion of $N(m)$ for the case (cf. eq. [10])

$$D(s) = D_0 e^{-s/h}. \tag{32}$$

For this purpose we need the first and the second moments of

$$\mathfrak{N} = \frac{\nu^a}{\Phi_0 D_0} e^{-a(b+m)} N(m) = \int_0^{\xi} e^{-\gamma r} r^{a-1} \prod_{i=1}^{n(r)} Q_i\, dr, \tag{33}$$

where

$$\gamma = (\nu h)^{-1}. \tag{34}$$

These moments can be found by using the lemma for $m = 1$ and 2 for the case

$$F(r) = e^{-\gamma r} r^{a-1}. \tag{35}$$

i) *The first moment of* $\mathfrak{N}$.—For $m = 1$, we conclude from equation (31) that

$$\mu_1(\xi; x) = \int_0^{\xi} dr F(r + x)\, e^{-(1-Q_1)r}, \tag{36}$$

since $\mu_0 \equiv 1$. For $F(r)$ given by equation (35), we have

$$\mu_1(\xi; x) = \int_0^{\xi} e^{-\gamma(r+x)} (r + x)^{a-1} e^{-(1-Q_1)r} dr. \tag{37}$$

Writing $(r + x) = y$ in this equation, we have

$$\mu_1(\xi; x) = e^{x(1-Q_1)} \int_x^{\xi+x} e^{-(\gamma+1-Q_1)y} y^{a-1} dy, \tag{38}$$

or, alternatively,

$$\mu_1(\xi; x) = \frac{e^{x(1-Q_1)}}{(\gamma + 1 - Q_1)^a} \int_{x(\gamma+1-Q_1)}^{(\xi+x)(\gamma+1-Q_1)} dy\, y^{a-1} e^{-y}. \tag{39}$$

In terms of the incomplete Γ-function,

$$\Gamma(a; z) = \int_0^z e^{-y} y^{a-1} dy, \tag{40}$$

we can express $\mu_1(\xi; x)$ in the form

$$\mu_1(\xi; x) = \frac{e^{x(1-Q_1)}}{(\gamma + 1 - Q_1)^a} \{\Gamma(a; [\xi + x][\gamma + 1 - Q_1]) - \Gamma(a; x[\gamma + 1 - Q_1])\}. \tag{41}$$

In particular, for $x = 0$, we have

$$\bar{\mathfrak{N}} = \mu_1(\xi; 0) = \frac{\Gamma(a; \xi[\gamma + 1 - Q_1])}{(\gamma + 1 - Q_1)^a}. \tag{42}$$

When $\gamma = 0$, $\xi = \infty$, and Q occurs with only one value, equation (42) reduces to a formula given by Markarian (*op. cit.*, eq. [5]).

Letting

$$\xi_1 = \xi\,(\gamma + 1 - Q_1)\,, \tag{43}$$

we can express equation (42) more conveniently in the form

$$\mu_1(\xi;\,0) = \left(\frac{\xi}{\xi_1}\right)^a \Gamma(a;\,\xi_1)\,. \tag{44}$$

The incomplete Γ-function (40) has the expansion

$$\Gamma(a;\,z) = e^{-z} z^a \sum_{j=0}^{\infty} \frac{z^j}{a_j} \qquad (a > 0)\,, \tag{45}$$

where

$$a_0 = a \qquad \text{and} \qquad a_j = a\,(a+1)\ldots(a+j) \qquad (j \geqslant 1)\,. \tag{46}$$

The corresponding expansion for $\mu_1(\xi;\,0)$ is

$$\mu_1(\xi;\,0) = \xi^a e^{-\xi_1} \sum_{j=0}^{\infty} \frac{\xi_1^j}{a_j}. \tag{47}$$

ii) *The second moment of* $\mathfrak{N}$.—Substituting for $\mu_1(\xi - r;\,r)$ in accordance with equation (39) in equation (31) for $m = 2$ and $F(r)$ given by equation (35), we have

$$\tfrac{1}{2}\mu_2(\xi;\,0) = \int_0^{\xi} d\,r\, r^{a-1} e^{-(1-Q_1)r - \gamma r}\, \frac{e^{r(1-Q_1)}}{(\gamma + 1 - Q_1)^a} \int_{r(\gamma+1-Q_1)}^{\xi(\gamma+1-Q_1)} dy\, y^{a-1} e^{-y}, \tag{48}$$

or

$$\mu_2(\xi;\,0) = \frac{2}{(\gamma + 1 - Q_1)^a} \int_0^{\xi} d\,r\, r^{a-1} e^{-(\gamma + Q_1 - Q_2)r} \int_{r(\gamma+1-Q_1)}^{\xi(\gamma+1-Q_1)} dy\, y^{a-1} e^{-y}. \tag{49}$$

An alternative form of this equation is

$$\mu_2(\xi;\,0) = \frac{2\,\xi^{2a}}{\xi_1^a \xi_2^a} \int_0^{\xi_2} d\,z\, z^{a-1} e^{-z} \int_{z\xi_1/\xi_2}^{\xi_1} dy\, y^{a-1} e^{-y}, \tag{50}$$

where, in addition to ξ_1 (eq. [43]), we have let

$$\xi_2 = \xi\,(\gamma + Q_1 - Q_2)\,. \tag{51}$$

Expressing the integral over y in equation (50) in terms of the incomplete Γ-function (40), we obtain

$$\mu_2(\xi;\,0) = \frac{2\,\xi^{2a}}{\xi_1^a \xi_2^a} \left\{ \Gamma(a;\,\xi_1)\,\Gamma(a;\,\xi_2) - \int_0^{\xi_2} d\,z\, z^{a-1} e^{-z} \Gamma\left(a;\,\frac{z\xi_1}{\xi_2}\right) \right\}. \tag{52}$$

Expanding $\Gamma(a;\,z\xi_1/\xi_2)$ according to equation (45), we can reduce the second term on the right-hand side of equation (52) as follows:

$$\frac{2\xi^{2\alpha}}{\xi_1^{\alpha}\xi_2^{\alpha}}\int_0^{\xi_2} dz\, z^{\alpha-1}e^{-z(1+\xi_1/\xi_2)}\left(\frac{z\xi_1}{\xi_2}\right)^{\alpha}\sum_{j=0}^{\infty}\left(\frac{z\xi_1}{\xi_2}\right)^{j}\frac{1}{a_j}$$

$$= 2\xi^{2\alpha}\sum_{j=0}^{\infty}\frac{\xi_1^j}{a_j}\int_0^1 e^{-z(\xi_1+\xi_2)}\, z^{2\alpha+j-1}dz$$

$$= 2\xi^{2\alpha}\sum_{j=0}^{\infty}\frac{\xi_1^j}{a_j(\xi_1+\xi_2)^{2\alpha+j}}\,\Gamma(2\alpha+j;\ \xi_1+\xi_2) \tag{53}$$

$$= 2\xi^{2\alpha}e^{-(\xi_1+\xi_2)}\sum_{j=0}^{\infty}\frac{\xi_1^j}{a_j}\left\{\sum_{k=0}^{\infty}\frac{(\xi_1+\xi_2)^k}{(2\alpha+j)_k}\right\}.$$

Combining this with the corresponding expansions for $\Gamma(\alpha;\xi_1)$ and $\Gamma(\alpha;\xi_2)$, we obtain

$$\mu_2(\xi;0) = 2\xi^{2\alpha}e^{-(\xi_1+\xi_2)}\left\{\left(\sum_{j=0}^{\infty}\frac{\xi_1^j}{a_j}\right)\left(\sum_{j=0}^{\infty}\frac{\xi_2^j}{a_j}\right)-\sum_{j=0}^{\infty}\frac{\xi_1^j}{a_j}\left[\sum_{k=0}^{\infty}\frac{(\xi_1+\xi_2)^k}{(2\alpha+j)_k}\right]\right\}. \tag{54}$$

For $\xi=\infty$, $\mu_2(\infty;0)$ can be reduced to an incomplete beta-function: When $\xi\to\infty$, both ξ_1 and $\xi_2\to\infty$, but ξ_1/ξ_2 tends to a finite limit, namely, $(\gamma+1-Q_1)/(\gamma+Q_1-Q_2)$. The corresponding expression for μ_2 is (cf. eq. [50])

$$\mu_2(\infty;0) = \frac{2}{(\gamma+1-Q_1)^{\alpha}(\gamma+Q_1-Q_2)^{\alpha}}\int_0^{\infty} dz\, z^{\alpha-1}e^{-z}\int_{zt}^{\infty} dy\, y^{\alpha-1}e^{-y}, \tag{55}$$

where we have written

$$t=\frac{\gamma+1-Q_1}{\gamma+Q_1-Q_2}. \tag{56}$$

Writing

$$J(t) = \int_0^{\infty} dz\, z^{\alpha-1}e^{-z}\int_{zt}^{\infty} dy\, y^{\alpha-1}e^{-y} \tag{57}$$

and differentiating with respect to t, we have

$$\frac{dJ}{dt} = -t^{\alpha-1}\int_0^{\infty} dz\, z^{2\alpha-1}e^{-z(1+t)}, \tag{58}$$

or

$$\frac{dJ}{dt} = -\frac{t^{\alpha-1}}{(1+t)^{2\alpha}}\,\Gamma(2\alpha). \tag{59}$$

Integrating this last equation over t and noting that $J\to 0$ as $t\to\infty$, we have

$$J(t) = \Gamma(2\alpha)\int_t^{\infty}\frac{x^{\alpha-1}}{(1+x)^{2\alpha}}\,dx. \tag{60}$$

With the substitution $y=x/(1+x)$, $J(t)$ becomes

$$J(t) = \Gamma(2\alpha)\int_{t/(1+t)}^{1} y^{\alpha-1}(1-y)^{\alpha-1}dy. \tag{61}$$

Alternatively, we can also write

$$J(l) = \Gamma(2a) \int_0^{1/(1+l)} x^{a-1}(1-x)^{a-1} dx . \tag{62}$$

Hence in this case the formula for the second moment takes the form

$$\mu_2(\infty\,;\,0) = \frac{2\Gamma(2a)}{(\gamma+1-Q_1)^a(\gamma+Q_1-Q_2)^a} \int_0^{(\gamma+Q_1-Q_2)/(1+2\gamma-Q_2)} x^{a-1}(1-x)^{a-1} dx . \tag{63}$$

When $\gamma = 0$ and Q occurs with only one value, equation (63) reduces to a formula given by Markarian (*op. cit.*, eq. [21]).

iii) *The dispersion in $N(m)$.*—Since $N(m)$ and $\mathfrak{N}$ differ only by a constant factor, the dispersion, δ^2, in $N(m)$ can be expressed in terms of the first two moments of $\mathfrak{N}$, which we have evaluated. Thus

$$\delta^2(\xi) = \frac{\mu_2(\xi;0)}{\mu_1^2(\xi;0)} - 1 . \tag{64}$$

Using expressions (47) and (54) for $\mu_1(\xi; 0)$ and $\mu_2(\xi; 0)$, we have

$$\delta^2(\xi) = 2e^{\xi_1-\xi_2}\left\{\frac{\sum_{j=0}^{\infty} \xi_2^j/a_j}{\sum_{j=0}^{\infty} \xi_1^j/a_j} - \frac{\sum_{j=0}^{\infty} (\xi_1^j/a_j)\left[\sum_{k=0}^{\infty} (\xi_1+\xi_2)^k/(2a+j)_k\right]}{\left(\sum_{j=0}^{\infty} \xi_1^j/a_j\right)^2}\right\} - 1 . \tag{65}$$

It is seen that the dispersion depends on γ, Q_1, and Q_2 only through the combinations ξ_1 and ξ_2.

For $\xi = \infty$ the expression for the dispersion takes the form (cf. eqs. [42] and [63])

$$\delta^2(\infty) = \frac{2\Gamma(2a)}{\Gamma^2(a)}\left(\frac{\gamma+1-Q_1}{\gamma+Q_1-Q_2}\right)^a \int_0^{(\gamma+Q_1-Q_2)/(1+2\gamma-Q_2)} x^{a-1}(1-x)^{a-1} dx - 1 . \tag{66}$$

In this case δ^2 depends on γ, Q_1, and Q_2 only through the single combination

$$\chi = \frac{\gamma+Q_1-Q_2}{1+2\gamma-Q_2} = \frac{\xi_2}{\xi_1+\xi_2}, \tag{67}$$

for we can write

$$\delta^2(\infty) = \frac{2\Gamma(2a)}{\Gamma^2(a)}\left(\frac{1-\chi}{\chi}\right)^a \int_0^{\chi} x^{a-1}(1-x)^{a-1} dx - 1 . \tag{68}$$

It is found that, for ξ_1 and ξ_2 each less than 2, equation (65) with not too many terms suffices to determine δ^2. In Table 1 we have listed the dispersions computed with the help of this formula for certain ranges of a, ξ_1, and ξ_2 which are required in the applications of the theory to be discussed in § 3. An examination of Table 1 shows that for $\xi_1 < 1$, the dependence of $\delta^2(a, \xi_1; \xi_1 - \xi_2)$ on ξ_1 is so slight that it effectively depends only on a and $\xi_1 - \xi_2$. Also the dependence on a is not very pronounced (see Fig. 1). These facts have an important bearing when we come to discuss the observations in § 3.

For $\xi = \infty$, the dispersion is given by equation (68) and depends only on χ. The dispersions evaluated with the aid of this formula for a range of values of χ and a are given in Table 2.

3. *An analysis of star counts based on the formulae of § 2.*—The paper by Markarian[4] to which we have already referred contains an analysis of the results of star counts tabu-

TABLE 1

VALUES OF $\delta^2(\alpha, \xi_1; \xi_1 - \xi_2)$

$\alpha=1.65$				$\alpha=1.50$			$\alpha=1.20$			
$\xi_1-\xi_2$	$\xi_1=0.3$	$\xi_1=0.4$	$\xi_1=0.5$	$\xi_1-\xi_2$	$\xi_1=0.4$	$\xi_1=0.8$	$\xi_1-\xi_2$	$\xi_1=0.5$	$\xi_1=1.0$	$\xi_1=2.0$
0.00	0	0	0	0.00	0	0	0.0	0	0	0
.02	0.0091	0.0089	0.0086	.05	0.0213	0.0197	.1	0.0354	0.0314	0.0246
.04	.0184	.0179	.0174	.10	.0431	.0399	.2	.0726	.0644	.0502
.06	.0278	.0271	.0264	.15	.0655	.0606	.3	.1117	.0990	.0769
.08	.0373	.0365	.0357	.20	.0885	.0819	.4	.1529	.1352	.1048
0.10	0.0470	0.0461	0.0453	0.25	0.1123	0.1039	0.5	0.1962	0.1730	0.1339

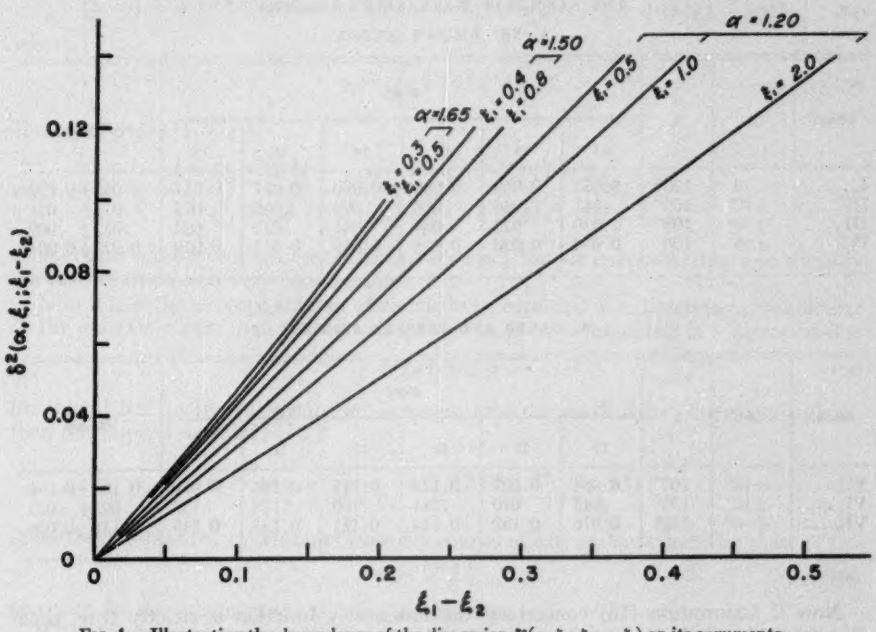

FIG. 1.—Illustrating the dependence of the dispersion $\delta^2(\alpha, \xi_1; \xi_1 - \xi_2)$ on its arguments

TABLE 2

THE DISPERSION $\delta^2(\alpha, \chi)$ FOR $\xi = \infty$

α	χ					
	0.50	0.48	0.46	0.44	0.42	0.40
1.0.....	0	0.0400	0.0800	0.1200	0.1600	0.2000
1.1.....	0	.0457	.0918	.1381	.1846	.2314
1.2.....	0	.0516	.1039	.1568	.2103	.2644
1.3.....	0	.0577	.1164	.1762	.2370	.2989
1.4.....	0	.0639	.1293	.1963	.2648	.3349
1.5.....	0	0.0702	0.1425	0.2170	0.2936	0.3724

lated by van Rhijn and by Baker and Kiefer.[7] Considering various regions with nearly the same galactic latitude but distributed over a range of galactic longitudes, Markarian determined the dispersions,

$$\delta^2(m) = \frac{\overline{N^2(m)}}{\overline{N(m)}^2} - 1, \tag{69}$$

of the tabulated counts. In view of the general inaccessibility of Markarian's paper, we have summarized the results of his analysis in Table 3.

TABLE 3

THE RESULTS OF MARKARIAN'S ANALYSIS

A. VAN RHIJN'S COUNTS

GROUP	β	λ	$\delta^2(m)$						$\delta^2_{\text{average}}$
			13	14	15	16	17	18	
I.....	0	100°	0.053	0.069	0.096	0.090	0.087	0.115	0.085±0.020
II.....	±10°	100°	.041	.046	.068	.092	.098	.078	.071± .021
III.....	±30°	100°	.030	.023	.034	.041	.042	.023	.032± .009
IV.....	±40°	100°	0.034	0.020	0.028	0.019	0.012	0.019	0.022±0.007

B. BAKER AND KIEFER'S COUNTS

GROUP	β	λ	$\delta^2(m)$						$\delta^2_{\text{average}}$
			10	11	12	13	14	15	
V.....	−10°	160°	0.084	0.107	0.124	0.117	0.106	0.079	0.103±0.016
VI.....	±10°	130°	.045	.070	.081	.100	.128	.133	.093± .031
VII.....	+ 0°	130°	0.076	0.133	0.144	0.151	0.135	0.149	0.131±0.026

Now if assumption (13) concerning the luminosity function is strictly true, then $\delta^2(m)$ should be independent of m. Actually, the dispersions as determined by Markarian show an appreciable scatter with m. But the averages for the different groups (given in the last column of Table 3) show such a marked dependence on β that we may suppose that the formulae of § 2 can be applied to these averages. This supposition also underlies Markarian's discussion, though, since he had developed the theory only for the case $\xi = \infty$, he was unable to use the dispersions except for the regions with very low galactic latitudes.[8] However, with the more general formulae we have derived, we can discuss the dispersions at all galactic latitudes; we shall see that this enables a check on the basic assumptions underlying the present method of analysis. Also we shall find that Markarian's conclusions based on the dispersions for $\beta = 0$ require revision.

Before we proceed to apply the formulae of § 2 to the dispersions listed in Table 3, we

[7] *Ap. J.*, **94**, 482, 1941.

[8] Actually, Markarian applied his formulae also for the groups at $\beta = \pm 10°$. But, as we shall see, this application of the formulae valid for $\xi = \infty$ to latitudes even as low as 10° is an invalid procedure.

shall relate the means Q_1 and Q_2 (eq. [24]), which occur in these formulae, with the corresponding means q_1 and q_2 introduced in Paper I. Since (cf. eq. [17])

$$Q = q^A, \qquad A = 1.0859a,$$

we have

$$Q_k = \int_0^1 \psi(q)\, q^{kA} dq, \tag{70}$$

where $\psi(q)$ governs the frequency of occurrence of interstellar clouds with a transparency factor q.

In practice we shall be interested only in values of $q_1 (= \bar{q})$ close to unity. In this case it readily follows from equations (70) that

$$Q_k = 1 - kA(1-q_1) + \tfrac{1}{2}kA(kA-1)(1-2q_1+q_2) + O[\overline{(1-q)^3}], \tag{71}$$

where

$$q_j = \int_0^1 \psi(q)\, q^j dq. \tag{72}$$

Hence, to order $\overline{(1-q)^3}$,

$$\begin{aligned} 1-Q_1 &= A(1-q_1) - \tfrac{1}{2}A(A-1)(1-2q_1+q_2), \\ \text{and} \quad 1-Q_2 &= 2A(1-q_1) - A(2A-1)(1-2q_1+q_2). \end{aligned} \tag{73}$$

These equations provide entirely sufficient accuracy for our purposes; they also simplify the further discussion very considerably.

Now if ξ_0 is the average number of clouds to be expected in a direction perpendicular to the galactic plane, then the number of clouds, ξ, to be expected in a direction β is

$$\xi = \xi_0 \operatorname{cosec} \beta. \tag{74}$$

Further, if Δ is the (mean) absorption in magnitudes perpendicular to the galactic plane, then (cf. Paper I, eqs. [67]–[70])

$$\xi_0 = -\frac{\Delta}{2.5 \log_{10} q_1} = 0.9210 \frac{\Delta}{1-q_1} + O(1). \tag{75}$$

It has been estimated by Hubble[9] from his counts of extragalactic nebulae that

$$\Delta = 0^m.25; \tag{76}$$

however, for the present we shall leave Δ unspecified.

With ξ given by equation (74), the (exact) expressions for ξ_1 and ξ_2 are (eqs. [43] and [51])

$$\begin{aligned} \xi_1 &= \xi_0(\gamma + 1 - Q_1) \operatorname{cosec} \beta \\ \text{and} \quad \xi_2 &= \xi_0(\gamma + Q_1 - Q_2) \operatorname{cosec} \beta. \end{aligned} \tag{77}$$

With $(1 - Q_1)$ given by equation (73), we have

$$\xi_1 = \xi_0\{\gamma + A(1-q_1) + O[\overline{(1-q)^2}]\} \operatorname{cosec} \beta. \tag{78}$$

Writing

$$\gamma = A(1-q_1)\, c \tag{79}$$

and substituting for ξ_0 from equation (73), we obtain

$$\xi_1 = 0.9210(1+c)\Delta A \operatorname{cosec} \beta. \tag{80}$$

[9] *Ap. J.*, 79, 8, 1934.

From this expression for ξ_1 it is evident that the principal uncertainty in estimating ξ_1 will arise from a lack of knowledge of c, i.e., of γ. Now we may safely exclude density gradients, which will lead us to expect appreciable differences in density over distances much less than a kiloparsec. According to equation (34), this excludes values of γ greater than 0.15 if we accept the currently estimated number of seven clouds per kiloparsec. We shall presently see that the values of A which we shall encounter are of order unity; and, since we expect values of $(1 - q_1)$ in the neighborhood of 0.15, we conclude that the uncertainty in our knowledge of the density gradients implies an uncertainty in ξ_1 of a factor of the order of 2. This must be kept in mind when we come to interpret the observed dispersions.

i) *The discussion of the groups centered at galactic latitudes* $\beta = \pm 10°$, $\pm 30°$, *and* $\pm 40°$.—In § 2 we saw that, for $\xi_1 < 1$, the principal argument on which the dispersion depends is

$$\xi_1 - \xi_2 = \xi_0 (1 - 2Q_1 + Q_2) \operatorname{cosec} \beta . \tag{81}$$

In the framework of the approximations represented by equations (73), this argument is

$$\xi_1 - \xi_2 = A^2 \xi_0 (1 - 2q_1 + q_2) \operatorname{cosec} \beta . \tag{82}$$

Consequently, if $(\xi_1 - \xi_2)/A^2$ *can be determined from the observed dispersions at various galactic latitudes, we shall find that it varies linearly with* cosec β. This is a definite prediction of the theory and is capable of verification. We shall analyze the dispersions for groups II–VI given in Table 3 with this in view.

The reduction of the data is exhibited in Table 4. The mean dispersions $(\delta^2)_{av}$ given in the third column are Markarian's values taken from Table 3. The constant a in the empirical representation of the luminosity function (eq. [13]) was determined for the regions included in each of the groups by the formula

$$a = 2.303 \, [\log \overline{N(m+1)} - \log \overline{N(m)}]_{\text{average}} . \tag{83}$$

The values of a determined in this fashion are given in the fourth column; estimates of the uncertainties in these constants were also made and are indicated. The constants A and α now follow from equations (70) and (15) and are given in the fifth and sixth columns. The values of ξ_1 given by equation (80) for $\Delta = 0^m.25$ and $c = 0$, and the values ξ_1 (in view of the uncertainty in γ which we have described earlier) for which $\xi_1 - \xi_2$ was determined according to equation (65) are given in the seventh and eighth columns. From the values of α and ξ_1 given in the sixth and eighth columns we observe that we are in the range of the parameters included in Table 1; the values of $\xi_1 - \xi_2$ determined with the aid of this table are given in the ninth column; the uncertainties in these entries are largely due to the scatter in $\delta^2(m)$. It will be noticed that the derived values of $\xi_1 - \xi_2$ are not sensitive to the assumed values of ξ_1; this is particularly true of the high galactic-latitude groups III and IV. Finally, the last column gives the values of $(\xi_1 - \xi_2)/A^2$.

In Figure 2 we have plotted the values of $(\xi_1 - \xi_2)/A^2$ given in Table 4 against cosec β. It is seen that the predicted linear relation between $(\xi_1 - \xi_2)/A^2$ and cosec β is confirmed very satisfactorily. If, for the sake of definiteness, we adopt for $|\beta| = 10°$ the mean of the $(\xi_1 - \xi_2)/A^2$ values determined for groups II, V, and VII for $\xi_1 = 1.0$, we find that the straight line,

$$\frac{\xi_1 - \xi_2}{A^2} = 0.06 \operatorname{cosec} \beta , \tag{84}$$

fits the observations as well as may be expected; this line is also shown in Figure 2.

Finally, combining equation (82) with the empirically determined relation (84), we have

$$\xi_0 (1 - 2q_1 + q_2) = 0.06 . \tag{85}$$

TABLE 4

THE REDUCTION OF THE DATA ON THE DISPERSIONS ($\beta = \pm 10°, \pm 30°, \pm 40°$)

GROUP	cosec β	$(\delta^2)_{av}$	a	A	ϵ	0.2303 A × cosec β	ξ_1	$\xi_1 - \xi_2$	$(\xi_1 - \xi_2)/A^2$
	A. Van Rhijn's Regions								
IV...	1.56	0.022	0.62±0.09	0.67±0.09	1.65	0.24	0.2 0.4	0.046 .048	0.102±0.050
III...	2.00	.032	.70± .04	.76± .04	1.48	0.35	0.4 0.8	.074 .080	.132± .045
II....	5.76	0.071	0.82±0.05	0.89±0.06	1.22	1.18	1.0 2.0	.22 0.28	.29 ± .10 0.35 ±0.10
	B. Baker and Kiefer's Regions								
V....	5.76	0.103	0.83±0.04	0.90±0.04	1.2	1.19	1.0 2.0	0.31 .39	0.39 ±0.09 .48 ± .09
VI...	5.76	0.093	0.83±0.12	0.90±0.13	1.2	1.19	1.0 2.0	.28 0.36	.35 ± .13 0.44 ±0.13

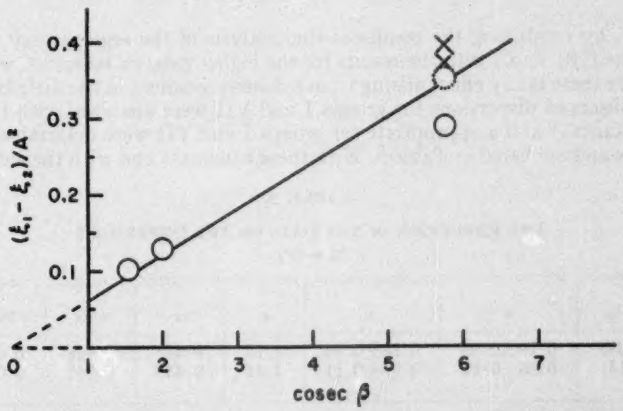

FIG. 2.—Illustrating the linear relation which exists between the observationally deduced values of $(\xi_1 - \xi_2)/A^2$ and cosec β. The circles and the crosses represent, respectively, the points deduced from van Rhijn's counts (groups II, III, and IV) and Baker and Kiefer's counts (groups V and VI). The straight line (eq. [85]) has been drawn to represent these points. The dotted circle refers to group II ($\beta = \pm 10°$) if a density gradient corresponding to $c = 1$ (eq. [80]) is assumed to exist.

ii) *The discussion of the groups on the galactic plane.*—Turning, now, to the dispersions for groups I and VII, which include only regions within 5° of the galactic plane, we first observe that, according to equation (68), the dispersion is expected to depend only on the single variable,

$$\chi = \frac{\gamma + Q_1 - Q_2}{2\gamma + 1 - Q_2}. \tag{86}$$

With Q_1 and Q_2 given by the approximate formulae (73), χ becomes

$$\chi = \frac{1}{2}\left\{1 - \tfrac{1}{2}A^2 \frac{1 - 2q_1 + q_2}{\gamma + A(1 - q_1)}\right\}. \tag{87}$$

Writing γ as in equation (79), we can rewrite equation (87) in the form

$$\tfrac{1}{2} - \chi = \tfrac{1}{4}A \frac{1 - 2q_1 + q_2}{(1 + c)(1 - q_1)}. \tag{88}$$

Multiplying the numerator and the denominator of the quantity on the right-hand side of equation (88) by ξ_0 and substituting for $\xi_0(1 - q_1)$ according to equation (75), we have

$$\tfrac{1}{2} - \chi \simeq 0.271 \frac{A}{\Delta(1 + c)} \xi_0 (1 - 2q_1 + q_2). \tag{89}$$

As we have already seen, $\xi_0(1 - 2q_1 + q_2)$ can be determined from the observed dispersions at the higher galactic latitudes. For $\Delta = 0.25$ and $\xi_0(1 - 2q_1 + q_2)$ given by equation (85), relation (89) reduces to

$$\tfrac{1}{2} - \chi = 0.065 \frac{A}{1 + c}. \tag{90}$$

Accordingly, by combining the results of the analysis of the regions very close to the galactic plane ($|\beta| < 5°$) with the results for the higher galactic latitudes, we can determine whether there is any effect arising from a density gradient in the distribution of the stars. The observed dispersions for groups I and VII were analyzed with this in view.

The constants A and α appropriate for groups I and VII were determined as for the other groups and are listed in Table 5. With these constants and with the aid of Table 2,

TABLE 5

THE REDUCTION OF THE DATA ON THE DISPERSIONS
($\beta = 0°$)

Group	$(\delta^2)_{av}$	a	A	α	χ	$\frac{1}{2} - \chi$	$0.065\,A$	c
I.....	0.085	0.79±0.05	0.86±0.06	1.28	0.472	0.028	0.056	1.0
VII....	0.131	0.86±0.12	0.93±0.14	1.14	0.448	0.052	0.060	0.2

the corresponding values of χ were determined. The values of $\frac{1}{2} - \chi$ are then compared with $0.065A$ (cf. eq. [90]). From this comparison it appears that the observed dispersion for the regions included in group I indicates a density gradient corresponding to $c = 1$; but the observed dispersion for group VII can be accounted for without assuming any appreciable density gradient. It is of interest to notice in this connection that a value of $c = 1$ would make the deduced value of $(\xi_1 - \xi_2)/A^2$ for group II (cf. Table 4 and Fig. 2) agree better with the values for groups V and VI and with the straight line (84). However, it should be stated that the uncertainties in δ^2, A, and α are such that too much

reliance cannot be placed on this conclusion; for the observations can be combined in a manner in which the difference in the values of c for groups I and VII can be made to appear illusory. In any event, we are here concerned only with illustrating the use of the formulae we have derived.

iii) *The mean transparency of the interstellar clouds.*—The foregoing discussion of the observed dispersions in $N(m)$ leads to the one definite result expressed by equation (85). Using equation (75) (with $\Delta = 0.25$), we can write it alternatively in the form

$$1 - 2q_1 + q_2 = \frac{0.06}{0.2303}(1 - q_1) = 0.260\,(1 - q_1)\,, \tag{91}$$

or

$$q_2 = 1.740q_1 - 0.740\,. \tag{92}$$

If we adopt the value $q_1 = 0.85$, then from equation (92) we deduce that

$$q_2 = 0.739\,. \tag{93}$$

This agrees with the value (0.733) determined in Paper I (eq. [74]) from the fluctuations in the total brightness of the Milky Way and confirms the importance of including the dispersion in the transparencies of the interstellar clouds in these discussions.

ON THE STELLAR DYNAMICS OF SPHERICAL GALAXIES*

J. BELZER, G. GAMOW,** AND G. KELLER
Ohio State University, George Washington University, and Perkins Observatory
Received September 5, 1950

ABSTRACT

The dynamical behavior of stars in spherical galaxies is studied on the basis of Hubble's luminosity distribution, with the assumption that the mass of material along any line of sight is proportional to the surface luminous intensity. It is concluded that the stars within 3 parsecs of the center have nearly *random motion* and may be in the state of dynamical equilibrium. On the other hand, it seems that at distances of more than 15 parsecs from the center the motion of stars is *largely radial*. It is suggested that in the outer region statistical equilibrium may have been achieved with regard to the radial component of the stellar momenta.

INTRODUCTION

It seems to be generally accepted now that elliptical galaxies, as well as the central bodies of spirals, are formed entirely from stars belonging to population II and that practically no gas or dust lies between them.[1, 2, 3] This fact makes it difficult to understand the regular shapes of these stellar systems, since, as was first indicated by Jeans many years ago,[4] the free paths of stars in such galaxies exceed their diameters by a factor of many millions. Indeed, Jeans was inclined to believe that the fact that elliptical galaxies possess the regular shapes of rotating bodies definitely proved their gaseous constitution, a conclusion which we now know to be incorrect. It seems that the only way to account for the regular shapes of elliptical galaxies is to assume that the stars which form these systems at the present time once condensed from primordial giant gaseous nebulae of past epochs and that the observed stellar distribution reflects the symmetry features of these primordial gaseous bodies. Thus it is interesting to study the stellar distribution which would result from the condensation of such primordial gaseous nebulae.

In the present paper we shall attack only the case of spherical galaxies,[5] which is mathematically simpler than that of elliptical ones.

Let it be assumed that the stars now present in spherical galaxies were created out of the primordial gas by some type of condensation process. As contraction within the star reduced the surface area of the star, the force exerted on the star by the gas still external to it must have been correspondingly reduced. The external force due to gas pressure must also have been reduced as a consequence of the depletion of the interstellar gas resulting from the star formation. Now in a gas sphere which is in hydrostatic equilibrium the gravitational attraction of an element of gas toward the center is counterbalanced by

* *Contribution from the Perkins Observatory*, No. 28.

** Summer lecturer at the Ohio State University, 1948.

[1] W. Baade, *Ap. J.*, **100**, 137, 1944.

[2] Baade, *ibid.*, p. 147.

[3] Baade, *A.J.*, **53**, 207, 1948.

[4] J. Jeans, *Astronomy and Cosmogony* (Cambridge: At the University Press, 1928), pp. 336, 343 ff.

[5] The fact that at least some of the galaxies which appear spherical are actually physical three-dimensional spheres, and not ellipsoids of revolution viewed parallel to the axis of symmetry, was proved by Hubble's statistical studies (*Ap. J.*, **64**, 321, 1926), which led to the conclusion that the elliptical galaxies are nearly uniformly distributed among the ellipticity classes. Hubble's results have been questioned by ten Bruggencate (*Zs. f. Ap.*, **1**, 275, 1930), but the latter's conclusions were based on a physical model which excluded stars as an important constituent of galaxies and thus are not tenable at the present time.

the radial gradient of the gas pressure. We have seen, however, that after star formation the forces due to gas pressure were largely removed. The result must have been that the stars "rained" in toward the center subsequent to their formation. As we shall see later (last column of Table 2), the average radial velocity which a star attains in falling from rest toward the center of the galaxy is fairly large. The question may be raised as to whether a star, once it is formed and starts to fall inward, may not travel so fast that it will fail to exchange enough energy with its neighbors to permit the aggregate of stars to arrive at a random distribution of velocities during the age of the galaxy.

Let us assume, for the moment, that the change in the energy of a star resulting from encounters with its neighbors is negligible. It will be shown that the falling-in times are short compared to the probable age of 3×10^9 years, and, since the periods of falling in are not isochronous, there will have been times when some stars originating at a large radial distance, S_2, will be found closer to the center than some stars which originated at a smaller distance, S_1. Now in view of the large number of stars and their presumed uniform distribution over the surface of the sphere, one would not expect tangential forces to arise from such an inversion. But nonconservative radial forces between the stars S_1 and S_2 must result, thus permitting an interchange of energy. Thus there is a mechanism for the mutual adjustment of the radial velocities, even though close encounters between individual stars may not be effective. On the other hand, close encounters appear to be the only mechanism by which the angular momenta of stars can be altered.

At the time of formation, stars must certainly have some angular momenta resulting from the turbulent motion in the primordial nebula. In the case of the spherical galaxies, with zero over-all angular momentum, the random angular momenta of stars are expected to be small. It is therefore worth while to investigate the structure of spherical galaxies on the assumptions that (*a*) the tangential velocities of stars may be neglected; (*b*) the interchange of energy through close encounters has been negligible, so that the angular distribution of material still corresponds to that of the primordial gaseous nebula; and (*c*) that enough readjustment of the radial velocities has already taken place through the agency of the inversion mechanism that at the present time stars are not altering their mode of radial motion appreciably during the course of several oscillations through the center.

After the stellar motions have been computed on the basis of these assumptions, it is then desirable to estimate the amount of energy which individual stars will exchange through close encounters. It is thereby possible to divide the galaxy into two parts, namely, that part in which the foregoing assumptions apply and that in which tangential motions of stars must be taken into account.

THE OBSERVATIONAL MATERIAL

A microphotometric study of plates taken on fifteen elliptical nebulae has been made by Hubble.[6] These objects are of the following types:

Type	No. of Objects	Type	No. of Objects	Type	No. of Objects
E0.....	4	E2.....	4	E5.....	1
E1.....	3	E4.....	2	E7.....	1

Hubble found that the surface intensity of light in the projected images varied with distance along either major or minor axis according to the empirical relation

$$\log I = \log I_0 - 2 \log \left(\frac{r}{a} + 1\right), \tag{1}$$

[6] *Ap. J.*, 71, 231, 1930.

where I_0 is the central surface intensity and a is an adjustable constant. The reliability of Hubble's technique has been questioned by De Vaucouleurs,[7, 8] who compares three of Hubble's intensity-curves with curves based on observations by himself, by Redman and Shirley,[9] and by Oort.[10] In Figure 1, De Vaucouleurs's and Hubble's observations on NGC 3379 have been plotted. Despite De Vaucouleurs's objections, the agreement between the two sets of data is, on the whole, not bad. The relation between the apparent surface intensity and distance as given by equation (1) has also been plotted, where the constant a has been set equal to 3″. The agreement between the formula and both observers is fairly good if one keeps in mind the extreme difficulty of measuring low surface

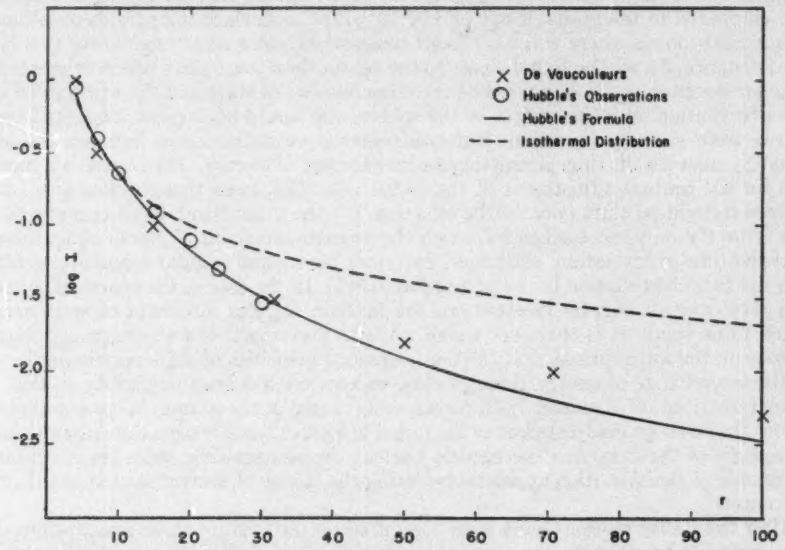

FIG. 1.—Logarithm of the apparent surface luminous intensity (I) in terms of distance from the center (r) for NGC 3379. I is in units of the central surface intensity and r is in seconds of arc. The dashed curve is the distribution to be expected from stars of equal mass which have achieved statistical dynamical equilibrium. Data for the latter curve are due to Hubble (*Ap. J.*, **71**, 231, 1930).

intensities against the sky background. The fit between the formula and De Vaucouleurs's data for NGC 4649 is about as satisfactory. In the latter case, also, the formula gives the steeper decline of intensity with distance.

It is concluded that, so far as is now known, equation (1) still gives a satisfactory representation of the data. This is particularly true in the region between $4a$ and $30a$, which is the region in which most of Hubble's measurements lie.

Assuming that there is no appreciable obscuration of light coming from any part of the galaxy, the light-intensity per unit volume may be computed by Von Zeipel's method. This has been done by Hubble, and the resultant space luminosities are given in his Table XII. We have used this table as a starting point for our own calculations.

We shall now assume that the luminosity distribution, as measured by Hubble, coincides with the true mass distribution of stars in the galaxy. This is based on two assumptions.

[7] *J. d. Obs.*, **31**, 113, 1948.

[8] *Ann d'ap.*, **11**, 247, 1948.

[9] *M.N.*, **98**, 613, 1938.

[10] *Ap. J.*, **91**, 273, 1940.

a) It is assumed that there is no appreciable obscuration of the light from any part of an elliptical galaxy by interstellar material associated with that galaxy. Hubble[9] arrived at this conclusion because of the sharpness of the nuclear images and the uniformity of color distribution over the images. Baade has remarked[3] that, in general, absorbing material seems to be very rarely associated with a pure type II population, a fact which is well known in respect to the globular clusters. Indeed, Russell[11] has made this fact the basis of an explanation of the absence of supergiant stars from type II populations. The question might be raised as to whether there may not be an appreciable amount of dark material in the transition types, such as E7, which may well partake of some of the characteristics of the Sa spirals. Oort's study[10] of NGC 3115 (E7) indicates a very marked increase in the ratio of mass density to luminosity (per unit volume) with increasing distances from the center along the major axis. A comparable variation in this ratio was found to be present in the Andromeda galaxy by Babcock.[12] Whether the effect is due to (1) obscuration by dark material, (2) the additional mass of the dark material, (3) a variation in the average mass/luminosity ratio of the stellar population, or (4) some combination of these or other causes remains an open question. In any event, it will be assumed here that NGC 3115 is not typical of the quasi-spherical galaxies.

b) It is assumed that the average mass/luminosity ratio of the stellar population is a constant throughout a spherical galaxy. Coupled with the assumption of negligible obscuration, this means that the surface intensity of light at any point in the galactic image should be proportional to the galactic mass lying along that line of sight. (It is also assumed here that scattering of light is inappreciable.) No direct determinations of the relation between the luminosity function and central distance for spherical galaxies appears to have been published. The uniformity of color distribution in elliptical galaxies would imply, however, that very large variations in the character of the stellar population are unlikely. The evidence from color studies is strengthened by Smith's finding[13] that no differences in the spectral type between different parts of M32 could be detected on low-dispersion spectra. There is evidence that in the case of globular clusters the giants tend to be more concentrated toward the center than somewhat fainter stars.[14] One would expect such a concentration if conditions of statistical equilibrium exist at the centers of globular clusters, as seems probable from the computed times of relaxation.[15] All in all, the assumption of a constant mass/luminosity ratio should probably be regarded as a crude working hypothesis, to be employed until sufficiently detailed luminosity data are available.

In order to translate the curve given in Figure 1 into the actual scale of densities and distances, we must know the masses and dimensions of the elliptical galaxies. Since galaxies have anything but sharp edges, the radii of their photographic images are markedly dependent on the exposure time. Hubble found that the radii of his images varied as the 0.42 power of the exposure time. In the present study we shall need to have available a value of the radius in parsecs which can be correlated with a specific value of r/a in equation (1). Hubble[6] estimates that the edges of the galaxies must lie beyond $r/a = 35$ on his long-exposure plates. If we associate the value $r/a = 35$ with a diameter of 1900 light-years (E0), also given by Hubble,[16] the corresponding radius $R_H = 290$ parsecs. The average radius found by Shapley[17] for elliptical nebulae by the use of microdensitom-

[11] *Pub. A.S.P.*, **60**, 202, 1948. Some revision of these ideas may soon be required, however. Hubble has recently remarked (*Observatory*, **70**, 129, 1950) that supergiant stars have been observed around the globular galaxy M87.

[12] *Lick Obs. Bull.*, **19**, 41, 1939.

[13] *Ap. J.*, **82**, 192, 1935.

[14] H. Shapley, *Pop. Astr.*, **57**, 203, 1949.

[15] S. Chandrasekhar, *Principles of Stellar Dynamics* (Chicago: University of Chicago Press, 1942).

[16] *The Realm of the Nebulae* (New Haven: Yale University Press, 1936), p. 178.

[17] *Proc. Nat. Acad. Sci.*, **26**, 186, 1942; *Harvard Rept.*, No. I-238.

eter tracings is much larger. His value is 2000 parsecs. Even this value must be regarded as merely a lower limit.

Only the most approximate estimates of the masses of elliptical galaxies can be made on the basis of the data now available, and there are rather serious discrepancies. Assuming that the stars in the outer regions of the Andromeda nebula move in circular Keplerian orbits, Babcock[12] obtains a mass of 1.11×10^{42} gm $= 5.6 \times 10^{8} \odot$ for the population II core. Since the radius of the core is approximately equal to 240 parsecs, it is reasonable to suppose that it may also be expected to have a mass M_H of the same order as that lying within a radius R_H of a spherical galaxy.

For a region of NGC 3115, 73 parsecs in radius, Oort[10] obtains a density of 365 $\odot$/parsec^3. If the ratio of major to minor axis is $\frac{2}{3}$, the total mass of the region would be $4 \times 10^{8} \odot$. The region in question has a very small mass/luminosity ratio, so that it may be a body which is physically analogous to the core of the Andromeda nebula.

A mass estimate may be based on Hubble's mean photographic magnitude of -15.3 for E0–E2 galaxies and on the crude assumption that all the stars are G5 dwarfs of $M_{pg} = 5.4$. These figures imply that there should be 5×10^{8} G5 stars, or a mass of about $5 \times 10^{8} \odot$. One would suspect this estimate of being on the low side because of the preponderance of faint dwarfs in type II populations. The estimate will apply only to the

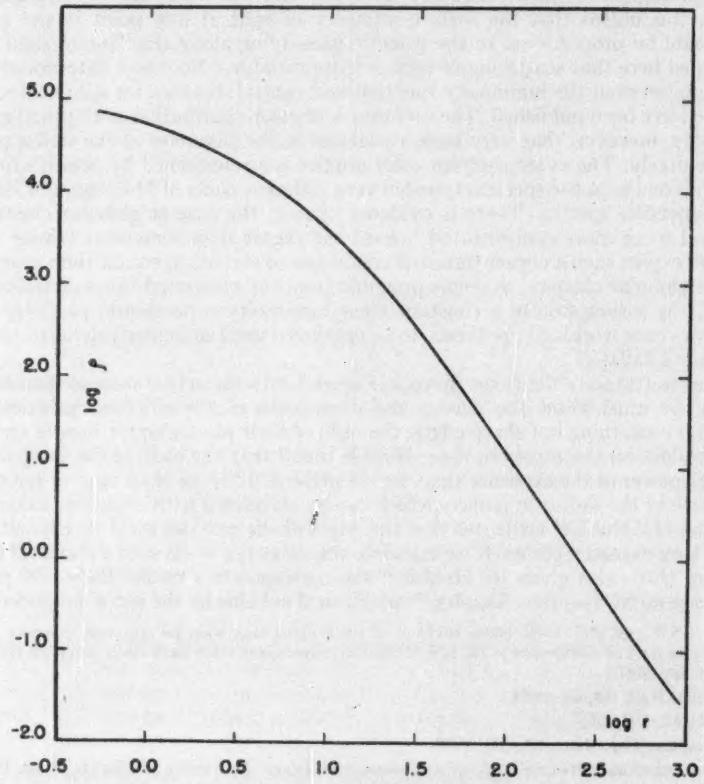

FIG. 2.—The adopted density distribution for spherical galaxies. The density ρ is measured in sun masses per cubic parsec, and the radius r is measured in parsecs.

portion of the galaxy over which the integrated light has been measured by Hubble.

Smith's study[13] of the random velocities in the Virgo cluster led him to the conclusion that the average galactic mass is $2 \times 10^{11} \odot$. This figure is reminiscent of mass estimates which have been made for NGC 3115 (E7, $2 \times 10^{11} \odot$, Oort[10]), the Andromeda nebula (Sb, $10^{11} \odot$, Babcock[12]), and the Milky Way (Sc, $2 \times 10^{11} \odot$). One might suspect that the spirals and intrinsically flattened elliptical systems are not only larger but brighter and very much more massive. The greater brightness would favor the selection of such objects. In the present study we shall direct our attention to the more spherical objects of smaller dimensions and adopt the mass of $5 \times 10^{8} \odot$ within the radius R_H. With these values, Figure 2 illustrates the relationship between the star density (in $\odot/\mathrm{pc}^3$) and radius (pc). It is not unlikely that, if one could determine the entire mass contained within the outermost limits of a spherical galaxy, the result would be very much larger than $5 \times 10^{8} \odot$.

Employing micrometric and interferometric measurements, Smith[13] estimated that the angular radius of the bright semistellar nucleus of M32 was $0''.4 \pm 0''.05$. If the distance of the galaxy is taken as 210,000 parsecs, the nuclear radius becomes about 0.4 parsec. The mean value of a, which is to be employed in formula (1) in the case of M32, is $2.8 \times (2''.03) = 5''.7$. The value of r/a at the edge of the nucleus is therefore 0.07. Smith also finds that the amount of light received from the nucleus is about 3 per cent of the luminosity of the galaxy (as determined by Hubble). In accordance with our general assumptions, we shall assume that the nuclear mass is also 3 per cent of the mass of the material upon which Hubble based his integrated magnitude determination.

THE TEST OF THE RADIAL-MOTION HYPOTHESIS

If the motion of stars in spherical galaxies is confined to radial anharmonic oscillations of different amplitudes, the observed density at a certain distance r from the center must be the sum of the density of stars which have reached their maximum elongation at this distance and the contributions due to transient stars with larger amplitudes of oscillation. In order to obtain from observational data the total number of stars with amplitudes of oscillation s, we must first calculate the distribution of gravitational potential $V(r)$ within the spherical galaxy. If the potential energy is taken as zero at the center of the galaxy, then

$$V(r) = G \int_0^r \frac{dr}{r^2} \int_0^r 4\pi r^2 \rho \, dr. \tag{2}$$

Using the density distribution corresponding to the empirical apparent intensity law (1), we have computed the potential $V(r)$. No correction was made for the concentrated mass of the nucleus. Integrations of equation (2) were performed numerically on International Business Machines. The results are given in Table 1, where R_H is the Hubble radius in centimeters, M_H is the mass of the galaxy in grams lying within R_H, ρ is the smoothed-out density in grams per cubic centimeter, and V is the potential in ergs per gram. If $v_r = dr/dt$ is the radial velocity of a star, if s is the radial distance at which the star was formed, and if we assume that the star was at rest at the instant of formation, then

$$\frac{1}{2}\left(\frac{dr}{dt}\right)^2 = V(s) - V(r), \tag{3}$$

and

$$t_r(s) = \int_0^s \{2[V(s) - V(r)]\}^{-1/2} dr, \tag{4}$$

where $t_r(s)$ is the time required for falling into the center of the galaxy.

[13] *Ap. J.*, 83, 23, 1936.

There is certainly no reason to believe that the potential $V(r)$ can be considered a time-independent function for any galaxy which is not in an equilibrium state or a steady dynamical state. On the other hand, if, on the assumption of a steady state, $t_F(s)$ turns out to be small compared to the probable lifetime of the galaxy, it seems most unlikely that the stars have remained essentially stationary since their time of formation.

Using the values of V in Table 1, the values of $t_F(s)$ given in Table 2 were obtained with the aid of equation (4). The average radial velocity, $\overline{v_r}$, is also given. The third and

TABLE 1

DENSITY AND POTENTIAL

r/R_H	$\rho/(M_H/R_H^3)$	$[V/(M_H/R_H)]\times 10^7$	r/R_H	$\rho/(M_H/R_H^3)$	$[V/(M_H/R_H)]\times 10^7$
0.00180	3720	0.0184	0.180	3.97	3.62
.00288	2910	0.0203	0.288	1.15	4.22
.00453	2160	0.0680	0.453	0.322	4.75
.00718	1480	0.164	0.718	0.0849	5.16
.0114	927	0.336	1.14	0.0217	5.50
.0180	505	0.619	1.80	0.00553	5.73
.0288	250	1.033	2.88	0.00144	5.92
.0453	106.7	1.584			
.0718	39.6	2.24			
0.114	13.2	2.94			

TABLE 2

FALLING TIMES AND AVERAGE RADIAL VELOCITIES

s/R_H	t_F (Sec)$\times$ $[M_H^{1/2}/R_H^{3/2}]$	t_F (Years)	$\overline{v_r}$ (Cm/Sec)$\times$ $[R_H^{1/2}/M_H^{1/2}]\times 10^4$	$\overline{v_r}$ (Km/Sec)
0.0104	72.3	59,300	1.43	48
0.0497	179	147,000	2.78	93
0.238	805	660,000	2.96	99
1.25	6050	4,960,000	2.07	69

fifth columns were obtained on the assumption that $R_H = 290$ parsecs, $M_H = 5 \times 10^8 \odot$.

It will be seen from the third column of Table 2 that the falling-in times are short compared with the probable age of the galaxy. Indeed, the average star has probably made a thousand or more oscillations since the time of its formation.

It follows from equation (3) that the amount of time which a star, originating at s, spends in an interval of radius dr during the course of one quarter-oscillation is given by

$$dt = \{2\,[V(s) - V(r)]\}^{-1/2} dr\,,$$

and the fraction of its total oscillation time spent in this interval is

$$\frac{dr}{t_F\{2\,[V(s) - V(r)]\}^{1/2}}. \tag{5}$$

Let us define the "stop density," $\phi(s)$, of stars which reach the ends of their oscillation at distances from the center between s and $s + ds$ so that the total number of such stars is $4\pi\phi(s)s^2 ds$. Then the space density of stars observed at any particular instant of

time (assuming that the stars from any s have become distributed at random with regard to their phase of oscillation) is given by

$$4\pi\rho(r)\,r^2 = \int_r^\infty \frac{4\pi s^2\phi(s)\,ds}{t_F\{2[V(s) - V(r)]\}^{1/2}}. \tag{6}$$

We now assume that $\rho(r)$ decreases sufficiently rapidly with large r so that $V(r)$ approaches a finite limit. For the sake of convenience in this particular calculation, let us take the value of V to be zero at $r = \infty$.

Changing to V as a variable of integration, we have

$$\begin{aligned}\rho(r)\,r^2 &= \int_{V(r)}^0 \frac{ds}{dV(s)}\frac{s^2\phi(s)\,dV(s)}{t_F\{2[V(s) - V(r)]\}^{1/2}} \\ &= \int_0^{V_1(r)} \left[\frac{s^2\phi(s)}{t_F\sqrt{2}}\left(-\frac{ds}{dV_1(s)}\right)\right]\frac{dV_1(s)}{[V_1(r) - V_1(s)]^{1/2}},\end{aligned} \tag{7}$$

where

$$V_1(r) = -V(r), \qquad V_1(s) = -V(s).$$

Now equation (7) may be regarded as an integral equation in which the quantity in brackets is the unknown. Since it is in the form of Volterra's equation of the first kind, we have

$$\left(-\frac{ds}{dV_1(s)}\right)\frac{s^2\phi(s)}{t_F\sqrt{2}} = \frac{1}{\pi}\frac{d}{dV_1(s)}\int_0^{V_1(s)} \frac{r^2\rho(r)\,dV_1(r)}{\{V_1(s) - V_1(r)\}^{1/2}}, \tag{8}$$

which is easily reduced to

$$\phi(s) = \frac{t_F\sqrt{2}}{\pi s^2}\frac{d}{ds}\int_\infty^s \frac{dV(r)}{dr}\frac{r^2\rho(r)\,dr}{\{V(r) - V(s)\}^{1/2}}. \tag{9}$$

Values of $\phi(s)$ corresponding to several values of s have been obtained with the aid of equation (9) and are listed in Table 3. Series approximations were employed when r

TABLE 3

STOP DENSITIES

s/R_H	$\phi(s)[R_H/M_H]$	s/R_H	$\phi(s)[R_H/M_H]$
0.0104	−608	0.238	+ 1.58
0.0497	+ 49.5	1.25	+ 0.0164

became nearly equal to s. The contributions to the integral for large values of r are small and may be estimated with all the accuracy that is needed. We see that for the large distances the stop densities have reasonable values, but that they become negative near the center of the galaxy. The reason for this failure is that, as one penetrates into the galaxy, a point is reached where the computed population due to transient stars is larger than the local observed density, thus leading to the negative value of computed stop density.

This difficulty implies that the motion of stars near the center cannot be entirely radial. If the stars do have appreciable tangential velocities, then these velocities may either have been inherited by the stars from the material from which they were created or else have been acquired through close encounters. Let us make the assumption that all tangential velocities arise from collisions. We shall endeavor to calculate how much the energy of a star, which is initially in a radial orbit of amplitude s, would change as a result of collisions during a time comparable to the supposed age of the galaxy. If this

change in energy is only a small fraction of the total energy of motion of the star and provided that the original contraction and redistribution of radial velocities has already taken place, the star will tend to remain in its present orbit. However, it will be shown that stars having amplitudes of oscillation smaller than a certain amount have actually exchanged an appreciable amount of energy through collisions. It is concluded that an appreciable number of stars has not survived in purely radial orbits.

THE RELAXATION TIME

The computation of the rate of energy exchange proceeds from the following expression:[19]

$$(\Delta E)^2 = 8\pi N G m^4 (0.18) \log_e \left[\frac{D_0 v^2}{2Gm}\right] dt, \tag{10}$$

where $(\Delta E)^2$ is the square of the average change in energy in the interval of time dt (energy in ergs), N is the number of stars per cubic centimeter, m is the mass of an individual star (assumed constant) in grams, (0.18) is the average value of a function which depends upon the ratio of the velocity of the star in question to the velocity of the average field star (since the function does not depend sensitively upon this ratio, we shall follow Chandrasekhar and employ the average value), and D_0 is the average distance between neighboring stars in centimeters. Since $D_0 \approx 1/N^{1/3}$, $N = \rho(r)/m$, $v^2 = 2[V(s) - V(r)]$, and $vdt = dr$, equation (10) may be written as follows:

$$(\Delta E)^2 = 8\pi (0.18) G^2 m^3 \rho(r) \{\log [V(s) - V(r)] - \tfrac{1}{3} \log \rho - \log G - \tfrac{2}{3} \log m\} dr. \tag{11}$$

If we introduce the new units

$$r' = \frac{r}{R_H}, \qquad \rho' = \rho\left[\frac{R_H^3}{M_H}\right], \qquad V' = V\left[\frac{R_H}{M_H}\right], \tag{12}$$

we may write equation (11) as follows:

$$(\Delta E)^2 = 8\pi (0.18) G^2 m^3 \left(\frac{M_H}{R_H^2}\right) \rho' \left\{\log [V'(s) - V'(r)] - \tfrac{1}{3} \log \rho' + \log\left[\frac{M_H^{2/3}}{G m^{2/3}}\right]\right\} dr'. \tag{13}$$

If the changes in energy due to individual encounters are random, then the square of the accumulated change over a longer period of time is, on the average, equal to the sum of the squares of the individual changes. The entire change during one quarter-oscillation may be obtained by integrating equation (13) from $r' = 0$ to $r' = s'$. If T is the probable age of the galaxy, then the square of the energy change during that time may be obtained by multiplying the energy change over a quarter-cycle by

$$\frac{T}{t_r} = \left(\frac{T}{t'_r}\right)\left(\frac{M_H^{1/2}}{R_H^{3/2}}\right) \quad \text{where} \quad t'_r = t_r \left(\frac{M_H^{1/2}}{R_H^{3/2}}\right). \tag{14}$$

Finally, we are interested in the ratio F of the entire energy change to the present energy of the star, the latter quantity being

$$mV(s) = mV'(s)\left(\frac{M_H}{R_H}\right). \tag{15}$$

[19] Chandrasekhar, *op. cit.*, p. 63.

Performing the indicated operations, we obtain

$$F^2 = J'(s')\left(\frac{m}{M_H}\right)\left(\frac{M_H^{1/2}}{R_H^{3/2}}\right)T, \tag{16}$$

where

$$J'(s') = \frac{8\pi(0.18)G^2}{[V'(s')]^2(l'_P)^2} \times \int_0^{s'} \rho' \left\{\log[V'(s') - V'(r')] - \tfrac{1}{3}\log\rho' + \log\left[\frac{M_H^{2/3}}{Gm^{2/3}}\right]\right\} dr'. \tag{17}$$

If we assume that $m = \odot$, $M_H = 5 \times 10^8\ \odot$, $T = 3 \times 10^9$ years, and $R_H = 290$ parsecs, then

$$F^2 = 7.05 \times 10^{-8} J'(s'). \tag{18}$$

Aside from the ratio M_H/m, $J'(s')$ can be computed without reference to the absolute dimensions or mass of the galaxy. This has been done by a graphical procedure on the basis of the data of the type illustrated in Table 1. The computation need be made with only two-figure accuracy, since the data and assumptions do not warrant a more elaborate procedure. The quantity in braces in equation (17) is nearly constant throughout the range of integration. The results are presented in Table 4.

TABLE 4

FRACTION OF ENERGY EXCHANGED THROUGH COLLISIONS

s/R_H	$J'(s')$	F^2	s/R_H	$J'(s')$	F^2
0.0104	81	0.57	0.238	0.078	5.5×10^{-4}
0.0497	0.67	0.0047	1.25	0.0055	3.9×10^{-5}

It may be seen from Table 4 that stars cannot have oscillated in orbits with amplitudes as small as 0.0104 R_H ($\approx$ 3 parsecs) for 3×10^9 years without having acquired appreciable tangential velocities. This would partly account for the results of the preceding section, which show that stars within $s' \approx 0.02$ cannot be moving in purely radial orbits. Since the stop density at any point is essentially computed by subtracting the density of transient stars from the observed density, a negative stop density implies that the computed transient density is too large. If the orbits of many stars are, in reality, not radial, then such stars will have a perigalacticon distance which is not zero and will not be found closer to the center than that distance. But we have computed the stop density on the assumption that all orbits are radial. The existence of nonradial orbits implies that the computed transient density is too high near the center, and consequently the stop density there should be increased, perhaps to the point where it becomes positive.

If stars with large amplitudes of radial oscillation have small components of tangential velocity at the extremities of their orbits, these stars will also avoid the central regions. For example, let us compute what these tangential velocities would have to be in order for such stars to move in orbits with a perigalacticon distance of 3 parsecs. From equation (2) the radial velocity of a star near the center is $\sqrt{[2V(s)]}$, and its angular momentum is $\approx m r_P \sqrt{[2V(s)]}$, where r_P is its perigalacticon distance. Assuming that angular momentum is nearly conserved during the period of a few revolutions, then one must have

$$m v_{TA} s = m r_P \sqrt{[2V(s)]}, \tag{19}$$

where v_{TA} is the tangential velocity at apgalacticon. Therefore,

$$v_{TA} = \left(\frac{2M_H}{R_H}\right)^{1/2} \left(\frac{r'_P}{s'}\right) \sqrt{V'(s)}\,. \tag{20}$$

Numerical results are given in Table 5, where v_{TA} is measured in kilometers per second.

TABLE 5

TANGENTIAL VELOCITIES AT APGALACTICON

s'	v_{TA}	s'	v_{TA}
0.0104	81	0.238	13.1
0.0497	41	1.25	2.9

It is not unlikely that there could be small apgalacticon tangential velocities due to turbulence in the primordial gas cloud. It is also possible that some angular momentum might be acquired as a result of close encounters. While we know that stars with large orbital amplitudes cannot exchange enough energy through encounters to acquire anything like a circular orbit, such stars might acquire enough angular momentum so that their perigalacticon distances would be considerable. The formulae necessary to make the computations of acquired angular momentum are similar to those used in the case of the energy exchange. One has[20]

$$\Sigma\Delta v_T^2 = 8\pi NG^2m^2H(x_0)\left(\frac{1}{v}\right)\log\left[\frac{D_0 v^2}{2Gm}\right]dt\,, \tag{21}$$

where $\Sigma\Delta v_T^2$ is the mean square tangential velocity acquired in the time interval dt. $H(x_0)$ is defined and tabulated by Chandrasekhar.[21] For $x_0 \ll 1$, it is approximately $4x_0/3\sqrt{\pi}$. The quantity $x_0 = v\sqrt{[3/(2\bar{v}^2)]}$, where $\bar{v}^2$ is the mean-square velocity of the field stars. Other quantities have the same meanings as before. The square of r'_P is

$$(r'_P)^2 = \frac{1}{2V'(s)R_H^2}\int_0^T r^2\Delta v^2 dt\,;$$

therefore

$$(r'_P)^2 = \left(\frac{m}{M_H}\right)\left(\frac{M_H^{1/2}}{R_H^{3/2}}\right)\left[\frac{2\pi G^2}{t'_P V'(s)}\right]T \tag{22}$$

$$\times\int_0^{s'} \frac{H(x_0)\,\rho'(r')^2 dr'}{[V'(s) - V'(r)]}\left\{\log[V'(s) - V'(r)] - \tfrac{1}{3}\log\rho' + \log\left[\frac{M_H^{2/3}}{Gm^{2/3}}\right]\right\}.$$

There are several objections to applying equation (22). First, it is based on equation (21), which was derived for a distribution of field-star velocities that is both spherically symmetric and Gaussian. Neither of these conditions seems likely to be satisfied in the present case. Moreover, one must know $\bar{v}^2$ before x_0 can be evaluated. However, with

[20] Chandrasekhar, *op. cit.*, p. 229. The writers are indebted to Dr. Lyman Spitzer for suggesting the importance of this calculation and for indicating the appropriate method. Cohen, Spitzer, and Routly (*Phys. Rev.*, **80**, 230, 1950) have shown that, instead of using $D_0 = 1/N^{1/3}$, one should use a dimension of the order of that in which the star density is constant. The latter distance is certainly larger than the value used in this paper. But, since the dependence on D_0 is logarithmic, it may be shown that the error is unimportant in these qualitative calculations.

[21] *Op. cit.*, p. 73.

only the roughest sort of estimates of the appropriate values of $\overline{v^2}$, the following results were obtained by graphical integration:

$$s = 3 \text{ parsecs}, \quad \frac{s}{R_H} = 0.0104, \quad \frac{r_P}{R_H} = 3.10^{-3}, \quad r_P \approx 0.9 \text{ parsec};$$

$$s = 290 \text{ parsecs}, \quad \frac{s}{R_H} = 1.25, \quad \frac{r_P}{R_H} = 10^{-3}, \quad r_P \approx 0.3 \text{ parsec}.$$

These numbers are probably correct within a factor of 2 either way.

In the case of $s = 3$ parsecs, one sees that the perigalacticon distance is an appreciable fraction of the apgalacticon distance, which means that the orbit is pretty far from being radial. This confirms our earlier results based on the energy transferred by collisions. For $s = 290$ parsecs, one sees that the perigalacticon distance due to angular momentum acquired in collisions is very small. On the other hand, Table 5 shows that only 3 km/sec of tangential velocity at apgalacticon is enough to give a perigalacticon distance of 3 parsecs. It would therefore seem probable that for the stars with large orbital amplitude the angular momentum is mostly primordial, whereas for stars of small orbital amplitude the angular momentum is acquired.

A word about the nucleus should be said at this point. In the calculations of this and preceding sections the nuclear concentration of stars has been neglected. For most of these exploratory calculations the neglect does not have any important effect on the results. Such may not be the case when it comes to the relaxation time. If one assumes the mass and density estimates given in an earlier section of this paper, one finds that the nuclear density ρ' is of the order of 10^7. It is not possible to compute $V(r)$ within the nucleus without detailed information concerning the internal density distribution. But, neglecting the alterations in $V(r)$ due to the nucleus, one can estimate the effect that the density alone would have on the computed value of F^2. The result is that F^2 is increased by a factor of 100, implying that orbits out to $s/R_H = 0.05$ are seriously disturbed as long as they pass through the nucleus. If $V(r)$ due to the nucleus could be taken into account, it would probably reduce the correction factor, since the velocities would be increased considerably.

SUGGESTION THAT SOME LIMITED REGIONS MAY BE IN STATISTICAL EQUILIBRIUM

Since motions with three degrees of freedom do exist near the center of the galaxy, it is worth while attempting to see how closely the situation there approximates that of an isothermal spherical distribution. It is well known that the frequency function for an isothermal spherical distribution of stars is

$$f = \left(\frac{3}{2\pi \overline{v^2}}\right)^{3/2} \rho_0 \exp\left\{\frac{-3v^2/2 - 3V(r)}{\overline{v^2}}\right\}, \tag{23}$$

$$\rho = \int_0^\infty 4\pi v^2 f \, dv = \rho_0 \exp\left[\frac{-3V(r)}{\overline{v^2}}\right], \tag{24}$$

where f is the density in phase space of stars having co-ordinates r and v, and ρ_0 is the space density at $r = 0$. From equation (24) we get

$$V(r) = \frac{-\overline{v^2}}{3 \text{ (Mod)}} \log_{10} \rho + \text{Const.}; \tag{25}$$

$$\therefore \quad \overline{v^2} = -3 \text{ (Mod)} \frac{\Delta V(r)}{\Delta (\log_{10} \rho)}, \tag{26}$$

$$\overline{v^2} = -3\,(\text{Mod})\left(\frac{M_H}{R_H}\right)\frac{\Delta V'(r)}{\Delta(\log_{10}\rho')}. \tag{27}$$

The Δ's on the right-hand side indicate corresponding differences. The difference quotient may be obtained graphically, provided that the relation between V' and $\log_{10}\rho'$ is linear, as equation (27) shows it should be for a true isothermal distribution. If one does not include the nucleus in the calculation of V', one sees from Figure 3 (curve for three degrees of freedom) that there is fair linearity in the region nearest the center

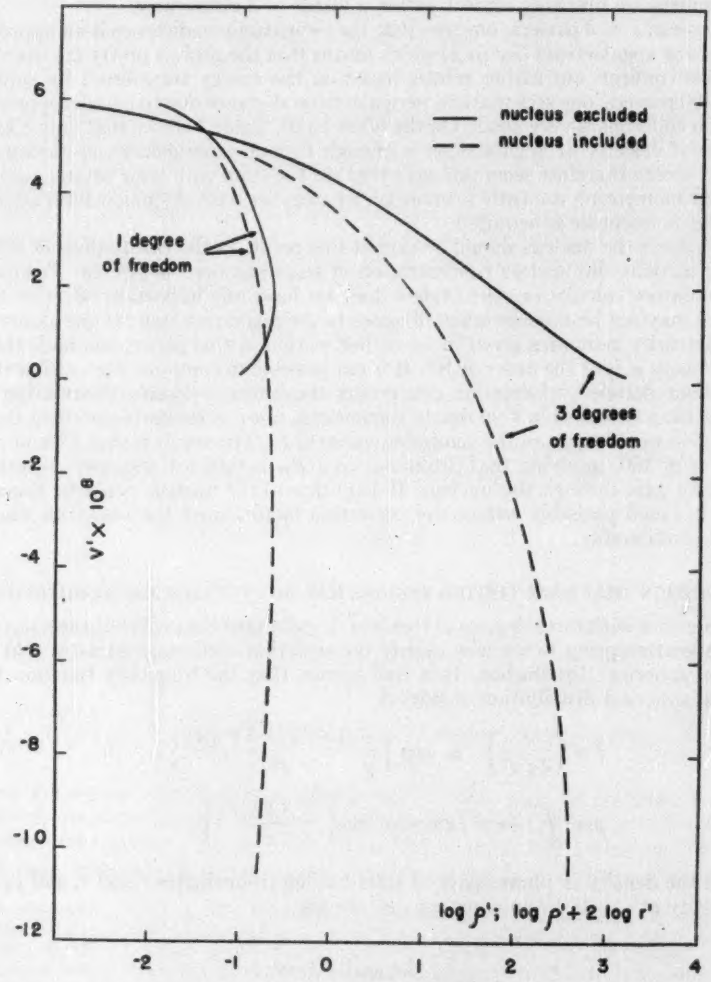

FIG. 3.—Potential energy as a function of density and (density) × (radius)^2; V', ρ', and r' are defined as in equation (12). For the dashed curves (nucleus included) V' is adjusted so that it has the same value at infinity as for the solid curves (nucleus excluded).

(right-hand side). The root mean square velocity computed from equation (27) is

$$\sqrt{(\bar{v}^2)} = 1.29 \times 10^{-4} \sqrt{\frac{M_H}{R_H}} \approx 433 \text{ km/sec}. \tag{28}$$

The component of this quantity along any particular direction (as, for instance, the line of sight) may be obtained by dividing it by $\sqrt{3}$, so the root mean square radial velocity would be

$$\sqrt{(\bar{v}_r^2)} = \frac{\sqrt{(\bar{v}^2)}}{\sqrt{3}} = 250 \text{ km/sec}. \tag{29}$$

If the stars comprising the outer part of the galaxy are, in fact, moving in largely radial orbits, it is interesting to speculate on whether they may have achieved statistical equilibrium with regard to the one degree of freedom that they do enjoy. It would be necessary to show that sufficient energy can be exchanged between such stars by the inversion process and, moreover, that the system will progress toward a state of maximum dynamical probability. Our attempts to demonstrate the last two points have not been successful. However, let us see what some of the consequences would be if equilibrium in one degree of freedom were attained.

The number of stars (having exclusively radial motion) which will be found at a distance r from the center of oscillation is proportional to

$$\exp\left[\frac{-V(r)}{\bar{v}_r^2}\right]; \tag{30}$$

but the space density can be obtained only by dividing by the area of the sphere over which such stars are distributed. Consequently,

$$\rho = \left(\frac{C}{r^2}\right) \exp\left[\frac{-V(r)}{\bar{v}_r^2}\right]; \tag{31}$$

$$\therefore\ 2 \log r + \log \rho = \frac{-V(r)}{\bar{v}_r^2} + \text{Const.}, \tag{32}$$

and

$$\bar{v}_r^2 = -\,(\text{Mod})\left(\frac{M_H}{R_H}\right) \frac{\Delta V'(r)}{\Delta [2 \log_{10} r' + \log_{10} \rho']}. \tag{33}$$

Now if $\bar{v}_r^2$, for the outer part of the galaxy where there is only one degree of freedom, is to be equal to $\bar{v}_r^2$ for the inner part, then from equations (27), (29), and (33) we see that we should have

$$\underset{\text{(outer part)}}{\frac{\Delta V'(r)}{\Delta [2 \log_{10} r' + \log_{10} \rho']}} = \underset{\text{(inner part)}}{\frac{\Delta V'(r)}{\Delta [\log_{10} \rho']}}. \tag{34}$$

In Figure 3, $V'(r)$ has been plotted against $2 \log_{10} r' + \log_{10} \rho'$ (see the curve marked "one degree of freedom"). If equation (34) is to be satisfied, it means that the upper left part of the one-degree-of-freedom-curve should have the same slope as the lower right part of the three-degrees-of-freedom-curve. This is seen to be the case, provided that the nuclear potential is omitted from the computation.

The nearly linear portion of the three-degrees-of-freedom-curve extends as far as $\log \rho' = 0.60$, which corresponds to $r/R_H = 0.180$, or about 50 parsecs. But from Table 4 it appears that the relaxation time for stars at this distance is too large to permit three-

dimensional equilibrium to have been established this far out, unless the nucleus is a very efficient scattering agent in this respect. On the basis of the relaxation-time estimates, it seems that one can really count on randomness of motion only as far out as $s/R_H = 0.0104$, or 3 parsecs.

If one assumes that the essentially flat portion of the one-degree-of-freedom-curve extends to the left of $\log \rho' + 2 \log r' = -1.35$, then the one-dimensional equilibrium region starts at $s/R_H = 0.72$, or 200 parsecs.

An attempt has been made to include the effect of the nucleus. Using Smith's estimate of the nuclear luminosity, we have m (nucleus) $= 0.03M_H$. The contribution of this matter to the potential was calculated on the assumption that it was all contained within a very small radius. The effect of this concentrated mass is very great at points close to the center, as the curves in Figure 3 show. The linear relation between $\bar{V}(r)$ and $\log \rho'$ becomes less secure, and $\overline{v_r^2}$ is increased by a factor of 2 or 3.

It is possible that more precise observations will reveal that the nuclear luminosity is not quite so large as supposed. Another possibility is that there is a disproportionate number of giants in that region, so that the mass of the nucleus is smaller than would be computed on the assumption of an average mass/luminosity ratio.

It will be noticed that the root mean square velocity given in equation (25) is considerably higher than those which appear in the last column of Table 2. The explanation is that in computing equation (25) we have used a slope which is somewhat greater than the mean slope of the right half of the upper right-hand curve in Figure 3. In so doing we have made a moderate allowance for the nuclear concentration.

SUMMARY

It is assumed that the elliptical galaxies were originally gaseous nebulae out of which the individual stars were later formed by a process of local condensation. It is then suggested that the present regular shapes of elliptical galaxies reflect the symmetry features of the primordial nebulae. In the particular case of spherical galaxies, the motion of newly formed stars may be in the nature of a radial anharmonic vibration.

Hubble's observations of the apparent luminosity distribution in elliptical nebulae have been taken as a starting point of the detailed calculations. It has been assumed that the mass distribution is proportional to the luminosity distribution, and only spherically symmetric configurations are considered in the analysis. In this connection the probable total masses and radii of the galaxies are also discussed.

The potential distribution and periods of stars having various amplitudes of orbital motion are computed. It is shown that the average star has made of the order of a thousand orbital oscillations in 3×10^9 years.

On the hypothesis of radial motion, the relative numbers of stars having different orbital amplitudes are computed. The result is not inconsistent with the hypothesis for amplitudes greater than 15 parsecs but is contradictory at smaller distances from the center.

Calculation of the amount of energy exchanged through close encounters shows that statistical equilibrium has been attained within 3 parsecs of the center for all three components of the velocity. For stars with orbital amplitudes greater than 15 parsecs, the energy exchanged through encounters is negligible. A statistical equilibrium may have been attained with regard to the radial component of the velocity for stars with orbital amplitudes greater than 200 parsecs.

The authors wish to express their appreciation to Drs. Martin Schwarzschild and Lyman Spitzer, Jr., for stimulating discussions. They are especially indebted to Dr. Walter Baade for his comments regarding the observational material.

RADIATION FIELD OF EXTENDED STELLAR ATMOSPHERES

S. MIYAMOTO
Institute of Astrophysics, University of Kyoto
Received June 5, 1950

ABSTRACT

In this paper the problem of the radiation field in an extended atmosphere in which the transformation of ultraviolet radiation into Lyman-α radiation is taking place is considered. In treating this problem the Lyman-α contour is assumed to consist of a core and a wing with different absorption coefficients; also, account is taken of the ionization from the second quantum state. It is shown that both these effects reduce the transformation into Lyman-α to an extent that the pressure resulting from the radiation is comparable to that due to the ultraviolet radiation. However, it appears that in the outermost parts of the nebula radiation pressure due to Lyman-α may be one hundred times that of the ultraviolet radiation. For planetary nebulae the main effect comes from the contour's not being strictly rectangular, while in the atmospheres of Be stars the ionization from the second quantum state is the principal factor. The two effects are comparable when the dilution factor is about 0.0016.

I. INTRODUCTION

The radiation field of planetary nebulae was first treated by V. A. Ambarzumian[1] and S. Chandrasekhar.[2] Inside the nebula the ultraviolet radiation from the central star is transformed to Lyman-α radiation by the operation of the Rosseland cycle. If the nebula is opaque to ultraviolet radiation, the transformation of the ultraviolet radiation is nearly complete and results in a large outward radiation pressure.

In the case of the atmospheres of Be stars, where dilution of radiation is not so strong as in the planetary nebulae, the writer has previously shown[3] that the transformation of the Lyman-α is arrested by a process which is the inverse of the Rosseland cycle; for the increased density in Lyman-α results in an increase in the population of the second quantum state and therefore also an increase in the ionization from that level. We shall call this latter process the "fluorescence effect."

H. Zanstra has recently pointed out[4] that the assumption of a rectangular contour of the Lyman-α made in these investigations may also lead to an exaggerated estimate of the pressure due to this radiation. He has suggested that the assumption of a less idealized form for the line contour will alter the Lyman-α radiation appreciably. The writer has also obtained[5] the solution for this latter problem when the contour of Lyman-α can be represented by a step function.

In this paper we shall treat the radiation field in extended atmospheres, taking into account both the effect of fluorescence and the effect of the line contour. Also we shall allow the dilution factor to have any value. The principal results of this analysis may be stated as follows: For planetary nebulae, where the dilution factor is very small, the effect of the line contour is predominant, while for Be stars, where the dilution is not so small, the fluorescence is much more effective. Both effects are comparable for a dilution factor equal to 0.0016. In both cases the intensity of the Lyman-α radiation is much reduced compared with the Ambarzumian solution, and the radiation pressure is cut down to an extent that makes it comparable to the radiation pressure due to the ultraviolet radiation.

[1] *M.N.*, **95**, 469, 1935.

[2] *Zs. f. Ap.*, **9**, 266, 1935.

[3] *Jap. J. Astr.*, **1**, 17, 1949; hereafter referred to as "Paper A."

[4] *B.A.N.*, Vol. **11**, No. 401, 1949.

[5] *Pub. Astr. Soc. Japan*, Vol. **2**, No. 1, 1950; hereafter referred to as "Paper B."

II. THE STATEMENT OF THE PROBLEM

We shall consider a gaseous shell of optical thickness τ_0 for the Lyman continuum. We shall suppose that this shell is illuminated by dilute Planck radiation from the central star. Further, we shall assume that the contour of the Lyman-α line can be approximated by two step functions (see Fig. 1). Let L_α and L'_α denote the central core and the "wings" of the contour, respectively. Let the absorption coefficient for L_α and L'_α be κ_α and κ'_α, respectively. Further, let the ratios of these coefficients to that for the ultraviolet radiation be $\varpi_\alpha = \kappa_\alpha/\kappa_c$ and $\varpi'_\alpha = \kappa'_\alpha/\kappa_c$. The optical depths for L_α and L'_α are then $\varpi_\alpha\tau$ and $\varpi'_\alpha\tau$. The choice of the wing L'_α is somewhat arbitrary, but from general considerations it would appear that the most favorable assumptions would be $\tau_0 \sim 1$, $\varpi_\alpha \sim 10^4$, and $\varpi'_\alpha \sim 1$.

In treating the transfer of the Lyman-α radiation, we shall make the following specific assumption: By the process of absorption and emission, a Lyman-α quantum is transformed to a Lyman-α' quantum with a probability p and to a Lyman-α quantum with a probability $1 - p$. In conformity with our choice of the extent of the wings made in the preceding paragraph, we shall take $p \sim 10^{-4}$.[6]

In treating the Rosseland cycle, we shall suppose that we have to deal with the three

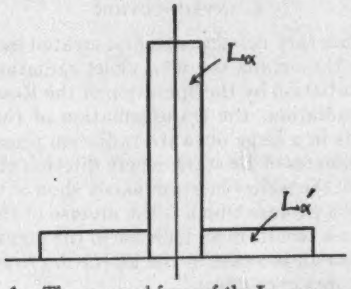

FIG. 1.—The assumed form of the Lyman-α contour

levels: the ground level, 1; the second level, 2; and the continuum, c. The radiation connecting the levels $1 \rightarrow c$, $2 \rightarrow c$, and $1 \rightarrow 2$ are, respectively, the ultraviolet radiation, the Balmer continuous radiation, and the Lyman-α radiation. For the division of the Lyman-α contour into the wings and the core in the manner we have used, the probabilities of spontaneous emissions are $A_{21}(1 - p)$ and $A_{21}p$ for L_α and L'_α, respectively; here A_{21} denotes the ordinary Einstein coefficients when the Lyman-α emission is considered in its entirety. The corresponding probabilities of absorption are $B_{12}(1 - p)J_\alpha$ and $B_{12}pJ'_\alpha$, where J_α and J'_α denote the mean intensities and B_{12} the Einstein coefficients corresponding to A_{21}.

In the following we shall distinguish the quantities relating to the Balmer continuous radiation, the Lyman-α, and the Lyman-α' with the suffixes β, α, and α', respectively; the unsuffixed quantities will refer to the ultraviolet radiation.

III. THE EQUATIONS OF TRANSFER AND OF RADIATIVE EQUILIBRIUM

Let N_j denote the population of the level j ($j = 1$, 2, and c), A_{ji} and B_{ij} the Einstein coefficients, and the J's the mean intensities. Then the equations expressing the conservation in the numbers of atoms in the different levels are

$$N_1\{B_{12}[(1 - p)J_\alpha + pJ'_\alpha] + B_{1c}J\} = N_2A_{21} + N_c^2A_{c1}, \quad (1)$$

[6] $p = 0.18 \times 10^{-4}$ is better numerically. I express my cordial thanks to Dr. H. Zanstra for his invaluable discussion (added Dec. 11, 1950).

$$N_2(A_{21}+B_{2c}J_\beta) = N_1B_{12}\{(1-p)J_\alpha + pJ'_\alpha\} + N_c^2A_{c2}\,, \tag{2}$$

and

$$N_c^2(A_{c1}+A_{c2}) = N_1B_{1c}J + N_2B_{2c}J_\beta\,. \tag{3}$$

And the equations of transfer, neglecting curvature, are

$$\cos\theta\frac{dI}{dz} = -\frac{h\nu}{4\pi}(N_1B_{1c}I - N_c^2A_{c1})\,, \tag{4}$$

$$\cos\theta\frac{dI_\alpha}{dz} = -\frac{h\nu_\alpha}{4\pi}(1-p)(N_1B_{12}I_\alpha - N_2A_{21})\,, \tag{5}$$

$$\cos\theta\frac{dI'_\alpha}{dz} = -\frac{h\nu_\alpha}{4\pi}p(N_1B_{12}I'_\alpha - N_2A_{21})\,, \tag{6}$$

and

$$\cos\theta\frac{dI_\beta}{dz} = -\frac{h\nu_\beta}{4\pi}(N_2B_{2c}I_\beta - N_c^2A_{c2})\,, \tag{7}$$

where z is the geometrical distance measured from the central star outward, θ the angle between the direction of radiation and the z-axis, and ν the frequency. In writing equations (5) and (6) we have neglected the frequency difference between L_α and L'_α.

In this paper we shall restrict ourselves to the case $\tau_0 \sim 1$. Then the atmosphere has only a small opacity in the Balmer continuum, and we need not consider the equation of transfer (7) for $B\alpha_c$. It must be remarked, however, that these circumstances do not necessarily mean the smallness of the ionization from the second level.

The optical depths for the ultraviolet radiation, L_α and L'_α, are, by definition,

$$d\tau = -\frac{h\nu}{4\pi}N_1B_{1c}dz\,; \qquad d\tau_\alpha = -\frac{h\nu_\alpha}{4\pi}N_1B_{12}(1-p)\,dz = -\varpi_\alpha d\tau \tag{8}$$

and

$$d\tau'_\alpha = -\frac{h\nu_\alpha}{4\pi}N_1B_{12}p\,dz = -\varpi'_\alpha d\tau\,, \tag{9}$$

where

$$\varpi_\alpha = \frac{\nu_\alpha B_{12}}{\nu B_{1c}}(1-p) \sim 10^4 \qquad \text{and} \qquad \varpi'_\alpha = \frac{\nu_\alpha B_{12}}{\nu B_{1c}}p \sim 1\,. \tag{10}$$

Changing the variable from z to τ, equations (4), (5), and (6) become

$$\mu\frac{dI}{d\tau} = I - \frac{N_c^2}{N_1}\frac{A_{c1}}{B_{1c}}\,; \qquad \mu\frac{dI_\alpha}{\varpi_\alpha d\tau} = I_\alpha - \frac{N_2}{N_1}\frac{A_{21}}{B_{12}}\,; \qquad \mu\frac{dI'_\alpha}{\varpi'_\alpha d\tau} = I'_\alpha - \frac{N_2}{N_1}\frac{A_{21}}{B_{12}}\,. \tag{11}$$

Performing the usual operations on these equations, we find:

$$\frac{1}{4}\frac{dF}{d\tau} = J - \frac{N_c^2}{N_1}\frac{A_{c1}}{B_{1c}}\,, \quad \frac{1}{4}\frac{dF_\alpha}{\varpi_\alpha d\tau} = J_\alpha - \frac{N_2}{N_1}\frac{A_{21}}{B_{12}}\,, \quad \text{and} \quad \frac{1}{4}\frac{dF'_\alpha}{\varpi'_\alpha d\tau} = J'_\alpha - \frac{N_2}{N_1}\frac{A_{21}}{B_{12}}\,; \tag{12}$$

and, further,

$$\frac{dK}{d\tau} = \tfrac{1}{4}F\,, \qquad \frac{dK_\alpha}{\varpi_\alpha d\tau} = \tfrac{1}{4}F_\alpha\,, \qquad \text{and} \qquad \frac{dK'_\alpha}{\varpi'_\alpha d\tau} = \tfrac{1}{4}F'_\alpha\,, \tag{13}$$

where

$$J = \frac{1}{2}\int_{-1}^{+1} I\,d\mu\,; \qquad F = 2\int_{-1}^{+1} I\mu\,d\mu\,; \qquad \text{and} \qquad K = \frac{1}{2}\int_{-1}^{+1} I\mu^2 d\mu\,; \tag{14}$$

and similar expressions for L_α and L'_α.

The inner surface of the shell atmosphere is illuminated by the incident radiation from the central star. Let us denote by πS the ultraviolet flux at the inner surface. We shall neglect the incident Lyman-α radiation, since the field in Lyman-α is controlled by the ultraviolet radiation.

On the Eddington-Milne approximation,

$$3K = J + \tfrac{1}{2}Se^{\tau-\tau_0}, \qquad 3K_\alpha = J_\alpha, \qquad \text{and} \qquad 3K'_\alpha = J'_\alpha; \tag{15}$$

and from equations (12) and (13) we obtain

$$\frac{d^2J}{d\tau^2} = 3J - 3\frac{N_c^2}{N_1}\frac{A_{c1}}{B_{1c}} - \tfrac{1}{2}Se^{\tau-\tau_0}, \tag{16}$$

$$\frac{d^2J_\alpha}{\varpi_\alpha^2 d\tau^2} = 3J_\alpha - 3\frac{N_2}{N_1}\frac{A_{21}}{B_{12}}, \qquad \text{and} \qquad \frac{d^2J'_\alpha}{\varpi_\alpha'^2 d\tau^2} = 3J'_\alpha - 3\frac{N_2}{N_1}\frac{A_{21}}{B_{12}}. \tag{17}$$

Solving equations (1)–(3), we find

$$\frac{N_2}{N_1} = \frac{(A_{c1}+A_{c2})B_{12}\{(1-p)J_\alpha + pJ'_\alpha\} + A_{c2}B_{1c}J}{A_{21}(A_{c1}+A_{c2}) + A_{c1}B_{2c}J_\beta} \tag{18}$$

and

$$\frac{N_c^2}{N_1} = \frac{B_{2c}J_\beta B_{12}\{(1-p)J_\alpha + pJ'_\alpha\} + (A_{21}+B_{2c}J_\beta)B_{1c}J}{A_{21}(A_{c1}+A_{c2}) + A_{c1}B_{2c}J_\beta}. \tag{19}$$

Within the scope of our approximation, J_β is constant and is equal to the incident Balmer continuous radiation. Therefore, these expressions are linear functions of J, J_α, and J'_α. Inserting these expressions in equations (16) and (17), we find, after some algebra, that

$$\frac{d^2J}{d\tau^2} = 3\frac{C_2}{1+\zeta}J - 3\frac{\zeta}{1+\zeta}\frac{p}{\nu_\alpha}(\varpi_\alpha J_\alpha + \varpi'_\alpha J'_\alpha) - \tfrac{1}{2}Se^{\tau-\tau_0}, \tag{20}$$

$$\frac{d^2J_\alpha}{\varpi_\alpha^2 d\tau^2} = 3\frac{\zeta+p}{1+\zeta}J_\alpha - 3\frac{p}{1+\zeta}J'_\alpha - 3\frac{(1-p)}{\varpi_\alpha}\frac{C_2}{1+\zeta}\frac{\nu_\alpha}{\nu}J, \tag{21}$$

and

$$\frac{d^2J'_\alpha}{\varpi_\alpha'^2 d\tau^2} = 3\left(1-\frac{p}{1+\zeta}\right)J'_\alpha - 3\frac{1-p}{1+\zeta}J_\alpha - \frac{3p}{\varpi'_\alpha}\frac{C_2}{1+\zeta}\frac{\nu_\alpha}{\nu}J, \tag{22}$$

where

$$C_1 = \frac{A_{c1}}{A_{c1}+A_{c2}}, \qquad C_2 = \frac{A_{c2}}{A_{c1}+A_{c2}}, \qquad \text{and} \qquad \zeta = \frac{C_1B_{2c}J_\beta}{A_{21}}. \tag{23}$$

The quantity ζ is characteristic of the fluorescence effect, while the effect of the line contour is determined by p. From the first term in the right-hand side of equation (21), we anticipate that the relative importance of the two effects will be determined by comparing ζ with p.

Now, since $\zeta \propto J_\beta \propto W$, we see that $\zeta < p$ for sufficiently small W, and, in this case, the solution valid for nebulae is obtained, while $\zeta > p$ for comparatively large W, and we get the solution appropriate for the atmospheres of the Be stars. The critical case arises when

$$\zeta = p. \tag{24}$$

Numerically we find $\zeta = 0.06\ W$ corresponding to a photospheric temperature of 19,600°. Putting $p = 10^{-4}$, we get, for the critical dilution factor, $W = 0.0016$.

According to the current estimates, the average dilution factor of the Be stars is $W = 0.01$. Therefore, we conclude that the Be-star field is quite different from that of nebulae.

We shall write down the integrals of equations (20)–(22) obtained by S. Chandrasekhar and L. G. Henyey. First, we have[7]

$$F + \frac{\nu}{\nu_a} F_a + \frac{\nu}{\nu_a} F'_a = \tfrac{4}{3} b \,, \tag{25}$$

where $4b/3$ is a constant of integration.

Second, using Eddington's approximation, we get[8, 7]

$$J = a + b\tau - \frac{\nu}{\nu_a \varpi_a} J_a - \frac{\nu}{\nu_a \varpi'_a} J'_a - \tfrac{1}{2} S e^{\tau - \tau_0} \,, \tag{26}$$

where a is another constant of integration.

By the aid of the last integral, we can eliminate the ultraviolet intensity J from equations (21) and (22). After the calculations, we finally get

$$\frac{d^2 J_a}{d\tau^2} = a_{11} J_a + a_{12} J'_a + a_{13}(a + b\tau) + a_{14} e^{\tau - \tau_0} \,, \tag{27}$$

$$\frac{d^2 J'_a}{d\tau^2} = a_{21} J_a + a_{22} J'_a + a_{23}(a + b\tau) + a_{24} e^{\tau - \tau_0} \,, \tag{28}$$

where we have used the following abbreviations:

$$\begin{aligned}
a_{11} &= 3\,\frac{\varpi_a^2(\zeta + p) + (1-p)C_2}{1+\zeta}; \qquad a_{21} = -3\,\frac{(1-p)\varpi_a'^2 - pC_2(\varpi'_a/\varpi_a)}{1+\zeta}; \\
a_{12} &= -3\,\frac{\varpi_a^2 p - (1-p)C_2(\varpi_a/\varpi'_a)}{1+\zeta}; \qquad a_{22} = 3\,\frac{\varpi_a'^2(1+\zeta-p) + pC_2}{1+\zeta}; \\
a_{13} &= -3\,\frac{1-p}{1+\zeta} C_2 \varpi_a \frac{\nu_a}{\nu}; \qquad a_{23} = -3\,\frac{p}{1+\zeta} C_2 \varpi'_a \frac{\nu_a}{\nu}; \\
a_{14} &= \tfrac{3}{2}\,\frac{1-p}{1+\zeta} C_2 \varpi_a \frac{\nu_a}{\nu} S; \qquad a_{24} = \tfrac{3}{2}\,\frac{p}{1+\zeta} C_2 \varpi'_a \frac{\nu_a}{\nu} S.
\end{aligned} \tag{29}$$

IV. THE GENERAL INTEGRALS

The general integrals of the simultaneous differential equations (27) and (28) can be obtained by well-known manipulations. Thus:

$$J_a = A e^{\lambda_1 \tau} + B e^{-\lambda_1 \tau} + C e^{\lambda_2 \tau} + D e^{-\lambda_2 \tau} + \gamma(a + b\tau) + \delta e^{\tau - \tau_0} \,, \tag{30}$$

$$J'_a = A k_1 e^{\lambda_1 \tau} + B k_1 e^{\lambda_1 \tau} + C k_2 e^{\lambda_2 \tau} + D k_2 e^{-\lambda_2 \tau} + \gamma'(a + b\tau) + \delta' e^{\tau - \tau_0} \,, \tag{31}$$

where λ_1 and λ_2 are two positive roots, given by

$$(\lambda_1^2, \lambda_2^2) = \tfrac{1}{2}\{(a_{11} + a_{22}) \pm \sqrt{[(a_{11} + a_{22})^2 - 4(a_{11}a_{22} - a_{21}a_{12})]}\}, \tag{32}$$

[7] L. G. Henyey, *Ap. J.*, **88**, 133, 1938.

[8] S. Chandrasekhar, *Ap. J.*, **87**, 476, 1938.

and, further,

$$k_1=\frac{\lambda_1^2-a_{11}}{a_{12}}=\frac{a_{21}}{\lambda_1^2-a_{22}},\qquad k_2=\frac{\lambda_2^2-a_{11}}{a_{12}}=\frac{a_{21}}{\lambda_2^2-a_{22}}; \tag{33}$$

$$\gamma=\frac{a_{12}a_{23}-a_{13}a_{22}}{a_{11}a_{22}-a_{12}a_{21}},\qquad \gamma'=\frac{a_{13}a_{21}-a_{11}a_{23}}{a_{11}a_{22}-a_{12}a_{21}}; \tag{34}$$

and

$$\delta=\frac{a_{12}a_{24}-a_{22}a_{14}+a_{14}}{a_{11}a_{22}-a_{12}a_{21}-a_{11}-a_{22}+1},\qquad \delta'=\frac{a_{14}a_{21}-a_{11}a_{24}+a_{24}}{a_{11}a_{22}-a_{12}a_{21}-a_{11}-a_{22}+1}, \tag{35}$$

and A, B, C, and D are four constants of integration. These equations, together with the ultraviolet intensity given by equation (26), complete the solution.

The fluxes can be derived from equations (30) and (31) by differentiations. Using equations (13) and (15) in the reductions, we get

$$F_a=\frac{4}{3\varpi_a}\frac{dJ_a}{d\tau}=\frac{4}{3\varpi_a}A\lambda_1e^{\lambda_1\tau}-\frac{4}{3\varpi_a}B\lambda_1e^{-\lambda_1\tau}+\frac{4}{3\varpi_a}C\lambda_2e^{\lambda_2\tau}$$
$$-\frac{4}{3\varpi_a}D\lambda_2e^{-\lambda_2\tau}+\frac{4\gamma}{3\varpi_a}b+\frac{4\delta}{3\varpi_a}e^{\tau-\tau_0}; \tag{36}$$

$$F'_a=\frac{4}{3\varpi'_a}\frac{dJ'_a}{d\tau}=\frac{4}{3\varpi'_a}A\lambda_1k_1e^{\lambda_1\tau}-\frac{4}{3\varpi'_a}B\lambda_1k_1e^{-\lambda_1\tau}+\frac{4}{3\varpi'_a}C\lambda_2k_2e^{\lambda_2\tau}$$
$$-\frac{4}{3\varpi'_a}D\lambda_2k_2e^{-\lambda_2\tau}+\frac{4\gamma'}{3\varpi'_a}b+\frac{4\delta'}{3\varpi'_a}e^{\tau-\tau_0}. \tag{37}$$

The flux in the ultraviolet is given by equation (25), providing the conservation of quanta.

V. BOUNDARY CONDITIONS

At the outer boundary there is no incident radiation. The corresponding boundary conditions are

$$2J_a(0)=F_a(0),\qquad 2J'_a(0)=F'_a(0),\qquad \text{and}\qquad 2J(0)=F(0)-\tfrac{1}{2}Se^{-\tau_0}. \tag{38}$$

At the inner surface the diffuse fluxes must vanish. Therefore,

$$F_a(\tau_0)=0,\qquad F'_a(\tau_0)=0,\qquad \text{and}\qquad F(\tau_0)=S. \tag{39}$$

The six constants of integration, A, B, C, D, a, and b, can be determined from these six conditions. The full expressions of them are too tedious to reproduce here. The approximate solutions useful in numerical computations will be given later.

VI. APPROXIMATE FORMULAE

For practical purposes, terms of order $1/\varpi_a$ may be neglected, compared with those of order unity. On this approximation the coefficients of the differential equations (27) and (28) become

$$\begin{aligned}
&a_{11}\simeq 3\varpi_a^2(\zeta+\phi)\ (\text{order }\varpi_a), && a_{21}\simeq -3\varpi'^2_a && (\text{order }1);\\
&a_{12}\simeq -3\left(\varpi_a^2\phi-C_2\frac{\varpi_a}{\varpi'_a}\right)(\text{order }\varpi_a), && a_{22}\simeq 3\varpi'^2_a && (\text{order }1);\\
&a_{13}\simeq -3C_2\varpi_a\frac{\nu_a}{\nu}\ (\text{order }\varpi_a), && a_{23}\simeq -3\phi C_2\varpi'_a\frac{\nu_a}{\nu} && (\text{order }\phi);\\
&a_{14}\simeq\tfrac{3}{2}C_2\varpi_a\frac{\nu_a}{\nu}S\ (\text{order }\varpi_aS), && \text{and} \quad a_{24}\simeq\tfrac{3}{2}\phi C_2\varpi'_a\frac{\nu_a}{\nu}S && (\text{order }\phi S).
\end{aligned} \tag{40}$$

The orders of magnitude of the respective terms given are for the case $\zeta \sim p \sim 10^{-4}$.

Similarly, from equation (32) we find

$$\lambda_1^2 \simeq 3\varpi_a^2(\zeta+p)\ (\text{order } \varpi_a), \quad \lambda_2^2 \simeq 3\,\frac{\varpi_a\varpi_a'^2\zeta + C_2\varpi_a'}{\varpi_a(\zeta+p)} \qquad (\text{order } 1) \tag{41}$$

and

$$k_1 \simeq -\frac{\varpi_a'^2}{\varpi_a^2(\zeta+p)}\left(\text{order } \frac{1}{\varpi_a}\right), \qquad k_2 \simeq \frac{\varpi_a(\zeta+p)}{\varpi_a p - (C_2/\varpi_a)} \quad (\text{order } 1)\,. \tag{42}$$

The coefficients of the particular integrals are

$$\gamma \simeq \frac{\nu_a}{\nu}\,\frac{C_2\varpi_a'}{(\varpi_a\varpi_a'\zeta + C_2)}, \qquad \gamma' \simeq \frac{\nu_a}{\nu}\,\frac{C_2\varpi_a'}{(\varpi_a\varpi_a'\zeta + C_2)} \qquad (\gamma,\ \gamma' \text{ order } 1)\,; \tag{43}$$

$$\delta \simeq -\frac{1}{2}\,\frac{\nu_a}{\nu}\,\frac{C_2(3\varpi_a' - 1)}{(3\varpi_a\varpi_a'^2\zeta + 3\varpi_a'C_2 - \varpi_a[\zeta+p])}\,S \qquad (\text{order } S)\,; \tag{44}$$

$$\delta' \simeq -\frac{3}{2}\,\frac{\nu_a}{\nu}\,\frac{C_2\varpi_a'^2}{(3\varpi_a\varpi_a'^2\zeta + 3\varpi_a'C_2 - \varpi_a[\zeta+p])}\,S \qquad (\text{order } S)\,. \tag{45}$$

By using equations (26), (30), (31), and (25), (36), (37), we can write down immediately the boundary conditions (38) and (39). In the present approximation we have

$$b = \tfrac{3}{4}S;\ \left(1 - \frac{2\lambda_1}{3\varpi_a}\right)A + \left(1 + \frac{2\lambda_1}{3\varpi_a}\right)B + C + D + \gamma a + \delta e^{-\tau_0} = 0\,, \tag{46}$$

$$\left(1 - \frac{2\lambda_1}{3\varpi_a'}\right)k_1A + \left(1 + \frac{2\lambda_1}{3\varpi_a'}\right)k_1B + \left(1 - \frac{2\lambda_2}{3\varpi_a'}\right)k_2C + \left(1 + \frac{2\lambda_2}{3\varpi_a'}\right)k_2D + \gamma' a - \gamma' b\,\frac{2}{3\varpi_a'} + \left(1 - \frac{2}{3\varpi_a'}\right)\delta' e^{-\tau_0} = 0\,, \tag{47}$$

$$\left(\frac{1}{\varpi_a} + \frac{k_1}{\varpi_a'}\right)\left(\frac{2}{3}\lambda_1 - 1\right)A - \left(\frac{1}{\varpi_a} + \frac{k_1}{\varpi_a'}\right)\left(\frac{2}{3}\lambda_1 + 1\right)B + \frac{k_2}{\varpi_a'}\left(\frac{2}{3}\lambda_2 - 1\right)C - \frac{k_2}{\varpi_a'} \times \left(\frac{2}{3}\lambda_2 + 1\right)D + \left(\frac{\nu_a}{\nu} - \frac{\gamma}{\varpi_a'}\right)a - \frac{1}{2}\,\frac{\nu_a}{\nu}\left(1 - \frac{\nu\gamma}{\nu_a\varpi_a'}\right)S - \frac{1}{4}\,\frac{\nu_a}{\nu}\,Se^{-\tau_0} - \frac{1}{3}\,\frac{\delta'}{\varpi_a'}e^{-\tau_0} = 0\,, \tag{48}$$

$$\lambda_1 e^{\lambda_1\tau_0}A - \lambda_1 e^{-\lambda_1\tau_0}B + \lambda_2 e^{\lambda_2\tau_0}C - \lambda_2 e^{-\lambda_2\tau_0}D + \tfrac{3}{4}\gamma S + \delta = 0\,, \tag{49}$$

and

$$\lambda_1k_1 e^{\lambda_1\tau_0}A - \lambda_1k_1 e^{-\lambda_1\tau_0}B + \lambda_2k_2 e^{\lambda_2\tau_0}C - \lambda_2k_2 e^{-\lambda_2\tau_0}D + \tfrac{3}{4}\gamma S + \delta' = 0\,. \tag{50}$$

From the solutions of the foregoing equation we find that A is of order $Se^{-\lambda_1\tau_0}/\sqrt{\varpi_a}$ and B, C, D, a, and b are all of order S.

From equations (30) and (31) we notice that the orders of magnitude of J_a and J_a' are equal to that of S. This is remarkable, since Ambarzumian's solution gave J_a to be of order $\varpi_a S$.

The flux F_a in the core Lyman-α is also reduced in equation (36), and the orders of magnitude of the respective terms can be expressed as follows:

$$F_a \text{ is of order } \left\{\frac{1}{\sqrt{\varpi_a}}\,e^{-\lambda_1\tau} + \frac{1}{\varpi_a}\,f(\tau)\right\}S\,, \tag{51}$$

where $f(\tau)$ stands for a slowly varying function of τ of order unity. The first term is small

compared with the second throughout the atmosphere except the outermost part, where $\lambda_1 \tau \lesssim 1$.

Hence the flux in the core of Lyman-α

$$F_a \text{ is of order } \frac{1}{\varpi_a} S . \tag{52}$$

This must be compared with the Ambarzumian solution, which gives F_a of order S. At the outermost part, the first term of equation (51) becomes dominant, and we have

$$F_a \text{ is of order } \frac{1}{\sqrt{\varpi_a}} S \qquad (\lambda_1 \tau \lesssim 1) . \tag{53}$$

For the flux in the wings of Lyman-α we find from equation (37) that

$$F'_a \text{ is of order } S . \tag{54}$$

This means that the most of the Lyman-α radiation is streaming out through the wings of the contour.

Parallel to the reduction of the flux, pressure due to Lyman-α is also cut down largely, compared with the current Ambarzumian solution. Let P, P_a, and P'_a be the radiation pressures of the ultraviolet, L_a and L'_a, respectively. Then, by multiplying equation (51) by ϖ_a, we get

$$P_a \text{ is of order } \{ \sqrt{\varpi_a} e^{-\lambda_1 \tau} + f(\tau) \} P , \tag{55}$$

and from equation (54), by multiplying it with ϖ'_a, we have

$$P'_a \text{ is of order } P . \tag{56}$$

Throughout most of the atmosphere, Lyman-α exerts a radiation pressure comparable to that due to the ultraviolet radiation. While in the outermost parts

$$P_a \text{ is of order } P\sqrt{\varpi_a} \qquad (\lambda_1 \tau \lesssim 1) , \tag{57}$$

the pressure is, therefore, about one hundred times stronger. Yet it is still about one-hundredth of the Ambarzumian solution: P_a is of order $\varpi_a P$.

VII. PLANETARY NEBULAE

We shall now treat in more detail the two extreme cases, viz., the planetary nebulae and the Be-star atmospheres.

For the planetary nebulae the dilution of the radiation from the central star is so large that the populations of the excited levels are small and the Rosseland cycle operates fully. Therefore, putting $\zeta = 0$ in equations (20)–(22), we get

$$\frac{d^2 J}{d\tau^2} = 3C_2 J - \tfrac{1}{2} S e^{\tau - \tau_0} , \tag{58}$$

$$\frac{d^2 J_a}{\varpi_a^2 d\tau^2} = 3pJ_a - 3pJ'_a - 3\frac{(1-p)C_2}{\varpi_a}\frac{\nu_a}{\nu} J , \tag{59}$$

and

$$\frac{d^2 J'_a}{\varpi'^2_a d\tau^2} = 3(1-p)J'_a - 3(1-p)J_a - 3\frac{pC_2}{\varpi'_a}\frac{\nu_a}{\nu} J . \tag{60}$$

From equation (58) we see that the ultraviolet field can be derived separately. The solutions satisfying the boundary conditions

$$F(\tau_0) = S \qquad \text{and} \qquad 2J(0) = F(0) - \tfrac{1}{2} S e^{-\tau_0} \tag{61}$$

can be obtained by the usual method, as follows:

$$J = \alpha e^{u\tau} + \beta e^{-u\tau} + \tfrac{1}{2}\frac{1}{(u^2-1)}\, e^{\tau-\tau_0} S\,, \tag{62}$$

and

$$F = \tfrac{4}{3}\alpha u e^{u\tau} - \tfrac{4}{3}\beta u e^{-u\tau} + \frac{2}{3}\frac{u^2}{u^2-1}\, e^{\tau-\tau_0} S\,, \tag{63}$$

where $u^2 = 3C_2$ and

$$\alpha = -\frac{\tfrac{2}{3} + u^{-1} + \tfrac{1}{3} e^{-(u+1)\tau_0}}{2\,(\cosh u\tau_0 + \tfrac{2}{3} u \sinh u\tau_0)}\,\frac{1}{4}\frac{3-u^2}{u^2-1}\, S\,, \tag{64}$$

and

$$\beta = -\frac{\tfrac{2}{3} - u^{-1} + \tfrac{1}{3} e^{(u-1)\tau_0}}{2\,(\cosh u\tau_0 + \tfrac{2}{3} u \sinh u\tau_0)}\,\frac{1}{4}\frac{3-u^2}{u^2-1}\, S\,. \tag{65}$$

Introducing equation (62) into equations (59) and (60) and eliminating the ultraviolet intensity J, we get

$$\frac{d^2 J_a}{d\tau^2} = a_{11} J_a + a_{12} J_a' + a_{13} e^{u\tau} + a_{14} e^{-u\tau} + a_{15} e^{\tau} \tag{66}$$

and

$$\frac{d^2 J_a'}{d\tau^2} = a_{21} J_a + a_{22} J_a' + a_{23} e^{u\tau} + a_{24} e^{-u\tau} + a_{25} e^{\tau}\,, \tag{67}$$

where

$$a_{11} = 3p\varpi_a^2\,, \qquad a_{12} = -a_{11}\,,$$

$$a_{13} = -3(1-p) C_2 \varpi_a \frac{\nu_a}{\nu}\,\alpha \simeq -3C_2\varpi_a \frac{\nu_a}{\nu}\,\alpha \qquad \text{(order } \varpi_a S)\,,$$

$$a_{14} = -3(1-p) C_2 \varpi_a \frac{\nu_a}{\nu}\,\beta \simeq -3C_2\varpi_a \frac{\nu_a}{\nu}\,\beta \qquad \text{(order } \varpi_a S)\,,$$

$$a_{15} = -3(1-p) C_2 \varpi_a \frac{\nu_a}{\nu}\,\frac{1}{2}\frac{1}{u^2-1}\, e^{-\tau_0} S \simeq$$
$$-3C_2\varpi_a \frac{\nu_a}{\nu}\,\frac{1}{2}\frac{1}{u^2-1}\, e^{-\tau_0} S \qquad \text{(order } \varpi_a S)\,, \tag{68}$$

$$a_{21} = -3(1-p)\varpi_a'^2 \simeq -3\varpi_a'^2\,, \qquad a_{22} = -a_{21}\,,$$

$$a_{23} = -3p\varpi_a' C_2 \frac{\nu_a}{\nu}\,\alpha\,, \qquad a_{24} = -3p\varpi_a' C_2 \frac{\nu_a}{\nu}\,\beta\,,$$

$$a_{25} = -3p\varpi_a' C_2 \frac{\nu_a}{\nu}\,\frac{1}{2}\frac{1}{u^2-1}\, e^{-\tau_0} S \qquad (a_{23}, a_{24}, a_{25} \text{ of order } pS)\,.$$

Solving these equations, we find

$$J_a = A e^{\lambda\tau} + B e^{-\lambda\tau} + a + b\tau + \Phi_a(\tau)\,, \tag{69}$$

$$J_a' = -\frac{\varpi_a'^2}{p\varpi_a^2}(A e^{\lambda\tau} + B e^{-\lambda\tau}) + a + b\tau + \Phi_a'(\tau)\,, \tag{70}$$

$$F_a = \frac{4\lambda}{3\varpi_a} A e^{\lambda\tau} - \frac{4\lambda}{3\varpi_a} B e^{-\lambda\tau} + \frac{4}{3\varpi_a}\, b + \frac{4}{3\varpi_a}\,\phi_a(\tau)\,, \tag{71}$$

and

$$F_a' = -\frac{\varpi_a'^2}{p\varpi_a^2}\left(\frac{4\lambda}{3\varpi_a'} A e^{\lambda\tau} - \frac{4\lambda}{3\varpi_a'} B e^{-\lambda\tau}\right) + \frac{4}{3\varpi_a'} b + \frac{4}{3\varpi_a'} \phi_a'(\tau), \tag{72}$$

where

$$\lambda = \sqrt{[3p\varpi_a^2 + 3(1-p)\varpi_a'^2]} \simeq \sqrt{(3p\varpi_a^2)} \qquad (\text{order } \sqrt{\varpi_a}), \tag{73}$$

$$-\Phi_a(\tau) = \frac{\nu_a}{\nu}\frac{(\varpi_a'^2 - C_2)}{p\varpi_a}(\alpha e^{u\tau} - \beta e^{-u\tau}) + \frac{\nu_a}{\nu}\frac{C_2(3\varpi_a'^2 - 1)}{2p\varpi_a}\frac{1}{u^2-1} S e^{\tau-\tau_0}, \tag{74}$$

$$-\Phi_a'(\tau) = \frac{\nu_a}{\nu}\frac{\varpi_a'^2}{p\varpi_a}(\alpha e^{u\tau} - \beta e^{-u\tau}) + \frac{\nu_a}{\nu}\frac{3}{2}\frac{C_2\varpi_a'^2}{p\varpi_a}\frac{1}{u^2-1} S e^{\tau-\tau_0}, \tag{75}$$

$$-\phi_a(\tau) = -\frac{d\Phi_a}{d\tau} = \frac{\nu_a}{\nu}\frac{(\varpi_a'^2 - C_2)}{p\varpi_a} u(\alpha e^{u\tau} - \beta e^{-u\tau}) + \frac{\nu_a}{\nu}\frac{C_2(3\varpi_a'^2 - 1)}{2p\varpi_a}\frac{1}{u^2-1} S e^{\tau-\tau_0}, \tag{76}$$

$$-\phi_a'(\tau) = -\frac{d\Phi_a'}{d\tau} = \frac{\nu_a}{\nu}\frac{\varpi_a'^2}{p\varpi_a} u(\alpha e^{u\tau} - \beta e^{-u\tau}) + \frac{\nu_a}{\nu}\frac{3}{2}\frac{C_2\varpi_a'^2}{p\varpi_a}\frac{1}{u^2-1} S e^{\tau-\tau_0} \text{ (all of order } S). \tag{77}$$

The boundary conditions,

$$2J_a(0) = F_a(0), \quad 2J_a'(0) = F_a'(0), \quad F_a(\tau_0) = 0, \quad \text{and} \quad F_a'(\tau_0) = 0, \tag{78}$$

determine the constants A, B, a, and b. Neglecting the terms of order $1\sqrt{\varpi_a}$ compared with those of order unity, we get the following approximate expressions:

$$A = -\{\phi_a(\tau_0) - \phi_a'(\tau_0)\}\frac{1}{\lambda} e^{-\lambda\tau_0} = \frac{1}{\lambda} e^{-\lambda\tau_0}\frac{\nu_a}{\nu}\frac{C_2}{p\varpi_a}\left\{u(\alpha e^{u\tau_0} + \beta e^{-u\tau_0}) + \frac{1}{2}\frac{1}{u^2-1} S\right\}; \tag{79}$$

$$B = \Phi_a'(0) - \Phi_a(0) + \frac{2}{3\varpi_a'}\{\phi_a'(\tau_0) - \phi_a'(0)\}$$
$$= -\frac{\nu_a}{\nu}\frac{C_2}{p\varpi_a}\left\{\alpha - \beta + \frac{1}{2}\frac{1}{u^2-1} S e^{-\tau_0}\right\} + \frac{2}{3}\frac{\nu_a}{\nu}\frac{\varpi_a'}{p\varpi_a}\Big[u\{\alpha(1 - e^{u\tau_0}) + \beta(1 - e^{-u\tau_0})\} + \tfrac{3}{2}C_2\frac{1}{u^2-1} S(1 - e^{-\tau_0})\Big]; \tag{80}$$

$$a = -\Phi_a'(0) + \frac{2}{3\varpi_a'}\{\phi_a'(0) - \phi_a'(\tau_0)\}$$
$$= \frac{\nu_a}{\nu}\frac{\varpi_a'^2}{p\varpi_a}\left\{\alpha - \beta + \tfrac{3}{2}C_2\frac{1}{u^2-1} S e^{-\tau_0}\right\} + \frac{\nu_a}{\nu}\frac{\varpi_a'}{p\varpi_a}\Big[\tfrac{2}{3}u\{\alpha(e^{u\tau_0} - 1) + \beta(e^{-u\tau_0} - 1)\} + C_2\frac{1}{u^2-1} S(1 - e^{-\tau_0})\Big]; \tag{81}$$

$$b = -\phi_a'(\tau_0) = \frac{\nu_a}{\nu}\frac{\varpi_a'^2}{p\varpi_a}\left\{u(\alpha e^{u\tau_0} + \beta e^{-u\tau_0}) + \tfrac{3}{2}C_2\frac{1}{u^2-1} S\right\}. \tag{82}$$

From these equations we find that A is of order $1/\sqrt{\varpi_a}e^{-\lambda\tau_0}S$ and B, a, and b are all of order S. Therefore, we obtain, for the planetary nebulae, the same conclusions mentioned at the end of Section VI:

$$\left.\begin{aligned} &J,\ J_a,\ J'_a,\ F,\ F'_a \qquad \text{of order } S\,, \\ &\text{while} \\ &F_a \text{ is of order } \begin{cases} 1/\varpi_a S & \text{for the most of the nebula} \\ 1/\sqrt{\varpi_a} S & \text{for the outermost part } \sqrt{\varpi_a}\tau \lesssim 1\,. \end{cases} \end{aligned}\right\} \tag{83}$$

Our results are in agreement with those of Paper B. Our formulae reduce to that case if we put $C_1 = 0$, $C_2 = 1$, and hence $\alpha = \beta = 0$.

VIII. Be-STAR ATMOSPHERES

For these atmospheres we can put $p = 0$ in equations (20)–(22), and, omitting the L'_a equation, we have the fundamental equations

$$\frac{d^2J}{d\tau^2} = 3\,\frac{C_2}{1+\zeta}\,J - 3\,\frac{\nu}{\nu_a}\,\frac{\zeta}{1+\zeta}\,\varpi_a J_a - \tfrac{1}{2}Se^{\tau-\tau_0} \tag{84}$$

and

$$\frac{d^2J_a}{d\tau^2} = -3\varpi_a\,\frac{C_2}{1+\zeta}\,\frac{\nu_a}{\nu}\,J + 3\varpi_a^2\,\frac{\zeta}{1+\zeta}\,J_a\,. \tag{85}$$

The solutions are given by

$$J = Ae^{v\tau} + Be^{-v\tau} + a + b\tau - \tfrac{1}{2}Se^{\tau-\tau_0} \tag{86}$$

and

$$J_a = -\frac{\nu_a}{\nu}\,\varpi_a\,(Ae^{v\tau} + Be^{-v\tau}) + \frac{\nu_a}{\nu}\,\frac{C_2}{\zeta\varpi_a}\,(a + b\tau - \tfrac{1}{2}Se^{\tau-\tau_0})\,, \tag{87}$$

where $v = \sqrt{(3\varpi_a^2\zeta)}$ and

$$F = \tfrac{4}{3}\,ve^{v\tau}A - \tfrac{4}{3}\,ve^{-v\tau}B + \tfrac{4}{3}b \tag{88}$$

and

$$F_a = -\frac{\nu_a}{\nu}\,\frac{4}{3}\,v\,(Ae^{v\tau} - Be^{-v\tau}) + \frac{4}{3}\,\frac{\nu_a}{\nu}\,\frac{C_2}{\zeta\varpi_a^2}\,(b - \tfrac{1}{2}Se^{\tau-\tau_0})\,. \tag{89}$$

The boundary conditions,

$$F(\tau_0) = S\,, \quad F_a(\tau_0) = 0\,, \quad 2J(0) = F(0) - \tfrac{1}{2}Se^{-\tau_0}\,, \quad 2J_a(0) = F_a(0)\,, \tag{90}$$

determine the constants A, B, a, and b. Neglecting the small terms, we get

$$A = \frac{C_2}{\zeta\varpi_a^2}\,\frac{1}{4v}\,Se^{-v\tau_0}\,, \qquad B = \frac{1}{2}\,\frac{C_2}{\zeta\varpi_a^2}\,S(1 - \tfrac{1}{2}e^{-\tau_0})\,, \tag{91}$$

$$a = \tfrac{1}{2}\,(1 + \tfrac{1}{2}e^{-\tau_0})\,S\,, \qquad \text{and} \qquad b = \tfrac{3}{4}S\,. \tag{92}$$

With these values, the formulae giving the intensity and the flux become

$$J = \tfrac{1}{2}\,(1 + \tfrac{1}{2}e^{-\tau_0} + \tfrac{3}{2}\tau - e^{\tau-\tau_0})\,S\,, \qquad F = S\,, \tag{93}$$

$$J_a = \frac{\nu_a}{\nu}\,\frac{C_2}{2\zeta\varpi_a}\{1 + \tfrac{1}{2}e^{-\tau_0} + \tfrac{3}{2}\tau - e^{\tau-\tau_0} - (1 - \tfrac{1}{2}e^{-\tau_0})\,e^{-v\tau}\}S\,, \tag{94}$$

$$F_\alpha = \frac{\nu_\alpha}{\nu}\frac{C_2}{\zeta\varpi_\alpha^2}\{\tfrac{2}{3}\sqrt{(\zeta\varpi_\alpha^2)}\,(1-\tfrac{1}{2}e^{-\tau_0})\,e^{-\sigma\tau}+1-\tfrac{2}{3}e^{\tau-\tau_0}\}S. \tag{95}$$

In the Be atmospheres the Lyman-α field is formed by the transformation of the ultraviolet radiation. But its transformation is checked by the inverse Rosseland cycle. The flux of ultraviolet radiation is thus conserved in a first approximation, and only a small fraction of it flows out as the Lyman-α radiation, as the above results actually show. These results are in agreement with those of Paper A.

The mean intensity of Lyman-α radiation, J_α, is not larger than the ultraviolet intensity.

The flux in Lyman-α is of order $S/\zeta\varpi_\alpha^2$ through most of the atmosphere. For $W = \frac{1}{2}$, 0.1, and 0.01 and the photospheric temperature 19,600°, we have

$$\zeta\varpi_\alpha^2 = 3\times10^6, \quad 6\times10^5, \quad \text{and} \quad 6\times10^4;$$

and hence

$$F_\alpha \sim 3\times10^{-7}S, \quad 2\times10^{-6}S, \quad \text{and} \quad 2\times10^{-5}S,$$

respectively. The corresponding radiation pressures are

$$P_\alpha \sim 0.003P, \quad 0.02P, \quad \text{and} \quad 0.2P,$$

respectively.

In the outermost part, where $\sqrt{(3\varpi_\alpha^2\zeta)} \sim 1$, F_α is of order $S/\varpi_\alpha\sqrt{\zeta}$ or

$$F_\alpha \sim 6\times10^{-4}S, \quad 10^{-3}S, \quad \text{and} \quad 4\times10^{-3}S,$$

respectively, for the three values of the dilution factor used earlier. The radiation pressure, P_α is of order $P/\sqrt{\zeta}$ or, numerically,

$$P_\alpha \sim 6P, \quad 10P, \quad \text{and} \quad 40P.$$

For smaller values of W, the field gradually changes to the nebular case, and the pressure attains the value $P_\alpha \sim 100P$; this is shown by equation (57).

The magnitude of the Lyman-α pressure seems appropriate to the formation of a tenuous atmosphere for the early-type stars. We shall give dynamical applications of these results in a separate paper.

PROPAGATION OF SHOCK WAVES IN THE GENERALIZED ROCHE MODEL*

PIERRE A. CARRUS, PHYLLIS A. FOX, FELIX HAAS, AND ZDENĚK KOPAL
Massachusetts Institute of Technology
Received August 11, 1950

ABSTRACT

The aim of the present paper has been to investigate the events which take place if the core of a generalized Roche model is made to expand as the result of an instantaneous central explosion. A sudden expansion of the core sets off a wave of condensation traveling through the envelope; and, if the initial explosion has been sufficiently strong, the outgoing disturbance will possess the characteristics of a shock wave. It is shown that, if the initial explosion has been instantaneous, the velocity, pressure, and density at any point of the disturbed medium can be made to depend on a single parameter, $\xi = r^{-3}t^2$, where t denotes the time and r the radial distance.

The equations of the problem have been rewritten in terms of ξ as the sole independent variable and integrated numerically for 18 cases corresponding to different Mach numbers of the shock waves and different ratios, γ, of specific heats of the gas constituting the envelope. The expanding regime forms a concentric shell, limited on the outside by the shock front of radius varying as $t^{2/3}$, while the interface of the core confronts us with a "contact discontinuity." For large values of the Mach number M, the thickness of the shell increases with increasing M and decreasing value of the ratio of specific heats; for $\gamma = \frac{7}{5}$ (corresponding to polyatomic gas) the radius of the core becomes zero for any strength of the shock. It is shown that, for $\gamma = \frac{5}{3}$ (corresponding to monatomic gas), a shock wave characterized by a Mach number $M = 2.877\ldots$ is just sufficiently strong to endow the mass particles immediately behind it with a velocity equal to one of escape from the gravitational field of the configuration, while for $M > 5.92\ldots$ the whole envelope will eventually be ejected.

Table 1 contains the numerical data describing the individual solutions in terms of nondimensional parameters which can be converted into absolute units by a suitable choice of the initial conditions; and Table 2 summarizes the physical properties of the respective shock waves.

In a previous paper, published recently in this *Journal* by one of us,[1] the radial oscillations of a generalized Roche model (consisting of a compressible massive core, of finite dimensions, surrounded by an infinitesimally thin envelope) were investigated in some detail. Such oscillations, of the nature of standing waves characterized by a node at the center and a loop at the surface of zero pressure, may be of astrophysical importance in connection with the pulsation of composite stellar models. The present investigation will, on the other hand, be concerned with the properties of running waves in stellar interiors. More specifically, we propose to consider the propagation, through a generalized Roche model and certain similar configurations, of spherical disturbances which are sufficiently energetic to give rise to expanding shock waves and whose impact may be sufficient actually to eject matter from the surface at speeds exceeding the velocity of escape from the gravitational field of the whole configuration. The astrophysical implications of the situation which we propose to consider lie clearly in the direction of the nova phenomenon. We do not claim, to be sure, to deal as yet very closely in this paper with the actual physical situation encountered in the nova outbursts. A great amount of preparatory work must, however, be done before a solution of the actual astrophysical problem can be even approached with any hope of success. The work summarized in the present paper should be regarded as a first contribution to the study of the propagation of shock waves in spherical-gas models of astrophysical interest and a first step toward our ultimate goal.

In order to describe the physical situation analyzed in the present work, let us consider, first, a classical generalized Roche model consisting of a massive core of finite

* An investigation performed under Contract N5ori-07843 with the Office of Naval Research.

[1] Z. Kopal, *Ap. J.*, 111, 395, 1950.

dimensions but arbitrary structure, surrounded by an envelope of infinitesimal weight, in which the density falls off as the inverse square of the distance from the center. Suppose, now, that such a configuration becomes disturbed from its state of equilibrium by an instantaneous explosion—whatever its origin—at the center, which causes the core suddenly to expand. Its expansion will, in turn, set off in the envelope an outward-going spherical wave of condensation; and if the impulse provided by the initial explosion is sufficiently strong, the outgoing disturbance will possess the characteristics of a shock wave and will propagate in accordance with well-known laws governing the propagation of such waves. Our aim will be, in brief, to investigate the way in which the energy liberated by the explosion is converted into motion and heat through the medium of shock waves propagating in the envelope of a generalized Roche model. In doing so, however, we shall be prevented by sheer weight of mathematical difficulties from considering the most general type of the motion which may result from an instantaneous central explosion. Instead, we shall limit ourselves to investigating solutions of the type of "progressing blast waves"—in the terminology of Courant and Friedrichs[2]—which are characterized by a shock wave on the head of the disturbed motion and which carry a sufficient impulse actually to cause an ejection of the matter from the surface. Progressing waves in compressible homogeneous media situated in the field of constant gravity have been previously studied by several writers.[3] Our present investigation may therefore be regarded as an extension of the previous work with terrestrial applications to the more difficult astronomical case of progressing blast waves in heterogeneous models, which propagate through a fluctuating gravitational field created by the disturbed mass itself. The main conclusions arrived at in the course of this investigation have already been summarized in the abstract; so that, in what follows, our task will be to substantiate them in detail.

EQUATIONS OF THE PROBLEM

Let u, p, and ρ denote the radial velocity, pressure, and density at any point inside our model at a distance r from the center and at a time t. If, moreover, m denotes the (constant) mass of the core, γ the ratio of specific heats of the gas constituting it, and G the gravitation constant, the Eulerian hydrodynamical equations reduce to

$$\frac{\partial u}{\partial t}+u\frac{\partial u}{\partial r}+\frac{1}{\rho}\frac{\partial p}{\partial r}+\frac{Gm}{r^2}=0, \tag{1}$$

the equation of continuity becomes

$$\frac{\partial \rho}{\partial t}+u\frac{\partial \rho}{\partial r}+\rho\left\{\frac{\partial u}{\partial r}+\frac{2u}{r}\right\}=0, \tag{2}$$

while the energy equation (appropriate for polytropic gas) assumes the form

$$\frac{\partial}{\partial t}(p\rho^{-\gamma})+u\frac{\partial}{\partial r}(p\rho^{-\gamma})=0. \tag{3}$$

The reader should keep in mind that, if shock waves are to occur in the flow governed by the foregoing equations, the flow behind such a wave will no longer be isentropic, and, in consequence, there will be no closed equation of state relating p and ρ. Such a relationship can be obtained only by a simultaneous integration of equations (1), (2),

[2] R. Courant and K. Friedrichs, *Supersonic Flow and Shock Waves* (New York: Interscience Publishers, 1948), secs. 160–161.

[3] G. I. Taylor, *The Formation of a Blast Wave by a Very Intense Explosion* (Ministry of Home Security, R.C. 210 [II–5–153] [1941]); *The Propagation and Decay of Blast Waves* (British Civilian Defense Research Committee [1944]); *Proc. R. Soc., London, A*, 201, 159, 1950; J. von Neumann, NDRC Report No. SR7/743 (1944).

and (3) for u, p, and ρ as functions of r and t, subject to appropriate boundary conditions.

In our present problem the outer boundary conditions are given over a moving surface (the shock wave), and the inner conditions are defined on the surface of the expanding core. In what follows, let p_0 and ρ_0 denote the undisturbed values of pressure and density in front of the shock wave (where they depend only on r), and u_1, p_1, and ρ_1 be the values of the respective quantities at any point immediately after the passage of the shock. If so, the well-known Rankine-Hugoniot conditions,[4] expressing the continuity of energy, mass, and momentum across the shock wave, permit us to express u_1, p_1, and ρ_1 in terms of the undisturbed values of these quantities by means of the following equations:

$$u_1 = \frac{2V}{\gamma+1} - \frac{2\gamma p_0}{(\gamma+1)\rho_0 V}, \tag{4}$$

$$p_1 = \frac{2\rho_0 V^2 - (\gamma-1)p_0}{\gamma+1}, \tag{5}$$

$$\rho_1 = \frac{(\gamma+1)\rho_0^2 V^2}{(\gamma+1)\rho_0 V^2 + 2\gamma p_0}, \tag{6}$$

where V denotes the velocity of propagation of the shock. On the other hand, consistent with our definition of the generalized Roche model, we should expect that the derivative $\partial\rho/\partial r$ would be discontinuous at the core; but the significant feature of our problem is that neither the position of the shock nor that of the core is known to us beforehand at any moment but must be ascertained by the compatibility of prescribed conditions as the integration proceeds.

The problem of solving equations (1)–(3) subject to the conditions just enumerated is one of considerable complexity: the system of partial differential equations is one of third order and of second degree, in two independent variables, with initial conditions defined over two moving boundaries. These equations cannot be linearized by any transformation of the variables, and the neglect of nonlinear terms would eliminate the essential features of the problem. A retention of the nonlinear terms precludes, on the other hand, any possibility of the construction of an analytical solution; so that numerical integrations appear to offer the only method of approach. Numerical integration of partial differential equations in two independent variables constitutes, however, no small task. Before embarking upon it, we propose, therefore, to investigate, first, the conditions for which the fundamental system of partial differential equations may be reducible to that of ordinary differential equations, which can be solved—numerically or otherwise—with much less difficulty.

In specific terms, let us seek such solutions of the system of equations (1)–(3) in which u, p, and ρ can be made to depend on r and t only through the product $r^\phi t^\psi$, where ϕ and ψ are suitably chosen constants. Accordingly, we shall assume that

$$u = \frac{r}{t} U(\xi), \tag{7}$$

$$p = r^{\alpha+2\beta-2} P(\xi), \tag{8}$$

$$\rho = r^{\alpha} t^{\beta} \Omega(\xi), \tag{9}$$

and the local velocity of sound

$$c^2 = \gamma \frac{p}{\rho} = \left(\frac{r}{t}\right)^2 C^2(\xi), \tag{10}$$

[4] Cf., e.g., Courant and Friedrichs, *op. cit.*, sec. 54.

where

$$\xi = r^{\phi} t^{\psi} \tag{11}$$

and the parameters κ, λ, ϕ, and ψ are to be determined by physical considerations.

The form of equation (1) imposes the ratio $\psi/\phi = -\frac{2}{3}$ if ξ is to replace r and t throughout as the independent variable. The other parameters, κ and λ, may be determined by considering the form of the total energy carried by the wave motion. If $R(t)$ denotes the radius, at any time, of the shock front and $a(t)$ that of the core of our generalized Roche model, it follows that the total energy E of the envelope (being the sum of its kinetic, thermal, and gravitational energies) will be given by

$$E = 4\pi \int_a^R \left\{ \tfrac{1}{2} \rho u^2 + \frac{p}{\gamma - 1} - G \frac{m \rho}{r} \right\} r^2 dr . \tag{12}$$

Now if the total energy of the initial explosion is to be released at an instant, the foregoing expression for E must obviously be independent of the time. Consistent with our foregoing assumptions, we have

$$R(t) = \xi_0^{1/\phi} t^{-\psi/\phi} \tag{13}$$

and

$$a(t) = \xi_1^{1/\phi} t^{-\psi/\phi} , \tag{14}$$

where ξ_0 and ξ_1 are values which the new independent variable ξ assumes at the shock and the core, respectively. Inserting the foregoing relations together with equations (7)–(9) into equation (12), we find the kinetic and thermal energies carried by the wave motion to be independent of the time, provided that

$$\lambda - (\kappa + 5)\left(\frac{\psi}{\phi}\right) = 2 , \tag{15}$$

and it follows that κ and λ are related by

$$\lambda = -\tfrac{2}{3}(\kappa + 2) . \tag{16}$$

It is interesting to note that this choice of parameters will automatically enforce the constancy of the gravitational contribution to the total energy. This constancy would impose, between κ, λ, ϕ, and ψ, the relation

$$\lambda - (\kappa + 2)\left(\frac{\psi}{\phi}\right) = 0 ,$$

which, together with equation (16), again yields

$$\frac{\psi}{\phi} = -\tfrac{2}{3} \quad \text{and} \quad \lambda = -\tfrac{2}{3}(\kappa + 2) . \tag{17}$$

It should be observed that the foregoing equations do not specify our parameters uniquely but provide only two relations between them. These relations are obviously satisfied by

$$\phi = -3 , \quad \psi = 2 , \quad \kappa = -2 , \quad \lambda = 0 , \tag{18}$$

the values which we shall hereafter adopt. It can be easily shown that no generality has been lost by this choice; for all other combinations of the four parameters consistent with equations (17) will lead to no new solutions.

Having thus specified the values of the arbitrary parameters in equations (7)–(9), we shall rewrite equations (1)–(3) in terms of the new independent variable $\xi = r^{-3} t^2$. If we abbreviate, for the sake of simplicity,

$$3U(\xi) - 2 = \Xi(\xi) \tag{19}$$

and

$$C^2(\xi) = S(\xi), \tag{20}$$

we establish, after some transformations, that the original system of equations (1)–(3) is equivalent to the following system of three ordinary differential equations:

$$\frac{1}{P}\frac{dP}{d\xi} = \frac{1}{3\xi\Xi}\left\{3(2\gamma-2) + 3\gamma\Xi - 3\gamma\xi\frac{d\Xi}{d\xi}\right\}, \tag{21}$$

$$\frac{1}{S}\frac{dS}{d\xi} = \frac{1}{3\xi\Xi}\left\{2(3\gamma-4) + (3\gamma-1)\Xi - 3(\gamma-1)\xi\frac{d\Xi}{d\xi}\right\}, \tag{22}$$

$$\frac{1}{\Xi}\frac{d\Xi}{d\xi} = \frac{1}{3\xi\Xi^2}\left\{\Xi^2 + \Xi - 2 + 9\xi Gm - \frac{27}{\gamma}\xi\frac{S}{P}\frac{dP}{d\xi}\right\}. \tag{23}$$

Once these equations have been solved, the last one of our four auxiliary functions in equation (9) follows from

$$\Omega(\xi) = \gamma\frac{P(\xi)}{S(\xi)}. \tag{24}$$

SOLUTION OF THE EQUATIONS

Having reduced the differential equations of the problem to tractable form, we have yet to specify the initial conditions which determine the nature of their solution. Consider, first, the boundary conditions at the shock front. On the passage through the shock, the velocity, pressure, and density are known to undergo a discontinuous change expressed by equations (4)–(6), where, consistent with the assumptions of the preceding section,

$$V = \frac{dR}{dt} = \frac{2}{3}\frac{R}{t}. \tag{25}$$

In front of the shock, in the undisturbed envelope of the generalized Roche model, we have, by definition,

$$\rho_0 = \beta r^{-2}, \tag{26}$$

where β is an arbitrary constant; and, if this envelope is to be in hydrostatic equilibrium, the integration of equation (1) discloses that the corresponding pressure must vary as

$$p_0 = \tfrac{1}{3}Gm\beta r^{-3}. \tag{27}$$

Insert now the foregoing relations in equations (4)–(6). If, furthermore, we replace u_1, p_1, and ρ_1 by expressions (7)–(9), which are expected to hold good from the shock inward, we find that immediately behind the shock front, when $\xi = \xi_0$,

$$U(\xi_0) = \frac{4(1-x)}{3(\gamma+1)}, \tag{28}$$

$$P(\xi_0) = \frac{4\beta(2\gamma-\gamma x+x)}{9\gamma(\gamma+1)}, \tag{29}$$

$$\Omega(\xi_0) = \frac{\beta(\gamma+1)}{\gamma-1+2x}, \tag{30}$$

and, therefore,

$$S(\xi_0) = \frac{4(2\gamma-\gamma x+x)(\gamma-1+2x)}{9(\gamma+1)^2}, \tag{31}$$

where

$$x = \tfrac{3}{4} G m \gamma \xi_0 . \tag{32}$$

In order to be able to integrate equations (21)–(23) from the shock inward, we still must ascertain the values of the derivatives of U, P, and Ω (or S) with respect to ξ immediately behind the shock wave. This can be done by means of the initial differential equations (1)–(3), which, rewritten in terms of U, P, and Ω, assume the forms

$$(2-3U)\,\xi\Omega U' - 3\xi P' = \Omega\{U(1-U) - Gm\xi\}, \tag{33}$$

$$(2-3U)\,\xi\Omega' - 3\Omega\xi U' = -\Omega U , \tag{34}$$

$$(2-3U)\,\Omega\xi P' - \gamma(2-3U)\,P\xi\Omega' = 2\Omega P(1-\gamma U) , \tag{35}$$

where primes denote differentiation with respect to ξ. If, in these equations, we set $\xi = \xi_0$ and insert for $U(\xi_0)$, $P(\xi_0)$, and $\Omega(\xi_0)$ from equations (28)–(30), we can solve the foregoing system of equations for $U'(\xi_0)$, $P'(\xi_0)$, and $\Omega'(\xi_0)$; doing so, we find that, immediately behind the shock,

$$U'(\xi_0) = -\frac{2(5+6\gamma x-3\gamma-2x)}{9(\gamma+1)^2\xi_0}, \tag{36}$$

$$P'(\xi_0) = -\frac{4\beta[8\gamma(\gamma-1)x^2-(21\gamma^2-8\gamma+3)x+2\gamma(5\gamma-3)]}{27\gamma(\gamma+1)^2(\gamma-1+2x)\xi_0}, \tag{37}$$

$$\Omega'(\xi_0) = \frac{\beta(4x-4\gamma x+\gamma-7)}{3(\gamma-1+2x)^2\xi_0}, \tag{38}$$

and, therefore,

$$27(\gamma+1)^3\xi_0 S'(\xi_0) = 8\{2(\gamma-1)(1-3\gamma)x^2+(15\gamma^2-12\gamma+5)x-\gamma(6\gamma-10)\} . \tag{39}$$

It may be noticed that, since the pressure occurs in equations (21)–(23) through its logarithmic derivative only, these equations are independent of β; the only parameters influencing the solution are γ, x, and ξ_0. Of these three parameters, ξ_0 determines the position of the shock at a given time t_0. In what follows we shall arbitrarily set $\xi_0 = 1$, which can be done without the loss of generality by a proper choice of our units of length and time. The ratio γ of specific heats is characteristic of the material which we are considering; so that x remains as the only arbitrary nondimensional constant characterizing our solutions. It is easy to show that this constant is intimately related with the Mach number M (i.e., with the strength) of the shock front. As is well known,

$$M = \frac{V}{c_0}, \tag{40}$$

where c_0 denotes the velocity of sound in the undisturbed medium in front of the shock wave. Now, in our present case, V is given by equation (25), while, by equations (26) and (27),

$$c_0^2 = \gamma\frac{p_0}{\rho_0} = \frac{Gm\gamma}{3r}. \tag{41}$$

Hence it transpires immediately that

$$M^2 = \frac{1}{x}, \tag{42}$$

which discloses that, if the expanding regime we are considering is to be characterized by a shock wave on its head, we must have

$$0 \leqslant x < 1 , \tag{43}$$

the strength of the shock being greater, the smaller the value of x.

Let us, furthermore, consider the relation between x and the ratio of the velocity of individual particles to the velocity of escape from the gravitational field of the star. As is well known,[5] the velocity of escape V_{esc} is defined by

$$V_{esc}^2 = \frac{2Gm}{r} ; \tag{44}$$

therefore, the ratio

$$\frac{u}{V_{esc}} = y = \frac{U(\xi)}{\sqrt{(2Gm\xi)}} \tag{45}$$

is given by equation (7). Immediately behind the shock wave we thus have

$$y = \frac{1-x}{\gamma+1}\sqrt{\frac{2\gamma}{3x}} , \tag{46}$$

relating x and y. If any ejection of matter is to take place, we must obviously have $y > 1$. If, therefore, we are interested only in such solutions as will lead to the actual ejection of matter from the gravitational field of the star, we must choose x so as to satisfy the inequality

$$0 \leqslant x < \frac{1}{4\gamma}\{3\gamma^2+10\gamma+3-\sqrt{[(3\gamma^2+10\gamma+3)^2-16\gamma^2]}\} , \tag{47}$$

the upper limit of which depends solely on γ. This upper limit corresponds to the velocity of ejection equal to that of the escape, while $x = 0$ would correspond to an infinite strength and Mach number of the shock and, therefore, to an infinite energy of the initial explosion.

Suppose, now, that a proper value of x has been chosen and an integration of equations (21)–(23) started from the initial conditions given earlier in this section for $\xi_0 = 1$ in the direction of increasing ξ, which, for fixed t, corresponds to a march from the surface inward (the center of our configuration corresponding to $\xi = \infty$). Such integrations can proceed until, for each value of x, we have reached a point $\xi = \xi_1$ at which $\Xi(\xi_1)$ vanishes. The point at which $\Xi(\xi_1) = 0$ turns out to be a singular point of our solution; for the compatibility of our system of equations requires that $\Omega'(\xi_1) = \infty$, though the pressure at $\xi = \xi_1$ remains continuous. When this point has been reached, we have evidently arrived at the interface of the core of our generalized Roche model. Owing to $\Xi(\xi_1) = 0$, the mass particles at $\xi = \xi_1$ are found to be moving with the velocity V—which means that there is no further energy transfer between the core and the envelope, in agreement with our basic premises. Thus the field of flow which we are considering is bounded by *two* surfaces of discontinuity; whereas, on the outer boundary (the shock wave), the pressure, density, *and* velocity are discontinuous with matter flowing freely across, the inner boundary is of the nature of a contact discontinuity in density but *not* in pressure or velocity. The flow of mass across this discontinuity is consequently zero.

It is easy to show that, for $\gamma \neq \frac{4}{3}$, the value of ξ_1 at which $\Xi(\xi_1)$ vanishes is always

[5] Cf., e.g., F. R. Moulton, *Celestial Mechanics* (New York: McGraw-Hill, 1939), p. 150.

finite. Consider the total energy of the envelope in its undisturbed state; it is given by

$$H = 4\pi \int_a^R \left\{ \frac{1}{\gamma - 1} \frac{p_0}{\rho_0} - \frac{Gm}{r} \right\} \rho_0 r^2 dr$$

$$= \frac{4\pi (4 - 3\gamma)}{3(\gamma - 1)} Gm\beta \log \frac{R}{a}, \tag{48}$$

by virtue of equations (26) and (27). For $\gamma \neq \frac{4}{3}$, this expression can remain finite only if $a \neq 0$. Hence, for $\gamma > \frac{4}{3}$, the discontinuity in $\Omega(\xi_1)$ is bound to occur for a finite value of ξ_1.

NUMERICAL INTEGRATIONS

Equations (21)–(23) as they stand are too involved to admit of the possibility of an analytical solution; so that, in order to investigate the properties of an expanding flow of gas defined by such equations, recourse must be had to numerical integration. We have performed 18 such integrations—14 for $\gamma = \frac{5}{3}$ (monatomic gas) and 4 for $\gamma = \frac{8}{5}$—corresponding to a series of Mach numbers ranging from $M^2 = 8.27924\ldots$ (which corresponds to $y = 1$) to $M^2 = \infty$. The details of such integrations are given in Table 1, the successive columns of which are self-explanatory. Each tabulation extends from $\xi = 1$ (assumed position of the shock wave) down to ξ_1, at which the core sets in and the density becomes discontinuous. As many decimals are retained in each tabulation as are regarded to be significant. The values so normalized permit the evaluation of the actual absolute properties of the expanding regime of gas flow corresponding to any explosion by choosing the appropriate absolute value of β. The accompanying diagram (Fig. 1) shows a plot of U against C, for a number of solutions corresponding to $\gamma = \frac{5}{3}$ and 6 different assumed Mach numbers of expansion.

As we surmised at the beginning, the field of flow considered in this investigation is not

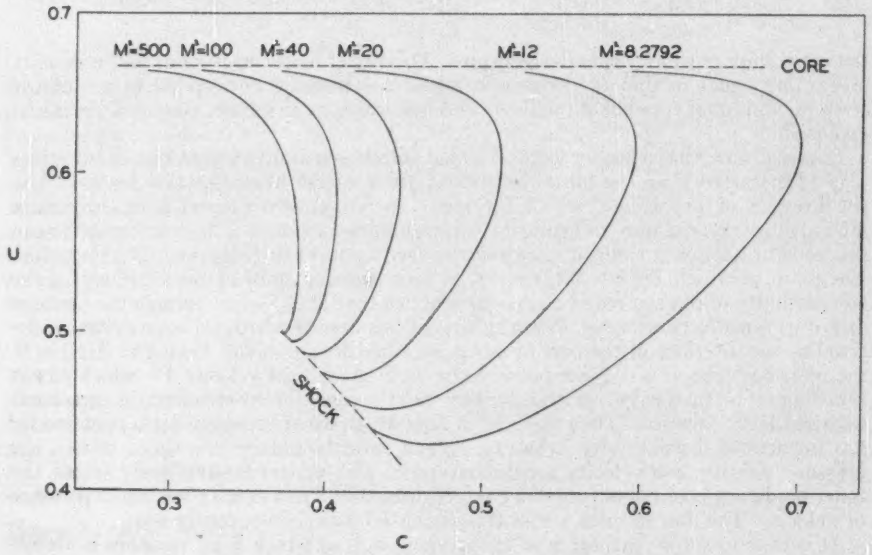

FIG. 1.—Vector field representing the solutions of our differential equations (21)–(23) for $U = r^{-1}lu$ and $C = r^{-1}lc$ of spherical progressing waves discussed in the present paper.

TABLE I

Physical Properties of the Expanding Field of Flow behind Shock Waves of Different Strengths

ξ	U	C	P/β	Q/β	γ	$PQ^{\gamma}/\beta^{1-\gamma}$	F
		$\gamma = 5/3$		$M^2 = 8.2792$			
1.00	0.4396	0.4297	0.3253	2.936	1.0000	0.0540	0.0000
1.02	0.4390	0.4309	0.3220	2.891	0.9689	0.0549	0.0094
1.04	0.4384	0.4320	0.3189	2.848	0.9781	0.0557	0.0185
1.06	0.4379	0.4331	0.3160	2.807	0.9676	0.0566	0.0277
1.08	0.4374	0.4343	0.3132	2.768	0.9576	0.0574	0.0366
1.10	0.4369	0.4354	0.3105	2.730	0.9477	0.0582	0.0450
1.10	0.4369	0.4354	0.3105	2.730	0.9477	0.0582	0.0450
1.14	0.4359	0.4377	0.3056	2.658	0.9288	0.0599	0.0616
1.18	0.4351	0.4399	0.3009	2.591	0.9112	0.0616	0.0778
1.22	0.4343	0.4422	0.2968	2.529	0.8946	0.0632	0.0937
1.26	0.4336	0.4445	0.2930	2.472	0.8788	0.0648	0.1095
1.30	0.4330	0.4467	0.2896	2.418	0.8638	0.0665	0.1274
1.34	0.4324	0.4490	0.2863	2.367	0.8497	0.0681	0.1456
1.38	0.4319	0.4512	0.2834	2.320	0.8364	0.0697	0.1639
1.42	0.4315	0.4535	0.2808	2.276	0.8238	0.0713	0.1196
1.46	0.4312	0.4557	0.2784	2.235	0.8119	0.0729	0.1256
1.50	0.4309	0.4579	0.2763	2.196	0.8005	0.0743	0.1312
1.54	0.4307	0.4601	0.2743	2.159	0.7896	0.0760	0.1363
1.58	0.4305	0.4624	0.2725	2.124	0.7792	0.0776	0.1410
1.62	0.4304	0.4646	0.2708	2.091	0.7694	0.0792	0.1455
1.66	0.4304	0.4668	0.2693	2.060	0.7600	0.0807	0.1495
1.70	0.4304	0.4690	0.2680	2.031	0.7510	0.0825	0.1530
1.74	0.4305	0.4712	0.2668	2.005	0.7424	0.0839	0.1564
1.78	0.4306	0.4734	0.2657	1.976	0.7342	0.0854	0.1596
1.82	0.4308	0.4756	0.2648	1.951	0.7264	0.0869	0.1625
1.86	0.4310	0.4777	0.2639	1.927	0.7189	0.0884	0.1652
1.90	0.4313	0.4799	0.2631	1.904	0.7118	0.0899	0.1678
1.94	0.4316	0.4821	0.2623	1.882	0.7050	0.0915	0.1702
1.98	0.4320	0.4842	0.2620	1.862	0.6984	0.0930	0.1724
2.02	0.4323	0.4864	0.2615	1.843	0.6920	0.0944	0.1745
2.02	0.4323	0.4864	0.2615	1.843	0.6920	0.0944	0.1745
2.18	0.4342	0.4948	0.2608	1.772	0.6690	0.1005	0.1816
2.34	0.4366	0.5031	0.2601	1.713	0.6498	0.1061	0.1871
2.50	0.4396	0.5112	0.2608	1.665	0.6325	0.1117	0.1914
2.66	0.4427	0.5192	0.2621	1.620	0.6176	0.1173	0.1949
2.82	0.4462	0.5271	0.2636	1.580	0.6045	0.1227	0.1977
2.98	0.4500	0.5348	0.2661	1.561	0.5930	0.1280	0.1999
3.14	0.4540	0.5425	0.2697	1.523	0.5828	0.1335	0.2017
3.30	0.4581	0.5498	0.2716	1.498	0.5737	0.1385	0.2031
3.46	0.4624	0.5569	0.2747	1.477	0.5655	0.1435	0.2043
3.62	0.4668	0.5638	0.2781	1.459	0.5581	0.1485	0.2052
3.78	0.4713	0.5707	0.2817	1.442	0.5514	0.1531	0.2059
3.94	0.4758	0.5774	0.2854	1.427	0.5453	0.1578	0.2065
4.10	0.4804	0.5840	0.2892	1.414	0.5397	0.1625	0.2069
4.10	0.4804	0.5840	0.2892	1.414	0.5397	0.1625	0.2069
4.42	0.4898	0.5968	0.2975	1.392	0.5300	0.1713	0.2074
4.74	0.4993	0.6086	0.3066	1.376	0.5217	0.1798	0.2075
5.06	0.5089	0.6200	0.3166	1.364	0.5146	0.1876	0.2074
5.38	0.5185	0.6308	0.3280	1.356	0.5085	0.1949	0.2072
5.70	0.5280	0.6410	0.3529	1.351	0.5031	0.2016	0.2068
6.02	0.5376	0.6505	0.3424	1.349	0.4984	0.2078	0.2062
6.34	0.5470	0.6594	0.3621	1.350	0.4942	0.2135	0.2055
6.66	0.5564	0.6677	0.3820	1.353	0.4905	0.2186	0.2047
6.98	0.5657	0.6755	0.3721	1.360	0.4871	0.2233	0.2039
7.30	0.5749	0.6828	0.3824	1.370	0.4840	0.2265	0.2029
7.62	0.5840	0.6892	0.3929	1.383	0.4813	0.2299	0.2018
7.94	0.5930	0.6934	0.4038	1.399	0.4788	0.2306	0.2007
8.26	0.6019	0.6975	0.4149	1.420	0.4765	0.2311	0.1996
8.58	0.6107	0.7002	0.4257	1.447	0.4745	0.2303	0.1985
8.90	0.6194	0.7014	0.4372	1.482	0.4725	0.2270	0.1970
9.22	0.6280	0.7005	0.4491	1.527	0.4705	0.2218	0.1956
9.54	0.6365	0.6965	0.4615	1.586	0.4686	0.2140	0.1941
9.86	0.6449	0.6882	0.4745	1.670	0.4672	0.2019	0.1925
10.18	0.6531	0.6716	0.4884	1.806	0.4657	0.1835	0.1906
10.50	0.6613	0.6322	0.5040	2.102	0.4643	0.1461	0.1885
10.7151	0.6667	0.0000	0.5184	∞	0.4633	0.0000	0.1862
		$\gamma = 5/3$		$M^2 = 10$			
1.00	0.4500	0.4807	0.3267	3.077	1.125	0.0808	0.0000
1.02	0.4495	0.4816	0.3230	3.023	1.112	0.1810	0.0108
1.04	0.4490	0.4826	0.3196	2.982	1.101	0.0817	0.0209
1.06	0.4486	0.4836	0.3161	2.937	1.089	0.0825	0.0305
1.08	0.4482	0.4845	0.3129	2.894	1.077	0.0832	0.0395
1.10	0.4477	0.4855	0.3098	2.852	1.067	0.0840	0.0480
1.12	0.4473	0.4865	0.3068	2.812	1.057	0.0848	0.0560
1.14	0.4470	0.4874	0.3041	2.774	1.047	0.0855	0.0636
1.16	0.4470	0.4874	0.3041	2.774	1.047	0.0855	0.0636
1.19	0.4461	0.4892	0.2976	2.684	1.022	0.0874	0.0809
1.24	0.4455	0.4923	0.2918	2.602	1.000	0.0892	0.0951
1.29	0.4446	0.4947	0.2863	2.528	0.979	0.0911	0.1095
1.34	0.4441	0.4970	0.2815	2.456	0.959	0.0929	0.1215
1.39	0.4437	0.4994	0.2771	2.392	0.941	0.0947	0.1319
1.44	0.4433	0.4418	0.2732	2.333	0.923	0.0965	0.1415
1.44	0.4433	0.4418	0.2732	2.333	0.923	0.0965	0.1415
1.54	0.4428	0.4466	0.2665	2.227	0.892	0.0701	0.1574
1.64	0.4424	0.4513	0.2610	2.135	0.864	0.0736	0.1706
1.74	0.4423	0.4560	0.2565	2.052	0.839	0.0771	0.1815
1.84	0.4423	0.4607	0.2528	1.986	0.817	0.0806	0.1904
1.94	0.4440	0.4653	0.2498	1.925	0.797	0.0840	0.1981
2.04	0.4450	0.4699	0.2474	1.887	0.779	0.0874	0.2048
2.04	0.4450	0.4699	0.2474	1.887	0.779	0.0874	0.2048
2.24	0.4476	0.4790	0.2441	1.774	0.748	0.0959	0.2150

ξ	U	C	P/β	Q/β	γ	$PQ^{\gamma}/\beta^{1-\gamma}$	F
		$\gamma = 5/3$		$M^2 = 10$			
2.44	0.4808	0.4879	0.2425	1.627	0.722	0.1005	0.2229
2.64	0.4845	0.4965	0.2417	1.554	0.700	0.1068	0.2290
2.84	0.4889	0.5048	0.2420	1.502	0.681	0.1127	0.2337
3.04	0.4936	0.5129	0.2430	1.459	0.665	0.1180	0.2375
3.24	0.4986	0.5209	0.2446	1.432	0.651	0.1242	0.2406
3.44	0.4788	0.5287	0.2467	1.471	0.639	0.1297	0.2430
3.64	0.4792	0.5362	0.2491	1.444	0.628	0.1350	0.2451
3.84	0.4848	0.5435	0.2518	1.421	0.618	0.1402	0.2467
4.04	0.4906	0.5506	0.2548	1.401	0.610	0.1453	0.2480
4.24	0.4964	0.5575	0.2580	1.384	0.603	0.1502	0.2491
4.44	0.5023	0.5642	0.2614	1.369	0.596	0.1549	0.2500
4.64	0.5082	0.5706	0.2650	1.356	0.590	0.1594	0.2507
4.84	0.5142	0.5768	0.2687	1.346	0.584	0.1637	0.2513
5.04	0.5202	0.5828	0.2725	1.337	0.579	0.1678	0.2518
5.24	0.5263	0.5886	0.2764	1.330	0.574	0.1718	0.2522
5.44	0.5325	0.5943	0.2805	1.324	0.571	0.1757	0.2525
5.64	0.5385	0.5998	0.2846	1.319	0.567	0.1794	0.2527
5.84	0.5444	0.6050	0.2888	1.316	0.565	0.1828	0.2528
6.04	0.5504	0.6098	0.2931	1.314	0.560	0.1859	0.2529
6.24	0.5564	0.6143	0.2975	1.314	0.557	0.1887	0.2529
6.44	0.5624	0.6185	0.3020	1.315	0.554	0.1913	0.2528
6.64	0.5683	0.6225	0.3065	1.318	0.551	0.1935	0.2527
6.84	0.5743	0.6262	0.3111	1.322	0.549	0.1953	0.2526
7.04	0.5802	0.6296	0.3158	1.328	0.547	0.1968	0.2524
7.24	0.5861	0.6327	0.3205	1.335	0.544	0.1980	0.2522
7.44	0.5919	0.6354	0.3255	1.343	0.542	0.1989	0.2520
7.64	0.5977	0.6377	0.3302	1.353	0.541	0.1995	0.2517
7.84	0.6035	0.6396	0.3352	1.364	0.539	0.1994	0.2514
8.04	0.6092	0.6409	0.3403	1.381	0.537	0.1987	0.2510
8.24	0.6149	0.6417	0.3455	1.396	0.536	0.1974	0.2506
8.44	0.6206	0.6418	0.3507	1.430	0.534	0.1955	0.2502
8.64	0.6262	0.6410	0.3560	1.445	0.533	0.1929	0.2497
8.84	0.6318	0.6392	0.3615	1.476	0.531	0.1891	0.2492
9.04	0.6374	0.6360	0.3671	1.512	0.530	0.1842	0.2486
9.24	0.6429	0.6310	0.3729	1.561	0.529	0.1775	0.2480
9.44	0.6483	0.6232	0.3790	1.626	0.527	0.1686	0.2473
9.64	0.6538	0.6110	0.3854	1.721	0.526	0.1559	0.2465
9.84	0.6591	0.5905	0.3925	1.878	0.525	0.1375	0.2456
10.04	0.6644	0.5298	0.4004	2.426	0.524	0.0948	0.2443
10.1242	0.6667	0.0000	0.4046	∞	0.523	0.0000	0.2435
		$\gamma = 5/3$		$M^2 = 12$			
1.0	0.4583	0.4132	0.3278	3.200	1.156	0.0472	0.0000
1.1	0.4564	0.4173	0.3091	2.958	1.192	0.0527	0.0520
1.2	0.4549	0.4214	0.2940	2.759	1.127	0.0542	0.0951
1.3	0.4538	0.4255	0.2816	2.592	1.089	0.0676	0.1241
1.4	0.4530	0.4296	0.2713	2.450	1.068	0.0909	0.1466
1.5	0.4526	0.4337	0.2627	2.328	1.012	0.0945	0.1662
1.6	0.4525	0.4378	0.2555	2.222	0.980	0.0975	0.1844
1.7	0.4526	0.4418	0.2495	2.130	0.951	0.0707	0.1977
1.8	0.4529	0.4458	0.2445	2.051	0.924	0.0728	0.2089
1.8	0.4529	0.4458	0.2445	2.051	0.924	0.0728	0.2089
2.0	0.4544	0.4537	0.2367	1.916	0.880	0.0801	0.2282
2.2	0.4567	0.4615	0.2312	1.809	0.845	0.0861	0.2391
2.4	0.4597	0.4692	0.2274	1.722	0.815	0.0919	0.2449
2.6	0.4635	0.4767	0.2249	1.650	0.787	0.0978	0.2486
2.8	0.4674	0.4841	0.2235	1.589	0.760	0.1035	0.2505
3.0	0.4718	0.4915	0.2229	1.538	0.745	0.1088	0.2514
3.05	0.4730	0.4931	0.2230	1.529	0.7417	0.1099	0.2514
3.25	0.4778	0.4995	0.2232	1.491	0.7258	0.1148	0.2722
3.45	0.4829	0.5060	0.2236	1.456	0.7120	0.1196	0.2763
3.65	0.4883	0.5126	0.2248	1.428	0.6999	0.1244	0.2779
3.85	0.4939	0.5192	0.2262	1.400	0.6891	0.1291	0.2801
4.05	0.4994	0.5260	0.2278	1.377	0.6795	0.1336	0.2820
4.25	0.5051	0.5329	0.2297	1.358	0.6708	0.1379	0.2836
4.45	0.5109	0.5397	0.2318	1.341	0.6632	0.1420	0.2850
4.65	0.5168	0.5422	0.2340	1.327	0.6563	0.1460	0.2862
4.85	0.5228	0.5474	0.2364	1.315	0.6501	0.1498	0.2872
5.05	0.5288	0.5524	0.2389	1.305	0.6444	0.1535	0.2881
5.05	0.5288	0.5524	0.2389	1.305	0.6444	0.1535	0.2881
5.45	0.5408	0.5620	0.2443	1.289	0.6344	0.1600	0.2896
5.85	0.5528	0.5708	0.2500	1.280	0.6259	0.1657	0.2905
6.25	0.5649	0.5791	0.2561	1.277	0.6187	0.1704	0.2912
6.65	0.5769	0.5845	0.2625	1.280	0.6128	0.1739	0.2917
7.05	0.5888	0.5898	0.2692	1.290	0.6075	0.1761	0.2920
7.45	0.6007	0.5929	0.2761	1.306	0.6027	0.1769	0.2921
7.85	0.6124	0.5961	0.2833	1.330	0.5986	0.1761	0.2921
8.25	0.6240	0.5965	0.2907	1.360	0.5950	0.1739	0.2919
8.65	0.6355	0.5912	0.2985	1.423	0.5918	0.1698	0.2915
8.65	0.6355	0.5912	0.2985	1.423	0.5918	0.1698	0.2915
8.85	0.6411	0.5868	0.3028	1.464	0.5901	0.1603	0.2912
9.05	0.6468	0.5769	0.3069	1.521	0.5889	0.1525	0.2909
9.25	0.6524	0.5694	0.3114	1.601	0.5875	0.1418	0.2905
9.45	0.6580	0.5515	0.3163	1.733	0.5862	0.1266	0.2900
9.65	0.6635	0.5235	0.3217	1.958	0.5849	0.1062	0.2894
9.7666	0.6667	0.0000	0.3265	∞	0.5842	0.0000	0.2880

TABLE I

Physical Properties of the Expanding Field of Flow behind Shock Waves of Different Strengths

ξ	U	C	P/β	Q/β	γ	$PQ^{\gamma}/\beta^{1-\gamma}$	F
		$\gamma = 5/3$		$M^2 = 15$			
1.0	0.4667	0.4065	0.3289	3.353	1.429	0.0442	0.0000
1.1	0.4652	0.4089	0.3063	3.074	1.368	0.0474	0.0586
1.2	0.4640	0.4123	0.2915	2.859	1.297	0.0506	0.1159
1.3	0.4631	0.4156	0.2776	2.676	1.244	0.0537	0.1725
1.4	0.4625	0.4190	0.2659	2.524	1.197	0.0568	0.1849
1.5	0.4622	0.4225	0.2560	2.393	1.155	0.0598	0.1870
1.6	0.4621	0.4257	0.2477	2.279	1.118	0.0628	0.2051
1.7	0.4622	0.4290	0.2408	2.179	1.085	0.0657	0.2201
1.8	0.4623	0.4323	0.2346	2.091	1.056	0.0686	0.2327
1.9	0.4632	0.4356	0.2292	2.013	1.029	0.0714	0.2434
2.0	0.4640	0.4388	0.2245	1.944	1.005	0.0742	0.2525
2.0	0.4640	0.4388	0.2245	1.944	1.005	0.0742	0.2525
2.2	0.4662	0.4453	0.2172	1.838	0.962	0.0796	0.2673
2.4	0.4690	0.4516	0.2117	1.750	0.927	0.0849	0.2786
2.6	0.4724	0.4578	0.2076	1.681	0.897	0.0900	0.2874
2.8	0.4762	0.4639	0.2046	1.624	0.871	0.0950	0.2945
3.0	0.4804	0.4699	0.2024	1.578	0.849	0.0998	0.3003
3.2	0.4849	0.4758	0.2009	1.479	0.830	0.1046	0.3051
3.4	0.4897	0.4815	0.2000	1.438	0.813	0.1092	0.3091
3.6	0.4947	0.4870	0.1995	1.402	0.798	0.1136	0.3125
3.8	0.4999	0.4923	0.1994	1.371	0.785	0.1178	0.3154
4.0	0.5053	0.4975	0.1996	1.344	0.774	0.1219	0.3179
4.2	0.5108	0.5025	0.2001	1.321	0.764	0.1258	0.3200
4.4	0.5164	0.5073	0.2008	1.301	0.756	0.1295	0.3219
4.4	0.5164	0.5073	0.2008	1.301	0.7637	0.1295	0.3219
4.6	0.5278	0.5163	0.2022	1.268	0.7376	0.1365	0.3250
4.8	0.5392	0.5245	0.2054	1.244	0.7244	0.1427	0.3274
5.0	0.5503	0.5319	0.2094	1.228	0.7133	0.1481	0.3293
5.2	0.5611	0.5384	0.2117	1.218	0.7040	0.1528	0.3308
5.4	0.5711	0.5439	0.2158	1.213	0.6961	0.1561	0.3320
5.6	0.5870	0.5482	0.2192	1.215	0.6893	0.1584	0.3330
5.8	0.5969	0.5514	0.2233	1.224	0.6834	0.1594	0.3337
7.6	0.6107	0.5527	0.2277	1.242	0.6783	0.1587	0.3344
8.0	0.6224	0.5517	0.2323	1.272	0.6738	0.1556	0.3348
8.0	0.6224	0.5517	0.2323	1.272	0.6738	0.1556	0.3348
8.2	0.6282	0.5501	0.2347	1.293	0.6717	0.1529	0.3349
8.4	0.6340	0.5474	0.2372	1.320	0.6698	0.1493	0.3350
8.6	0.6398	0.5432	0.2396	1.356	0.6680	0.1445	0.3350
8.8	0.6455	0.5369	0.2426	1.402	0.6663	0.1381	0.3351
9.0	0.6512	0.5276	0.2453	1.469	0.6646	0.1292	0.3351
9.00	0.6512	0.5275	0.2453	1.469	0.6646	0.1292	0.3351
9.05	0.6526	0.5243	0.2460	1.491	0.6642	0.1264	0.3351
9.10	0.6540	0.5207	0.2467	1.516	0.6638	0.1233	0.3350
9.15	0.6554	0.5167	0.2474	1.545	0.6634	0.1198	0.3350
9.20	0.6569	0.5122	0.2482	1.579	0.6631	0.1160	0.3350
9.25	0.6583	0.5072	0.2490	1.618	0.6627	0.1117	0.3350
9.30	0.6597	0.4997	0.2498	1.667	0.6624	0.1066	0.3349
9.35	0.6611	0.4914	0.2508	1.728	0.6620	0.1005	0.3349
9.40	0.6625	0.4803	0.2515	1.817	0.6617	0.0930	0.3348
9.40	0.6625	0.4803	0.2515	1.817	0.6617	0.0930	0.3348
9.42	0.6631	0.4747	0.2519	1.863	0.6615	0.0895	0.3348
9.44	0.6637	0.4683	0.2523	1.916	0.6614	0.0852	0.3348
9.46	0.6642	0.4606	0.2527	1.987	0.6612	0.0805	0.3347
9.48	0.6648	0.4507	0.2531	2.077	0.6611	0.0749	0.3347
9.50	0.6653	0.4373	0.2535	2.210	0.6610	0.0676	0.3346
9.52	0.6659	0.4166	0.2540	2.440	0.6608	0.0574	0.3346
9.54	0.6664	0.3654	0.2545	3.177	0.6607	0.0371	0.3345
9.5476	0.6667	0.0000	0.2548	∞	0.6606	0.0000	0.3345
		$\gamma = 5/3$		$M^2 = 20$			
1.00	0.4760	0.3976	0.3300	3.479	1.479	0.0413	0.0000
1.02	0.4748	0.3982	0.3251	3.418	1.462	0.0419	0.0146
1.04	0.4745	0.3987	0.3204	3.359	1.445	0.0425	0.0291
1.06	0.4743	0.3992	0.3159	3.303	1.429	0.0431	0.0411
1.08	0.4741	0.3998	0.3115	3.249	1.413	0.0437	0.0553
1.09	0.4739	0.4005	0.3073	3.197	1.398	0.0443	0.0646
1.10	0.4737	0.4006	0.3033	3.147	1.383	0.0449	0.0727
1.12	0.4735	0.4013	0.2994	3.099	1.368	0.0454	0.0861
1.14	0.4733	0.4018	0.2957	3.053	1.354	0.0460	0.0959
1.16	0.4731	0.4023	0.2921	3.008	1.340	0.0466	0.1052
1.18	0.4730	0.4029	0.2886	2.964	1.326	0.0472	0.1141
1.20	0.4730	0.4029	0.2886	2.964	1.326	0.0472	0.1141
1.22	0.4728	0.4042	0.2852	2.922	1.494	0.0486	0.1343
1.24	0.4725	0.4054	0.2820	2.881	1.404	0.0500	0.1525
1.26	0.4720	0.4067	0.2862	2.881	1.436	0.0514	0.1684
1.40	0.4719	0.4080	0.2598	2.601	1.410	0.0528	0.1825
1.45	0.4718	0.4093	0.2540	2.527	1.385	0.0542	0.1957
1.50	0.4717	0.4106	0.2486	2.458	1.361	0.0556	0.2078
1.55	0.4716	0.4119	0.2436	2.394	1.339	0.0569	0.2178
1.60	0.4717	0.4132	0.2390	2.334	1.318	0.0582	0.2274
1.65	0.4718	0.4144	0.2347	2.277	1.299	0.0594	0.2362
1.70	0.4719	0.4157	0.2306	2.224	1.280	0.0609	0.2441
1.75	0.4720	0.4170	0.2268	2.174	1.261	0.0622	0.2515
1.80	0.4722	0.4183	0.2233	2.127	1.244	0.0635	0.2582
1.85	0.4725	0.4195	0.2201	2.083	1.228	0.0648	0.2644
1.90	0.4728	0.4208	0.2170	2.042	1.213	0.0660	0.2701
1.95	0.4731	0.4221	0.2141	2.003	1.198	0.0673	0.2754
2.00	0.4735	0.4234	0.2114	1.966	1.184	0.0685	0.2803
2.0	0.4735	0.4234	0.2114	1.966	1.184	0.0685	0.2803
2.1	0.4744	0.4259	0.2065	1.898	1.157	0.0710	0.2891

ξ	U	C	P/β	Q/β	γ	$PQ^{\gamma}/\beta^{1-\gamma}$	F
		$\gamma = 5/3$		$M^2 = 20$			
2.2	0.4784	0.4283	0.2021	1.836	1.133	0.0734	0.2968
2.3	0.4796	0.4308	0.1982	1.780	1.111	0.0758	0.3038
2.4	0.4779	0.4333	0.1946	1.730	1.091	0.0781	0.3096
2.5	0.4793	0.4358	0.1916	1.684	1.072	0.0804	0.3149
2.6	0.4808	0.4382	0.1891	1.642	1.054	0.0827	0.3196
2.7	0.4825	0.4406	0.1868	1.603	1.039	0.0850	0.3238
2.8	0.4843	0.4429	0.1844	1.567	1.023	0.0872	0.3276
2.9	0.4860	0.4453	0.1825	1.534	1.009	0.0894	0.3310
3.0	0.4880	0.4476	0.1807	1.503	0.996	0.0916	0.3341
3.0	0.4880	0.4476	0.1807	1.503	0.996	0.0916	0.3341
3.2	0.4920	0.4522	0.1778	1.449	0.972	0.0958	0.3396
3.4	0.4964	0.4566	0.1754	1.402	0.951	0.0999	0.3442
3.6	0.5010	0.4608	0.1736	1.362	0.933	0.1037	0.3481
3.8	0.5058	0.4648	0.1722	1.328	0.917	0.1073	0.3515
4.0	0.5107	0.4687	0.1711	1.298	0.903	0.1108	0.3544
4.2	0.5158	0.4725	0.1703	1.271	0.890	0.1142	0.3570
4.4	0.5210	0.4762	0.1698	1.248	0.878	0.1174	0.3593
4.6	0.5263	0.4799	0.1694	1.227	0.867	0.1205	0.3613
4.8	0.5317	0.4838	0.1693	1.207	0.858	0.1237	0.3630
5.0	0.5372	0.4877	0.1693	1.189	0.849	0.1269	0.3646
5.2	0.5428	0.4913	0.1694	1.172	0.841	0.1300	0.3660
5.4	0.5484	0.4945	0.1697	1.158	0.834	0.1328	0.3673
5.6	0.5541	0.4972	0.1700	1.147	0.828	0.1353	0.3685
5.8	0.5598	0.4995	0.1705	1.139	0.822	0.1374	0.3696
6.0	0.5655	0.5017	0.1710	1.132	0.816	0.1395	0.3706
6.2	0.5712	0.5038	0.1717	1.126	0.811	0.1409	0.3715
6.4	0.5769	0.5058	0.1724	1.122	0.806	0.1423	0.3723
6.6	0.5827	0.5076	0.1731	1.120	0.802	0.1434	0.3730
6.8	0.5885	0.5092	0.1739	1.119	0.798	0.1444	0.3737
7.0	0.5942	0.5104	0.1748	1.118	0.794	0.1450	0.3743
7.2	0.6000	0.5109	0.1757	1.122	0.790	0.1450	0.3749
7.4	0.6058	0.5109	0.1766	1.128	0.787	0.1446	0.3754
7.6	0.6115	0.5103	0.1776	1.135	0.784	0.1439	0.3759
7.8	0.6173	0.5098	0.1787	1.145	0.781	0.1428	0.3763
8.0	0.6230	0.5089	0.1798	1.157	0.778	0.1410	0.3767
8.2	0.6288	0.5072	0.1809	1.172	0.776	0.1388	0.3771
8.4	0.6345	0.5045	0.1821	1.193	0.774	0.1357	0.3774
8.6	0.6402	0.5003	0.1833	1.221	0.772	0.1314	0.3777
8.8	0.6459	0.4942	0.1846	1.260	0.770	0.1258	0.3780
9.0	0.6515	0.4840	0.1860	1.323	0.768	0.1187	0.3782
9.2	0.6572	0.4675	0.1876	1.430	0.766	0.1093	0.3784
9.4	0.6628	0.4368	0.1891	1.681	0.764	0.0912	0.3785
9.5280	0.6667	0.0000	0.1901	∞	0.763	0.0000	0.3786
		$\gamma = 5/3$		$M^2 = 30$			
1.0	0.4823	0.3896	0.3311	3.638	2.093	0.0385	0.0000
1.1	0.4806	0.3913	0.3061	3.331	1.995	0.0412	0.0713
1.2	0.4820	0.3931	0.2854	3.078	1.906	0.0438	0.1256
1.3	0.4816	0.3949	0.2680	2.865	1.829	0.0464	0.1679
1.4	0.4813	0.3966	0.2532	2.685	1.762	0.0489	0.2015
1.5	0.4812	0.3984	0.2405	2.529	1.702	0.0513	0.2287
1.6	0.4812	0.4002	0.2295	2.389	1.648	0.0537	0.2510
1.7	0.4814	0.4019	0.2199	2.269	1.599	0.0561	0.2695
1.8	0.4817	0.4037	0.2115	2.163	1.555	0.0585	0.2851
1.9	0.4822	0.4054	0.2040	2.068	1.515	0.0608	0.2983
2.0	0.4827	0.4072	0.1974	1.984	1.478	0.0630	0.3096
2.0	0.4827	0.4072	0.1974	1.984	1.478	0.0630	0.3096
2.2	0.4843	0.4107	0.1862	1.840	1.414	0.0674	0.3279
2.4	0.4862	0.4141	0.1771	1.721	1.359	0.0716	0.3420
2.6	0.4884	0.4175	0.1695	1.622	1.312	0.0757	0.3532
2.8	0.4913	0.4208	0.1634	1.538	1.272	0.0797	0.3622
3.0	0.4943	0.4241	0.1582	1.466	1.237	0.0836	0.3695
3.2	0.4976	0.4273	0.1539	1.406	1.206	0.0875	0.3756
3.4	0.5013	0.4304	0.1502	1.352	1.177	0.0909	0.3807
3.6	0.5051	0.4334	0.1471	1.305	1.153	0.0944	0.3851
3.8	0.5091	0.4364	0.1444	1.264	1.131	0.0977	0.3889
3.8	0.5091	0.4364	0.1444	1.264	1.131	0.0977	0.3889
4.1	0.5186	0.4407	0.1411	1.210	1.103	0.1027	0.3932
4.4	0.5292	0.4448	0.1386	1.166	1.078	0.1072	0.3971
4.7	0.5392	0.4486	0.1364	1.129	1.057	0.1114	0.4004
5.0	0.5364	0.4521	0.1348	1.098	1.039	0.1153	0.4032
5.3	0.5438	0.4554	0.1336	1.072	1.023	0.1189	0.4058
5.6	0.5514	0.4584	0.1328	1.050	1.009	0.1221	0.4076
5.9	0.5591	0.4611	0.1317	1.032	0.997	0.1250	0.4094
6.2	0.5669	0.4635	0.1309	1.016	0.986	0.1276	0.4110
6.5	0.5748	0.4656	0.1305	1.002	0.976	0.1299	0.4124
6.8	0.5827	0.4675	0.1300	0.992	0.968	0.1318	0.4135
7.1	0.5907	0.4694	0.1298	0.984	0.960	0.1339	0.4147
7.4	0.5988	0.4686	0.1298	0.976	0.953	0.1351	0.4157
7.7	0.6068	0.4676	0.1296	0.969	0.947	0.1364	0.4166
8.0	0.6149	0.4663	0.1299	0.966	0.942	0.1369	0.4174
8.3	0.6230	0.4640	0.1301	1.007	0.937	0.1366	0.4182
8.6	0.6311	0.4606	0.1303	1.024	0.932	0.1352	0.4189
8.9	0.6392	0.4547	0.1308	1.053	0.928	0.1330	0.4195
9.2	0.6475	0.4460	0.1309	1.097	0.924	0.1292	0.4201
9.2	0.6475	0.4460	0.1309	1.097	0.9243	0.1292	0.4201
9.3	0.6500	0.4421	0.1310	1.117	0.9231	0.1269	0.4203
9.4	0.6527	0.4359	0.1312	1.145	0.9220	0.1247	0.4205
9.5	0.6554	0.4302	0.1313	1.183	0.9209	0.1223	0.4206
9.6	0.6581	0.4213	0.1315	1.235	0.9198	0.1195	0.4208
9.7	0.6608	0.4089	0.1317	1.313	0.9188	0.1157	0.4209
9.8	0.6635	0.3900	0.1319	1.445	0.9179	0.1114	0.4211
9.9	0.6662	0.3576	0.1321	1.831	0.9170	0.1041	0.4212
9.9189	0.6667	0.0000	0.1325	∞	0.9168	0.0000	0.4212

TABLE I

Physical Properties of the Expanding Field of Flow behind Shock Waves of Different Strengths

ξ	U	C	P/β	Q/β	γ	$P\Sigma^{\gamma}/\beta^{1-\gamma}$	F
		$\gamma = 5/3$		$M^2 = 40$			
1.00	0.4875	0.3954	0.3217	5.721	2.438	0.0871	0.0000
1.04	0.4873	0.3940	0.3206	5.596	2.380	0.0852	0.0328
1.08	0.4870	0.3926	0.3195	5.482	2.343	0.0836	0.0617
1.12	0.4868	0.3871	0.3008	5.346	2.300	0.0802	0.0877
1.16	0.4867	0.3876	0.2919	5.228	2.259	0.0812	0.1111
1.20	0.4865	0.3861	0.2827	5.138	2.221	0.0792	0.1322
1.24	0.4864	0.3847	0.2740	5.045	2.184	0.0451	0.1515
1.28	0.4862	0.3832	0.2658	2.957	2.149	0.0441	0.1686
1.32	0.4861	0.3827	0.2620	2.875	2.116	0.0451	0.1844
1.36	0.4861	0.3803	0.2567	2.798	2.084	0.0460	0.1986
1.40	0.4860	0.3808	0.2497	2.735	2.054	0.0470	0.2120
1.44	0.4860	0.3814	0.2441	2.656	2.025	0.0476	0.2241
1.48	0.4859	0.3819	0.2398	2.591	1.997	0.0489	0.2353
1.52	0.4859	0.3824	0.2328	2.530	1.971	0.0498	0.2456
1.56	0.4859	0.3830	0.2291	2.472	1.945	0.0507	0.2551
1.60	0.4860	0.3836	0.2248	2.417	1.921	0.0516	0.2639
1.80	0.4860	0.3865	0.2248	2.417	1.921	0.0516	0.2639
1.72	0.4862	0.3861	0.2124	2.268	1.854	0.0543	0.2898
1.84	0.4865	0.3907	0.2020	2.139	1.793	0.0569	0.3065
1.96	0.4870	0.3965	0.1929	2.026	1.738	0.0595	0.3209
2.08	0.4877	0.3998	0.1849	1.927	1.691	0.0619	0.3338
2.20	0.4885	0.4015	0.1779	1.839	1.647	0.0644	0.3447
2.32	0.4894	0.4031	0.1717	1.761	1.606	0.0669	0.3540
2.44	0.4904	0.4047	0.1661	1.690	1.570	0.0693	0.3620
2.56	0.4916	0.4065	0.1611	1.627	1.536	0.0716	0.3690
2.68	0.4929	0.4078	0.1567	1.570	1.506	0.0739	0.3751
2.80	0.4943	0.4093	0.1527	1.518	1.477	0.0762	0.3806
2.92	0.4958	0.4109	0.1490	1.471	1.451	0.0783	0.3855
3.04	0.4974	0.4124	0.1457	1.428	1.427	0.0805	0.3900
3.16	0.4991	0.4139	0.1427	1.389	1.404	0.0826	0.3939
3.28	0.5008	0.4153	0.1399	1.352	1.383	0.0846	0.3997
3.40	0.5027	0.4168	0.1374	1.319	1.363	0.0867	0.3998
3.52	0.5046	0.4182	0.1351	1.287	1.345	0.0887	0.4029
3.64	0.5066	0.4197	0.1330	1.258	1.328	0.0907	0.4057
3.76	0.5087	0.4210	0.1310	1.232	1.312	0.0925	0.4076
3.88	0.5109	0.4224	0.1292	1.207	1.297	0.0944	0.4096
4.00	0.5131	0.4238	0.1275	1.184	1.283	0.0962	0.4116
4.00	0.5131	0.4238	0.1275	1.184	1.283	0.0962	0.4116
4.24	0.5178	0.4264	0.1245	1.142	1.257	0.0999	0.4151
4.48	0.5224	0.4289	0.1220	1.105	1.234	0.1033	0.4181
4.72	0.5274	0.4313	0.1198	1.073	1.215	0.1065	0.4207
4.96	0.5325	0.4335	0.1178	1.045	1.196	0.1095	0.4230
5.20	0.5377	0.4357	0.1162	1.020	1.179	0.1124	0.4250
5.44	0.5431	0.4377	0.1147	0.998	1.164	0.1151	0.4268
5.68	0.5486	0.4396	0.1134	0.979	1.151	0.1176	0.4284
5.92	0.5541	0.4412	0.1125	0.962	1.139	0.1198	0.4299
6.16	0.5598	0.4426	0.1113	0.947	1.128	0.1218	0.4312
6.40	0.5655	0.4438	0.1104	0.934	1.118	0.1237	0.4324
6.64	0.5713	0.4449	0.1096	0.923	1.109	0.1255	0.4335
6.88	0.5771	0.4460	0.1089	0.913	1.100	0.1269	0.4345
7.12	0.5830	0.4469	0.1083	0.904	1.093	0.1281	0.4354
7.36	0.5889	0.4474	0.1078	0.897	1.085	0.1291	0.4363
7.60	0.5949	0.4476	0.1073	0.891	1.079	0.1298	0.4371
7.84	0.6009	0.4470	0.1068	0.891	1.073	0.1295	0.4378
8.08	0.6069	0.4460	0.1065	0.892	1.068	0.1288	0.4385
8.32	0.6129	0.4444	0.1061	0.896	1.062	0.1276	0.4391
8.56	0.6190	0.4432	0.1058	0.902	1.058	0.1267	0.4397
8.80	0.6250	0.4396	0.1055	0.911	1.053	0.1254	0.4403
9.04	0.6311	0.4366	0.1053	0.922	1.050	0.1208	0.4408
9.28	0.6372	0.4329	0.1051	0.937	1.046	0.1171	0.4413
9.52	0.6433	0.4278	0.1049	0.957	1.042	0.1128	0.4418
9.76	0.6494	0.4196	0.1048	0.987	1.039	0.1071	0.4422
10.00	0.6556	0.4079	0.1046	1.035	1.037	0.0998	0.4426
10.24	0.6617	0.3886	0.1045	1.183	1.034	0.0884	0.4430
10.4282	0.6667	0.0000	0.1044	∞	1.032	0.0000	0.4433
		$\gamma = 5/3$		$M^2 = 60$			
1.0	0.4917	0.3813	0.3332	3.809	3.011	0.0887	0.0000
1.1	0.4915	0.3822	0.3047	3.477	2.869	0.0822	0.0779
1.2	0.4910	0.3851	0.2818	3.201	2.746	0.0405	0.1373
1.3	0.4908	0.3840	0.2628	2.967	2.638	0.0428	0.1863
1.4	0.4907	0.3848	0.2469	2.768	2.540	0.0451	0.2197
1.5	0.4906	0.3858	0.2328	2.596	2.454	0.0475	0.2686
1.6	0.4907	0.3867	0.2194	2.445	2.376	0.0494	0.2741
1.7	0.4908	0.3876	0.2082	2.313	2.305	0.0515	0.2945
1.8	0.4910	0.3886	0.1986	2.196	2.241	0.0536	0.3125
1.9	0.4913	0.3896	0.1903	2.091	2.182	0.0557	0.3288
2.0	0.4916	0.3904	0.1828	1.997	2.129	0.0577	0.3332
2.0	0.4916	0.3904	0.1828	1.997	2.129	0.0577	0.3332
2.2	0.4925	0.3922	0.1694	1.838	2.038	0.0615	0.3585
2.4	0.4937	0.3939	0.1586	1.702	1.962	0.0653	0.3787
2.6	0.4951	0.3957	0.1494	1.590	1.901	0.0690	0.3958
2.8	0.4968	0.3976	0.1417	1.496	1.848	0.0725	0.3955
3.0	0.4987	0.3995	0.1351	1.418	1.793	0.0760	0.4084
3.2	0.5009	0.4010	0.1294	1.341	1.715	0.0794	0.4154
3.4	0.5032	0.4027	0.1244	1.279	1.671	0.0827	0.4154
3.6	0.5057	0.4044	0.1201	1.224	1.632	0.0858	0.4200
3.8	0.5084	0.4060	0.1163	1.176	1.597	0.0888	0.4240
4.0	0.5113	0.4078	0.1129	1.133	1.565	0.0917	0.4276
4.0	0.5113	0.4078	0.1129	1.133	1.565	0.0917	0.4276
4.4	0.5174	0.4108	0.1071	1.059	1.511	0.0975	0.4332
4.8	0.5240	0.4135	0.1025	0.999	1.468	0.1028	0.4376
5.2	0.5310	0.4162	0.0987	0.950	1.432	0.1076	0.4411
5.6	0.5384	0.4186	0.0956	0.909	1.398	0.1120	0.4440
ξ	U	C	P/β	Q/β	γ	$P\Sigma^{\gamma}/\beta^{1-\gamma}$	F
		$\gamma = 5/3$		$M^2 = 60$			
6.0	0.5461	0.4207	0.0929	0.874	1.365	0.1162	0.4464
6.4	0.5541	0.4225	0.0905	0.845	1.341	0.1196	0.4484
6.8	0.5623	0.4239	0.0886	0.821	1.320	0.1228	0.4502
7.2	0.5707	0.4250	0.0869	0.802	1.302	0.1255	0.4517
7.6	0.5792	0.4257	0.0854	0.786	1.287	0.1276	0.4530
8.0	0.5878	0.4258	0.0841	0.774	1.275	0.1290	0.4542
8.4	0.5965	0.4253	0.0830	0.765	1.260	0.1297	0.4553
8.8	0.6054	0.4240	0.0820	0.760	1.249	0.1296	0.4562
9.2	0.6144	0.4220	0.0811	0.759	1.240	0.1286	0.4570
9.6	0.6234	0.4189	0.0802	0.762	1.232	0.1262	0.4578
10.0	0.6324	0.4139	0.0794	0.773	1.225	0.1220	0.4585
10.0	0.6324	0.4139	0.0794	0.773	1.225	0.1220	0.4585
10.2	0.6370	0.4104	0.0790	0.782	1.221	0.1190	0.4589
10.4	0.6416	0.4061	0.0786	0.795	1.218	0.1153	0.4592
10.6	0.6461	0.4008	0.0782	0.812	1.215	0.1107	0.4595
10.8	0.6507	0.3937	0.0778	0.837	1.212	0.1047	0.4598
11.0	0.6553	0.3838	0.0774	0.876	1.210	0.0965	0.4601
11.2	0.6600	0.3681	0.0770	0.947	1.208	0.0845	0.4604
11.4	0.6648	0.3328	0.0766	1.165	1.205	0.0604	0.4607
11.4898	0.6667	0.0000	0.0749	∞	1.204	0.0000	0.4609
		$\gamma = 5/3$		$M^2 = 75$			
1.0	0.4935	0.3796	0.3554	3.946	3.377	0.0952	0.0000
1.1	0.4930	0.3805	0.3243	3.607	3.218	0.0878	0.0801
1.2	0.4928	0.3810	0.2810	3.328	3.080	0.0590	0.1411
1.3	0.4926	0.3817	0.2613	2.989	2.958	0.0421	0.1862
1.4	0.4925	0.3822	0.2442	2.783	2.850	0.0445	0.2244
1.5	0.4925	0.3832	0.2289	2.610	2.753	0.0476	0.2549
1.6	0.4925	0.3839	0.2172	2.456	2.666	0.0486	0.2819
1.7	0.4927	0.3847	0.2060	2.320	2.587	0.0507	0.3027
1.8	0.4928	0.3854	0.1961	2.200	2.515	0.0527	0.3201
1.9	0.4931	0.3861	0.1875	2.094	2.449	0.0546	0.3340
2.0	0.4935	0.3869	0.1794	1.998	2.388	0.0566	0.3476
2.0	0.4935	0.3869	0.1794	1.998	2.388	0.0566	0.3476
2.2	0.4941	0.3885	0.1653	1.832	2.281	0.0604	0.3679
2.4	0.4951	0.3900	0.1541	1.696	2.194	0.0641	0.3835
2.6	0.4965	0.3912	0.1452	1.581	2.107	0.0677	0.3967
2.8	0.4977	0.3927	0.1372	1.485	2.036	0.0711	0.4065
3.0	0.4993	0.3941	0.1303	1.398	1.974	0.0745	0.4135
3.2	0.5011	0.3955	0.1243	1.324	1.919	0.0776	0.4201
3.4	0.5031	0.3969	0.1192	1.261	1.868	0.0810	0.4256
3.4	0.5031	0.3969	0.1192	1.261	1.868	0.0810	0.4256
3.6	0.5076	0.3998	0.1106	1.154	1.782	0.0871	0.4343
3.8	0.5126	0.4022	0.1038	1.069	1.712	0.0928	0.4407
4.0	0.5181	0.4047	0.0981	1.001	1.654	0.0982	0.4457
5.0	0.5841	0.4070	0.0859	0.844	1.805	0.1053	0.4497
5.4	0.5304	0.4091	0.0900	0.896	1.565	0.1081	0.4539
5.8	0.5371	0.4111	0.0849	0.858	1.527	0.1125	0.4566
6.2	0.5441	0.4128	0.0841	0.855	1.496	0.1164	0.4577
6.6	0.5515	0.4142	0.0818	0.795	1.469	0.1196	0.4596
7.0	0.5588	0.4154	0.0798	0.771	1.448	0.1231	0.4612
7.4	0.5665	0.4165	0.0780	0.750	1.425	0.1259	0.4626
7.8	0.5742	0.4168	0.0764	0.733	1.407	0.1283	0.4638
8.2	0.5821	0.4170	0.0750	0.719	1.390	0.1301	0.4649
8.6	0.5901	0.4169	0.0737	0.707	1.376	0.1314	0.4659
9.0	0.5982	0.4160	0.0726	0.699	1.365	0.1319	0.4668
9.4	0.6065	0.4145	0.0715	0.694	1.354	0.1315	0.4676
9.8	0.6148	0.4122	0.0705	0.692	1.344	0.1302	0.4683
10.2	0.6233	0.4089	0.0696	0.694	1.335	0.1279	0.4690
10.6	0.6316	0.4043	0.0688	0.701	1.328	0.1244	0.4696
11.0	0.6401	0.3976	0.0680	0.717	1.321	0.1186	0.4702
11.0	0.6401	0.3976	0.0680	0.717	1.321	0.1186	0.4702
11.2	0.6444	0.3931	0.0676	0.729	1.318	0.1145	0.4705
11.4	0.6487	0.3872	0.0672	0.747	1.316	0.1086	0.4707
11.6	0.6530	0.3798	0.0668	0.770	1.313	0.1023	0.4710
11.8	0.6573	0.3689	0.0664	0.813	1.310	0.0942	0.4712
12.0	0.6616	0.3484	0.0660	0.908	1.307	0.0754	0.4715
12.2	0.6660	0.2013	0.0656	2.898	1.305	0.0185	0.4719
12.2812	0.6667	0.0000	0.0656	∞	1.305	0.0000	0.4720
		$\gamma = 5/3$		$M^2 = 100$			
1.0	0.4950	0.3778	0.3527	3.884	3.913	0.0547	0.0000
1.1	0.4948	0.3784	0.3041	3.540	3.729	0.0370	0.0817
1.2	0.4946	0.3790	0.2803	3.254	3.569	0.0382	0.1439
1.3	0.4945	0.3795	0.2602	3.011	3.438	0.0414	0.1924
1.4	0.4944	0.3801	0.2430	2.803	3.305	0.0436	0.2308
1.5	0.4944	0.3806	0.2281	2.624	3.191	0.0457	0.2620
1.6	0.4944	0.3812	0.2151	2.468	3.090	0.0477	0.2876
1.7	0.4945	0.3818	0.2037	2.330	2.998	0.0497	0.3088
1.8	0.4946	0.3823	0.1936	2.207	2.914	0.0517	0.3265
1.9	0.4948	0.3829	0.1845	2.097	2.837	0.0537	0.3413
2.0	0.4950	0.3834	0.1763	1.999	2.767	0.0556	0.3541
2.0	0.4950	0.3834	0.1763	1.999	2.767	0.0556	0.3541
2.2	0.4953	0.3845	0.1623	1.839	2.641	0.0593	0.3742
2.4	0.4958	0.3856	0.1507	1.709	2.533	0.0629	0.3897
2.6	0.4965	0.3867	0.1410	1.601	2.438	0.0664	0.4021
2.8	0.4974	0.3878	0.1327	1.471	2.355	0.0698	0.4130
3.0	0.4987	0.3889	0.1257	1.384	2.281	0.0731	0.4210

TABLE I

Physical Properties of the Expanding Field of Flow behind Shock Waves of Different Strengths

ξ	U	C	P/β	Q/β	γ	PQ^γ/β^γ	F
		γ = 5/3		M² = 100			
3.2	0.5011	0.3900	0.1195	1.801	2.215	0.0784	0.4277
3.4	0.5027	0.3911	0.1139	1.841	2.155	0.0795	0.4292
3.4	0.5027	0.3911	0.1139	1.841	2.155	0.0795	0.4292
3.8	0.5063	0.3931	0.1048	1.920	2.053	0.0815	0.4418
4.2	0.5104	0.3951	0.0976	1.982	1.969	0.0812	0.4462
4.6	0.5149	0.3971	0.0918	0.970	1.898	0.0966	0.4532
5.0	0.5198	0.3989	0.0870	0.911	1.839	0.1016	0.4571
5.4	0.5251	0.4006	0.0830	0.862	1.786	0.1063	0.4605
5.8	0.5307	0.4021	0.0796	0.820	1.742	0.1106	0.4629
6.2	0.5366	0.4035	0.0768	0.783	1.704	0.1150	0.4650
6.6	0.5428	0.4047	0.0740	0.755	1.670	0.1189	0.4668
7.0	0.5492	0.4058	0.0718	0.727	1.641	0.1222	0.4684
7.4	0.5557	0.4067	0.0698	0.704	1.615	0.1254	0.4697
7.8	0.5624	0.4074	0.0680	0.685	1.592	0.1284	0.4709
8.2	0.5692	0.4079	0.0664	0.665	1.572	0.1311	0.4719
8.6	0.5763	0.4081	0.0650	0.650	1.553	0.1335	0.4729
9.0	0.5834	0.4079	0.0637	0.638	1.537	0.1348	0.4736
9.4	0.5908	0.4073	0.0625	0.628	1.523	0.1357	0.4744
9.8	0.5980	0.4065	0.0614	0.620	1.510	0.1362	0.4751
10.2	0.6054	0.4049	0.0604	0.614	1.498	0.1362	0.4757
10.6	0.6129	0.4030	0.0594	0.610	1.488	0.1364	0.4763
11.0	0.6205	0.4004	0.0585	0.609	1.479	0.1338	0.4768
11.4	0.6281	0.3967	0.0576	0.610	1.471	0.1313	0.4773
11.8	0.6358	0.3916	0.0568	0.617	1.463	0.1270	0.4777
12.2	0.6436	0.3839	0.0560	0.628	1.457	0.1200	0.4781
12.6	0.6514	0.3729	0.0552	0.662	1.451	0.1098	0.4785
13.0	0.6595	0.3525	0.0544	0.730	1.445	0.0919	0.4789
13.3767	0.6667	0.0000	0.0537	∞	1.440	0.0000	0.4792
		γ = 5/3		M² = 200			
1.0	0.4975	0.3752	0.3520	3.942	5.592	0.0898	0.0000
1.1	0.4974	0.3754	0.3243	3.797	5.302	0.0860	0.0849
1.2	0.4973	0.3756	0.2998	3.305	5.076	0.0882	0.1684
1.3	0.4972	0.3759	0.2689	3.052	4.875	0.0805	0.1984
1.4	0.4972	0.3762	0.2409	2.835	4.698	0.0694	0.2281
1.5	0.4972	0.3765	0.2253	2.646	4.539	0.0445	0.2701
1.6	0.4972	0.3768	0.2116	2.482	4.395	0.0465	0.2922
1.7	0.4972	0.3771	0.1995	2.337	4.264	0.0455	0.3180
1.8	0.4973	0.3774	0.1889	2.210	4.144	0.0504	0.3362
1.9	0.4974	0.3777	0.1797	2.099	4.054	0.0522	0.3616
2.0	0.4975	0.3780	0.1717	2.001	3.953	0.0540	0.3848
2.0	0.4976	0.3780	0.1717	2.001	3.953	0.0540	0.3848
2.2	0.4976	0.3784	0.1569	1.825	3.752	0.0576	0.3960
2.4	0.4983	0.3789	0.1448	1.679	3.595	0.0810	0.4021
2.6	0.4988	0.3794	0.1348	1.557	3.468	0.0844	0.4147
2.8	0.4994	0.3800	0.1262	1.453	3.367	0.0877	0.4248
3.0	0.5001	0.3805	0.1186	1.362	3.226	0.0709	0.4330
3.2	0.5008	0.3811	0.1116	1.281	3.120	0.0740	0.4397
3.4	0.5016	0.3817	0.1068	1.210	3.041	0.0770	0.4453
3.6	0.5025	0.3824	0.1006	1.147	2.981	0.0800	0.4500
3.8	0.5034	0.3830	0.0961	1.092	2.938	0.0829	0.4540
4.0	0.5043	0.3837	0.0924	1.046	2.912	0.0857	0.4574
4.0	0.5043	0.3837	0.0924	1.046	2.912	0.0857	0.4574
4.5	0.5079	0.3860	0.0838	0.942	2.877	0.0938	0.4642
5.0	0.5115	0.3882	0.0770	0.861	2.857	0.0999	0.4691
5.5	0.5155	0.3874	0.0715	0.795	2.847	0.1049	0.4728
6.0	0.5199	0.3885	0.0670	0.740	2.873	0.1107	0.4757
6.5	0.5246	0.3895	0.0632	0.694	2.801	0.1162	0.4780
7.0	0.5305	0.3904	0.0599	0.655	2.828	0.1214	0.4799
7.5	0.5349	0.3915	0.0571	0.621	2.185	0.1294	0.4815
8.0	0.5404	0.3921	0.0547	0.591	2.136	0.1314	0.4828
8	0.5404	0.3921	0.0547	0.591	2.136	0.1314	0.4828
9	0.5522	0.3930	0.0507	0.547	2.068	0.1396	0.4848
10	0.5647	0.3932	0.0475	0.512	1.996	0.1450	0.4864
11	0.5778	0.3925	0.0449	0.485	1.948	0.1499	0.4876
12	0.5913	0.3906	0.0427	0.466	1.909	0.1525	0.4886
13	0.6053	0.3872	0.0408	0.454	1.877	0.1522	0.4894
14	0.6197	0.3816	0.0391	0.449	1.852	0.1485	0.4900
15	0.6344	0.3728	0.0376	0.451	1.831	0.1418	0.4905
15.0	0.6344	0.3728	0.0376	0.451	1.831	0.1418	0.4905
15.5	0.6419	0.3656	0.0369	0.460	1.823	0.1348	0.4908
16.0	0.6494	0.3563	0.0363	0.479	1.815	0.1259	0.4910
16.5	0.6570	0.3396	0.0354	0.512	1.806	0.1080	0.4912
17.0	0.6647	0.2985	0.0345	0.645	1.802	0.0717	0.4915
17.1948	0.6667	0.0000	0.0343	∞	1.801	0.0000	0.4916
		γ = 5/3		M² = 300			
1.0	0.4983	0.3744	0.3351	3.980	6.680	0.0838	0.0000
1.1	0.4983	0.3746	0.3054	3.804	6.602	0.0858	0.0849
1.2	0.4982	0.3748	0.2788	3.308	6.284	0.0880	0.1686
1.3	0.4982	0.3750	0.2577	3.055	5.980	0.0401	0.1988
1.4	0.4981	0.3752	0.2397	2.839	5.782	0.0421	0.2286
1.5	0.4981	0.3754	0.2242	2.652	5.586	0.0441	0.2720
1.6	0.4981	0.3755	0.2108	2.489	5.389	0.0460	0.2984
1.7	0.4981	0.3757	0.1986	2.348	5.229	0.0479	0.3203
1.8	0.4981	0.3759	0.1881	2.218	5.082	0.0498	0.3397
1.9	0.4983	0.3761	0.1785	2.105	4.948	0.0517	0.3545
2.0	0.4984	0.3763	0.1699	2.000	4.823	0.0535	0.3676
ξ	U	C	P/β	Q/β	γ	PQ^γ/β^γ	F
		γ = 5/3		M² = 300			
2.0	0.4984	0.3763	0.1699	2.000	4.823	0.0535	0.3676
2.2	0.4985	0.3767	0.1552	1.825	4.601	0.0570	0.3869
2.4	0.4989	0.3771	0.1429	1.678	4.407	0.0604	0.4052
2.6	0.4992	0.3774	0.1325	1.551	4.237	0.0637	0.4179
2.8	0.4996	0.3778	0.1236	1.444	4.086	0.0670	0.4280
3.0	0.5001	0.3782	0.1159	1.351	3.951	0.0702	0.4362
3.2	0.5006	0.3786	0.1092	1.270	3.830	0.0733	0.4439
3.4	0.5012	0.3790	0.1033	1.199	3.720	0.0765	0.4485
3.6	0.5019	0.3793	0.0981	1.136	3.620	0.0792	0.4532
3.8	0.5026	0.3797	0.0935	1.081	3.529	0.0821	0.4572
4.0	0.5034	0.3800	0.0893	1.031	3.445	0.0849	0.4606
4.0	0.5034	0.3800	0.0893	1.031	3.445	0.0849	0.4606
4.5	0.5056	0.3809	0.0806	0.935	3.302	0.0917	0.4675
5.0	0.5081	0.3818	0.0736	0.861	3.211	0.0983	0.4721
5.5	0.5110	0.3828	0.0678	0.771	2.982	0.1048	0.4757
6.0	0.5141	0.3834	0.0631	0.713	2.872	0.1104	0.4785
6.5	0.5176	0.3842	0.0592	0.665	2.778	0.1158	0.4806
7.0	0.5212	0.3850	0.0559	0.629	2.696	0.1210	0.4822
7	0.5212	0.3850	0.0559	0.629	2.696	0.1210	0.4822
8	0.5293	0.3861	0.0505	0.564	2.561	0.1312	0.4849
9	0.5382	0.3870	0.0463	0.515	2.456	0.1400	0.4868
10	0.5477	0.3876	0.0430	0.477	2.370	0.1477	0.4882
11	0.5579	0.3877	0.0404	0.447	2.302	0.1545	0.4893
12	0.5686	0.3872	0.0381	0.423	2.248	0.1598	0.4902
13	0.5796	0.3861	0.0362	0.404	2.200	0.1640	0.4909
14	0.5910	0.3842	0.0345	0.389	2.162	0.1666	0.4915
15	0.6028	0.3812	0.0330	0.378	2.130	0.1670	0.4920
16	0.6148	0.3770	0.0317	0.372	2.104	0.1648	0.4924
16.0	0.6148	0.3770	0.0317	0.372	2.104	0.1648	0.4924
16.5	0.6209	0.3739	0.0311	0.372	2.092	0.1627	0.4926
17.0	0.6271	0.3705	0.0305	0.371	2.082	0.1593	0.4928
17.5	0.6334	0.3667	0.0299	0.373	2.072	0.1547	0.4929
18.0	0.6397	0.3617	0.0293	0.377	2.064	0.1487	0.4931
18.5	0.6461	0.3519	0.0287	0.385	2.058	0.1409	0.4933
19.0	0.6525	0.3418	0.0281	0.401	2.049	0.1289	0.4934
19.0	0.6525	0.3418	0.0281	0.401	2.049	0.1289	0.4934
19.1	0.6539	0.3395	0.0280	0.406	2.047	0.1263	0.4934
19.2	0.6552	0.3368	0.0279	0.410	2.045	0.1233	0.4934
19.3	0.6565	0.3338	0.0277	0.416	2.044	0.1198	0.4935
19.4	0.6577	0.3303	0.0276	0.423	2.043	0.1158	0.4935
19.5	0.6590	0.3262	0.0275	0.432	2.042	0.1114	0.4935
19.6	0.6603	0.3213	0.0274	0.443	2.041	0.1064	0.4935
19.7	0.6616	0.3153	0.0273	0.458	2.040	0.1003	0.4936
19.8	0.6629	0.3077	0.0272	0.480	2.039	0.0924	0.4936
19.9	0.6643	0.2963	0.0271	0.515	2.038	0.0819	0.4937
20.0	0.6656	0.2771	0.0269	0.584	2.037	0.0659	0.4937
20.0822	0.6667	0.0000	0.0267	∞	2.036	0.0000	0.4938
		γ = 5/3		M² = 500			
1.00	0.4990	0.3737	0.3322	3.976	8.921	0.0834	0.0000
1.06	0.4990	0.3738	0.3146	3.752	8.647	0.0847	0.0843
1.12	0.4989	0.3739	0.2980	3.552	8.324	0.0860	0.1001
1.18	0.4989	0.3739	0.2830	3.372	8.119	0.0873	0.1291
1.24	0.4989	0.3740	0.2694	3.210	7.920	0.0886	0.1728
1.30	0.4989	0.3740	0.2571	3.063	7.736	0.0896	0.2016
1.36	0.4989	0.3741	0.2460	2.929	7.565	0.0410	0.2286
1.42	0.4989	0.3742	0.2358	2.806	7.401	0.0422	0.2489
1.48	0.4989	0.3743	0.2264	2.693	7.249	0.0434	0.2684
1.54	0.4989	0.3743	0.2177	2.589	7.107	0.0446	0.2856
1.60	0.4989	0.3744	0.2097	2.494	6.973	0.0457	0.3010
1.60	0.4989	0.3744	0.2097	2.494	6.973	0.0457	0.3010
1.72	0.4989	0.3745	0.1954	2.321	6.725	0.0480	0.3270
1.84	0.4989	0.3746	0.1829	2.171	6.502	0.0502	0.3481
1.96	0.4990	0.3748	0.1720	2.041	6.301	0.0525	0.3654
2.08	0.4991	0.3749	0.1625	1.926	6.118	0.0544	0.3798
2.20	0.4991	0.3750	0.1538	1.822	5.949	0.0564	0.3920
2.32	0.4992	0.3752	0.1459	1.728	5.795	0.0586	0.4025
2.44	0.4993	0.3753	0.1390	1.644	5.660	0.0606	0.4111
2.56	0.4995	0.3755	0.1328	1.569	5.519	0.0626	0.4187
2.56	0.4995	0.3755	0.1328	1.569	5.519	0.0626	0.4187
2.80	0.4998	0.3758	0.1218	1.438	5.280	0.0665	0.4311
3.04	0.5002	0.3760	0.1128	1.327	5.071	0.0705	0.4407
3.28	0.5006	0.3763	0.1048	1.230	4.886	0.0740	0.4483
3.52	0.5010	0.3766	0.0981	1.151	4.723	0.0775	0.4544
3.76	0.5015	0.3768	0.0922	1.081	4.572	0.0809	0.4595
4.00	0.5021	0.3771	0.0869	1.020	4.437	0.0841	0.4634
4.24	0.5027	0.3774	0.0823	0.966	4.315	0.0873	0.4669
4.48	0.5034	0.3777	0.0783	0.917	4.204	0.0905	0.4698
4.72	0.5042	0.3780	0.0747	0.872	4.103	0.0775	0.4723
4.96	0.5050	0.3782	0.0713	0.831	4.008	0.0970	0.4745
5.20	0.5059	0.3784	0.0682	0.794	3.921	0.1002	0.4764
5.44	0.5068	0.3787	0.0654	0.760	3.841	0.1033	0.4780
5.68	0.5077	0.3789	0.0629	0.730	3.766	0.1065	0.4794
5.92	0.5086	0.3792	0.0606	0.704	3.696	0.1091	0.4807
6.16	0.5096	0.3794	0.0585	0.681	3.630	0.1117	0.4818
6.40	0.5107	0.3796	0.0571	0.660	3.569	0.1142	0.4828
6.64	0.5118	0.3799	0.0555	0.639	3.511	0.1167	0.4837
6.88	0.5130	0.3801	0.0535	0.619	3.457	0.1192	0.4845
7.12	0.5142	0.3803	0.0519	0.599	3.406	0.1220	0.4852
7.36	0.5154	0.3805	0.0505	0.580	3.358	0.1247	0.4859
7.60	0.5167	0.3807	0.0490	0.563	3.315	0.1276	0.4865
7.84	0.5180	0.3809	0.0478	0.548	3.270	0.1303	0.4871

TABLE I

Physical Properties of the Expanding Field of Flow behind Shock Waves of Different Strengths

ξ	U	C	P/β	Q/β	γ	$PQ^{\gamma}/\beta^{1-\gamma}$	F
		$\gamma = 5/3$		$M^0 = 500$			
7.84	0.5180	0.3809	0.0478	0.548	3.270	0.1303	0.4871
8.80	0.5236	0.3817	0.0433	0.496	3.130	0.1295	0.4882
9.76	0.5286	0.3823	0.0399	0.456	2.998	0.1482	0.4902
10.72	0.5265	0.3838	0.0371	0.422	2.827	0.1585	0.4912
11.68	0.5438	0.3830	0.0348	0.396	2.812	0.1636	0.4920
12.64	0.5510	0.3850	0.0328	0.373	2.740	0.1700	0.4926
13.60	0.5568	0.3858	0.0311	0.354	2.679	0.1767	0.4931
14.56	0.5669	0.3822	0.0296	0.338	2.627	0.1806	0.4936
15.52	0.5763	0.3815	0.0283	0.324	2.582	0.1846	0.4940
16.48	0.5839	0.3799	0.0271	0.313	2.543	0.1876	0.4944
17.44	0.5927	0.3779	0.0261	0.305	2.509	0.1923	0.4947
18.40	0.6017	0.3754	0.0252	0.298	2.479	0.1960	0.4949
19.36	0.6109	0.3721	0.0243	0.293	2.454	0.1980	0.4951
20.32	0.6208	0.3676	0.0235	0.290	2.433	0.1846	0.4953
21.28	0.6298	0.3614	0.0227	0.290	2.414	0.1767	0.4955
22.24	0.6395	0.3531	0.0219	0.293	2.397	0.1694	0.4957
22.24	0.6395	0.3531	0.0219	0.293	2.397	0.1694	0.4957
22.48	0.6420	0.3507	0.0217	0.294	2.394	0.1669	0.4957
22.72	0.6444	0.3477	0.0215	0.296	2.390	0.1635	0.4958
22.96	0.6469	0.3444	0.0213	0.299	2.387	0.1593	0.4958
23.20	0.6494	0.3407	0.0211	0.304	2.383	0.1544	0.4959
23.44	0.6518	0.3365	0.0209	0.309	2.380	0.1489	0.4960
23.68	0.6544	0.3313	0.0207	0.314	2.377	0.1435	0.4960
23.92	0.6569	0.3246	0.0205	0.325	2.374	0.1344	0.4960
24.16	0.6594	0.3158	0.0203	0.339	2.372	0.1227	0.4961
24.40	0.6620	0.3038	0.0201	0.363	2.369	0.1091	0.4961
24.64	0.6645	0.2853	0.0199	0.407	2.366	0.0890	0.4962
24.8411	0.6667	0.0000	0.0197	∞	2.365	0.0000	0.4962
		$\gamma = 7/5$		$M^0 = 100$			
1.0	0.5280	0.3328	0.3660	4.808	3.960	0.0287	0.0000
1.1	0.5281	0.3276	0.3194	4.204	3.782	0.0371	0.1139
1.2	0.5243	0.3423	0.2910	3.725	3.590	0.0405	0.1962
1.3	0.5227	0.3469	0.2678	3.337	3.438	0.0439	0.2694
1.4	0.5212	0.3514	0.2485	3.018	3.304	0.0474	0.3124
1.5	0.5198	0.3556	0.2322	2.751	3.184	0.0509	0.3520
1.6	0.5186	0.3601	0.2184	2.528	3.075	0.0544	0.3840
1.7	0.5175	0.3643	0.2065	2.334	2.977	0.0574	0.4103
1.8	0.5165	0.3684	0.1961	2.167	2.887	0.0615	0.4321
1.9	0.5156	0.3724	0.1870	2.022	2.806	0.0660	0.4505
2.0	0.5148	0.3763	0.1790	1.896	2.730	0.0686	0.4661
2.0	0.5148	0.3763	0.1790	1.896	2.730	0.0686	0.4661
2.2	0.5135	0.3838	0.1656	1.685	2.596	0.0767	0.4910
2.4	0.5125	0.3911	0.1546	1.515	2.481	0.0829	0.5098
2.6	0.5118	0.3981	0.1457	1.378	2.381	0.0900	0.5244
2.8	0.5113	0.4047	0.1383	1.266	2.292	0.0971	0.5363
3.0	0.5110	0.4110	0.1320	1.172	2.213	0.1040	0.5455
3.2	0.5110	0.4171	0.1268	1.092	2.142	0.1109	0.5533
3.4	0.5111	0.4229	0.1219	1.025	2.078	0.1178	0.5598
3.6	0.5114	0.4284	0.1178	0.963	2.021	0.1246	0.5653
3.8	0.5118	0.4337	0.1142	0.911	1.969	0.1315	0.5700
4.0	0.5124	0.4388	0.1110	0.865	1.922	0.1380	0.5741
4.0	0.5124	0.4388	0.1110	0.865	1.922	0.1380	0.5741
4.4	0.5139	0.4484	0.1056	0.786	1.837	0.1510	0.5809
4.8	0.5156	0.4572	0.1012	0.726	1.765	0.1637	0.5862
5.2	0.5177	0.4654	0.0976	0.676	1.703	0.1760	0.5906
5.6	0.5202	0.4732	0.0946	0.635	1.649	0.1878	0.5938
6.0	0.5229	0.4805	0.0920	0.598	1.601	0.1991	0.5965
6.4	0.5257	0.4871	0.0896	0.568	1.559	0.2100	0.5989
6.8	0.5287	0.4931	0.0879	0.542	1.521	0.2204	0.6009
7.2	0.5319	0.4982	0.0862	0.520	1.487	0.2299	0.6027
7.6	0.5352	0.5029	0.0847	0.501	1.456	0.2389	0.6042
8.0	0.5386	0.5079	0.0834	0.485	1.428	0.2469	0.6056
8.0	0.5386	0.5079	0.0834	0.485	1.428	0.2469	0.6056
8.8	0.5457	0.5157	0.0812	0.458	1.380	0.2620	0.6079
9.6	0.5531	0.5217	0.0795	0.438	1.339	0.2743	0.6097
10.4	0.5607	0.5259	0.0780	0.423	1.304	0.2835	0.6112
11.2	0.5685	0.5286	0.0768	0.413	1.274	0.2898	0.6124
12.0	0.5765	0.5294	0.0758	0.406	1.248	0.2928	0.6143
12.8	0.5848	0.5284	0.0749	0.403	1.226	0.2928	0.6151
13.6	0.5933	0.5254	0.0741	0.404	1.206	0.2891	0.6151
14.4	0.6011	0.5205	0.0734	0.408	1.188	0.2820	0.6158
15.2	0.6095	0.5126	0.0728	0.416	1.172	0.2713	0.6164
16.0	0.6179	0.5020	0.0723	0.430	1.158	0.2568	0.6169
16.8	0.6264	0.4880	0.0718	0.453	1.146	0.2380	0.6174
17.6	0.6349	0.4694	0.0714	0.487	1.135	0.2101	0.6178
18.4	0.6435	0.4445	0.0710	0.539	1.125	0.1769	0.6182
19.2	0.6521	0.4030	0.0706	0.652	1.116	0.1341	0.6186
20.0	0.6607	0.3339	0.0701	0.945	1.108	0.0765	0.6190
20.5666	0.6667	0.0000	0.0698	∞	1.103	0.0000	0.6192

ξ	U	C	P/β	Q/β	γ	$PQ^{\gamma}/\beta^{1-\gamma}$	F
		$\gamma = 3/2$		$M^0 = 200$			
1.0	0.5807	0.3897	0.3552	4.902	5.629	0.0327	0.0000
1.1	0.5888	0.3548	0.3185	4.277	5.348	0.0360	0.1175
1.2	0.5871	0.3395	0.2891	3.784	5.104	0.0393	0.2042
1.3	0.5856	0.3427	0.2650	3.386	4.890	0.0428	0.2701
1.4	0.5841	0.3467	0.2450	3.058	4.699	0.0459	0.3215
1.6	0.5827	0.3505	0.2281	2.786	4.527	0.0491	0.3619
1.6	0.5814	0.3542	0.2137	2.554	4.372	0.0524	0.3947
1.7	0.5802	0.3579	0.2013	2.357	4.232	0.0556	0.4216
1.8	0.5191	0.3615	0.1906	2.187	4.104	0.0588	0.4437
1.9	0.5181	0.3649	0.1810	2.039	3.988	0.0621	0.4623
2.0	0.5171	0.3683	0.1726	1.909	3.878	0.0654	0.4781
2.0	0.5171	0.3683	0.1726	1.909	3.878	0.0654	0.4781
2.2	0.5153	0.3747	0.1584	1.682	3.685	0.0720	0.5032
2.4	0.5137	0.3809	0.1468	1.519	3.517	0.0785	0.5221
2.6	0.5125	0.3869	0.1374	1.377	3.370	0.0850	0.5368
2.8	0.5111	0.3927	0.1294	1.259	3.240	0.0916	0.5484
3.0	0.5101	0.3982	0.1226	1.160	3.124	0.0981	0.5578
3.2	0.5092	0.4035	0.1166	1.078	3.019	0.1046	0.5655
3.4	0.5084	0.4087	0.1117	1.005	2.924	0.1112	0.5719
3.6	0.5076	0.4138	0.1075	0.940	2.839	0.1177	0.5773
3.8	0.5073	0.4187	0.1034	0.885	2.760	0.1242	0.5819
4.0	0.5068	0.4235	0.0999	0.835	2.688	0.1309	0.5858
4.0	0.5068	0.4235	0.0999	0.835	2.688	0.1309	0.5858
4.4	0.5065	0.4328	0.0940	0.758	2.560	0.1439	0.5922
4.8	0.5060	0.4416	0.0892	0.698	2.450	0.1570	0.5971
5.2	0.5060	0.4500	0.0852	0.651	2.354	0.1701	0.6010
5.6	0.5062	0.4582	0.0818	0.614	2.269	0.1833	0.6042
6.0	0.5067	0.4662	0.0789	0.584	2.194	0.1966	0.6068
6.4	0.5074	0.4738	0.0764	0.560	2.127	0.2097	0.6090
6.8	0.5082	0.4811	0.0743	0.541	2.067	0.2229	0.6108
7.2	0.5092	0.4883	0.0724	0.526	2.013	0.2359	0.6124
7.6	0.5103	0.4954	0.0707	0.512	1.965	0.2489	0.6138
8.0	0.5115	0.5022	0.0692	0.502	1.918	0.2617	0.6150
8	0.5115	0.502	0.0692	0.412	1.918	0.262	0.6150
9	0.5150	0.518	0.0661	0.389	1.821	0.295	0.6174
10	0.5191	0.533	0.0637	0.374	1.741	0.328	0.6192
11	0.5235	0.548	0.0618	0.365	1.674	0.361	0.6206
12	0.5282	0.562	0.0603	0.358	1.617	0.394	0.6217
13	0.5333	0.575	0.0590	0.355	1.569	0.427	0.6226
14	0.5385	0.588	0.0580	0.351	1.528	0.460	0.6233
15	0.5439	0.600	0.0572	0.348	1.490	0.492	0.6239
16	0.5495	0.611	0.0565	0.347	1.457	0.524	0.6244
17	0.5552	0.622	0.0559	0.347	1.428	0.557	0.6249
18	0.5610	0.634	0.0554	0.347	1.402	0.590	0.6253
19	0.5668	0.645	0.0549	0.348	1.379	0.623	0.6257
20	0.5727	0.655	0.0545	0.349	1.358	0.656	0.6260
21	0.5787	0.665	0.0541	0.354	1.339	0.689	0.6263
22	0.5848	0.675	0.0538	0.357	1.322	0.722	0.6266
23	0.5909	0.684	0.0535	0.361	1.306	0.755	0.6268
24	0.5970	0.693	0.0533	0.366	1.292	0.787	0.6270
25	0.6032	0.701	0.0530	0.371	1.279	0.819	0.6272
26	0.6094	0.709	0.0528	0.377	1.267	0.850	0.6274
27	0.6156	0.717	0.0526	0.383	1.256	0.880	0.6276
28	0.6218	0.725	0.0524	0.389	1.246	0.910	0.6277
29	0.6281	0.732	0.0523	0.396	1.237	0.939	0.6278
30	0.6343	0.740	0.0522	0.403	1.228	0.968	0.6280
31	0.6406	0.747	0.0521	0.410	1.220	0.996	0.6281
32	0.6469	0.754	0.0520	0.417	1.213	1.023	0.6282
33	0.6532	0.762	0.0519	0.424	1.206	1.050	0.6283
34	0.6595	0.775	0.0518	0.429	1.200	1.118	0.6284
35.1259	0.6667	0.000	0.0517	∞	1.192	0.000	0.6285
		$\gamma = 7/5$		$M^0 = 500$			
1.00	0.5325	0.3278	0.3564	4.961	8.927	0.0322	0.0000
1.02	0.5319	0.3287	0.3472	4.819	8.832	0.0328	0.0272
1.04	0.5315	0.3296	0.3394	4.696	8.740	0.0335	0.0528
1.06	0.5312	0.3305	0.3319	4.589	8.652	0.0341	0.0765
1.08	0.5309	0.3313	0.3248	4.497	8.566	0.0348	0.0989
1.10	0.5305	0.3322	0.3180	4.321	8.483	0.0354	0.1200
1.12	0.5302	0.3331	0.3114	4.211	8.402	0.0360	0.1398
1.14	0.5298	0.3339	0.3052	4.106	8.322	0.0367	0.1585
1.16	0.5295	0.3347	0.2992	4.008	8.245	0.0373	0.1761
1.18	0.5292	0.3356	0.2934	3.909	8.170	0.0380	0.1927
1.20	0.5289	0.3364	0.2879	3.817	8.097	0.0386	0.2084
1.20	0.5289	0.3364	0.2879	3.817	8.097	0.0386	0.2084
1.25	0.5281	0.3384	0.2760	3.603	7.921	0.0402	0.2442
1.30	0.5273	0.3404	0.2654	3.410	7.758	0.0418	0.2765
1.35	0.5266	0.3423	0.2557	3.235	7.601	0.0434	0.3051
1.40	0.5259	0.3442	0.2469	3.076	7.454	0.0450	0.3304
1.45	0.5252	0.3461	0.2390	2.930	7.314	0.0467	0.3524
1.50	0.5245	0.3479	0.2317	2.797	7.182	0.0483	0.3719
1.55	0.5238	0.3497	0.2251	2.674	7.057	0.0499	0.3894
1.60	0.5232	0.3515	0.2190	2.561	6.937	0.0515	0.4051
1.65	0.5226	0.3533	0.2045	2.457	6.823	0.0531	0.4195
1.70	0.5220	0.3550	0.1983	2.360	6.714	0.0547	0.4326
1.75	0.5214	0.3567	0.1926	2.270	6.610	0.0563	0.4449
1.80	0.5209	0.3584	0.1873	2.187	6.511	0.0579	0.4516
1.8	0.5209	0.3584	0.1873	2.187	6.511	0.0579	0.4516
1.9	0.5198	0.3617	0.1776	2.032	6.324	0.0611	0.4704
2.0	0.5188	0.3649	0.1690	1.904	6.152	0.0643	0.4865

TABLE I

Physical Properties of the Expanding Field of Flow behind Shock Waves of Different Strengths

ξ	U	C	P/β	Ω/β	γ	$P\Omega^{\gamma}/\beta^{\gamma}$	F
		$\gamma = 3/2$		$M^2 = 500$			
2.1	0.5179	0.3680	0.1814	1.787	5.998	0.0675	0.4999
2.2	0.5169	0.3711	0.1545	1.685	5.844	0.0708	0.5116
2.3	0.5160	0.3741	0.1485	1.590	5.706	0.0740	0.5218
2.4	0.5151	0.3770	0.1427	1.506	5.576	0.0772	0.5307
2.4	0.5151	0.3770	0.1427	1.506	5.576	0.0772	0.5307
2.5	0.5135	0.3827	0.1320	1.362	5.341	0.0837	0.5454
2.6	0.5121	0.3881	0.1249	1.243	5.132	0.0901	0.5570
2.7	0.5108	0.3934	0.1179	1.143	4.946	0.0965	0.5663
2.8	0.5096	0.3985	0.1119	1.057	4.778	0.1030	0.5739
3.4	0.5046	0.4234	0.1087	0.894	4.238	0.1093	0.5802
3.5	0.5079	0.4282	0.1021	0.923	4.487	0.1187	0.5865
3.6	0.5057	0.4129	0.0981	0.864	4.359	0.1222	0.5900
4.0	0.5068	0.4174	0.0945	0.814	4.241	0.1287	0.5939
4.2	0.5051	0.4218	0.0913	0.770	4.135	0.1351	0.5972
4.4	0.5044	0.4261	0.0884	0.731	4.052	0.1416	0.6002
4.6	0.5039	0.4303	0.0858	0.695	3.959	0.1481	0.6028
4.8	0.5032	0.4344	0.0834	0.663	3.862	0.1545	0.6051
5.0	0.5027	0.4384	0.0812	0.634	3.770	0.1608	0.6071
5.0	0.5027	0.4384	0.0812	0.634	3.770	0.1608	0.6071
5.5	0.5017	0.4480	0.0765	0.572	3.587	0.1769	0.6115
6.0	0.5009	0.4573	0.0726	0.521	3.439	0.1931	0.6145
6.5	0.5004	0.4661	0.0694	0.479	3.291	0.2093	0.6171
7.0	0.5001	0.4745	0.0667	0.444	3.169	0.2255	0.6192
7.5	0.4999	0.4826	0.0643	0.414	3.061	0.2417	0.6209
8.0	0.4999	0.4905	0.0623	0.388	2.964	0.2578	0.6223
8.5	0.5000	0.4981	0.0605	0.366	2.876	0.2737	0.6235
9.0	0.5003	0.5055	0.0589	0.346	2.797	0.2896	0.6245
9.5	0.5007	0.5128	0.0575	0.328	2.725	0.3055	0.6254
10.0	0.5011	0.5198	0.0563	0.313	2.657	0.3215	0.6262
10	0.5011	0.5198	0.0563	0.313	2.657	0.321	0.6262
11	0.5035	0.5329	0.0542	0.286	2.540	0.354	0.6276
12	0.5058	0.5458	0.0524	0.264	2.439	0.386	0.6285
13	0.5065	0.5576	0.0509	0.245	2.351	0.418	0.6295
14	0.5076	0.5690	0.0497	0.230	2.275	0.450	0.6300
15	0.5096	0.5800	0.0486	0.217	2.207	0.482	0.6306
16	0.5118	0.5909	0.0476	0.205	2.146	0.513	0.6311
18	0.5118	0.5909	0.0476	0.205	2.146	0.513	0.6311
19	0.5167	0.6109	0.0461	0.186	2.042	0.575	0.6319
20	0.5220	0.6294	0.0449	0.170	1.957	0.641	0.6325
22	0.5276	0.6469	0.0439	0.157	1.886	0.706	0.6330
24	0.5334	0.6639	0.0431	0.147	1.826	0.765	0.6334
26	0.5394	0.6805	0.0424	0.138	1.774	0.818	0.6337
28	0.5456	0.6961	0.0419	0.130	1.729	0.894	0.6339
30	0.5519	0.7103	0.0414	0.123	1.690	0.960	0.6341
30	0.5519	0.710	0.0414	0.123	1.690	0.96	0.6341
34	0.5647	0.727	0.0406	0.112	1.624	1.08	0.6345
38	0.5779	0.759	0.0400	0.104	1.572	1.19	0.6348
42	0.5913	0.778	0.0396	0.097	1.530	1.29	0.6350
46	0.6048	0.794	0.0392	0.092	1.496	1.39	0.6352
50	0.6185	0.811	0.0389	0.090	1.467	1.45	0.6353
54	0.6322	0.840	0.0386	0.086	1.443	1.55	0.6354
58	0.6460	0.884	0.0384	0.078	1.423	1.75	0.6355
62	0.6599	0.922	0.0382	0.068	1.405	2.13	0.6356
65.9659	0.6697	0.000	0.0381	∞	1.396	0.00	0.6357
		$\gamma = 3/2$		$M^2 = \infty$			
1.0	0.5523	0.3066	0.3656	5.000	∞	0.0318	0.0000
1.1	0.5516	0.3309	0.3176	4.302	∞	0.0380	0.1215
1.2	0.5300	0.3349	0.2871	3.840	∞	0.0382	0.2110
1.3	0.5286	0.3388	0.2623	3.487	∞	0.0413	0.2789
1.4	0.5271	0.3426	0.2416	3.087	∞	0.0445	0.3315
1.5	0.5257	0.3462	0.2242	2.804	∞	0.0477	0.3731
1.6	0.5244	0.3497	0.2093	2.566	∞	0.0509	0.4066
1.7	0.5232	0.3531	0.1964	2.363	∞	0.0541	0.4339
1.8	0.5220	0.3564	0.1852	2.187	∞	0.0573	0.4565
1.9	0.5209	0.3596	0.1754	2.035	∞	0.0604	0.4754
2.0	0.5198	0.3627	0.1667	1.901	∞	0.0636	0.4914
2.0	0.5198	0.3627	0.1667	1.901	∞	0.0636	0.4914
2.2	0.5179	0.3687	0.1520	1.677	∞	0.0700	0.5167
2.4	0.5160	0.3744	0.1401	1.499	∞	0.0763	0.5357
2.6	0.5143	0.3798	0.1302	1.363	∞	0.0827	0.5504
2.8	0.5127	0.3851	0.1219	1.253	∞	0.0890	0.5620
3.0	0.5112	0.3902	0.1148	1.151	∞	0.0954	0.5715
3.2	0.5098	0.3951	0.1087	1.045	∞	0.1018	0.5788
3.4	0.5084	0.3998	0.1034	0.970	∞	0.1082	0.5851
3.6	0.5072	0.4044	0.0987	0.905	∞	0.1146	0.5904
3.8	0.5060	0.4088	0.0946	0.849	∞	0.1209	0.5949
4.0	0.5049	0.4131	0.0909	0.799	∞	0.1273	0.5987

ξ	U	C	P/β	Ω/β	γ	$P\Omega^{\gamma}/\beta^{\gamma}$	F
		$\gamma = 3/2$		$M^2 = \infty$			
4.0	0.5049	0.4131	0.0909	0.799	∞	0.1273	0.5987
4.4	0.5028	0.4215	0.0848	0.714	∞	0.1401	0.6049
4.8	0.5009	0.4294	0.0796	0.647	∞	0.1528	0.6096
5.2	0.4992	0.4369	0.0752	0.591	∞	0.1655	0.6135
5.6	0.4976	0.4441	0.0715	0.544	∞	0.1783	0.6165
6.0	0.4961	0.4511	0.0684	0.504	∞	0.1912	0.6187
6.4	0.4947	0.4579	0.0657	0.470	∞	0.2040	0.6207
6.8	0.4935	0.4643	0.0633	0.440	∞	0.2168	0.6224
7.2	0.4923	0.4705	0.0612	0.414	∞	0.2296	0.6239
7.6	0.4912	0.4765	0.0593	0.391	∞	0.2425	0.6250
8.0	0.4902	0.4825	0.0576	0.371	∞	0.2549	0.6261
8.4	0.4892	0.4882	0.0560	0.353	∞	0.2676	0.6270
8.8	0.4883	0.4938	0.0546	0.336	∞	0.2805	0.6278
9.2	0.4874	0.4993	0.0534	0.321	∞	0.2951	0.6286
9.6	0.4866	0.5045	0.0522	0.308	∞	0.3060	0.6291
10.0	0.4858	0.5096	0.0511	0.296	∞	0.3189	0.6297
10.0	0.4858	0.5096	0.0511	0.296	∞	0.319	0.6297
11.2	0.4838	0.5244	0.0484	0.264	∞	0.357	0.6311
12.4	0.4817	0.5383	0.0462	0.239	∞	0.396	0.6322
13.6	0.4801	0.5516	0.0444	0.219	∞	0.433	0.6330
14.8	0.4787	0.5642	0.0428	0.202	∞	0.471	0.6337
16.0	0.4774	0.5762	0.0415	0.188	∞	0.509	0.6343
17.2	0.4763	0.5876	0.0404	0.176	∞	0.547	0.6346
18.4	0.4752	0.5985	0.0394	0.165	∞	0.586	0.6350
19.6	0.4743	0.6089	0.0385	0.156	∞	0.625	0.6353
20.8	0.4734	0.6190	0.0377	0.148	∞	0.665	0.6356
22.0	0.4726	0.6288	0.0370	0.140	∞	0.706	0.6358
22.0	0.4726	0.6288	0.0370	0.1406	∞	0.706	0.6358
24.4	0.4712	0.6474	0.0358	0.1285	∞	0.782	0.6362
26.8	0.4700	0.6647	0.0349	0.1183	∞	0.857	0.6365
29.2	0.4690	0.6811	0.0340	0.1100	∞	0.933	0.6368
31.6	0.4680	0.6967	0.0333	0.1029	∞	1.010	0.6370
34.0	0.4672	0.7117	0.0327	0.0965	∞	1.087	0.6371
36.4	0.4665	0.7260	0.0321	0.0914	∞	1.163	0.6373
38.8	0.4659	0.7398	0.0317	0.0868	∞	1.239	0.6374
41.2	0.4654	0.7530	0.0312	0.0828	∞	1.316	0.6375
43.6	0.4648	0.7658	0.0308	0.0790	∞	1.394	0.6376
46.0	0.4644	0.7783	0.0305	0.0758	∞	1.473	0.6377
46.0	0.4644	0.7783	0.0305	0.0756	∞	1.473	0.6377
50.8	0.4638	0.8021	0.0299	0.0697	∞	1.635	0.6379
55.6	0.4629	0.8243	0.0294	0.0649	∞	1.797	0.6379
60.4	0.4624	0.8450	0.0289	0.0608	∞	1.959	0.6380
65.2	0.4620	0.8646	0.0285	0.0573	∞	2.082	0.6381
70.0	0.4616	0.8834	0.0282	0.0542	∞	2.256	0.6382
74.8	0.4613	0.9017	0.0279	0.0515	∞	2.420	0.6382
79.6	0.4610	0.9194	0.0277	0.0491	∞	2.544	0.6383
84.4	0.4608	0.9367	0.0274	0.0469	∞	2.908	0.6383
89.2	0.4607	0.9534	0.0272	0.0449	∞	2.952	0.6384
94.0	0.4606	0.9691	0.0270	0.0432	∞	3.007	0.6384
94.0	0.4606	0.969	0.0270	0.0432	∞	3.01	0.6384
103.6	0.4604	0.998	0.0267	0.0401	∞	3.32	0.6384
113.2	0.4603	1.026	0.0264	0.0376	∞	3.62	0.6385
122.8	0.4603	1.053	0.0262	0.0354	∞	3.93	0.6386
132.4	0.4604	1.078	0.0260	0.0335	∞	4.24	0.6386
142.0	0.4605	1.102	0.0258	0.0318	∞	4.55	0.6386
151.6	0.4606	1.126	0.0256	0.0305	∞	4.85	0.6388
161.2	0.4608	1.148	0.0254	0.0290	∞	5.15	0.6386
170.8	0.4611	1.169	0.0253	0.0278	∞	5.46	0.6387
180.4	0.4615	1.189	0.0252	0.0267	∞	5.78	0.6387
190.0	0.4616	1.208	0.0251	0.0257	∞	6.09	0.6387
199.6	0.4619	1.228	0.0250	0.0248	∞	6.40	0.6387
209.2	0.4622	1.247	0.0249	0.0240	∞	6.70	0.6387
218.8	0.4625	1.266	0.0248	0.0233	∞	7.00	0.6387
228.4	0.4629	1.285	0.0247	0.0225	∞	7.31	0.6388
238.0	0.4632	1.300	0.0247	0.0219	∞	7.62	0.6388
238	0.4632	1.300	0.0247	0.0219	∞	7.6	0.6388
286	0.4662	1.378	0.0244	0.0192	∞	9.1	0.6388
334	0.4674	1.447	0.0241	0.0173	∞	10.6	0.6388
382	0.4697	1.511	0.0240	0.0158	∞	12.1	0.6388
430	0.4710	1.570	0.0238	0.0145	∞	13.6	0.6388
478	0.4744	1.626	0.0237	0.0134	∞	15.2	0.6389
526	0.4768	1.680	0.0236	0.0125	∞	16.8	0.6389
574	0.4793	1.731	0.0235	0.0118	∞	18.3	0.6389
622	0.4818	1.778	0.0234	0.0112	∞	19.8	0.6389
670	0.4844	1.820	0.0234	0.0106	∞	21.4	0.6389
718	0.4870	1.856	0.0233	0.0101	∞	23.0	0.6389
.	.	.	.	.	.	.	.
.	.	.	.	.	.	.	.
.	.	.	.	.	.	.	.

isentropic. As is well known, the difference between the entropy $s(\xi)$ at any point within the shock wave and that of the undisturbed medium in front of the shock is given by

$$s(\xi) - s_0 = \frac{\Re}{\gamma - 1} \log \frac{K}{K_0}, \tag{49}$$

where $\Re$ denotes the gas constant and K_0 and K are the values of the adiabatic constants in front of and behind the shock wave. Now, in front of the shock wave,

$$K_0 = p_0 \rho_0^{-\gamma} = \tfrac{1}{3} G m \beta^{1-\gamma} r^{-(3-2\gamma)} \tag{50}$$

by virtue of equations (26) and (27); while, behind the shock,

$$K = p \rho^{-\gamma} = r^{2\gamma} l^{-2} P \Omega^{-\gamma} \tag{51}$$

by virtue of equations (8) and (9). These equations disclose that the undisturbed medium itself will not be isentropic unless $\gamma = 1.5$; and that behind the shock wave will not be so even if the entropy in front of the wave is constant. In general, we find that

$$\frac{K}{K_0} = \frac{3\beta^{\gamma-1}}{Gm} \frac{P\Omega^{-\gamma}}{\xi} = \frac{9\gamma}{4x} \left(\frac{P}{\beta\xi}\right) \left(\frac{\Omega}{\beta}\right)^{-\gamma}. \tag{52}$$

In particular, if K_1 denotes the value of the adiabatic constant immediately behind the shock, an appeal to equations (29) and (30) discloses that

$$\frac{K_1}{K_0} = \frac{2\gamma - \gamma x + x}{x(\gamma - 1 + 2x)^{-\gamma} (\gamma + 1)^{\gamma+1}}, \tag{53}$$

which, for $x = 1$ (i.e., the Mach number $M = 1$), reduces indeed to 1; in this case, there is no entropy change across the incipient shock. If, however, $x > 1$, then $K_1 > K_0$, and the corresponding increase in entropy can be evaluated by means of equation (49). The penultimate column of Table 1 lists the auxiliary quantity $(P/\beta\xi)(\Omega/\beta)^{-\gamma}$, tabulated as a function of ξ, which should facilitate the computation of the entropy at any point of the field of flow under investigation.

The last column of Table 1 ultimately contains the values of the integral

$$F(\xi) = \int_{\xi_0}^{\xi} \left\{ \frac{U^2}{2} \frac{\Omega}{\beta} + \frac{1}{\gamma - 1} \frac{P}{\beta} - \frac{4x\xi\Omega}{3\gamma\xi_0} \right\} \frac{\xi_0 d\xi}{\xi^2}, \tag{54}$$

which is related to the total energy $E(\xi)$ contained at any time within a concentric shell extending from the shock inward by means of the equation

$$E(\xi) = \frac{4\pi\beta}{3\xi_0} F(\xi). \tag{55}$$

In particular, the total energy of wave motion in the envelope of our generalized Roche model can be obtained from the preceding equation (55) by setting, in the latter, $\xi = \xi_1$.

A knowledge of $E(\xi_1)$ puts us, in turn, in a position to determine the amount of energy which had to be released by the instantaneous initial explosion in order to produce a shock wave of requisite strength. A sum H of the thermal and gravitational energy originally stored in the envelope has already been given by equation (48), where, by virtue of equations (13) and (14), we are entitled to set $R/a = (\xi_1/\xi_0)^{1/3}$. The difference $|E(\xi_1) - H(\xi_1)|$ furnishes, therefore, the absolute amount of energy whose instantaneous release was adequate for giving rise to the computed phenomena; and the ratio $|E - H|/|H|$ expresses this amount in terms of the energy originally contained in the envelope.

The numerical values of the quantity $|E - H|/|H|$ corresponding to each one of our solutions can be found in the last column of Table 2, which summarizes the physical characteristics of the solutions presented in Table 1. The headings of the first eight columns of Table 2 are self-explanatory. The ratios $\xi_0/\xi_1 \equiv (a/R)^3$, compiled in the tenth column, are identical with the ratios of mean density of our configuration as a whole (limited by the radius R) to that of its core; while the eleventh column contains the fraction of the mass of the envelope which has been endowed with a velocity greater than that of escape from the gravitational field of the core.

TABLE 2

SUMMARY OF THE PHYSICAL PROPERTIES OF THE SHOCK WAVES

M^2	a/R	y	p_1/p_0	ρ_1/ρ_0	$(t/\tau)u_1$	$(t/\tau)c_1$	T_1/T_0	K_1/K_0	ξ_0/ξ_1	Mass Ejected Divided by Mass Total	$\frac{\lvert E-H\rvert}{\lvert H\rvert}$
	$\gamma=\frac{5}{3}$										
8.27924	0.4536	1.000	10.10	2.936	0.4396	0.4297	3.44	1.677	0.0933	0.000	2.625
10.....	.4623	1.125	12.25	3.077	.4500	.4307	3.98	1.882	.0988	0.196	3.630
12.....	.4678	1.255	14.75	3.200	.4583	.4132	4.61	2.123	.1024	0.363	4.803
15.....	.4714	1.429	18.50	3.333	.4667	.4055	5.55	2.486	.1047	0.537	6.566
20.....	.4715	1.679	24.75	3.479	.4750	.3976	7.11	3.099	.1048	0.717	9.395
30.....	.4654	2.093	37.25	3.636	.4833	.3896	10.24	4.332	.1008	0.905	14.77
40.....	.4576	2.438	49.76	3.721	.4875	.3854	13.37	5.568	.0958	1.000	19.86
60.....	.4432	3.011	74.74	3.809	.4917	.3813	19.62	8.042	.0870	1.000	29.28
75.....	.4340	3.377	93.49	3.846	.4933	.3796	24.31	9.900	.0818	1.000	36.22
100.....	.4213	3.913	124.76	3.884	.4950	.3779	32.13	13.001	.0748	1.000	47.08
200.....	.3880	5.562	249.75	3.942	.4975	.3752	63.36	25.372	.0584	1.000	85.76
300.....	.3679	6.820	374.74	3.960	.4983	.3744	94.63	37.811	.0498	1.000	127.6
500.....	0.3427	8.821	624.75	3.976	.4990	.3737	157.13	62.606	0.0403	1.000	199.5
∞.....	0	∞	∞	4.000	0.5000	0.3727	∞	∞	0	1.000	∞
	$\gamma=\frac{7}{5}$										
100.....	0.3651	3.960	119.81	4.808	0.5280	0.3328	24.92	11.367	0.0486	1.000	70.11
200.....	0.3053	5.629	239.83	4.902	.5307	.3297	48.92	22.093	0.0285	1.000	120.26
∞.....	0	∞	∞	5.000	0.5333	0.3266	∞	∞	0	1.000	∞

In conclusion, the writers wish to express their indebtedness to Miss Virginia K. Brenton and Mrs. Margaret D. Hill for carrying out most of the numerical integrations presented in this paper and to Mr. Francis G. Davoren for editorial help in the preparation of the tables.

APPENDIX

In conclusion of the present investigation, we wish to point out that, if the Mach number of the shock front which we are considering were infinite (which amounts to an assumption that the pressure p_0 in front of the shock wave can be ignored in comparison with the pressure p behind the shock), and if the density ρ_0 in the undisturbed medium varies as

$$\rho_0 = \beta r^\nu , \tag{36}$$

where ν is an arbitrary constant exponent, there exists a certain value of γ for which the equations of motion of our problem, rewritten in terms of a single independent variable $\xi = r^\phi t^\psi$, admit of a solution in a closed form.

In order to prove this statement, we may recall that $M = \infty$ corresponds to $x = 0$ and, therefore, to $Gm = 0$ (implying our motion to be so rapid that no finite central mass can decelerate

it significantly). If so, the Rankine-Hugoniot shock-wave conditions, simplified by ignoring p_0 in comparison with p_1, yields

$$U(\xi_0) = -(1-\mu^2)\frac{\psi}{\phi}, \tag{57}$$

$$P(\xi_0) = (1-\mu^2)\left(\frac{\psi}{\phi}\right)^2\beta, \tag{58}$$

and

$$\Omega(\xi_0) = \mu^{-2\beta}, \tag{59}$$

where we have let

$$\mu^2 = \frac{\gamma-1}{\gamma+1}. \tag{60}$$

On the other hand, it may be readily verified that the solution of the fundamental equations in this particular case yields

$$U(\xi) = -(1-\mu^2)\frac{\psi}{\phi} = \frac{-2}{\gamma+1}\frac{\psi}{\phi}, \tag{61}$$

$$P(\xi) = P(\xi_0)\left(\frac{\xi}{\xi_0}\right)^{2(3\psi+\phi)/\phi\psi}, \tag{62}$$

$$\Omega(\xi) = \Omega(\xi_0)\left(\frac{\xi}{\xi_0}\right)^{2(3\psi+\phi)/\phi\psi}, \tag{63}$$

for any value of ξ. For these equations to be consistent with equations (57)–(59) immediately behind the shock wave (i.e., when $\xi = \xi_0$), it is obviously necessary that

$$\gamma = \frac{1-(\phi/\psi)}{3+(\phi/\psi)}, \tag{64}$$

and the constancy of the energy requires, on the other hand, that

$$\nu + 5\frac{\psi}{\phi} + 2 = 0, \tag{65}$$

i.e., that

$$\nu = -5 - 2\frac{\phi}{\psi} = \frac{\gamma-7}{\gamma+1}. \tag{66}$$

In the particular case discussed in this paper, $\phi/\psi = -\frac{4}{3}$ by equation (17) and $\nu = -2$, in accordance with equation (65). The value of γ, corresponding to these parameters by equation (64), turns out to be $\frac{5}{3}$ (the one appropriate for monatomic gas); and in this case the closed solution of our equations describing the properties of a gas flow behind a shock wave of an infinite strength takes the explicit form

$$u = \frac{1}{2}\frac{r}{t}, \qquad \rho = 4\beta\xi_0\frac{r}{t^3}, \qquad p = \frac{\beta}{3}\xi_0\frac{r^3}{t^4}, \tag{67}$$

respectively.

It is interesting to note that another particular case of the family of solutions just deduced, corresponding to strong progressing blast waves in water, was previously discovered by Primakoff.[6] In his case the medium in front of his shock was supposed to be homogeneous ($\nu = 0$), and the constancy of the energy of the whole explosion led to $\psi/\phi = -\frac{2}{5}$. If so, the value of γ required to yield a solution in a closed form turned out to be 7 (which corresponds, very approximately, to the ratio of specific heats in water under normal conditions), exactly in agreement with our equations (64)–(66). It transpires, therefore, that Primakoff's solution happens to be a particular member of the whole family of closed solutions whose explicit form has been given above and whose existence has so far escaped notice.

[6] As quoted by Courant and Friedrichs, *op. cit.*, sec. 161.

TWO NEW BAND SYSTEMS OF THE *AlCl* MOLECULE

DEVENDRA SHARMA
Division of Physics, National Research Council, Ottawa, Canada
Received August 22, 1950

ABSTRACT

An uncondensed discharge in a tube containing $AlCl_3$ vapor and helium shows two groups of bands in the regions λλ 4154–3970 and λλ 5612–5265, the former ones being degraded to shorter and the latter to longer wave lengths. The λλ 4154–3970 bands are found to be analogous to the Cameron bands of *CO*, being due to a transition from the first excited triplet state $a^3\Pi$ to the ground state $X^1\Sigma^+$ of *AlCl*. The other bands have the $a^3\Pi$ state as their lower state and probably $a^3\Sigma$ state as their upper state. Only the $(0, v'')$ progression of these bands is observed, possibly indicating a predissociation at $v' = 1$ in the $^3\Sigma$ state.

A. INTRODUCTION

The band spectrum of the diatomic aluminum chloride (*AlCl*) molecule has been investigated by Bhaduri and Fowler,[1] Mahanti,[2] and Holst[3] in emission, and by Miescher[4] in absorption. It consists of the well-known ultraviolet bands λλ 2810–2555 corresponding to the transition $A^1\Pi \rightarrow X^1\Sigma^+$.

The present investigations, originally started with a view to obtaining *AlO* bands in a discharge tube, have given further information regarding the spectrum of the *AlCl* molecule. In addition to the ultraviolet system, bands degraded to shorter wave lengths in the violet region (λλ 4154–3970) and bands degraded to longer wave lengths in the green region (λλ 5612–5265) have been observed. Vibrational analyses given below show that the emitter of these bands is the diatomic *AlCl* molecule. In addition, we have observed bands degraded to longer wave lengths in the regions λλ 3510–2950 and λλ 4500–3900, but these have not yet been assigned unambiguously.

B. EXPERIMENTAL

The new bands were obtained in a conventional discharge tube which was used end-on. It contained hollow cylindrical electrodes about 7 cm long and 2.5 cm in diameter, and the discharge passed through a 20 cm long and 1.5 cm wide tube coaxial with the electrodes. At the lower middle part of the discharge tube a tube containing $AlCl_3$ was attached. As aluminum chloride is fairly hygroscopic, it was necessary to distil it in vacuum in a few stages to get rid of the water vapor. After evacuating the discharge tube, helium was let in from a bulb through a pair of stopcocks joined near the front part of the tube, and the requisite amount of $AlCl_3$ vapor was produced by warming the tube containing aluminum chloride. A transformer, carrying a current of from 4 to 8 amp. at 110 volts in the primary and capable of giving 3000 volts in the secondary, was used to run the discharge. The spectrum was photographed on medium Hilger quartz and glass spectrographs and in the first order of a 21-foot grating.

C. RESULTS

VIOLET BANDS

The violet bands are reproduced in Figure 1, *a*. Some of these bands show both *P* and *Q* heads (designated as P_2 and Q_2), whereas the others show only *P* heads (P_1). In Table 1

[1] B. N. Bhaduri and A. Fowler, *Proc. R. Soc. London, A*, **145**, 321, 1934.
[2] P. C. Mahanti, *Zs. f Phys.*, **88**, 550, 1934.
[3] W. Holst, *Zs. f. Phys.*, **93**, 55, 1934.
[4] E. Miescher, *Helvetica Phys. Acta*, **9**, 693, 1936.

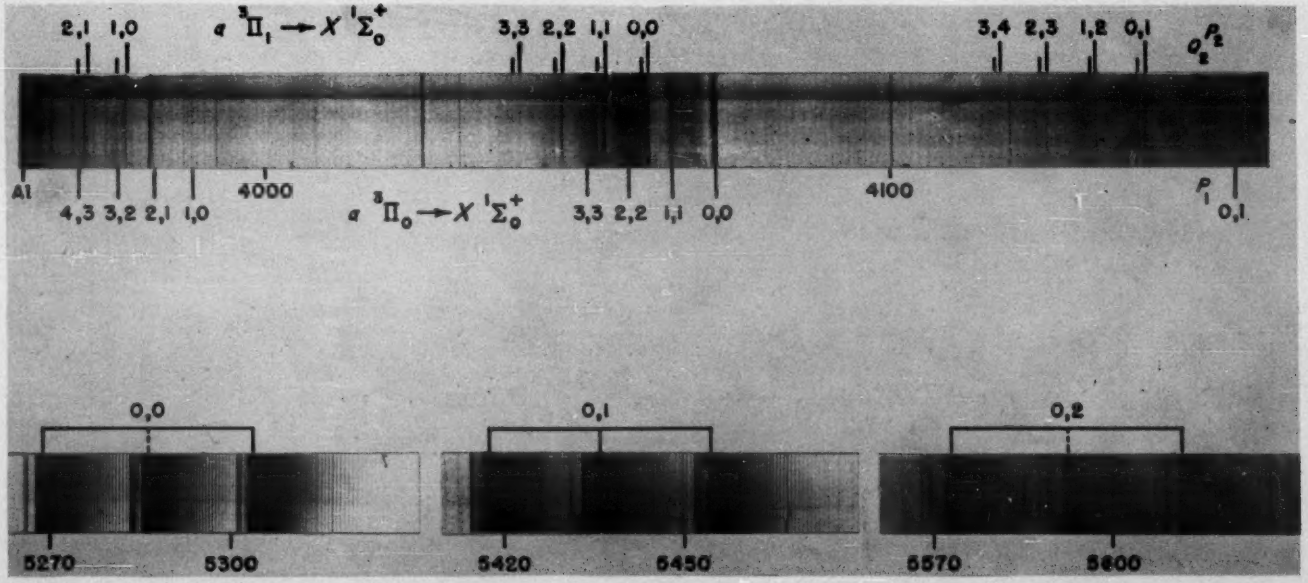

FIG. 1.—*Upper*, the violet bands of *AlCl; lower*, the green bands of *AlCl*. Only the *Q*-form heads are marked. The other heads can be identified easily

are listed the wave lengths and wave numbers of all the measured band heads, along with their estimated intensities. These bands form three separate sequences, and evidently the middle one, which is the strongest of the three, is the $\Delta v = 0$ sequence. On arranging the Q heads in a Deslandres scheme and finding out the average values of $\Delta G''_{v+1/2}$, one finds that they agree well with the average $\Delta G''_{v+1/2}$ values determined from the Q-head measurements of the ultraviolet bands[1] of the *AlCl* molecule, as shown in Table 2, indicating that both the systems in question have a common lower state, viz., $X^1\Sigma^+$.

As the violet system of bands is not very extensive, only four $\Delta G''_{v+1/2}$ values can be determined, while eighteen are known for the ultraviolet system. Further, each of the $\Delta G''_{v+1/2}$ in the present case is an average of only a few first differences. Therefore, it

TABLE 1

THE VIOLET BAND SYSTEM OF *AlCl*

λ_{air} (A)	Intensity	ν_{vac} (Cm^{-1})	Assignments	O−C (Cm^{-1})
3971.30.....	1	25173.58	2, 1 Q_2; 4, 3 P_1	+0.02; +0.80
3972.76.....	3	25164.32	2, 1 P_2	−0.20
3973.80.....	1	25157.74		−0.17
3977.39.....	3	25135.03	1, 0 Q_2; 3, 2 P_1	−0.28; −0.88
3978.74.....	3	25126.50	1, 0 P_2	+0.07
3979.80.....	1	25119.81		−0.23
3983.38.....	1	25097.24	2, 1 P_1	−1.19
3989.43.....	2	25059.18	1, 0 P_1	−1.16
3990.30.....	0	25053.71		−0.24
4040.70.....	0	24741.22	3, 3 Q_2	−0.54
4041.86.....	2	24734.12	3, 3 P_2	+0.18
4047.39.....	2	24700.33	2, 2 Q_2	+0.27
4048.67.....	3	24692.52	2, 2 P_2	+0.04
4052.57.....	2	24668.76	3, 3 P_1	+0.91
4054.34.....	5	24657.99	1, 1 Q_2	+0.08
4055.58.....	7	24650.45	1, 1 P_2	+0.04
4059.50.....	4	24626.65	2, 2 P_1	+0.26
4061.37.....	8	24615.31	0, 0 Q_2	0.00
4062.62.....	10	24607.73	0, 0 P_2	0.00
4066.50.....	5	24584.25	1, 1 P_1	−0.07
4073.56.....	8	24541.65	0, 0 P_1	+0.01
4118.09.....	0	24276.28	3, 4 Q_2	+0.22
4119.19.....	0	24269.79	3, 4 P_2	−0.07
4125.95.....	1	24230.03	2, 3 Q_2	−0.43
4126.91.....	2	24224.39	2, 3 P_2	−0.03
4133.79.....	1	24184.08	1, 2 Q_2	−0.33
4134.76.....	3	24178.41	1, 2 P_2	+0.04
4141.78.....	2	24137.43	0, 1 Q_2	−0.48
4142.78.....	4	24131.60	0, 1 P_2	−0.11
4154.03.....	1	24066.25	0, 1 P_1	+0.63

TABLE 2

$\Delta G_{v+1/2}$ VALUES FOR THE LOWER STATES OF THE ULTRAVIOLET AND VIOLET BANDS

State	$\Delta G''_{1/2}$	$\Delta G''_{3/2}$	$\Delta G''_{5/2}$	$\Delta G''_{7/2}$
$X^1\Sigma^+$ state of the ultraviolet bands.....	477.3$_3$	473.1$_8$	469.3$_2$	465.7$_3$ cm^{-1}
Lower state of the violet bands.....	477.4$_6$	473.5$_8$	470.3$_0$	464.9$_4$ cm^{-1}

seemed advisable to use the vibrational constants, ω_e'' and $\omega_e''x_e''$, obtained from the analysis of the more extensive main system.[1, 3] The following equation represents all the Q heads of the violet bands satisfactorily:

$$\nu_{Q_2} = 24593.84 + (524.35u' - 2.175u'^2) - (481.30u'' - 1.95u''^2), \quad (1)$$

where $u = v + \frac{1}{2}$. The Q heads give the most accurate vibrational constants obtainable from band-head measurements. Since the P- and Q-head separations are not negligible, it seems worth while to give a separate equation for the P heads:

$$\left.\begin{matrix}\nu_{P_2}\\ \nu_{P_1}\end{matrix}\right\} = \left\{\begin{matrix}24586.16\\ 24520.07\end{matrix}\right\} + (523.29u' - 2.295u'^2) - (480.00u'' - 1.99u''^2). \quad (2)$$

The vibrational assignments of all the band heads are given in the second-last column of Table 1, and the differences between the observed wave numbers and those calculated on the basis of equations (1) and (2) are entered in the last column. The agreement between the observed and calculated values is fairly satisfactory.

The bands due to the heavier $Al^{27}Cl^{37}$ isotope are marked i in Table 1. The isotope effect has been observed with certainty only for the 1, 0 P_2, 2, 1 P_2, and 1, 0 P_1 heads. As the bands due to the heavier isotope will move toward the system origin, it will be possible to observe them only in the $\Delta v = +1$ sequence, because in the $\Delta v = -1$ sequence they will be masked by the bands of the more abundant lighter isotope. The agreement between the observed and calculated isotope shifts is satisfactory.

Assuming B_e'' and α_e'', which are known from the rotational analysis of the main $AlCl$ bands,[3] one obtains from the separations of the P and Q heads of the $a^3\Pi - X^1\Sigma^+$ bands the following approximate B_v' values:

B_0'	B_1'	B_2'	B_3'
0.249	0.247	0.245	0.242 cm^{-1}

which give $B_e' = 0.250$ cm^{-1} and $\alpha_e' = 0.002$ cm^{-1}.

GREEN BANDS

The green bands shown in Figure 1, *b*, consist of only the first three members[5] of a v''-progression of triplet bands. Each component of these triplet bands shows several heads. Table 3 contains the measurements of all these heads, along with their estimated intensities and their vibrational assignments. The components due to the heavier isotope $Al^{27}Cl^{37}$ have been marked with i. It will be observed that the $\Delta G''_{v+1/2}$ values for these bands and their triplet separations are, within experimental errors, the same as the corresponding quantities for the upper state of the violet bands. One can therefore represent the heads marked Q (see below) in the three progressions by

$$b^3\Sigma - \left\{\begin{matrix}a^3\Pi_0\\ a^3\Pi_1\\ a^3\Pi_2\end{matrix}\right\}: \quad \nu = \left\{\begin{matrix}19236.84\\ 19172.65\\ 19108.64\end{matrix}\right\} - (524.35u'' - 2.175u''^2), \quad (3)$$

where ω_e'' and $\omega_e''x_e''$ are the same as the ω_e' and $\omega_e'x_e'$ for the Q heads of the violet bands in equation (1).

[5] Some low-dispersion plates show faintly the fourth member of the progression also.

TABLE 3

THE GREEN BAND SYSTEM OF *AlCl*

λ_{air} (A)	Intensity	ν_{vac} (Cm^{-1})	Assignments* (Forms of Heads)	O−C (Cm^{-1})
		0, 0 Band		
5265.78....	4	18985.27	S	+0.27
65.98....	4	84.55	S	− .45
67.48....	4	79.14	iR $b^3\Sigma-a^3\Pi_0$	+ .48
67.82....	10	77.92	R	+ .26
68.63....	5	75.00	Q	− .21
83.41....	3	921.92	iS	+ .11
83.74....	6	20.74	S	− .07
85.42....	4	14.72	iR $b^3\Sigma-a^3\Pi_1$	+ .25
85.77....	9	13.47	R	.00
5301.37....	2	857.82	iS	+ .02
01.83....	4	56.18	S	− .62
03.37....	3	50.70	iR $b^3\Sigma-a^3\Pi_2$	+ .24
03.74....	8	49.39	R	− .07
04.30....	5	47.40	Q	+0.39
		0, 1 Band		
5411.83....	1	18472.92	iS	−0.08
13.87....	3	65.96	S	+ .11
14.16....	3	64.97	iR $b^3\Sigma-a^3\Pi_0$	− .05
15.00....	1	62.10	iQ	− .26
16.28....	7	57.74	R	− .13
17.14....	3	54.81	Q	− .40
30.73....	2	408.63	iS	− .18
32.89....	6	01.31	S, iR $b^3\Sigma-a^3\Pi_1$	− .35, +0.48
35.21....	7	393.45	R	− .23
35.93....	3	91.02	Q	.00
49.91....	2	343.84	iS	− .96
51.93....	6	37.05	S, iR $b^3\Sigma-a^3\Pi_2$	− .60, +0.23
54.10....	7	29.75	R	+ .08
54.92....	3	26.99	Q	−0.02
		0, 2 Band		
5567.70....	2	17955.76	iR	+0.03
69.08....	2	51.31	S	+0.09
69.44....	2	50.16	Line? $b^3\Sigma-a^3\Pi_0$	
71.83....	4	42.46	R	−0.02
72.28....	3	41.01	Line?	
72.85....	2	39.17	Q	−0.39
84.92....	2	900.40	iS	+0.12
87.68....	2	891.56	iR $b^3\Sigma-a^3\Pi_1$	+0.02
89.20....	4	86.69	S	−0.34
91.83....	5	78.28	R	−0.01
5607.59....	2	828.04	iR	+0.51
09.41....	3	22.25	S $b^3\Sigma-a^3\Pi_2$	−0.77
11.82....	5	14.60	R	+0.32
12.49....	2	12.47	Q	+1.11

* The significance of the symbols Q, R, and S is explained in the text.

UNASSIGNED BANDS

The red degraded bands in the region λλ 3510–2950, measured on spectrograms taken with the quartz spectrograph, approximate roughly to the relation

$$\nu = 31450.8 + (391.4u' - 0.9u'^2) - (592.0u'' - 3.0u''^2)\,. \tag{4}$$

It is not possible to draw from this an unambiguous conclusion as to the nature of the emitter; but ω_e'' is of an order of magnitude compatible with what one would expect for the Al_2 molecule.

D. DISCUSSION

THE VIOLET BANDS

It has been shown earlier (eq. [1]) that the lower state of the violet bands is the same as the lower state of the well-known ultraviolet bands of *AlCl*. The fact that some of the sub-bands of a given band show both *Q* and *P* heads, whereas others show only *P* heads, suggests that the bands are due to an intercombination between an upper $^3\Pi$ state and the $^1\Sigma^+$ ground state (see, e.g., Herzberg).[6] Assuming Hund's case *a*, the selection rule $\Delta\Omega = 0, \pm 1$ with $\Delta J = 0$ forbidden for $\Omega = 0 \rightarrow \Omega = 0$ restricts the transitions in such an intercombination to $^3\Pi_0 - {}^1\Sigma^+$ (P_1 and R_1 branches) and $^3\Pi_1 - {}^1\Sigma^+$ (P_2, Q_2, and R_2 branches, all of comparable intensities) in agreement with the observed band structure. However, as case *b* is approached, the selection rule for Ω holds less rigorously, and, in addition to the above five branches, the Q_1, P_3, Q_3, and R_3 branches also occur, as in the Cameron bands of *CO*.[7]

If *A* is the multiplet separation and B_v the rotation constant, the ratio A/B_v denoted by *Y* is a measure of the strength of the coupling of the spin to the internuclear axis.[6] For small values of *Y* we are close to case *b;* and, as *Y* increases in magnitude, we approach case *a*. Now, for the upper state of the Cameron bands, $Y_{CO} \cong 25$, whereas, for the violet *AlCl* bands, $Y_{ALCL} \cong 260$, indicating a much stronger coupling of the spin to the internuclear axis (case *a*) in the latter molecule. This explains the occurrence of only the P_1, P_2, and Q_2 heads in the violet *AlCl* bands.

Similar $^3\Pi - {}^1\Sigma$ transitions have been recorded in other halides of the *Al* group, namely, in *AlI*,[8] *GaCl*, *GaBr*, *GaI*,[9] *InCl*, *InBr*, and *In I*.[10] Figure 2 shows a plot of the electronic energies of the $^3\Pi_0$ and $^3\Pi_1$ states against number of electrons, n_e, for these molecules. We observe here that the curves for the three chlorides are very similar to those for the three iodides. Among the bromides, *AlBr* is still missing, and one can see from the diagram that the $^3\Pi$ state of this molecule will lie roughly at 24,000 cm^{-1}.

In Figure 3 the ω_e values of the $^1\Sigma$ ground state and the first excited $^3\Pi$ state of the chlorides of *Al*, *Ga*, and *In* are plotted against n_e. The value of 524.35 cm^{-1} for the ω_e of the $^3\Pi$ state of *AlCl* fits well with the rest of the data.

THE GREEN BANDS

As we have seen earlier, the lower state of the λλ 5612–5265 bands is the same as the upper state of the violet bands, i.e., $a^3\Pi$. Also, since the triplet separations of the green bands are, within experimental errors, the same as the $^3\Pi_0 - {}^3\Pi_1$ separations of the

[6] G. Herzberg, *Molecular Spectra and Molecular Structure*, Vol. I: *Spectra of Diatomic Molecules* (New York: D. Van Nostrand Co., Inc., 1950).

[7] K. N. Rao, *Ap. J.*, **110**, 304, 1949.

[8] E. Miescher, *Helvetica Phys. Acta*, **8**, 279, 1935.

[9] E. Miescher and M. Wehrli, *Helvetica Phys. Acta*, **7**, 331, 1934.

[10] M. Wehrli and E. Miescher, *Helvetica Phys. Acta*, **7**, 298, 1934.

violet bands, the upper state of the green bands is, in all probability, a $^3\Sigma$ state, designated $b^3\Sigma$. This could be established unambiguously only if the rotational structure were fully resolved.

Since no detailed rotational analysis is possible on the basis of the present spectrograms, accurate B'_e values cannot be obtained. However, an approximate B'_0 value can be determined from a partially resolved branch which occurs at the longward end of each sub-band of the 0, 0 band. These branches yield $B'_0 - B''_0 = -0.023$ cm^{-1}, and, since B''_0 is known from the violet bands to be 0.249 cm^{-1}, it follows that $B'_0 = 0.226$ cm^{-1}.

Since we are dealing here with Hund's case *a*, there will be nine branches in each of the three $^3\Sigma - {}^3\Pi_0$, $^3\Sigma - {}^3\Pi_1$, and $^3\Sigma - {}^3\Pi_2$ sub-bands. If the triplet splitting in the $^3\Sigma$

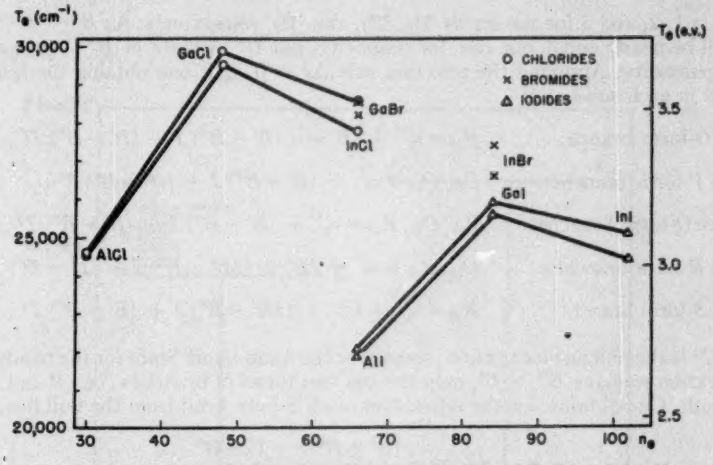

FIG. 2.—T_e values of the first excited $^3\Pi$ states of some of the diatomic halides of the *Al* group plotted against n_e, the number of electrons in the molecules.

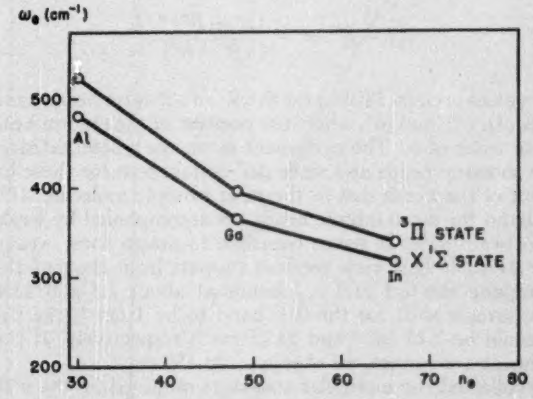

FIG. 3.—ω_e values of the ground and the first excited $^3\Pi$ states of the chlorides of *Al*, *Ga*, and *In* versus n_e.

state is very small, some of these branches will almost coincide and there will be only five effective branches of the forms O, P, Q, R, and S. It is easy to see which branches overlap and how many form heads. Writing the rotational energies in the two states in the usual way,[6] we have

$$^3\Sigma: \quad \begin{cases} F_1'(J) = B'K'(K'+1) = B'(J'-1)J', \\ F_2'(J) = B'K'(K'+1) = B'J'(J'+1), \\ F_3'(J) = B'K'(K'+1) = B'(J'+1)(J'+2), \end{cases}$$

$$^3\Pi: \quad F_k''(J) = B^{(k)''}J''(J''+1),$$

where k is 1, 2, and 3 for the states $^3\Pi_0$, $^3\Pi_1$, and $^3\Pi_2$, respectively. As $B^{(1)''}$, $B^{(2)''}$, and $B^{(3)''}$ will be nearly equal, one can, for simplicity, put B'' in place of $B^{(k)''}$ without any loss of generality. Applying the selection rule $\Delta J = 0, \pm 1$, one obtains the following branches in each sub-band:

One O-form branch: $P_{1k} = \nu_0^{(k)} + 2B' - (3B' + B'')J + (B' - B'')J^2$,

Two P-form branches: $P_{2k}, Q_{1k} = \nu_0^{(k)} - (B' + B'')J + (B' - B'')J^2$,

Three Q-form branches: $P_{3k}, Q_{2k}, R_{1k} = \nu_0^{(k)} + (B' - B'')J + (B' - B'')J^2$,

Two R-form branches: $Q_{3k}, R_{2k} = \nu_0^{(k)} + 2B' + (3B' - B'')J + (B' - B'')J^2$,

One S-form branch: $R_{3k} = \nu_0^{(k)} + 6B' + (5B' - B'')J + (B' - B'')J^2$,

where $\nu_0^{(k)}$ is the null line for the first, second, or third sub-band. Since for the bands under consideration we have $B'' > B'$, only the last two forms of branches (i.e., R and S) will form heads. One obtains, for the separation of an S-form head from the null line,

$$\nu_{hS} - \nu_0^{(k)} = -\frac{(B' + B'')^2 + 12B'B''}{4(B' - B'')}, \tag{5}$$

which in the present case is roughly four times the corresponding separation for the R-form heads,

$$\nu_{hR} - \nu_0^{(k)} = -\frac{(B' + B'')^2}{4(B' - B'')}. \tag{6}$$

The calculated values used in Table 3 for the S- and R-form heads have been obtained by using equations (3), (5), and (6), where the position of the Q-form head has been used for an approximate value of ν_0. The agreement is, on the whole, satisfactory.

Since there are so many heads and since $\Delta G'$ is unknown for these bands, an unambiguous assignment of the heads due to the rarer isotopic molecule $Al^{27}Cl^{37}$ is not possible. In the 0, 0 band the more intense heads are accompanied by weaker heads about 1 cm^{-1} to the shortward side. It seems plausible to assign these weaker heads to the isotopic molecule $Al^{27}Cl^{37}$. This view receives support from the fact that similar weak band heads accompany the 0, 1 and 0, 2 bands at about 7.3 and 13.4 cm^{-1}. Indeed, if we assume the isotopic shift for the 0, 0 band to be 1 cm^{-1}, the shifts for the 0, 1 and 0, 2 bands should be 7.15 cm^{-1} and 13.25 cm^{-1}, respectively. If these assignments of isotopic band heads are correct, we obtain $\omega_e' \cong 350$ cm^{-1}.

In Table 4 are collected the molecular constants obtained for the $a^3\Pi$ and $b^3\Sigma$ states of the $AlCl$ molecule.

Figure 4 shows the energy-level diagram of the $AlCl$ molecule. The fact that only

TABLE 4

MOLECULAR CONSTANTS FOR THE $a^3\Pi$ AND $b^3\Sigma$ STATES OF *AlCl*

STATE	T_e (Cm^{-1})	ω_e (Cm^{-1})	$\omega_e x_e$ (Cm^{-1})	B_e (Cm^{-1})	α_e (Cm^{-1})	r_e (10^{-8} Cm)	OBSERVED TRANSITIONS	
							Designation	ν_{00} (Cm^{-1})
$b^3\Sigma$.....	~43590	~350	.....	$B_0=0.226$	.....	$r_0=2.21$	$b^3\Sigma \rightarrow a^3\Pi_2$	18847.40
							$b^3\Sigma \rightarrow a^3\Pi_1$	18911*
							$b^3\Sigma \rightarrow a^3\Pi_0$	18975.00
$a^3\Pi$.....	24658	524.35	2.175	0.250	0.002	2.10	$a^3\Pi_2 \rightarrow X^1\Sigma$	24680 Q_2*
	24593.84						$a^3\Pi_1 \rightarrow X^1\Sigma$	24615.31 Q_1
	24528						$a^3\Pi_0 \rightarrow X^1\Sigma$	24541.65 P_1

* Calculated ν_{00} value.

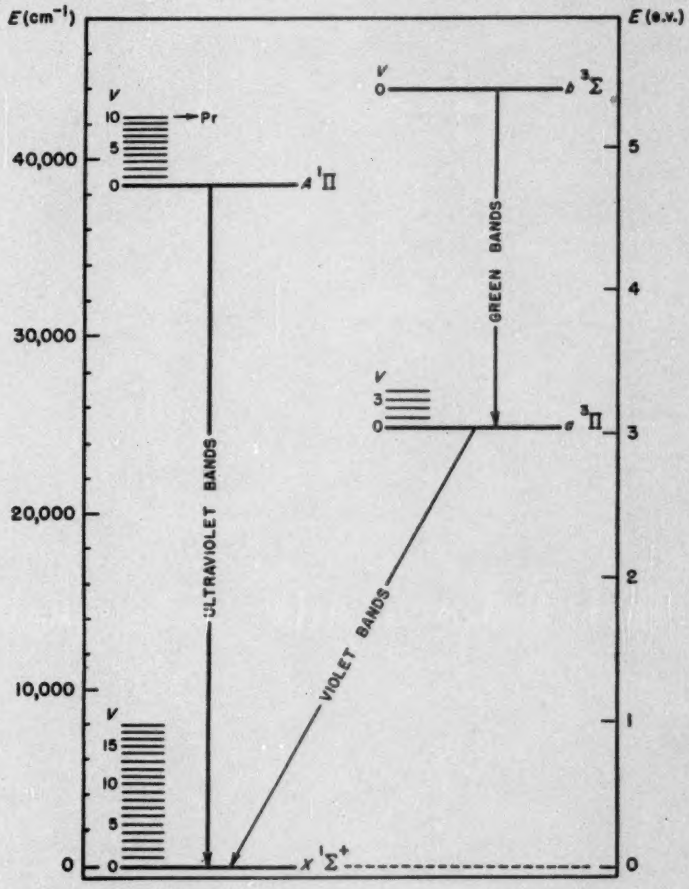

FIG. 4.—The energy-level diagram of the *AlCl* molecule

$v' = 0$ has been observed in the $b^3\Sigma$ state indicates that higher vibrational levels are probably predissociated. It may be recalled here that Holst[8] records a predissociation in the level $v' = 10$ of the $A^1\Pi$ state of *AlCl*.

The author extends his sincere thanks to Dr. G. Herzberg for his kind interest and numerous valuable suggestions during the course of the work and to Dr. A. E. Douglas for many helpful discussions.

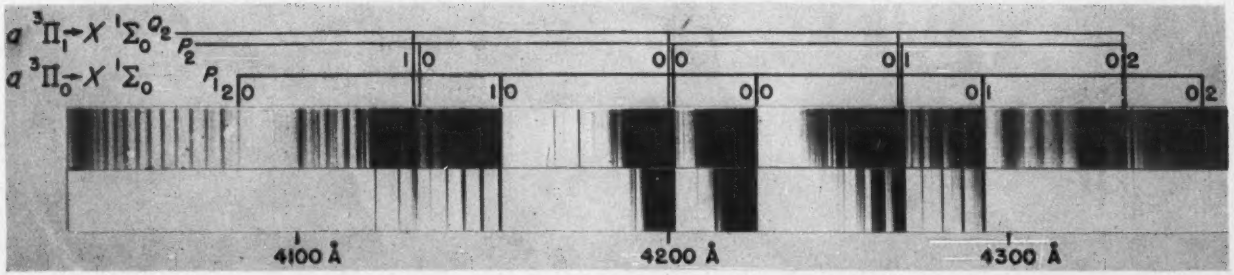

FIG. 1.—The $a^3\Pi \rightarrow X^1\Sigma$ band system of *AlBr*. Two different exposures are shown. Only the first band heads of each sequence are marked

A NEW BAND SYSTEM OF THE *AlBr* MOLECULE

DEVENDRA SHARMA
Division of Physics, National Research Council, Ottawa, Canada
Received October 2, 1950

ABSTRACT

New bands, shaded to shorter wave lengths, in the region λλ 4370–4040 have been observed in a discharge tube containing *AlBr* vapor and helium. They have been analyzed and found to belong to the intercombination $^3\Pi \rightarrow {}^1\Sigma$ transition.

Recently an intercombination band system of the *AlCl* molecule has been studied.[1] This new system, lying in the violet region, is due to a transition from the first excited triplet state, $a^3\Pi$, to the ground state, $X^1\Sigma^+$, of *AlCl*. The corresponding transition in *AlBr* by comparison with *AlCl* and *AlI* was predicted to occur at about 24,000 cm^{-1} or near 4200 A. When investigating the spectrum of *AlBr* in a discharge tube similar to the one used for *AlCl*, in addition to the well-known $A^1\Pi - X^1\Sigma$ bands (λλ 3000–2750),[2, 3, 4] a new band system shaded to shorter wave lengths was indeed found in the region 4370–4040 A. Spectrograms of the new bands, taken on a Hilger E-1 spectrograph with glass optics, are reproduced in Figure 1. There are two central sequences. The bands of the one to the longward side have only one head (marked P_1), whereas the bands of the other one have two heads (marked P_2 and Q_2). These can easily be identified as corresponding to the components $^3\Pi_0 \rightarrow {}^1\Sigma$ and $^3\Pi_1 \rightarrow {}^1\Sigma$, respectively, of a $^3\Pi \rightarrow {}^1\Sigma$ transition in Hund's coupling case *a*.[5] The $^3\Pi_2 \rightarrow {}^1\Sigma$ component does not occur on account of the selection rule $\Delta\Omega = 0, \pm 1$.

The wave lengths of all the band heads of the new system, along with their wave numbers in vacuum, are listed in Table 1. Arranging these bands in a Deslandres scheme, one finds that, as expected, the $\Delta G''_{v+1/2}$ values for the Q_2 heads are, within experimental error, the same as those for the lower state of the main $A^1\Pi - X^1\Sigma$ system of *AlBr*. Therefore, the ω_e'' and $\omega_e''x_e''$ values determined from the measurements[3] of the main system have been used. The Q_2 heads, which lie very near the band origins, are found to correspond to the equation

$$\nu_{Q_2} = 23779.3 + (410.32u' - 1.75u'^2) - (378.00u'' - 1.28u''^2), \qquad (1)$$

where $u = v + \frac{1}{2}$. The P_2 heads are slightly to the longward side from the corresponding Q_2 heads. As no Q heads occur in the $^3\Pi_0 \rightarrow {}^1\Sigma$ transition, the corresponding constants have to be evaluated from P heads only. The P_2 and P_1 heads conform to the following equations:

$$\nu_{P_2} = 23773.6 + (410.40u' - 1.85u'^2) - (377.28u'' - 1.26u''^2), \qquad (2)$$

$$\nu_{P_1} = 23641.3 + (411.25u' - 1.85u'^2) - (377.28u'' - 1.26u''^2). \qquad (3)$$

It will be observed from the last two equations that the ω_e' values in the two components $^3\Pi_1$ and $^3\Pi_0$ differ by 0.85 cm^{-1}. This is not unlikely in view of a triplet splitting of 132 cm^{-1}. The vibrational assignments of the heads are given in the third column of Table 1.

[1] D. Sharma, *Ap. J.*, 113, 210, 1951.
[2] H. G. Howell, *Proc. R. Soc. London, A*, 148, 696, 1935.
[3] C. G. Jennergren, *Ark. Mat. Astr. Fys.*, Vol. 35A, No. 22, 1948.
[4] P. C. Mahanti, *Indian J. Phys.*, 9, 369, 1935.
[5] G. Herzberg, *Molecular Spectra and Molecular Structure*, Vol. I: *Spectra of Diatomic Molecules* (New York: D. Van Nostrand Co., Inc., 1950).

TABLE 1

THE $^3\Pi \rightarrow {}^1\Sigma$ BANDS OF *AlBr*

λ_{air} (A)	ν_{vac} (Cm^{-1})	Assignments	O−C (Cm^{-1})	λ_{air} (A)	ν_{vac} (Cm^{-1})	Assignments	O−C (Cm^{-1})
4052.64.....	24668.3	12, 10 P_1	−2.0	4131.83.....	24195.6	1, 0 P_2	+0.2
53.09.....	65.6	12, 10 P_1*	−1.5	35.29.....	75.3	5, 4 P_1	+0.3
54.84.....	54.9	11, 9 P_1	−0.7	35.59.....	73.6	5, 4 P_1	+0.2
55.34.....	51.9	11, 9 P_1	−0.5	39.62.....	50.0	4, 3 P_1	+0.6
57.38.....	39.6	10, 8 P_1	0.0	39.89.....	48.4	4, 3 P_1	+0.5
57.83.....	36.8	10, 8 P_1	+0.3	44.32.....	22.6	3, 2 P_1	−0.1
60.15.....	22.7	9, 7 P_1	+0.2	44.57.....	21.2	3, 2 P_1	0.0
60.64.....	19.7	9, 7 P_1	+0.2	49.08.....	095.0	2, 1 P_1	+0.2
63.15.....	04.5	8, 6 P_1	+0.3	49.36.....	93.3	2, 1 P_1	−0.1
63.60.....	01.8	8, 6 P_1	+0.6	54.06.....	66.1	1, 0 P_1	+0.4
66.37.....	585.0	7, 5 P_1	+0.3	54.33.....	64.5	1, 0 P_1	+0.1
66.85.....	82.1	7, 5 P_1	+0.3	85.22.....	23886.9	3, 3 Q_2	+0.2
69.85.....	64.0	6, 4 P_1	0.0	86.12.....	81.8	3, 3 P_2	−0.5
70.32.....	61.2	6, 4 P_1	0.0	90.46.....	57.0	2, 2 Q_2	−0.2
73.53.....	41.8	5, 3 P_1	−0.4	91.30.....	52.2	2, 2 P_2	−0.5
74.01.....	38.9	5, 3 P_1	−0.5	95.79.....	26.7	1, 1 Q_2	0.0
77.37.....	18.7	4, 2 P_1	−0.4	96.68.....	21.7	1, 1 P_2	−0.2
77.83.....	15.9	4, 2 P_1	−0.5	4201.36.....	795.1	0, 0 Q_2	−0.2
81.33.....	494.9	3, 1 P_1	0.0	02.28.....	89.9	0, 0 P_2	−0.1
81.84.....	91.9	3, 1 P_1	−0.4	03.54.....	82.8	4, 4 P_1	+0.6
85.52.....	69.8	2, 0 P_1	+0.3	08.81.....	53.0	3, 3 P_1	0.0
86.03.....	66.8	2, 0 P_1	−0.2	14.24.....	22.4	2, 2 P_1	−0.1
4108.52†.....	332.8	6, 5 Q_2	+0.6	19.85.....	690.9	1, 1 P_1	0.0
08.85†.....	30.9	.....	.....	25.74.....	57.9	0, 0 P_1;	−0.2;
09.76†.....	25.5	6, 5 P_2	−0.6			8, 9 P_2	0.0
10.06†.....	23.7	6, 5 P_2	−0.7	29.69.....	35.8	7, 8 Q_2	−1.9
10.62†.....	20.4	12, 11 P_1	−0.4	30.43.....	31.6	7, 8 P_2	−0.1
10.93†.....	18.6	12, 11 P_1	−0.1	34.48.....	09.0	6, 7 Q_2	−0.4
12.90†.....	06.9	5, 4 Q_2	−1.1	35.33.....	04.3	6, 7 P_2	0.0
13.76†.....	01.8	5, 4 P_2;	−0.8;	39.69.....	580.0	5, 6 Q_2	−0.2
		11, 10 P_1	+0.3	40.48‡.....	75.6	5, 6 P_2	−0.1
14.09†.....	299.9	5, 4 P_2	−1.1	45.08‡.....	50.1	4, 5 Q_2	+0.1
16.41†.....	86.2	.....	.....	45.84.....	45.9	4, 5 P_2	−0.1
16.71†.....	84.4	10, 9 P_1;	−0.6;	50.54.....	19.8	3, 4 Q_2	+0.9
		4, 3 Q_2	+1.4	51.31‡.....	15.6	3, 4 P_2	+0.5
17.96†.....	77.0	4, 3 P_2	−0.9	56.41.....	487.4	2, 3 Q_2	+0.6
18.19†.....	75.7	4, 3 P_2	−0.6	57.21.....	83.0	2, 3 P_2	0.0
19.70†.....	66.8	9, 8 P_1	+1.4	62.36‡.....	54.6	1, 2 Q_2	+0.8
19.98†.....	65.1	9, 8 P_1	+1.6	63.27.....	49.6	1, 2 P_2	−0.1
22.30.....	51.5	3, 2 P_2	−0.5	68.62.....	20.2	0, 1 Q_2	+0.3
22.52.....	50.2	3, 2 P_2	−0.4	69.42.....	15.8	0, 1 P_2	+0.5
23.26†.....	45.8	8, 7 P_1	+1.3	74.79.....	386.4	3, 4 P_1	+0.6
23.57†.....	44.0	8, 7 P_1	+1.3	80.87.....	53.2	2, 3 P_1	+0.4
24.15†.....	40.6	.....	.....	87.13.....	19.1	1, 2 P_1	+0.4
24.46†.....	38.8	.....	.....	93.60.....	284.0	0, 1 P_1	+0.6
25.27†.....	34.0	.....	.....	4306.16.....	16.0	5, 7 P_2	−0.1
25.68†.....	31.6	.....	.....	12.13.....	183.9	4, 6 P_2	0.0
26.04.....	29.5	2, 1 Q_2	−0.5	18.34.....	50.6	3, 5 P_2	+0.2
26.87.....	24.6	2, 1 P_2	−0.3	24.61.....	17.0	2, 4 P_2	+1.2
27.10.....	23.3	7, 6 P_1;	+0.8;	31.64.....	079.5	1, 3 P_2	−0.5
		2, 1 P_2	−0.3	38.45.....	43.3	0, 2 P_2	+0.3
30.72.....	02.0	1, 0 Q_2	−0.2	49.11.....	22986.8	2, 4 P_1	+1.2
30.91.....	00.9	6, 5 P_1	+1.6	56.35.....	48.6	1, 3 P_1	−0.4
31.51.....	197.4	1, 0 P_2;	+0.7;	63.43.....	11.3	0, 2 P_1	+0.2
		6, 5 P_1	−0.2				

* Indicates the heads due to the heavier isotope $Al^{27}Br^{81}$.

† Lines or bands of doubtful origin due to several other lines in that region.

‡ Heads coincident with lines of the 4241 A *AlH* band.

The differences between the observed and calculated values, entered in the last column of the table, show that the agreement is quite satisfactory.

Since B_e'' and α_e'' are known[8] to be 0.1591 and 0.000853 cm^{-1}, respectively, one obtains from the P_2- and Q_2-head separations the approximate values $B_e' = 0.164$ cm^{-1} and $\alpha_e' = 0.001$ cm^{-1}.

The bands of the sequence $\Delta v = +2$ at first sight appear like the rotational structure of a hydride band, with lines in pairs and the structure breaking off suddenly. The two lines in each pair are almost equally intense and have a separation of about 2.5–3 cm^{-1}. This is indeed equal to the calculated isotope shift for bands due to the two equally abundant isotopic molecules $AlBr^{79}$ and $AlBr^{81}$. The linelike structure of these bands can be accounted for by the fact that, as Δv increases, B_v' and B_v'' become more and more nearly equal, as can be seen from the rough values of B_e' and α_e' found above. Incidentally, the head of heads of this sequence is visible at about 4045 A. The isotopic heads of the $\Delta v = +1$ sequence are just resolved and have the correct shift of about 1.5 cm^{-1}. Since the difference between B_v' and B_v'' for the bands of the $\Delta v = -2$ sequence is greater than that for the bands of the $\Delta v = +2$ sequence, the bands of the former sequence are not so linelike as are those of the $\Delta v = +2$ sequence, and consequently the two isotopic heads are not resolved. To some extent similar considerations hold for the bands of the $\Delta v = -1$ sequence also.

Comparing, in Table 2, the molecular constants determined for the $a^3\Pi$ state of *AlBr*

TABLE 2

THE MOLECULAR CONSTANTS FOR THE $a^3\Pi$ STATE OF *AlCl*, *AlBr*, AND *AlI*
(All Values Are in Cm^{-1})

Molecule	State	T_e	A	ω_e	$\omega_e x_e$	B_e	α_e
AlCl.....	$^3\Pi_2$ $^3\Pi_1$ $^3\Pi_0$	24658 24593.8 24528	65	524.35	2.175	0.250	0.002
AlBr.....	$^3\Pi_1$ $^3\Pi_0$*	23779.3 23647	132	410.32 411.2	1.75 1.75	0.164	0.001
AlI.....	$^3\Pi_1$ $^3\Pi_0$	22089.5 21889.3	200	333.4 337.2	2.0 2.0	.....	.....

* These constants have been calculated for the origins from those for the P_1 heads.

with the corresponding values for *AlCl*[1] and *AlI*,[6] one finds that they fit well into the sequence.

The author has great pleasure in recording his thanks to Dr. G. Herzberg and Dr. A. E. Douglas for their kind interest and helpful suggestions during the course of the work.

[8] E. Miescher, *Helvetica Phys. Acta*, **8**, 279, 1935.

NOTES

PHOTOGRAPHS WITH THE HENYEY-GREENSTEIN WIDE-ANGLE CAMERA

The photographs illustrated in Figures 1–6 were obtained with a camera designed by L. G. Henyey, now of the University of California, and J. L. Greenstein, now of the California Institute of Technology, when both were members of the staff of the Yerkes Observatory.

The camera was constructed in the optical shop of the observatory by Messrs. Fred Pearson and Charles Ridell. In principle it consists of a lens which photographs the image formed by a spherical mirror; it has a field of approximately 140° and works at an effective aperture ratio of $f/2$. The lens and plateholder are supported in a position several feet in front of the mirror by means of three struts; the shadows of the plateholder and struts are visible in all the plates. The diameter of the field on the original plates is 21.5 mm; the enlargement of the plates is therefore approximately six times.

Figures 1, 2, and 3 illustrate the appearance of the Milky Way from Sagittarius to Canis Major. Figure 4 shows the Gegenschein, and Figures 5 and 6 illustrate the great aurora of August 19–20, 1950. The position of the center of the Gegenschein on Figure 4 agrees closely with the longitude of the antisolar point; this result is at variance with the recent determination of D. A. Rojkovsky.[1]

We are indebted to Dr. W. W. Morgan for advice and assistance in preparing the reproductions.

DONALD OSTERBROCK*
STEWART SHARPLESS

YERKES OBSERVATORY
October 23, 1950

ROTATIONAL STRUCTURE IN THE *R* BRANCH OF THE ATMOSPHERIC NITROUS OXIDE BAND AT 8.6 μ

In a recent contribution to this *Journal*, Migeotte discusses the feeble fine structure in the *R* branch of the very weak nitrous oxide band at 8.6 μ in the atmospheric spectrum.[1] Repeating an earlier error by Sutherland and Callendar,[2] Migeotte mistakenly asserts that the faint fine structure of this weak and minor band is completely absent from the author's grating map of the infrared solar spectrum, published a decade ago.[3] Migeotte has obviously overlooked Figure 28 of the map, for even a cursory examination of this segment unmistakably reveals ten lines in the *R* branch of the weak 8.6 μ band. These atmospheric lines, positions taken from Figure 28, are listed in Table 1 below, together with their laboratory comparisons.[4]

[1] *A.J. Acad. Sci. U.S.S.R.*, **27**, 34, 1950.

* Atomic Energy Commission Pre-doctoral Fellow in Astrophysics.

[1] M. V. Migeotte, *Ap. J.*, **112**, 136, 1950.

[2] G. B. B. M. Sutherland and G. S. Callendar, *Rep. Prog. Phys.*, **9**, 18, 1943.

[3] A. Adel, *Ap. J.*, **94**, 451, 1941.

[4] E. K. Plyler and E. F. Barker, *Phys. Rev.*, **38**, 1827, 1931.

FIG. 1.—The Milky Way from Sagittarius to Perseus, October 12, 1950. Exposure, 15 minutes on Eastman 103*a*-O emulsion.

FIG. 2.—The Milky Way from Sagitta to Auriga, October 10, 1950. Exposure, 15 minutes on Eastman 103*a*-O emulsion.

FIG. 3.—The Milky Way from Cassiopeia to Canis Major, October 12, 1950. Exposure, 15 minutes on Eastman 103*a*-F emulsion. The zodiacal light appears in the lower left part of the plate.

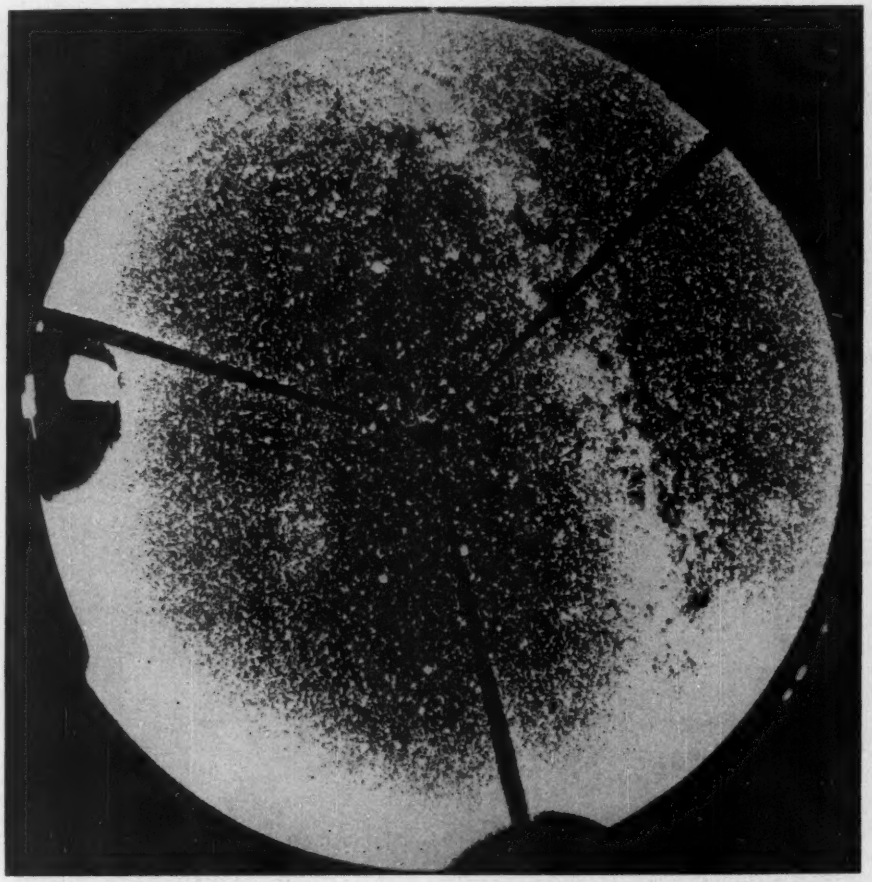

FIG. 4.—The Gegenschein, October 10, 1950. Exposure, 15 minutes on Eastman 103*a*-F emulsion. The Gegenschein and a small part of the zodiacal band are visible in the lower left-central part of the plate. The plate has been copied to high contrast.

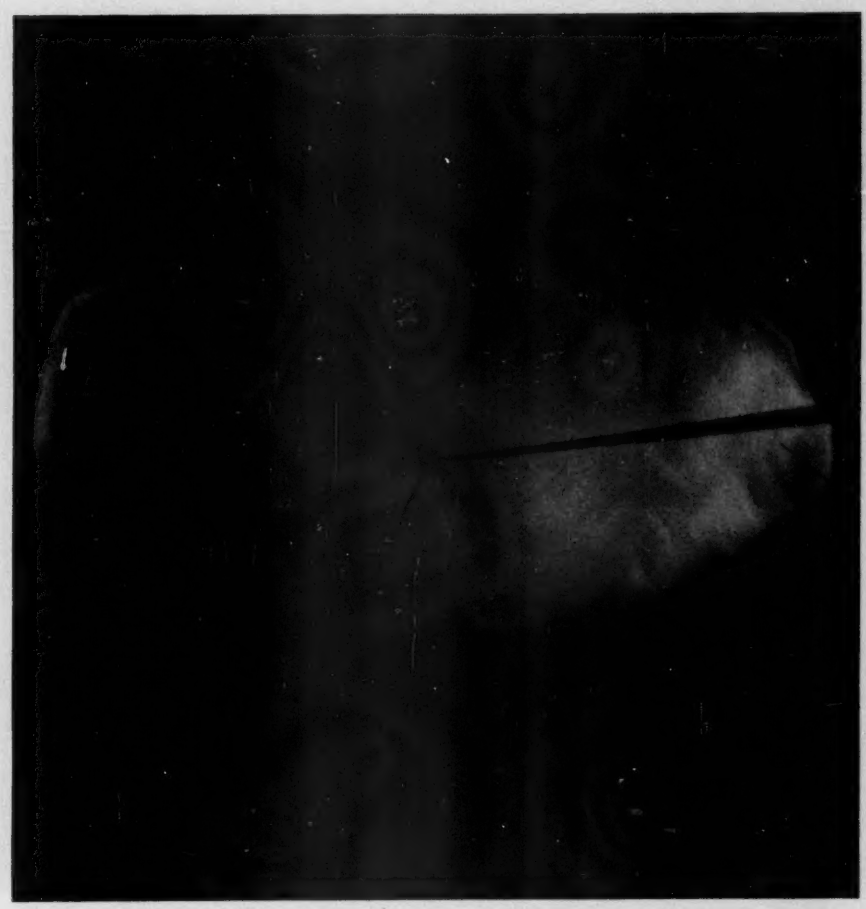

FIG. 5.—The aurora of August 20, 1950. Exposure, 10 seconds on Eastman 103*a*-F emulsion. The star Vega is in the upper right-central part of the plate.

FIG. 6.—The aurora of August 20, 1950. Exposure, 10 seconds on Eastman 103*a*-F emulsion. The star Vega is in the right-central part of the plate.

TABLE 1

R BRANCH LINES IN ATMOSPHERIC
N_2O AT 8.6μ

Solar Spectrum* (Cm^{-1})	Laboratory† (Cm^{-1})	Laboratory *minus* Solar Spectrum (Cm^{-1})	Solar Spectrum* (Cm^{-1})	Laboratory† (Cm^{-1})	Laboratory *minus* Solar Spectrum (Cm^{-1})
1171.2.....	1171.4	0.2	1181.6.....	1181.8	0.2
1172.1.....	1172.2	.1	1182.5.....	1182.7	.2
1176.3.....	1176.7	.4	1183.4.....	1183.6	.2
1177.4.....	1177.5	.1	1184.2.....	1185.4	.2
1178.5‡.....	1179.2	.7	1185.2.....	1185.3	0.1
1179.7.....	1180.0	0.3			

* Adel, *Ap. J.*, **94**, 451, 1941.
† Plyler and Barker, *Phys. Rev.*, **38**, 1827, 1931.
‡ N_2O line perturbed by additional absorption of independent origin.

ARTHUR ADEL

ARIZONA STATE COLLEGE
FLAGSTAFF, ARIZONA
October 9, 1950

A LIST OF NEWLY DISCOVERED PECULIAR OBJECTS

In the classification of Harvard objective-prism spectral plates (dispersion 95 A/mm at $H\gamma$) I have found the objects with peculiar spectra shown in the accompanying tabulation.

Star	α 1855	δ 1855	m	Spectral Type
BD+60°114.....	$0^h41^m.7$	+60° 7'.1	9.5	Be
BD+30°4282.....	20 55.1	+30 42.7	9.2	Be
BD+51°3330.....	22 13.5	+51 23.7	8.5	Bnne
BD+44°3607.....	20 46.8	+44 44.3	8.9	Composite
BD+45°3741.....	21 51.4	+45 54.2	6.9	Composite
BD+53°2849.....	22 15.0	+53 4.9	8.3	Composite
	23 26.2	+61 13.0	9.5?	WN6:
BD+60°2613.....	23 37.1	+60 59.2	9.5	WN8:

The stars classified as emission-line B stars are not included in any of Merrill's lists of Be stars. Each of them shows an emission component on the red side of $H\beta$; the spectra of the first two appear very faint, so that it is not possible to describe them further. All the hydrogen lines in BD+51°3330 are very much widened.

None of the composites in the above list have been classified as such in the *HD Catalogue;* nor do they appear in Hynek's list[1] of composite spectra. The spectra, in general, correspond respectively to classes F2, G2 III, and F5, while the relatively weak K lines are appropriate to an early A star.

The objects identified as Wolf-Rayet stars appear as very faint spectra on one plate,

[1] J. A. Hynek, *Contr. Perkins Obs.*, No. 10, 1938.

though the visible emission bands suffice for assigning approximate spectral types.[2] In the first star the features at λλ 4605–4622 (*N* v), λ 4638 (*N* III), λ 4686 (*He* II), and *Hβ* are characteristic of class WN6. The spectrum of BD+60°2613 is much fainter, and the classification is more uncertain.

MIRIAM E. WALTHER JAFFE

HARVARD COLLEGE OBSERVATORY
June 30, 1949

CONCERNING EGGEN'S PARALLAXES AND SCHLESINGER'S PROBABLE ERRORS

In a recent paper on the color-luminosity array[1] Olin J. Eggen published his photoelectric measures of magnitudes and colors for 180 stars in the region of the sun. In Table 4 he lists the parallaxes of seventeen subgiants as derived on the assumption of a uniform absolute photographic magnitude equal to +3.60; these "photometric" parallaxes are compared with the corresponding trigonometric parallaxes given in Schlesinger's *Catalogue*.[2] Eggen finds that the agreement between the two sets is much better than could be expected from the probable errors published in the parallax catalogue. Thus the average difference between the individual values in the two sets amounts to only $\pm 0''.0032$, whereas the average of the seventeen tabulated probable errors of the trigonometric parallaxes alone amounts to $\pm 0''.0061$. Eggen remarks that "a study of the probable errors given by Schlesinger on the basis of agreements between different determinations for each star shows that his probable errors should be reduced by an average factor of 0.7."

I should like to point out that Eggen's explanation is not admissible, since it is well established that there was once a tendency among parallax observers to withhold publication of a determination which differed greatly from previously published determinations.[3] Thus the interagreement of various determinations for one star does not yield a reliable value of the probable error of the combined parallax. The consensus among parallax workers is that Schlesinger's probable errors are just about right and that they have been derived in a sound statistical manner. A reduction of these errors by a factor of 0.7 is out of the question. The exceptionally close agreement between the trigonometric and "photometric" parallaxes must be explained in a different manner.

A. N. VYSSOTSKY

LEANDER MCCORMICK OBSERVATORY
September 12, 1950

[2] *Trans. I.A.U.*, **6**, 248–253, 1938.

[1] *Ap. J.*, **112**, 141, 1950.

[2] *General Catalogue of Stellar Parallaxes* (2d ed.; New Haven: Yale University Observatory, 1935).

[3] J. Schilt, *A.J.*, **48**, 53, 1939 (see Table 12).

THE OBSERVATORY

FOUNDED 1877

* * *

A Magazine presenting current developments in Astronomy by means of Articles, Correspondence, Notes on discoveries and Reviews of important astronomical books. The papers read at the Meetings (Astronomical & Geophysical) of the Royal Astronomical Society and the discussions which follow are also fully reported.

* * *

Annual subscription for 6 issues, post free, £1 should be sent to

The Editors, ROYAL OBSERVATORY
Greenwich, London S.E., 10

Now available . . .

MICROFILMS

of the

ASTROPHYSICAL JOURNAL

Complete Journal volumes may now be obtained in a single roll of positive microfilm on adequately labeled metal reels at a cost of approximately one-fourth of a cent per page, which is about equal to that of preserving them in conventional library binding. Sales will be restricted to those subscribing to the paper edition, and the film copy will be distributed only at the end of the calendar year, after publication of the November issue.

Inquiries should be directed to

UNIVERSITY MICROFILMS
313 N. FIRST ST. ANN ARBOR, MICH.

POPULAR ASTRONOMY

A magazine now in its fifty-ninth year, devoted to the elementary aspects of Astronomy and allied sciences.

Published monthly, except July and September.

Yearly subscription rates: Domestic $4.00; Canadian $4.25; Foreign $4.50 (U.S. dollars).

Address

POPULAR ASTRONOMY
CARLETON COLLEGE
NORTHFIELD, MINNESOTA, U.S.A.

ASTROPHYSICAL MONOGRAPHS

Sponsored by the Editors of the Astrophysical Journal

PRINCIPLES OF STELLAR DYNAMICS

By S. CHANDRASEKHAR

In this monograph the dynamical methods of interpreting the distribution of the galaxy, spiral nebulae, and star clusters are developed from a coherent point of view. "This book should exert a profound influence on the future development of the field of galactic dynamics. I can recommend its study unreservedly to newcomers in the field and to those who already have a passing acquaintance with its problems. The experts can profit from reading it."—BART J. BOK, in *Science*. 1942. $3.00

SPECTRA OF LONG-PERIOD VARIABLE STARS

By PAUL W. MERRILL

This monograph is devoted largely to the observational side of the subject, but some discussion of the physical significance of various spectral features is included. A brief introduction and a historical chapter are inserted for the benefit of the reader who is not a specialist in stellar spectra. "To one wishing an intimate view of our present knowledge of the spectra of long-period variable stars, whether he be student, astronomer, physicist, or chemist, the present monograph is indispensable."—J. H. MOORE in *Astronomical Society of the Pacific*. 1940. *Paper*, $3.00

THE MASSES OF THE STARS, WITH AN APPENDIX: A GENERAL CATALOGUE OF DYNAMICAL PARALLAXES

By HENRY NORRIS RUSSELL *and* CHARLOTTE E. MOORE

"Astrophysicists will be grateful to the authors for so thorough and critical a compilation of available knowledge. . . . We may be permitted to congratulate the senior author on this magnificent outgrowth from an idea which germinated in his mind thirty years ago."—PROFESSOR A. S. EDDINGTON, *The Observatory* (England). 1940. *Paper*, $4.50

THE DISTRIBUTION OF THE STARS IN SPACE

By BART J. BOK

". . . an extremely important contribution to the field of galactic structure, invaluable alike to both students and research workers in the field."—*Science*. The large number and variety of researches carried out in this field during the past fifteen years are discussed critically in this study with clarity and dispatch. 1937. *Paper*, $2.50

THE UNIVERSITY OF CHICAGO PRESS